Friedrich-Schiller-Universität Jena

Chemisch-Geowissenschaftlichen Fakultät

Characterization of macromolecular systems by mass spectrometry and hyphenated techniques

Dissertation

(kumulativ)

zur Erlangung des akademischen Grades

doctor rerum naturalium (Dr. rer. nat.)

vorgelegt dem Rat der Chemisch-Geowissenschaftlichen Fakultät der Friedrich-Schiller-Universität Jena

von M.Sc. Sarah Charlotte Crotty

geboren am 5. Mai 1987 in Ambilly (Frankreich)

Gutachter:

1. .....
2. .....

Tag der öffentlichen Verteidigung: .....

Continue to grow and evolve

Mahatma Gandhi

Table of Contents

Documentation of authorship

This section contains a list of the individual author contributions to the publications reprinted in this thesis

P1) S. Crotty,[1] S. Gerişlioğlu,[2] K. J. Endres,[3] C. Wesdemiotis,[4] U. S. Schubert,[5] Polymer architectures *via* mass spectrometry and hyphenated techniques: A review, *Anal. Chim. Acta* **2016**, *932*, 1-21.

Author	**1**	**2**	**3**	**4**	**5**
Conceptual development	X				
Preparation of the manuscript	X	X	X		
Correction of the manuscript				X	X
Supervision S. Crotty					X
Proposed publication equivalent	0.5				

P2) M. J. Barthel,[#1] T. Rudolph,[#2] S. Crotty,[3] F. H. Schacher,[4] U. S. Schubert,[5] Homo- and diblock copolymers of poly(furfuryl glycidyl ether) by living anionic polymerization: Towards reversibly core-crosslinked micelles, *J. Polym. Sci., Part A: Polym. Chem.* **2012**, *50*, 4958-4965.

Author	**1**	**2**	**3**	**4**	**5**
Conceptual development	X	X		X	
Polymer synthesis and characterization	X	X			
MALDI-ToF MS measurements			X		
Cross-linking studies	X	X			
DLS measurements		X			
Preparation of the manuscript	X	X			
Correction of the manuscript				X	X
Supervision				X	X
Proposed publication equivalent			0.25		

[#] equal contribution

P3) C. von der Ehe,[1] F. Kretschmer,[2] C. Weber,[3] S. Crotty,[4] S. Stumpf,[5] S. Hoeppener,[6] M. Gottschaldt,[7] U. S. Schubert,[8] RAFT copolymerization of thioglycosidic glycomonomers with *N*iPAm and subsequent immobilization onto gold nanoparticles, in *ACS Symposium Series, Issue Controlled Radical Polymerization* (Eds.: K. Matyjaszewski, B.S. Summerlin, N.V. Tsarevsky, J. Chiefari), Wiley-VH Verlag GmbH & Co. KGaA, 2015, pp. 221-256.

Author	**1**	**2**	**3**	**4**	**5**	**6**	**7**	**8**
Conceptual development	X		X				X	
Preparation of the manuscript	X							
Polymer synthesis	X							
Characterization by MALDI-ToF MS				X				
Gold nanoparticle synthesis	X	X						
TEM measurement					X	X		
Correction of the manuscript		X	X	X	X	X	X	X
Supervision S. Crotty								
Proposed publication equivalent				0.25				

P4) S. Crotty,[1] C. von der Ehe,[2] C. Weber,[3] U. S. Schubert,[4] Detailed MALDI comparison of *N*iPAm glycopolymers, *Eur. Polym. J.* **2015**, *71*, 325-335.

Author	**1**	**2**	**3**	**4**
Conceptual development	X		X	
Preparation of the manuscript	X			
Characterization by MALDI-ToF MS	X			
Polymer synthesis		X		
Correction of the manuscript		X	X	X
Supervision S. Crotty				X
Proposed publication equivalent	1.0			

P5) G. M.-E. Pozza,[1] S. Crotty,[2] M. Rawiso,[3] U. S. Schubert,[4] P. J. Lutz,[5] Molecular and structural characterization of hybrid poly(ethylene oxide)-polyhedral oligomeric silesquioxanes star-shaped macromolecules, *J. Phys. Chem. B* **2015**, *119*, 1669-1680.

Author	**1**	**2**	**3**	**4**	**5**
Conceptual development	X				X
Polymer synthesis and characterization	X				
Characterization by MALDI-ToF MS		X			
Characterization by SAXS			X		
Preparation of the manuscript	X				
Correction of the manuscript		X	X	X	X
Supervision G. M.-E. Pozza				X	X
Supervision S. Crotty				X	
Proposed publication equivalent		0.25			

P6) T. Rudolph,[1] S. Crotty,[2] M. von der Luehe,[3] D. Pretzel,[4] U. S. Schubert,[5] F. H. Schacher,[6] Synthesis and solution properties of double hydrophilic poly(ethylene oxide)-*block*-poly(2-ethyl-2-oxazoline) (PEO-*b*-PEtOx) star block copolymers, *Polymers* **2013**, *5*, 1081-1101.

Author	**1**	**2**	**3**	**4**	**5**	**6**
Conceptual development	X					
Synthesis and characterization of polymers	X		X			
Characterization by 2D (LCCC × SEC), MALDI-ToF MS		X				
Preparation of the manuscript	X			X		X
Correction of the manuscript	X	X	X	X	X	X
Supervision of T. Rudolph						X
Supervision of M. von der Luehe	X					X
Supervision S. Crotty					X	
Proposed publication equivalent		0.5				

P7) S. Crotty,[1] C. Weber,[2] A. Baumgaertel,[3] N. Fritz,[4] E. Altuntaş,[5] K. Kempe,[6] U. S. Schubert,[7] Semi-automated multi-dimensional characterization of synthetic copolymers, *Eur. Polym. J.* **2014**, *60*, 153-162.

Author	**1**	**2**	**3**	**4**	**5**	**6**	**7**
Conceptual development	X						
Characterization by LCCC, MALDI-ToF MS, spotting	X			X			
Characterization by ESI MS					X		
Polymer synthesis		X				X	
Preparation of the manuscript	X						
Correction of the manuscript		X	X		X		X
Supervision S. Crotty							X
Proposed publication equivalent	1.0						

P8) M. S. Engler,[#1] S. Crotty,[#2] M. J. Barthel,[3] C. Pietsch,[4] K. Knop,[5] U. S. Schubert,[6] S. Boecker,[7] COCONUT − an efficient tool for estimating copolymer compositions from mass spectra, *Anal. Chem.* **2015**, *57*, 5223-5231.

Author	**1**[#]	**2**[#]	**3**	**4**	**5**	**6**	**7**
Conceptual development	X	X					
Polymer synthesis			X				
Polymer characterization		X					
Development of algorithms	X						
Preparation of the manuscript	X	X					
Correction of the manuscript			X	X	X	X	X
Supervision M. S. Engler							X
Supervision S. Crotty					X	X	X
Proposed publication equivalent		1.0					

[#] equal contribution

P9) M. S. Engler,[#1] S. Crotty,[#2] M. J. Barthel,[3] C. Pietsch,[4] U. S. Schubert,[5] S. Boecker,[6], Abundance correction for mass discrimination effects in polymer spectra, *Rapid Commun. Mass Spectrom.* **2016**, *30*, 1233-1241.

Author	**1**	**2**	**3**	**4**	**5**	**6**
Conceptual development	X	X				
Synthesis of polymers			X			
Characterization by SEC, NMR, MALDI-ToF MS		X				
Algorithm development	X					
Preparation of the manuscript	X	X				
Correction of the manuscript			X	X	X	X
Supervision of S. Crotty				X	X	
Supervision of M. S. Engler						X
Proposed publication equivalent		1.0				

[#] equal contribution

Erklärung zu den Eigenanteilen des Promovenden/der Promovendin sowie der weiteren Doktoranden/Doktorandinnen als Koautoren an den Publikationen und Zweitpublikationsrechten bei einer kumulativen Dissertation

Für alle in dieser kumulativen Dissertation verwendeten Manuskripte liegen die notwendigen Genehmigungen der Verlage („Reprint permissions") für die Zweitpublikation vor.

Die Co-Autoren der in dieser kumulativen Dissertation verwendeten Manuskripte sind sowohl über die Nutzung, als auch über die oben angegebenen Eigenanteile informiert und stimmen dem zu.

Die Anteile der Co-Autoren an den Publikationen sind in diesem Kapitel aufgeführt (Documentation of authorship).

Ich bin mit der Abfassung der Dissertation als publikationsbasiert, d.h. kumulativ, einverstanden und bestätige die vorstehenden Angaben. Eine entsprechend begründete Befürwortung mit Angabe des wissenschaftlichen Anteils des Doktoranden/der Dokorandin an den verwendeten Publikationen werde ich parallel an den Rat der Falkultät der Chemisch-Geowissenschaftlichen Fakultät richten.

Sarah C. Crotty	Datum	Ort	Unterschrift
Prof. Ulrich S. Schubert	Datum	Ort	Unterschrift

1. Introduction

Synthetic polymers are of great interest due to their use on a daily basis. Different polymer classes and architectures play a key role in a wide range of applications such as packaging, clothes, vehicles, drug delivery, etc..[1-3] Specific architectures and well-defined polymers are essential to be designed for precise applications from linear, star-shaped to branched copolymers. A number of polymerization techniques are used to tailor and engineer different structures and monomers for polymers. Several polymerization techniques have been developed throughout the years, which can be used to tailor smart polymers.[4-10]

Besides these synthetic routes, analytical methods are of great importance to characterize polymers. Numerous separation and structural techniques have been developed to obtain information about molar masses, dispersities, compositions, end groups and architectures (Figure 1.1).

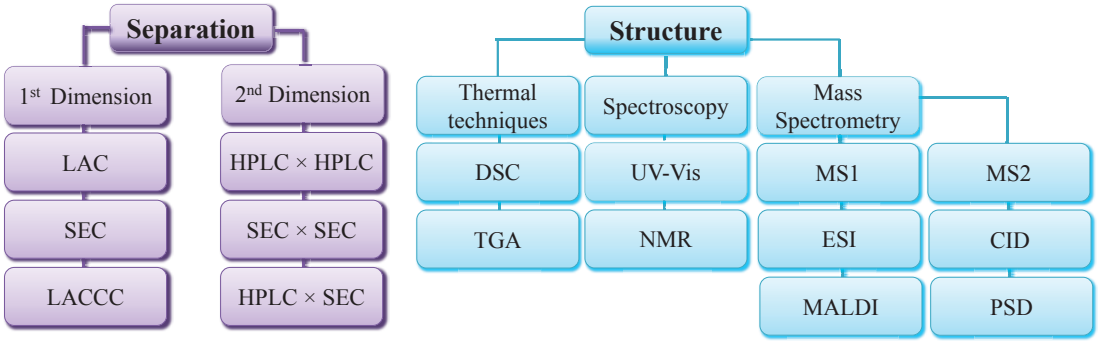

Figure 1.1 Schematic overview of selected analytical techniques used for the characterization of various (co)polymer architectures.

Besides the selected techniques shown in Figure 1.1, less traditional methods are applied such as analytical ultracentrifugation (AUC), asymmetrical flow field-flow fractionation (AF4) and mass spectrometry (MS). Several MS ionization techniques have been used over the last 30 years to obtain an in depth knowledge of polymer systems.[11, 12] Examples are is matrix-assisted laser desorption/ionization (MALDI)[13, 14] as well as electrospray ionization (ESI),[15] which are used constantly to obtain detailed information on side products and polymerization processes.[16-19] MALDI is very frequently used due to its ability to ionize singly charged species, which represents an advantage in comparison to ESI (discussed in Chapter 3).[12, 20] Moreover, tandem

mass spectrometry (MS/MS) has also evolved to sequence polymers, a technique which was initially used for end group determination. Collision induced dissociation (CID) and post source decay (PSD) are the two mainly applied techniques used for the fragmentation of polymers, and were firstly utilized in the field of proteomics.[21, 22] During PSD, fragments are formed after the source, *i.e.* in the flight tube. This actually means that the collision energy is not dependent on the ionization parameters, but on the extraction voltage. High-energy CID is equivalent to PSD in terms of collision energy, which is in the range of keV. CID promotes more fragments than PSD, which makes it harder to select the parent ion and complicates the spectrum, however, providing also additional information. Moreover, ion mobility-mass spectrometry (IM-MS) is a recently developed technique, which can provide architectural information (*e.g.* the shape) of polymers. This technique is extremely powerful because of its speed and fruitful information, which would be normally acquired by MS/MS or liquid chromatography (LC)-MS/MS.

Aside using MS methods for determining structure, functionality and molar masses, additional characterization methods are of essence for synthetic polymers.[23] As a consequence, combined techniques *i.e.* online or offline hyphenated systems to MS have expanded the knowledge of chemists (discussed in Chapter 4).[18, 24-26] Nonetheless, considering hyphenation as an important tool to develop clarity upon synthetic polymers, computational methods have grown to accelerate our knowledge of polymer systems. Mostly MS spectra have been used to compute chain lengths, average compositions, architectures.

The focus of this thesis was to gain in-depth structural information of synthetic polymers by the application of several combined techniques. Traditional methods such as size exclusion chromatography (SEC) and nuclear magnetic resonance (NMR) are now complemented with more complex techniques such as mass spectrometry, advanced chromatographic and computational methods.

The second chapter provides an overview about the state of the art considering the influence of the polymer architecture on its characterization by mass spectrometry, thereby providing a general overview of the field. Homopolymers, *i.e.* polymers obtained from one monomer only, were investigated with MS evaluating their architecture. Secondly, linear copolymers were investigated and complementary methods were required for a detailed characterization. Finally, the most complex polymers with special architectures, *i.e.* nonlinear polymers, were also analyzed with

MS. However, such systems demand extensive knowledge of the polymer class and complementary methods to elucidate the architecture.

In the third chapter, we demonstrate the use of MS for molar mass distributions in comparison to SEC, which requires specific standards if absolute values are to be obtained. MALDI-ToF MS is superior due to its diverse use of matrices for specific species. The first example shows how MALDI-ToF MS could be a fast and informative method for high molar masses polymers and, thus, provides molar masses and dispersity values for poly(furfuryl glycidyl ether) (PFGE), a polymer with self-healing properties. The second example is the study of poly(*N*-*iso*propyl acrylamide) (P*N*iPAm) copolymers with protected or deprotected glyco-monomers, including detailed studies about the ionization, with specific combinations of matrices and cationization agents.

The fourth chapter will combine three different examples regarding linear, star-shaped and hybrid polymers, which were analyzed by advanced techniques. The linear copolymers were analyzed by separating them according to their chemical heterogeneity using liquid absorption chromatography at critical conditions (LACCC) of poly(2-ethyl-2-oxazoline) (PEtOx), followed by automated spotting onto a MALDI target, which was subsequently analyzed by MALDI-time-of-flight (ToF) MS. In addition, this spotting method allows a high-throughput sample preparation and facilitates the analysis. Secondly, star-shaped polymers: [poly(ethylene oxide) (PEO)-*b*-PEtOx]$_8$ were firstly separated using LACCC of linear PEO as first separation dimension and were furthermore injected onto an SEC column confirming the conversion of the click reaction between the PEO core and the PEtOx arms. Lastly, a hybrid PEO star-shaped polymer was investigated in detail using MALDI-ToF MS due to its high molar masses in the range of *m/z* 10,000 up to 20,000 to verify the complete functionality of the core with PEO arms.

Finally, the last chapter will focus upon the development of computational methods for the analysis of copolymers, concentrating on linear copolymers. The main focus was to create a free software for all users in polymer sciences to obtain information regarding average composition, overcoming isotopic, overlapping peaks and isobaric species from MS spectra. Moreover, the architecture of linear polymers (random or gradient) can also be obtained through 2D composition maps, which prevents the synthetic chemist to carry out kinetic studies. Moreover, the quantitative studies were carried out by correction of the mass discrimination and isotopic abundance. A more

challenging work is the sequencing of copolymers to evaluate the most probable chain composition.

Consequently, modern polymer science has demonstrated that traditional methods such as SEC and NMR are not sufficient for a detailed characterization of the molecular structure. Thus advanced analytical techniques such as different ionization techniques within MS, a range of chromatographic hyphenation and computational methods are implemented for elucidating the complexity of synthetic polymers. This expansion in knowledge will be of great importance for further challenges in polymer science.

2. Polymer architecture *via* mass spectrometry

Parts of this chapter have been published **P1)** S. Crotty, S. Gerişlioğlu, K. J. Endres, C. Wesdemiotis, U. S. Schubert, Polymer architectures *via* mass spectrometry and hyphenated techniques: A review, *Anal. Chim. Acta* **2016**, *932*, 1-21.

The relation between synthetic polymers´ architecture and mass spectrometry and hyphenated techniques will be covered in this chapter. Synthetic polymers have been classified in different ways: homopolymers, linear copolymers and complex polymers. A homopolymer is a linear polymer composed of only one type of monomer. Further, linear copolymers are composed of at least two monomers that can be arranged in different ways but in a linear fashion. In general, this includes of block, random, gradient copolymers, and other specific arrangements throughout the polymer chain. In addition, polymers can also have a higher complexity *e.g.* star-shaped, graft, cyclic, comb, branched etc. (Figure 2.1). Throughout this chapter, recent developments from mass spectrometry and hyphenated systems applied to polymers will be discussed, thus presenting studies and prospects in polymer architecture.

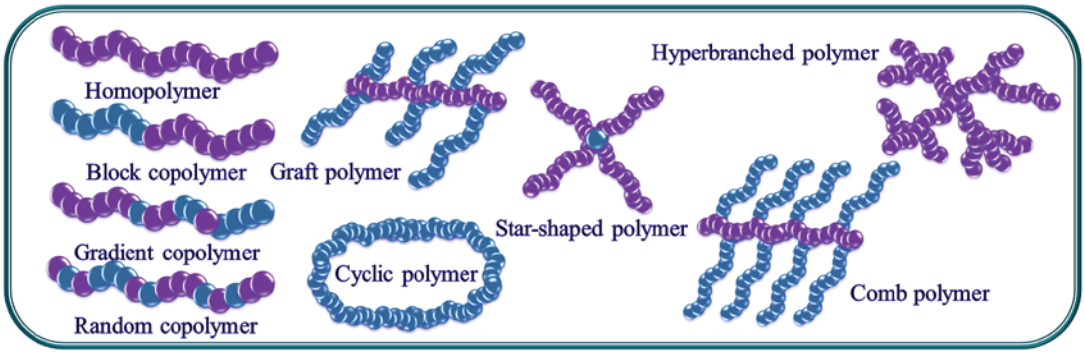

Figure 2.1. Schematic overview of various (co)polymer architectures.

In more detail, the structural complexity arises from the architectures. However also other aspects come into play, such as the chemical nature of the monomers, the length of the polymer, the dispersity, the molar mass distribution as well as the α- and ω- end groups. Moreover, difficulties can arise from defects from synthetic procedures. Several traditional techniques have been used to evaluate the polymer architectures, furthermore complemented by recently developed methods during the last years.

2.1. Linear homopolymers

In this part of this chapter, homopolymers will be investigated by different methods. Homopolymers being the simplest polymer chains existing still remain a challenge in polymer science. The detailed investigations of homopolymers can be a fundamental starting point to then obtain libraries and finally facilitate the interpretation of more complex polymer analytes. The traditional methods are based on thermal degradation to obtain architectural information especially regarding end groups and the sequence of the monomers. Furthermore, tandem mass spectrometry (MS/MS), LC-MS, field-flow fractionation (FFF) and IM-MS have developed over the decades to further establish properties such as conformation, defects etc..

Thermal degradation methods have been used since 1948 and are still applied today.[27, 28] For linear homopolymers, they are used for the determination of defects in microstructures and the investigation of pyrolysis mechanisms. Both physical and structural properties are provided by these and help to improve robustness of products. Furthermore, MS/MS techniques were developed throughout the years, which involved the fragmentation of an analyte ion to gain architectural information. Different activation methods have been developed, however, collision induced dissociation (CID) is the one that is the most widely used for polymers. The review by Wesdemiotis *et al.* have discussed in detail the fragmentation mechanisms of a variety of polymer types.[29] The structural information such as end groups and the sequence is very useful for homopolymers. It also has the possibility to determine isobaric and isomeric species of polymers systems. Nonetheless, hyphenated techniques, with a pre separation, represent an advantage in comparison to only MS/MS or thermal methods.

Moreover, hyphenated systems such liquid adsorption chromatography at critical conditions, such as (LACCC)-ESI MS, have enabled to differentiate poly(methyl metacrylate (PMMA) homopolymers with different end groups. This difference was due to the separation according to the chemical heterogeneity by LACCC. Secondly, the quantification of the different homopolymers was performed by evaporative light scattering detector (ELSD) and thirdly, MS for identification.[30] In addition, the group of Barner-Kowolik have implemented a polymer model created by PREDICI® to investigate polymer propagation and the determination of cross termination reactions using the RAFT polymerization technique.[31, 32] The newly adopted technique within mass spectrometry is ion mobility because of its powerful ability to establish conformation.

Furthermore, hyphenated systems and recent ionization techniques were applied to PEO polymeric systems. As described above, LACCC hyphenated to either an ESI or MALDI spectrometer showed that different end groups with different molar mass of PEOs could be elucidated.[33] In addition, both FFF-ESI-MS and IM-MS techniques were applied to low molar mass PEO systems. The FFF-ESI-MS technique separated different molar masses and compositions, which gives similar results as to LACCC-ESI-MS.[34] A faster technique to obtain the identical results as LACCC-ESI-MS and MS/MS is IM-MS, which can separate different compositions, isobaric species and architectures in the gas-phase (Figure 2.2).[35]

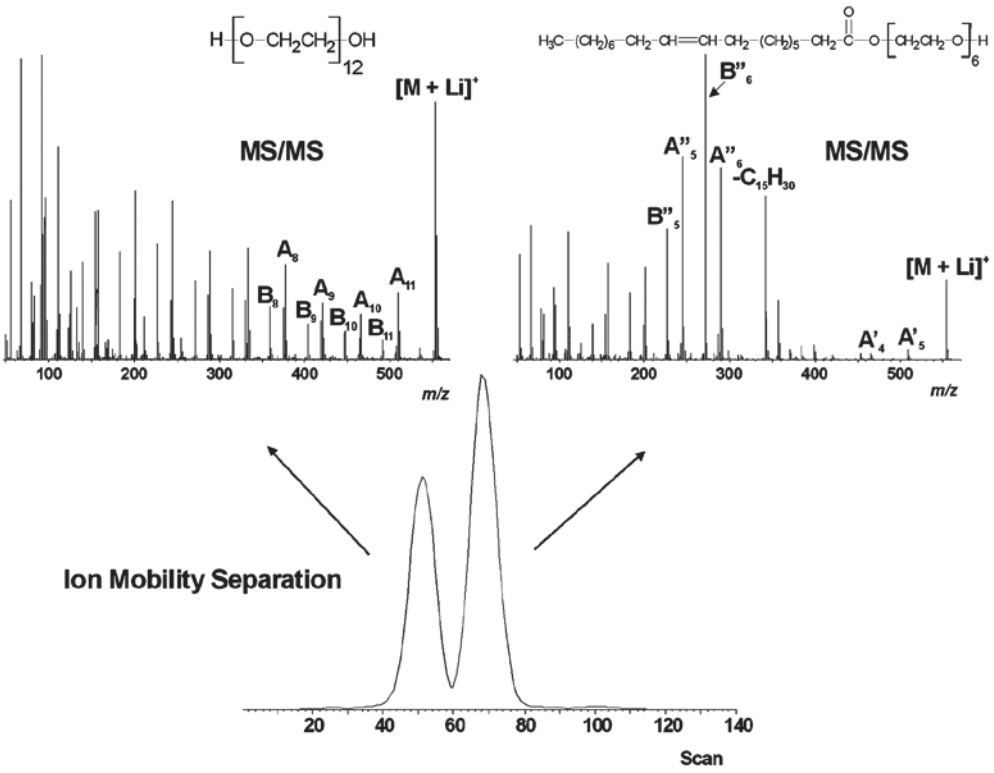

Figure 2.2. Arrival time distribution (bottom) of *m/z* 553 from a mixture of PEO 1000 and PEO monooleate and IM-MS/MS spectra (top) from the two peaks noted. Peaks in the IM-MS/MS spectra are partially annotated. IM-MS/MS spectra are very similar to those noted from MS/MS data (without IM separation) of the same oligomers, obtained from PEO 1000 and PEO monooleate separately.

Hyphenated techniques have proven to be promising to solve actual analytical issues. Throughout the years computational methods have arose and showed to facilitate

the analysis. For example, the polymer labeling using mass spectrometry (PLUMS) software could determine the fragments obtained without prior knowledge of the chemical structure of the monomer and the end groups.[36] This software demonstrated its ability by the analysis of several poly(2-oxazoline)s with varying side groups which have been studied with MS and MS/MS. The different ionization sources and fragmentation have enabled to establish degradation products and side products formed during the synthesis procedures.[36] Another software Polymerator developed by Jackson *et al.* has been used with poly(propylene glycol) PPG,[37] poly(hydroxyethylmethacrylate) PHEMA,[38] PEO,[39] which is dependent on the polymer class and the knowledge of individual fragments.

The growth of these techniques will help chemists to evaluate complex polymers in a more in-depth manner by making them less time-consuming.

2.2. Linear copolymers

The second degree of complexity is represented by linear copolymer, which include block, random, gradient copolymers. Block copolymers of linear architecture are composed of (at least) two segments/domains bound together and can undergo microphase separation due to their different miscibilities in specific solvents. Mass spectrometry has shown to be useful in determining block lengths, sequences as well as microstructures.[40]

Similar approaches as for homopolymers have been applied to linear copolymers to establish architectural information. Traditional thermal degradation techniques have been applied to numerous polymer classes such as PMMA, PS, PEO, poly(propylene oxide) (PPO), P2VP, polyisoprene (PI). However, the focus will be on direct MS and hyphenated techniques. Direct MS for block copolymers has helped to elucidate side products, end groups, degree of polymerization of each block. For example, many PS block copolymers have been investigated with different polymerization techniques and different lengths to determine structural defects and sequences.[41, 42] Willemse *et al.* portrayed that microstructures of PS-*b*-PI could be determined *via* direct MS in addition to block lengths, composition.[43] The other important polymer class is poly(meth)acrylates, which are usually nowadays synthesized in a fast way by the RAFT polymerization. The power of different fragmentation techniques enabled to differentiate between block and random copolymers. The PMMA-*b*-Poly(butyl methacrylate) (BMA) showed BMA units in comparison to PMMA-*r*-P*n*BMA where

MMA and *n*BMA units were randomly cleaved.[44] Polyesters represent another attractive polymer class due to their biodegradable and biocompatible properties. Poly(lactide-*co*-glycolide) (PLGA) has been studied by MALDI to differentiate topologies such as random or block like microstructures. These differences are important properties for chemists, which indicate the rate of incorporation of the monomers (Figure 2.3).[45, 46]

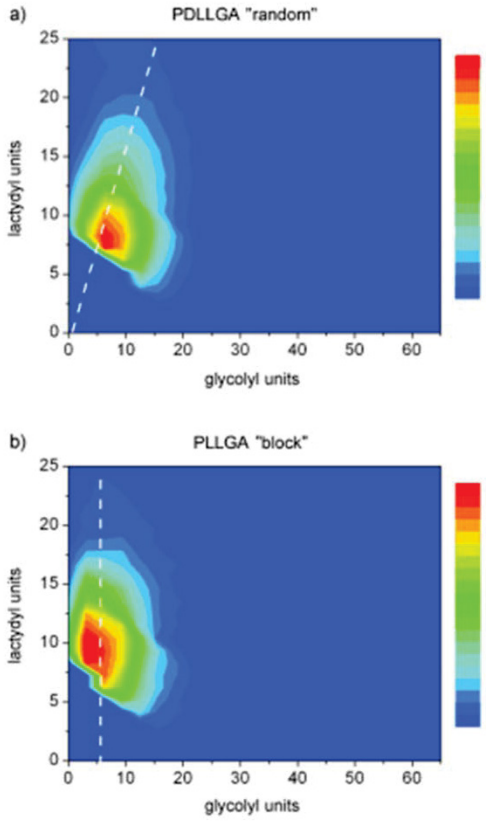

Figure 2.3. Contour plots of a) PDLLGA and b) PLLGA for cyclic structures plotted with lactydyl units.

As described before, PEO has shown extraordinary properties and has been exploited further with copolymers and formed specific shapes such as micelles, vesicles etc.. The focus was the known issue of isobaric species within copolymer spectra, which are present in PEO-*b*-PPO-*b*-PEO. Weidner *et al.* have developed the software MassChrom2D, to on one hand provide quantitative data and on the other hand separate isobaric species.[47] This software is a major step forward towards quantifying polymer species and separate different end groups (Figure 2.4).

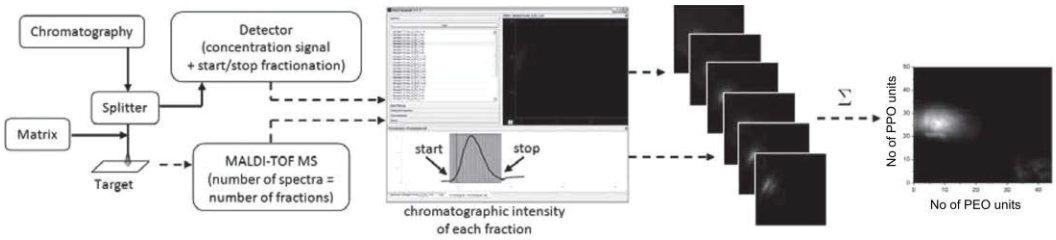

Figure 2.4. Scheme of measurement procedure using MassChrom2D to combine chromatography MALDI data for determining the copolymer composition.

Finally, Baumgaertel *et al.* have focused on establishing the LACCC of PEtOx to separate different end groups from block copolymers independently of their molar masses. Moreover, a 2D-LC (LACCC × SEC) with an ELSD has shown that the quantification of different species was possible and that the block length was determined (Figure 2.5). However, isobaric species had to be distinguished by CID.[48]

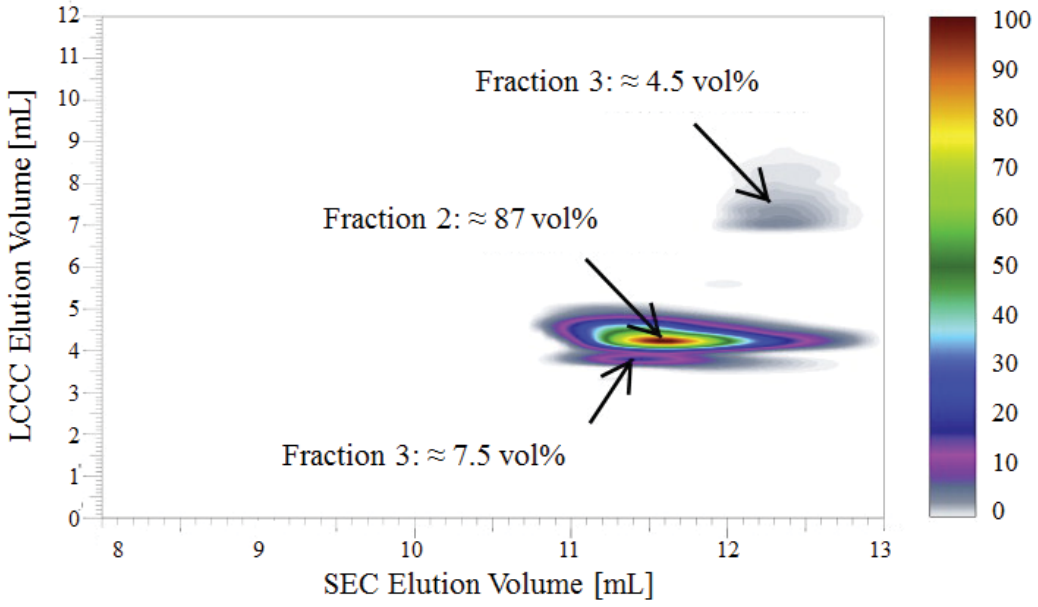

Figure 2.5. 2D contour plot of the poly(2-ethyl-2-oxazoline-*b*-2-(2,6-difluorophenyl)-2-oxazoline) (p(EtOx-*b*-*o*DFOx)) copolymer: 1st dimension LACCC for PEtOx (eluent: 2-propanol/H_2O = 91/9 (v/v)); 2nd dimension SEC (eluent: 0.07% triethylamine in THF).

To conclude, linear copolymers, especially block copolymers, are architecturally important. Furthermore, random, gradient copolymers are of interest in polymer science, however, quite challenging to analyze in comparison to blocks. Nevertheless,

hyphenated techniques or complementary techniques have proven to be essential to verify the architecture of linear copolymers.

2.3. Complex polymers

Polymer science has increased its innovative polymer architectures due to their potential in various applications. Complex architectures have developed throughout the decades such as cyclic, star-shaped, graft 'like' and branched polymers. These architectures have been analyzed by the analytical methods established for the linear copolymers. In this part, the focus of the current research will be star-shaped and branched polymers.

Different methods can be used to synthesize star-shaped polymers (for example, "core-first", "arm-first" or "graft-onto" methodologies). These structures have drawn the attention of scientists because of their attractive properties for diverse applications *e.g.* carriers in drug delivery or material science. A few examples that are portrayed show that MS can be used to establish architectural information. However, their characterization is – due to their chemical structure – scarce and not facile. MS has proven to be a powerful tool to enlighten the star-shaped conformation and their possible defects by IM-MS,[49] the completion of the reaction was shown by 2D-LC[50] and or direct MS.[32] In addition, these techniques are also used to differentiate between star-shaped and other conformations *e.g.* linear species.

Finally, the last mentioned architecture in this chapter is branched and dendritic polymers, which are highly complex. A few examples, which reached great importance due to their application, will be described here for example poly(amidoamine) PAMAM amongst others. PAMAM – trade name is Starburst – exhibit a good biocompatibility. Fourier transform-ion cyclotron resonance (FT-ICR) MS and diverse fragmentation techniques were used to identify dendrimers. PDI values were determined by high-resolution spectra of low and high molar mass considering their rather polydisperse nature.[51] MS/MS of these dendrimers have found to identify present defects and non-defects.[52] Furthermore, small angle X-ray scattering (SAXS) and IM-MS have also shown to be able to provide complementary results to those of MS/MS with this particular example.[53]

To conclude, polymer science includes a very broad range of macromolecular species due to the possible increase in structural complexity and molar masses. In the past 50 years, macromolecules have grown and been applied to material science and

drug delivery amongst other fields. The magnitude of information regarding the properties of polymers has increased because of mass spectrometry. Furthermore, diverse techniques have arisen in mass spectrometry but also in liquid chromatography and computational methods. In the upcoming years, all these potential tools will help to investigate copolymers, which is still a challenging matter.

3. Mass spectrometry for polymers with biological function

Parts of this chapter will be/have been published **P2)** M. J. Barthel, T. Rudolph, S. Crotty, F. H. Schacher, U. S. Schubert, Homo- and diblock copolymers of poly(furfuryl glycidyl ether) by living anionic polymerization: Towards reversibly core-crosslinked micelles *J. Polym. Sci., Part A: Polym. Chem.* **2012**, *50*, 4958-4965. **P3)** C. von der Ehe, F. Kretschmer, C. Weber, S. Crotty, S. Stumpf, S. Höppener, M. Gottschaldt, U. S. Schubert, RAFT copolymerization of thioglycosidic glycomonomers with *N*iPAm and subsequent immobilization onto gold nanoparticles, *in* ACS Symposium Series, Issue Controlled Radical Polymerization *(Eds.: K. Matyjaszewski, B.S. Summerlin, N.V. Tsarevsky, J. Chiefari), Wiley-VH Verlag GmbH & Co. KGaA,* 2015*, pp. 221-256.* **P4)** S. Crotty, C. von der Ehe, C. Weber, U. S. Schubert, Detailed MALDI comparison of *N*iPAm glycopolymers, *Eur. Polym. J.* **2015**, *71*, 325-335.

Synthetic polymers are a challenging type of compounds due to their dispersity, composition and architecture. Mass spectrometry is a powerful analytical technique and provides polymer chemists information such as molar mass distribution, chemical composition, end groups and structure. Various MS techniques such as ESI, MALDI, APCI and others have been used extensively since their introduction for the characterization of proteins and DNA. MALDI-ToF MS has been used and discovered in the 1980's by Hillenkamp,[54] Karas[54] and Tanaka (Figure 3.1).[13] MALDI-ToF MS has proven to be advantageous relative to other ionization methods due to the theoretical ionization of infinite *m/z* values. Moreover, MALDI-ToF MS provides access to a good mass resolution through the analyte embedment by the matrix. A large number of matrices have since been developed for biological matter and later been expanded to organic ligands, complexes and polymers. The matrix is the key item because it has to be transferred from a solid phase to a gas phase by absorbing the wavelength of the laser.[55] In addition, the matrix is also a way to volatilize the analyte by embedment and separation of the analytes by co-crystallization. However, the matrix choice is still a trial and error process due to the lack of systematic structure-properties correlations. Nonetheless, the general factor is the polarity, *i.e.* its hydrophobicity or hydrophilicity, of a matrix to its analyte.[56, 57]

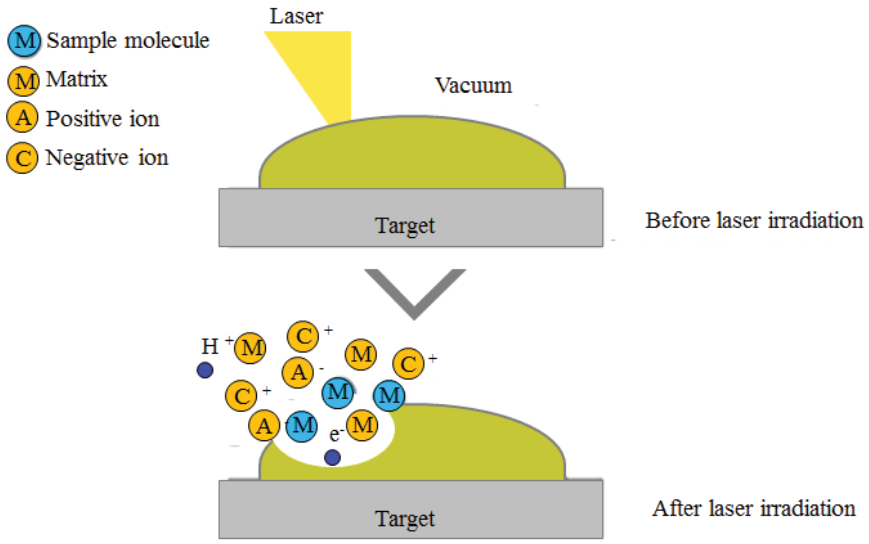

Figure 3.1. Schematic representation of the ionization process in MALDI-MS (adapted from ref.[58]).

Beyond the transition into the gas phase, the sample preparation remains the crucial step for the acquisition of a good spectrum. The crucial aspect is the co-crystallization of the matrix, the analyte and the cationization agent. Over the years the sample preparation has developed and the most common techniques are the dried droplet method,[59] the layering method[60] and the spraying methods amongst others.[11] The dried droplet is the simplest and fastest method, however, also prone to the formation of heterogeneous crystals so called 'hot spots' and, thus, producing a so called coffee 'ring effect'.[61]

As a first example, PFGE homopolymer as well as diblock copolymers of PEO-*b*-PFGE were investigated with MALDI-ToF MS. PFGE is an interesting polymer due to its possible application as self-healing material.[62] PEO has been demonstrated to behave as a stealth polymer within drug delivery investigations.[3, 63] PEO alone is an easy polymer to ionize due to its neutrality and rich oxygen content. These polymers synthesized by anionic ring-opening polymerization (AROP) are well-defined, have narrow dispersities and neutrality of PEO. Figure 3.2. displays the MALDI-ToF MS of the PFGE homopolymer. In this particular case, the molar mass distribution was investigated resulting an M_p value of 8,200 g·mol^{-1} with a corresponding repeating unit of 154 g·mol^{-1}. Two distributions were observed: A major one with sodiated adducts and another minor distribution. Moreover, PEO-*b*-PFGE, having a high degree of

polymerization of EO in comparison to PFGE, was investigated by MALDI. The obtained spectrum at high molar mass values was successful in both reflector and linear mode due to its advantageous PEO block, a highly ionizable polymer.

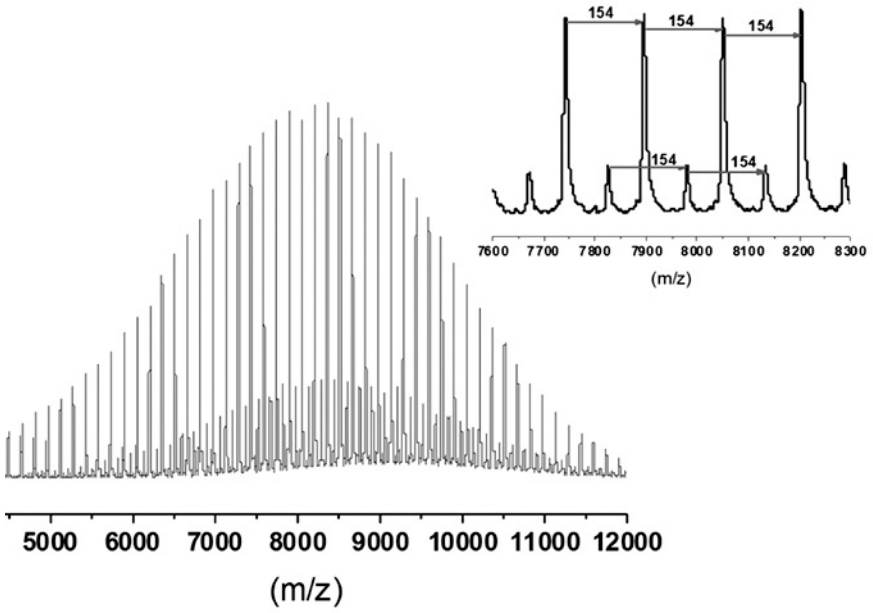

Figure 3.2. MALDI-ToF MS spectrum of a PFGE homopolymer (matrix: DCTB).

This result differed slightly from the SEC values; however, the values from NMR are in good accordance with the ones from MALDI-ToF MS. This discrepancy is originated most probably by solvent and column interactions of the polymers during the chromatographic separation. This demonstrates that high molar mass polymers can be analyzed with MALDI and, even with these high *m/z* values and the resolution from the detector, the end groups can be obtained. Detectors for high molar masses have recently been introduced to the market, which will be of great interest for polymer science.[64]

Moreover, glycopolymers are of great interest because of their interaction with lectins.[65] For this purpose, statistical copolymers of P*N*iPAm were synthesized by the RAFT polymerization process bearing either glucose or mannose in the side chain. The polymers are important because of their role that saccharides play on cell-surfaces, while *N*iPAm introduces a lower critical solution temperature (LCST) behavior, resulting in thermoresponsive properties of the polymer.

The synthesis of the glycopolymers included the polymerization of protected glycomonomers and a subsequent deprotection step. Both polymers were investigated with mass spectrometry to gain information about the copolymer composition since the

application of NMR spectroscopy was difficult due to overlapping signals (Figure 3.3). Using MALDI-ToF MS, the presence of polymer chains with 0 to 4 sugar units per chain as well as the end group fidelity could be confirmed (Figure 3.4).[66]

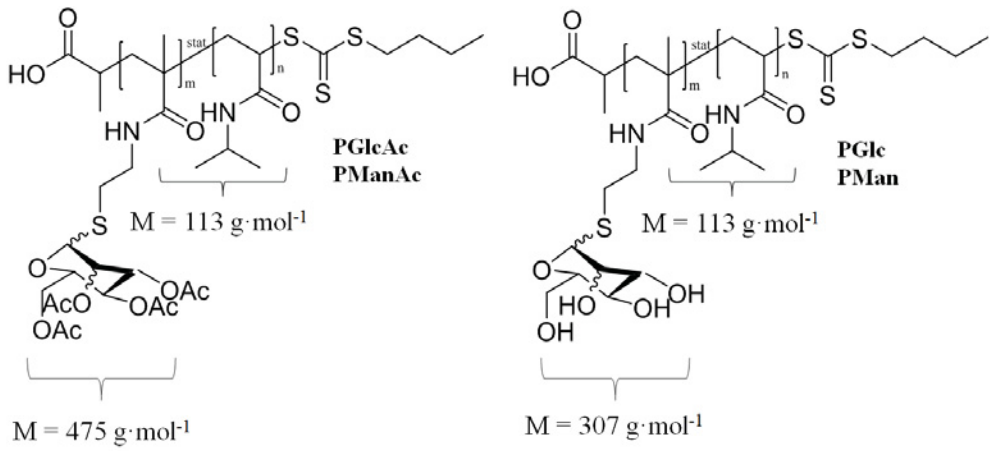

Figure 3.3. Schematic representation of the glycopolymers: Protected (left) and deprotected (right) polymers investigated in this study.

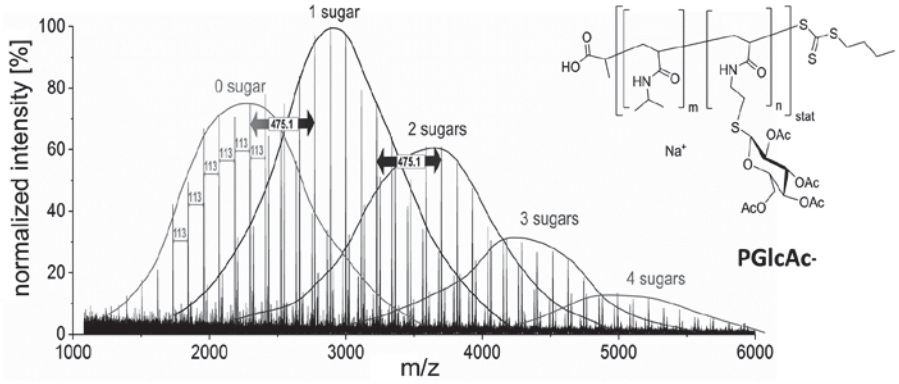

Figure 3.4. MALDI-ToF MS spectrum of the protected glycopolymer PGlcAc (Matrix: DCTB).

Furthermore, both the protected (PGlcAc and PManAc) and the deprotected (PGlc and PMan) polymers were screened by using MALDI-ToF MS. A systematic difference regarding the ionization behavior of these polymers was observed by the use of different matrices and cationization agents. In this case the dried droplet technique was used to facilitate and fasten the sample preparation thus leading to a minor segregation of the polymer and the matrix on the target.[61]

Tables 3.1 and 3.2 show the optimum measurement conditions for the protected and deprotected polymers respectively.

Table 3.1. Screening of matrices and cationization agents for PGlcAc (top) and PManAc (bottom).

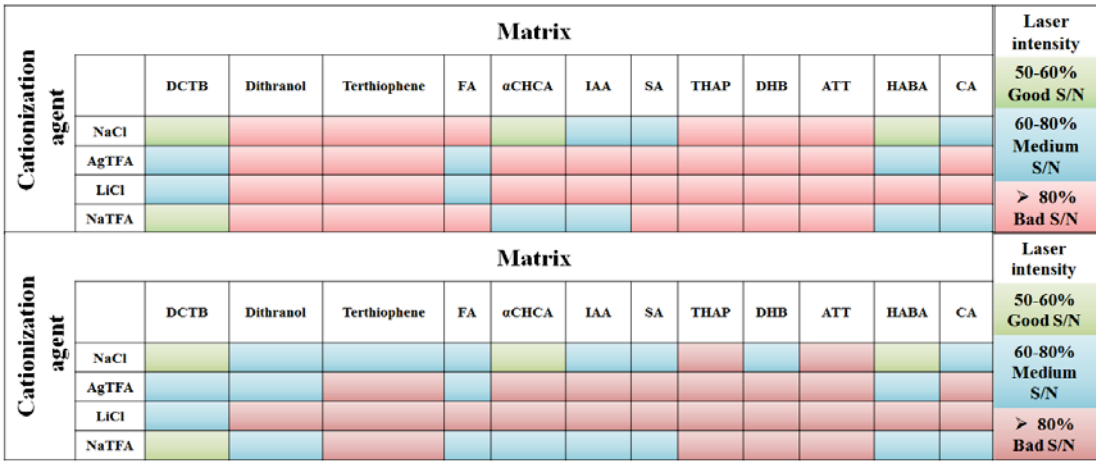

Table 3.2. Screening of matrices and cationization agents for PGlc (top) and PMan (bottom).

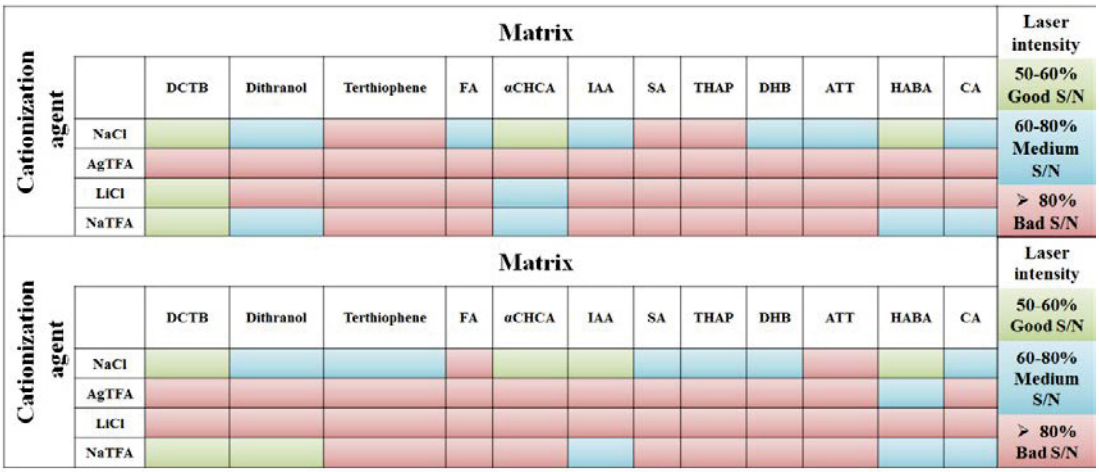

This screening resulted in 48 permutations and similar solvents were used to ensure a sufficient co-crystallization. The color code represents the capacity of each matrix / combination to ionize the analyte. The red color represents no ionization or a very high laser intensity for an optimum spectrum. The blue color signifies that the chains of the polymers were ionized but certain aspects were not fulfilled. Finally, the green color indicates the best conditions *i.e.* that the baseline is lowest, a good signal to noise ratio or no suppression of high or low molar masses.

In most cases *trans*-2-[3-(4-*tert*-butylphenyl)-2-methyl-2-propenylidene]malononitrile (DCTB) with a sodium salt resulted in the best ionization for both protected glycopolymers, which indicates that the sugar moieties do not influence the optimum matrix/salt combination. Both protected and deprotected polymers did not ionize with either Li^+ or Ag^+ cations, however, the sodium cations gave useful results. The salts such as sodium trifluoroacetate (NaTFA) and sodium chloride (NaCl) were slightly different in their ionization characteristics, nevertheless presented in similar results.

Furthermore, all four glycopolymers were subsequently compared in detail with their best four matrices. These were DCTB, 4'-hydroxyazobenzene-2-carboxylic acid (HABA), 3-indoleacrylic acid (IAA) and α-cyano-4-hydroxycinnamic acid (αCHCA) with NaCl as cationization agent for PGlcAc and PManAc (Figure 3.5).

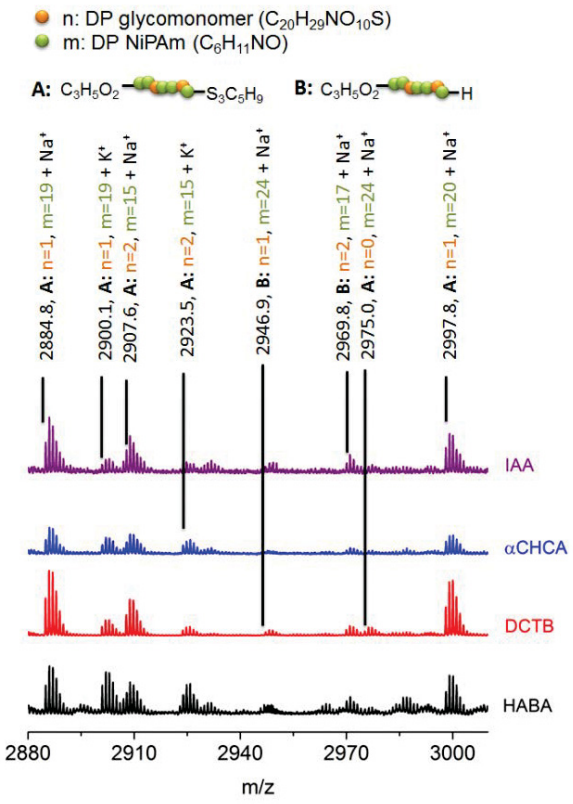

Figure 3.5. Overlay of the normalized MALDI-ToF mass spectra of PManAc obtained with different matrices using NaCl as cationization agent. The zoom covers a *m/z* difference of 113.1 corresponding to one *N*iPAm repeating unit.

DTCB and αCHCA show at first glance high intense signals in comparison to IAA and HABA having both lower signal intensities. All major peak were assigned with a

m/z difference of 113.1, which corresponds to a *N*iPAm unit. The main series A corresponds to the intact trithiocarbonate end group with *N*iPAm and sugar units. Another series B was observed, which originate from a RAFT end group cleavage. However, it is not as abundant as the A series.

Moreover, the deprotected polymers PMan and PGlc were scrutinized with the successful four matrices DCTB, dithranol, 2,5 di-hydroxybenzoic acid (DHB) and αCHCA with NaCl as cationization agent (Figure 3.6). Basically the same trend was observed regarding the series, however, the series B was more pronounced than in the protected ones. This cleavage was in particular observed with the use of DHB and dithranol and has been readily observed before with RAFT polymers having a labile end group.[67] Fewer fragmentations were observed whilst analyzed with DCTB and αCHCA. Finally, DCTB amongst the two last matrices gave the best result to obtain a good signal to noise ratio with no ion suppression. The type of sugar moiety did not influence the observed trends. In general not many detailed investigations regarding matrices and polymer class ionization have been studied so far and in particular the relationship between polarity of the polymer and the matrix.[56]

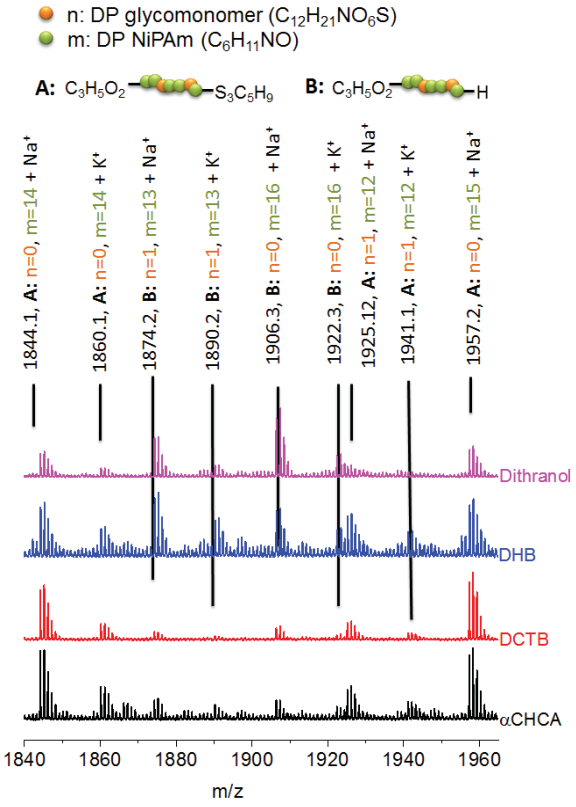

Figure 3.6. Overlay of the normalized MALDI-ToF mass spectra of PMan obtained with different matrices using NaCl as cationization agent. The zoom covers a *m/z* difference of 113.1 corresponding to one *N*iPAm repeating unit.

In conclusion, MALDI-ToF MS represents an advanced tool for the determination of the absolute and high molar masses and molecular structure beside of the traditional relative characterization methods. Furthermore, the systematic studies presented in this chapter allowed the establishment of specific trends such as the RAFT end group cleavage, the different ionization in comparison to different matrices. DCTB, a not well known matrix for proteins, has shown to be successful for a wide range of polymer classes. Moreover, MALDI-ToF MS, has been applied for many years, in the polymer science field to investigate the relationship between the choice of the matrix and the polymer class. This is still a trial to error process due to none systematic research studies.

4. Polymer characterization: MS and its complementary methods

Parts of this chapter have been published **P5)** G. M.-E. Pozza, S. Crotty, M. Rawiso, U. S. Schubert, P. J. Lutz, Molecular and structural characterization of hybrid poly(ethylene oxide)-polyhedral oligomeric silesquioxanes star-shaped macromolecules, *J. Phys. Chem. B* **2015**, *119*, 1669-1680. **P6)** T. Rudolph, S. Crotty, M. von der Luehe, D. Pretzel, U. S. Schubert, F. H. Schacher, Synthesis and solution properties of double hydrophilic poly(ethylene oxide)-*block*-poly(2-ethyl-2-oxazoline) (PEO-*b*-PEtOx) star block copolymers, *Polymers* **2013**, *5*, 1081-1101. **P7)** S. Crotty, C. Weber, A. Baumgaertel, N. Fritz, E. Altuntaş, K. Kempe, U. S. Schubert, Semi-automated multi-dimensional characterization of synthetic copolymers, *Eur. Polym. J.* **2014**, *60*, 153-162.

A complex synthetic polymer is described by having different functionalities, composition, architecture and chain length. For them to be analyzed in detail, advanced separation and or complementary methods have to be utilized. MS/MS methods can provide information such as end groups, monomer sequences, composition, architecture, block lengths. SAXS and static light scattering (SLS) have also been used to identify architecture/shape and molar mass distribution but require polymers with sufficiently high molar masses. A combination of SAXS and MALDI was applied for the analysis of the hybrid PEO star-shaped macromonomers, which are of great interest for surface modifying agents to enhance the biocompatibility of surfaces for medicinal applications[68-70] and also applicable for hydrogels.[71] AROP is the preferred method to polymerize PEO thus producing well-defined polymers. Moreover, polyhydral oligomeric silesquioxanes (POSS) are of interest due to the ability of producing water-soluble materials when combined with PEO.[72, 73] These hybrid stars have been constructed upon a POSS core, which was further coupled to PEO segments. The challenge was to evaluate the architecture, molar mass, and functionality. SEC with refractive index (RI) detection was used to calculate the amount of grafting of the PEO arms onto the POSS core. Light scattering (LS) and MALDI-ToF MS have proven suitable to obtain an absolute value whereas SEC had to rely on the use of linear standards, whose hydrodynamic volume largely differs from that of star-shaped

polymers. Thus, MS was used to identify the composition and molar mass of the star-shaped polymer $Q_8M_8^{PEO}$.

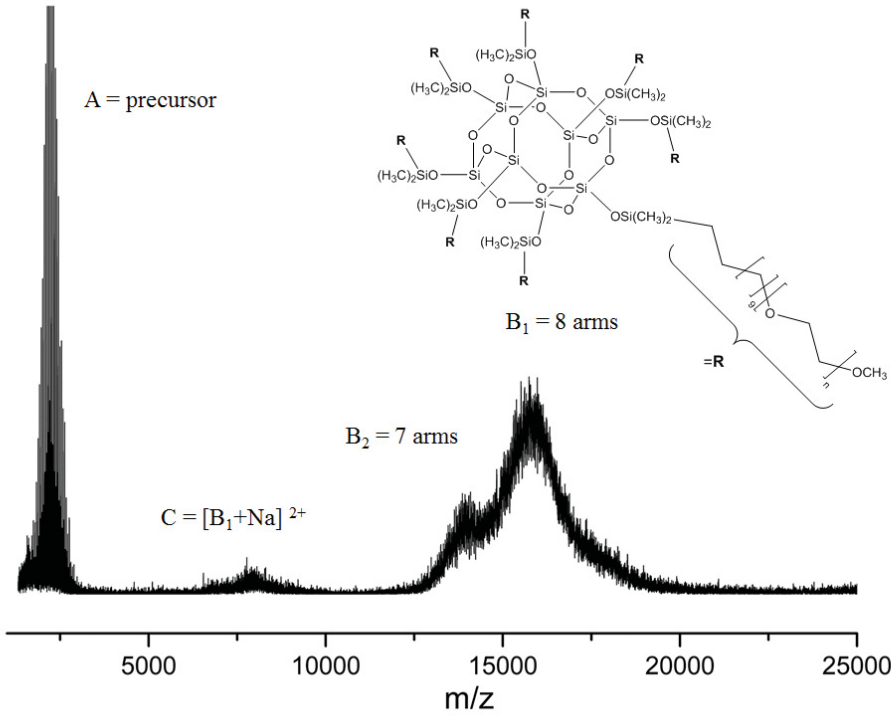

Figure 4.1. MALDI-ToF MS of $Q_8M_8^{PEO}$ (matrix: DCTB, cationization agent: NaI).

In Figure 4.1 several peaks have been highlighted such as *m/z* 2,234 (A) corresponding to the PEO precursor macromonomer indicating a slight residue present in the analyte, which however is not detected by NMR and SEC. The other peaks such as *m/z* 15,974 (B_1) indicate a fully functionalized star and *m/z* 14,040 (B_2) shows that the arms are of similar lengths, which are coupled to the POSS core. However, it could either be a star which had only seven arms or a cleaved arm either formed during the synthesis or cleaved inside the MS source. The peak (C) at *m/z* 7,773 only indicates the doubly charged species of (B_1). SAXS was used to investigate the average conformation. Both the arms as linear PEOs and the star-shaped $Q_8M_8^{PEO}$ polymers were analyzed. For the arms, SAXS confirmed their linearity and a degree of polymerization of 40.[74, 75] Furthermore, the star-shaped polymer was analyzed and the scattering behavior revealed a star-branched conformation.[74, 76-78]

Several chromatographic techniques have been developed to facilitate the elucidation of these aspects. Moreover, the combination of two of these techniques

namely 2D chromatography can also enable the analysis. Liquid adsorption chromatography (LAC), LACCC,[79] gradient polymer elution chromatography (GPEC), SEC and temperature gradient interaction chromatography (TPIC) are all different types of chromatographic separation methods, which can be coupled to gain knowledge from the polymer systems.[80] The most commonly used are LACCC × SEC setups in terms of its informative aspect, which provides two dimensions at once. The LACCC dimension separates according to differences in functionality irrespective of the molar mass and SEC separates according to the molar mass.[79, 81] This 2D setup can be applied to all polymers: Homopolymer, block, random, gradient as well as star-shaped and branched copolymers. Despite the different powerful abilities of each separation capability, certain drawbacks and limitations are present, which makes even 2D × LC alone not sufficient to investigate complex polymers.[82, 83] As a consequence, MS can be used as a third dimension to compliment the 2D analyses. Thus, through decades offline and online coupling have been developed. Mostly spraying and spotting[84, 85] are applicable for MALDI-MS, while ESI-MS can be coupled directly to chromatographic systems.[86]

Star-shaped polymers are of interest due to the type of architecture which plays a key role in the physical properties and different morphologies can be produced upon solvent selection.[87-89] The absence of a critical micellar concentration (cmc) in the system provides a great potential for drug delivery applications to encapsulate drugs and or use the 'stealth' effect in case of PEO containing stars.[3, 69, 90, 91] The eight arms star block copolymers discussed here have as core a PEO material for medicinal application and the outer shell PEtOx as non-toxic and pseudo-peptide character[92-94] polymerized *via* CROP. Star-shaped polymers can either be synthesized by the 'arm first' or the 'core first' method. Both were applied for this system and reveal different behaviors.[95] The 'arm first' route, which is based on a copper catalyzed azide alkyne click reaction produced aggregates while the 'core first' approach resulted in molecularly dissolved polymers.[96] The focus will be only on the 'arm first' approach where the high molar mass star-shaped polymers were investigated by 2D-LC (LACCC × SEC), MALDI, and SLS. The core is constituted of a commercial star-shaped PEO with eight arms with hydroxyl end group $[PEO_{28}\text{-}OH]_8$, which was further tosylated $[PEO_{28}\text{-}Ts]_8$. Furthermore, sodium azide was used to convert the tosyl group into an azide group yielding $[PEO_{28}\text{-}N_3]_8$. To monitor the conversion efficiency of each step ^{13}C-NMR and

2D-LC (LACCC × SEC) were applied. LACCC of linear PEO with α,ω-H were used to quantify and verify the purity of the core modifications (Figure 4.2).

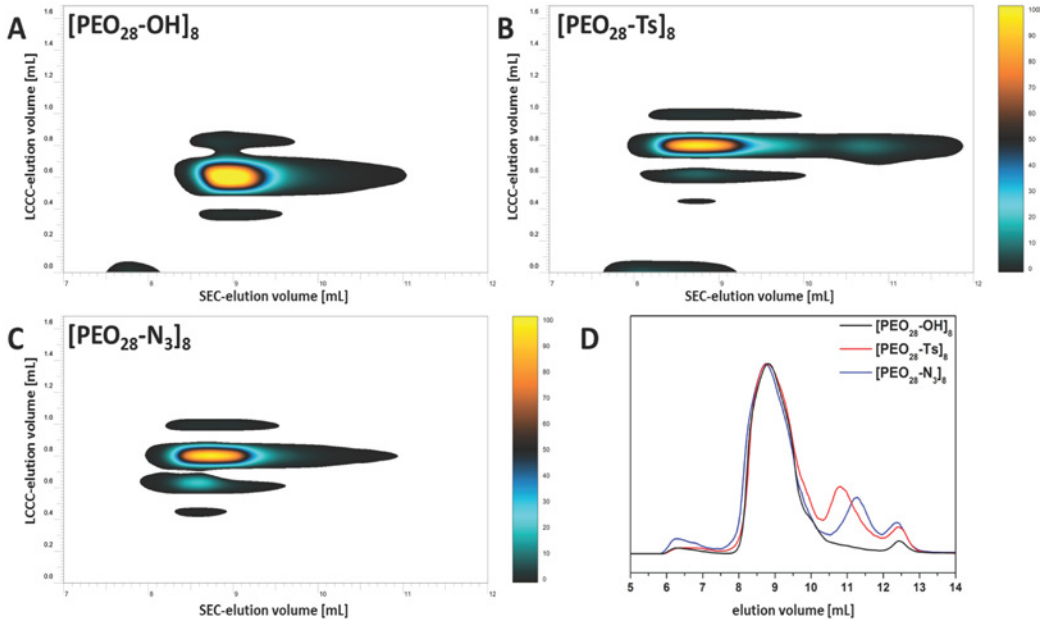

Figure 4.2. 2D-LC results (ACN/H_2O 55/45 v/v) for $[PEO_{28}\text{-}OH]_8$ (A), $[PEO_{28}\text{-}Ts]_8$ (B), and $[PEO_{28}\text{-}N_3]_8$ (C); in comparison with the SEC traces obtained for $[PEO_{28}\text{-}OH]_8$ (solid black line), $[PEO_{28}\text{-}Ts]_8$ (solid red line), and $[PEO_{28}\text{-}N_3]_8$ (solid blue line, THF was used as eluent).

As shown in Figure 4.2, 2D-LC was effective to verify the purity of the commercial material using the ELSD detector hyphenated to the HPLC. Only one distribution was observed, whereas $[PEO_{28}\text{-}Ts]_8$ shows two distributions, which correlates to a 3% remaining unfunctionalized material. This value is in good agreement with the data from NMR spectroscopy which shows a 100% conversion. Furthermore, $[PEO_{28}\text{-}N_3]_8$ was analyzed and 10% of the educt was detected by the ELSD. This could be due to the experimental conditions where a possible exchange between azide and hydroxyl groups could occur.[97, 98] Moreover, MALDI and SLS were used to investigate the molar mass of the star-shaped polymers because SEC measurements show a lower elution volume due to its more compact form in solution. Both MALDI and SLS could evoke a molar mass M_n of 50,000 and 54,000 $g \cdot mol^{-1}$ respectively for a 'core first' approach.

Another part of this chapter consists of the analysis through multidimensional characterization techniques of block copolymers with different monomer types. Complementary methods, further automated to one another, have a major advantage in

polymer characterization to enable a fast and reproducible way of analyzing polymers. At first the critical conditions of PEtOx were established to be able to differentiate end groups from one another independently from the molar mass. Subsequently, the eluates were separated and then spotted onto a MALDI target *via* a robotic instrument. Finally the samples were then measured by MALDI-MS and ESI-MS as well as MS/MS to establish the structural information.

Two block copolymers were analyzed that are composed of a moderately hydrophilic PEtOx block and a short hydrophobic poly(2-(1-ethyl-pentyl)-2-oxazoline) P(EPOx) or a fluorophilic P*o*DFOx block.[99] These polymers are attractive due to their potential application as potential drug delivery vehicles.[100-103] The eluted species were thus spotted in a continuous fashion with the Proteineer fc (Figure 4.3).

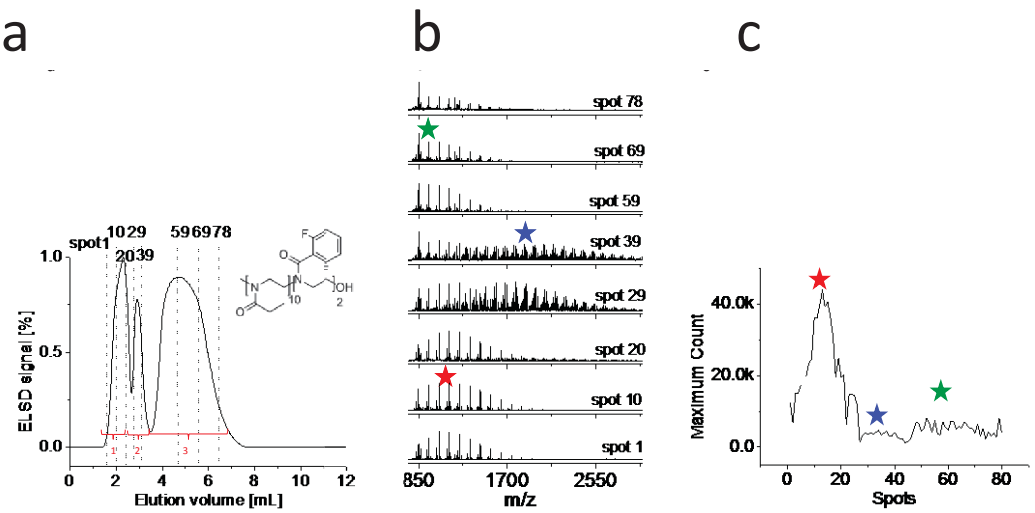

Figure 4.3. (a) LACCC chromatogram PEtOx-*b*-P*o*DFOx, (b) stacked MALDI-ToF MS spectra of the spots generated by the Proteineer fc (none normalized) and (c) maximum count at three specific m/z values. (★ *m/z* = 1243, ★ *m/z* = 2144, ★ *m/z* = 1144).

The focus in this chapter will be on the PEtOx-*b*-P*o*DFOx sample applied to this analytical setup. Three peak were observed in the chromatogram (Figure 4.3 (a)), which were then spotted and measured with MALDI MS (Figure 4.3 (b)). Furthermore, Figure 4.3 (c) shows the maximum count for each spot with three chosen maxima values. Thus as depicted, three species were assigned. The PEtOx amino/ester homopolymer is labelled with (★), the copolymer with (★) and the hydroxyl homopolymer PEtOx is indicated with (★). In general, the peaks 1 and 3 correspond to a PEtOx homopolymer and the peak 2 corresponds to the copolymer. A straightforward assignment was the

block copolymer, which displays many peaks in the MS, a common aspect for copolymers in general (Figure 4.4 (b)). In detail the copolymer was a $-CH_3$ and a $-OH$ end group. In addition, proton initiated block copolymers were also elucidated, which is a result from chain transfer reactions during cationic ring opening polymerization (CROP).

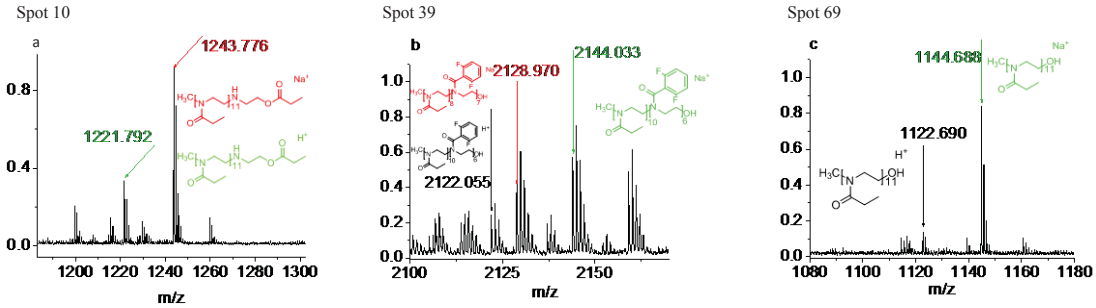

Figure 4.4. MALDI-ToF MS spectra of different spots of PEtOx-*b*-P*o*DFOx and the maximum count for each spot: (a) First spot of the PEtOx amino/ester homopolymer, (b) PEtOx-*b*-P*o*DFOx copolymer and (c) PEtOx homopolymer with hydroxyl end group (matrix: DCTB, cationization agent: NaCl).

A less obvious assignment was made for the peaks 1 and 3, which evidently have different end groups due to their different elution behavior. The presence of isobaric species is the explanation for this observation, which readily occurs during termination reaction in the CROP. Thus, to differentiate the isobaric species ESI-Q-ToF MS/MS was used, after offline fractionation, which showed different fragmentation patterns of the end group.[48] Therefore, the peak 1 contains PEtOx with amino/ester end groups and the peak 3 corresponds to PEtOx-OH. In this study, complementary methods were used and required to distinguish differences in the structural elucidation, a recurring aspect with copolymers.

Finally, these numerous studies showed that complementary characterization techniques, coupled either online or offline, have shown to be important for a detailed investigations for systems such as block up to star-shaped copolymers. As a consequence, advanced setups represent an important step towards high-throughput multidimensional measurements for complex copolymers because of its reproducibility, quantifiability and structurally informative aspect, making it amenable for pharmaceutical polymers. This highly developed approach can be transferred to other polymer classes as well, which is also very useful for complementing 2D-LC

experiments. Finally, and most importantly, this allows new ways for an intellectual property (IP) protection. The next steps would be to monitor and analyze pharmaceutical polymers and drug loaded carriers.

5. Software development for copolymers

Parts of this chapter will be/have been published **P8)** M. S. Engler, S. Crotty, M. J. Barthel, C. Pietsch, K. Knop, U. S. Schubert, S. Boecker, COCONUT - an efficient tool for estimating copolymer compositions from mass spectra, *Anal. Chem.* **2015**, *57*, 5223-5231. **P9)** M. S. Engler, S. Crotty, M. J. Barthel, C. Pietsch, U. S. Schubert, S. Boecker, Abundance correction for mass discrimination effects in polymer spectra, *Rapid Commun. Mass Spectrom.* **2016**, *30*, 1233-1241.

In depth copolymer analysis represents a major challenge as shown in the previous chapter.[104] Many scientists use online or offline hyphenation (2D-LC)[84] and other sophisticated techniques (IM-MS,[105] AUC,[106] AF4[107] and MS/MS[29]) to elaborate detailed information. However, mass spectrometry can profit from computational methods. Moreover, not only molar mass distribution and end groups can be determined by MS1 but chemical composition,[108] the topology,[45, 46] the chain length distributions, the block lengths of copolymers[43, 109, 110] as well as reactivity of monomers.[111] However, mass spectrometry of copolymers results in overlapping peaks and isobaric species. Over a few decades, software tools have been designed to overcome these difficulties.

Several research groups have developed different computational methods focusing on specific issues arising from copolymers spectra. Wilczek-Vera *et al.*[112] have used a copolymer composition matrix for the evaluation of relative abundances and architectures of copolymer chains. Terrier *et al.* have also used a 2D composition matrix to evaluate degradation of copolymers *i.e.* the compositional drift.[113] Weidner *et al.* presented a hyphenated system with on the one hand LACCC and on the other hand MS determination. By an offline method, *i.e.* fractionation of the LACCC separation, the copolymer was then evaluated according to their abundance by MS.[47] Furthermore, Vivó-Truyols *et al.* presented a computational method to resolve overlapping isotopes.[114]

The quantification of polymers with MS has been addressed, however, much less frequently than for structural elucidations[115-118] and mass discrimination effects.[119, 120] One way to approach this issue is the use of hyphenation, *e.g.* with HPLC and 2D-LC.[47] However, mass discrimination is a crucial disadvantage, which hampers MS

investigations. Nonetheless, an open software has been developed to resolve these major issues.

Within this chapter, computational methods have been exploited to resolve several issues: Baseline, peak shapes, isobars and overlaps. Moreover, simulated data have been also included to evaluate the power of the method. As a result, a copolymer composition numbering tool (COCONUT) was created as open access software.[121] As suitable analytes, copolymers were synthesized *via* anionic polymerization with different ratios of isoprene and styrene in both first marcromer (I_n) and second marcromer (P_n) (Figure 5.1).

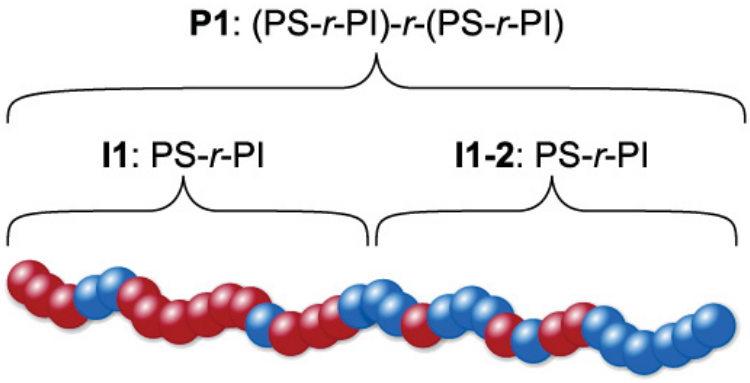

Figure 5.1. Schematic representation of the synthesized (PS-*r*-PI)-*r*-(PS-*r*-PI) copolymers **P1**; **P2** and **P3** have the same architecture but different PS to PI ratios.

This polymerization technique allows the preparation of well-defined polymers with low dispersities, which is favorable for MS characterization to have an efficient ionization of all polymer chains. The copolymers shown in Figure 5.2 were characterized with ^{1}H NMR as well as MALDI-ToF MS and subsequently computed with COCONUT. All these methods reveal a good correlation of the isoprene and styrene ratios. The MS spectra show overlapping and isobaric species, which were resolved. Consequently, the most abundant copolymer was detected, which was confirmed by the use ^{1}H NMR. Moreover, the microstructures of the analytes were determined with block structures for **I1-I3** and random copolymers for **P1-P3**. These were evaluated by the slope of the line crossing the most abundant chains.[45]

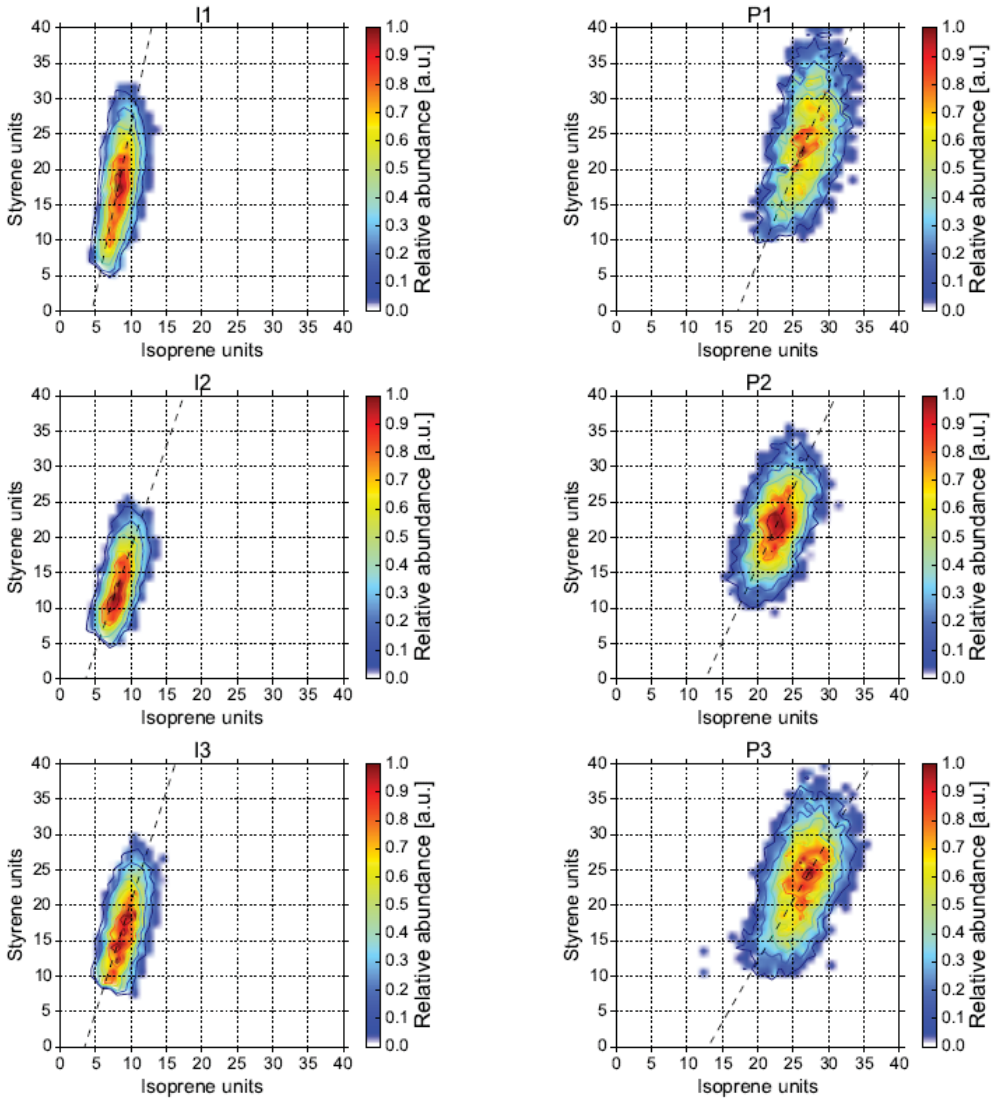

Figure 5.2. Copolymer composition matrix of the (PS-*r*-PI) macromers **I1** to **I3** (left) and the final (PS-*r*-PI)-*r*-(PS-*r*-PI) copolymers **P1** to **P3** (right).

Furthermore, mass spectra were simulated where the reconstruction of all isotopes was calculated for two types of copolymers: PMMA-*co*-PnBA and PMMA-*co*-PHEMA. As shown in Figure 5.3, COCONUT chose the correct distribution located in the center of the composition matrix and could resolve overlapping peaks by using the area under the isotopic patterns. Moreover, the peak shape in mass spectra and the way it is selected is crucial and, thus, the software centroids all peaks and filters off the background noise.

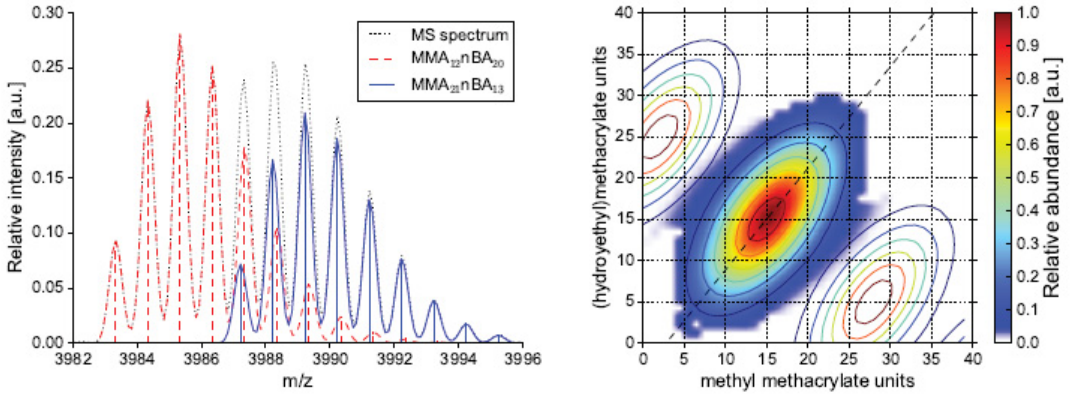

Figure 5.3. Left: Detail of the simulated MS spectrum of PMMA-*co*-PnBA showing overlapping isotopes. The relative molecule abundances estimated by COCONUT are represented by the centroid intensities. Right: Copolymer composition matrix estimated from a simulated MS spectrum of PMMA-*co*-PHEMA copolymer overlaid with all isobaric distributions (contours).

Nonetheless all these results are semi-quantitative, which remains a challenge in polymer science to quantify each chain within one copolymer. Thus the second part of this chapter addresses the intensity correction and the mass discrimination of polymer chains. The quantification is complex with a single MS spectrum due the inhomogenous sample preparation and the poor reproducibility. Moreover, the ionization of copolymers and their respective homopolymers require different matrices, even when keeping the measurements constant, to enable the correction of the isotopic abundances. The copolymers mentioned above were also used in this part and thus newly characterized homopolymers were studied. In particular PS and PI homopolymers required a different matrix to enable the transport of the ions into the gas phase. In this particular case the measurement conditions were the same, the only difference was that for PS dithranol was used and for PI DCTB. Two homopolymers with a molar mass of 2,500 g·mol^{-1} and 5,000 g·mol^{-1} were mixed with an equimolar ratio and an expected mass discrimination was observed for the high *m/z* values.

The Figure 5.4 shows the correction for the mass discrimination before and after for both PS (top) and PI (bottom).

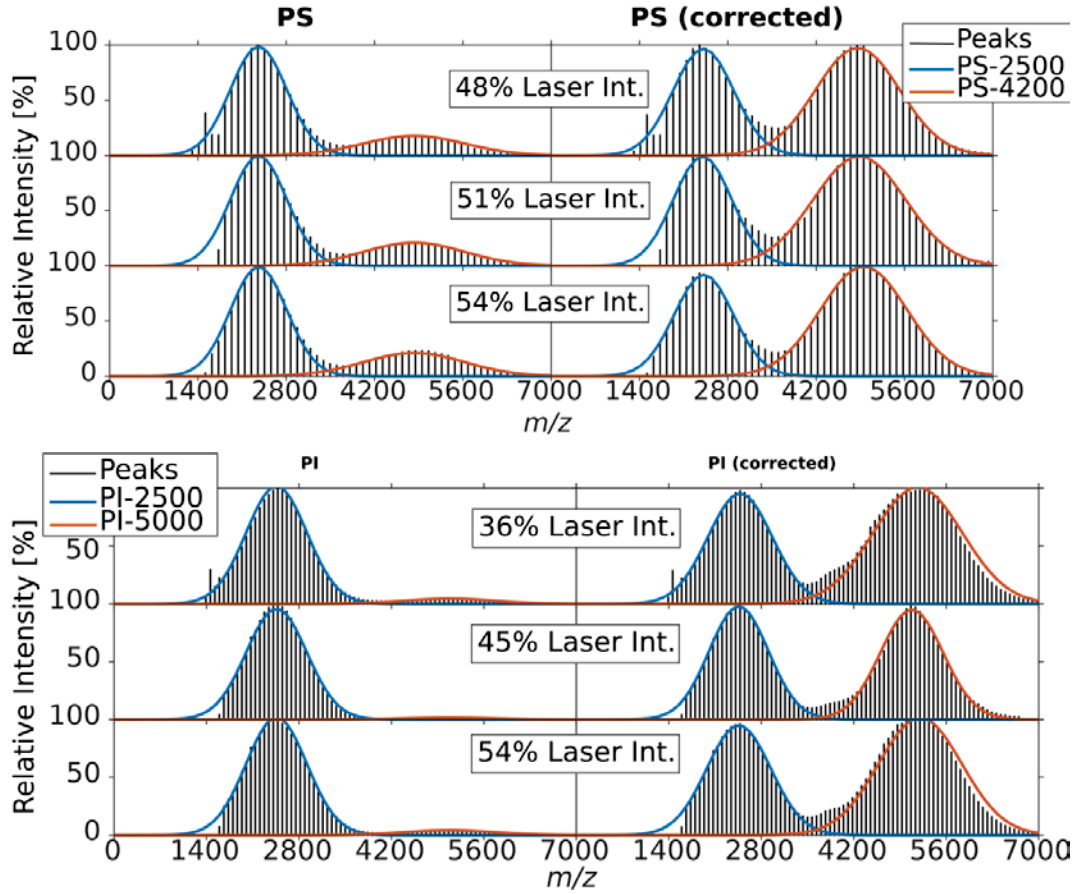

Figure 5.4. PS (top) and PI (bottom) homopolymers before and after the correction for the mass discrimination.

As shown, a strong mass discrimination for high *m/z* values before correction was observed and was, thus, corrected to obtain equal areas under the curve for both homopolymers in both mixtures. The correction factors were then applied to the three copolymers: **P1**, **P2** and **P3**. However, the M_n values reported in this part are slightly lower due to degradation of the styrene and isoprene over time. This singularity is common for this type of copolymers. Nonetheless, the correction of the spectra for the copolymers was successful (Figure 5.5).

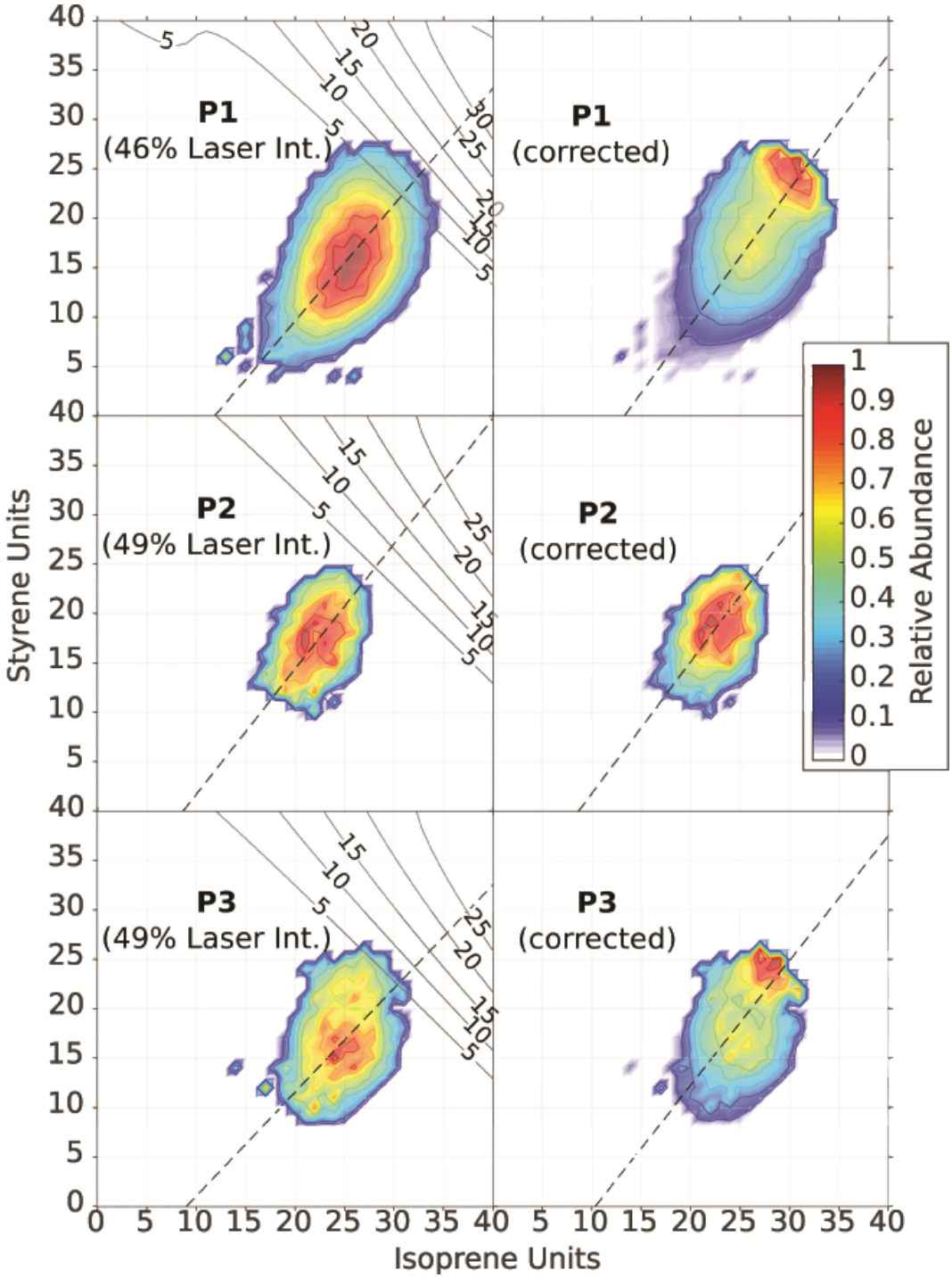

Figure 5.5. Measured (left) and corrected (right) copolymer compositions of **P1** to **P3**. The overlaid contour lines on the left side represent the estimated intensity correcting function. Dashed lines represent the average compositions obtained by fitting a line through the most abundant isotopes.

The corrected 2D composition maps show a higher number of PS and PI. The average composition before correction was an circular shape and after the correction it showed a narrow oval shape characteristic of a living polymerization.

Copolymer MS spectra are challenging in comparison to homopolymers. However, several computational methods were developed to help chemists to identify their copolymer architectures as well as to quantify and qualify the most abundant copolymer. This tool (free-ware) has a remarkable efficiency and accelerates the manual analysis. In the future, sequencing of copolymers will be investigated to explore the exact structure of the polymer chains.

6. Summary

The objectives of the presented thesis were the investigations of a range of complex architectural copolymers using mass spectrometry (MS) and advanced chromatographic techniques. The field of polymer science includes a very broad range of macromolecular species due to the possibility to increase structural complexity and molar masses. Synthetic polymers have various specific properties such as heterogeneity, topology, composition, functionality or molar mass. MS techniques such as electrospray ionization (ESI), matrix-assisted laser desorption/ionization (MALDI), atmospheric pressure chemical ionization (APCI) and their hyphenation to liquid chromatography (LC) systems have helped to improve the analysis of polymers (Chapter 2). Furthermore, IM-MS and Fourier transform (FT)-MS techniques have a great potential in the characterization of macromolecules. In the future, all these tools will help to investigate copolymers, still a challenging topic.

MALDI-ToF MS represents an advanced tool for the determination of the absolute molar masses, for a wide range of polymer classes: poly(ethylene oxide) (PEO), poly(furfuryl glycidyl ether) (PFGE), poly(*N*-isopropyl acrylamide) (P*N*iPAm) being highly relevant due to their specific properties (Chapter 3). Nonetheless, asymmetric field flow field fractionation (AF4) and analytical ultracentrifugation (AUC) are powerful techniques for absolute molar mass determination however, not to the molecular level. However, these two techniques have a greater potential for higher molar mass polymers. Moreover, research using MALDI-MS has tried to investigate the relationship between the matrix choice and the polymer class for many years. In addition, it can be also applied as analysis method to monitor the reaction progress and to gain additional information regarding possible side reactions during the polymerization process.

In Chapter 4, complex synthetic polymers were investigated by complementary characterization techniques either online or offline. These have shown to be important for detailed investigations for block up to star-shaped copolymers. The first example discussed in this chapter portrayed hybrid stars such as polyhydral oligomeric silesquioxanes (POSS) cage with eight PEO arms, which were investigated with MALDI and static light scattering (SLS), techniques characterizing high molar mass polymers, and elucidated the importance of applying complementary methods. Furthermore, [PEO-*b*-PEtOx]$_8$ as a block like star-shaped polymer was analyzed *via*

two-dimensional-liquid chromatography (2D-LC) (LACCC × SEC) and offline MALDI MS to detect the functionalization and the molar mass. Moreover, poly(2-ethyl-2-oxazoline)-*b*-poly(2-(2,6-difluorophenyl)2-oxazoline)) (PEtOx-*b*-P*o*DFOx) was studied by an advanced setup representing an important step towards high-throughput multidimensional measurements and revealed its reproducibility, quantifiability aspect and structurally informative, thus making it applicable for pharmaceutical polymers. Finally, and most importantly this allows new ways for an intellectual property (IP) protection. The next steps would be to analysis of pharmaceutical polymers and drug loaded carriers.

The combination of computational methods and mass spectrometry has proved to be very productive (Chapter 5). Copolymer spectra are challenging in comparison to those of homopolymers. However, new computational methods were developed to identify copolymer architectures, and to quantify as well as qualify the most abundant species. The newly developed tool COCONUT and others have a remarkable efficiency in accelerating the manual analysis, the software was applied to PS-*r*-PI with different amounts of monomers. The sequencing of copolymers will be an important future target.

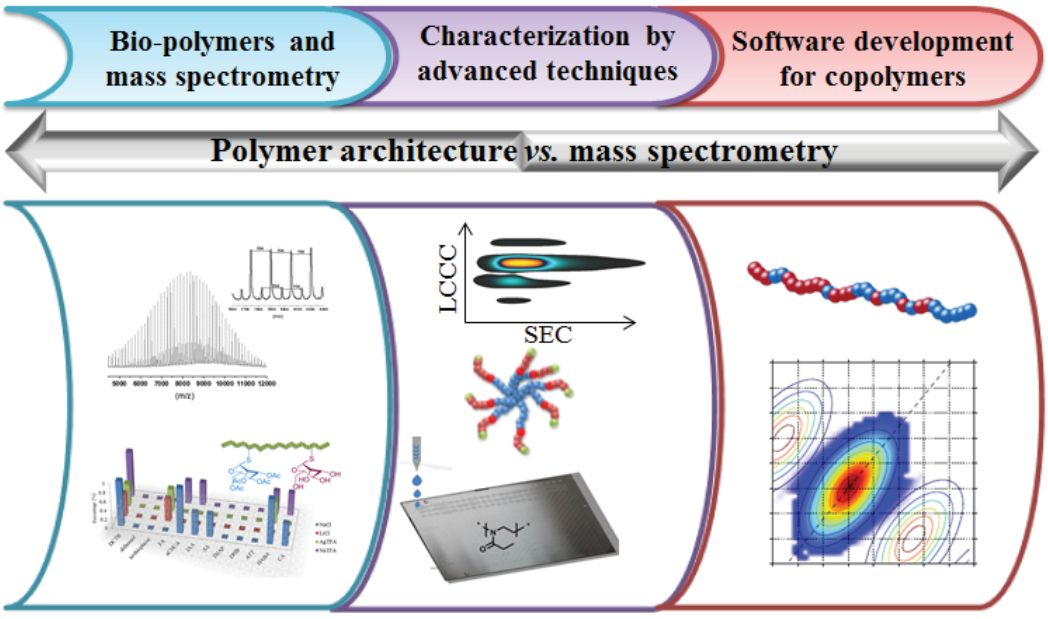

Figure 6.1. Overview of techniques and macromolecules discussed in this thesis.

To conclude, this thesis shows the potential of MS techniques as well as chromatographic techniques and computational methods for synthetic polymers. All

these different methods enable a detailed investigation of polymers, which is of essence to engineer smart polymers. Future work will continue on developing additional software techniques for non-linear copolymers. Furthermore, sequencing of linear copolymers with block, random, gradient like microstructures will be in the focus.

7. Zusammenfassung

Ziel dieser Arbeit war es, unterschiedliche Copolymere mit komplexer Architektur mittels massenspektrometrischer (MS) und spezieller chromatographischer Techniken zu untersuchen, um die Vielfältigkeit dieser Methoden im Hinblick auf detaillierte Charakterisierung zu demonstrieren. Wegen der zunehmenden Möglichkeiten, die strukturelle Komplexität und Molmassen synthetischer Polymere weiter zu entwicklen, bietet die moderne Polymerchemie eine sehr breite Auswahl von makromolekularen Spezies. Synthetische Polymere besitzen eine Vielzahl an wichtigen Eigenschaften wie Heterogenität, Topologie, Zusammensetzung, Funktionalität oder Molmasse. MS Techniken wie Elektrospray-Ionisierung (ESI), Matrix-unterstützte Laser Desorption-Ionisierung (MALDI), chemische Ionisation bei Atmosphärendruck (APCI) und ihre Kopplung mit Flüssigchromatographie (LC) haben dazu beigetragen, die Analytik solcher Polymere wesentlich zu verbessern (Kapitel 2). Des Weiteren haben Ionenmobilitätsspektrometrie und Fourier-Transformations (FT)-MS Techniken ein großes Potenzial zur Charakterisierung von Makromolekülen. Zukünftig werden auch diese Techniken zur Untersuchung von Copolymeren verstärkt genutzt werden, so dass dies weiterhin ein anspruchsvolles Forschungsfeld darstellen wird.

Neben den traditionellen relativen Methoden stellt MALDI-ToF MS ein fortgeschrittenes Werkzeug für die Bestimmung von absoluten Molmassen dar, und zwar für viele Polymerklassen, die aufgrund ihrer Eigenschaften höchste Relevanz besitzen u. a. (Polyethylenoxid (PEO), Poly(furfuryl glycidyl ether) (PFGE) und Poly(*N*-isopropyl acrylamide) (P*n*iPAm)), Kapitel 3). Trotzdem sind Asymmetrischer-Fluss-Feld-Fluss-Fraktionierung (AF4) und Analytischer Ultrazentrifugation (AUC) Techniken, die ein größeres Potenzial für die Bestimmung besonders hoher Molmassen besitzen. Diese haben jedoch den Nachteil, dass strukturelle Informationen bis hin zu dem molekularen Level nicht geliefert werden können. Außerdem hat sich die Forschung im Bereich von MALDI für viele Jahre damit beschäftigt, den Zusammenhang zwischen Auswahl von Matrix und Polymerklasse zu untersuchen. Des Weiteren kann diese Technik aber auch dazu eingesetzt werden, den Verlauf von Reaktionen oder das Auftreten und die Art von Nebenreaktionen während der Polymerisation aufzuklären.

In Kapitel 4 wurden synthetische Polymere mit komplexen Architekturen mittels komplementärer Techniken, die entweder direkt oder indirekt miteinander gekoppelt

sind, untersucht. Diese Herangehensweise hat sich schon bei detaillierten Untersuchungen recht einfacher Systeme wie von Blockcopolymeren als sehr wichtig herausgestellt und lässt sich bis auf die Untersuchung sternförmiger Copolymere hin ausdehnen. Als erstes Beispiel in diesem Kapitel wurde die Untersuchung von sternförmigen Hybrid-Polymeren, die aus einem Poly(hydral oligomeric silesquioxane)-(POSS) Käfig und acht PEO Armen bestehen, beschrieben. Die Anwendung von MALDI und statischer Lichtstreuung (SLS), zwei Techniken für die Charakterisierung von Polymeren mit hohen Molmassen, zeigt klar die Wichtigkeit von komplementären Methoden auf. Letzteres wurde mit [PEO-*b*-PEtOx]$_8$ als einem Beispiel für ein sternförmiges Blockcopolymer mittels Zweidimensionalität-Flüssigchromatographie (2D-LC) (LACCC × SEC) und offline MALDI MS-Kopplung untersucht, um die Funktionaliäten und die molare Massen zu bestimmen. Zudem wurde Poly(2-ethyl-2-oxazoline)-*b*-poly(2-(2,6-difluorophenyl)-2-oxazoline) (PEtOx-*b*-P*o*DFOx) untersucht. Der dazu angewendete multidimensionale Hochdurchsatz-Aufbau der Analytik zeigte ein hohes Maß an Reproduzierbarkeit, war quantitativ, lieferte zugleich strukturelle Informationen und stellt somit einen wichtigen Schritt im Hinblick auf die Anwendbarkeit für Pharmapolymere dar. Eine zukünftige Anwendung für beispielsweise beladene polymere Trägersysteme für Wirkstoffe eröffnet neue Wege zum Schutz geistigen Eigentums (IP).

Die Kombination von Berechnungsmethoden mit Massenspektrometrie hat sich als essenziell für die Polymerwissenschaft herausgestellt (Kapitel 5), da die Spektren von Copolymeren eine wesentlich größere Herausforderung im Vergleich zu denen von Homopolymeren darstellen. Es existieren mehrere Computer-basierte Methoden, die Chemikern dabei helfen, ihre Spektren so auszuwerten, dass Copolymer-Architekturen identifiziert und das hauptsächlich auftretende Copolymer in gewissem Maße auch quantifiziert werden kann. Das neu entwickelte Programm COCONUT und andere haben hierbei eine bemerkenswerte Effizienz bei der Interpretation von Spektren von PS-*r*-PI gezeigt und ist der manuellen Auswertungwert überlegen. Wie bei Proteinen wird hier die Sequenzierung von Copolymeren der nächste Schritt sein, um die Zusammensetzung einzelner Polymerketten untersuchen zu können.

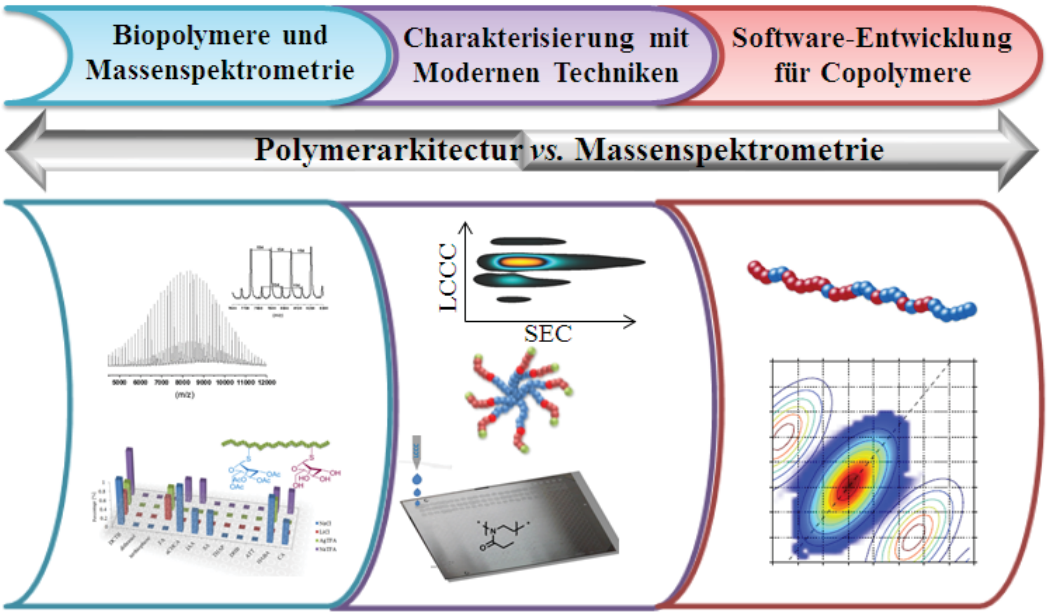

Abbildung 7.1. Übersicht über die Techniken und Makromoleküle, die im Rahmen dieser Arbeit diskutiert wurden.

Abschließensd lässt sich sagen, dass in dieser Arbeit gezeigt werden konnte, wie leistungsstark die Kombination aus MS und chromatographischen Techniken in Kombination mit eigens entwickelten Software-Methoden für die Strukturaufklärung unterschiedlicher synthetischer Polymerarchitekturen sein kann. Alle diese Methoden ermöglichen eine detaillierte Untersuchung von Polymeren, welches eine Grundlage für den Aufbau „smarter“ Polymere darstellt. In Fortführung dieses Themas wird die Entwicklung von Software für nichtlineare Systeme und in der Sequenzierung von linearen Copolymeren stehen, um die Mikrostrukturen (random, gradient, block) dieser mittels MS Techniken aufklären zu können.

8. References

[1] C. d. l. H. Alarcon, S. Pennadam, C. Alexander, *Chem. Soc. Rev.* **2005**, *34*, 276-285.

[2] G. R. Whittell, M. D. Hager, U. S. Schubert, I. Manners, *Nature Mater.* **2011**, *10*, 176-188.

[3] K. Knop, R. Hoogenboom, D. Fischer, U. S. Schubert, *Angew. Chem. Int. Ed.* **2010**, *49*, 6288-6308.

[4] N. Hadjichristidis, M. Pitsikalis, S. Pispas, H. Iatrou, *Chem. Rev.* **2001**, *101*, 3747-3792.

[5] R. Hoogenboom, *Angew. Chem. Int. Ed.* **2009**, *48*, 7978-7994.

[6] M. Szwarc, *Nature* **1956**, *178*, 1168-1169.

[7] R. B. Grubbs, *Polym. Rev.* **2011**, *51*, 104-137.

[8] G. Moad, E. Rizzardo, S. H. Thang, *Aus. J. Chem.* **2009**, *62*, 1402-1472.

[9] C. Barner-Kowollik, S. Perrier, *J. Polym. Sci., Part A: Polym. Chem.* **2008**, *46*, 5715-5723.

[10] W. Jakubowski, N. V. Tsarevsky, P. McCarthy, K. Matyjaszewski, *Mater. Matters.* **2010**, *5*, 16-24.

[11] S. D. Hanton, *Chem. Rev.* **2001**, *101*, 527-570.

[12] G. Montaudo, F. Samperi, M. S. Montaudo, *Prog. Polym. Sci.* **2006**, *31*, 277-357.

[13] K. Tanaka, H. Waki, Y. Ido, S. Akita, Y. Yoshida, T. Yoshida, T. Matsuo, *Rapid Commun. Mass Spectrom.* **1988**, *2*, 151-153.

[14] M. Karas, D. Bachmann, F. Hillenkamp, *Anal. Chem.* **1985**, *57*, 2935-2939.

[15] J. B. Fenn, *Angew. Chem. Int. Ed.* **2003**, *42*, 3871-3894.

[16] D. R. Maloney, K. H. Hunt, P. M. Lloyd, A. V. G. Muir, S. N. Richards, P. J. Derrick, D. M. Haddleton, *J. Chem. Soc., Chem. Commun.* **1995**, 561-562.

[17] C. N. McEwen, P. M. Peacock, *Anal. Chem.* **2002**, *74*, 2743-2748.

[18] P. M. Peacock, C. N. McEwen, *Anal. Chem.* **2004**, *76*, 3417-3428.

[19] J. H. Scrivens, A. T. Jackson, *Int. J. Mass Spectrom.* **2000**, *200*, 261-276.

[20] J. C. Blais, M. Tessier, G. Bolbach, B. Remaud, L. Rozes, J. Guittard, A. Brunot, E. Maréchal, J. C. Tabet, *Int. J. Mass Spectrom. Ion Process.* **1995**, *144*, 131-138.

[21] A. P. Gies, M. J. Vergne, R. L. Orndorff, D. M. Hercules, *Macromolecules* **2007**, *40*, 7493-7504.

[22] D. Suckau, A. Resemann, M. Schuerenberg, P. Hufnagel, J. Franzen, A. Holle, *Anal. Bioanal. Chem.* **2003**, *376*, 952-965.

[23] H. Pasch, *Adv. Polym. Sci.* **2000**, *150*, 1-66.

[24] P. M. Peacock, C. N. McEwen, *Anal. Chem.* **2006**, *78*, 3957-3964.

[25] S. M. Weidner, S. Trimpin, *Anal. Chem.* **2008**, *80*, 4349-4361.

[26] S. M. Weidner, S. Trimpin, *Anal. Chem.* **2010**, *82*, 4811-4829.

[27] S. L. Madorsky, S. Straus, *Ind. Eng. Chem.* **1948**, *40*, 848-852.

[28] L.A. Wall, *J. Res. Natl. Bur. Stand. (U.S.)* **1948**, *41*, 315-322.

[29] C. Wesdemiotis, N. Solak, M. J. Polce, D. E. Dabney, K. Chaicharoen, B. C. Katzenmeyer, *Mass Spectrom. Rev.* **2011**, *30*, 523-559.

[30] R. Peters, Y. Mengerink, S. Langereis, M. Frederix, H. Linssen, H. J. van, d. W. S. van, *J. Chromatogr. A* **2002**, *949*, 327-335.

[31] M. Dietrich, M. Glassner, T. Gruendling, C. Schmid, J. Falkenhagen, C. Barner-Kowollik, *Polym. Chem.* **2010**, *1*, 634-644.

[32] A. Feldermann, A. Ah Toy, T. P. Davis, M. H. Stenzel, C. Barner-Kowollik, *Polymer* **2005**, *46*, 8448-8457.
[33] S. Trimpin, S. M. Weidner, J. Falkenhagen, C. N. McEwen, *Anal. Chem.* **2007**, *79*, 7565-7570.
[34] M. Hassellöv, G. Hulthe, B. Lyvén, G. Stenhagen, *J. Liq. Chromatogr. Relat. Technol.* **1997**, *20*, 2843-2856.
[35] G. R. Hilton, A. T. Jackson, K. Thalassinos, J. H. Scrivens, *Anal. Chem.* **2008**, *80*, 9720-9725.
[36] A. Baumgaertel, K. Scheubert, B. Pietsch, K. Kempe, A. C. Crecelius, S. Böcker, U. S. Schubert, *Rapid Commun. Mass Spectrom.* **2011**, *25*, 1765-1778.
[37] A. Jackson, S. Slade, K. Thalassinos, J. Scrivens, *Anal. Bioanal. Chem.* **2008**, *392*, 643-650.
[38] A. T. Jackson, K. Thalassinos, R. O. John, N. McGuire, D. Freeman, J. H. Scrivens, *Polymer* **2010**, *51*, 1418-1424.
[39] J. P. Williams, G. R. Hilton, K. Thalassinos, A. T. Jackson, J. H. Scrivens, *Rapid Commun. Mass Spectrom.* **2007**, *21*, 1693-1704.
[40] M. S. Montaudo, *Mass Spectrom. Rev.* **2002**, *21*, 108-144.
[41] T. Orhan, J. Hacaloglu, *Polym. Degrad. Stabil.* **2013**, *98*, 356-360.
[42] A. C. Crecelius, C. R. Becer, K. Knop, U. S. Schubert, *J. Polym. Sci., Part A: Polym. Chem.* **2010**, *48*, 4375-4384.
[43] R. X. E. Willemse, B. B. P. Staal, E. H. D. Donkers, A. M. van Herk, *Macromolecules* **2004**, *37*, 5717-5723.
[44] S. M. Miladinović, C. J. Kaeser, M. M. Knust, C. L. Wilkins, *Int. J. Mass Spectrom.* **2011**, *301*, 184-194.
[45] S. Huijser, B. B. P. Staal, J. Huang, R. Duchateau, C. E. Koning, *Biomacromolecules* **2006**, *7*, 2465-2469.
[46] S. Huijser, B. B. P. Staal, J. Huang, R. Duchateau, C. E. Koning, *Angew. Chem. Int. Ed.* **2006**, *118*, 4210-4214.
[47] S. M. Weidner, J. Falkenhagen, I. Bressler, *Macromol. Chem. Phys.* **2012**, *213*, 2404-2411.
[48] A. Baumgaertel, C. Weber, N. Fritz, G. Festag, E. Altuntaş, K. Kempe, R. Hoogenboom, U. S. Schubert, *J. Chromatogr. A* **2011**, *1218*, 8370-8378.
[49] D. Morsa, T. Defize, D. Dehareng, C. Jérôme, E. De Pauw, *Anal. Chem.* **2014**, *86*, 9693-9700.
[50] T. Rudolph, S. Crotty, M. von der Lühe, D. Pretzel, U. Schubert, F. Schacher, *Polymers* **2013**, *5*, 1081-1101.
[51] L. P. Tolic, G. A. Anderson, R. D. Smith, H. M. Brothers, II, R. Spindler, D. A. Tomalia, *Int. J. Mass Spectrom. Ion Processes* **1997**, *165/166*, 405-418.
[52] M. He, S. A. McLuckey, *Rapid Commun. Mass Spectrom.* **2004**, *18*, 960-972.
[53] F. Maire, G. Coadou, L. Cravello, C. Lange, *J. Am. Soc. Mass Spectrom.* **2013**, *24*, 238-248.
[54] M. Karas, F. Hillenkamp, *Anal. Chem.* **1988**, *60*, 2299-2301.
[55] S. M. A. B. Batoy, E. Akhmetova, S. Miladinovic, J. Smeal, C. L. Wilkins, *Appl. Spectrosc. Rev.* **2008**, *43*, 485-550.
[56] A. J. Hoteling, W. J. Erb, R. J. Tyson, K. G. Owens, *Anal. Chem.* **2004**, *76*, 5157-5164.
[57] S. D. Hanton, K. G. Owens, *J. Am. Soc. Mass Spectrom.* **2005**, *16*, 1172-1180.
[58] http://www.shimadzu.com/about/nobel/noblesoul/images/tec_img02.gif, (last accessed 02/04/2015).
[59] H. Räder, W. Schrepp, *Acta Polymerica* **1998**, *49*, 272-293.

[60] M. A. R. Meier, U. S. Schubert, *Rapid Commun. Mass Spectrom.* **2003**, *17*, 713-716.
[61] S. Gabriel, C. Schwarzinger, B. Schwarzinger, U. Panne, S. Weidner, *J. Am. Soc. Mass Spectrom.* **2014**, *25*, 1356-1363.
[62] Q. Tian, M. Z. Rong, M. Q. Zhang, Y. C. Yuan, *Polym. Int.* **2010**, *59*, 1339-1345.
[63] J. M. Harris, R. B. Chess, *Nat. Rev. Drug Discov.* **2003**, *2*, 214-221.
[64] http://www.covalx.com/hm2, (last accessed 18/07/2016).
[65] V. Vázquez-Dorbatt, J. Lee, E.-W. Lin, H. D. Maynard, *ChemBioChem* **2012**, *13*, 2478-2487.
[66] C. v. d. Ehe, F. Kretschmer, C. Weber, S. Crotty, S. Stumpf, S. Hoeppener, M. Gottschaldt, U. S. Schubert, in *Controlled Radical Polymerization: Materials, Vol. 1188*, American Chemical Society, **2015**, pp. 221-256.
[67] A. Favier, C. Ladavière, M.-T. Charreyre, C. Pichot, *Macromolecules* **2004**, *37*, 2026-2034.
[68] Y. Gnanou, P. Lutz, P. Rempp, *Makromol. Chem.* **1988**, *189*, 2885-2892.
[69] G. Lapienis, *Prog. Polym. Sci.* **2009**, *34*, 852-892.
[70] E. Alexandre, B. Schmitt, K. Boudjema, E. W. Merrill, P. J. Lutz, *Macromol. Biosci.* **2004**, *4*, 639-648.
[71] K. B. Keys, F. M. Andreopoulos, N. A. Peppas, *Macromolecules* **1998**, *31*, 8149-8156.
[72] G. M. E. Pozza, H. Harris, M. J. Barthel, J. Vitz, U. S. Schubert, P. J. Lutz, *Macromol. Chem. Phys.* **2012**, *213*, 2181-2191.
[73] P. Maitra, S. L. Wunder, *Chem. Mater.* **2002**, *14*, 4494-4497.
[74] M. Rawiso, *J. Phys. IV* **1999**, *09*, 147-195.
[75] J. P. Cotton, *J. Phys. IV* **1999**, *09*, 21-49.
[76] M. Daoud, J. P. Cotton, *J. Phys.* **1982**, *43*, 531-538.
[77] G. S. Grest, K. Kremer, T. A. Witten, *Macromolecules* **1987**, *20*, 1376-1383.
[78] G. S. Grest, *Macromolecules* **1994**, *27*, 3493-3500.
[79] B. G. Belenky, E. S. Gankina, M. B. Tennikov, L. Z. Vilenchik, *J. Chromatogr. A* **1978**, *147*, 99-110.
[80] M. Malik, H. Ahmed, B. Trathnigg, *Anal. Bioanal. Chem.* **2009**, *393*, 1797-1804.
[81] A. A. Gorbunov, A. M. Skvortsov, *Adv. Colloid Interface Sci.* **1995**, *62*, 31-108.
[82] E. Beaudoin, A. Favier, C. Galindo, A. Lapp, C. Petit, D. Gigmes, S. Marque, D. Bertin, *Eur. Polym. J.* **2008**, *44*, 514-522.
[83] P. J. Schoenmakers, G. Vivó-Truyols, W. M. C. Decrop, *J. Chromatogr. A* **2006**, *1120*, 282-290.
[84] S. Weidner, J. Falkenhagen, R.-P. Krueger, U. Just, *Anal. Chem.* **2007**, *79*, 4814-4819.
[85] M. I. Malik, B. Trathnigg, K. Bartl, R. Saf, *Anal. Chimi. Acta* **2010**, *658*, 217-224.
[86] J. Falkenhagen, S. Weidner, *Anal. Chem.* **2009**, *81*, 282-287.
[87] Z. Iatridi, C. Tsitsilianis, *Polymers* **2011**, *3*, 1911-1933.
[88] F. H. Schacher, U. Freier, F. Steiniger, *Soft Matter* **2012**, *8*, 6968-6978.
[89] A. A. Steinschulte, B. Schulte, M. Erberich, O. V. Borisov, F. A. Plamper, *ACS Macro Lett.* **2012**, *1*, 504-507.
[90] K. Knop, G. M. Pavlov, T. Rudolph, K. Martin, D. Pretzel, B. O. Jahn, D. H. Scharf, A. A. Brakhage, V. Makarov, U. Mollmann, F. H. Schacher, U. S. Schubert, *Soft Matter* **2013**, *9*, 715-726.

[91] F. Quaglia, L. Ostacolo, G. Nese, M. Canciello, G. De Rosa, F. Ungaro, R. Palumbo, M. I. La Rotonda, G. Maglio, *J. Biomed. Mater. Res. A* **2008**, *87A*, 563-574.
[92] M. Bauer, C. Lautenschlaeger, K. Kempe, L. Tauhardt, U. S. Schubert, D. Fischer, *Macromol. Biosci.* **2012**, *12*, 986-998.
[93] J.-S. Park, K. Kataoka, *Macromolecules* **2007**, *40*, 3599-3609.
[94] H. Schlaad, C. Diehl, A. Gress, M. Meyer, A. L. Demirel, Y. Nur, A. Bertin, *Macromol. Rapid Commun.* **2010**, *31*, 511-525.
[95] O. Altintas, A. P. Vogt, C. Barner-Kowollik, U. Tunca, *Polym. Chem.* **2012**, *3*, 34-45.
[96] C. Tsitsilianis, P. Lutz, S. Graff, J. P. Lamps, P. Rempp, *Macromolecules* **1991**, *24*, 5897-5902.
[97] H. Sharghi, R. Khalifeh, M. M. Doroodmand, *Adv. Synth. Catal.* **2009**, *351*, 207-218.
[98] V. V. Rostovtsev, L. G. Green, V. V. Fokin, K. B. Sharpless, *Angew. Chem. Int. Ed.* **2002**, *114*, 2708-2711.
[99] B. M. Rosen, C. J. Wilson, D. A. Wilson, M. Peterca, M. R. Imam, V. Percec, *Chem. Rev.* **2009**, *109*, 6275-6540.
[100] F. C. Gaertner, R. Luxenhofer, B. Blechert, R. Jordan, M. Essler, *J. Control. Release* **2007**, *119*, 291-300.
[101] A. Mero, G. Pasut, L. D. Via, M. W. M. Fijten, U. S. Schubert, R. Hoogenboom, F. M. Veronese, *J. Control. Release* **2008**, *125*, 87-95.
[102] T. X. Viegas, M. D. Bentley, J. M. Harris, Z. Fang, K. Yoon, B. Dizman, R. Weimer, A. Mero, G. Pasut, F. M. Veronese, *Bioconjucate. Chem.* **2011**, *22*, 976-986.
[103] R. Luxenhofer, A. Schulz, C. Roques, S. Li, T. K. Bronich, E. V. Batrakova, R. Jordan, A. V. Kabanov, *Biomaterials* **2010**, *31*, 4972-4979.
[104] M. S. Montaudo, *Mass Spectrom. Rev.* **2002**, *21*, 108-144.
[105] S. Trimpin, M. Plasencia, D. Isailovic, D. E. Clemmer, *Anal. Chem.* **2007**, *79*, 7965-7974.
[106] G. M. Pavlov, I. Perevyazko, U. S. Schubert, *Macromol. Chem. Phys.* **2010**, *211*, 1298-1310.
[107] H. Cölfen, M. Antonietti, *Field-flow fractionation techniques for polymer and colloid analysis*, Springer, Berlin Heidelberg, **2000**.
[108] M. S. Montaudo, *J. Am. Soc. Mass Spectrom.* **2004**, *15*, 374-384.
[109] G. Wilczek-Vera, Y. Yu, K. Waddell, P. O. Danis, A. Eisenberg, *Rapid Commun. Mass Spectrom.* **1999**, *13*, 764-777.
[110] G. Wilczek-Vera, Y. Yu, K. Waddell, P. O. Danis, A. Eisenberg, *Macromolecules* **1999**, *32*, 2180-2187.
[111] S. Huijser, G. D. Mooiweer, R. van der Hofstad, B. B. P. Staal, J. Feenstra, A. M. van Herk, C. E. Koning, R. Duchateau, *Macromolecules* **2012**, *45*, 4500-4510.
[112] G. Wilczek-Vera, P. O. Danis, A. Eisenberg, *Macromolecules* **1996**, *29*, 4036-4044.
[113] P. Terrier, W. Buchmann, G. Cheguillaume, B. Desmazières, J. Tortajada, *Anal. Chem.* **2005**, *77*, 3292-3300.
[114] G. Vivó-Truyols, B. Staal, P. J. Schoenmakers, *J. Chromatogr. A* **2010**, *1217*, 4150-4159.
[115] W. Yan, J. A. Gardella Jr, T. D. Wood, *J. Am. Soc. Mass Spectrom.* **2002**, *13*, 914-920.

[116] R. R. Hensel, R. C. King, K. G. Owens, *Rapid Commun. Mass Spectrom.* **1997**, *11*, 1785-1793.
[117] H. Chen, M. He, J. Pei, H. He, *Anal. Chem.* **2003**, *75*, 6531-6535.
[118] Z. Walterová, J. Horský, *Anal. Chim. Acta* **2011**, *693*, 82-88.
[119] D. C. Schriemer, L. Li, *Anal. Chem.* **1997**, *69*, 4169-4175.
[120] D. C. Schriemer, L. Li, *Anal. Chem.* **1997**, *69*, 4176-4183.
[121] http://bio.informatik.uni-jena.de/software/coconut/, (last accessed 20/06/2015).

9. List of abbreviations

AF4	Asymmetrical flow field-flow fractionation
APCI	Atmospheric pressure chemical ionization
API	Atmospheric pressure ionization
APPI	Atmospheric pressure photoionization
AROP	Anionic ring-opening polymerization
ATRP	Atom transfer radical polymerization
AUC	Analytical ultracentrifugation
BMA	Butyl methacrylate
CA	Caffeic acid
αCHCA	α-Cyano-4-hydroxycinnamic acid
CI	Chemical ionization
CID	Collision induced dissociation
COCONUT	Copolymer composition numbering tool
CROP	Cationic ring-opening polymerization
Đ	Dispersity
DCTB	*trans*-2-[3-(4-*tert*-Butylphenyl)-2-methyl-2-propenylidene]malononitrile
DHB	2,5-Dihydroxybenzoic acid
DSC	Differential scanning calorimetry
ECD	Electron capture dissociation
EI	Electron ionization
ELSD	Evaporative light scattering detector
EO	Ethylene oxide
EPOx	2-(1-Ethyl-pentyl)-2-oxazoline
ESI	Electrospray ionization
ETD	Electron-transfer dissociation
FA	Ferrulic acid
FAB	Fast atom bombardment
FFF	Field flow fractionation
FT	Fourier transform
FT-ICR	Fourier transform-ion cyclotron resonance
GPEC	Gradient polymer elution chromatography
GTP	Group transfer polymerization

HABA	Hydroxyazobenzene-2-carboxylic acid
HPLC	High performance liquid chromatography
IAA	3-Indoleacrylic acid
IM-MS	Ion mobility-mass spectrometry
I_n	First macromer
IP	Intellectual property
IR	Infrared
ISD	In-source decay
LAC	Liquid adsorption chromatography
LACCC	Liquid absorption chromatography at critical conditions
LC	Liquid chromatography
LCST	Lower critical solution temperature
LiCl	Lithium chloride
LS	Light scattering
MALDI	Matrix-assisted laser desorption/ionization
MS	Mass spectrometry
MS/MS	Tandem mass spectrometry
NaTFA	Sodium trifluoroacetate
NaCl	Sodium chloride
NMP	Nitroxide mediated polymerization
NMR	Nuclear magnetic resonance
PBA	Poly(butyl acrylate)
P2VP	Poly(2-vinylpyridine)
P*o*DFOx	Poly(2-(2,6-difluorophenyl)-2-oxazoline))
PAMAM	Poly(amidoamine)
PCL	Poly(*ε*-caprolactone)
PEG	Poly(ethylene glycol)
PEO	Poly(ethylene oxide)
PEtOx	Poly(2-ethyl-2-oxazoline)
PEPOx	Poly(2-(1-ethyl-pentyl)-2-oxazoline)
PFGE	Poly(furfuryl glycidyl ether)
PHEMA	Poly(2-hydroxyethyl methacrylate)
PI	Polyisoprene
PLA	Poly(lactide)

PLGA	Poly(lactide-*co*-glycolide)
PLUMS	Polymer labeling using mass spectrometry
PMA	Poly(methylacrylate)
PMMA	Poly(methyl methacrylate)
P_n	Second marcromer
P*n*BA	Poly(*n* butyl acrylate)
P*N*iPAm	Poly(*N*-*iso*propyl acrylamide)
PO	Propylene oxide
POSS	Polyhydral oligomeric silesquioxanes
PPO	Poly(propylene oxide)
PS	Polystyrene
PSD	Post source decay
PS-*r*-PI	Poly(styrene-*r*-isoprene)
RAFT	Reversible addition-fragmentation chain transfer
RI	Refractive index
SA	Sinapinic acid
SAXS	Small angle X-ray scattering
SEC	Size exclusion chromatography
SID	Surface-induced dissociation
SLS	Static light scattering
TGA	Thermogravimetric analysis
THAP	2',4',6'-Trihydroxyacetophenone monohydrate
ToF	Time-of-flight
TPIC	Temperature gradient interaction chromatography
UV-Vis	Ultraviolet-visible

Curriculum Vitae

Sarah C. Crotty

Personal Information

Date of Birth	5th of May 1987
Place of Birth	Ambilly, France
Citizenship	British / French

Education

Since 01 2012-present	**Ph.D. student**, Friedrich Schiller University Jena, Germany Laboratory of Organic and Macromolecular Chemistry (IOMC) *Characterization of macromolecular systems with mass spectrometry and hyphenated techniques.* Supervisor: Prof. Dr. Ulrich S. Schubert
09 2010 / 09 2011	**M.Sc**., University of Warwick, U.K. *Characterization of synthetic polymers via MALDI-ToF MS/MS.* Supervisor: Prof. Dr. David. M. Haddleton and Dr. C. Remzi Becer
08 2008 / 08 2009	**Industrial placement:** Advinus Therapeutics Pvt. Ltd., India.
09 2006 / 09 2010	**B.Sc.**, Loughborough University, U.K. *Analysis of calixarenes via ESI-Q-ToF MS.* Supervisor: Prof. Dr. Colin. S. Creaser

Jena, den……2016

Sarah C. Crotty

Publication List

Peer-reviewed publications

1. M. J. Barthel, T. Rudolph, S. Crotty, F. H. Schacher, U. S. Schubert, Homo- and diblock copolymers of poly(furfuryl glycidyl ether) by living anionic polymerization: Towards reversibly core-crosslinked micelles, *J. Polym. Sci., Part A: Polym. Chem.* **2012**, *50*, 4958-4965.

2. R. Schroot, C. Friebe, E. Altuntas, S. Crotty, M. Jäger, U. S. Schubert, Nitroxide-mediated polymerization of styrenic triarylamines and chain-end functionalization with a ruthenium complex: Toward tailored photoredox-active architectures, *Macromolecules* **2013**, *46*, 2039-2048.

3. T. Rudolph, K. Kempe, S. Crotty, R. M. Paulus, U. S. Schubert, I. Krossing, F. H. Schacher, A strong cationic Brønsted acid, [H(OEt2)2]-[Al{OC(CF3)3}4], as an efficient initiator for the cationic ring-opening polymerization of 2-alkyl-2-oxazolines, *Polym. Chem.* **2013**, *4*, 495-505.

4. T. Rudolph, S. Crotty, M. von der Luehe, D. Pretzel, U. S. Schubert, F. H. Schacher, Synthesis and solution properties of double hydrophilic poly(ethylene oxide)-*block*-poly(2-ethyl-2-oxazoline) (PEO-*b*-PEtOx) star block copolymers, *Polymers* **2013**, *5*, 1081-1101.

5. G. M.-E. Pozza, M. J. Barthel, S. Crotty, J. Vitz, F. H. Schacher, P. J. Lutz, U. S. Schubert, Precise synthesis of undecenyl poly(ethylene oxide) macromonomers as heterofunctional building blocks for the synthesis of linear diblocks or of branched materials, *Eur. Polym. J.* **2014**, *57*, 221-236.

6. S. Crotty, C. Weber, A. Baumgaertel, N. Fritz, E. Altuntaş, K. Kempe, U. S. Schubert, Semi-automated multi-dimensional characterization of synthetic copolymers, *Eur. Polym. J.* **2014**, *60*, 153-162.

7. G. M.-E. Pozza, S. Crotty, M. Rawiso, U. S. Schubert, P. J. Lutz, Molecular and structural characterization of hybrid poly(ethylene oxide)-polyhedral oligomeric silesquioxanes star-shaped macromolecules, *J. Phys. Chem. B* **2015**, *119*, 1669-1680.

8. M. S. Engler,[#] S. Crotty,[#] M. J. Barthel, C. Pietsch, K. Knop, U. S. Schubert, S. Boecker, COCONUT − an efficient tool for estimating copolymer compositions from mass spectra, *Anal. Chem.* **2015**, *57*, 5223-5231.
   [#] equal contribution

9. C. von der Ehe, F. Kretschmer, C. Weber, S. Crotty, S. Stumpf, S. Hoeppener, M. Gottschaldt, U. S. Schubert, RAFT copolymerization of thioglycosidic glycomonomers with *N*iPAm and subsequent immobilization onto gold nanoparticles, in *ACS Symposium Series, Controlled Radical Polymerization* (Eds.: K. Matyjaszewski, B. S. Summerlin, N.V. Tsarevsky, J. Chiefari), Wiley-VCH Verlag GmbH & Co, 2015, pp. 221-256.

10. T. Rudolph, S. Crotty, U. S. Schubert, F. H. Schacher, Star-shaped poly(2-ethyl-2-oxazoline) featuring a porphyrin core: synthesis and metal complexation, *ePolymers* **2015**, *15*, 227-235.

11. I. Yildirim, S. Crotty, C. H. Loh, G. Festag, C. Weber, P.-F. Caponi, M. Gottschaldt, M. Westerhausen, U. S. Schubert, End-functionalized polylactides using a calcium based pre-catalyst: Synthesis and insights by mass spectrometry, *J. Polym. Sci., Part A: Polym. Chem.* **2016**, *54*, 437-448.

12. S. Crotty, C. von der Ehe, C. Weber, U. S. Schubert, Detailed MALDI comparison of *N*iPAm glycopolymers, *Eur. Polym. J.* **2015**, *71*, 325-335.

13. M. S. Engler,[#] S. Crotty,[#] M. J. Barthel, C. Pietsch, U. S. Schubert, S. Boecker, Abundance correction for mass discrimination effects in polymer spectra, *Rapid Commun. Mass Spectrom.* **2016**, *30*, 1233-1241.
   [#] equal contribution

14 S. Crotty, S. Gerişlioğlu, K. J. Endres, C. Wesdemiotis, U. S. Schubert, Polymer architectures *via* mass spectrometry and hyphenated techniques: A review, *Anal. Chim. Acta* **2016**, 932, 1-21.

Oral contributions

S. Crotty, C. Weber, A. Baumgaertel, N. Fritz, E. Altuntaş, K. Kempe, U. S. Schubert, Semi-automated multi-dimensional characterization of synthetic copolymers, **Kolloquium MALDI- und ESI-ToF Massenspektrometrie zur Untersuchung von Polymeren**, *Berlin*, Germany, May 2012.

Poster contributions

S. Crotty, C. Weber, A. Baumgaertel, N. Fritz, E. Altuntaş, K. Kempe, U. S. Schubert, Semi-automated multi-dimensional characterization of synthetic copolymers, **SCM-6**, *Dresden*, Germany, February 2013.

M. S. Engler, S. Crotty, M. J. Barthel, C. Pietsch, K. Knop, U. S. Schubert, S. Boecker COCONUT sequencing of copolymers using mass spectrometry, **DGMS**, *Berlin*, Germany, March 2013.

M. S. Engler, S. Crotty, M. J. Barthel, C. Pietsch, K. Knop, U. S. Schubert, S. Boecker COCONUT sequencing of copolymers using mass spectrometry, **IMSC**, *Geneva*, Switzerland, August 2014.

Acknowledgment / Danksagung

Lastly, I would like to thank the people who helped me a great deal over the last years during my Ph.D. studies.

Firstly, I want to express my sincere gratitude to my supervisor Prof. Dr. Ulrich S. Schubert. I would like to thank him for the very interesting topics regarding mass spectrometry and the possibility to pursue multidisciplinary themes. Furthermore, I thank him to develop and have the freedom to carry out personal ideas within the context of the given topics. Alongside of the scientific projects, I was able to discuss the recent developments of my research on numerous occasions during conferences and with project partners from all around world. I'm gratefully thankful for his continuous support and his trust over the years.

Further, I would like to thank Prof. Dr. Sebastian Boecker and Martin Engler for a very fruitful and stimulating cooperation over the years with the informatics applied to copolymers. I would also like to thank Prof. Dr. Pierre J. Lutz and Dr. Gladys M.-E. Pozza for their cooperation and visit from Strasbourg over the years regarding PEO and mass spectrometry. A great thanks goes to Prof. Dr. Felix H. Schacher and Tobias Rudolph for the diverse inspiring topics and discussions. Moreover, I would like to thank Prof. Dr. Chrys Wesdemiotis and his students for the fruitful cooperation.

Then, I would like to acknowledge all the co-workers within the Schubert-group who have significantly contributed to this work over all these years. I would like to thank in particular Dr. Christian Pietsch (Pietscher) for teaching and giving me an introduction into the RAFT polymerization technique and many discussions with and without the robots! Further, for many suggestions, ideas and your time over the years to achieve the scientific goals. I would also like to thank Dr. Christine Weber for your support, ideas and discussions during the last years. A thank you to Dr. Katrin Knop for your time, scientific input and late nights in the office (TO).

Furthermore, a great thanks goes to Dr. Markus J. Barthel, Tobias Rudolph, Christian von der Ehe, Dr. Christine Weber, Dr. Kristian Kempe and Dr. Gladys M.-E. Pozza for the diverse and numerous polymers over these years! Thank you Dr. Stephanie Schubert

for your support and involvement in various topics with the Evonik projects. Renzo M. Paulus and Dr. Juergen Vitz for the IT support and help with the Chemspeed robots. Thank you Dr. Grit Festag and Nicole Fritz for keeping the SEC systems running. The NMR team Dr. Wolfgang Guenther and Gabriele Sentis for the continuous running spectrometers. Thank you to the MS team for the discussions and the office time in the TO and the ZAF. I would like to thank Cornelia Bader for the synthesis of DCTB. I also would like to thank Dr. Uwe Koehn for all the orders. I thank Anette Kuse and Sandra Koehn for making sure that their shops were always nicely stocked up.

I also would like to thank Tanja Wagner, Sylvia Braunsdorf, Simone Burchardt and Franca Frister for your continuous help and support for diverse administrative aspects and Doreen Kuechler and Jeannette Frommhold for all the support regarding finances.

I would like to also thank the whole TO building within the Schubert and Schacher group for the great evenings together, the support and the great atmosphere. I would also like to thank the new ZAF colleagues for the nice ambiance.

Then, I would like to thank Alexandra Rinkenauer, Dr. Christian Pietsch, Dr. Michael Wagner, Dr. Ulrike Guenther, Kristin Memm and Stefanie Berthold for long conversations about science and private topics. Thank you for making my German better over the years! Thank you for your support during these years in Germany without you this work would have not been possible. Thank you to Emily Baron and Louise Hopkins for your support over these years.

A special thank you goes to my family, mostly, living in France but always there for me during the hard times and successful ones. Thank you for the continuous discussions and guidance. An immense thank you goes to Clinton for always having faith in me and your continuous motivation during the hard times even if you were on the other side of the world! Without your support and your strength over these years this thesis would have not been possible.

Declaration of authorship / Selbständigkeitserklärung

Ich erkläre, dass ich die vorliegende Arbeit selbständig und unter Verwendung der angegebenen Hilfsmittel, persönlichen Mitteilungen und Quellen angefertigt habe.

I certify that the work presented here is, to the best of my knowledge and belief, original and the result of my own investigations, except as acknowledged, and has not been submitted, either in part or whole, for a degree at this or any other university.

……..... Jena, …….... 2016

Sarah C. Crotty

Publications P1-P9

P1 *Anal. Chim. Acta* **2016**, *932*, 1-21. Reprinted with permission. Copyright 2016 Elsevier.

P2 *J. Polym. Sci., Part A: Polym. Chem.* **2012**, *50*, 4958-4965. Reprinted with permission. Copyright 2012 © Wiley Periodical, Inc.

P3 Reprinted with permission from *ACS Symp. Ser. Issue Controlled Radical Polymerization*, **2016**, *1188*, 221-256. Copyright 2015 American Chemical Society.

P4 *Eur. Polym. J.* **2015**, *71*, 325-335. Reprinted with permission. Copyright 2015 Elsevier.

P5 Reprinted with permission from *J. Phys. Chem. B* **2015**, *119*, 1669-1680. Copyright 2015 American Chemical Society.

P6 Reprinted with permission from *Polymers* **2013**, *5*, 1081-1101. Copyright 2013 MDPI.

P7 *Eur. Polym. J.* **2014**, *60*, 153-162. Reprinted with permission. Copyright 2014 Elsevier.

P8 Reprinted with permission from *Anal. Chem.* **2015**, *57*, 5223-5231. Copyright 2015 American Chemical Society.

P9 *Rapid Commun. Mass Spectrom.* **2016**, *30*, 1233-1241. Reprinted with permission Copyright 2016 © Wiley Periodical, Inc.

Publication 1

Polymer architectures *via* mass spectrometry and hyphenated techniques: A review

S. Crotty, S. Gerişlioğlu, K. J. Endres, C. Wesdemiotis, U. S. Schubert

Anal. Chim. Acta **2016**, *932*, 1-21.

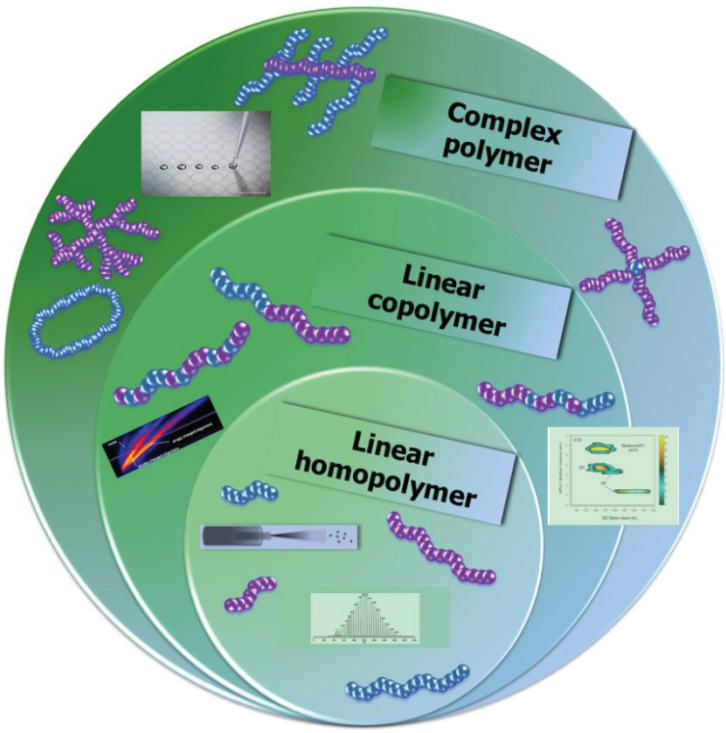

Analytica Chimica Acta 932 (2016) 1–21

Contents lists available at ScienceDirect

Analytica Chimica Acta

journal homepage: www.elsevier.com/locate/aca

Review

Polymer architectures *via* mass spectrometry and hyphenated techniques: A review

Sarah Crotty [a, b], Selim Gerişlioğlu [c], Kevin J. Endres [d], Chrys Wesdemiotis [c, d, **], Ulrich S. Schubert [a, b, *]

[a] Laboratory of Organic and Macromolecular Chemistry (IOMC), Friedrich Schiller University Jena, Humboldstr. 10, 07743 Jena, Germany
[b] Jena Center for Soft Matter (JCSM), Friedrich Schiller University Jena, Philosophenweg 7, 07743 Jena, Germany
[c] Department of Chemistry, The University of Akron, Akron, OH 44325, USA
[d] Department of Polymer Science, The University of Akron, Akron, OH 44325, USA

HIGHLIGHTS

- Novel approaches in MS characterization of polymers are discussed.
- Publications on MS and hyphenated strategies toward analysis of polymers architectures are reviewed.
- Computational methods for the interpretation of polymer MS data are encouraged.
- Upcoming expectances using MS-based methods on polymer analysis are suggested.

GRAPHICAL ABSTRACT

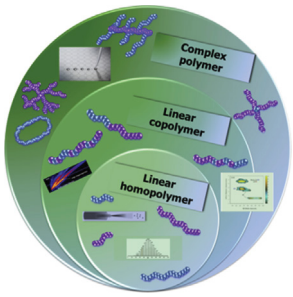

ARTICLE INFO

Article history:
Received 13 July 2015
Received in revised form
7 April 2016
Accepted 16 May 2016
Available online 24 May 2016

Keywords:
Mass spectrometry
Liquid chromatography
Ion mobility
Tandem mass spectrometry
Polymers
Hyphenation

ABSTRACT

This review covers the application of mass spectrometry (MS) and its hyphenated techniques to synthetic polymers of varying architectural complexities. The synthetic polymers are discussed as according to their architectural complexity from linear homopolymers and copolymers to stars, dendrimers, cyclic copolymers and other polymers. MS and tandem MS (MS/MS) has been extensively used for the analysis of synthetic polymers. However, the increase in structural or architectural complexity can result in analytical challenges that MS or MS/MS cannot overcome alone. Hyphenation to MS with different chromatographic techniques (2D × LC, SEC, HPLC etc.), utilization of other ionization methods (APCI, DESI etc.) and various mass analyzers (FT-ICR, quadrupole, time-of-flight, ion trap etc.) are applied to overcome these challenges and achieve more detailed structural characterizations of complex polymeric systems. In addition, computational methods (software: MassChrom2D, COCONUT, 2D maps etc.) have also reached polymer science to facilitate and accelerate data interpretation. Developments in technology and the comprehension of different polymer classes with diverse architectures have significantly improved, which allow for smart polymer designs to be examined and advanced. We present specific examples covering diverse analytical aspects as well as forthcoming prospects in polymer science.

* Corresponding author. Laboratory of Organic and Macromolecular Chemistry (IOMC), Friedrich Schiller University Jena, Humboldstr. 10, 07743 Jena, Germany.
** Corresponding author. Department of Chemistry, The University of Akron, Akron, OH 44325, USA.
E-mail addresses: wesdemiotis@uakron.edu (C. Wesdemiotis), ulrich.schubert@uni-jena.de (U.S. Schubert).

http://dx.doi.org/10.1016/j.aca.2016.05.024
0003-2670/

Abbreviations

AUC	Analytical ultracentrifuge
AF4	Asymmetric flow field-flow fractionation
APCI	Atmospheric pressure chemical ionization
AROP	Anionic ring opening polymerization
ASAP	Atmospheric solid analysis probe
ATRP	Atom transfer radical polymerization
CCS	Collisional cross section
CE	Capillary electrophoresis
CI	Chemical ionization
CAD	Collision activated dissociation
CZE	Capillary zone electrophoresis
Đ	Dispersity
DESI	Desorption electrospray ionization
DMSS	Dimethylsilylstyrene
ECD	Electron capture dissociation
EI	Electron ionization
ELSD	Evaporative light scattering detector
EO	Ethylene oxide
ESI	Electrospray ionization
ETD	Electron transfer dissociation
FFF	Field-flow fractionation
FT-ICR	Fourier transform-ion cyclotron resonance
GC	Gas chromatography
HPLC	High-performance liquid chromatography
ICR	Ion cyclotron resonance
IM-MS	Ion mobility-mass spectrometry
IR	Infrared
ISD	In-source decay
LAC	Liquid adsorption chromatography
LACCC	Liquid adsorption chromatography at critical conditions
LC	Liquid chromatography
LDI	Laser desorption ionization
LS	Light scattering
MALDI	Matrix-assisted laser desorption/ionization
MD	Molecular dynamics
MS	Mass spectrometry
MS/MS	Tandem mass spectrometry
NMP	Nitroxide-mediated radical polymerization
NMR	Nuclear magnetic resonance
NP	Normal phase
PAA	Poly(acrylic acid)
PAMAM	Poly(amidoamine)
PB	Poly(butadiene)
PBS	Poly(butadiene succinate)
PBT	Poly(butylene terephthalate)
PCL	Poly(caprolactone)
PDMS	Poly(dimethylsiloxane)
PE	Poly(ethylene)
PEEK	Poly(ether ether ketone)
PEI	Poly(ethylenimine)
PEO	Poly(ethylene oxide)
PET	Poly(ethylene terephthalate)
PHEMA	Poly(hydroxyethylmethacrylate)
PI	Poly(*iso*prene)
PIB	Poly(*iso*butylene)
PLA	Poly(lactide)
PLGA	Poly(lactic-*co*-glycolic acid)
PLUMS	Polymer labeling using mass spectrometry
PMA	Poly(methyl acrylate)
PMAA	Poly(methacrylic acid)
PMMA	Poly(methyl methacrylate)
P*n*BA	Poly(*n*-butyl acrylate)
PO	Propylene oxide
POM	Poly(oxymethylene)
PP	Polypropylene
PPG	Poly(propylene glycol)
PPI	Poly(propylene imine)
PPO	Poly(propylene oxide)
PS	Polystyrene
PSD	Post-source decomposition
PSS	Poly(styrene sulphonate)
P*t*BA	Poly(*t*-butyl acrylate)
P*t*BMA	Poly(*t*-butyl methacrylate)
PVAc	Poly(vinyl acetate)
PVAl	Poly(vinyl alcohol)
PVP	poly(*N*-vinyl pyrrolidone)
Py/GC	pyrolysis/gas chromatography
Q	Quadrupole
RAFT	Reversible addition-fragmentation chain transfer
RI	Refractive index
RP	Reversed phase
RP-TGIC	Reverse phase-temperature gradient interaction chromatography
SAXS	Small angle X-ray scattering
SEC	Size exclusion chromatography
SG1	*N*-*tert*-butyl-*N*-(1-diethylphosphono-2,2-dimethyl propyl)
SID	Surface-induced dissociation
SIMS	Secondary ionization mass spectrometry
SORI	Sustained off resonance irradiation
SL	Surface layer
SPME/GC	Solid phase microextraction/gas chromatography
TA-APGD	Thermal-assisted atmospheric pressure glow discharge
ThFFF	Thermal field-flow fractionation
TMPO	Trimethylolpropaneoxetane
ToF	Time-of-flight
UV	Ultraviolet

Contents

1. Introduction

Wherever we look in everyday life, we see polymers in a multitude of forms, *e.g.* as simple plastic bags, as packing material, as molded forms in toys, computers, seats, pens, in cars, trains, bikes, in shampoo and clothes, various household furniture, windows and in the paint on the wall. Nonetheless, polymers do not exclusively satisfy basic requirements; but high-tech materials are designed from polymers to challenge societal problems in medicine, energy generation and storage nowadays.

Depending on the application of the material (for example, polystyrenes as applied in construction and foam material or polylactides for the use in drug delivery systems), structurally distinct polymers with different macroscopic properties are prepared from a large library of structurally diverse monomers. This first level of structural complexity is not only influenced by the chemical nature of the monomer, but also by the length of the macromolecules and their molar mass distribution, expressed in the dispersity (Đ), as well as their end groups. By using two or more monomers, a second degree of structural complexity is reached for copolymers. Tuning the molar ratio of the monomers and their organization, such as in block, gradient or random copolymers, plays an important role in the resulting material having different chemical and/or physical properties. A third stage of structural complexity is reached by the arrangement of the monomers into a cyclic, star-shaped, comb-shaped or dendritic structure (Fig. 1). These different architectures enable the engineering of highly complex molecules for high-end applications, *e.g.* micelles, amphiphilic block copolymers, polyion complexes, which encapsulate or entrap agents for tumor targeting applications [1].

However, by increasing the structural or architectural complexity of the polymeric system, the construction of the desired features results in far more demanding synthetic procedures, which increase the probability of defects. On the other hand, high-tech applications require well-defined and very reproducible products. To solve these opposing exigencies of synthesis reality and application requirements, a thorough and profound characterization of the polymer's architecture is required.

Mass spectrometry (MS) and tandem mass spectrometry (MS/MS) are extensively used to provide detailed information on structural properties of polymers [2–7]. Furthermore, many techniques that can be hyphenated to MS can provide greater insight on the polymer architectural information [8]. In particular, high-performance liquid chromatography (HPLC) techniques such as normal and reverse-phase HPLC and size exclusion chromatography (SEC) systems provide preseparation of complex mixtures and highly disperse samples for MS analysis [2,4,5,7,9]. Liquid adsorption chromatography at critical conditions (LACCC) is a specific HPLC condition, which enables the differentiation of end groups irrespective of the molar mass. First, the critical conditions

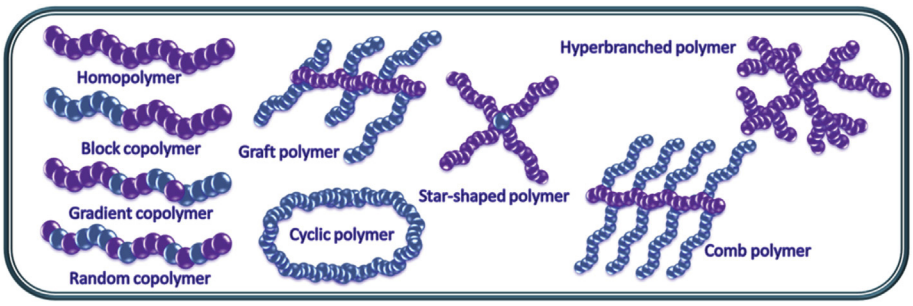

Fig. 1. Schematic overview of various (co)polymer architectures.

are determined with a minimum of three polymer standards with the same end groups, but different molar masses and dissolved in a "good solvent". Then the "bad" solvent is added step by step, therefore promoting the elution of the standards from SEC towards adsorption mode. The critical conditions are reached when all standards have the same retention time. In addition to one-dimensional separation, 2D-liquid chromatography (LC) is utilized by combining multiple chromatographic techniques to separate samples by their inherent chemical and physical properties prior to MS. Moreover, the shape of a polymer can be investigated by field-flow fractionation (FFF), and although it is ideal for the separation of higher molar mass polymers, its connection to MS is not exploited extensively [10]. A more recently applied technique to polymers is ion mobility-mass spectrometry (IM-MS), which shows great promise because of its ability to separate gas-phase ions depending on their shape, size and charge state [11]. The main advantages of IM-MS are the ability to rapidly separate and differentiate isobaric and isomeric species without the need for MS/MS. Finally, in addition to hyphenated techniques, computational methods are being employed increasingly in polymer science for detailed data interpretation essentially facilitating the spectral analysis [12].

Within this feature, MS techniques and hyphenated MS setups that were used to acquire information on macromolecular architectures are discussed in view of their benefit and disadvantages, as well as the desired future developments needed for obtaining more detailed insight on the molecular composition and the structure of polymers.

2. First dimension of complexity: linear homopolymers with MS

The complexity of homopolymers is mainly determined by the chemical identity of the monomer, the length of the polymer chains, its Đ value and the α- and ω-end groups, which might show an immense diversity depending on the applied synthesis technique. Additionally, the analyses of homopolymers is seen as the fundamental starting point for studies striving to develop and improve methods for more complex structures, to create libraries, facilitate predictions and enable interpretations of more complex data sets. In essence, the lengths of the polymer chains and Đ values can be acquired by a one-dimensional MS technique. By degradation or fragmentation of the polymer, information regarding the end groups as well as the chemical nature of the repeating unit can be obtained [3,13].

2.1. Thermal-MS techniques

Thermal-MS based techniques have the ability to decompose polymers by heat [13]. Subsequently, decomposed materials are analyzed by the mass spectrometer to obtain information regarding synthetic defects in the polymer chain and degradation products of the material. Several co-workers have used diverse techniques to investigate the polymer structure and pyrolysis products. For example, Zhang et al. utilized thermal-assisted atmospheric pressure glow discharge (TA-APGD) for structural characterization of polystyrene (PS) and poly(oxymethylene) (POM) [14]. The analysis of the degradation products by TA-APGD-MS provided information on the structural composition of the polymer without any sample pretreatment which can particularly be important for the analysis of polymer materials that are difficult to dissolve. Barton et al. used electrospray ionization (ESI)-MS in addition to matrix-assisted laser desorption/ionization (MALDI)-MS to investigate the degradation mechanisms of poly(propylene oxide) (PPO) by heating the polymer prior to MS analysis [15]. One of the notable advantages of thermal methods is that it allows insoluble polymers to be analyzed by mass spectrometry. Tsai et al. used stepwise pyrolysis/gas chromatography (Py/GC)-MS method to investigate the thermal degradation of poly(aryl-ether-ether-ketone) PEEK. This study shows that Py/GC-MS can be a very useful analytical tool to separate and characterize, even the isomeric temperature dependent pyrolysis products by applying a stepwise temperature program [16]. Another application of thermal methods with mass spectrometry was on lacquer films. Lu et al. analyzed and compared the laccol components of natural and synthetic *Rhus succedanea* lacquer films, which also enabled the confirmation of the polymerization mechanism and structure of the macromolecule [17].

For linear homopolymers, thermal-MS techniques have mostly been used for determination of defects in microstructures and investigation of pyrolysis mechanisms since 1948 [18,19]. Characterization of the temperature dependent degradation products by thermal-MS techniques can provide information regarding both physical and structural properties, thus helping the manufacturing of robust products.

2.2. MS/MS techniques

MS/MS techniques involve fragmentation of analyte ions in the mass spectrometer to obtain more detailed structural and/or architectural information. An MS/MS analysis can be carried out by using diverse scanning modes such as: product ion scan, precursor ion scan, neutral loss scan and selected reaction monitoring. Out of all these modes, the product ion scan is one of the most common MS/MS modes used for structural characterization of various synthetic polymers. During this mode of MS/MS analysis, a precursor analyte ion is isolated and this is followed by its activation and fragmentation inside the mass spectrometer. Finally, all of the fragmentation products are scanned and analyzed for more detailed investigation of the precursor ion structure. Many activation methods have been developed, such as collision activated dissociation (CAD), surface-induced dissociation (SID), photodissociation, electron capture dissociation (ECD), electron transfer dissociation (ETD), and post-source decay (PSD). Although numerous fragmentation techniques exist and are applied to synthetic polymers, the most widely used technique is CAD, which is closely related to PSD and in-source decay (ISD) techniques. However, it does not always suffice for the full characterization of polymer architectures. Applications of MS/MS to a wide variety of polymer types and their fragmentation mechanisms have been discussed in detail in a review by Wesdemiotis et al. and several representative examples of such work are highlighted below [20].

For example, aromatic side chain based polymers such as PS has numerous different applications due to their importance in life science, and poly(2-vinylpyridine) (P2VP), for instance, in membranes as well as in batteries, and features a similar structure to PS, with only a slightly different side chain [20]. Furthermore, poly(-acrylate)s are also important for contact lenses, membranes [21] as well as nanoparticles for energy storage [22]; MS/MS studies have been reported on poly(methyl acrylate) (PMA) [20,23], poly(methyl methacrylate) (PMMA) [20,24,25], poly(*t*-butyl methacrylate) (P*t*BMA), poly(*t*-butyl acrylate) P*t*BA and poly(*n*-butyl acrylate) (P*n*BA) [20,26]. Other important polymers that have been investigated include poly(vinyl acetate) (PVA) [20,27], poly(methacrylic acid) (PMAA) and poly(acrylic acid) (PAA) [20,28], polyesters [29–34], poly(lactide) (PLA) [35–38], poly(ethylene oxide) (PEO) [20,39,40], and poly(oxazoline)s [41–44], all of which show remarkable promise in biodegradable and biocompatible materials [21,45–47]. Beyond these examples, many other polymer classes have been investigated under diverse ionization and fragmentation techniques, including poly(ethylenimine)s (PEI) [48,49],

poly(dimethylsiloxane)s (PDMS) [20,39], complexes of PMMA with polyglycine [20], polyisocyanates [50], polyisobutylenes [51], and *N-iso*propylacrylamides [52], poly(ethylene/butylene terephthalate)s [29,30], polysulfide [53], polysulfones [54], polyesteramides [55], etc.

The above mentioned studies illustrate that, the differentiation between a pure polymer and its side products is a complex issue. MS/MS for homopolymers can be a very useful method for structural identification of the end groups and the sequence, *i.e.* the detection of defects in the polymer. Additionally MS/MS can also be used for determination of isobaric and isomeric species, and differences within a mixture of linear and nonlinear systems. However, in such cases, preseparation by hyphenated techniques might be necessary. Despite the diversity of the fragmentation techniques that can be used, MS/MS might not be enough to provide the necessary information to fully distinguish architectural differences. The use of LC as an analytic technique in the liquid phase prior to ionization enables the separation of polymer mixtures due to differences in polarity or hydrophobicity, which can provide complementary information and simplify the MS/MS data obtained from mixtures. Also, ion mobility (IM) spectrometry can provide additionally gas-phase separation of polymers before and/or after fragmentation. The combination of MS/MS with either one of these techniques makes it possible to obtain more detailed information on the nature of the end groups, presence of isomeric architectures, monomer sequences and degree of substitutions. However, these hyphenated techniques are mostly applicable on oligomers with a *m*/*z* around 4000; thus, MS hyphenation techniques have to progress towards materials with higher molar masses and high dispersity.

3. First dimension of complexity: linear homopolymers with hyphenated techniques

3.1. LC-MS based techniques

Traditional analytical techniques for polymer characterization are pyrolysis MS, SEC and nuclear magnetic resonance (NMR) spectroscopy. The direct injection of a sample into the mass spectrometer without preseparation, known as direct MS, has been used as an analytical technique for polymers as well, but it has been proven that there are some cases where MS alone is insufficient for a comprehensive characterization of end groups, copolymer composition sequences, Đ etc. Thus techniques involving hyphenation with HPLC either separating by polarity or size and 2D-LC have been developed to provide a more detailed polymer characterization [8]. The hyphenation to MS is a versatile tool and many different types of LC-MS techniques were introduced over the past 20 years making LC-MS hyphenated methods important in polymer characterization and empowering them for sophisticated polymer analysis [8].

Many different 1D-LC systems hyphenated with MS are reported, particularly, for optimizing the transfer of the sample from a chromatographic system to the mass spectrometer. The main advantage of ESI is its compatibility with continuous hyphenation to diverse HPLC modes in comparison to MALDI, where most of the hyphenation techniques are carried out offline. Different hyphenations and different detectors are used to obtain extra knowledge regarding polymers, such as chemical heterogeneity and differentiation of (isomeric) architectures, thus enabling the chemist to improve the synthetic routes. A solvent free technique with an automated system was established for analyzing PEO under LACCC using a dry spraying technique [56]. PEO mixtures with different molar masses and different end groups were mixed and fractionated by using the LACCC technique prior to analysis of each fraction by solvent-free MALDI-MS. This tool allows an offline hyphenation of MALDI-MS with LACCC with much more convenient sample preparation procedure. Different spotting and simultaneous multisample deposition techniques were used to automate this hyphenation. Three different analytical methods have been combined to analyze PMMA homopolymers having different end groups [57]. LACCC-ESI MS with NMR spectroscopy and titration were used to investigate end group heterogeneity. Quantification of the components in the mixture was completed using an evaporative light scattering detector (ELSD) and identification of the different species was carried out *via* MS. Additionally, NMR spectroscopy was utilized for investigating the composition and titration for the quantification of OH groups. These complementary methods help to validate both structures and composition. The group of Barner-Kowollik hyphenated SEC with ESI-MS to analyze synthetic polymers that showed chromatographic broadening [58]. This hyphenation enables the determination of the structure *via* MS and of the molar masses *via* the refractive indices (RIs), as shown for PMMA oligomers used for calibration standards. SEC is widely used for molar mass determination of synthesized polymers; in this case band broadening was corrected through an in-house algorithm built for both detectors. This led to several observations: for lower molar masses (<7 kDa), weak band broadening is present; however, with the algorithm, band broadening for 10 kDa PMMA is corrected successfully. The resulting values were also in fair agreement with the manufacturer's value within an error of 15%. In conclusion, the method shows consistency between the two detectors. Since conventional calibrations can be false, multi-detection is critical and important. Furthermore, in a follow-up contribution from the same group, important synthetic facts for tuning a polymerization, such as propagation rate coefficients (k_p), were elucidated through pulsed laser polymerization and further analyzed *via* SEC-ESI MS [59]. This was found to be an accurate way to determine the molar mass of a polymer of any class, provided the polymer is ionizable by ESI. Propagation rates can be measured by such experiments which are important determinants for polymer chain lengths. The reversible addition-fragmentation chain transfer (RAFT) polymerization technique is used widely by many polymer groups in the world due to its facile 'one pot' polymer synthesis ability and the availability of a wide range of monomers that are capable of reacting. A series of acrylates were prepared using different initiators, and the reaction rates of the systems were investigated *via* SEC-ESI MS. The results were also compared with the predictions of the polymer model PREDICI® [60]. Furthermore, CAD was used to analyze the intermediate reaction mixtures to obtain information concerning the end groups and macromolecular structures. MS is essential for the investigation of polymer propagation and for establishing whether the proposed transformations occur. SEC-ESI MS followed by the application of the PREDICI® simulation tool is also used to determine the cross termination reactions in the RAFT polymerization of acrylates [61].

A 2D (RP-LC × SEC) chromatography system can also be coupled to MALDI and ESI. Even if this cannot be an online hyphenation, the procedure is still fully automated and very versatile. The RP-LC × SEC combination alone proves to be one of the most important analytical methods when specific conditions are applied in the first dimension, for example, LACCC. Linear poly(caprolactone) PCL with high and low molar masses were investigated by LACCC to identify end group heterogeneity, and the SEC dimension was used for molar mass separation [62]. As a result of hyphenating this technique to ESI and MALDI, the MS data served as the third dimension. High ionization efficiencies and multiply charged ion distributions were observed in ESI-MS spectra of the investigated PCL samples. Whereas in MALDI, prominently singly charged species, with low abundance, were observed because of the lower ionization

efficiency and matrix interference. Pretorius et al. conducted a comprehensive RP-LC × SEC analysis to investigate the relationship between the chemical composition and molecular mass distributions of model phthalic anhydride/propylene glycol polyesters synthesized with a 30% molar excess of glycol [63]. Gradient RP-LC allowed the isolation of homogenous fractions based on their chemical composition, which were then transferred to SEC for separation by hydrodynamic volume (Fig. 2). The 2D (RP-LC × SEC) contour plots show that the samples have different M_n and M_w values: s23 (135, 216), s25 (283, 837), s28 (569, 1520), respectively. The numbers shown are peaks associated with the one-dimensional gradient RP-LC analysis. Furthermore, each fraction was also analyzed with MALDI-ToF MS to elucidate the various stages of the polyesterification reaction in terms of molar mass, chemical composition, and end groups [63].

Depending on both chemical and physical properties of polymers, the RP-LC × SEC technique's ability of two-dimensional separation demonstrates its versatility, which makes it a very sophisticated and useful tool for polymer analysis. Therefore, its hyphenation to mass spectrometry can provide many advantages for polymer analysis, most importantly reducing the complexity of analysis of a highly heterogeneous polymer mixture having high dispersity: it will promote technology and insight for chemists to further develop smarter polymer designs.

3.2. Field-flow fractionation (FFF)-MS techniques

Field-flow fractionation is a separation technique, used mostly for aqueous solutions of disperse and charged or neutral species, dependent upon differing velocities in a field [64]. FFF is used for synthetic polymers but is less commonly applied in combination with the MS technique. Coupling this technique to a mass spectrometer is challenging due to the high molar masses of the investigated materials. Hassellöv et al. reported the analysis of low molar mass poly(styrene sulphonate) (PSS) and PEO standards by FFF-ESI MS [65]. After the low molar mass polymers were separated by FFF, they were analyzed by ESI MS to obtain compositional information. Further studies to obtain end group compositions were carried out by applying MS/MS. However, the technical online hyphenation was also highlighted and high salt concentrations caused clogging of the ESI-MS and high background signals for an efficient separation. Another example for the combination of FFF with MS was the coupling of a thermal field-flow fractionation (ThFFF) setup to MALDI-ToF MS for the analysis of high molar mass PS standards [10]. ThFFF enabled the separation and the fractionation of polymers that were further analyzed by MALDI-ToF MS. After the

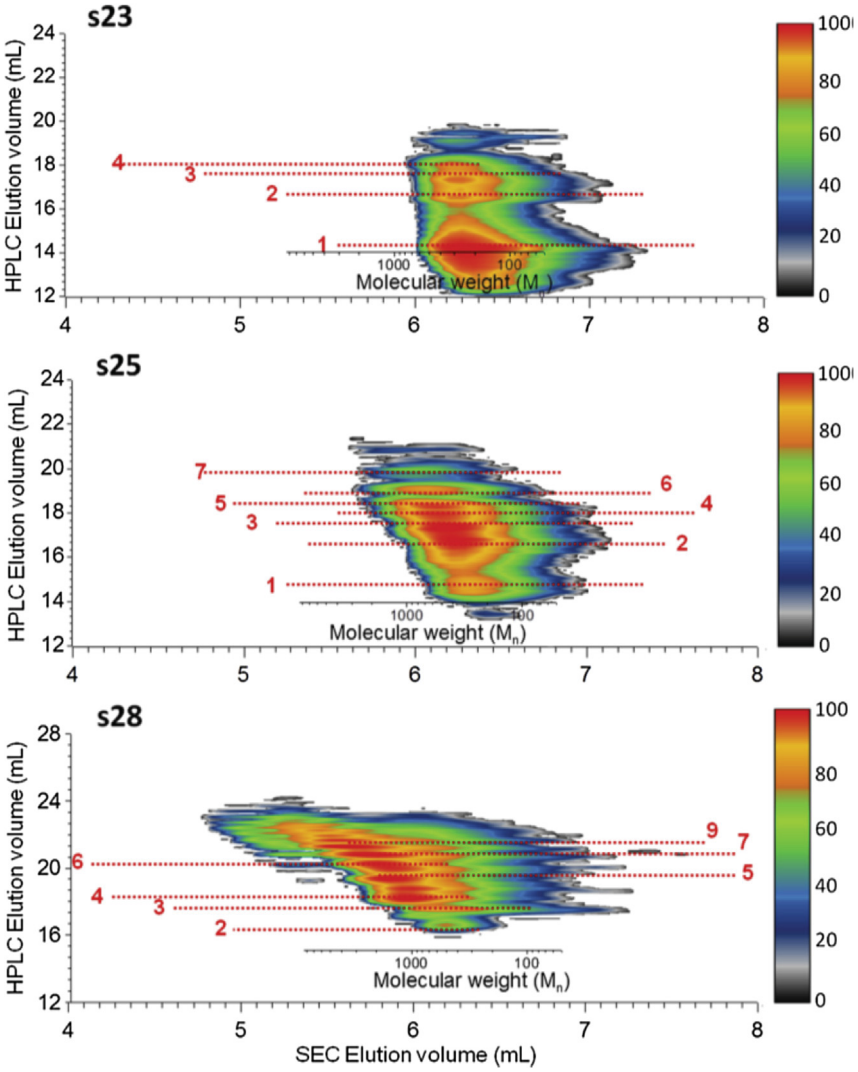

Fig. 2. 2D (RP-LC × SEC) contour plots of polyester samples: s23, s25, s28. Reproduced from Ref. [63].

separation and analysis with both ThFFF and MALDI-ToF MS, it was shown that both techniques have correlating results; in addition, FFF confirmed the macromolecular conformations. The resolution obtained was <15 kDa for the ThFFF separation and a maximum molar mass of 575 kDa by MALDI-ToF MS. To conclude, FFF is a promising technique for obtaining architectural information such as conformation and size of complex polymeric systems. Furthermore, the FFF-MS hyphenation shows that numerous dimensions expand the comprehensive characterization of polymers. This particular hyphenation needs further improvements and additional applications, specifically for more complex architectures of synthetic polymers where it is essential to characterize the composition and conformation.

3.3. Ion mobility-mass spectrometry (IM-MS) techniques

Previously used for 'omics', IM-MS has recently been applied to polymers and metallo(supramolecular) materials [11], and its applications to polymer science continue to increase. IM spectrometry provides an additional dimension for elucidating different conformations or architectures present in an analyte. With IM-MS, gas-phase ions are separated according to their mobility and composition. Information obtained by IM separation can be used to render collision cross-sections, which relate directly to the macromolecular shape.

Isobaric ions, which are two different chemical species having the same nominal mass (mass difference at ppm level) but different elemental composition, are often encountered in polymer analysis and can only be resolved with high resolution spectra. If isobaric species are not resolved, obtaining a more detailed structural characterization with MS/MS experiments can be very difficult. This can result in very complicated MS/MS data, having fragment ions from both species in the same spectrum. Preseparation by a LC technique might be an option for a situation such as this. However, the most important advantage of IM over LC techniques is that the separation occurs within milliseconds in the gas phase, and does not require excessive solvent usage. IM separation is an ideal technique for hyphenation to MS since the separation takes place in the gas phase. Isobaric species can be separated depending on conformational or architectural differences at a much faster rate in the gas phase. After IM separation, these isobaric species can further be investigated separately by MS/MS for more detailed structural characterization, if needed. Furthermore, having higher resolution in IM-MS/MS (for example by employing Q/ToF instrumentation) enables better mass accuracy in MS/MS studies. For example, Hilton et al. were able to investigate a poly(ethylene glycol) (PEG)s mixture composed of two PEG chains having different end groups by IM-MS/MS [66]. In this particular example, these two isobaric PEG chains have diol and monooleate end groups, and result in the same nominal m/z values. However, the structural difference at the end group of these two chains results in two distinct drift time values in the IM spectrum. Separation was therefore accomplished before MS/MS analysis. Fig. 3 shows the IM separation of these two chains at an isolated m/z value of 553. Further MS/MS characterization of these separated PEG chains reveals the structural difference at the end groups (Fig. 3). One can see that IM-MS could separate polymers having different end groups from both PEGs in the millisecond range when compared to LACCC, which requires a longer time approximately 1–2 h to perform. As a result, IM-MS is highlighted as being fast, comparable in terms of separation to LC-MS and rich in image information, which is beneficial to both academia and industry.

Synthetic inorganic polymers, such as polysiloxane and polyphosphazene based polymers, were investigated with ESI-IM-MS by Scionti et al. [67]. IM-MS provided information on the existence of higher order assemblies for the polysiloxanes. It also confirmed that the reaction of NH_4Cl with PCl_5 under aerobic conditions produces poly(dichlorophosphazene)s with both

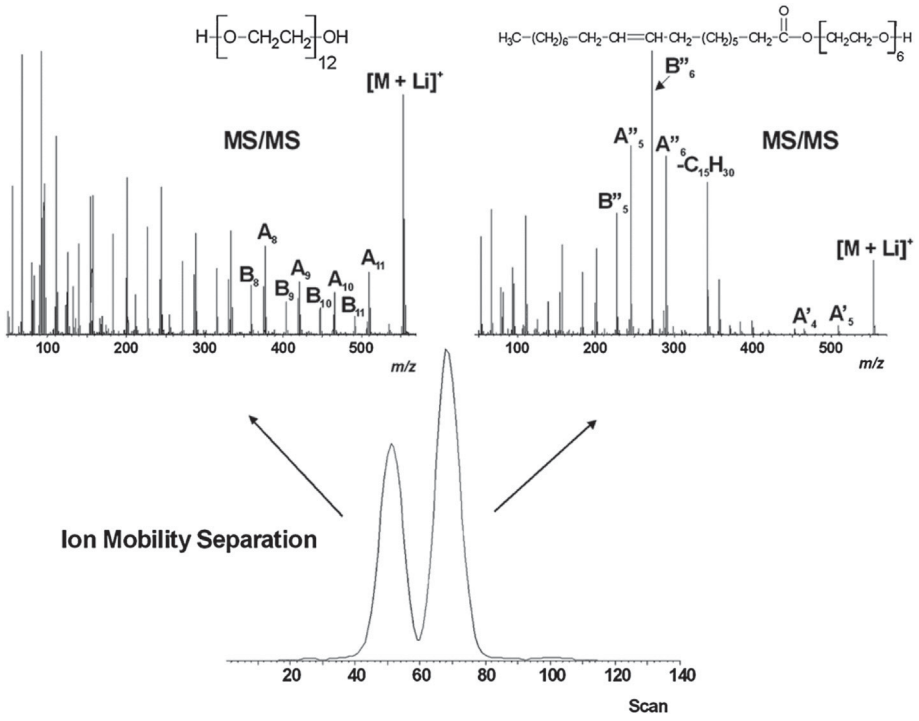

Fig. 3. Arrival time distribution (bottom) of m/z 553 from a mixture of PEG 1000 and PEG monooleate and IM-MS/MS spectra (top) from the two peaks noted. Peaks in the IM-MS/MS spectra are partially annotated. IM-MS/MS spectra are very similar to those noted from MS/MS data (without IM separation) of the same oligomers, obtained from PEG 1000 and PEG monooleate separately. Reproduced from Ref. [66].

tadpole as well as linear architectures.

Waters being the manufacturer of the first commercial IM-MS instruments (Synapt line of models) published a report on the analysis of polymers with IM-MS and MS/MS. Compared to traditional MS techniques, added IM dimension, shown to facilitate the determination of physical properties and sequences [68]. Kim et al. applied ESI-IM-MS combined with molecular dynamics (MD) simulations on PLAs having different stereoregularities, formed from cyclic lactide dimers by ring-opening polymerization [69]. The gas-phase conformation of PLAs is affected by stereoregularity and architecture (linear or cyclic), both of which influence collision cross-section value trends. Poly-LD-lactide (PLDLA) has more structural flexibility in comparison to poly-L-lactide (PLLA), thus PLDLA is able to maximize intramolecular interactions, showing lower energies and higher degrees of weak hydrogen bond interactions, which lead to more compact structures for PLDLA with the exception of small macrocycles. These differences in stereoregularity result in different physical properties and structure. IM-MS in conjunction with computational analysis is a powerful tool to differentiate these structural differences. Therefore, it is expected that IM-MS analysis can be a promising technique to characterize polymers with different structures and stereoregularities. Trimpin et al. used IM-MS to characterize PEO polymers of relatively high molar masses using ESI as the ion source [70]. Simulated and experimental cross-sections were compared and evaluated. High charge states were found to have an open and dynamic conformation. The intrinsic limitation with ESI is the accessible molar mass range, which is less restricted with MALDI. These two different sources coupled to IM-MS are becoming increasingly more attractive for polymer chemists as a faster way to obtain dense and rich information on polymer architectures. IM-MS has also been used to provide supportive architectural information to ETD fragmentation patterns for linear polyester samples by obtaining collision cross-section values of the major fragment series [36]. Another type of polymer, poly(propylene) (PP), was investigated using pyrolysis with an atmospheric solid analysis probe (ASAP) and IM-MS [71]. Pyrolysis was used to decompose polymers and IM-MS was used to determine their *m*/*z* values as well as to separate the polymer from any additives. The pyrolysis products were established and compared to prior studies. These two methods coupled to each other help to segregate species and confirm their structure. Barrère et al. showed that ASAP-IM-MS can be used to successfully distinguish between polyester and polyethylene blends [72]. ASAP as an ionization source is an effective technique for the characterization of polymer blends with different polarities without the need of complex sample preparation, which is particularly useful for samples that are difficult to dissolve. Therefore, the combination of ASAP and the structural separation provided by IM allows the clear identification of relatively large pyrolysis products from different polymers such as in PLA-polyethylene (PE) blends. Song et al. reported a detailed study using ESI-IM-MS on a PMMA homopolymer prepared by radical polymerization [73]. The small end group differences in the resulting PMMA system, could be discriminated by IM without the need of a time consuming LC separation. Finally, Hoskins et al. used IM-MS to differentiate between linear and cyclic PCL polymers [74]. The study shows that the IM step is capable of separating linear and cyclic architectures in a blend since the individual structures result in different drift time values (Fig. 4). Fig. 4c also displays that ions having same *m*/*z* values in mass spectrum were differentiated clearly according to their architectural differences.

All the reported examples show that, as a hyphenated technique, IM-MS can be a very valuable analytical technique for polymer science as it already is for 'omics' fields. Its capability of differentiating architectural differences in the gas phase provides an advantage over other chromatographic techniques and makes it a very promising hyphenated technique for solving current and future analytical problems that can be faced during the characterization of complex polymeric systems.

3.4. Computational methods

Computational methods are becoming more prominent in facilitating the analysis of MS and MS/MS spectra. For example, different poly(hydroxyethylmethacrylate) (PHEMA) backbone structures were analyzed *via* ESI by Jackson et al. The data analysis was done by the Polymerator software (Fig. 5 (a)) [75]. End group analysis was performed, and different fragmentation series were obtained and analyzed with the Polymerator software to identify polymer fragments (Fig. 5 (b)). The Polymerator enabled an easier and faster interpretation of the MS/MS data. Moreover, the information obtained can also support the formation of future libraries of fragments.

Another advantage of the Polymerator software is that it is dependent on the polymer class and the knowledge of individual fragments. This feature makes it possible to apply it to different polymers to allow the validation of manual and computed fragmentations [76]. Jackson et al. also used this software to distinguish between end group cleavage and the fragmentation of the polymer chain, and performed detailed end group analysis of poly(-propylene glycol) (PPG) by ESI with low energy MS/MS [77]. Williams et al. used the Polymerator software to analyze the CAD spectra of PEO ions having different end groups and different cationization agents, formed by desorption electrospray ionization (DESI) [78]. The authors emphasize the ability to determine microstructures for 'polymers'. However, prior knowledge of the fragmentation mechanisms is a requirement for utilizing the software. On the other hand, software based analysis can benefit from polymer libraries and is quicker than manual interpretation. In addition to the Polymerator, the polymer labeling using mass spectrometry (PLUMS) software is another computational method developed for the interpretation of fragmentation spectra [79]. This software was used to determine the fragment series formed, knowing that no prior knowledge on the chemical behavior of the polymer class was required. Using PLUMS, practically all of the possible fragments were determined with an attached probability, in contrast to the Polymerator, where chemical parameters are preidentified.

In conclusion, all discussed studies represent an immense step

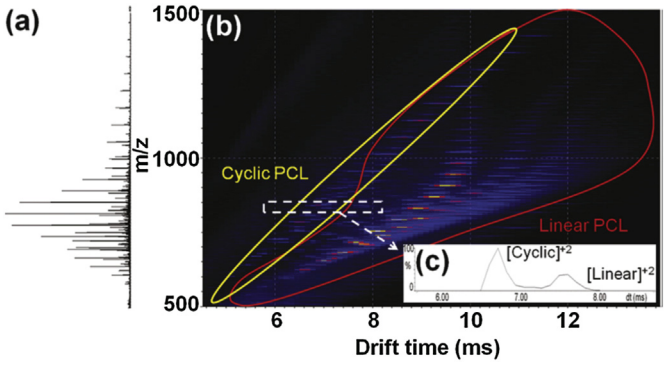

Fig. 4. Mass spectrum (a) and IM-MS 2-D plot (b) of a PCL blend having both cyclic and linear structures. The intensities of the ions detected are incorporated as a false color plot with red as the most abundant and blue as the least abundant ions. The inset (c) shows the drift time scale of a separated peak at 893.13 *m*/*z*. Reproduced from Ref. [74]. (For interpretation of the references to color in this figure legend, the reader is referred to the web version of this article.)

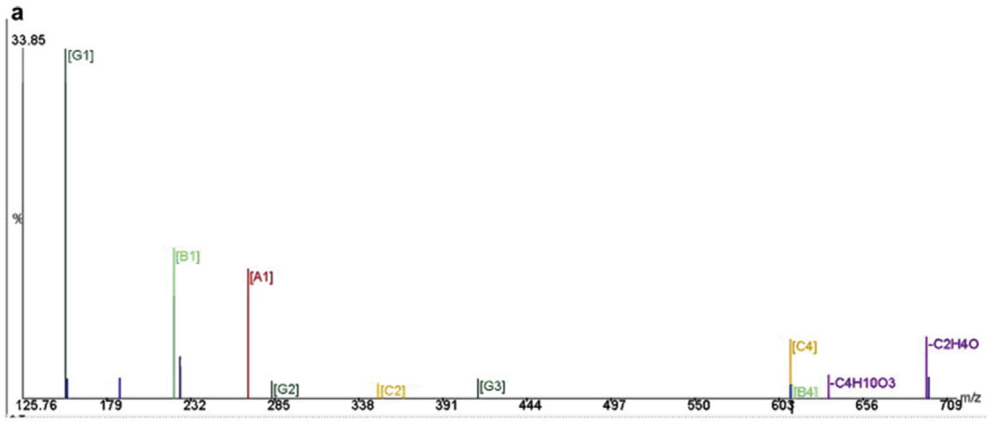

b

Theoretical Mass	Description	Observed Mass	Error (Da)	Intensity	min Intensity	max Da Error	Highlight Color
153.053	[G1]	153.054	0.001	33.853	0.5	0.01	
221.103	[B1]	221.102	0.001	14.434	0.5	0.01	
268.092	[A1]	268.093	0	12.445	0.5	0.01	
283.116	[G2]	283.117	0.002	1.589	0.5	0.01	
350.158	[C2]	350.16	0.002	1.38	0.5	0.01	
413.178	[G3]	413.18	0.001	1.848	0.5	0.01	
480.221	[C3]	480.222	0.001	0.561	0.5	0.01	
610.284	[C4]	610.284	0	5.661	0.5	0.01	
740.347	[M+Na]+	740.35	0.003	100	0.5	0.01	
696.321	-C2H4O	696.32	0.001	0	0.5	0.01	
634.284	-C4H10O3	634.282	0.002	0	0.5	0.01	

Fig. 5. (a) Screenshot from Polymerator software of annotated ESI-MS/MS spectrum from the sodiated tetramer of PHEMA. (b) The details of the annotated fragment ions are displayed by the Polymerator software in the table. Reproduced from Ref. [75].

forward in polymer science in view of a detailed characterization of polymer architecture and conformation. The growth of these techniques will help chemists to evaluate complex polymers in a more in-depth manner by making them less time-consuming.

4. Second dimension of complexity: linear copolymers

4.1. Block copolymers

Block copolymers of linear architecture are composed of at least two segments/domains bound together. Block copolymers may undergo microphase separation due to differences in the solubility of the different segments in a specific solvent. This results in different morphologies in solution, for example, the formation of micellar structures. Furthermore, the morphologies of the formed nanostructures can be tuned *via* the relative length of the individual blocks. Such types of polymers are widely used in the fields of drug delivery, thin films, membranes etc. [1,80]. The use of MS and specific hyphenations allow the determination of block lengths and sequences, as well as the differentiation between different architectures/microstructures [81].

4.1.1. Direct MS techniques

Direct MS analysis of copolymers helps to elucidate side products, end groups and the degree of polymerization of each block. For example, Houshia et al. analyzed high molar mass block copolymers comprising of EO and PO segments *via* MALDI-FTMS [82]. The authors use correlation functions and probability functions to evaluate diverse copolymer components overlapping isotopic patterns, which is required for polymers having high molar masses where the loss of resolution is predominant and the certitude of copolymer composition becomes weak.

MS analyses are generally more complex for linear copolymers than for homopolymers because the ionization efficiency can significantly differ as a result of the different lengths and comonomers structures in each block. Nonetheless, direct MS can provide elements of a comprehensive characterization of copolymers, though additional methods such as thermal-MS, MS/MS and hyphenated techniques are needed for further elucidation of the architecture.

4.1.2. Thermal-MS based techniques

Similarly to homopolymers, thermal degradation techniques are useful for accomplishing detailed evaluations of block copolymer structures. For example, Zhang et al. used thermal-assisted atmospheric pressure glow discharge mass spectrometry (TA-APGDMS) to evaluate block copolymer fragments [14]. The block copolymers were based on POM and poly(butadiene succinate) (PBS) segments. Firstly, fragmentation pathways were established for standard homopolymers, and later for the corresponding copolymers. Characteristic degradation patterns from the POM homopolymers were also observed in the POM-containing copolymers; however, this did not hold for PBS homopolymers and its block copolymers. This study proved that thermal degradation is applicable to copolymers and helps to elucidate their structure and chemical composition. PEO-*b*-(PPO)-*b*-PEO triblock copolymers were also studied using thermal degradation [83]. SEC, NMR spectroscopy and MALDI-MS were used to characterize poloxamer 407. The products of heat induced degradation were analyzed by MALDI-MS and by solid phase microextraction/gas chromatography (SPME/GC) MS. These complementary methods are essential in revealing the oxidation mechanism of poloxamers and their structures. Ohran et al. have investigated three kinds of block copolymers: PS-*b*-P2VP, P2VP-*b*-PMMA and poly(*iso*prene) (PI)-*b*-P2VP *via* direct pyrolysis-MS [84]. This method allows the evaluation of backbone cleavages and, as a consequence, the determination of the sequence and possible crosslinks formed.

Lattimer et al. investigated the pyrolysis products of segmented polyurethanes with MALDI-MS after thermal degradation. In this study, different temperatures were used during pyrolysis to investigate thermal degradation mechanisms by analyzing the pyrolysis products (up to 10,000 Da) with MALDI-MS [85]. Whitson et al. characterized commercial polyurethanes by atmospheric pressure chemical ionization (APCI)-MS in combination with a direct insertion probe (DP). By slowly increasing the temperature, the thermal degradation products and the other components in the

blend, such as additives were successfully separated. The temporal separation that took place in this method was based on compound volatilities and bond stabilities. As a result, combining thermal method by using DP allowed these insoluble materials to be directly analyzed by MS [86]. Another application of this method was done on cross-linked amphiphilic conetworks composed by graft copoly(*N*,*N*-dimethyl acrylamide-*g*-dimethylsiloxane) (PDMAAm-*g*-PDMS) and their blends [87]. The different compositions of hydrophobic and hydrophilic components in these graft copolymer blends were distinguished by utilizing DP-APCI-MS. In addition to different comonomer compositions, information on the thermal stability of the different domains within the copolymer was obtained with the help of precise pyrolysis temperature control by DP [87].

In accordance with the studies discussed above, thermal-MS techniques have great potential for providing important information on structural (block lengths, defects in sequences) and physical properties such as thermal degradation characteristics. Additionally, utilizing a thermal based technique can be essential for MS characterization of polymers that are insoluble (for ESI) or too large to be desorbed (for solvent-free MALDI), and unable to form gas-phase ions due to the lack of functional groups to attract and bind a charged particle, such as a proton or metal cation.

4.1.3. MS/MS techniques

MS/MS techniques have proven to be very useful for the investigation of sequences and block lengths of different copolymer structures. Cerda et al. subjected $[PPG\text{-}b\text{-}PEG]^{2+}$ to both ECD and CAD analysis, which allows for detailed structural characterization of this copolymer [40]. The product ions generated from the ECD experiments showed that all of the copolymers studied consist of diblock structures, and not triblock structures that are designated by the polymer manufacturer. Furthermore, Baumgaertel et al. analyzed different poly(2-alkyl-2-oxazoline) block copolymers (variation of the alkyl side group), *via* ESI- and MALDI-MS using CAD for fragmentation [88]. The usage of both ionization methods revealed detailed information regarding the side products, monomer sequence and block length. The fragmentation patterns of block copolymers in such studies are mostly derived by using prior knowledge of the behavior of the analogous homopolymers under the same MS/MS conditions. Crecelius et al. studied *m*PEG-*b*-PS block copolymers prepared *via* atom transfer radical polymerization (ATRP) [89]. MALDI-ToF MS/MS was used for detailed structural characterization. For this reason, the homopolymers of each comonomer were investigated separately prior to the MS/MS analysis of the block copolymers to facilitate the interpretation of the fragmentation results. Detailed structural analysis by MALDI-MS/MS on these copolymers revealed accurate block lengths of PS and *m*PEG. The authors claimed to observe only fragments from both blocks individually, thus, concluding that a scission between the blocks takes place. The main fragmentation mechanisms observed were 1,4-hydrogen elimination and McLafferty rearrangement within the PEG chain.

In addition to CAD, different ion activation methods, such as ECD, can also provide useful MS/MS data for architectural analysis of copolymers. One of the earlier examples is the application of both CAD and ECD for sequence analysis of PEG-*b*-PPG-*b*-PEG copolymer mixtures. According to the results presented by Cerda et al., CAD can lead to misleading rearrangements, however, as mentioned before, ECD causes minimal rearrangements thus preventing internal fragment formation [90]. Therefore, extensive structural details such as sequence information on complex mixtures of low abundance block copolymers can be obtained by using ECD as an ion activation method for MS/MS. Another study that involves the comparison between CAD and ECD fragmentation patterns was performed on random and block polyacrylate and polyether copolymers [91]. The study shows that CAD alone is able to differentiate random and block copolymers. Random poly(-methyl methacrylate)-*r*-poly(*n*-butyl methacrylate) (PMMA-*r*-P*n*BMA) oligomers tend to undergo random losses of MMA or BMA monomeric units, but block poly(methyl methacrylate)-*b*-poly(*n*-butyl methacrylate) (PMMA-*b*-P*n*BMA) oligomers lose BMA monomeric units preferentially [91].

Based on the examples portrayed, MS/MS provides essential details on structural properties of copolymeric systems such as comonomer sequences, microstructural differences, and block lengths. Accurate determination of such properties of copolymers is essential for the assessment of material's quality.

4.1.4. LC-MS and computational based techniques

As described previously, copolymers are rather heterogeneous and disperse systems. For copolymer structures of high complexity, analysis on additional dimensions may be essential for detailed characterization. Direct MS characterization is not always sufficient to elucidate the architecture of block copolymers. As a consequence, hyphenated analytical techniques have been employed to facilitate the analysis of such polymer systems.

The following selected examples highlight the successful characterization of block copolymers using 1D-LC-MS. Pyrolysis-GC-MS hyphenated to either a gradient reversed-phase (RP) LC or a SEC instrument were used in a study by Kaal et al. on PEG-*b*-PPO copolymers [92]. While SEC or RP-LC separated the copolymers according to their hydrodynamic volume or polarity, respectively, the quantitative information for different compositions was obtained by pyrolysis-GC-MS. Furthermore, this method also permits the calculation of monomer feed ratios, which is important for a validation of the composition, as well. Leeuwen et al. analyzed block copolymers composed of *m*PEO and PCL blocks *via* ESI-MS and APCI MS combined with RP-LC fractionation [93]. Mass spectrometric analysis was performed both in the positive and negative mode. Further, gradient elution was applied for low molar mass copolymers and used to determine the block lengths as well as the comonomer composition. *m*PEO-*b*-PCL was investigated under APCI ionization conditions as a complementary method to ESI and for hyphenation to a HPLC system in order to evaluate the block length of both species present in this biocompatible polymer that can form micellar structures. Hayen et al. applied RP-LC-ESI MS to poly(ether-*b*-ester) block copolymers, *i.e.* PEO-*b*-poly(butylene terephthalate) (PBT) [94]. Application of RP-LC prior to MS analysis provided a separation of the side products having different segments, but similar molar masses. Girod et al. analyzed PEO-*b*-PS block copolymers by hyphenating LACCC to ESI-MS/MS [95]. The LACCC conditions were optimized by tuning the salt concentration in the mobile phase for better separation of the species with different end groups present in the sample, independent of their molar mass. Additionally, the length of the PS block was analyzed and also confirmed by CAD MS/MS. As a result, combination of these complementary methods allowed both the determination of the PS block length and end group analysis. A better understanding of RAFT polymerization of poly(*N*-vinyl pyrrolidone) (PVP) and poly(vinyl acetate) (PVAc) block copolymers (PVP-*b*-PVAc) and its byproducts was provided by Fandrich et al. who used gradient LC-MALDI and LC-Fourier transform-infrared (FT-IR) spectroscopy [96]. Hyphenation of various LC techniques to MALDI-MS and FT-IR made it possible to differentiate the main products from the by-products. Additionally, the results obtained throughout the study essentially helped to derive the possible changes in the reaction mechanism that could cause formation of copolymer blends containing long blocks of either PVP or PVAc.

Separation of compounds in complex mixtures can also be

carried out by utilizing two different LC methods in combination to obtain two dimensional separation (2D-LC). 2D-LC is a time-consuming technique; however, it is a very informative method and can be effectively used for copolymer analysis. Baumgaertel et al. used 2D (LACCC × SEC) in combination with MALDI- and ESI-MS/MS for the analysis of poly(2-ethyl-2-oxazoline-*b*-2-(2,6-difluorophenyl)-2-oxazoline) (p (EtOx-*b*-*o*DFOx)) block co-polymers, which have potential medicinal applications. In this study, the application of LACCC allowed separation of the polymers containing different end groups with varying polarity as well as the series with different block lengths. Further analysis of the LC fractions with MALDI-MS and ESI-MS/MS allowed full structural characterization of PEtOx chain transfer and termination products. Finally, quantification of the separated components were carried out by addition of SEC dimension. The 2D contour plot in Fig. 6 shows three fractions: fraction 1 corresponds to the PEtOx homopolymer with an ester end group (7.5 vol%), fraction 2 corresponds to the copolymer (p(EtOx-*b*-*o*DFOx)) (87 vol%) and fraction 3 corresponds to the PEtOx homopolymer with a hydroxyl end group (4.5 vol%) [97]. As a result, combination of the essential information obtained from all three methods was used to ensure that all products are comprehensively characterized.

Other studies from the Weidner group involved imaging of similar copolymer architectures by having specific RP-LC conditions hyphenated to a MALDI target *via* a spray to separate and identify different compositions within one copolymer [98]. Weidner et al. introduced this technique to study copolymers comprised of propylene oxide (PO) and ethylene oxide (EO) blocks, which contained isobaric species or species with very similar masses (within 2 Da). The separation of components differ in PPO and PEO content by LACCC could differentiate compositions from a sample that has overlapping *m*/*z* values, hence composition specific calibration curves were constructed based on the number of PO and EO co-monomers. Subsequently, more complex structures could be thoroughly separated, and characterized, thereby setting the foundation for the next step: sequencing of copolymer structures present in the blend.

Barqawi et al. used an automated system to deposit fractions of a triblock copolymers, that were separated in 2D LC/SEC run, onto a MALDI target [99]. Firstly, the critical conditions of poly(*iso*butylene) (PIB) homopolymers were identified, which was used as the first RP-LC dimension for the identification of the end group heterogeneity. In the second dimension, a SEC column was utilized to determine the molar mass of the polymer and to quantify the products as well as the undesired side products. The 2D-LC eluents were mixed with the salt and the matrix solutions and then sprayed onto a MALDI target with the help of an automated transfer module. This whole automated system allowed a continuous MS data collection at the various 2D-LC elution volumes, which essentially yielded numerous time-dependent spectra. This system is a major achievement in automation and characterization of complex polymer samples due to the fact that the first two dimensions are hyphenated to a MALDI-MS. It also allows a facile way to interpret spectra due to less overlapping peaks, an estimation of composition, chain length, and architecture of symmetrical and non-symmetrical triblock copolymers. In a different offline technique 2D-LC was combined with MALDI-MS to analyze EO based block copolymers [100]. LACCC was used as the first dimension to separate polymers bearing different functionalities. The second dimension was either a SEC or a LAC system which gave evidence for the molar mass of all products present with varying functionality. The setup was hyphenated to MALDI-MS in an offline manner. Raw copolymer samples are very complex to analyze due to high heterogeneity, however, advanced 2D fractionation prior to MS analysis makes the characterization of architectural details possible. It should also be considered that, this is a time-consuming method since optimization of numerous factors (solvent, column, temperature etc.) for separation is needed.

Over the years, computational methods have grown and make the analysis of polymeric materials faster and more straightforward. Weidner et al. have extensively studied PEO-*b*-PPO-type block copolymers [101]. They have developed a software-based chromatographic separation of block copolymers that are subsequently analyzed *via* MALDI-ToF MS. MALDI mass spectra of complex copolymeric systems can result in overlapping isotope patterns of ions comprising different monomeric compositions in the mass spectra. Therefore, preseparation of these species prior to MS data collection become essential for more accurate determination of monomer composition. In this case PEO-*b*-PPO-*b*-PEO was investigated thoroughly, by first establishing the critical conditions

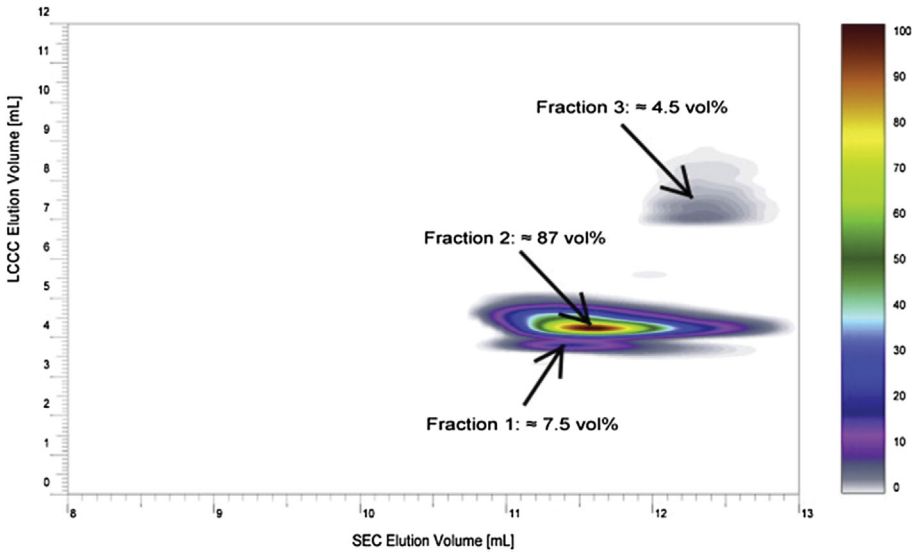

Fig. 6. 2D contour plot of the (p(EtOx-*b*-*o*DFOx)) copolymer: 1st dimension LACCC for PEtOx (eluent: 2-propanol/H_2O = 91/9 (v/v)); 2nd dimension SEC (eluent: 0.07% triethylamine in THF). Reproduced from Ref. [97].

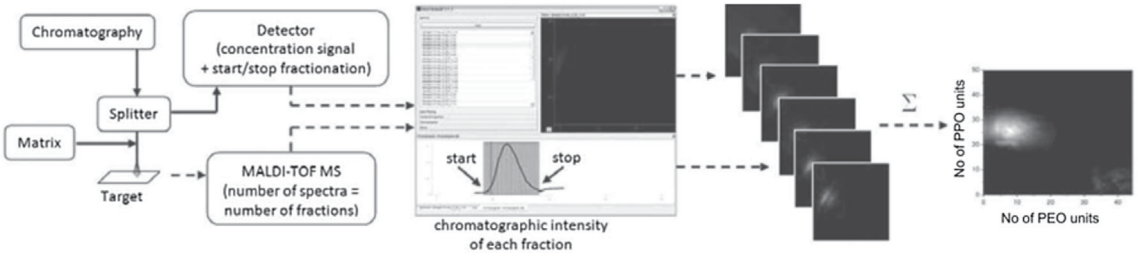

Fig. 7. Scheme of measurement procedure using MassChrom2D to combine chromatography MALDI data for determining the copolymer composition. Modified from Ref. [101].

of PPO which was followed by separation of the components with LAC according to their monomer compositions. All of the fractions obtained from the separation were then sprayed onto a MALDI target for MS analysis of each component. These MS data were then processed by the MassChrom2D algorithm and provided the number of EO and PO units present in each specific fraction. In addition, the intensity obtained from chromatographic data was inserted in the 2D composition plots formed by the MALDI spectra. The entire workflow of the protocol is summarized in Fig. 7. This method is a major step forward in quantifying and identifying the copolymers with different monomeric compositions present in complex mixtures.

Huijser et al. developed a software to establish the composition and topology of different linear chains of poly(lactide-*co*-glycolide) (PLLGA) which is used in drug delivery implants due to its advantageous properties as biodegradable and biocompatible materials [102]. The contour maps generated from the MALDI-MS analysis by using an in house developed software. The results show a significant difference in average composition between random and block copolymer chains. In the case of PLLGA, the line with a constant slope crossing the average composition do not pass through the origin, underlining a block-like structure, in contrast to PDLLGA which reveals a random like copolymer (Fig. 8). Such analytical results are very useful for synthetic chemists, as they indicate an influence in the incorporation rate of a monomer between D-lactide and L-lactide. As it is shown in this study, 1-D MS can also have potential for the detailed analysis of polymer architectures with the help of a powerful data interpretation software.

In a contribution by Vivo-Truyols et al., a PS-*b*-PI block copolymer was analyzed by SEC and, subsequently, MALDI-ToF MS [103]. The overall architecture was then determined from the combined analysis of each fractions. This approach can only be used for non-overlapping isotopic patterns, otherwise regression is used to deconvolute the overlap. The limitation of this method is that the whole spectrum cannot be fitted, and regression can only be applied to the center, which is not representative for the total polymer composition. Complications in both mass resolution and processing power of the computer have also to be taken into account. Nonetheless, this method can produce high-throughput data, offering a fast analysis and yielding kinetic information on copolymers – satisfying both analysts and synthetic chemists. In a related study, Willemse et al. portrayed the analysis and microstructure of PS-*b*-PI block copolymers [104]. The authors showed that MALDI-ToF MS can provide information on parameters such as chain length, composition, block properties or microstructures. It was also shown that overlapping peaks in a copolymer distribution can be interpreted by using NMR as a feedback method if the integrals do not overlap excessively, and thus are not affecting the evaluation of the average composition. In addition, contour plots were produced revealing the number of monomer units of each monomer and their microstructures. Wilczek-Vera et al. analyzed PS-*b*-*α*mPS by MALDI-MS and ^{1}H NMR spectroscopy, where both techniques were required for determination of the block lengths and chemical composition [105]. The Schulz-Zimm model correlates both experimental and theoretical distributions, and can also be applied to triblock copolymers. The model is a rapid method to obtain a complete composition of the copolymer. It was pointed out that anionic ring-opening polymerization (AROP) produces polymers with narrow Đ values. However, it should be noted that the

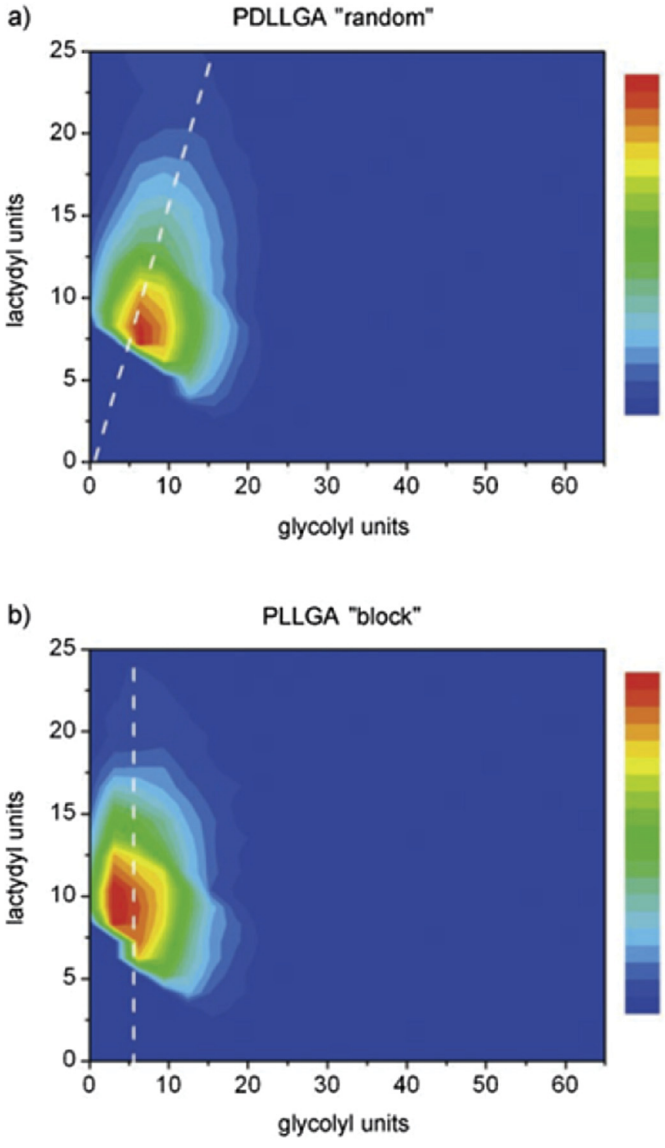

Fig. 8. Contour plots of a) PDLLGA and b) PLLGA for cyclic structures plotted with lactydyl units. Reproduced from Ref. [102].

narrowness does not mean that the copolymer is structurally less complex.

Block copolymers are very important in polymer science and have found many applications in diverse fields. Different block copolymer materials have successfully characterized by utilizing various analytical techniques (thermal techniques or LC methods) in combination with MS. Additionally, the urge to have more automated systems to produce data in a faster manner and understand block copolymer structures and architectures, has brought advanced informatics into polymer science.

4.2. Statistical copolymers

Statistical copolymers are composed of monomers, which form a sequence according to a statistical rule. Many copolymers form statistical sequences, such as poly(2-phenyl-2-oxazoline)-*stat*-(2(dec-9-enyl-2-oxazoline)). These are cationic polymers and due to their importance in biology and medicine, different analytical methods have been utilized in combination for their detailed characterization. The first example where statistical polymers were studied using a 2D setup was reported by the Schoemakers group, who analyzed block and statistical copolymers *via* gradient elution liquid chromatography (GELC), Pyrolysis-GC MS, SEC and capillary electrophoresis-ultraviolet (CE-UV) [106]. All four of these separation techniques provided different complementary information, none of which were conclusive on their own, thus, showing that hyphenated techniques can be essential to characterize complex statistical copolymers. First, Py-GC–MS was used to determine the average chemical composition. Subsequently, GELC was applied to further study the chemical-composition distribution. Offline GELC of these statistical copolymers showed two separated fractions, which were both bimodal in nature. An addition of a SEC dimension revealed that separation of these fractions in GELC dimension was not based on differences in the molar mass (Fig. 9). This was rationalized by the presence of an ionic fraction in the samples of statistical copolymers, resulting from either chain-transfer reactions or termination by addition of water. Confirmation of this rationale was obtained by further analysis with CE and the results revealed that cationically charged polymers were predominant with only a minority being neutral. All of these analyses show that the statistical copolymers are not monomodal in comparison to block copolymers, but had different end groups and probably a different chemical composition per polymer chain.

4.3. Random copolymers

Random copolymers are quite challenging to analyze – in particular when aiming for a sequence determination [81]. An example of MS/MS analysis of random copolymers was recently reported which involved MALDI-ToF-MS/MS on samples containing styrene and dimethylsilylstyrene (DMSS) repeating units [107]. MS/MS provided detailed structural information and sequence coverage by revealing comonomer localization along the copolymer chains. A polystyrene oligomer end-capped by a block DMSS was easily differentiated from the random samples by isolating and fragmenting individual lithiated oligomers. From the MS/MS data, it was found that the localization of the DMSS block differs depending on whether *p*-DMSS or *m*-DMSS is used during the synthesis. Sequence information could be obtained by following the mass shifts occurring on the different fragment series containing either the terminating or the initiating end of the precursor oligomer ion that was being fragmented.

Huijser et al. used MALDI-ToF MS spectra to determine the reactivity ratios of the employed monomers, even with a long chain length model, for random, gradient, alternating and block-like copolymers [108]. This study represents a way to establish kinetic analysis by simply acquiring mass spectra. It was shown that, if analyzed and used properly, a MALDI-MS method can reveal many details such as: reactivity ratios, composition, length of all chains and microstructures. Additionally, ESI-MS also shows a great promise for characterization of such complex copolymer mixtures with the addition of an IM dimension. Different blends of homopolymers and random copolymers have been studied by ESI-IM-MS [109]. Even from samples containing relatively low molar mass analytes, ESI produces ions in many different charge states readily, making the spectra harder to analyze without the IM dimension.

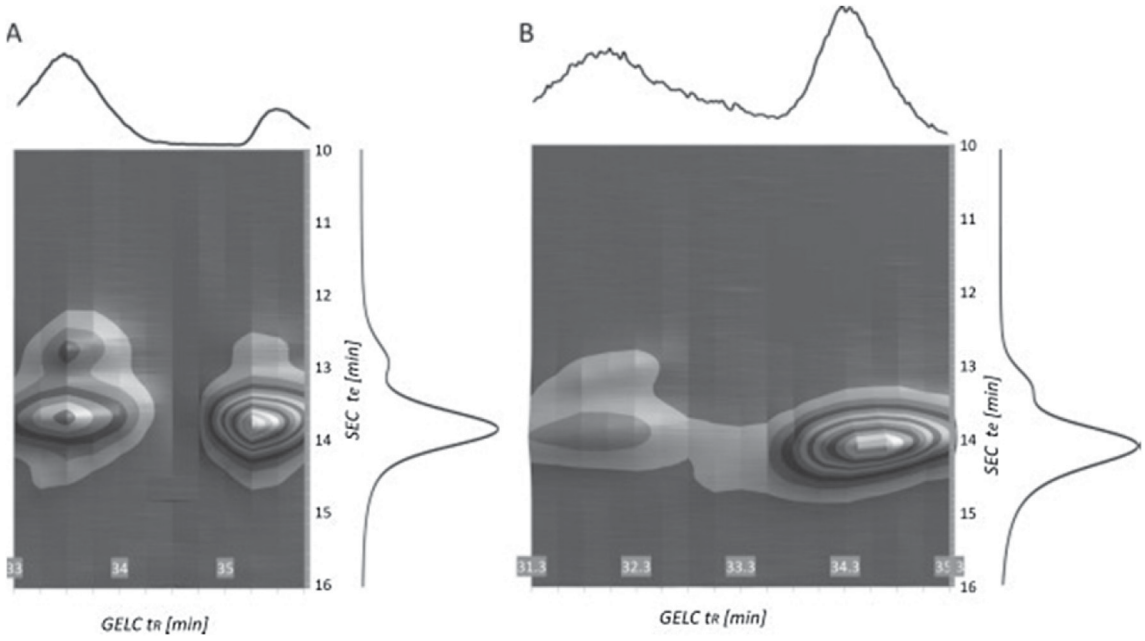

Fig. 9. Off-line comprehensive 2D (GELC)/×/SEC chromatograms of (polyPhOx$_{20}$-*stat*-DecEnOx$_{40}$) (A) and polyPhOx$_{40}$-*stat*-DecEnOx$_{20}$ (B). Reproduced from Ref. [106].

Furthermore, folding transitions of the polymer chain can also be detected in the IM-MS spectra of mobility separated charge states. One aspect to highlight is the investigation of random copolymers PEO-*r*-PPG and PEO-*r*-PPO and their blends. This demonstrates that ESI-IM-MS can be a cost effective analytical method where the component in a complex mixture can be separated and investigated according to their architectural differences. In addition, Engler et al. used copolymer composition numbering tool (COCONUT), a computational method to establish the compositional distribution from MS spectra and the microstructures of random/block copolymers of PS-*co*-PI *via* AROP [110]. Isobaric species and overlapping isotopes could also be resolved using a method based on linear programming. Nonetheless, this method is only semi-quantitative, which is a remaining challenge in polymer science and mass spectrometry.

Overall, different hyphenated analytical techniques, combined with computer-based data processing methods, provides an effective tool to determine the lengths of the blocks and distinguishing between different architectures and sequences of block, random or statistical copolymer chains. The goal of these techniques and hyphenations is to aid chemists in tuning their polymers for their industrial and/or biological applications, as well as understanding and optimizing their chemical reactions.

5. Third dimension of complexity: complex polymers

With increasing demand on advanced polymer architectures for diverse applications, polymers are becoming more and more complex in their architecture, and at the same time, more challenging to characterize. Star-shaped, graft 'like' and branched polymers in particular are in the focus of current research efforts. Even these non-linear architectures are analyzed by many of the established methods presented above.

5.1. Graft 'like' polymers

So far, only a few graft copolymers have jointly been investigated by MS and hyphenated techniques. One such example was PEO-*g*-poly(vinyl alcohol) (PEO-*g*-PVAl), which was used for instant-release tablet coatings due to its mechanical properties [111]. This particular graft copolymer was analyzed by 2D (LACCC × SEC) experiments, which showed that no free PEO was left after the radical polymerization. In addition, MALDI-ToF MS experiments were performed and confirmed this finding. Both complementary methods yielded the same basic results and furthermore, 2D-LC allowed the quantification of the degree of grafting. Comb-like polymers are of wide interest due to their unique architecture, however, they have not been analyzed widely either by MS or liquid chromatography. As an example, Adler et al. showed that such copolymers based on hydrophilic PEO and PMAA units, could be characterized *via* hyphenated MS techniques [112]. Firstly, the LACCC conditions for PEOs were established in order to identify the presence of possible different end groups, followed by SEC for the molar mass measurement of PEO-*comb*-PMAA. The presence of the PEO macromonomer was confirmed by this method, as complemented by FT-IR. To conclude this analysis of hydrophilic copolymers, the authors showed that hyphenation and complementary methods are of necessity to evaluate their architecture, thereby quantifying the degree of grafting and, in addition, determining the monomer feed.

Graft 'like' copolymers have, to the best of our knowledge, hardly been analyzed *via* MS, nonetheless, 2D chromatography has been performed fairly often. In this respect, the 2D-LC based technique is very powerful for polymer analysis, especially with LACCC for one of the employed monomers. Moreover, the offline analysis by MALDI-ToF MS allows an additional dimension and, thus, provides further characteristics of the observed architectures. Both 2D-LC and MS as hyphenated methods are versatile tools for the architecture characterization of graft 'like' polymers. The major drawbacks of a 2D chromatographic system are its expense, time-requirement, and the lack of appropriate standards, leading to erroneous results.

5.2. Cyclic polymers

Cyclic polymers have very different physical properties when compared to their linear homologues and are applied in a wide range of fields, for example, commercial polycarbonates and polyesters for the perfume industry. In contrast to linear species, no chain ends are present as a result from ring closure. Many groups have studied the difference between linear and cyclic polymers using several different ionization methods, hyphenations and complementary methods to obtain as much knowledge and architectural information as possible. For example, Yol et al. have compared both linear and cyclic homopolymers of PS and poly(-butadiene) (PB), which showed significant differences in their MALDI MS/MS spectra [113]. In particular, in the case of linear polymers, a noticeable "depolymerization" was observed, and low mass radical ions were predominant; in comparison, cyclic polymers of similar molar masses gave fragments of higher molar mass with higher relative abundance. In either case, MALDI-ToF MS/MS can determine the end group (for linear polymers) or the linker (for cyclic polymers) used, and is applicable to polymers prepared *via* different polymerization techniques. Maslinska-Solich et al., was able to differentiate linear and macrocyclic oxazolidine-based polymers just by analyzing their MS spectra, and assigning specific peaks to polymer chains with and without end groups [114,115]. Wachsen et al., used three complementary methods to compare linear and cyclic polymers [116]. PLA was used due to its importance as a synthetic polymer, since it is extensively used in biocompatible and biodegradable materials. SEC, LACCC, and MALDI-MS were used to perform a detailed characterization of PLAs. These complementary methods were essential to either determine the structure or separate the different architectures formed during various polymerization techniques. LACCC is a very beneficial technique, however, it is very time consuming due to the many parameters that need to be optimized. Nevertheless, it allows the differentiation between the components with different end groups independently from their molar mass. Osaka et al. studied PLA by ESI- and MALDI-MS where differences between linear and cyclic architectures become apparent [37]. Different fragment ion series were observed in the ESI-MS/MS spectra: three series for the linear and one for the cyclic polymers. Compared to ESI-MS/MS results, MALDI-MS/MS spectra showed the same fragment series for cyclic architectures but differed for linear architectures (only one fragment series was formed). A less common technique was used by McDonnell et al. for the same purpose: sustained off resonance irradiation (SORI)-CAD-FT-ion cyclotron resonance (ICR). In contrast to the previous approaches, this method has very high mass resolution [117]. This allowed to carry out high accuracy mass measurements of the fragment ions which essentially helped to derive different fragmentation mechanisms observed for both linear and cyclic architectures.

Although MS techniques are widely used for the analysis of linear and cyclic polymers, quantification of cyclic and linear chains in an analyte mixture has hardly been addressed by using a hyphenated method. As an exception, Wang et al. applied surface layer (SL)-MALDI-ToF MS to quantify and determine different architectures (linear and cyclic) in PS films that were spin cast from blends [118]. Since the linear and cyclic polymers in the blend differ

in mass, no MS/MS was required, but its use with either ESI- or MALDI-MS would make it possible to differentiate architectures and/or sequences that have the same mass. MALDI- and ESI-MS can cause chemical changes to labile polymers, leading to erroneous data when an inappropriate solvent, salt or matrix is used. Such changes can be detected using IM-MS where charge states and/or overlapping components with different architecture can be deconvoluted [119].

In conclusion, 2D chromatography methods, MS, MS/MS and/or IM-MS have been used to characterize cyclic synthetic (co)polymers. Direct ESI- and MALDI-MS can be enough to differentiate between linear and cyclic oligomers, if there is high enough resolution. However, this is difficult to achieve for high molar masses. CAD is also used for this specific differentiation, however, the poor fragmentation efficiency at higher *m*/*z* values, typically limits its application to lower molecular weight polymers. IM-MS, on the contrary, is a much faster technique that can be used to differentiate linear and cyclic polymers.

5.3. Star-shaped polymers

Star-shaped polymers are synthesized *via* different techniques (for example "core-first", "arm-first" or "graft-onto" methodologies) and are attractive materials for diverse applications, such as drug delivery or material science. However, their characterization is not facile due to their chemical structure. Several analytical techniques have been used to establish a full characterization of star-shaped polymers.

The RAFT polymerization technique is one of the commonly used methods for the preparation of star-shaped polymers [61,120,121]. Star-shaped polymers of *para*-acetoxystyrene and its by-products obtained during RAFT polymerization was analyzed by Chaffey-Millar et al. with MS techniques [120]. In this example, ESI-MS proved to be a powerful tool to differentiate between "star-star couples", terminated with initiator fragments and linear polymers. In addition to ESI-MS analysis, a kinetic model for the polymerization had to be utilized to aid the interpretation of the MS data. Based on these facts, one can conclude that complementary methods are vital to explain experimental observations.

A number of other polymerization techniques are also available for the synthesis of star-shaped copolymers, depending on the employed monomer class and the (targeted) molar mass. PB-based star-shaped polymers were synthesized by Allgaier et al. and the products were analyzed with MALDI-ToF MS [122]. The investigation was limited to low molar masses, however, it was still sufficient to confirm the star-shaped architecture of the polymers. The results were extrapolated to high molar masses through the use of a theoretical modeling. A four-arm PEO-based star-shaped polymer was obtained from AROP and subsequently transformed into an eight-shaped polymer *via* end group modification and two-fold intramolecular ring closure [123]. The final products as well as all intermediates are unambiguously identified by MALDI-MS. IM-MS was also used to examine the conformations of linear PCLs and star shaped PCLs having different topologies [124]. By using theoretical molecular dynamics calculations, two major conformations were found for such polymers (near-spherical and elongated) depending on the charge state and the length of the polymer. Furthermore, these findings were supported by CAD experiments. In light of the results that were obtained by both experiments and simulations, it was concluded that the final conformations depend on the degree of polymerization, charge state, and the branching ratio of the polymer.

Star-shaped block copolymers can also be prepared through the coupling to a core, and are of great interest for drug delivery applications. Li et al. showed that characterization of such star-shaped polymers is difficult [125]. Star-shaped PCL-*b*-PEGs were characterized *via* SEC and MALDI-ToF MS, where MALDI analyses provided information on both the molar masses and the structural identity. The SEC analyses provided additional confirmation and complementary information on the molar masses. One has to be cautious when a star is composed of two different monomers due to differences in the ionization behavior. In this case, a study with a 2D (LACCC × SEC) system would be appealing, taking the critical conditions of both homopolymers (PEG and PCL) into account to ensure that the star is not missing an arm. Furthermore, Rudolph et al. showed that MALDI, static light scattering (SLS) and 2D-LC are essential to obtain absolute molar masses, and to confirm the architecture of their star-shaped $[PEO_{28}$-*b*-PEtOx$]_8$, which was synthesized by the copper-catalyzed azide-alkyne cycloaddition reaction (CuAAC). These techniques are necessary considering that NMR spectroscopy and SEC are not satisfactory to fully characterize these systems [126].

Another type of architecture, branched-based star polymers, was investigated by Yu et al. by MALDI-MS, even at high molar masses [127]. The monomer employed here was EO, which – due to its neutral properties and high ionization efficiency – enables an investigation of polymers even at high molar masses and non-linear architectures. Here, MALDI-MS proves to be a powerful tool to identify stars with different numbers of arms.

Despite the successful characterizations of star-shaped polymer systems in the above examples, analysis of such materials still remains complex in nature. From the diverse examples portrayed, it is clear that star-shaped polymers and their possible side products *e.g.* star-star couples, are distinguishable by MS only. However, IM-MS and 2D-LC can provide additional information to differentiate topologies, and moreover this can be supported by MS/MS or other complementary techniques such as LS or small angle X-ray scattering (SAXS), to determine branching ratios, charge states and the degree of polymerization. The analytical potential of IM-MS is increasingly being appreciated and its speed in analysis is being remarkably acknowledged. Although some methods are still more suitable for high molar masses *e.g.* LS, asymmetric flow field-flow fractionation (AF4) and analytical ultracentrifuge AUC. It is envisaged that complementary techniques such as IM-MS, 2D-LC, LS, AF4 should further support the characterization of these polymer systems.

5.4. Branched polymers

The analysis of dendritic materials with MALDI-ToF MS has been carried out utilizing different matrices, doping agents, solvents, delayed extractions and polymer concentrations. Many examples based on different types of polymers and different numbers of dendritic generations as well as branched or hyperbranched polymers have been characterized *via* direct MALDI MS and also by a range of hyphenated techniques.

5.4.1. Amidoamines and imines

Numerous methods are used to analyze and evaluate different architectures of such compounds. FT-ICR MS was utilized to characterize poly(amidoamine) (PAMAM) based dendrimers – their trade name is Starburst – which exhibit good biocompatibility [128]. High-resolution spectra can be used to determine the Đ values of dendrimers, at least for those of low molar masses. Moreover, this specific instrumentation offers resolving power for high molar masses even of rather disperse samples. MS/MS is useful in this particular case to determine the faults introduced in the synthetic route and to identify the detailed architecture by the specific fragmentation reactions of defect and non-defect dendrimers. This can be done using fragments resulting from

competitive *retro*-Michael additions on the PAMAM: from multiply charged dendrimer ions, two major types of fragments are formed during MS/MS experiments due to the separation of charges [129]. Amide-based dendrimers have been used widely in studies designed to fully understand the ECD mechanism [130]. Unexpected results were discovered such as b•/y cleavages (cleavage after C═O towards the outer layer), S,E dissociations (direction of the cleavage start, end respectively) and minor c,z• (cleavage after N—H towards the outer layer) fragmentations. The fragmentation patterns were compared to poly(propylene imine) (PPI) dendrimers, which lack the amide groups. The comparison showed that macromolecular properties, intramolecular charge-solvation and energy barriers are important determinants for the fragmentation pathways observed, and thus, for the architecture deduced from them. In addition, IM-MS has been used to separate dendrimer constituents and turned out to be much faster than LC or capillary zone electrophoresis (CZE) [131]. Unique cross-sections would be assigned to 'perfect' and 'imperfect' dendrimers, thus unveiling their architectures and complementing the MS/MS data. Furthermore, the results correlated with NMR spectroscopy and SAXS, thus emphasizing the versatility of this technique. Another application of IM-MS in combination with molecular modeling on PAMAM dendrimers concerns the dependence of conformation on the degree of protonation. The results obtained by theoretical calculations show that changes in the conformation are dictated by electrostatic repulsion, which is in agreement with the experimental IM-MS results. On the basis of these findings, IM-MS supported by computational chemistry is a promising tool for future studies on the architectures of higher generation dendrimers [132]. PAMAM dendrimers of higher molar mass were also studied by MALDI-MS and ISD [133]. Different matrices were found to result in different fragmentation patterns. The fragments obtained from ISD of PAMAM dendrimers correlate well with those from ECD of such materials.

Dendrimers of the PPI-type have been studied using different fragmentation techniques to elucidate their architectures. For example, Adhiya et al. examined the conformation of such dendrimers in solution and the gas phase by ESI-CAD and MALDI-PSD-MS [134]. Solutions in different solvents were used and diverse fragmentation pathways, such as the cleavage of outer branches from singly protonated ions, were monitored as a function of the solvent (polar/protic *vs.* non-polar). Lower intensities were observed with non-polar solvents, indicating differences in the dendrimer architectures and the conformations probed. Meijer and co-workers have reviewed the same type of dendrimers in detail by using ESI-CAD, and similar pathways were observed [135]. Further, low energy ESI-MS has been applied to monitor the growth, fragmentations and shape of such dendrimers [136,137]. In addition, HPLC was hyphenated to ESI-MS and used to detect defects in the dendrimers, however, this represents a demanding task due to co-elution of components and isomerism of structures. Adding MS/MS experiments should at least partly resolve these problems by providing information on the different architectures eluting [138]. Branched PEI was investigated under ESI- and MALDI-MS conditions with CAD. These polymers were widely studied due to their reputation as a "golden standard" for gene delivery applications [49]. Three low abundant fragmentation series are detected, arising from a C—N bond cleavage. Their relative abundances provide useful insight on the branching architectural features of the examined PEI samples.

5.4.2. Ethers and esters

Ether based dendrimers have several application domains and MALDI-ToF MS is the traditionally used method for their characterization. MALDI-MS has been utilized to determine the structure and end groups of hyperbranched systems and, thus, differentiate cyclic structures of poly(3-{2-[2-(2-hydroxyethoxy) ethoxy] ethoxy}methyl-3'-methyloxetane (PHEMO), which is used as polymer electrolyte for reinforcement of polyelectrolyte membranes [139]. FT-ICR combined with liquid secondary ion mass spectrometry (SIMS) was used to evaluate, the fragmentation behavior of poly(ether)-type dendrimers with lateral terpyridine moieties and their complexes with iron(II) ions, for an architectural investigation [140]. Hyperbranched 3-ethyl-3-hydroxymethyloxetane trimethylolpropaneoxetane (TMPO)-based polyethers of low molar masses were investigated with ToF-SIMS [141]. The use of this technique with dendrimers of early generations allowed the determination of the degree of branching. However, high molar masses are not accessible with this method.

The Haddleton group investigated aryl ester dendrimers by MALDI-ToF MS. Their low homogeneity, disperse nature and the high laser power requirement for their ionization made the analysis of the spectra of such dendrimers intricate [142]. Fragmentations are induced in-source due to the high laser intensity, indirectly affirming the architecture by the presence of a series of cleaved off branch units. In a different study, MALDI-MS was applied to verify the synthetic route to such dendrimers [143]. The findings pointed out that traditional solution-based methods, such as NMR spectroscopy and SEC, are not powerful enough, and that hyphenated techniques and/or direct MS is required. Polyesteramides, as biodegradable polymers, were studied with MALDI- and ESI-MS giving different results, such as OH groups being present in the ESI spectra but not in the MALDI spectra [144]. This study demonstrated the need for using more than one ionization technique in order to determine architecture through direct MS. The other observation was that ISD is observed with MALDI and not with ESI; thus the analysis of the MALDI data should be carried out carefully due to fragments that lead to erroneous architecture deduction. Finally, Koster et al. used both ECD and low energy CAD to analyze hyperbranched oligomers and concluded that ECD produces more fragments, because it deposits higher internal energies to cause consecutive fragmentations; however, ECD did not produce complementary sequence information, because the new fragments were internal [145]. Thus one has to be aware, when using the data of different fragmentation techniques, that the fragment production mechanisms permit the derivation of the correct architecture.

Hyperbranched polyacrylates, in which the branches grow out of the ester groups, have been prepared by ATRP of acrylate inimers (an inimer can react as an initiator or monomer) [26]. Their architectures were analyzed by MS/MS. Fragmentation occurs by sigmatropic 1,5-H rearrangements over the ester groups, but not by rearrangement of H atoms in the polyacrylate chain. The rearrangements over the side chain provide information about the branching architecture. The fragments produced reveal branching sites and branch sizes, and are completely different from fragments generated by the isomeric linear architecture.

5.4.3. Aromatic ring based

Aromatic monomers with a variety of structures have been polymerized to form dendrimers. Such dendrimers, or branched systems, were analyzed *via* MS techniques (as well as other methods). For example, the Fréchet group applied MALDI-MS to study the functionalities at the surface and the focal point of dendritic aromatic poly(ether)s [146,147]. This method allowed monitoring of the purity and the growth unlike other standard polymer characterization methods. Aromatic poly(ether)s and block-like dendrimers with potential biological applications were characterized by MALDI-ToF MS, which enabled confirmation of the architecture generated using different monomers [148]. In this study, the

choice of matrix and the sample preparation method were critical for obtaining informative mass spectra. Aromatic polyester dendrimers were analyzed by MALDI and laser desorption ionization (LDI) in the presence of different metal salts, which enabled the polymer to be ionized by cation attachment, so that the different generations formed could be identified and verified [149]. In a more recent study, branched and linear poly(aramide)s were compared by MALDI-IM-MS. Synthesized poly(aramide)s were compared to commercial Kevlar® and was found that in Kevlar® both linear and branched species are present [150]. Furthermore, IM separation enabled the distinction between branched *meta-para* aramide and *para* aramide (Kevlar®). In addition, CAD of both branched and linear products was performed and distinct fragments appeared from each sample, thus enabling differentiation between different architectures. This example demonstrates that how a fast and facile these techniques can be to control the production and quality of the material and how polymer characterization can improve in the future. A highly branched PS was synthesized by linking polystyrene anions with 4-chlorodimethyl-silylstyrene and analyzed by MALDI-MS and HPLC [151]. Reverse phase temperature gradient interaction chromatography (RP-TGIC) was used first to fractionate the polymer according to the number of PS branches. The fractions were then characterized by MALDI-ToF MS. Resolution was higher with a RP column in comparison to a normal phase (NP) one, and increased with the number of branches. LACCC resulted in lower resolution than RP-TGIC. Non-aromatic branched polymers were investigated by Liu et al. who analyzed the compositions, sequences and architectures of small oligomers of a hyperbranched glycopolymer, prepared by atom transfer radical copolymerization of an acrylate monomer (A) and an acrylate inimer (B), both carrying mannose ester pendants [152]. MALDI-MS and/or ESI-MS data confirmed the incorporation of multiple inimer repeat units, which lead to formation of a hyperbranched material. MS^n studies elucidated the atomic connectivity in various *n*-mers and specific sequences were distinguished from isomers based on the characteristic elimination of a bromomethane molecule. This provided definitive information about the comonomer connectivity in the copolymeric AB_2 trimer and A_2B_2 tetramer isomers. Consistent with the MS/MS data, IM-MS studies confirmed that only one of the possible A_2B_2 structures was formed (Fig. 10). A comparison of the experimentally determined collision cross-section (CCS) of the detected isomer with the theoretical predictions for the two sequences conclusively showed that BBA_2 is the prevalent tetrameric architecture.

MALDI-ToF MS is extremely beneficial for characterizing branched polymers. By utilizing a higher laser power and fragmentation for the determination of branching points. Various ionization techniques with different fragmentation methods should be used to support hypotheses. In some of the cases, CAD, ECD or ISD were used to establish possible defects in architectures. Specific cleavages enable the verification of the synthetic routes *e.g.* outer layer cleavages of specific bonds. Therefore, tandem mass spectrometry remains an important technique in characterizing the structural features in branched polymers. Furthermore, addition of IM dimension and molecular modeling to the analysis are useful for confirming their respective results regarding conformation changes and for providing complementary information on architectural differences.

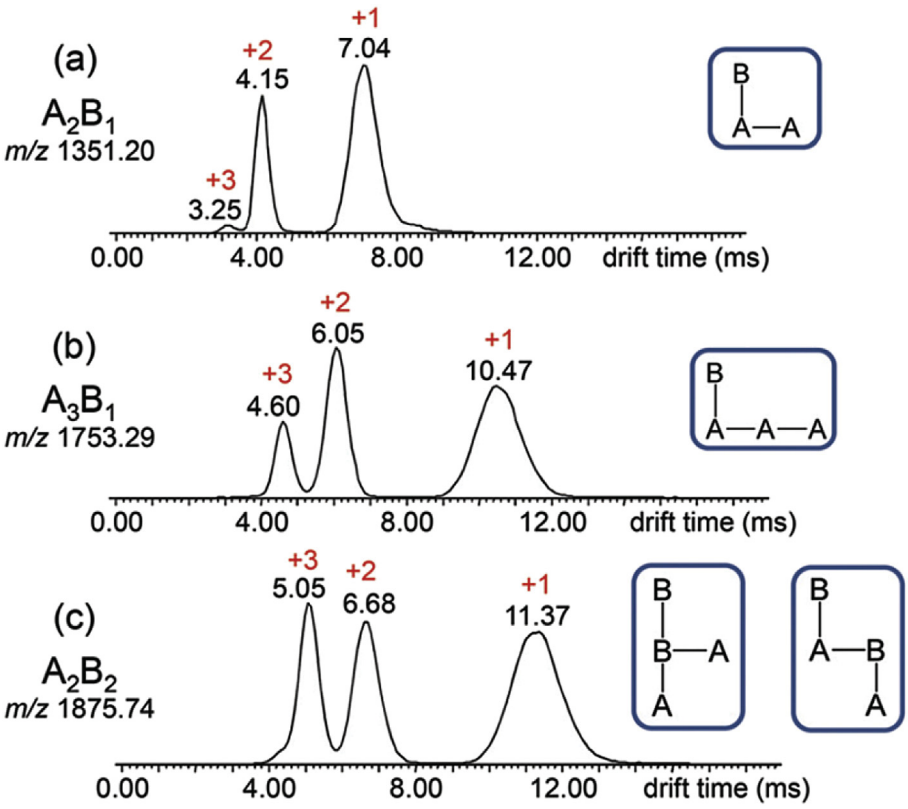

Fig. 10. (a–c) ESI-IM-MS drift time distributions of sodiated, $[M+nNa]^{n+}$, glycopolymer samples having different comonomeric ratios. Three peaks are observed for all three samples, corresponding to ions with +1 to +3 sodium charges. The A_2B_1 trimer and A_3B_1 tetramer can only have the sequence shown, as they contain only one inimer unit. Based on MS/MS, the A_2B_2 tetramer loses CH_3Br, which is compatible with the two sequences shown. Only the first, BBA_2, has a simulated collision cross-section that matches the measured one. Reproduced from Ref. [152].

6. Conclusion

The field of polymer science includes a very broad range of macromolecular species, with diverse structural complexity and molar masses. In the past 20 years, many applications involved synthetic polymers, which experience growing interest in the fields of biology and medicine. Many properties of synthetic polymers are important such as heterogeneity, topology, composition, functionality and/or molar mass. ESI-MS and MALDI-MS have been extensively used in the last two decades and have provided a great magnitude of information on the above-mentioned properties. Numerous developments have arisen recently in MS concerning high-resolution mass analyzers and higher sensitivity, which will boost MS applications in polymer science. Hyphenation of other analytical techniques to MS, for example LC, facilitates the determination of chemical heterogeneity and molar mass, and thus, enhances MS analysis. Furthermore, IM-MS is found to be of potential equivalence to LC, by separating molecules in the gas-phase relatively quickly according to their architectural differences without the need of excessive amounts of solvent consumption. In the future, further improvement and application of all these potential tools will help to investigate more complex architectures of different polymeric materials, which is still a challenging topic in terms of characterization. Moreover, automated software are being developed and continue to be implemented to support complicated data interpretation. MS remains to be a versatile technique and has a promising future in combination with other analytical and computational methods for an improved analysis, and a better understanding of polymer systems with different architectures.

Acknowledgement

Financial support from the Thüringer Ministerium für Bildung, Wissenschaft und Kultur (grants no. B515-07008 and B715-08011) and from the National Science Foundations (CHE-1308307) is gratefully acknowledged. S. Crotty thanks Dr. A. Winter and Dr. K. Knop for discussions and corrections of this work.

References

[1] K. Kataoka, A. Harada, Y. Nagasaki, Block copolymer micelles for drug delivery: design, characterization and biological significance, Adv. Drug Deliv. Rev. 47 (2001) 113–131.
[2] A.P. Gies, Mass Spectrometry in Polymer Chemistry, Wiley, Weinheim, 2011, pp. 33–56.
[3] V. Scionti, C. Wesdemiotis, Mass Spectrometry in Polymer Chemistry, Wiley, Weinheim, 2011, pp. 57–84.
[4] J.B. Fenn, Electrospray wings for molecular elephants, Angew. Chem. Int. Ed. 42 (2003) 3871–3894.
[5] M. Karas, F. Hillenkamp, Laser desorption ionization of proteins with molecular masses exceeding 10,000 daltons, Anal. Chem. 60 (1988) 2299–2301.
[6] D.I. Carroll, I. Dzidic, R.N. Stillwell, K.D. Haegele, E.C. Horning, Atmospheric pressure ionization mass spectrometry. Corona discharge ion source for use in a liquid chromatograph-mass spectrometer-computer analytical system, Anal. Chem. 47 (1975) 2369–2373.
[7] K. Tanaka, H. Waki, Y. Ido, S. Akita, Y. Yoshida, T. Yoshida, T. Matsuo, Protein and polymer analyses up to m/z 100 000 by laser ionization time-of-flight mass spectrometry, Rapid Commun. Mass Spectrom. 2 (1988) 151–153.
[8] J. Falkenhagen, S. Weidner, Mass Spectrometry in Polymer Chemistry, Wiley, Weinheim, 2011, pp. 209–235.
[9] M. Dole, L.L. Mack, R.L. Hines, R.C. Mobley, L.D. Ferguson, M.B. Alice, Molecular beams of macroions, J. Chem. Phys. 49 (1968) 2240–2249.
[10] G.E. Kassalainen, S.K. Ratanathanawongs Williams, Coupling thermal field-flow fractionation with matrix-assisted laser desorption/ionization time-of-flight mass spectrometry for the analysis of synthetic polymers, Anal. Chem. 75 (2003) 1887–1894.
[11] X. Li, Y.-T. Chan, G.R. Newkome, C. Wesdemiotis, Gradient tandem mass spectrometry interfaced with ion mobility separation for the characterization of supramolecular architectures, Anal. Chem. 83 (2011) 1284–1290.
[12] A.C. Crecelius, U.S. Schubert, Mass Spectrometry in Polymer Chemistry, Wiley, Weinheim, 2011, pp. 281–318.
[13] P. Rizzarelli, S. Carroccio, C. Puglisi, Mass Spectrometry in Polymer Chemistry, Wiley, Weinheim, 2011, pp. 437–465.
[14] N. Zhang, Y. Zhou, C. Zhen, Y. Li, C. Xiong, J. Wang, H. Li, Z. Nie, Structural characterization of synthetic polymers using thermal-assisted atmospheric pressure glow discharge mass spectrometry, Analyst 137 (2012) 5051–5056.
[15] Z. Barton, T.J. Kemp, A. Buzy, K.R. Jennings, Mass spectral characterization of the thermal degradation of poly(propylene oxide) by electrospray and matrix-assisted laser desorption ionization, Polymer 36 (1995) 4927–4933.
[16] C.J. Tsai, L.H. Perng, Y.C. Ling, A study of thermal degradation of poly(aryl-ether-ether-ketone) using stepwise pyrolysis/gas chromatography/mass spectrometry, Rapid Commun. Mass Spectrom. 11 (1997) 1987–1995.
[17] R. Lu, Y. Kamiya, Y.-Y. Wan, T. Honda, T. Miyakoshi, Synthesis of Rhus succedanea lacquer film and analysis by pyrolysis-gas chromatography/mass spectrometry, J. Anal. Appl. Pyrolysis 78 (2007) 117–124.
[18] S.L. Madorsky, S. Straus, High vacuum pyrolytic fractionation of polystyrene, Ind. Eng. Chem. 40 (1948) 848–852.
[19] L.A. Wall, Mass spectrometric investigation of the thermal decomposition of polymers, J. Res. Natl. Bur. Stand. (U.S.) 41 (1948) 315–322.
[20] C. Wesdemiotis, N. Solak, M.J. Polce, D.E. Dabney, K. Chaicharoen, B.C. Katzenmeyer, Fragmentation pathways of polymer ions, Mass Spectrom. Rev. 30 (2011) 523–559.
[21] E. Caló, V.V. Khutoryanskiy, Biomedical applications of hydrogels: a review of patents and commercial products, Eur. Polym. J. 65 (2015) 252–267.
[22] T. Hanemann, D.V. Szabó, Polymer-nanoparticle composites: from synthesis to modern applications, Materials 3 (2010) 3468.
[23] E. Altuntaş, A. Krieg, A. Baumgaertel, A.C. Crecelius, U.S. Schubert, ESI, APCI, and MALDI tandem mass spectrometry of poly(methyl acrylate)s: a comparison study for the structural characterization of polymers synthesized via CRP techniques and the software application to analyze MS/MS data, J. Polym. Sci. Part A Polym. Chem. 51 (2013) 1595–1605.
[24] O. Laine, S. Trimpin, H.J. Raeder, K. Muellen, Changes in post-source decay fragmentation behavior of poly(methyl methacrylate) polymers with increasing molecular weight studied by matrix-assisted laser desorption/ionization time-of-flight mass spectrometry, Eur. J. Mass Spectrom. 9 (2003) 195–201.
[25] C.D. Borman, A.T. Jackson, A. Bunn, A.L. Cutter, D.J. Irvine, Evidence for the low thermal stability of poly(methyl methacrylate) polymer produced by atom transfer radical polymerisation, Polymer 41 (2000) 6015–6020.
[26] K. Chaicharoen, M. Polce, A. Singh, C. Pugh, C. Wesdemiotis, Characterization of linear and branched polyacrylates by tandem mass spectrometry, Anal. Bioanal. Chem. 392 (2008) 595–607.
[27] M.-S. Giguère, P.M. Mayer, Climbing the internal energy ladder: the unimolecular decomposition of ionized poly(vinyl acetate), Int. J. Mass Spectrom. 231 (2004) 59–68.
[28] R. Giordanengo, S. Viel, B. Allard-Breton, A. Thévand, L. Charles, Positive mode electrospray tandem mass spectrometry of poly(methacrylic acid) oligomers, Rapid Commun. Mass Spectrom. 23 (2009) 1557–1562.
[29] J.J.L. Bryant, J.A. Semlyen, Cyclic polyesters: 6. Preparation and characterization of two series of cyclic oligomers from solution ring-chain reactions of poly(ethylene terephthalate), Polymer 38 (1997) 2475–2482.
[30] J.J.L. Bryant, J.A. Semlyen, Cyclic polyesters: 7. Preparation and characterization of cyclic oligomers from solution ring-chain reactions of poly(-butylene terephthalate), Polymer 38 (1997) 4531–4537.
[31] P. Kilz, W. Radke, Application of two-dimensional chromatography to the characterization of macromolecules and biomacromolecules, Anal. Bioanal. Chem. 407 (2015) 193–215.
[32] K. Yamanaka, Y. Kimura, T. Aoki, T. Kudo, End-group analysis of bacterially produced poly(3-hydroxybutyrate): discovery of succinate as the polymerization starter, Macromolecules 42 (2009) 4038–4046.
[33] P. Rizzarelli, Matrix-assisted laser desorption ionization time-of-flight/time-of-flight tandem mass spectra of biodegradable polybutylenesuccinate, Rapid Commun. Mass Spectrom. 27 (2013) 2213–2225.
[34] O. Laine, T. Laitinen, P. Vainiotalo, Characterization of polyesters prepared from three different phthalic acid isomers by CID-ESI-FT-ICR and PSD-MALDI-TOF mass spectrometry, Anal. Chem. 74 (2002) 4250–4258.
[35] V. Scionti, C. Wesdemiotis, Electron transfer dissociation versus collisionally activated dissociation of cationized biodegradable polyesters, J. Mass Spectrom. 47 (2012) 1442–1449.
[36] B.C. Katzenmeyer, L.R. Cool, J.P. Williams, K. Craven, J.M. Brown, C. Wesdemiotis, Electron transfer dissociation of sodium cationized polyesters: reaction time effects and combination with collisional activation and ion mobility separation, Int. J. Mass Spectrom. 378 (2015) 303–311.
[37] I. Osaka, M. Watanabe, M. Takama, M. Murakami, R. Arakawa, Characterization of linear and cyclic polylactic acids and their solvolysis products by electrospray ionization mass spectrometry, J. Mass Spectrom. 41 (2006) 1369–1377.
[38] W.J. De, O. Coulembier, P. Dubois, P. Gerbaux, Collision-induced dissociation of polymer ions: charge driven decomposition for sodium-cationized polylactides and isomeric end-group distinction, Int. J. Mass Spectrom. 308 (2011) 11–17.
[39] P. Terrier, B. Desmazieres, J. Tortajada, W. Buchmann, APCI/APPI for synthetic polymer analysis, Mass Spectrom. Rev. 30 (2011) 854–874.
[40] G. Hart-Smith, A review of electron-capture and electron-transfer dissociation tandem mass spectrometry in polymer chemistry, Anal. Chim. Acta 808 (2014) 44–55.
[41] A. Baumgaertel, C. Weber, K. Knop, A. Crecelius, U.S. Schubert,

Characterization of different poly(2-ethyl-2-oxazoline)s via matrix-assisted laser desorption/ionization time-of-flight tandem mass spectrometry, Rapid Commun. Mass Spectrom. 23 (2009) 756–762.
[42] E. Altuntaş, K. Kempe, A. Crecelius, R. Hoogenboom, U.S. Schubert, ESI-MS & MS/MS analysis of poly(2-oxazoline)s with different side groups, Macromol. Chem. Phys. 211 (2010) 2312–2322.
[43] E. Altuntas, C. Weber, K. Kempe, U.S. Schubert, Comparison of ESI, APCI and MALDI for the (tandem) mass analysis of poly(2-ethyl-2-oxazoline)s with various end-groups, Eur. Polym. J. 49 (2013) 2172–2185.
[44] E. Altuntas, C. Weber, U.S. Schubert, Detailed characterization of poly(2-ethyl-2-oxazoline)s by energy variable collision-induced dissociation study, Rapid Commun. Mass Spectrom. 27 (2013) 1095–1100.
[45] K. Knop, R. Hoogenboom, D. Fischer, U.S. Schubert, Poly(ethylene glycol) in drug delivery: pros and cons as well as potential alternatives, Angew. Chem. Int. Ed. 49 (2010) 6288–6308.
[46] A.J.R. Lasprilla, G.A.R. Martinez, B.H. Lunelli, A.L. Jardini, R.M. Filho, Poly-lactic acid synthesis for application in biomedical devices — a review, Biotech. Adv. 30 (2012) 321–328.
[47] N. Adams, U.S. Schubert, Poly(2-oxazolines) in biological and biomedical application contexts, Adv. Drug Deliv. Rev. 59 (2007) 1504–1520.
[48] E. Altuntaş, K. Knop, L. Tauhardt, K. Kempe, A.C. Crecelius, M. Jäger, M.D. Hager, U.S. Schubert, Tandem mass spectrometry of poly(ethylene imine)s by electrospray ionization (ESI) and matrix-assisted laser desorption/ionization (MALDI), J. Mass Spectrom. 47 (2012) 105–114.
[49] E. Rivera-Tirado, C. Wesdemiotis, Characterization of polyethylenimine by electrospray ionization and matrix-assisted laser desorption/ionization, J. Mass Spectrom. 46 (2011) 876–883.
[50] V. Mass, W. Schrepp, B. von Vacano, H. Pasch, Sequence analysis of an isocyanate oligomer by MALDI-TOF mass spectrometry using collision induced dissociation, Macromol. Chem. Phys. 210 (2009) 1957–1965.
[51] K.M. Wollyung, C. Wesdemiotis, A. Nagy, J.P. Kennedy, Synthesis and mass spectrometry characterization of centrally and terminally amine-functionalized polyisobutylenes, J. Polym. Sci. Part A Polym. Chem. 43 (2005) 946–958.
[52] C. Schilli, M.G. Lanzendoerfer, A.H.E. Mueller, Benzyl and cumyl dithiocarbamates as chain transfer agents in the RAFT polymerization of N-isopropylacrylamide. In situ FT-NIR and MALDI-TOF MS investigation, Macromolecules 35 (2002) 6819–6827.
[53] A. Mahon, T.J. Kemp, J.E. Varney, P.J. Derrick, Ions derived from linear polysulfide oligomers using matrix-assisted laser desorption/ionisation time-of-flight mass spectrometry, Polymer 39 (1998) 6213–6217.
[54] S.T. Ellison, A.P. Gies, D.M. Hercules, S.L. Morgan, Py–GC/MS and MALDI–TOF/TOF CID study of polysulfone fragmentation reactions, Macromolecules 42 (2009) 3005–3013.
[55] P. Rizzarelli, C. Puglisi, Structural characterization of synthetic poly(ester amide) from sebacic acid and 4-amino-1-butanol by matrix-assisted laser desorption ionization time-of-flight/time-of-flight tandem mass spectrometry, Rapid Commun. Mass Spectrom. 22 (2008) 739–754.
[56] S. Trimpin, S.M. Weidner, J. Falkenhagen, C.N. McEwen, Fractionation and solvent-free MALDI-MS analysis of polymers using liquid adsorption chromatography at critical conditions in combination with a multisample on-target homogenization/transfer sample preparation method, Anal. Chem. 79 (2007) 7565–7570.
[57] R. Peters, Y. Mengerink, S. Langereis, M. Frederix, H. Linssen, J. van Hest, S. van der Wal, Quantitation of functionality of poly(methyl methacrylate) by liquid chromatography under critical conditions followed by evaporative light-scattering detection. Comparison with NMR and titration, J. Chromatogr. A 949 (2002) 327–335.
[58] T. Gruendling, M. Guilhaus, C. Barner-Kowollik, Quantitative LC–MS of polymers: determining accurate molecular weight distributions by combined size exclusion chromatography and electrospray mass spectrometry with maximum entropy data processing, Anal. Chem. 80 (2008) 6915–6927.
[59] T. Gruendling, D. Voll, M. Guilhaus, C. Barner-Kowollik, A perfect couple: PLP/SEC/ESI-MS for the accurate determination of propagation rate coefficients in free radical polymerization, Macromol. Chem. Phys. 211 (2010) 80–90.
[60] M. Dietrich, M. Glassner, T. Gruendling, C. Schmid, J. Falkenhagen, C. Barner-Kowollik, Facile conversion of RAFT polymers into hydroxyl functional polymers:a detailed investigation of variable monomer and RAFT agent combinations, Polym. Chem. 1 (2010) 634–644.
[61] A. Feldermann, A.A. Toy, T.P. Davis, M.H. Stenzel, C. Barner-Kowollik, An in-depth analytical approach to the mechanism of the RAFT process in acrylate free radical polymerizations via coupled size exclusion chromatography-electrospray ionization mass spectrometry (SEC-ESI-MS), Polymer 46 (2005) 8448–8457.
[62] H. Barqawi, E. Ostas, B. Liu, J.-F. Carpentier, W.H. Binder, Multidimensional characterization of α,ω-telechelic poly(ε-caprolactone)s via online coupling of 2D chromatographic methods (LC/SEC) and ESI-TOF/MALDI-TOF-MS, Macromolecules 45 (2012) 9779–9790.
[63] N. Pretorius, K. Rhode, J. Simpson, H. Pasch, Characterization of complex phthalic acid/propylene glycol based polyesters by the combination of 2D chromatography and MALDI-TOF mass spectrometry, Anal. Bioanal. Chem. 407 (2015) 217–230.
[64] H. Cölfen, M. Antonietti, New Developments in Polymer Analytics I (Advances in Polymer Science), Springer Berlin Heidelberg, 2000, pp. 67–187.
[65] M. Hassellöv, G. Hulthe, B. Lyvén, G. Stenhagen, Electrospray mass spectrometry as online detector for low molecular weight polymer separations with flow field-flow fractionation, J. Liq. Chromatogr. Relat. Technol. 20 (1997) 2843–2856.
[66] G.R. Hilton, A.T. Jackson, K. Thalassinos, J.H. Scrivens, Structural analysis of synthetic polymer mixtures using ion mobility and tandem mass spectrometry, Anal. Chem. 80 (2008) 9720–9725.
[67] V. Scionti, B.C. Katzenmeyer, N. Solak, X. Li, C. Wesdemiotis, Interfacing multistage mass spectrometry with liquid chromatography or ion mobility separation for synthetic polymer analysis, Eur. J. Mass Spectrom. 18 (2012) 113–137.
[68] http://www.waters.com/waters/library.htm?locale=en_US&lid=134757057&cid=511436 (last accessed 24.05.15).
[69] K. Kim, J. Lee, T. Chang, H. Kim, Characterization of polylactides with different stereoregularity using electrospray ionization ion mobility mass spectrometry, J. Am. Soc. Mass Spectrom. 25 (2014) 1771–1779.
[70] S. Trimpin, M. Plasencia, D. Isailovic, D.E. Clemmer, Resolving oligomers from fully grown polymers with IMS–MS, Anal. Chem. 79 (2007) 7965–7974.
[71] C. Barrere, F. Maire, C. Afonso, P. Giusti, Atmospheric solid analysis probe-ion mobility mass spectrometry of polypropylene, Anal. Chem. 84 (2012) 9349–9354.
[72] C. Barrere, W. Selmi, M. Hubert-Roux, T. Coupin, B. Assumani, C. Afonso, P. Giusti, Rapid analysis of polyester and polyethylene blends by ion mobility-mass spectrometry, Polym. Chem. 5 (2014) 3576–3582.
[73] J. Song, C.H. Grün, R.M.A. Heeren, H.-G. Janssen, O.F. van den Brink, High-resolution ion mobility spectrometry–mass spectrometry on poly(methyl methacrylate), Angew. Chem. Int. Ed. 49 (2010) 10168–10171.
[74] J.N. Hoskins, S. Trimpin, S.M. Grayson, Architectural differentiation of linear and cyclic polymeric isomers by ion mobility spectrometry-mass spectrometry, Macromolecules 44 (2011) 6915–6918.
[75] A.T. Jackson, K. Thalassinos, R.O. John, N. McGuire, D. Freeman, J.H. Scrivens, Characterisation of end groups in poly(2-hydroxyethyl methacrylate) by means of electrospray ionisation-mass spectrometry/mass spectrometry (ESI-MS/MS), Polymer 51 (2010) 1418–1424.
[76] K. Thalassinos, A.T. Jackson, J.P. Williams, G.R. Hilton, S.E. Slade, J.H. Scrivens, Novel software for the assignment of peaks from tandem mass spectrometry spectra of synthetic polymers, J. Am. Soc. Mass Spectrom. 18 (2007) 1324–1331.
[77] A. Jackson, S. Slade, K. Thalassinos, J. Scrivens, End-group characterisation of poly(propylene glycol)s by means of electrospray ionisation–tandem mass spectrometry (ESI-MS/MS), Anal. Bioanal. Chem. 392 (2008) 643–650.
[78] J.P. Williams, G.R. Hilton, K. Thalassinos, A.T. Jackson, J.H. Scrivens, The rapid characterisation of poly(ethylene glycol) oligomers using desorption electrospray ionisation tandem mass spectrometry combined with novel product ion peak assignment software, Rapid Commun. Mass Spectrom. 21 (2007) 1693–1704.
[79] A. Baumgaertel, K. Scheubert, B. Pietsch, K. Kempe, A.C. Crecelius, S. Böcker, U.S. Schubert, Analysis of different synthetic homopolymers by the use of a new calculation software for tandem mass spectra, Rapid Commun. Mass Spectrom. 25 (2011) 1765–1778.
[80] F.H. Schacher, P.A. Rupar, I. Manners, Functional block copolymers: nanostructured materials with emerging applications, Angew. Chem. Int. Ed. 51 (2012) 7898–7921.
[81] M.S. Montaudo, Mass spectra of copolymers, Mass Spectrom. Rev. 21 (2002) 108–144.
[82] O.J. Houshia, C. Wilkins, Compositional analysis of the high molecular weight ethylene oxide propylene oxide copolymer by MALDI mass spectrometry, Int. J. Chem. 4 (2012) 14–23.
[83] G. Gallet, S. Carroccio, P. Rizzarelli, S. Karlsson, Thermal degradation of poly(ethylene oxide–propylene oxide–ethylene oxide) triblock copolymer: comparative study by SEC/NMR, SEC/MALDI-TOF-MS and SPME/GC-MS, Polymer 43 (2002) 1081–1094.
[84] T. Orhan, J. Hacaloglu, Thermal degradation of poly(2-vinylpyridine) copolymers, Polym. Degrad. Stab. 98 (2013) 356–360.
[85] R.P. Lattimer, M.J. Polce, C. Wesdemiotis, MALDI-MS analysis of pyrolysis products from a segmented polyurethane, J. Anal. Appl. Pyrolysis 48 (1998) 1–15.
[86] S.E. Whitson, C. Wesdemiotis, R.P. Lattimer, Characterization of polyurethane formulations by direct probe atmospheric pressure chemical ionization mass spectrometry, Rubber Chem. Technol. 83 (2010) 35–45.
[87] S.E. Whitson, G. Erdodi, J.P. Kennedy, R.P. Lattimer, C. Wesdemiotis, Direct probe-atmospheric pressure chemical ionization mass spectrometry of cross-linked copolymers and copolymer blends, Anal. Chem. 80 (2008) 7778–7785.
[88] A. Baumgaertel, E. Altuntaş, K. Kempe, A. Crecelius, U.S. Schubert, Characterization of different poly(2-oxazoline) block copolymers by MALDI-TOF MS/MS and ESI-Q-TOF MS/MS, J. Polym. Sci. Part A Polym. Chem. 48 (2010) 5533–5540.
[89] A.C. Crecelius, C.R. Becer, K. Knop, U.S. Schubert, Block length determination of the block copolymer mPEG-b-PS using MALDI-TOF MS/MS, J. Polym. Sci. Part A Polym. Chem. 48 (2010) 4375–4384.
[90] B.A. Cerda, D.M. Horn, K. Breuker, F.W. McLafferty, Sequencing of specific copolymer oligomers by electron-capture-dissociation mass spectrometry, J. Am. Chem. Soc. 124 (2002) 9287–9291.
[91] S.M. Miladinović, C.J. Kaeser, M.M. Knust, C.L. Wilkins, Tandem Fourier transform mass spectrometry of block and random copolymers, Int. J. Mass

Spectrom. 301 (2011) 184–194.
[92] E.R. Kaal, M. Kurano, M. Geißler, H.-G. Janssen, Hyphenation of aqueous liquid chromatography to pyrolysis-gas chromatography and mass spectrometry for the comprehensive characterization of water-soluble polymers, J. Chromatogr. A 1186 (2008) 222–227.
[93] S.M. van Leeuwen, B. Tan, D.W. Grijpma, J. Feijen, U. Karst, Characterization of the chemical composition of a block copolymer by liquid chromatography/mass spectrometry using atmospheric pressure chemical ionization and electrospray ionization, Rapid Commun. Mass Spectrom. 21 (2007) 2629–2637.
[94] H. Hayen, A.A. Deschamps, D.W. Grijpma, J. Feijen, U. Karst, Liquid chromatographic-mass spectrometric studies on the in vitro degradation of a poly(ether ester) block copolymer, J. Chromatogr. A 1029 (2004) 29–36.
[95] M. Girod, T.N.T. Phan, L. Charles, Tuning block copolymer structural information by adjusting salt concentration in liquid chromatography at critical conditions coupled with electrospray tandem mass spectrometry, Rapid Commun. Mass Spectrom. 23 (2009) 1476–1482.
[96] N. Fandrich, J. Falkenhagen, S.M. Weidner, B. Staal, A.F. Thünemann, A. Laschewsky, Characterization of new amphiphilic block copolymers of N-vinylpyrrolidone and vinyl acetate, 2-chromatographic separation and analysis by MALDI-TOF and FT-IR coupling, Macromol. Chem. Phys. 211 (2010) 1678–1688.
[97] A. Baumgaertel, C. Weber, N. Fritz, G. Festag, E. Altuntaş, K. Kempe, R. Hoogenboom, U.S. Schubert, Characterization of poly(2-oxazoline) homo- and copolymers by liquid chromatography at critical conditions, J. Chromatogr. A 1218 (2011) 8370–8378.
[98] S.M. Weidner, J. Falkenhagen, LC-MALDI-TOF imaging MS: a new approach in combining chromatography and mass spectrometry of copolymers, Anal. Chem. 83 (2011) 9153–9158.
[99] H. Barqawi, M. Schulz, A. Olubummo, V. Saurland, W.H. Binder, 2D-LC/SEC-(MALDI-TOF)-MS characterization of symmetric and nonsymmetric biocompatible PEOm–PIB–PEOn block copolymers, Macromolecules 46 (2013) 7638–7649.
[100] M.I. Malik, B. Trathnigg, R. Saf, Characterization of ethylene oxide–propylene oxide block copolymers by combination of different chromatographic techniques and matrix-assisted laser desorption ionization time-of-flight mass spectroscopy, J. Chromatogr. A 1216 (2009) 6627–6635.
[101] S.M. Weidner, J. Falkenhagen, I. Bressler, Copolymer composition determined by LC-MALDI-TOF MS coupling and "MassChrom2D" data analysis, Macromol. Chem. Phys. 213 (2012) 2404–2411.
[102] S. Huijser, B.B.P. Staal, J. Huang, R. Duchateau, C.E. Koning, Chemical composition and topology of poly(lactide-co-glycolide) revealed by pushing MALDI-TOF MS to its limit, Angew. Chem. Int. Ed. 118 (2006) 4210–4214.
[103] G. Vivó-Truyols, B. Staal, P.J. Schoenmakers, Strip-based regression: a method to obtain comprehensive co-polymer architectures from matrix-assisted laser desorption ionisation-mass spectrometry data, J. Chromatogr. A 1217 (2010) 4150–4159.
[104] R.X.E. Willemse, B.B.P. Staal, E.H.D. Donkers, A.M. van Herk, Copolymer fingerprints of polystyrene-block-polyisoprene by MALDI-ToF-MS, Macromolecules 37 (2004) 5717–5723.
[105] G. Wilczek-Vera, P.O. Danis, A. Eisenberg, Individual block length distributions of block copolymers of polystyrene-block-poly(α-methylstyrene) by MALDI/TOF mass spectrometry, Macromolecules 29 (1996) 4036–4044.
[106] A. Chojnacka, K. Kempe, H.C. van de Ven, C. Englert, R. Hoogenboom, U.S. Schubert, H.-G. Janssen, P. Schoenmakers, Molar mass, chemical-composition, and functionality-type distributions of poly(2-oxazoline)s revealed by a variety of separation techniques, J. Chromatogr. A 1265 (2012) 123–132.
[107] A.M. Yol, J. Janoski, R.P. Quirk, C. Wesdemiotis, Sequence analysis of styrenic copolymers by tandem mass spectrometry, Anal. Chem. 86 (2014) 9576–9582.
[108] S. Huijser, G.D. Mooiweer, R. van der Hofstad, B.B.P. Staal, J. Feenstra, A.M. van Herk, C.E. Koning, R. Duchateau, Reactivity ratios of comonomers from a single MALDI–ToF–MS measurement at one feed composition, Macromolecules 45 (2012) 4500–4510.
[109] S. Trimpin, D.E. Clemmer, Ion mobility spectrometry/mass spectrometry snapshots for assessing the molecular compositions of complex polymeric systems, Anal. Chem. 80 (2008) 9073–9083.
[110] M.S. Engler, S. Crotty, M.J. Barthel, C. Pietsch, K. Knop, U.S. Schubert, S. Böcker, COCONUT—an efficient tool for estimating copolymer compositions from mass spectra, Anal. Chem. 87 (2015) 5223–5231.
[111] R. Gutzler, M. Smulders, R.F.M. Lange, The role of synthetic pharmaceutical polymer excipients in oral dosage forms – poly(ethylene oxide)-graft-poly(vinyl alcohol) copolymers in tablet coatings, Macromol. Symp. 225 (2005) 81–94.
[112] M. Adler, F. Rittig, S. Becker, H. Pasch, Multidimensional chromatographic and hyphenated techniques for hydrophilic copolymers, 1, Macromol. Chem. Phys. 206 (2005) 2269–2277.
[113] A.M. Yol, D.E. Dabney, S.-F. Wang, B.A. Laurent, M.D. Foster, R.P. Quirk, S.M. Grayson, C. Wesdemiotis, Differentiation of linear and cyclic polymer architectures by MALDI tandem mass spectrometry (MALDI-MS2), J. Am. Soc. Mass Spectrom. 24 (2013) 74–82.
[114] J. Maslinska-Solich, E. Kudrej-Gibas, Electrospray mass spectrometry determination of poly(oxazolidine acetal), Rapid Commun. Mass Spectrom. 17 (2003) 1769–1774.
[115] J. Maslinska-Solich, E. Gibas, Electrospray mass spectrometry studies of macromolecules containing 1,3-oxazolidine moieties, Rapid Commun. Mass Spectrom. 18 (2004) 2619–2628.
[116] O. Wachsen, K.H. Reichert, R.P. Krueger, H. Much, G. Schulz, Thermal decomposition of biodegradable polyesters. III. Studies on the mechanisms of thermal degradation of oligo-L-lactide using SEC, LACCC and MALDI-TOF-MS, Polym. Degrad. Stab. 55 (1997) 225–231.
[117] L.A. McDonnell, P.J. Derrick, B.B. Powell, P. Double, Sustained off-resonance irradiation collision-induced dissociation of linear, substituted and cyclic polyesters using a 9.4 T Fourier transform ion cyclotron resonance mass spectrometer, Eur. J. Mass Spectrom. 9 (2003) 117–128.
[118] S.-F. Wang, X. Li, R.L. Agapov, C. Wesdemiotis, M.D. Foster, Probing surface concentration of cyclic/linear blend films using surface layer MALDI-TOF mass spectrometry, ACS Macro Lett. 1 (2012) 1024–1027.
[119] X. Li, L. Guo, M. Casiano-Maldonado, D. Zhang, C. Wesdemiotis, Top-down multidimensional mass spectrometry methods for synthetic polymer analysis, Macromolecules 44 (2011) 4555–4564.
[120] H. Chaffey-Millar, G. Hart-Smith, C. Barner-Kowollik, Living star polymer formation (RAFT) studied via electrospray ionization mass spectrometry, J. Polym. Sci. Part A Polym. Chem. 46 (2008) 1873–1892.
[121] A.A. Toy, P. Vana, T.P. Davis, C. Barner-Kowollik, Reversible addition fragmentation chain transfer (RAFT) polymerization of methyl acrylate: detailed structural investigation via coupled size exclusion chromatography-electrospray ionization mass spectrometry (SEC-ESI-MS), Macromolecules 37 (2004) 744–751.
[122] J. Allgaier, K. Martin, H.J. Raeder, K. Muellen, Many-arm star polymers synthesized using chlorosilane linking agents: their structural quality concerning arm number and polydispersity, Macromolecules 32 (1999) 3190–3194.
[123] G. Wang, X. Fan, B. Hu, Y. Zhang, J. Huang, Synthesis of eight-shaped poly(ethylene oxide) by the combination of glaser coupling with ring-opening polymerization, Macromol. Rapid Commun. 32 (2011) 1658–1663.
[124] D. Morsa, T. Defize, D. Dehareng, C. Jérôme, E. De Pauw, Polymer topology revealed by ion mobility coupled with mass spectrometry, Anal. Chem. 86 (2014) 9693–9700.
[125] Y. Li, B. Zhang, J.N. Hoskins, S.M. Grayson, Synthesis, purification, and characterization of "perfect" star polymers via "Click" coupling, J. Polym. Sci. Part A Polym. Chem. 50 (2012) 1086–1101.
[126] T. Rudolph, S. Crotty, M. von der Lühe, D. Pretzel, U.S. Schubert, F.H. Schacher, Synthesis and solution properties of double hydrophilic poly(ethylene oxide)-block-poly(2-ethyl-2-oxazoline) (PEO-b-PEtOx) star block copolymers, Polymers 5 (2013) 1081–1101.
[127] D. Yu, N. Vladimirov, J.M.J. Frechet, MALDI-TOF in the characterizations of dendritic-linear block copolymers and stars, Macromolecules 32 (1999) 5186–5192.
[128] L.P. Tolic, G.A. Anderson, R.D. Smith, H.M. Brothers II, R. Spindler, D.A. Tomalia, Electrospray ionization Fourier transform ion cyclotron resonance mass spectrometric characterization of high molecular mass Starburst dendrimers, Int. J. Mass Spectrom. Ion. Process. 165/166 (1997) 405–418.
[129] M. He, S.A. McLuckey, Tandem mass spectrometry of half-generation PAMAM dendrimer anions, Rapid Commun. Mass Spectrom. 18 (2004) 960–972.
[130] S. Lee, S.Y. Han, T.G. Lee, G. Chung, D. Lee, H.B. Oh, Observation of pronounced b•,y cleavages in the electron capture dissociation mass spectrometry of polyamidoamine (PAMAM) dendrimer ions with amide functionalities, J. Am. Soc. Mass Spectrom. 17 (2006) 536–543.
[131] F. Maire, G. Coadou, L. Cravello, C.M. Lange, Traveling wave ion mobility mass spectrometry study of low generation polyamidoamine dendrimers, J. Am. Soc. Mass Spectrom. 24 (2013) 238–248.
[132] A. Tintaru, S. Pricl, L. Denbigh, X. Liu, L. Peng, L. Charles, Conformational changes of small PAMAM dendrimers as a function of their charge state: a combined electrospray mass spectrometry, traveling-wave ion mobility and molecular modeling study, Int. J. Mass Spectrom. 354–355 (2013) 235–241.
[133] H. So, J. Lee, S.Y. Han, H.B. Oh, MALDI in-source decay mass spectrometry of polyamidoamine dendrimers, J. Am. Soc. Mass Spectrom. 23 (2012) 1821–1825.
[134] A. Adhiya, C. Wesdemiotis, Poly(propylene imine) dendrimer conformations in the gas phase: a tandem mass spectrometry study, Int. J. Mass Spectrom. 214 (2002) 75–88.
[135] J.-W. Weener, J.L.J. van Dongen, J.C. Hummelen, E.W. Meijer, Fragmentation studies of poly(propylene imine) dendrimers in the gas-phase by using electrospray ionization mass spectrometry (ESI-MS), Polym. Mater. Sci. Eng. 77 (1997) 147–148.
[136] J.-W. Weener, J.L.J. van Dongen, E.W. Meijer, Electrospray mass spectrometry studies of poly(propylene imine) dendrimers: probing reactivity in the gas phase, J. Am. Chem. Soc. 121 (1999) 10346–10355.
[137] M.A.C. Broeren, J.L.J. van Dongen, M. Pittelkow, J.B. Christensen, M.H.P. van Genderen, E.W. Meijer, Multivalency in the gas phase: the study of dendritic aggregates by mass spectrometry, Angew. Chem. Int. Ed. 43 (2004) 3557–3562.
[138] S. van der Wal, Y. Mengerink, J.C. Brackman, E.M.M. de Brabander, C.M. Jeronimus-Stratingh, A.P. Bruins, Compositional analysis of nitrile terminated poly(propylene imine) dendrimers by high-performance liquid chromatography combined with electrospray mass spectrometry, J. Chromatogr. A 825 (1998) 135–147.

[139] L. Ye, Z.-G. Feng, Y.-M. Zhao, F. Wu, S. Chen, G.-Q. Wang, Synthesis and application as polymer electrolyte of hyperbranched polyether made by cationic ring-opening polymerization of 3-{2-[2-(2-hydroxyethoxy)ethoxy] ethoxymethyl}-3'-methyl-oxetane, J. Polym. Sci. Part A Polym. Chem. 44 (2006) 3650–3665.
[140] R.L.C. Lau, T.W.D. Chan, I.Y.K. Chan, H.-F. Chow, Fourier transform ion cyclotron resonance studies of terpyridine-based polyether dendrimers and their iron(II) metallocomplexes by liquid secondary ion mass spectrometry, Eur. Mass Spectrom. 1 (1995) 371–380.
[141] G. Coullerez, H.J. Mathieu, S. Lundmark, M. Malkoch, H. Magnusson, A. Hult, Cationization of dendritic macromolecule adsorbates on metals studied by time-of-flight secondary ion mass spectrometry, Surf. Interface Anal. 35 (2003) 682–692.
[142] A.J. Clark, A.A. Coleshill, D.M. Haddleton, S.J. Isles, H.S. Sahota, P.C. Taylor, Changes in the homogeneity of poly(arylester) dendrimers during the matrix-assisted laser desorption/ionization mass spectrometry experiment, Eur. Mass Spectrom. 5 (1999) 273–277.
[143] H. Sahota, P.M. Lloyd, S.G. Yeates, P.J. Derrick, P.C. Taylor, D.M. Haddleton, Characterization of aromatic polyester dendrimers by matrix-assisted laser desorption ionization mass spectrometry, J. Chem. Soc. Chem. Commun. (1994) 2445–2446.
[144] D. Muscat, H. Henderickx, G. Kwakkenbos, R. van Benthem, C.G. de Koster, R. Fokkens, N.M.M. Nibbering, In-source decay of hyperbranched poly-esteramides in matrix-assisted laser desorption/ionization time-of-flight mass spectrometry, J. Am. Soc. Mass Spectrom. 11 (2000) 218–227.
[145] S. Koster, M.C. Duursma, J.J. Boon, R.M.A. Heeren, S. Ingemann, R.A.T.M. van Benthem, C.G. de Koster, Electron capture and collisionally activated dissociation mass spectrometry of doubly charged hyperbranched poly(ester-amide)s, J. Am. Soc. Mass Spectrom. 14 (2003) 332–341.
[146] W. Hayes, A.W. Freeman, J.M.J. Frechet, Matrix-assisted laser desorption ionization mass spectrometric analysis of aromatic polyether dendritic systems, Polym. Mater. Sci. Eng. 77 (1997) 136–137.
[147] N. Yamazaki, I. Washio, Y. Shibasaki, M. Ueda, Facile synthesis of poly(phenylene-ether) dendrimers from unprotected AB2-building block using thionyl chloride as a condensing agent, Polym. Prepr. 46 (2005) 645–646.
[148] J.W. Leon, J.M.J. Frechet, Analysis of aromatic polyether dendrimers and dendrimer-linear block copolymers by matrix-assisted laser desorption ionization mass spectrometry, Polym. Bull. 35 (1995) 449–455.
[149] I.A. Mowat, R.J. Donovan, M. Bruce, W.J. Feast, N.M. Stainton, Matrix assisted laser desorption/ionization mass spectrometry of aryl ester dendrimers, Eur. Mass Spectrom. 4 (1998) 451–458.
[150] A.P. Gies, M. Kliman, J.A. McLean, D.M. Hercules, Characterization of branching in aramid polymers studied by MALDI–ion mobility/mass spectrometry, Macromolecules 41 (2008) 8299–8301.
[151] K. Im, S. Park, D. Cho, T. Chang, K. Lee, N. Choi, HPLC and MALDI-TOF MS analysis of highly branched polystyrene: resolution enhancement by branching, Anal. Chem. 76 (2004) 2638–2642.
[152] X. Liu, L.R. Cool, K. Lin, A.M. Kasko, C. Wesdemiotis, Tandem mass spectrometry and ion mobility mass spectrometry for the analysis of molecular sequence and architecture of hyperbranched glycopolymers, Analyst 140 (2015) 1182–1191.

Sarah Crotty was born in Ambilly (France) in 1987. She studied chemistry and analytical chemistry in Loughborough (B.Sc. in 2010) and Warwick (M.Sc. in 2011) (both UK). She worked in India for one year in R&D investigating the synthesis and characterization of potential drugs for tropical diseases. She joined in 2012 the research group of Prof. Ulrich S. Schubert as a PhD student at the Friedrich Schiller University Jena. Her research focuses on the characterization of synthetic polymers by the use of diverse techniques 2D-LC, liquid adsorption chromatography at critical conditions (LACCC), spotting, mass spectrometry (MALDI-, ESI- & MS/MS) and software algorithm.

Selim Gerişlioğlu was born in Izmir (Turkey) in 1989. He studied chemistry at Hacettepe University (B.Sc. in 2010) (Ankara, Turkey). He completed his MSc degree on physical chemistry in 2012 at Hacettepe University where he investigated ionization mechanisms in MALDI-MS. He moved to Akron, USA and joined the research group of Prof. Chrys Wesdemiotis as a PhD student at The University of Akron in 2013. His current research focuses on investigation of fragmentation mechanisms and structural characterization of copolymers by utilizing different tandem mass spectrometric techniques such as electron transfer dissociation and collisionally activated dissociation.

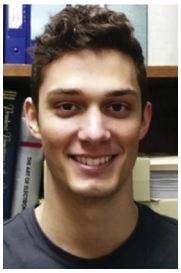

Kevin Endres was born in Addison, IL (U.S.) in 1992. He studied Specialized Chemistry at the University of Illinois at Urbana-Champaign (B.Sc. in 2014), and conducted synthetic research on self-assembling nanoparticles for potential self-healing applications. He joined the research group of Prof. Chrys Wesdemiotis as a PhD student at the University of Akron. His research focuses on the characterization of synthetic polymers with mass spectrometry (ESI and MALDI), polymer and supramolecular structures with IM-ESI-MS, and polymer blended films using SL-MALDI-ToF.

Chrys Wesdemiotis was born in Thessaloniki (Greece) in 1952. He completed his B.S., M.S. and Ph.D. at Technische Universität Berlin (1979). After a postdoctoral fellowship with Fred W. McLafferty at Cornell University (1980) and military service in Greece (1981–1983), he returned to Cornell as senior research associate (1983–1989). In 1989, he joined the University of Akron, where he currently is Distinguished Professor of Chemistry, Polymer Science, and Integrated Bioscience. Wesdemiotis is AAAS fellow, Editor of the European Journal of Mass Spectrometry, and member of the Editorial Boards of Mass Spectrometry Reviews, International Journal of Mass Spectrometry, and the Journal of the American Society for Mass Spectrometry. Research in the Wesdemiotis group focuses on the development and applications of multidimensional mass spectrometry methodologies for the characterization of new synthetic polymers and polymer-biomolecule interfaces.

Ulrich S. Schubert was born in Tubingen (Germany) in 1969. He studied chemistry in Frankfurt and Bayreuth (both Germany) as well as in Richmond (USA). His PhD studies were performed at the Universities of Bayreuth and South Florida/Tampa (USA). After a postdoctoral training with Jean-Marie Lehn at the University of Strasbourg (France), he moved to the TU Munich (Germany) and obtained his Habilitation in 1999. From 1999 to 2000 he was Professor at the Center for NanoScience, University of Munich (Germany), and from 2000 to 2007 Full-Professor at Eindhoven University of Technology (The Netherlands). Currently, he holds a chair at the Friedrich Schiller University Jena with research interest in nanoparticle systems as sensor and drug delivery devices, supramolecular chemistry, inkjet printing of polymers, polymers for energy storage, and self-healing materials.

Publication 2

Homo- and diblock copolymers of poly(furfuryl glycidyl ether) by living anionic polymerization: Towards reversibly core-crosslinked micelles

M. J. Barthel, T. Rudolph, S. Crotty, F. H. Schacher, U. S. Schubert

J. Polym. Sci., Part A: Polym. Chem. **2012**, *50*, 4958-4965.

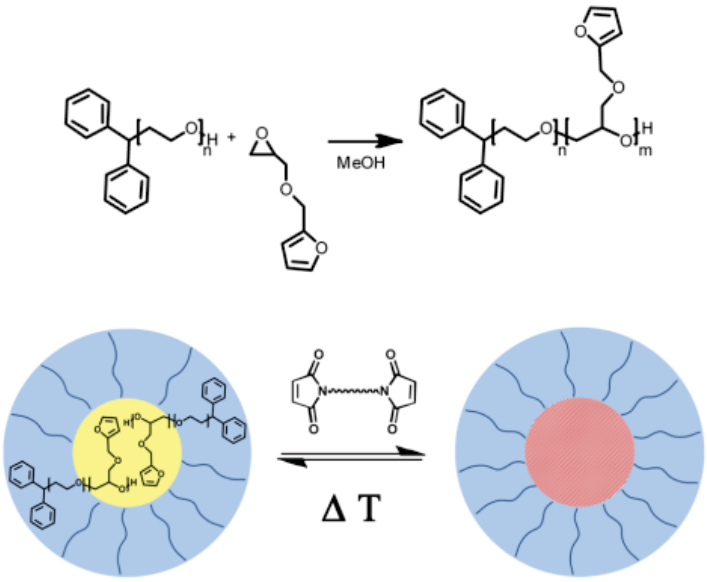

Homo- and Diblock Copolymers of Poly(furfuryl glycidyl ether) by Living Anionic Polymerization: Toward Reversibly Core-Crosslinked Micelles

Markus J. Barthel,[1,2,3]* Tobias Rudolph,[1,2]* Sarah Crotty,[1,2,3] Felix H. Schacher,[1,2] Ulrich S. Schubert[1,2,3]

[1]Laboratory of Organic and Macromolecular Chemistry (IOMC), Friedrich-Schiller-University Jena, Humboldtstr 10, 07743 Jena, Germany
[2]Jena Center for Soft Matter (JCSM), Friedrich-Schiller-University Jena, Humboldtstr. 10, 07743 Jena, Germany
[3]Dutch Polymer Institute (DPI), John F. Kennedylaan 2, 5612 AB Eindhoven, The Netherlands
Correspondence to: U. S. Schubert (E-mail: ulrich.schubert@uni-jena.de) or F. H. Schacher (E-mail: felix.schacher@uni-jena.de)

Received 26 July 2012; accepted 6 August 2012; published online 29 August 2012
DOI: 10.1002/pola.26327

ABSTRACT: We report the synthesis and characterization of well-defined homo- and diblock copolymers containing poly(furfuryl glycidyl ether) (PFGE) via living anionic ring-opening polymerization using different initiators. The obtained materials were characterized by SEC, MALDI-TOF MS, and ^{1}H NMR spectroscopy and molar masses of up to 9400 g/mol were obtained for PFGE homopolymers. If the amphiphilic diblock copolymer PEG-*block*-PFGE was dissolved in water, micelles with a PFGE core and a PEG corona were formed. Hereby, the hydrophobic PFGE core domains were used for the incorporation of a suitable bismaleimide and heating to 60 °C induced the crosslinking of the micellar core via Diels-Alder chemistry. This process was further shown to be reversible. © 2012 Wiley Periodicals, Inc. J Polym Sci Part A: Polym Chem 50: 4958–4965, 2012

KEYWORDS: anionic polymerization; block copolymers; crosslinking; furfuryl glycidyl ether; poly(ethylene glycol); ring-opening polymerization; self-assembly; self-healing

INTRODUCTION The preparation of micellar structures with controlled size, solubility, and surface chemistry for example, the controlled uptake and/or delivery of guest substances in selected compartments has rapidly increased over the last years.[1,2] Quite often, poly(ethylene glycol) (PEG) has been employed as the hydrophilic block, as PEG is non-toxic, chemically inert and highly water-soluble.[3,4]

For the preparation of well-defined, functionalized PEG and related poly(glycidyl ethers) with controlled molar masses, low polydispersity indices (PDIs), and predictable architectures, living anionic ring-opening polymerization (ROP) represents a powerful tool. Poly(glycidyl ethers) offer the possibility to introduce additional side-chain functionality into polyether-based polymers and block copolymers. This has been shown for example, PEG-*block*-poly(allyl glycidyl ether) block copolymers and their self-assembly into micelles in aqueous solution.[5] The PAGE segment enables post-polymerization modifications using thiol-ene chemistry and, therefore, the covalent attachment of drugs or bioactive moieties.[6–10] In that respect, Hrubý reported the attachment of doxorubicin, a drug commonly used in cancer therapy, to the PAGE compartment featuring a pH-sensitive linker to enable the selective cleavage of the drug at the target.[11] Besides PAGE, ethoxy ethyl glycidyl ether (EEGE),[12,13] or isopropyliden glyceryl glycidyl ether can be used for the synthesis of functional polyethers.[14]

An additional possibility for a (reversible) post-polymerization functionalization is the introduction of furfuryl groups. Kavita et al. used furfuryl methacrylate as a comonomer in the ATRP of methacrylates.[15] After polymerization, the furfuryl groups could be used in a subsequent Diels-Alder reaction for example, cross-linking and network formation.[16,17] Further heating above a certain temperature can be used to induce a retro-Diels-Alder reaction, resulting in a cleavage of the network junctions. Subsequent cooling restores the network and the process was shown to be fully reversible. One possible application field for these systems are self-healing materials, as recently demonstrated for PEG-based networks.[18,19] As an example for polyethers carrying furfuryl moieties in the side-chain, poly(furfuryl glycidyl ether) (PFGE) has been prepared using condensation reactions but with limited control over molar mass, molecular architecture, and PDI values.[20]

*Author Markus J. Barthel and Author Tobias Rudolph contributed equally to this work.

Additional Supporting Information may be found in the online version of this article.

Here, we report the synthesis of well-defined PFGE homopolymers and the corresponding poly(ethylene glycol)-*block*-poly(furfuryl glycidyl ether) (PEG_{139}-*b*-$PFGE_{12}$) diblock copolymer by living anionic ROP using different initiators [Diphenylmethyl potassium DPMK, sodium hydride (NaH), cesium hydroxide monohydrate (CsOH), and potassium *t*-butanolate (*t*-BuOK)]. Due to the hydrophobic nature of the PFGE block, poly(ethylene glycol)-*block*-PFGE (PEG-*b*-PFGE) diblock copolymers undergoes self-assembly in dilute aqueous solution into micelles with a PFGE core and a PEG corona. We show that a suitable crosslinker, 1-1′-(methylenedi-4,1-phenylene)bismaleimide (BMA), can be successfully encapsulated within the PFGE core domains and used for core-crosslinking upon heating of the micellar solution to 60 °C. This could be verified by dialysis of the aggregates into non-selective solvents (THF, DMF) where the micellar structure could be retained. We further demonstrate that the crosslinking process is reversible to a certain extent.

EXPERIMENTAL

Instruments

^{1}H NMR spectra were recorded on a Bruker AC 300 MHz. Size exclusion chromatography was performed on either a Shimadzu SCL-10 A system (with a LC-10AD pump, a RID-10 A refractive index detector, and a PL gel 5 μm mixed-D column at 25 °C) where the eluent was a mixture of chloroform:triethylamine:isopropanol (94:4:2) with a flow rate of 1 mL/min or on an Agilent Technologies 1200 Series SEC system equipped with a G131A isocratic pump, a G1329A autosampler, a G1362A refractive index detector, and both a PSS Gram 30 and a PSS Gram 1000 columns in series. 2.1% LiCl solution in DMA was used as eluent at 1 mL/min flow rate at a column oven temperature of 40 °C. Both systems were calibrated with PEG standards from PSS (M_n = 1470–42000 g/mol).

MALDI-TOF mass spectra were obtained using an Ultraflex III TOF/TOF mass spectrometer (Bruker Daltonics) with *trans*-2-[3-(4-*tert*-butylphenyl)-2-methyl-2-propenylidene] malononitrile or 2,5-dihydroxybenzoic acid as matrix in reflector as well as in linear mode. The instrument was calibrated prior to each measurement with an external PMMA standard from PSS Polymer Standards Services GmbH.

DLS was performed at a scattering angle of 90° on an ALV CGS-3 instrument and a He–Ne laser operating at a wavelength of λ = 633 nm at 25 °C. The CONTIN algorithm was applied to analyze the correlation functions obtained. Apparent hydrodynamic radii were calculated according to the Stokes–Einstein equation. All CONTIN plots are number-weighted.

Transmission electron microscopy (TEM) was performed on a Zeiss-CEM 902A, Oberkochen, Germany operating at 80 kV. Images were recorded using a 1k TVIPS FastScan CCD camera. No staining of the samples was necessary. For sample preparation, a drop of the micellar solution was cast onto carbon-coated TEM grids, the solvent was blotted away using filter paper, and the structures were imaged after drying.

Materials

Ethylene oxide (EO), furfuryl glycidyl ether (FGE), sodium hydride in mineral oil, potassium *t*-butanolate, cesium hydroxide monohydrate, *N, N*-dimethylformamide (DMF), tetrahydrofuran (THF), and toluene were purchased from Aldrich. Toluene was used directly from a solvent purification system (PureSolv, Innovative Technology). THF was distilled from sodium/benzophenone. EO was distilled from sodium. FGE was purified by column chromatography (eluent: ethylacetate/*n*-hexane 5/1) and vacuum drying before usage. Diphenylmethyl potassium (DPMK) was synthesized as reported previously.[1] Sodium hydride was washed with dry cyclohexane to remove the mineral oil and stored under argon. Cesium hydroxide was suspended in dry toluene and the solvent was removed under vacuum at 90 °C to dry the cesium hydroxide. The PEG precursor was synthesized via living anionic ROP of EO with DPMK in THF in a BüchiGlasUster PicoClave and dried via azeotropic distillation under vacuum from dry toluene. *t*-BuOK was used as received.

Polymerization of FGE in the Bulk

t-BuOK (5.6 mg, 0.05 mmol) were transferred into a Schlenk flask under inert conditions and 0.45 mL FGE (3.24 mmol, the ratio M:I was 65:1, $M_{n,theo}$ = 10,000 g/mol) were added. The mixture was kept for 24 h at 45 °C under vigorous stirring. The reaction was terminated by the addition of 0.1 mL methanol and the product was dried under vacuum. SEC: M_n = 5500 g/mol, PDI = 1.18. The synthesis of PFGE using NaH, CsOH, and DPMK as initiators was carried out using the same procedure.

Polymerization of FGE in Solution

Four milliliter of freshly prepared THF were transferred into a Schlenk flask and 0.071 mL DPMK (0.05 mmol) were added. Afterwards, 0.45 mL (FGE, 3.24 mmol, ratio of M:I was 65:1, and $M_{n,theo}$ = 10,000 g/mol) were introduced and the reaction was allowed to stir for 24 h at 45 °C. The reaction was terminated by the addition of 0.5 mL methanol and the product was dried under vacuum.

^{1}H NMR (300 MHz, DMSO-d_6, δ, ppm): 3.6–3.2 (br, 5H), 3.9 (t, 1H), 4.42 (s, 2H), 6.28 (m, 2H), 7.26–7.1 (m, 10H), and 7.36 (s, 1H). SEC: M_n = 2900 g/mol, PDI = 1.09; MALDI-TOF MS: M_p = 8200 g/mol.

The synthesis of PFGE using NaH, CsOH, and DPMK as initiators was carried out using the same procedure.

Synthesis of PEG-*b*-PFGE

One gram monohydroxy-functionalized PEG ($M_{p,MALDI}$ = 6100 g/mol, 0.16 mmol) was dried under vacuum at 75 °C for 2 h and dissolved in 10 mL freshly prepared THF. To activate the hydroxyl group, a stoichiometric amount of DPMK was added until the solution remained slightly red. FGE (0.73 mL, 5.3 mmol) were added and the reaction mixture was stirred for 24 h at 45 °C. The reaction was terminated by the addition of 0.5 mL methanol and the crude polymer was purified by precipitation in cold diethyl ether and dried under vacuum.

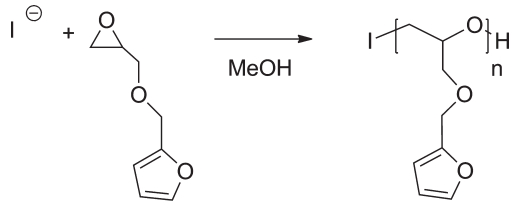

FIGURE 1 Schematic representation of the homopolymerization of FGE.

^{1}H NMR (300 MHz, DMSO-d_6, δ, ppm): 3.65–3.15 (br, PEG-backbone), 3.95 (t, 1H), 4.3 (s, 2H), 6.3 (m, 2H), 7.2–7.05 (m, 10H), 7.5 (s, 1H). SEC: M_n = 6000 g/mol, PDI = 1.06; MALDI-TOF MS: M_p = 8050 g/mol

RESULTS AND DISCUSSION

Synthesis of PFGE

The living anionic ring-opening polymerization (AROP) of allyl glycidyl ether (AGE) or EEGE represents a facile strategy for the introduction of functional groups into polyether-based materials, thus enabling post-polymerization functionalizations.[14] In most cases, click chemistry is used to modify the polymer and to adjust its properties, either in solution or in the bulk. FGE is another promising monomer for anionic ROP and subsequent post-polymerization functionalization via the pendant furane ring by, for example, Diels-Alder reactions. However, FGE was up to now only used in condensation reactions, exhibiting limited control over molar masses or PDI values.[20]

FGE was purified by column chromatography, followed by vacuum drying before usage in anionic ROP reactions. The homopolymerization in THF was first studied using DPMK as initiator, synthesized according to literature procedures.[21] For this system lower molar masses than expected were observed, even if longer reaction times (48 h) were used. Therefore, a general study of the FGE homopolymerization was performed. Hereby, we focused on different initiators for the AROP [DPMK, sodium hydride (NaH), cesium hydroxide monohydrate (CsOH), and potassium *t*-butanolate (*t*-BuOK)] (Fig. 1).

TABLE 1 Characterization Data for the PFGE Homopolymers Initiated Using Different Initiators in Bulk and in Solution

	In Bulk			In THF		
Initiator	M_n[a]	M_w[a]	PDI[a]	M_n[a]	M_w[a]	PDI[a]
NaH	2700	3200	1.18	–	–	–
CsOH	2800	3300	1.18	865	900	1.06
DPMK	3100	3500	1.11	2800	3150	1.09
t-BuOK	5500	7000	1.28	2900	3100	1.10

[a] Obtained by SEC ($CHCl_3$:*i*-Prop.:TEA 94:4:2, using PEG standards).

In addition, to study the influence of THF as solvent, the reactions were performed in solution as well as in the bulk. It can be clearly seen from the SEC traces [Fig. 2(a); Table 1] that *t*-BuOK (solid black line, $M_{n,app}$ = 5500 g/mol) lead to (apparently) higher molar masses than DPMK (dashed black line, $M_{n,app}$ = 3100 g/mol) under bulk conditions. CsOH (dotted black line, $M_{n,app}$ = 2800 g/mol), and NaH (black line with alternating dots and dashes, $M_{n,app}$ = 2700 g/mol) lead to even lower molar masses. However, coupling products were observed in case of *t*-BuOK, DPMK, and CsOH (bimodal distributions), as well as a broadening of the molar mass distribution using NaH as initiator.

To obtain a full picture, all initiators for the anionic ROP were also tested in THF. The results are displayed in Figure 2(b) and Table 1. The best results were obtained in case of *t*-BuOK (solid black line, $M_{n,app}$ = 2900 g/mol), leading to well-defined PFGE with higher molar masses as DPMK (dotted black line, $M_{n,app}$ = 2800 g/mol). No polymer was obtained for NaH, whereas CsOH (dashed black line, $M_{n,app}$ = 865 g/mol) again yielded lower molar masses.

For a detailed characterization of the obtained homopolymers, the DPMK initiated sample was studied using MALDI-TOF MS and ^{1}H NMR spectroscopy [Fig. 3(a,b)].

In this case, a molar mass (M_p) of 8200 g/mol could be determined by MALDI-TOF MS. The observed isotopic pattern in MALDI-TOF MS [Fig. 3(a), inset] corresponds well to

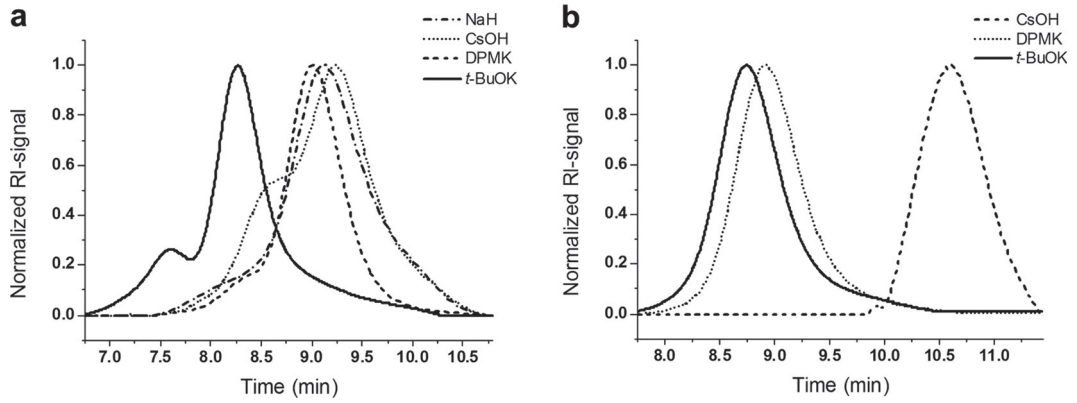

FIGURE 2 SEC traces for PFGE obtained by homopolymerization in bulk (a) and in THF (b) using different initiators for living anionic ROP.

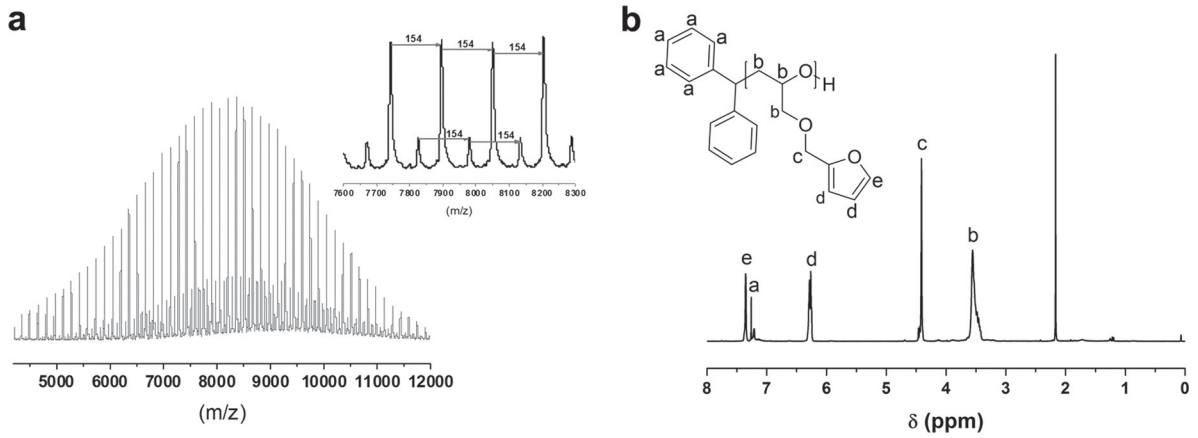

FIGURE 3 MADLI-TOF MS spectrum (a) and ^{1}H NMR (DMSO-d_6, 300 MHz) spectrum (b) of PFGE.

the calculated mass distribution with a repeating unit of 154 g/mol. The small second distribution can be attributed to side-reactions occurring during the measurement. In the ^{1}H NMR spectrum [Fig. 3(b)], the characteristic peaks for the furane ring at 7.36 and 6.26 ppm (e and d), as well as the signals for the phenyl groups of the initiator at 7.26 ppm (a) could be detected. It could be observed that the polymer shows significantly lower molar masses in the SEC measurements in comparison to the values determined by NMR and MALDI-TOF MS.

To probe the reaction kinetics for FGE, a polymerization aiming at a molar mass (M_n) of 10,000 g/mol (ratio of M:I was 65:1) using *t*-BuOK as initiator was performed in THF and monitored by a combination of SEC and ^{1}H NMR measurements. The results are displayed in Figure 4 and Table 2.

As shown in Figure 4(a) in the SEC measurements, almost no increase in the molar mass can be seen after 12 h. The conversion of the monomer was simultaneously monitored by ^{1}H NMR spectroscopy (Supporting Information Figure S1a) via the decrease of the characteristic signal of the proton next to the oxirane ring at 3.05 ppm. The signal of the two protons of the furane ring [Fig. 2(d)] was used as an internal standard. For the T24 sample ($M_{n,app}$ = 3450 g/mol) a monomer conversion of ~100% could be obtained, whereas T12 ($M_{n,app}$ = 3450 g/mol) yielded 90% FGE consumption. The living character of the polymerization is demonstrated by the semilogarithmic plot of the monomer concentration at t = 0 (M_0) divided by the concentration at $t = n$ (M_n) as displayed in Supporting Information Figure S1b. As shown in Figure 4(b), MALDI-TOF MS measurements yielded a molar mass (M_p) of 9400 g/mol for T24, being in good agreement with the targeted value of 10,000 g/mol. The small differences can be attributed to the handling of the initiator in very small amounts (6 mg *t*-BuOK) in the glovebox.

Synthesis of PEG-*b*-PFGE

For the synthesis of an AB diblock copolymer, PEG-*b*-PFGE, sequential anionic ROP of EO and FGE, respectively [Fig. 5(a)] was performed. As initiator, DPMK was used due to the possibility of an exact titration of the hydroxyl groups of the PEG macroinitiator, presumably avoiding the formation of homopolymer due to an excess of initiator. The PEG

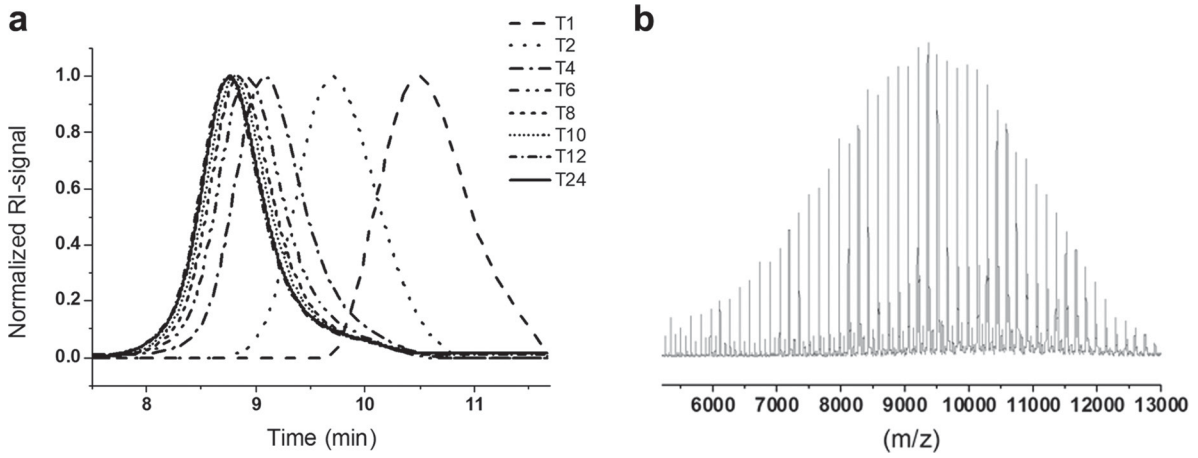

FIGURE 4 SEC traces for a kinetic study of the PFGE homopolymerization (a) and the corresponding MALDI-TOF MS spectrum of the final product (b, M_p = 9400 g/mol).

TABLE 2 Characterization Data for the Kinetic Study of the PFGE Homopolymerization

Sample	M_n[a]	M_w[a]	PDI[a]	Conversion[b] (%)
PFGE T1	900	1000	1.11	11
PFGE T2	1800	1900	1.07	30
PFGE T4	2750	3050	1.11	45
PFGE T6	3150	3500	1.10	64
PFGE T8	3300	3700	1.11	77
PFGE T10	3400	3800	1.12	82
PFGE T12	3450	3850	1.12	90
PFGE T24	3450	3850	1.12	100

[a] Obtained by SEC ($CHCl_3$:*i*-Prop.:TEA 94:4:2, using PEG standards).
[b] Determined by ^{1}H NMR.

precursor was prepared using DPMK as initiator for EO in THF.[21] The corresponding macroinitiator, PEG-OH with a molar mass (M_n) of 6100 g/mol and a PDI value of 1.05, was subsequently reactivated using DPMK, followed by the addition of FGE. MALDI-TOF MS [Fig. 5(b)] revealed a molar mass (M_n) of 8050 g/mol for the obtained PEG-*b*-PFGE diblock copolymer. Both PEG-OH and PEG-*b*-PFGE were further analyzed by SEC [Fig. 5(c)] and a shift to lower elution volume as well as a narrow PDI of 1.06 was obtained for the diblock copolymer.

The characteristic signals of the PEG backbone (3.5–3.2 ppm) and the furfuryl groups in the side-chain (7.5, 6.3, and 4.3 ppm) are also visible in the ^{1}H NMR spectrum (Supporting Information Fig. S2), resulting in a composition of PEG_{139}-*b*-$PFGE_{12}$, where the subscripts denote the degrees of polymerization of the respective segment.

As shown in Table 3 for PEG-*b*-PFGE, the obtained molar mass (M_n) of 8200 g/mol is significantly lower than the calculated one with 10,000 g/mol. One possible explanation for this could be the formation of aggregates during the polymerization in THF, thus limiting the molar mass. If the diblock copolymer is directly dissolved in THF, dynamic light scattering (DLS) yields mainly unimolecular polymer chains ($R_{h,app}$ = 4 nm), but also larger aggregates ($R_{h,app}$ = 300 nm) after 24 h (Supporting Information Fig. S3). This confirms the results obtained for the homopolymerization of FGE using different initiators, that is, that the ROP of FGE in THF does not reach full conversion if DPMK is used as an initiating system. Nevertheless, THF remained the solvent of choice due the even larger aggregates (~100 nm) formed immediately after dissolving PEG-*b*-PFGE in toluene and the insolubility of PEG-*b*-PFGE in cyclohexane or ethylbenzene.

Self-Assembly of PEG-*b*-PFGE in Water

Due to its amphiphilic nature, PEG_{139}-*b*-$PFGE_{12}$ forms micelles in dilute aqueous solution, as demonstrated using DLS experiments. The structures presumably consist of a hydrophobic PFGE core and a hydrophilic PEG corona [Fig. 6(a)] and we assume a spherical shape of the particles.

Directly after dissolution in water, micelles of $R_{h,app}$ = 10 nm and with a rather narrow size-distribution were obtained

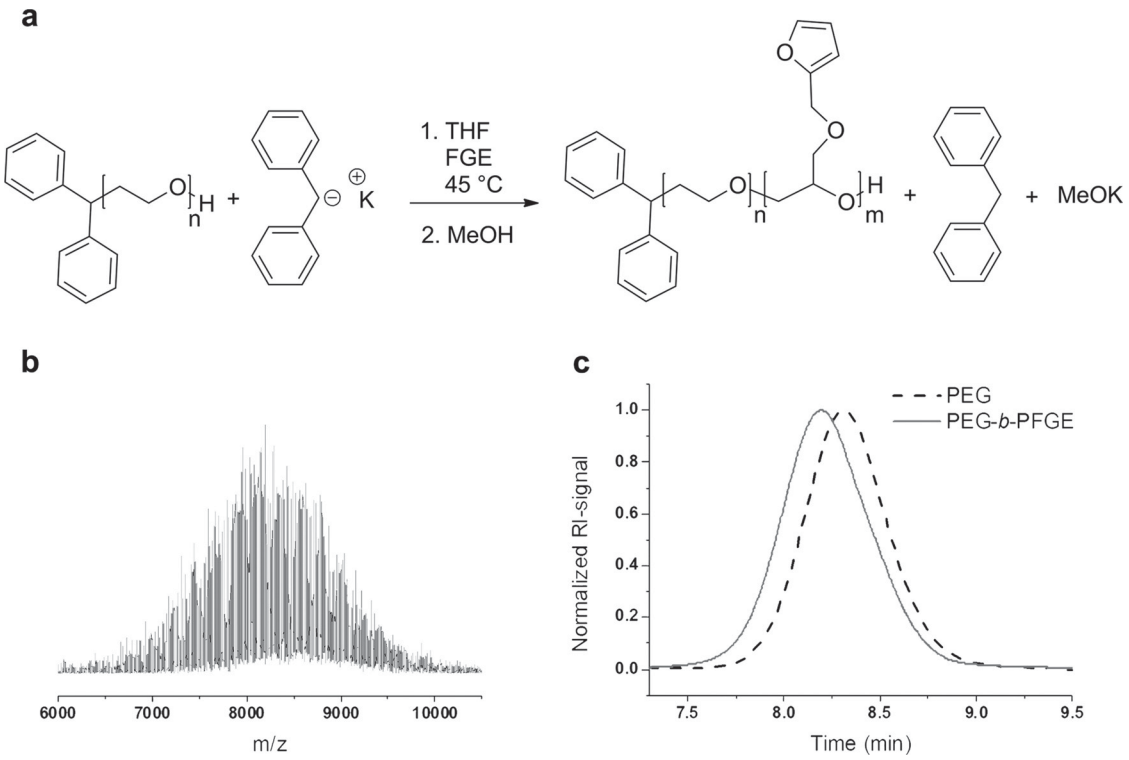

FIGURE 5 Synthesis of PEG-*b*-PFGE using sequential living anionic ROP (a), MALDI-TOF MS spectrum (b), and SEC traces for the PEG precursor (dashed black line) and PEG-*b*-PFGE (c, solid gray line).

TABLE 3 Characterization Data for Homopolymers and Block Copolymers

Sample	$M_{n,theo}$ (g/mol)	$M_{n,SEC}$ (g/mol)	$M_{p,MALDI}$ (g/mol)	PDI
PEG[a]	5000	5100[b]	6100	1.05[b]
PEG_{139}-*b*-$PFGE_{12}$[c]	10,000	6000[b]	8050	1.06[b]

[a] Precursor.
[b] Obtained by SEC ($CHCl_3$:*i*-Prop.:TEA 94:4:2, using PEG standards).
[c] Subscripts denote the degrees of polymerization of the corresponding block determined by ^1H NMR spectroscopy.

(Supporting Information Fig. S3a). The core-forming block, PFGE, can now be crosslinked via a Diels-Alder reaction, using a bisfunctional crosslinker, for example, a bismaleimide [Reaction scheme in Fig. 6(a)]. The controlled crosslinking of selected domains in micellar structures is desirable and can be used to enhance their resistance against degradation, limit the diffusion of guest molecules into or out of the core domains, or ensure the stability within desired environments.[22–24]

In our case, crosslinking of the micellar core was achieved by a [4 + 2] cycloaddition reaction [Fig. 6(a)]. For this purpose, PEG_{139}-*b*-$PFGE_{12}$ and a bisfunctional crosslinker, 1-1′-(methylenedi-4,1-phenylene)bismaleimide (BMA), were dissolved in DMF at a concentration of 15 g/L and a molar ratio crosslinker/PFGE of 50/1. To encapsulate the BMA linker within the hydrophobic PFGE core domains, water was slowly added until a turbid solution was obtained (water:DMF = 2:1). The remaining DMF was then removed by dialysis against water and the resulting aqueous solution was analyzed by DLS. The exact amount of encapsulated material is difficult to estimate, as BMA is insoluble in water and partially precipitated during dialysis. For the PEG_{139}-*b*-$PFGE_{12}$ micelles containing BMA in the core, a radius of $R_{h,app}$ = 6 nm was detected in water afterwards. To induce crosslinking of the core domains, the solution was subsequently heated to 60 °C for several hours. According to DLS, the micellar size did not change significantly upon the crosslinking procedure [Fig. 6(b)]. To prove the successful crosslinking of the PFGE core, the micelles were transferred to nonselective solvents for both blocks, THF and DMF. Therefore, the aqueous micellar solution was poured into an excess of, for example, THF so that the ratio was THF:H_2O = 6:1 (concentration = 0.8 g/L), dialyzed against THF and again analyzed by DLS [Fig. 6(c)]. Here, micelles with a radius of $R_{h,app}$ = 15 nm could be detected. The increase in size can be explained by a certain swelling of the crosslinked PFGE core in THF as a nonselective solvent. In a next step, the solvent was removed under vacuum and DMF as an alternative nonselective solvent was added (concentration = 1.6 g/L). Again, DLS studies revealed micelles with a solvent-swollen PFGE core and a radius of $R_{h,app}$ = 10 nm even after several days [Fig. 6(d)]. These results clearly indicate a successful crosslinking of the PFGE core. The structure of the PEG-*b*-PFGE micelles was also investigated using TEM (Fig. 7). As can be seen, spherical structures with diameters of ~20 nm but also larger species, most probably due to aggregation occurring during the drying process, can be

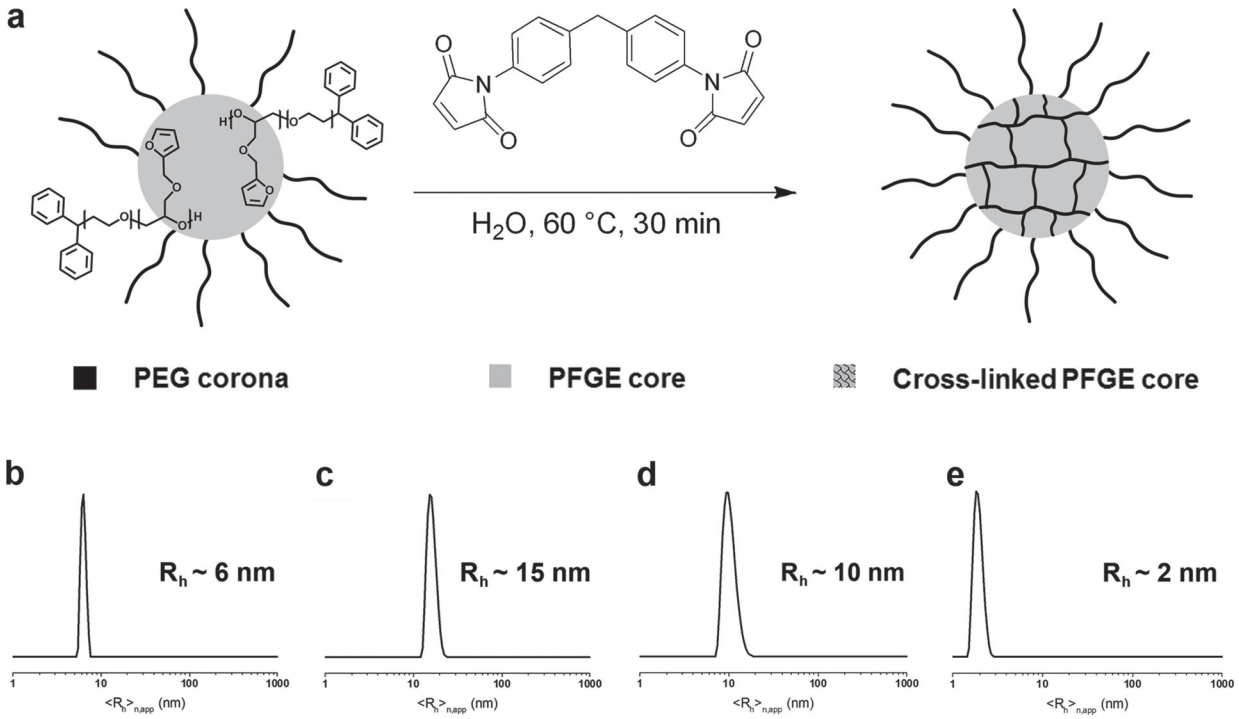

FIGURE 6 Crosslinking of the micellar core (a), number-weighted DLS CONTIN plots for PEG-*b*-PFGE micelles in water after crosslinking (b), in THF (c), and DMF (d), and after the retro-Diels-Alder reaction in DMF (e).

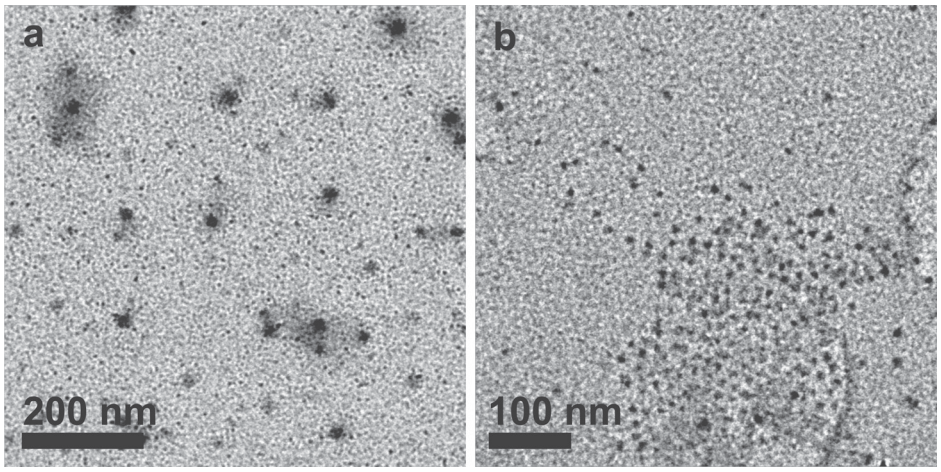

FIGURE 7 TEM micrographs of PEG_{139}-*b*-$PFGE_{12}$ micelles cast from aqueous solution (a) or after crosslinking of the PFGE core and subsequent dialysis to THF (b) onto carbon-coated TEM grids.

observed directly after dissolution of PEG_{139}-*b*-$PFGE_{12}$ in water [Fig. 7(a)]. The dark spots represent the PFGE core; the PEG corona is not visible under these conditions. After crosslinking of the PFGE core and subsequent dialysis into THF, again spherical micelles can be observed [Fig. 7(b)]. Here, core sizes of 10–20 nm are observed, again proving a successful crosslinking of the PFGE core domains.

Additionally, the crosslinking could be proven by the disappearance of the furan signals (6.3 and 4.3 ppm, Fig. 8) in ^{1}H NMR after prolonged heating at 60 °C (Fig. 8). Moreover, a new signal (5.3 ppm) appears which can be assigned to the double bond formed during the DA reaction. Although this indicates complete consumption of the furan moieties, the exact amount of encapsulated BMA is unknown and the presence of unreacted PFGE cannot be excluded. As the crosslinking via Diels-Alder chemistry should be reversible, the micellar solution was further heated to higher temperatures (150 °C) for 30 min in DMSO. As shown in Figure 8, the signals for the furan ring reappear, but also the signal for the cross-linked species is still present. Integration suggests that ~50% of the core undergo retro-DA reactions under these conditions, also for longer reaction times (6 h). Nevertheless, DLS after 2 h shows that unimolecular block copolymer chains are present [$R_{h,app}$ = 2 nm, Fig. 6(e)]. Presumably, the dissolution of the micellar core leads increases the conformational freedom of the polymer chains and decreases the concentration of reaction sites, which might explain the incomplete retro-DA reaction.

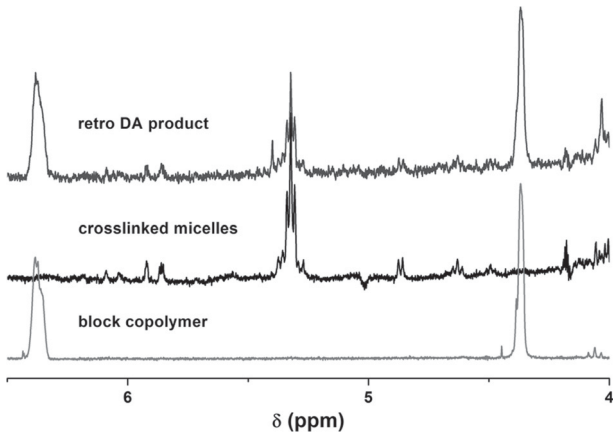

FIGURE 8 Characteristic region of the ^{1}H NMR (DMSO, 300 MHz) spectrum of PEG-*b*-PFGE, core-crosslinked micelles, and the retro-Diels-Alder product.

CONCLUSION

In summary, we synthesized well-defined homo- and diblock copolymers containing FGE with a narrow molar mass distribution (PDI < 1.1), molar masses (M_p) of up to 9400 g/mol for PFGE, and studied the influence of different initiators and the reaction kinetics in detail. For the PEG_{139}-*b*-$PFGE_{12}$ diblock copolymer, self-assembly in aqueous solution resulted in the formation of well-defined spherical micelles with a PFGE core and a PEG corona. One intriguing feature of the herein employed hydrophobic domain, PFGE, is that it can be reversibly crosslinked using Diels-Alder chemistry. The core-crosslinked micelles retain their structure in nonselective solvents like THF or DMF. For the retro-DA process, however, high temperatures are necessary and only a conversion of 50% could be observed. Nevertheless, the micellar cores were shown to disassemble into unimolecular chains. One possible improvement regarding the crosslinking process could be the use of a bismaleimide linker with a less rigid or pH-labile spacer, improving either the solubility or a triggered dissolution of the micellar cores. Although the initial results reported here describe only one single diblock copolymer (PEG_{139}-*b*-$PFGE_{12}$), the concept could be convincingly demonstrated. In the future, we will extend this to block copolymers with different weight fractions, giving access to other and also more complex morphologies in solution.[25] Whereas the reversible crosslinking of the core in spherical core-corona systems might be interesting for controlled release or surface patterning from non-selective solvents, such processes would be very

appealing if applied to vesicular,[26] tubular, or cylindrical structures.[27]

ACKNOWLEDGMENTS

The authors wish to acknowledge the Dutch Polymer Institute (DPI, technology area high-throughput-experimentation, project #690) and the Thuringian Ministry for Education, Science and Culture (grant #B514-09051, NanoConSens) for financial support of this study. F. H. S. and T. R. are grateful to the Thuringian Ministry for Education, Science, and Culture (TMBWK; #B515-10065, ChaPoNano) for financial support.

REFERENCES AND NOTES

1 Tyrrell, Z. L.; Shen, Y. Q.; Radosz, M. *Prog. Polym. Sci.* **2010**, *35*, 1128–1143.

2 Schacher, F. H.; Rupar, P. A.; Manners, I. *Angew. Chem. Int. Ed.* **2012**, *51*, 7898–7921.

3 Harris, J. M.; Chess, R. B. *Nat. Rev. Drug. Discov.* **2003**, *2*, 214–221.

4 Knop, K.; Hoogenboom, R.; Fischer, D.; Schubert, U. S. *Angew. Chem. Int. Ed.* **2010**, *49*, 6288–6308.

5 Hruby, M.; Konak, C.; Ulbrich, K. *J. Appl. Polym. Sci.* **2005**, *95*, 201–211.

6 Koyama, Y.; Umehara, M.; Mizuno, A.; Itaba, M.; Yasukouchi, T.; Natsume, K.; Suginaka, A.; Watanabe, K. *Bioconjugate Chem.* **1996**, *7*, 298–301.

7 Obermeier, B.; Frey, H. *Bioconjugate Chem.* **2011**, *22*, 436–444.

8 Ozdemir, F.; Keul, H.; Mourran, A.; Möller, M. *Macromol. Rapid. Commun.* **2011**, *32*, 1007–1013.

9 Hunt, J. N.; Feldman, K. E.; Lynd, N. A.; Deek, J.; Campos, L. M.; Spruell, J. M.; Hernandez, B. M.; Kramer, E. J.; Hawker, C. J. *Adv. Mater.* **2011**, *23*, 2327–2331.

10 Barthel, M. J.; Babiuch, K.; Rudolph, T.; Vitz, J.; Hoeppener, S.; Gottschaldt, M.; Hager, M. D.; Schacher, F. H.; Schubert, U. S. *J. Polym. Sci. Part A: Polym. Chem.* **2012**, *50*, 2914–2923.

11 Hruby, M.; Konak, C.; Ulbrich, K. *J. Controlled Release* **2005**, *103*, 137–148.

12 Reinicke, S.; Schmelz, J.; Lapp, A.; Karg, M.; Hellweg, T.; Schmalz, H. *Soft Matter* **2009**, *5*, 2648–2657.

13 Toy, A. A.; Reinicke, S.; Müller, A. H. E.; Schmalz, H. *Macromolecules* **2007**, *40*, 5241–5244.

14 Obermeier, B.; Wurm, F.; Mangold, C.; Frey, H. *Angew. Chem. Int. Ed.* **2011**, *50*, 7988–7997.

15 Kavitha, A. A.; Singha, N. K. *J. Polym. Sci. Part A: Polym. Chem.* **2007**, *45*, 4441–4449.

16 Kavitha, A. A.; Singha, N. K. *Macromolecules* **2010**, *43*, 3193–3205.

17 Bergman, S. D.; Wudl, F. *J. Mater. Chem.* **2008**, *18*, 41–62.

18 Imbesi, P. M.; Fidge, C.; Raymond, J. E.; Cauet, S. I.; Wooley, K. L. *ACS Macro Lett.* **2012**, *1*, 473–477.

19 Tian, Q. A.; Rong, M. Z.; Zhang, M. Q.; Yuan, Y. C. *Polym. Int.* **2010**, *59*, 1339–1345.

20 Pratama, P. A.; Peterson, A. M.; Palmese, G. R. *Macromol. Chem. Phys.* **2012**, *213*, 173–181.

21 Normant, H.; Angelo, B. *Bull. Soc. Chim. Fr.* **1960**, *2*, 354–359.

22 Kim, Y.; Pourgholami, M. H.; Morris, D. L.; Stenzel, M. H. *Biomacromolecules* **2012**, *13*, 814–825.

23 Schacher, F.; Walther, A.; Ruppel, M.; Drechsler, M.; Müller, A. H. E. *Macromolecules* **2009**, *42*, 3540–3548.

24 O'Reilly, R. K.; Hawker, C. J.; Wooley, K. L. *Chem. Soc. Rev.* **2006**, *35*, 1068–1083.

25 Percec, V.; Wilson, D. A.; Leowanawat, P.; Wilson, C. J.; Hughes, A. D.; Kaucher, M. S.; Hammer, D. A.; Levine, D. H.; Kim, A. J.; Bates, F. S.; Davis, K. P.; Lodge, T. P.; Klein, M. L.; DeVane, R. H.; Aqad, E.; Rosen, B. M.; Argintaru, A. O.; Sienkowska, M. J.; Rissanen, K.; Nummelin, S.; Ropponen, J. *Science* **2010**, *328*, 1009–1014.

26 Discher, B. M.; Won, Y.-Y.; Ege, D. S.; Lee, J. C.-M.; Bates, F. S.; Discher, D. E.; Hammer, D. A. *Science* **1999**, *284*, 1143–1146.

27 Zhang, X.; Tanner, P.; Graff, A.; Palivan, C. G.; Meier, W. *J. Polym. Sci. Part A: Polym. Chem.* **2012**, *50*, 2293–2318.

Supporting information for

"Homo- and Block Copolymers of Poly(furfuryl glycidyl ether) by Living Anionic Polymerization: Towards Reversibly Core-Crosslinked Micelles"

Markus J. Barthel,[1,2,3§] Tobias Rudolph,[1,2§] Sarah Crotty,[1,2] Felix H. Schacher[1,2]* and Ulrich S. Schubert[1,2,3]*

[1] Laboratory of Organic and Macromolecular Chemistry (IOMC), Friedrich-Schiller-University Jena, Humboldtstr. 10, 07743 Jena, Germany.

[2] Jena Center for Soft Matter (JCSM), Friedrich-Schiller-University Jena, Philospophenweg, 07743 Jena, Germany.

[3] Dutch Polymer Institute (DPI), John F. Kennedylaan 2, 5612 AB Eindhoven, The Netherlands.

§ These authors contributed equally to this work.

Materials and methods:

^{1}H NMR spectra were recorded on a Bruker AC 300 MHz using the residual solvent signal as an internal standard.

DLS was performed at a scattering angle of 90° on an ALV CGS-3 instrument and a He–Ne laser operating at a wavelength of λ = 633 nm at 25 °C. The CONTIN algorithm was applied to analyze the correlation functions obtained. Apparent hydrodynamic radii were calculated according to the Stokes–Einstein equation. All CONTIN plots are number-weighted.

Kinetic study of PFGE:

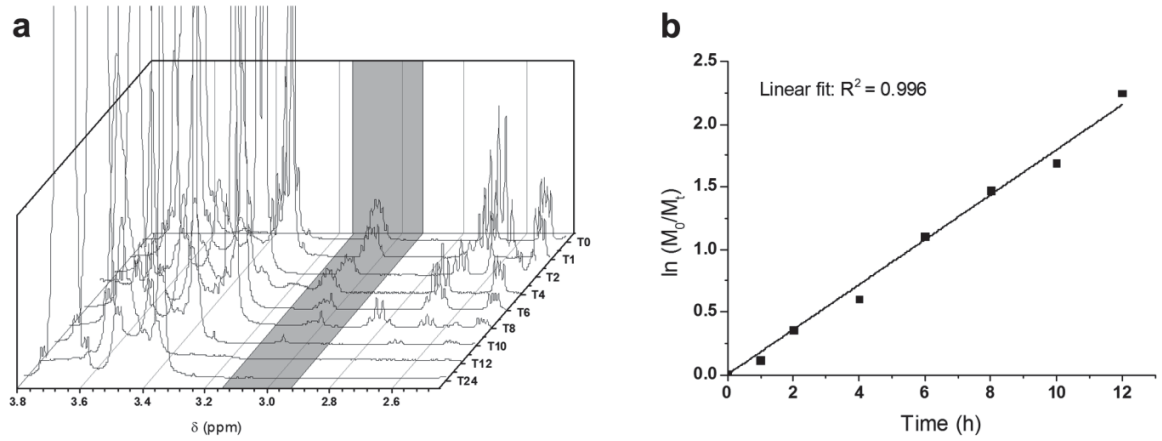

Figure S1. ^{1}H NMR traces of the kinetic study of the PFGE homopolymerization (a) and logarithmic plot of conversion against time (b).

PEG-*b*-PFGE:

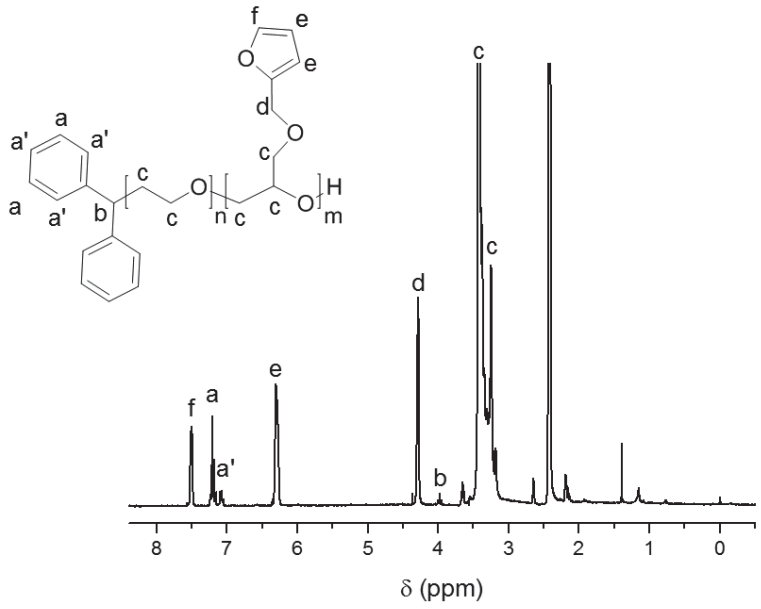

Figure S2: ^{1}H NMR (DMSO-d_6, 300 MHz) spectrum of PEG-*b*-PFGE.

DLS investigations of the diblock copolymer:

For DLS investigations 5 mg of the diblock copolymer PEG-*b*-PFGE were directly dissolved in 1 mL of a selective (H_2O), a non-selective solvent (DMF), as well as in the reaction solvent (THF). The corresponding behavior in solution was investigated and depicted in **Figure S2**. In water the amphiphilic block copolymer forms spherical micelles with a radius of $R_{h,app}$ = 10 nm.

For the reaction solvent, THF, particles with a radius of $R_{h,app}$ = 4 nm were obtained directly after dissolution. Over 24 h, this size increased up to several hundreds of nm and the solution turned slightly turbid, which indicates the formation of large agglomerates/micelles, which might also be an explanation for the lower degree of polymerization for PFGE during the polymerization.

As a non-selective solvent DMF was further used for the investigation of the diblock copolymer in solution showing a monomodal size distribution of $R_{h,app}$ = 2 nm.

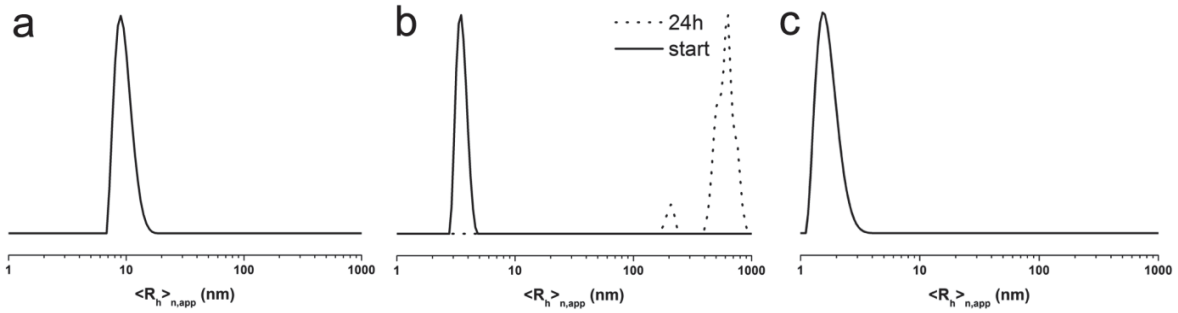

Figure S3: Number-weighted DLS CONTIN plots for PEG-*b*-PFGE in water (a), as well as directly after dissolving in THF and after 24 h in THF (b) or DMF (c).

1. H. Normant, B. Angelo, B. *Bull. Soc. Chim. Fr.* **1960**, 354.

Publication 3

RAFT copolymerization of thioglycosidic glycomonomers with *N*iPAm and subsequent immobilization onto gold nanoparticles

C. von der Ehe, F. Kretschmer, C. Weber, S. Crotty, S. Stumpf,
S. Hoeppener, M. Gottschaldt, U. S. Schubert

in *ACS Symposium Series, Issue Controlled Radical Polymerization*
(Eds.: K. Matyjaszewski, B.S. Summerlin, N.V. Tsarevsky, J. Chiefari),
Wiley-VH Verlag GmbH & Co. KGaA, 2015, pp. 221-256.

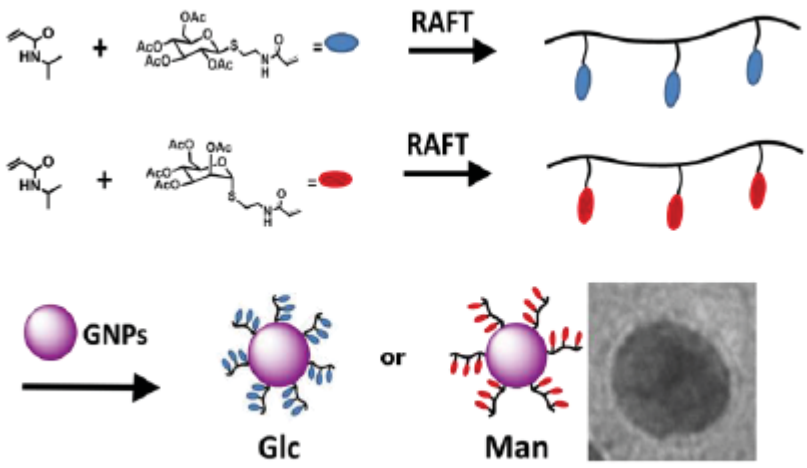

Chapter 15

RAFT Copolymerization of Thioglycosidic Glycomonomers with *N*iPAm and Subsequent Immobilization onto Gold Nanoparticles

C. von der Ehe,[1,2,3] F. Kretschmer,[1,2] C. Weber,[1,2] S. Crotty,[1,2] S. Stumpf,[1,2] S. Hoeppener,[1,2] M. Gottschaldt,[1,2] and U. S. Schubert[1,2,3,*]

[1]Laboratory of Organic and Macromolecular Chemistry (IOMC), Friedrich Schiller University Jena, Humboldtstraße 10, 07743 Jena, Germany
[2]Jena Center for Soft Matter (JCSM), Friedrich Schiller University Jena, Philosophenweg 7, 07743 Jena, Germany
[3]Dutch Polymer Institute (DPI), P.O. Box 902, 5600 AX Eindhoven, The Netherlands
[*]E-mail: ulrich.schubert@uni-jena.de

The synthesis of a new acetyl-protected *S*-glycosidic mannose glycomonomer is reported as well as the copolymerization with *N*-isopropyl acrylamide *via* reversible addition fragmentation chain transfer (RAFT) polymerization. The glycopolymers were deprotected and analyzed *via* ^{1}H NMR spectroscopy, size exclusion chromatography, elemental analysis, FT-IR spectroscopy as well as asymmetric flow field-flow fractionation (AF4) coupled with multi-angle laser light scattering (MALLS). Turbidimetric studies revealed the thermoresponsive properties of the glycopolymers. Subsequent immobilization onto gold nanoparticles was achieved without cleavage of the RAFT endgroup, leading to stable glycosylated nanoparticles, which were investigated towards their protein recognition capabilities, revealing that the mannosylated nanoparticles were able to detect the lectin Concanavalin A at very low concentrations.

In Controlled Radical Polymerization: Materials; Tsarevsky, et al.;
ACS Symposium Series; American Chemical Society: Washington, DC, 2015.

Introduction

Glycopolymers have attracted significant scientific interest in the last decades because of their ability to interact with natural occurring proteins (lectins). This enables synthetic glycopolymers to mimic the role that saccharides on cell-surfaces play in many biological processes (*1*). In order to optimize their properties as receptor mimics, the investigation of these materials is often facilitated by their immobilization, *e.g.* on microarrays (*2–4*). In particular gold nanoparticles (GNPs) with surface-immobilized glycopolymers are very promising for the detection of such interactions due to the surface plasmon resonance of gold nanoparticles (*5–9*). Therefore, glycopolymer-functionalized gold nanoparticles have shown to be very efficient sensors: An immobilized mannose glycopolymer, *e.g.*, was able to detect Concanavalin A (ConA) (*6*). A glycopolymer carrying *O*-glycosidic bound *N*-acetyl glucosamine was used for the detection of wheat germ agglutinin (WGA) (*8*) and a lactose glycopolymer immobilized to gold nanoparticles was able to efficiently detect *ricinus communis* agglutinin (RCA) (*9*).

The synthesis of such GNP-immobilized glycopolymers requires a glycopolymer possessing a thiol- or thioester endgroup. Thus, the reversible addition fragmentation chain transfer (RAFT) polymerization procedure represents the ideal strategy for the design of these materials due to the chemical structure of the RAFT endgroup, which can easily be converted into a thiol endgroup.

The immobilization of such glycopolymers onto gold surfaces, like nanoparticles, has been widely studied in literature, for example using disulfide-bridged glycopolymers (*9–11*), glycopolymers with pendant thiol-groups (*12*) or glycopolymers with thiol-endgroup (*13–15*). However, it was also shown by Ebeling and Vana that polymers with trithiocarbonate endgroups, prepared by RAFT polymerization, can be immobilized directly onto gold nanoparticles without the necessity of endgroup transformation (*16*, *17*). This method has, to the best of our knowledge, not been applied for glycopolymers up to now.

The successful application of immobilized glycopolymers depends also on the stability of the systems. The utilization of methacrylic glycomonomers with *O*-glycosidic linkage at the anomeric position is well-known in literature (*18–20*). However, *S*-glycosidic bound sugars have been shown to be more stable towards enzymatic degradation (*21*, *22*), which would be an advantage for their later application in aqueous systems. Thioglycosidic linked glycopolymers are accessible by, *e.g.*, the post-polymerization modification of polymers *via* thiol-ene reaction (*23–26*). However, the difficult polymerization of alkene functional acrylate or acrylamide monomers favors their synthesis by the polymerization of glycomonomers, at least as far as radical polymerization techniques are adressed.

Therefore, we present a new mannose glycomonomer with *S*-glycosidic instead of *O*-glycosidic linkage between the sugar and the polymerizable group.

Another interesting feature of certain synthetic polymers is the ability to undergo a lower critical solution temperature (LCST) transition, which results in thermoresponsive polymers that undergo a coil-to-globule transition upon exceeding a certain temperature. Thermoresponsive glycopolymers have already

been reported in literature (*27*–*36*). In some of these reports it was shown that the interaction of the respective glycopolymer with an analyte (*e.g.* lectin) could be controlled *via* the temperature (*30*, *33*, *36*).

As a consequence, thermoresponsive glycopolymers which can bind to certain analytes (*e.g.* lectins) could be promising candidates for later applications like affinity chromatography or temperature responsive drug delivery applications.

The LCST behavior of immobilized polymers is difficult to investigate, since common techniques involve the determination of the temperature where the polymer solution becomes turbid (cloud point temperature, T_{CP}). This technique cannot be applied on GNP immobilized systems. Alternatively, the surface plasmon resonance of the GNPs can be exploited for the analysis of the LCST feature (*37*, *38*).

In this contribution, we present new thioglycosidic-linked glucose- and mannose-bearing monomers, which were copolymerized with *N*-*iso*propylacrylamide (*N*iPAm) by RAFT polymerization and subsequently subjected to deprotection reactions. The resulting thermoresponsive glycopolymers were immobilized onto gold nanoparticles, representing - to the best of our knowledge - the first report of thermoresponsive glycopolymers immobilized on the surface of gold nanoparticles. This approach allows to investigate the LCST behavior of the immobilized glycopolymer as well as the lectin binding interaction with the same GNP sensor system.

Experimental Section

Materials and Instrumentation

All chemicals were purchased from Fluka, Sigma Aldrich or Acros Organics and were used without further purification unless otherwise stated. 2-(Butylthiocarbonothioylthio)propanoic acid (BTTCP) was kindly provided by BASF SE. 1,2,3,4,6-Penta-*O*-acetyl-α-d-mannopyranose (ManOAc) was purchased from Carbosynth, 1,2,3,4,6-penta-*O*-acetyl-β-D-glucopyranose (GlcOAc) was purchased from Alfa Aesar. 4,4′-Azobis(4-cyanovaleric acid) (ACVA) was of ≥98% purity (Sigma Aldrich). Spectra/Por® 3 dialysis membranes with molecular weight cut off (MWCO) 3,500 g/mol were purchased from VWR. 2-Mercaptoethylacrylamide was synthesized according to a literature procedure (*39*).

1D (^{1}H, ^{13}C) and 2D nuclear magnetic resonance spectra were recorded at 298 K on a Bruker AC 300 (300 MHz) or a Bruker AC 250 (250 MHz) spectrometer, respectively. The chemical shifts are given in parts per million (ppm) and the residual solvent resonance was used as an internal standard. FT-IR spectra were recorded on an IRAffinity-1 spectrometer from Shimadzu. Elemental analyses were carried out on a CHN-932 Automat Leco instrument. Size exclusion chromatograms (SEC) were measured using an Agilent 1200 series system with a PSS GRAM 1000/30 Å (10 μm particle size) column, a G1310A pump, a G1362A refractive index detector at 40 °C with a flow rate of 1 mL/min. *N,N*-Dimethylacetamide with 0.21% LiCl was used as eluent. Matrix-assisted laser desorption ionization time-of-flight (MALDI-TOF) mass spectra were

measured on an Ultraflex III TOF/TOF mass spectrometer (Bruker Daltonics) with *trans*-2-[3-(4-*tert*-butylphenyl)-2-methyl-2-propenylidene]malononitrile (DCTB) as matrix. The instrument was equipped with a Nd:YAG laser and a collision cell. All spectra were measured in the positive reflector mode. The instrument was calibrated prior to each measurement with an external poly(methyl methacrylate) standard from PSS Polymer Standards Services GmbH in the required measurement range. The MALDI-TOF mass spectra were measured from aliquots of the reaction solutions. BioBeads® S-X1 support for size exclusion chromatography was purchased from Bio Rad, swollen in THF, which was also used as eluent.

Asymmetric flow field-flow fractionation (AF4) was performed on an AF2000 MT System (Postnova Analytics, Landsberg, Germany) coupled to an UV (PN3211, 260 nm), RI (PN3150), MALLS (PN3070, 633 nm) and DLS (ZetaSizer Nano ZS) detector. The eluent is delivered by three different pumps (tip, focus, cross-flow) and the sample is injected by an autosampler (PN5300) into the channel. The channel has a trapezoidal geometry and an overall area of 31.6 cm^2. The nominal height of the spacer was 500 µm and a regenerated cellulose membrane with a molar mass cut-off of 10 kDa was used as accumulation wall. All experiments were carried out at 25 °C and the eluent was degassed water containing 5 mM NaCl. For all samples, the detector flow rate was set to 0.5 mL/min and 20 µL (10 mg/mL) were injected with an injection flow rate of 0.2 mL/min for 7 min. The cross-flow was set to 2.2 mL/min and after a constant period of 5 min it was decreased under an exponential gradient (0.5) to 0 mL/min within 35 min. Afterwards the cross-flow was kept constant at 0 mL/min for at least 45 min to ensure complete elution. For calculation of the molar mass Zimm plots were used. All measurements were done in triplicate. The refractive index increment (dn/dc) of all samples was measured by manual injection of a known concentration directly into the channel without any focusing or cross-flow. The dn/dc was calculated as the average of at least three injections from the area under the RI curve (AUCRI).

TEM measurements were performed on a FEI Technai G2 20 cryo-Transmission Electron Microscope at 200 kV. 15 µL of the sample solution were blotted onto carbon coated TEM grids (Mesh 400, Quantifoil) and excess material was removed by a filter paper (Whatman No. 1) under ambient conditions. Grid cleaning was performed by argon plasma treatment for 30 seconds prior to the preparation of the solutions. The samples were allowed to dry prior to the transfer to the microscope. After the sample solution was blotted onto the grid it was placed upside down onto a drop of uranyl acetate (1 wt%) for 30 minutes. A filter paper was used to remove excess material and the grid was dried for some minutes under ambient conditions.

UV-Vis spectra were recorded on a SPECORD® 250 UV-Vis spectrometer from Analytik Jena in 1 cm quartz cuvettes using the peltier temperature-controlled 8-cell changer. Measurements were performed at 25.0 °C unless stated otherwise. Turbidimetry was measured using a Crystal 16 from Avantium Technologies, connected to a chiller (Julabo FP 40) using a wavelength of 500 nm and a heating ramp of 1 K min^{-1}. Unless otherwise stated, cloud point temperatures (T_{CP}) are reported for 50% transmittance of the second heating run for a solution containing

5 mg/mL polymer in 1 mM *tris*(hydroxymethyl)aminomethane (TRIS)-buffered saline (TBS) buffer.

Glycomonomer Synthesis

General Procedure

2-Mercaptoethylacrylamide was dissolved in anhydrous dichloromethane (50 mL/g) and degassed by purging with nitrogen for 15 min. Peracetylated monosaccharide (1 equivalent) was added and the solution was cooled in an ice-water bath. Boron trifluoride diethyl etherate (48%) was slowly added (5 mL/h) to this solution. Subsequent to stirring at room temperature for 24 h the solution was washed with aqueous $NaHCO_3$ solution and brine, dried over anhydrous sodium sulfate and the solvent was evaporated under reduced pressure. The monomer was purified by column chromatography on silica gel (ethylacetate:hexane 3:1).

ManMAm

5.7 g (39.3 mmol) 2-Mercaptoethylacrylamide were reacted with 15.4 g (39.5 mmol) ManOAc and 26 mL boron trifluoride diethyl etherate (48%) according to the general procedure. R_f = 0.47 (ethylacetate:hexane 3:1). Yield: 3.11 g (17%).

^{1}H NMR (300 MHz, $CDCl_3$, δ): 1.96-2.15 (m, 15H, -CH_3), 2.75-2.93 (m, 2H, -CH_2-S-), 3.44-3.69 (m, 2H, -CH_2-NHCO), 4.09-4.14 (m, 1H, H6), 4.25-4.41 (m, 2H, H6, H4), 5.20-5.35 (m, 5H, H1,H2,H3,H5, C=CH_2), 5.70 (s, 1H, C=CH_2), 6.36 (s, 1H, NHCO). ^{13}C NMR (75 MHz, $CDCl_3$, δ): 18.6, 20.6, 20.7, 20.9, 31.8, 39.0, 62.6, 66.3, 71.0, 82.7, 119.9, 139.8, 168.4, 169.7, 169.8, 169.9, 170.5. Elemental analysis: Calculated for $C_{20}H_{29}NO_{10}S$: C 50.52%, H 6.15%, N 2.95%, S 6.74%; Found: C 50.34%, H 6.41%, N 2.85%, S 6.35%.

GlcMAm

5.2 g (35.8 mmol) 2-Mercaptoethylacrylamide were reacted with 14.0 g (35.9 mmol) GlcOAc and 14 mL boron trifluoride diethyl etherate (48%) according to the general procedure. R_f = 0.53 (ethylacetate:hexane 3:1). Yield: 3.73 g (22%).

^{1}H NMR (300 MHz, $CDCl_3$, δ): 1.95-2.06 (m, 15H, -CH_3), 2.76-2.99 (m, 2H, -CH_2-S-), 3.37-3.68 (m, 2H, -CH_2-NHCO), 3.70-3.76 (m, 1H, H5), 4.08-4.24 (m, 2H, H6), 4.53 (d, ^{3}J = 10.0 Hz, 1H, H1), 4.99-5.08 (m, 2H, H3, H4), 5.22 (t, ^{3}J = 9.36 Hz, 1H, H2), 5.33 (s, 1H, C=CH_2), 5.71 (s, 1H, C=CH_2), 6.39 (s, 1H, NHCO). ^{13}C NMR (75 MHz, $CDCl_3$, δ): 19.0, 21.0, 21.1, 31.0, 39.4, 62.4, 68.6, 70.1, 74.1, 76.4, 84.2, 120.1, 168.8, 169.9, 169.9, 170.5, 171.0. Elemental analysis: Calculated for $C_{20}H_{29}NO_{10}S$: C 50.52%, H 6.15%, N 2.95%, S 6.74%; Found: C 50.68%, H 6.25%, N 2.99%, S 6.70%.

In Controlled Radical Polymerization: Materials; Tsarevsky, et al.;
ACS Symposium Series; American Chemical Society: Washington, DC, 2015.

RAFT Polymerization Reactions

General Procedure for RAFT Polymerization

The monomers as well as BTTCP and ACVA were dissolved in DMF ([monomer] = 2 mol/L) and the mixture was degassed by purging with argon for 1.5 h. After removal of an aliquot for conversion analysis the polymerization mixture was stirred at 80 °C for 15 h. Another aliquot (100 µL) was removed for conversion analysis by ^{1}H NMR spectroscopy, using the integral of the isopropyl proton signal at 4 ppm as internal standard. The polymer was purified by precipitation into diethyl ether (P*N*iPAm) or a mixture of *n*-hexane and *tert*-butylmethyl ether 1:4 (glycopolymers), collected by filtration and dried under reduced pressure.

PNiPAm-1

4.0 g *N*iPAm (35.5 mmol) were polymerized according to the general procedure ([M]:[I]:[ACVA]=200:1:0.1). Conversion: 94%, yield: 3.63 g (91%).

AF4-MALLS: dn/dc = 0.180 ± 0.0012 mL/g, M_n = 16,600 ± 800 g/mol, M_w = 18,400 ± 700 g/mol, PDI = 1.11.

SEC: M_n = 26,300 g/mol, M_w = 33,000 g/mol, PDI = 1.26.

PManAc-1

1.286 mg (11.36 mmol) *N*iPAm and 600 mg (0.63 mmol) **ManMAm** were polymerized according to the general procedure ([M]:[CTA]:[AVCA]=200:1:0.1). Conversion$_{NiPAm}$: 91%, conversion$_{ManMAm}$: 98%. Yield: 1.63 g (86%).

SEC: M_n = 31,800 g/mol, M_w = 37,900 g/mol, PDI = 1.19.

PGlcAc-1

2.142 mg (18.93 mmol) *N*iPAm and 1.000 mg (2.10 mmol) **GlcMAm** were polymerized according to the general procedure ([M]:[CTA]:[AVCA]=200:1:0.1). Conversion$_{NiPAm}$: 88%, conversion$_{GlcMAm}$: 93%. Yield: 2.51 g (80%).

SEC: M_n = 33,000 g/mol, M_w = 36,800 g/mol, PDI = 1.12.

Kinetic Investigation

For kinetic investigation of the copolymerization reactions, the same general procedure was applied with [M]:[CTA]:[AVCA]=200:1:0.1. Hydroquinone dimethyl ether (HDME) was added as internal standard (30 mol% of monomer) and samples were taken periodically with a degassed syringe for analysis by SEC and ^{1}H NMR spectroscopy. For integration of the signals in the ^{1}H NMR

spectra, the peak at 6.2 ppm corresponding to two double bond protons of *N*iPAm was used for determination of the *N*iPAM conversion, whereas the double bond signal at 5.7 ppm was used to determine the glycomonomer conversion, using the HDME signal at 6.85 ppm as internal standard.

PGlcAc-2

128.5 mg (1.14 mmol) *N*iPAm and 60 mg (126 µmol) **GlcMAm** 94.53 µL DMF were polymerized according to the general procedure [M]:[CTA]:[AVCA]=25:1:0.1. $Conversion_{NiPAm}$: 94%, $conversion_{GlcMAm}$: 100%. The polymer was purified by preparative size exclusion chromatography (BioBeads® column S-X1, eluent: THF) followed by precipitation into 15 mL of *n*-hexane and subsequently dried under reduced pressure. Yield: 95 mg (50%).

MALDI-TOF MS (matrix: DCTB): M_n = 3,110 g/mol, M_w = 3,530 g/mol, PDI = 1.13.

SEC: M_n = 7,400 g/mol, M_w = 8,560 g/mol, PDI = 1.16.

PManAc-2

201 mg (1.78 mmol) *N*iPAm and 94 mg (198 µmol) **GlcMAm** were polymerized according to the general procedure [M]:[CTA]:[AVCA]=25:1:0.1. $Conversion_{NiPAm}$: 96%, $conversion_{ManMAm}$: 100%. The polymer was purified by preparative size exclusion chromatography (BioBeads® column S-X1, eluent: THF) followed by precipitation into 20 mL of *n*-hexane and subsequently dried under reduced pressure. Yield: 186 mg (63%).

MALDI-TOF MS (matrix: DCTB): M_n = 2,860 g/mol, M_w = 3,210 g/mol, PDI = 1.12.

SEC: M_n = 6,000 g/mol, M_w = 6,770 g/mol, PDI = 1.13.

Glycopolymer Deprotection

General Procedure for Glycopolymer Deprotection

The protected glycopolymer was dissolved in anhydrous methanol (4 mg/mL) and sodium methoxide solution (0.5 M in methanol) were added. After the solution was stirred for 2 h at room temperature, the mixture was neutralized with 1 M hydrochloric acid. The polymerization mixtures with [M]:[CTA]=200 were subjected to dialysis against deionized water (MWCO 3,500 g/mol). The polymerization mixtures with [M]:[CTA]=25 were purified by evaporation of the solvent, taking up the residue in ethanol, followed by filtration in order to remove the salt. After evaporation of the solvent the residue was re-dissolved in deionized water. Finally, all polymers were lyophilized.

PManOH-1

1,462 mg **PManAc-1** were deprotected with 1.6 mL sodium methoxide solution (0.5 M in methanol) according to the general procedure. Yield: 1.22 g (95%).

Elemental analysis: C 55.70%, H 9.38%, N 9.75%, S 1.90%.

AF4-MALLS: dn/dc = 0.182 ± 0.0015 mL/g, M_n = 18,700 ± 130 g/mol, M_w = 22,200 ± 300 g/mol, PDI = 1.19.

SEC: M_n = 31,100 g/mol, M_w = 41,700 g/mol, PDI = 1.34.

PGlcOH-1

2,207 mg **PGlcAc-1** were deprotected with 2.35 mL sodium methoxide solution (0.5 M in methanol) according to the general procedure. Yield: 1.59 g (82%).

Elemental analysis: C 53.92%, H 9.07%, N 9.61%, S 1.77%.

AF4-MALLS: dn/dc = 0.181 ± 0.0017 mL/g, M_n = 16,300 ± 1,000 g/mol, M_w = 20,000 ± 500 g/mol, PDI = 1.23.

SEC: M_n = 31,700 g/mol, M_w = 41,500 g/mol, PDI = 1.31.

PManOH-2

160 mg **PManAc-2** were deprotected with 170 µL sodium methoxide solution (0.5 M in methanol) according to the general procedure. Yield: 145 mg (99%).

Elemental analysis: C 52.47%, H 8.51%, N 8.76%, S 4.02%.

MALDI-TOF MS (matrix: DCTB): M_n = 2,650 g/mol, M_w = 2,760 g/mol, PDI = 1.04.

SEC: M_n = 6,730 g/mol, M_w = 7,840 g/mol, PDI = 1.16.

PGlcOH-2

61 mg **PGlcAc-2** were deprotected with 65 µL sodium methoxide solution (0.5 M in methanol) according to the general procedure. Yield: 45 mg (96%).

Elemental analysis: C 51.51%, H 8.43%, N 8.42%, S 3.48%.

MALDI-TOF MS (matrix: DCTB): M_n = 3,180 g/mol, M_w = 3,320 g/mol, PDI = 1.05.

SEC: M_n = 8,770 g/mol, M_w = 10,100 g/mol, PDI = 1.15.

Synthesis of Citrate Stabilized Gold Nanoparticles

The particles were synthesized as reported previously (*40*). Shortly, in a 250 mL round bottom flask 200 mL of a $HAuCl_4 \times 3H_2O$ (1 mM) solution was heated to 100 °C. 1 mL of a sodium citrate solution (0.78 M) was added at once while stirring under reflux. The color of the solution turned red after approximately 30 seconds, and heating was continued for 30 minutes. Subsequently, 1 mL of the citrate stabilized nanoparticles were centrifuged in a plastic vial at 5000 rpm for 90 min and 950 µL of the supernatant solution were removed. Afterwards 950 µL of distilled water were added and the particles were redispersed by simple shaking and short ultrasonication.

Immobilization of Glycopolymers onto Nanoparticles and Lectin Interaction

10 µL of polymer solution (1 mg/mL) were added to 1 mL of the obtained gold nanoparticle solution and incubated at room temperature for 1 h.

For the lectin interaction experiments, 200 µL of the functionalized nanoparticle solution (without centrifugation and re-dispersion) were diluted with 600 µL deionized water and 190 µL of TRIS buffered saline (pH 7.4, 5mM TRIS, 26 mM NaCl, 0.5 mM KCl) containing 5 mM Ca^{2+}, 5 mM Mn^{2+} and 5 mM Mg^{2+} (final gold concentration 40 µg/mL, final polymer concentration 2 µg/mL). Subsequently, ConA solution (0.1 mg/mL in TRIS buffered saline) was added to nanoparticle solution and the changes were monitored by UV-Vis spectroscopy.

Results and Discussion

Synthesis of Glycomonomer

S-Linked mannose and glucose bearing glycomonomers, **GlcMAm** and **ManMAm**, were synthesized as outlined in Scheme 1. First, 2-aminoethanethiol was reacted with methacryloylchloride to yield 2-mercaptoethylmethacrylamide (*39*). This compound was used as building block towards glycomonomers, exemplarily presented for glucose and mannose in this work. The obtained monomer with the nucleophilic thiol-group can react with peracetylated monosaccharides in a substitution reaction selectively at the anomeric position, retaining the α- or β-anomeric structure. The methacrylamide is less susceptible to side reactions (Michael addition), which immediately occurred for the acrylamide analogue monomer. 2-Mercaptoethylmethacrylamide only underwent Michael addition (polymerization) after extended storage time. Glycomonomer synthesis from this monomer was performed with peracetylated α-D-mannose and β-D-glucose, respectively, according to Scheme 1.

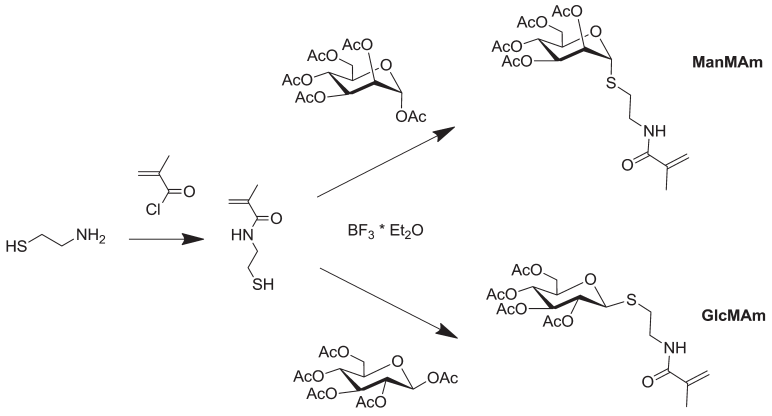

Scheme 1. Schematic representation of the glycomonomer synthesis.

The ^{1}H NMR spectra of the two purified monomers are depicted in Figure A1 (Appendix), proving the assumed structure of the two glycomonomers. The signals of the double bond protons could be clearly distinguished from the sugar ring protons *via* the heteronuclear single quantum coherence (HSQC) NMR spectrum (^{1}H, ^{13}C), depicted in Figure A2 and Figure A3, respectively (Appendix).

Synthesis of Glycopolymers by RAFT Polymerization

The protected glycomonomers were copolymerized with *N*iPAm *via* RAFT polymerization (Scheme 2), using 10 mol% of glycomonomer. BTTCP was used as chain transfer agent (CTA) and ACVA as initiator with a ratio of BTTCP:CTA of 10:1. In order to take advantage of the cluster glycoside effect by multivalent binding to biological receptors, polymers with several sugar repeating units are required. Therefore, glycopolymers with a target degree of polymerization (DP) of 200 were synthesized, controlling the chain length by the ratio of monomer to CTA ([M]:[CTA]).

For later application of the glycopolymer (*i.e.*, immobilization) it is necessary to gain knowledge about the fate of the trithiocarbonate endgroup. Since the endgroup analysis is always easier for short polymers, glycopolymers with a target DP of 25 were also synthesized in the same way to obtain short model polymers.

The polymerizations with DP = 200 (**PManAc-1** and **PGlcAc-1**) were performed in DMF at 80 °C followed by purification via precipitation. Size exclusion chromatography (SEC) revealed narrow and monomodal molar mass distributions (Figure A4, Appendix) with low PDI values (PDI = 1.19 for **PManAc-1** and PDI = 1.12 for **PGlcAc-1**, respectively). However, these values as well as the molar mass values obtained by SEC alone (Table 1) are not reliable since no suitable calibration is available for the measured copolymers (see below for a discussion of the molar masses obtained from absolute methods).

In Controlled Radical Polymerization: Materials; Tsarevsky, et al.;
ACS Symposium Series; American Chemical Society: Washington, DC, 2015.

Table 1. Summary of selected characterization data for the polymers synthesized by RAFT polymerization.

Polymer	*[M]:[CTA]*	*Conversion NiPAm [%][a]*	*Conversion glyco-monomer [%][a]*	$M_{n,theo}$ *[g/mol]*	M_n *[g/mol][b]*	*PDI[b]*
PManAc-1	200	91	98	28,090	31,800	1.19
PGlcAc-1	200	88	93	27,000	33,000	1.12
P*N*iPAm-1	200	94	-	21,500	26,300	1.26
PManAc-2	25	96	100	3,870	6,000	1.13
PGlcAc-2	25	94	100	3,820	7,400	1.16

[a] obtained by ^{1}H NMR spectroscopy [b] obtained by SEC measurement

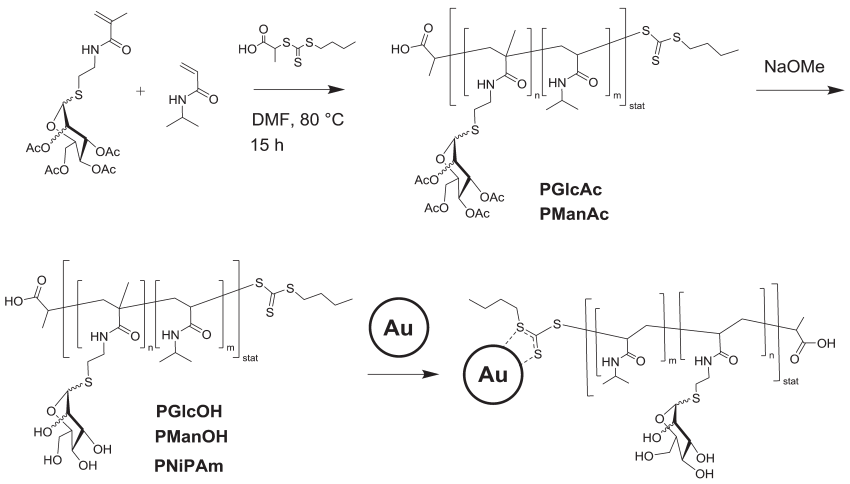

Scheme 2. Schematic representation of the glycopolymer synthesis via RAFT polymerization followed by deprotection of the sugar moieties and immobilization onto gold nanoparticles.

The conversions of the glycomonomers are slightly higher than the conversions of *N*iPAm, which is a indication for a slightly higher reactivity of the glycomonomer (Table 1). Therefore, the kinetics of the copolymerization reactions were studied (Figure A5, Appendix). As can be concluded from the pseudo-first order kinetic plot, the polymerization rate of the glycomonomers **ManMAm** and **GlcMAm** are indeed slightly higher than the polymerization rate of *N*iPAm. As a consequence, the statistical distribution of the glycomonomer repeating units in the final polymer chain is not strictly random but a small gradient in the monomer distribution is expected. As can be concluded from the initially linear slope of the kinetic plots (Figure A5 (left), Appendix) as well as the linear increase of the molar mass (M_n) with conversion (Figure A5 (right),

Appendix), the copolymerization is controlled up to conversions of 70%. A slight loss of control is observed for higher conversions, which can be ascribed to termination reactions, however, even for higher conversions the resulting PDI values are lower than 1.25.

The chemical structure of the copolymers was confirmed by ^{1}H NMR spectroscopy (Figure 1 and Figure A6, Appendix), showing the acetyl protecting groups of the sugar moieties in the protected glycopolymers **PManAc-1** and **PGlcAc-1**, respectively, as well as the signals arising from the sugar ring protons and the poly(*N*iPAm) (P*N*iPAm) protons (the ^{1}H NMR spectrum of the analogue P*N*iPAm homopolymer **P*N*iPAm-1** is shown in Figure A7, Appendix).

Deprotection of the glycopolymers was achieved with sodium methoxide in anhydrous methanol (Scheme 2). With respect to end-group determination (see below) it is important to note that the short glycopolymers, **PManAc-2** and **PGlcAc-2**, were subjected to the same deprotection reaction as their longer analogues **PManAc-1** and **PGlcAc-1**. After purification by dialysis, the ^{1}H NMR spectra of the purified polymers **PManOH-1** and **PGlcOH-1** (Figure 1 and Figure A6, Appendix) reveal the disappearance of the acetyl protecting groups as well as a shift of the sugar ring protons to higher field, showing the successful deprotection of the glycopolymers. Due to this shift the signals of the sugar ring protons overlap with the isopropyl proton signal of *N*iPAm. Therefore, a HSQC NMR spectrum (^{1}H, ^{13}C) was measured (Figure 1). This allows the assignment of the peaks in the region between 3 and 4 ppm (the complete spectra are depicted in Figure A8, Appendix, for **PManOH-1** and Figure A9 for **PGlcOH-1**, respectively). These spectra also reveal that the signals of the anomeric protons do not shift. Deprotection of the short glycopolymers **PGlcAc-2** and **PManAc-2** is confirmed in the same manner by ^{1}H NMR spectroscopy (Figure A10, Appendix).

Since the sugar proton signals in the ^{1}H NMR spectra overlay the methin proton signal of the isopropyl group (Figure 1 and Figure A6, Appendix), the sugar content of the glycopolymers **PManOH-1** and **PGlcOH-1** could not be determined by integration of the ^{1}H NMR spectra. Therefore, the sugar content was estimated by elemental analysis, using the ratio of sulfur to nitrogen content to obtain the number of sugar repeating units (in mol%), yielding 8.5 mol% mannose repeating units for **PManOH-1** and 8.0 mol% repeating units for **PGlcOH-1** (Table 2). These values are lower than expected from the monomer feed ratio, keeping in mind that the conversions of the glycomonomers were higher than the conversions of *N*iPAm for the RAFT copolymerization reactions. The reason for this is presumably the purification step of the protected glycopolymers by precipitation in *tert*-butyl methyl ether. During this step the glycopolymer chains with a higher sugar content than 10% are more hydrophobic and more prone to dissolve in the hydrophobic precipitation medium. This results in a lowering of the average sugar content of the precipitated polymer.

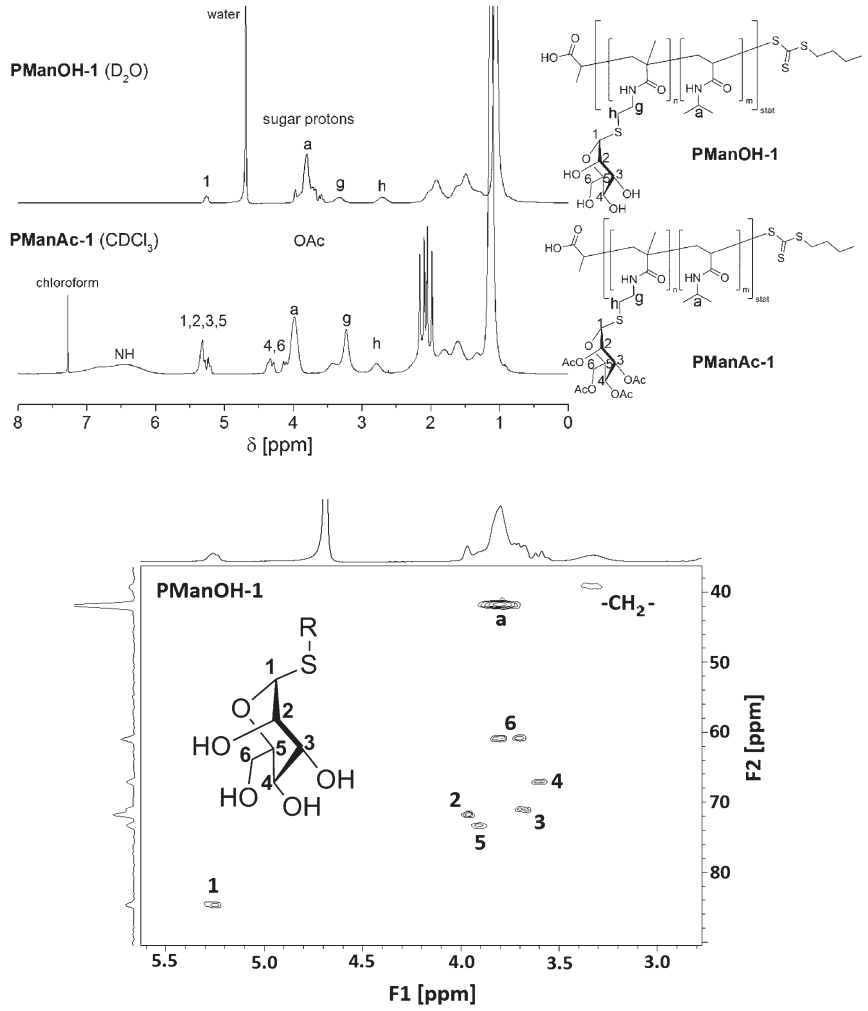

*Figure 1. [1]H NMR spectra of the two glycopolymers **PManAc-1** and **PManOH-1** (top) and zoom into the HSQC NMR spectrum ([1]H, [13]C) of the glycopolymer **PManOH-1** (bottom) showing the region of the sugar proton signals which overlap with the signal of the isopropyl methin protons of the NiPAm repeating units (300 MHz, $CDCl_3$ or D_2O).*

In Controlled Radical Polymerization: Materials; Tsarevsky, et al.;
ACS Symposium Series; American Chemical Society: Washington, DC, 2015.

Table 2. Summary of selected characterization data of the deprotected glycopolymers.

Polymer	*M_n [g/mol]*[a]	*PDI* [a]	*M_n [g/mol]*	*Sugar content [mol%]*	*Sugar DP*[e]	*T_{CP} [°C]*
PManOH-1	31,100	1.19 [b]	18,700 [b]	8.5 [d]	12.1	45.4
PGlcOH-1	31,700	1.23 [b]	16,300 [b]	8.0 [d]	10.0	47.4
PManOH-2	6,730	1.04 [c]	2,650 [c]	8.0 [f]	1.5	51.7
PGlcOH-2	8,770	1.05 [c]	3,180 [c]	7.6 [f]	1.7	53.0

[a] obtained by SEC measurement, linear PS calibration [b] obtained by AF4-MALLS measurement [c] obtained from the MALDI-TOF mass spectra [d] determined *via* elemental analysis [e] calculated from the molar mass obtained by AF4-MALLS or MALDI-TOF MS and the sugar content [f] calculated from the elemental analysis and correction of the results by subtraction of the RAFT endgroup using the molar masses obtained from the MALDI-TOF mass spectra

In addition to ^{1}H NMR spectroscopy the successful deprotection is confirmed by the disappearance of the peak derived from the carbonyl groups of the acetyl protecting groups (1750 cm^{-1}) in the FT-IR spectrum of the deprotected glycopolymers compared to the protected precursors (Figure A11, Appendix).

The SEC traces of the deprotected glycopolymers **PGlcOH-1** and **PManOH-1** show a very small shift towards lower elution volumes compared to the protected precursors (Figure A4, Appendix), which is an indication for an increase of the hydrodynamic volume of the deprotected, more polar glycopolymer in the polar solvent of the chromatography system (*N,N*-dimethylacetamide). Also for the deprotection of the short glycopolymers **PGlcAc2** and **PManAc-2**, the analogue shift in the size exclusion chromatograms is observed (Figure A12, Appendix), indicating successful deprotection.

Since also for the determination of the molar masses of **PManOH-1** and **PGlcOH-1** by SEC no valid calibration was available, the M_n of these longer glycopolymers were determined by asymmetric flow field-flow fractionation (AF4) coupled to multi-angle laser light scattering (MALLS) detector (*41*). In the gentle characterization technique AF4 separation is achieved by a liquid cross-flow through a semipermeable membrane in a channel without any stationary phase. Together with MALLS, this technique gives access to the molar mass distribution (M_n, M_w, PDI) of the glycopolymers. The values of the sugar repeating units obtained by elemental analysis together with the molar masses obtained by the AF4-MALLS measurements were used to calculate the degree of polymerization of the glycomonomers (sugar DP), yielding 12 mannose repeating units per chain for **PManOH-1** and 10 glucose repeating units for **PGlcOH-1**, respectively (Table 2). These amounts of statistically incorporated sugar repeating units should be high enough to enable multivalent binding of one polymer chain.

The AF4 method, which could be used for the determination of the absolute molar masses of the long glycopolymer chains, cannot be applied for the short

analogues. Therefore, the short glycopolymers **PManAc-2** and **PGlcAc-2** were analyzed by MALDI-TOF mass spectrometry (Figure 2), which revealed the molar masses of **PGlcOH-2** and **PManOH-2**, for which no valid calibration was available for SEC (Table 2). Although MALDI-TOF mass spectrometry is an absolute technique for the determination of molar masses, the obtained M_n values are assumed to be lower than the real values because in MALDI-TOF mass spectrometry the smaller molecules are ionized more easily. Therefore, the real molar mass is expected to be in between the values obtained by MS and SEC (Table 2). Like for the long analogue glycopolymers, the sugar content of the short glycopolymers was estimated by elemental analysis. Here, since the polymers are much shorter, the influence of the endgroup has to be taken into account. Calculation of the sugar content, therefore, required the amount of trithiocarbonate endgroups per given amount of polymer, which is accessible *via* the molar mass obtained by mass spectrometry, revealing 8.0 mol% sugar repeating units for **PManOH-2** and 7.6 mol% sugar repeating units for **PGlcOH-2**, respectively. These values are in the same range as the values of the longer glycopolymers, which was not expected since the purification steps for the short polymers were performed differently (preparative size exclusion chromatography instead of precipitation) and should, therefore, result in higher sugar contents closer to the feed ratio of the copolymerization reactions. It has to be taken into account that the M_n values obtained by MS are expected to be slightly too low, therefore, a too high sulfur content is subtracted in the calculation step correcting the influence of the RAFT endgroup, leading to a corrected sulfur content, which is slightly lower than the real value.

A major advantage of MALDI-TOF MS is the possibility to obtain knowledge of the structure of the polymer in hand. The obtained MALDI-TOF mass spectra of the two protected glycopolymers (Figure 2) show very similar features. The main distance between two peaks corresponds to the molar mass of *N*iPAm. Furthermore, different P*N*iPAm distributions could be observed in both cases, which correspond to the P*N*iPAm polymers with 0 to 3 protected sugar units (distance m/z = 475.1), which is confirmed by the comparison of calculated and measured isotopic patterns for both polymers **PManAc-2** and **PGlcAc-2** (Figure 2). In this way, MALDI-TOF mass spectrometry provides knowledge about the polymer endgroups, indicating that the carboxyl- and the trithiocarbonate endgroups are both attached to the polymer chains of all distributions found in the spectra.

The MALDI-TOF mass spectra of the deprotected glycopolymers **PGlcOH-2** and **PManOH-2** are very similar as well (Figure 3). In these spectra, different distributions are observed, all of them show the repeating unit of *N*iPAm and are separated by an offset of 307.1, which corresponds to the molar mass of the deprotected sugar repeating unit. The peak assignment is validated by the calculated isotopic patterns, which fit to the observed isotopic patterns, as shown exemplarily for each distribution in Figure 3. Most importantly, the MALDI-TOF mass spectra of **PGlcOH-2** and **PManOH-2** show the peaks corresponding to the polymer chains with the RAFT endgroup still attached after the deprotection step. No peaks were found corresponding to a product where the trithiocarbonate endgroups were cleaved by sodium methoxide.

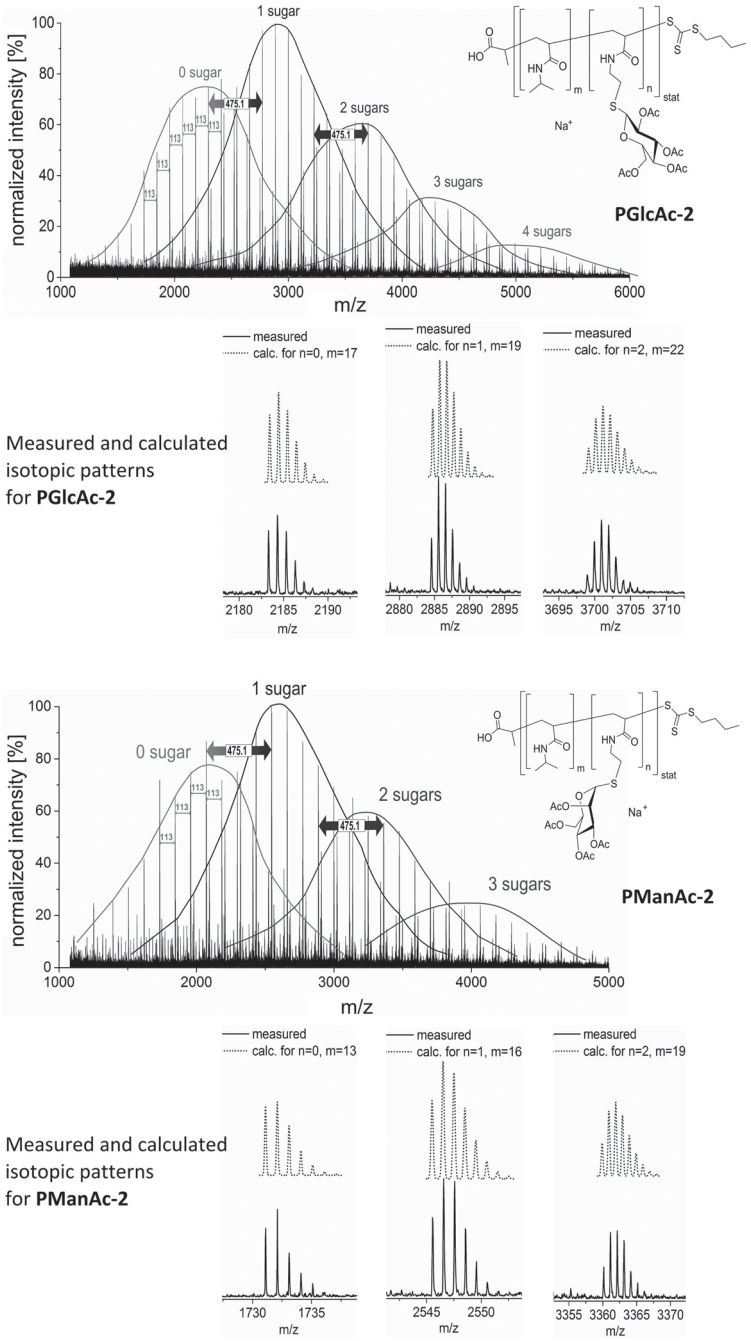

*Figure 2. MALDI-TOF mass spectra of the protected glycopolymers **PGlcAc-2** (top) and **PManAc-2** (bottom, matrix DCTB) and selected isotopic patterns (right, calculated and measured).*

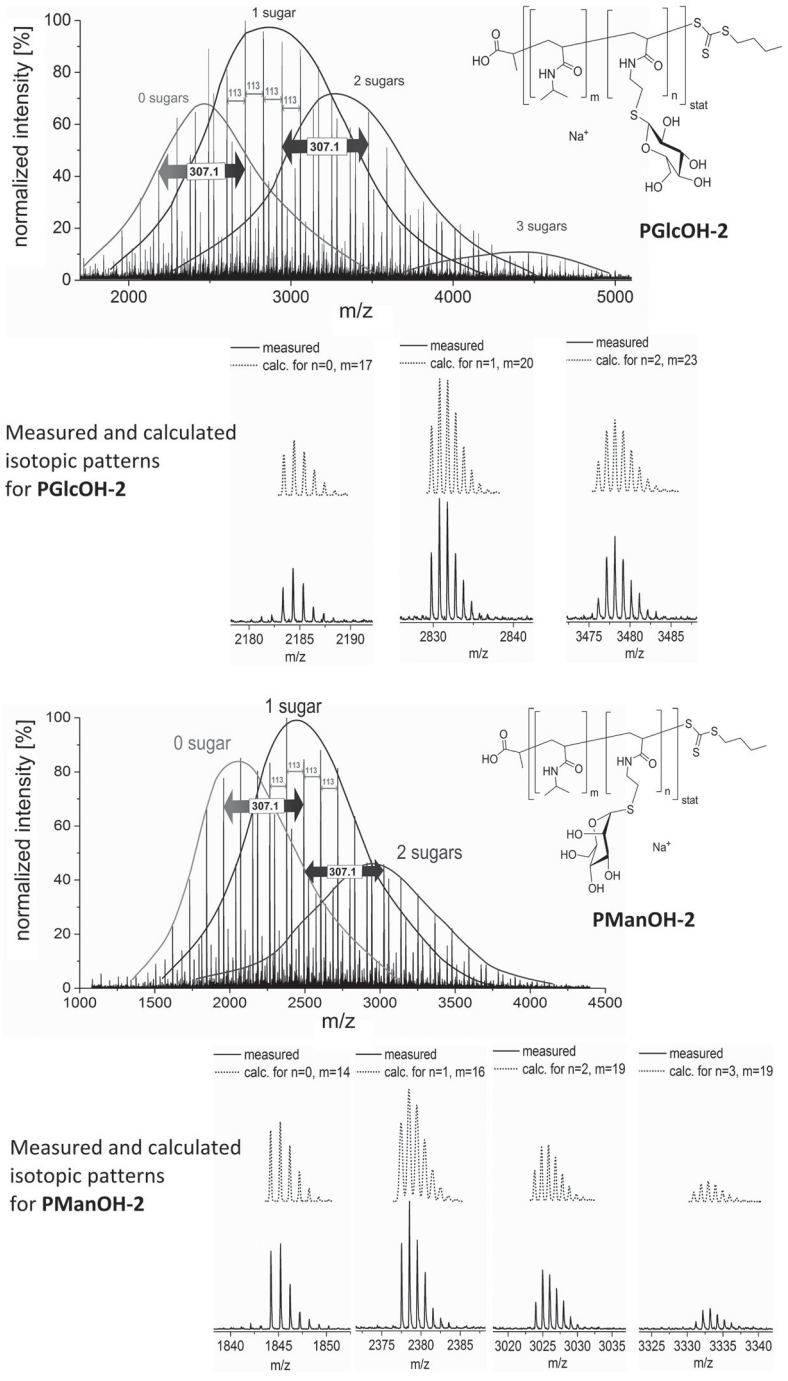

Figure 3. MALDI-TOF mass spectra of the deprotected glycopolymers ***PGlcOH-2*** *(top) and* ***PManOH-2*** *(bottom, matrix DCTB) and selected isotopic patterns (right, calculated and measured).*

These spectra in combination with the comparison of the measured and calculated isotopic patterns (Figure A13 to A20, Appendix) clearly proof the assumed structure of the synthesized glycopolymer with both endgroups, the carboxyl group and the trithiocarbonate, still attached to the polymer after deprotection. It is not possible to obtain such well resolved MALDI-TOF mass spectra for the longer analogue glycopolymers **PManOH-1** and **PGlcOH-1**, however, it can be assumed that the influence of the deprotection step and, therefore, the chemical identity of the endgroups is the same for the longer polymers.

Synthesis of Glycopolymer Coated Gold Nanoparticles

Citrate-stabilized nanoparticles for immobilization of the glycopolymers were prepared according to a literature procedure (*40*). Subsequently, the glycopolymers **PGlcOH-1** and **PManOH-1** as well as the *N*iPAm homopolymer **P*N*iPAm-1** were immobilized onto the surface of the gold nanoparticles (Scheme 2).

This immobilization was achieved *via* the trithiocarbonate RAFT endgroups of the polymers, as reported in literature for the direct immobilization of polymers derived from RAFT polymerization (*16*). The resulting polymer coated nanoparticles are stable over weeks.

Characterization of the functionalized nanoparticles by dynamic light scattering (DLS) revealed an increase of the particle diameter from 20.6 nm to 24 nm (Table 3). Additionally, the ζ-potential of the nanoparticle solutions shifted to lower negative values for the samples which were incubated with the polymers **PGlcOH-1**, **PManOH-1** and **P*N*iPAm-1**, respectively. This change of the ζ-potential shows that the polymers are immobilized onto the nanoparticle surface leading to replacement of the negatively charged citrate ions by non-charged polymer chains.

Table 3. DLS charaterization data of the nanoparticles stabilized by the different polymers.

Polymer	*diameter [nm]*	*ζ-potential [mV]*	λ_{max} *(UV-Vis) [nm]*
-	20.62 ± 0.08	-45.37 ± 0.65	520.5
PManOH-1	22.92 ± 0.05	-39.0 ± 3.2	523.0
PGlcOH-1	22.45 ± 0.02	-39.27 ± 0.17	523.0
P*N*iPAm-1	23.79 ± 0.16	-36.17 ± 0.53	522.9

TEM imaging of a sample stained with uranylacetate (Figure 4) clearly showed the presence of the polymer shell with a thickness between 1 to 2 nm. This is in good agreement with the DLS results, which show a difference of the diameter of functionalized and unfunctionalized nanoparticles, which is in the

same order of magnitude. However, the nanoparticle diameter determined by DLS (Table 3) is slightly larger than by TEM measurement, which is ascribed to the swelling of the nanoparticles in the solvent for DLS measurement, which was also described in literature for a similar case (*13*).

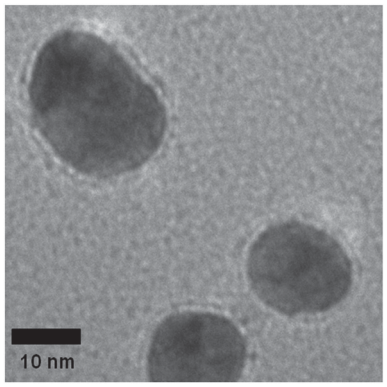

Figure 4. TEM image of gold particles coated with PManOH-1.

A further proof that the polymer is immobilized on the nanoparticle surface is the fact that the nanoparticles without polymer addition were not stable upon addition of TRIS buffered saline. This is indicated by a color change from red to blue, which shows aggregation of the particles. When gold nanoparticles are brought into close proximity the surface plasmon resonance shifts to higher wavelengths and also additional resonances arise. This is also obvious from the UV-Vis spectra, which immediately change drastically upon addition of the buffer solution to the nanoparticle solution (Figure A21, Appendix). On the other hand, the nanoparticles stabilized by **PGlcOH-1** and **PManOH-1** are stable under these conditions. A small shift of the maximum in the UV-Vis spectrum of the nanoparticles was observed upon addition of polymer (Table 3), reflecting the change in the direct environment of the gold nanoparticle surface. A higher concentration (10 fold) of polymer **P*N*iPAm-1** is required to stabilize the nanoparticles against addition of buffer solution. The reason for this might be the higher hydrophilic character of the glycopolymers **PGlcOH-1** and **PManOH-1.**

LCST Behavior

Since the temperature responsive behavior of the glycopolymers is of interest for potential applications, such as temperature-switchable affinity chromatography, this feature of the synthesized glycopolymers was investigated by turbidimetric studies.

The aqueous solutions of the glycopolymers display a very sharp transition from 100% to 0% transmission at 45.4 °C for **PManOH-1** and 47.4 °C for **PGlcOH-1** (Figure A22, Appendix). Furthermore, the cloud point temperatures (T_{CP}) are stable during repeated heating/cooling cycles (Figure A23, Appendix).

The increase of the transmittance upon cooling is observed approximately 2 °C lower than for the heating runs (Figure A24, Appendix). This kind of heating-cooling hysteresis of P*N*iPAm chains is known in literature and caused by the formation of hydrogen bonds between the amide bonds of the polymer chains, which have to be broken again upon cooling (*42*). Although the sugar content of **PManOH-1** is slightly higher than the sugar content of **PGlcOH-1**, the T_{CP} of the latter is slightly higher than the T_{CP} of the mannose glycopolymer. The same observations were made for the analogue shorter glycopolymers **PGlcOH-2** and **PManOH-2** (Table 2, Figure A25, Appendix). The T_{CP}s of the short glycopolymers **PManOH-2** and **PGlcOH-2** are slightly higher than the T_{CP}s of the analogue longer glycopolymers **PManOH-1** and **PGlcOH-1**, respectively (Table 2). This can be explained by the lower DP of these polymers. The lower chain length results in a more pronounced influence of the hydrophilic carboxylic endgroup compared to the longer polymers.

T_{CP} determination *via* turbidimetry relies on the decrease in transmittance that occurs upon phase separation of the binary polymer/water mixture upon heating. Therefore, it comes to no surprise that this method for T_{CP} determination has an inherent concentration dependence, since a lower amount of sample in the same volume cannot lead to the same turbidity simply because there is not enough material (the concentrated phase droplets) below certain concentrations. This is illustrated by the turbidity curves for solutions containing different concentrations of **PManOH-1** in Figure 5 (left), showing a decreased turbidity with decreasing concentration. Furthermore, this effect on the determined T_{CP} (Figure 5, right), which is due to the measurement technique, cannot be separated from the inherent concentration dependence. Consequently, below certain concentrations this method is not suitable for determination of cloud point temperatures. However, a method which does not rely on turbidity can be free from this concentration related limitation. As indicated earlier, the synthesized gold nanoparticles allow for determination of changes in the direct surface surrounding by change of the surface plasmon resonance detectable *via* UV-Vis spectroscopy.

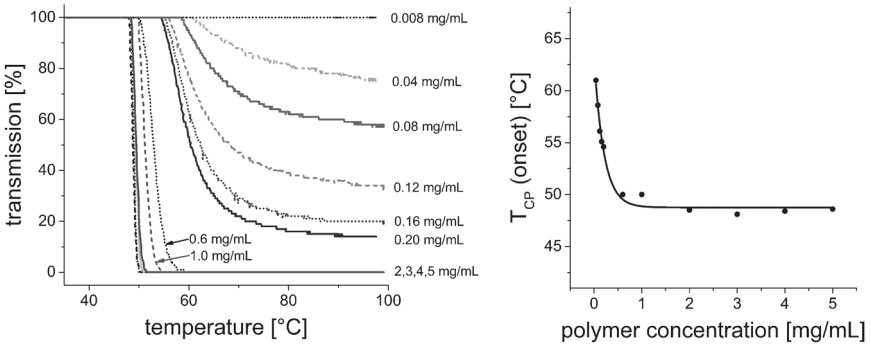

Figure 5. Turbidity curves (left) and cloud point temperatures of the glycopolymer ***PManOH-1*** *(right, T_{CP} defined here as onset of transmission decrease) at different concentrations (1 K×min^{-1} in TBS).*

In Controlled Radical Polymerization: Materials; Tsarevsky, et al.;
ACS Symposium Series; American Chemical Society: Washington, DC, 2015.

Consequently, to evaluate if the LCST behavior of the glycopolymer **PManOH-1** is still present after immobilization onto the gold nanoparticles, UV-Vis spectra of the functionalized GNPs were measured at different temperatures. The increase of absorbance as well as the shift of the peak maximum show a significant increase above 47 °C, which can be attributed to the coil to globule transition of the glycopolymer. Interestingly, the nanoparticles do not aggregate immediately upon exceeding the coil to globule temperature. The first observation is a very pronounced and sudden increase of the wavelength of the peak maximum (λ_{max}), followed by a second increase upon further heating (Figure 6). The first increase is attributed to the coil to globule transition at the surface, which changes the surrounding of the nanoparticles. In contrast, the second increase is attributed to the aggregation of the nanoparticles, which is supported by a decrease of the peak upon introducing a 60 seconds equilibration time before each measurement (Figure 6, 3rd and 4th heating run). Furthermore, from Figure 6 it can be concluded that the coil to globule transition at the GNP surface is fully reversible upon cooling.

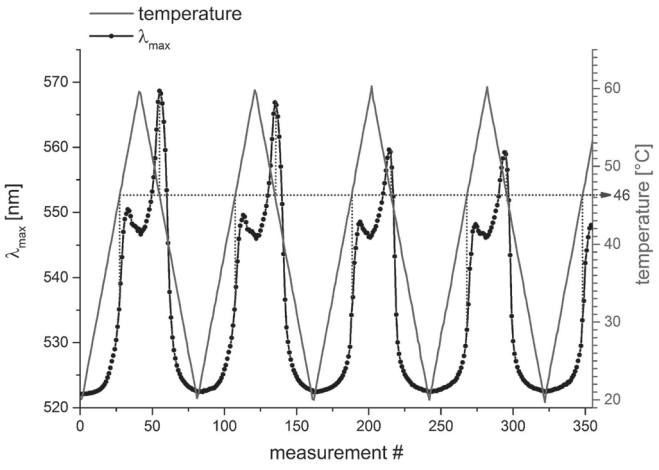

Figure 6. Change of the wavelength of the maximum in the UV-Vis spectra (λ_{max}) of the gold nanoparticles functionalized with PManOH-1 upon temperature change (polymer concentration: 2 µg/mL, gold concentration: 40 µg/mL; 1st and 2nd heating run: immediate measurement upon reaching the temperature, 3rd to 5th heating run: 60 seconds equilibration time before measurement).

These data show that the cloud point temperature of the immobilized glycopolymer is still present and can be conveniently analyzed by exploiting the surface plasmon resonance of the gold nanoparticles *via* UV-Vis spectroscopy. Another very advantageous aspect is the very low concentration, for which the determination of the coil to globule transition temperature is possible (the used polymer concentration was 2 µg/mL and the applied gold concentration 40 µg/mL).

Lectin Interaction Experiments

In order to investigate the ability of the glycopolymer-functionalized nanoparticles to selectively recognize proteins, lectin interaction studies were performed *via* UV-Vis spectroscopy. A solution of ConA was added to a solution of gold nanoparticles (200 μg_{Au}/mL) stabilized by glycopolymer or the homopolymer, respectively. A buffer containing Mn^{2+}, Mg^{2+} and Ca^{2+} ions was used (final concentration 1 mM) because these ions are required by the used lectin to interact with carbohydrates. Upon lectin addition to the mannose glycopolymer, the nanoparticles aggregated, revealing interaction with the surface-immobilized glycopolymers. The aggregation, visible as turbidity followed by settling down of the aggregates, could be observed with the naked eye. However, for a more detailed investigation this phenomenon was followed *via* UV-Vis spectroscopy. This method is in particular suitable since the UV-Vis spectrum of the gold nanoparticles, which shows a pronounced peak due to the surface plasmon resonance, is very sensitive to the direct environment of the nanoparticle surface. A redshift of the UV-Vis spectrum could, therefore, be observed upon interaction (Figure 7 (a)). Moreover, a steady decrease of the absorbance was observed after lectin addition (Figure 7 (a)), which is caused by increasing aggregation and sedimentation of the nanoparticles. In contrast, no change of the UV-Vis absorption spectra could be observed for the particles stabilized by the glucose copolymer **PGlcOH-1** or the homopolymer **P*N*iPAm-1** (Figure 7 (b) and (c)), because the lectin ConA is binding specifically to α-mannose or α-glucose only. In order to study the binding interaction of ConA to the mannosylated nanoparticles in more detail, the wavelength of the peak maximum in the UV-Vis spectra is plotted against the interaction time in Figure 8. The plot clearly shows the increasing interaction of the nanoparticles stabilized with **PManOH-1** with increasing ConA concentration, whereas the peak maximum stays constant for the other polymers **PGlcOH-1** and **P*N*iPAm-1**. Furthermore, due to the high sensitivity of the SPR of the gold nanoparticles, these experiments could show interactions between polymer and lectin using polymer concentrations as low as 2 μg/mL.

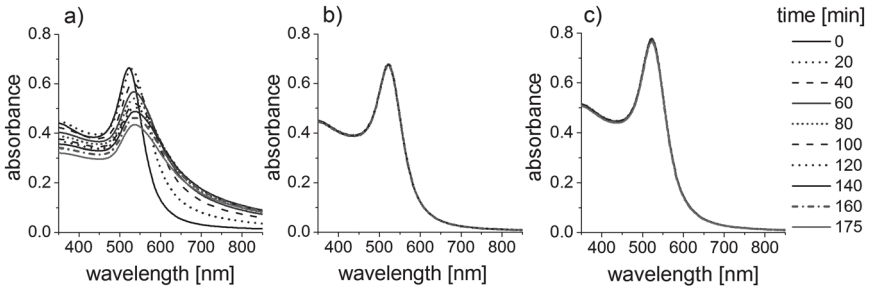

*Figure 7. Overlay of the UV-Vis spectra recorded after different time intervals following lectin addition to nanoparticles stabilized by **PManOH-1** (a), **PGlcOH-1** (b) and **PNiPAm-1** (c).*

In Controlled Radical Polymerization: Materials; Tsarevsky, et al.;
ACS Symposium Series; American Chemical Society: Washington, DC, 2015.

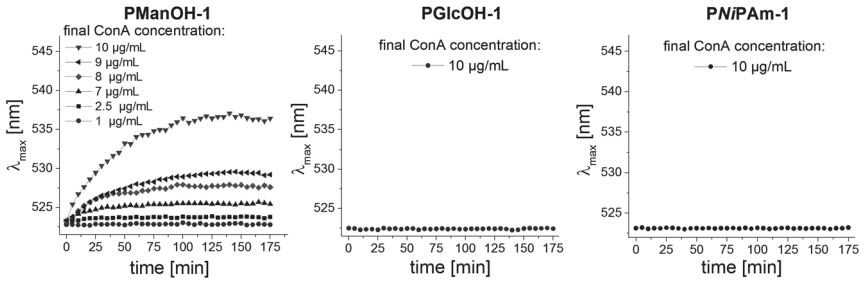

Figure 8. Change of the peak maxima of the UV-Vis spectra with time after addition of different amounts of ConA for glycopolymers stabilized by ***PManOH-1*** *(left),* ***PGlcOH-1*** *(middle) and* ***PNiPAm-1*** *(right). The polymer concentrations were 2 µg/mL in all cases, the gold concentration was 40 µg/mL.*

As stated earlier, the LCST behavior of the immobilized glycopolymers also affects the UV-Vis spectrum and ultimately leads to aggregation of the GNPs. Therefore, the influence of the LCST transition on the binding interaction between the functionalized gold nanoparticles and the lectin cannot be studied using this system in solution. The next steps for an in-depth investigation of the influence of the LCST transition on the binding interaction will involve immobilization of the nanoparticles onto glass slides (*6*, *9*, *11*).

Conclusion

New acetyl-protected *S*-glycosidic mannose- and glucose bearing monomers were polymerized *via* reversible addition fragmentation chain transfer (RAFT) polymerization. The obtained glycopolymers were deprotected using sodium methoxide, leading to well-defined glycopolymers which were analyzed *via* ^{1}H NMR spectroscopy, size exclusion chromatography, MALDI-TOF mass spectrometry, AF4-MALLS, elemental analysis as well as FT-IR spectroscopy, confirming the expected polymer structure. Turbidimetric studies revealed the thermoresponsive properties of the glycopolymers with sharp coil-to-globule transitions in buffered aqueous solution. Subsequent immobilization of the glycopolymers as well as the *N*iPAm homopolymer onto gold nanoparticles was achieved without reduction of the RAFT endgroup, leading to stable glyco-nanoparticles. Subsequent spectroscopic studies showed the LCST feature of the immobilized mannose-functionalized polymer at concentrations not detectable with, *e.g.*, turbidimetry. Furthermore, the glycopolymer-functionalized gold nanoparticles were investigated towards their protein recognition capabilities, revealing binding of the mannosylated nanoparticles to the lectin Concanavalin A. Also for this study, very low polymer concentrations were sufficient, in contrast to turbidimetry, which is one of the commonly used techniques for determination of lectin interactions. However, unlike comparably sensitive methods like quartz crystal microbalance (QCM) or specialized surface plasmon resonance (SPR) devices, this method only requires a standard UV-Vis spectrophotometer.

In summary, a new mannose monomer as well as the analogue glucose monomer were synthesized and polymerized by RAFT polymerization. This synthetic strategy was shown to represent a versatile route towards well-defined thermoresponsive glycopolymers which can selectively recognize lectins.

The glycopolymer immobilized gold nanoparticles were shown to be an efficient sensor to determine LCST behavior as well as lectin interaction at very low polymer concentrations where turbidity measurements are not possible anymore.

Appendix

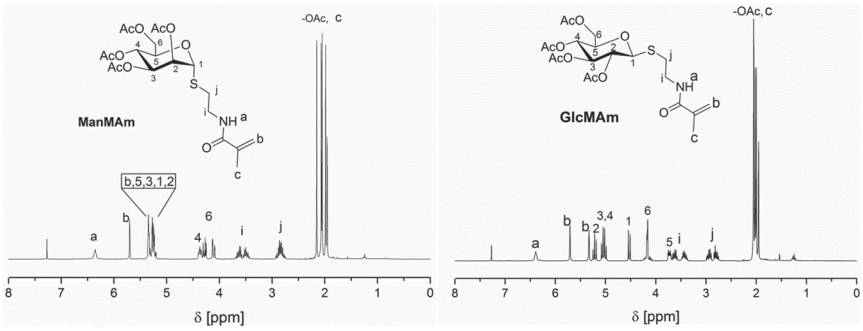

*Figure A1. [1]H NMR spectra of the two glycomonomers **ManMAm** (left) and **GlcMAm** (right) (300 MHz, $CDCl_3$).*

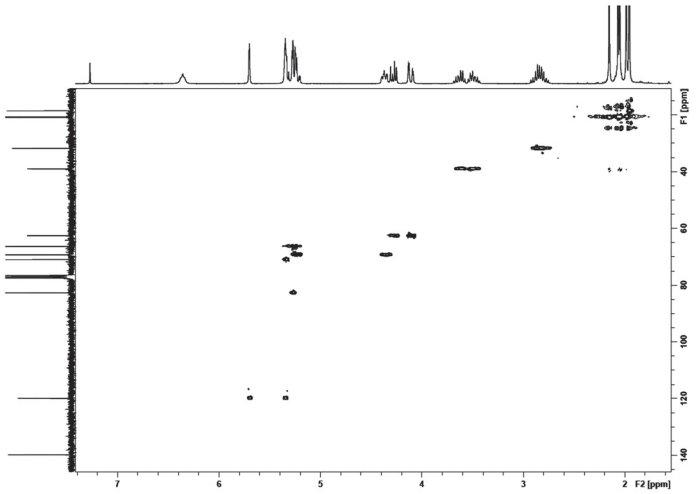

Figure A2. HSQC NMR spectrum of ManMAm (300 MHz, $CDCl_3$).

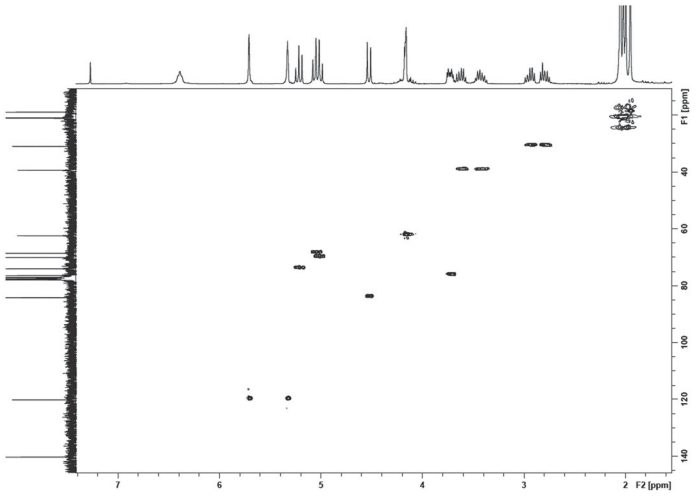

Figure A3. HSQC NMR spectrum of GlcMAm (300 MHz, $CDCl_3$).

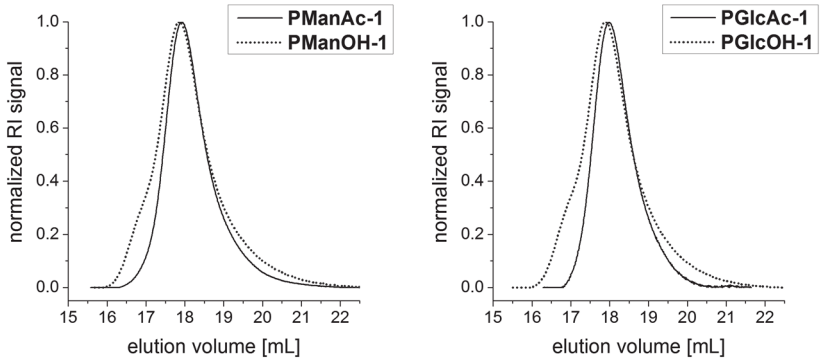

Figure A4. Overlay of the size exclusion chromatograms of selected protected and deprotected mannose carrying glycopolymers (left) and glucose carrying glycopolymers, (right) (DMAc/LiCl).

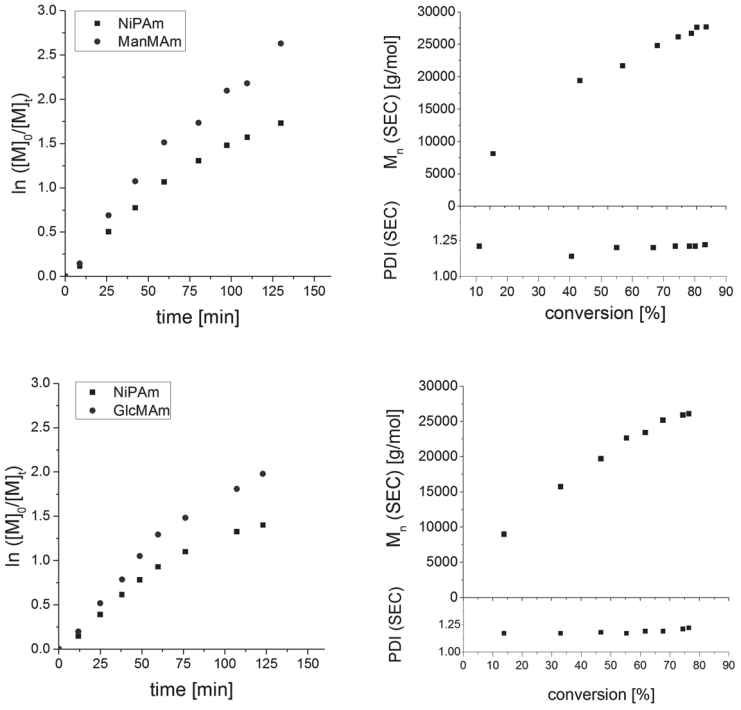

Figure A5. Pseudo-first order kinetic plot and molar mass versus conversion for the two copolymerizations of NiPAm with ManMAm (top) and GlcMAm (bottom), ([M]:[CTA]:[ACVA] = 200:1:0.1, [M] = 2 mol/L in DMF, T = 80 °C).

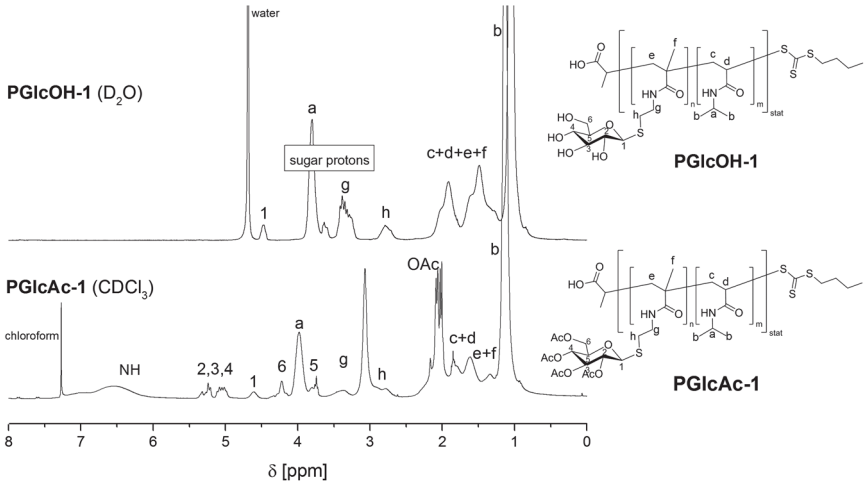

*Figure A6. [1]H NMR spectra of the two glycopolymers **PGlcAc-1** and **PGlcOH-1** (300 MHz, $CDCl_3$ or D_2O).*

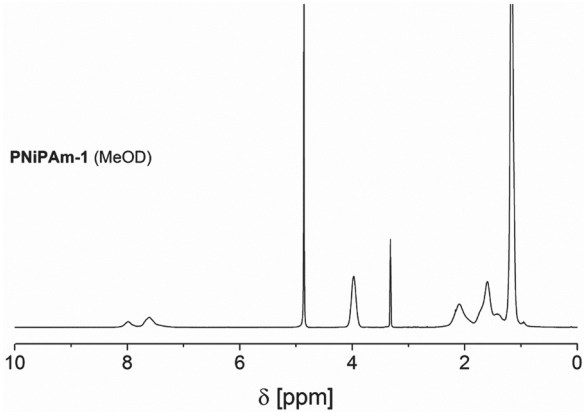

*Figure A7. [1]H NMR spectrum of **PNiPAm-1** (300 MHz, MeOD).*

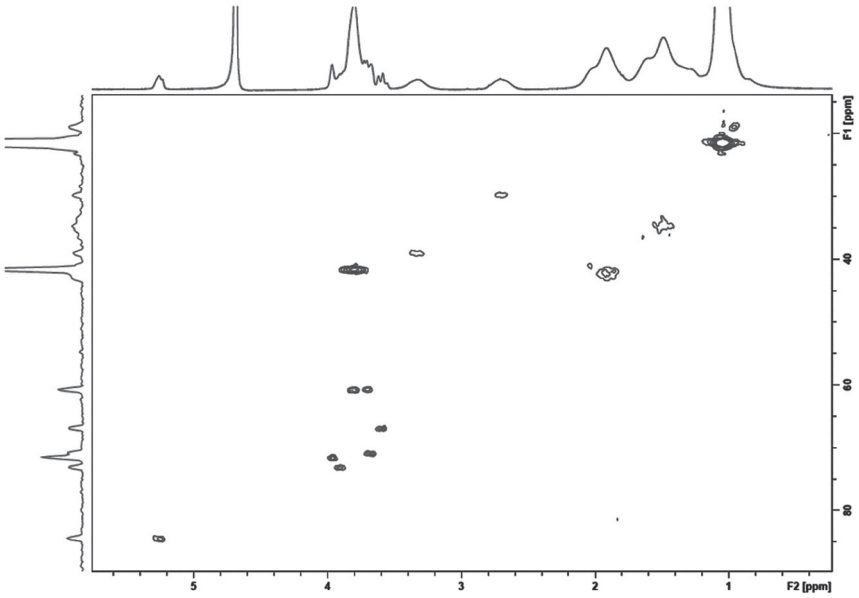

Figure A8. HSQC NMR spectrum of PManOH-1 (300 MHz, D_2O).

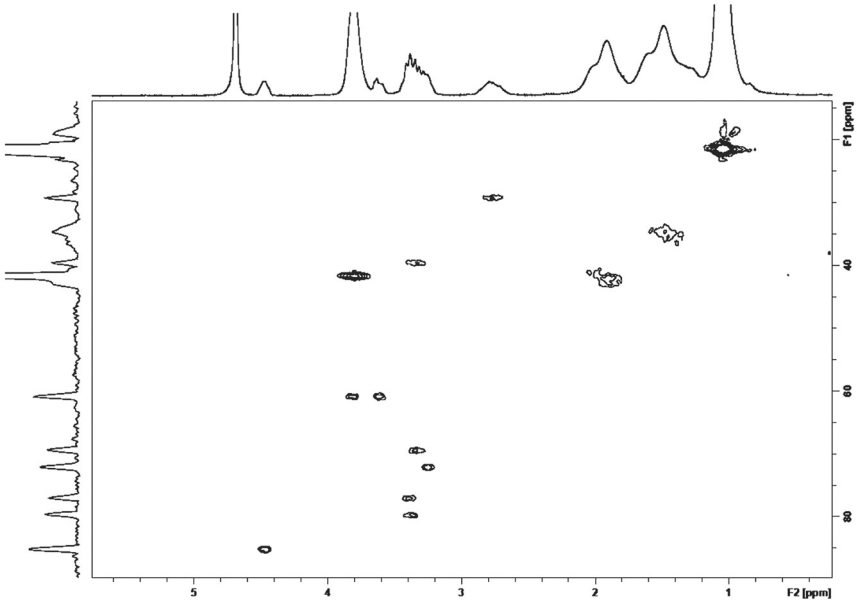

Figure A9. HSQC NMR spectrum of PGlcOH-1 (300 MHz, D_2O).

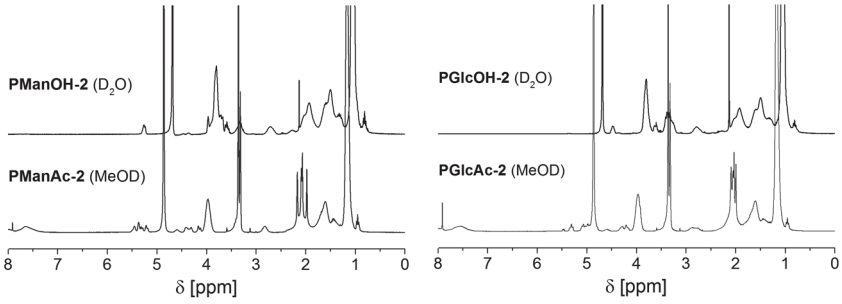

Figure A10. Overlay of ^1H NMR spectra of PManAc-2 and PManOH-2 (left) as well as PGlcAc-2 and PGlcOH-2 (right, 300 MHz, MeOD or D_2O).

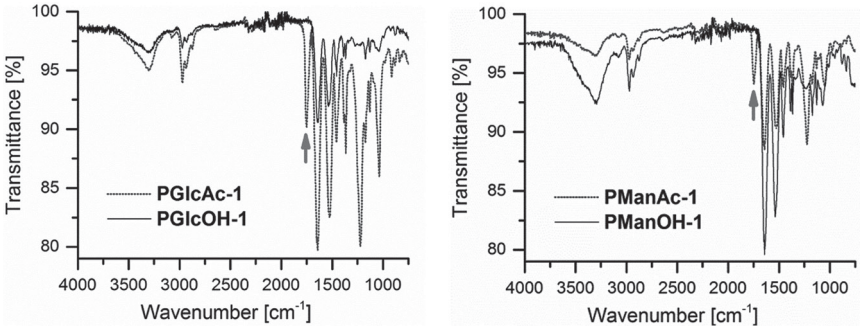

Figure A11. Overlay of the ATR FT-IR spectra of the protected and deprotected glucose glycopolymer (left) and overlay of the protected as well as the deproteded mannose glycopolymers (right).

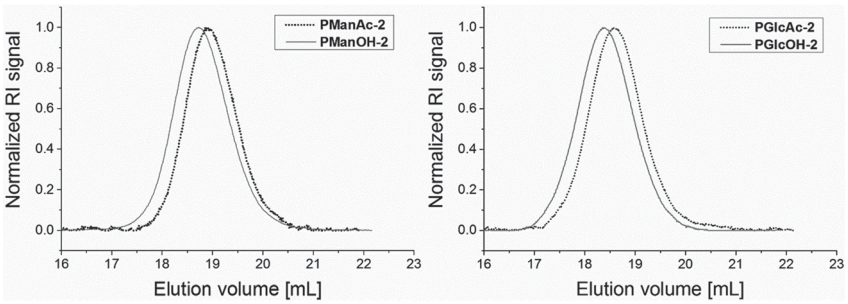

*Figure A12. Overlay of the size exclusion chromatograms of **PManAc-2** and **PManOH-2** (left) as well as **PGlcAc-2** and **PGlcOH-2** (right).*

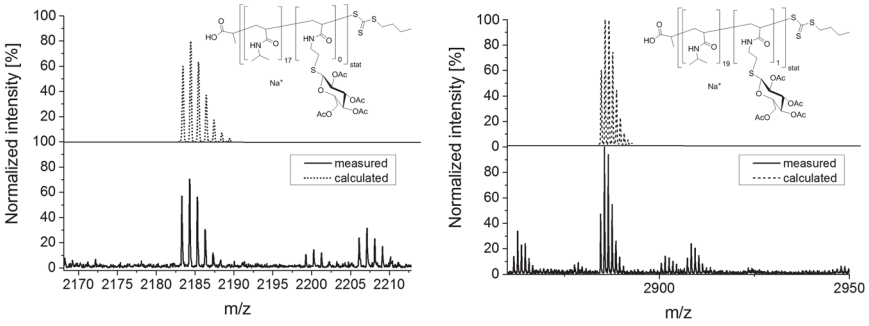

Figure A13. Overlay of the measured and calculated isotopic patterns without protected glucose repeating unit (left) and with one protected glucose repeating unit (right), calculated for $C_3H_5O_2(C_6H_{11}NO)_{17}C_5H_9S_3 + Na^+$ (left) and $C_3H_5O_2(C_{20}H_{29}NO_{10}S)_1(C_6H_{11}NO)_{19}C_5H_9S_3 + Na^+$ (right).

In Controlled Radical Polymerization: Materials; Tsarevsky, et al.;
ACS Symposium Series; American Chemical Society: Washington, DC, 2015.

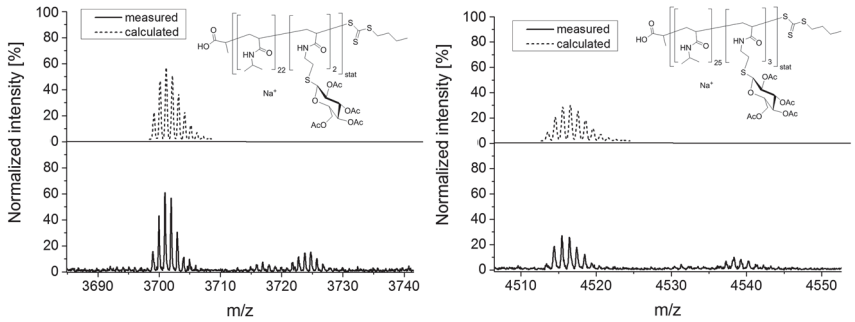

Figure A14. Overlay of the measured and calculated isotopic patterns with two protected glucose repeating units (left) and three protected glucose repeating units (right), calculated for $C_3H_5O_2(C_{20}H_{29}NO_{10}S)_2(C_6H_{11}NO)_{22}C_5H_9S_3 + Na^+$ (left) and $C_3H_5O_2(C_{20}H_{29}NO_{10}S)_3(C_6H_{11}NO)_{25}C_5H_9S_3 + Na^+$ (right).

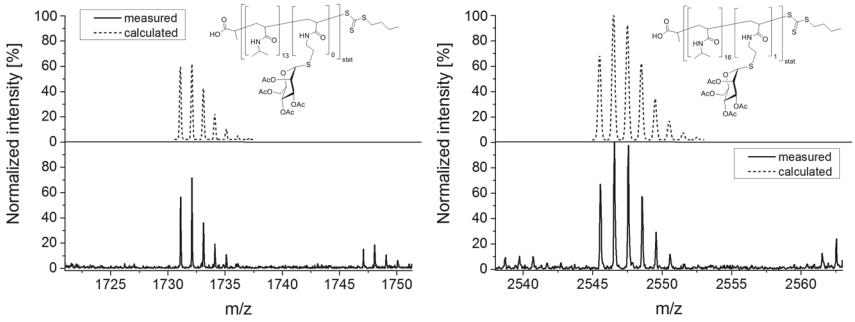

Figure A15. Overlay of the measured and calculated isotopic patterns without mannose repeating unit (left) and with one protected mannose repeating unit (right), calculated for $C_3H_5O_2(C_6H_{11}NO)_{13}C_5H_9S_3 + Na^+$ (left) and $C_3H_5O_2(C_{20}H_{29}NO_{10}S)_1(C_6H_{11}NO)_{16}C_5H_9S_3 + Na^+$ (right).

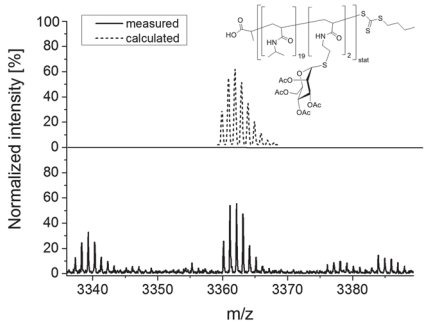

Figure A16. Overlay of the measured and calculated isotopic patterns with two protected mannose repeating units, calculated for $C_3H_5O_2(C_{20}H_{29}NO_{10}S)_2(C_6H_{11}NO)_{19}C_5H_9S_3 + Na^+$.

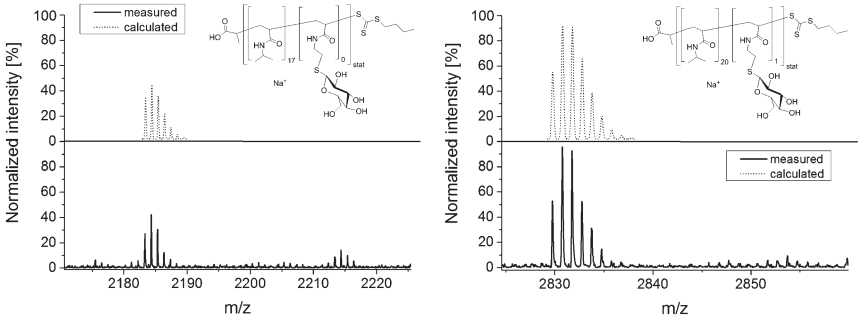

Figure A17. Overlay of the measured and calculated isotopic patterns without (left) and with one (right) glucose repeating unit. Calculated for $C_3H_5O_2(C_6H_{11}NO)_{17}C_5H_9S_3 + Na^+$ (left) and $C_3H_5O_2(C_{12}H_{21}NO_6S)(C_6H_{11}NO)_{20}C_5H_9S_3 + Na^+$ (right).

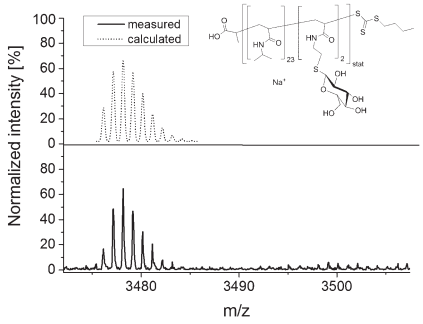

Figure A18. Overlay of the measured and calculated isotopic pattern with two repeating units of glucose, calculated for $C_3H_5O_2(C_{12}H_{21}NO_6S)_2(C_6H_{11}NO)_{23}C_5H_9S_3 + Na^+$.

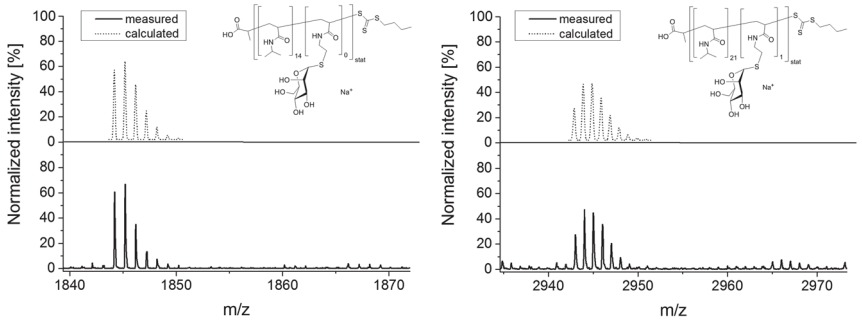

Figure A19. Overlay of the measured and calculated isotopic patterns without (left) and with one (right) deprotected mannose repeating unit, calculated for $C_3H_5O_2(C_6H_{11}NO)_{14}C_5H_9S_3 + Na^+$ (left) and $C_3H_5O_2(C_{12}H_{21}NO_6S)_1(C_6H_{11}NO)_{21}C_5H_9S_3 + Na^+$ (right).

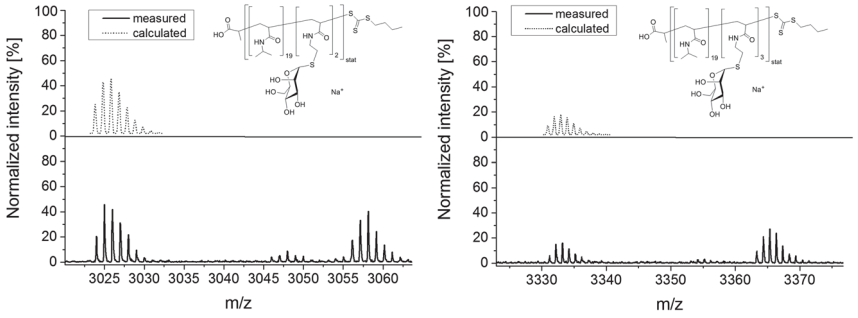

Figure A20. Overlay of the measured and calculated isotopic patterns with two (left) and three (right) deprotected mannose repeating units, calculated for $C_3H_5O_2(C_{12}H_{21}NO_6S)_2(C_6H_{11}NO)_{19}C_5H_9S_3 + Na^+$ (left) and $C_3H_5O_2(C_{12}H_{21}NO_6S)_3(C_6H_{11}NO)_{19}C_5H_9S_3 + Na^+$ (right).

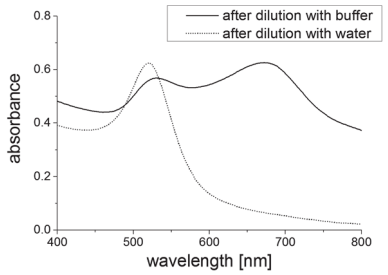

Figure A21. Overlay of UV/Vis spectra of the nanoparticle solution (same concentrations as for the lectin experiment) with and without buffer.

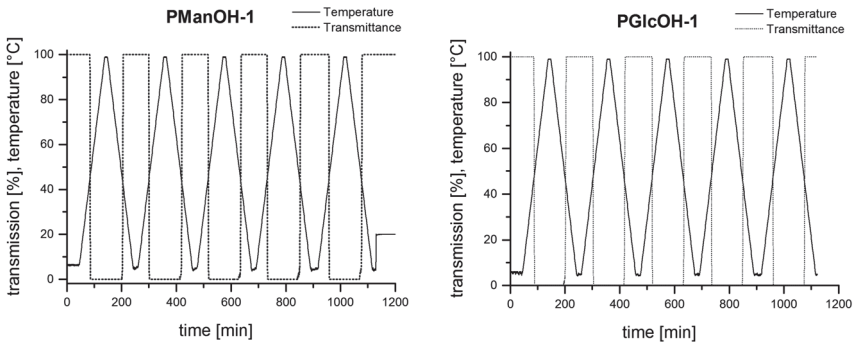

*Figure A22. Turbidimetric determination of the cloud point temperatures of the two glycopolymers **PManOH-1** (left) and **PGlcOH-1** (right) (5 mg/mL in TBS).*

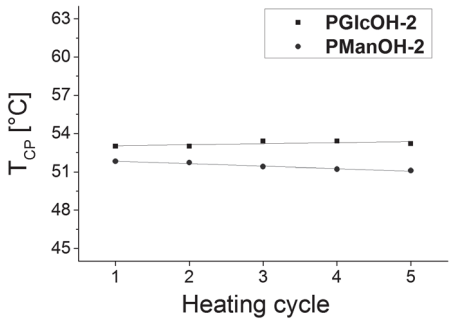

*Figure A23. T_{CP}s of **PGlcOH-2** and **PManOH-2** of successive heating cycles.*

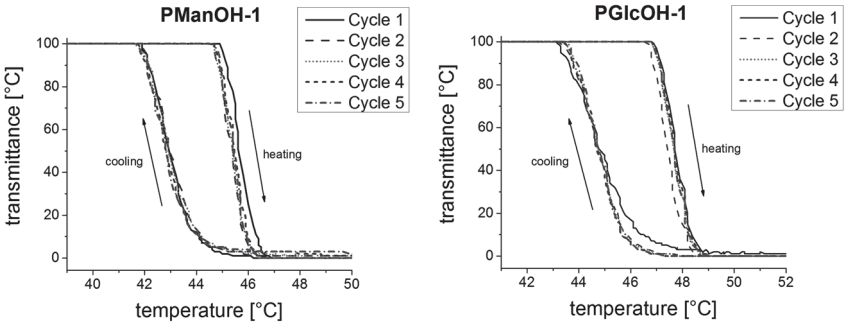

Figure A24. Transmittance plotted vs. temperature to show the heating-cooling hysteresis of the association and dissociation of the polymer chains in aqueous solution (5 mg/mL in TBS, heating rate 1 K×min^{-1}).

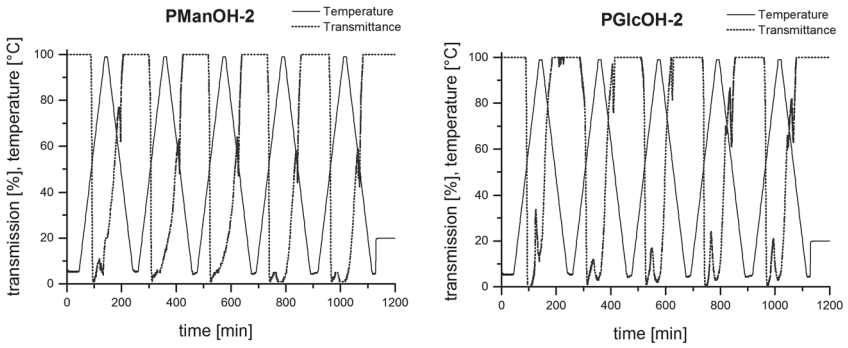

*Figure A25. Turbidimetric study of aqueous solutions of **PManOH-2** (left) as well as **PGlcOH-2** (right) (5 mg/mL in TBS).*

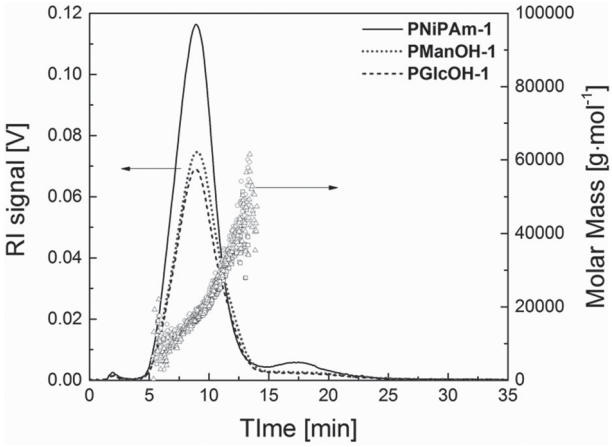

*Figure A26. Overlay of the AF4-MALLS fractograms of **PNiPAm-1**, **PManOH-1** and **PGlcOH-1** with 5 mM NaCl as eluent.*

Acknowledgments

This research forms part of the research program of the Dutch Polymer Institute (DPI), project #686. CW is thankful to the Carl Zeiss Foundation. Financial support from the research initiative PhoNa (Photonic nanomaterials), which is supported by the German Federal Ministry of Education and Research in the program "Spitzenforschung und Innovation in den Neuen Ländern" (support code 03IS2101A), is acknowledged. The authors also acknowledge the Thüringer Ministerium für Bildung, Wissenschaft und Kultur (grant no. B515-07008) for financial support. M. Wagner is acknowledged for the AF4 measurements. The authors also thank Bruker Daltonics for their help and support. TEM measurements were performed at the JSCM facilities, which were financed by the DFG and the European Fonds for Regional Development (EFRE).

References

1. Vázquez-Dorbatt, V.; Lee, J.; Lin, E.-W.; Maynard, H. D. *ChemBioChem* **2012**, *13*, 2478–2487.
2. Godula, K.; Bertozzi, C. R. *J. Am. Chem. Soc.* **2012**, *134*, 15732–15742.
3. Godula, K.; Bertozzi, C. R. *J. Am. Chem. Soc.* **2010**, *132*, 9963–9965.
4. Narla, S. N.; Sun, X.-L. *Lab Chip* **2012**, *12*, 1656–1663.
5. Narain, R.; Housni, A.; Gody, G.; Boullanger, P.; Charreyre, M.-T.; Delair, T. *Langmuir* **2007**, *23*, 12835–12841.
6. Anraku, Y.; Takahashi, Y.; Kitano, H.; Hakari, M. *Colloids Surf., B* **2007**, *57*, 61–68.
7. Housni, A.; Cai, H.; Liu, S.; Pun, S. H.; Narain, R. *Langmuir* **2007**, *23*, 5056–5061.
8. Kitano, H.; Nakada, H.; Mizukami, K. *Colloids Surf., B* **2008**, *61*, 17–24.

9. Mizukami, K.; Takakura, H.; Matsunaga, T.; Kitano, H. *Colloids Surf., B* **2008**, *66*, 110–118.
10. Vázquez-Dorbatt, V.; Tolstyka, Z. P.; Chang, C.-W.; Maynard, H. D. *Biomacromolecules* **2009**, *10*, 2207–2212.
11. Kitano, H.; Saito, D.; Kamada, T.; Gemmei-Ide, M. *Colloids Surf., B* **2012**, *93*, 219–225.
12. Huang, M.; Shen, Z.; Zhang, Y.; Zeng, X.; Wang, P. G. *Bioorg. Med. Chem. Lett.* **2007**, *17*, 5379–5383.
13. Toyoshima, M.; Miura, Y. *J. Polym. Sci., Part A: Polym. Chem.* **2009**, *47*, 1412–1421.
14. Spain, S. G.; Albertin, L.; Cameron, N. *Chem. Commun.* **2006**, 4198–4200.
15. Ishii, J.; Toyoshima, M.; Chikae, M.; Takamura, Y.; Miura, Y. *Bull. Chem. Soc. Jpn.* **2011**, *84*, 466–470.
16. Ebeling, B.; Vana, P. *Macromolecules* **2013**, *46*, 4862–4871.
17. Rossner, C.; Vana, P. *Angew. Chem.* **2014**, *126*, 1–5.
18. Pearson, S.; Chen, G.; Stenzel, M. H. Synthesis of Glycopolymers. In *Engineered Carbohydrate-based Materials for Biomedical Applications: Polymers, Surfaces, Dendrimers, Nanoparticles, and Hydrogels*; Narain, R., Ed.; John Wiley & Sons, Inc.: Hoboken, NJ, USA, 2011; pp 1–118.
19. Ting, S. R. S.; Min, E. H.; Escalé, P.; Save, M.; Billon, L.; Stenzel, M. H. *Macromolecules* **2009**, *42*, 9422–9434.
20. Ghadban, A.; Albertin, L. *Polymers* **2013**, *5*, 431–526.
21. Shen, H.; Byers, L. D. *Biochem. Biophys. Res. Commun.* **2007**, *362*, 717–720.
22. Wilson, J. C.; Kiefel, M. J.; Angus, D. I.; von Itzstein, M. *Org. Lett.* **1999**, *1*, 443–446.
23. Chen, G.; Amajjahe, S.; Stenzel, M. H. *Chem. Commun.* **2009**, 1198–1200.
24. Diehl, C.; Schlaad, H. *Chem. Eur. J.* **2009**, *15*, 11469–11472.
25. Diehl, C.; Schlaad, H. *Macromol. Biosci.* **2009**, *9*, 157–161.
26. Von der Ehe, C.; Czaplewska, J. A.; Gottschaldt, M.; Schubert, U. S. *Eur. Polym. J.* **2013**, *49*, 2660–2669.
27. Eissa, A. M.; Khosravi, E. *Eur. Polym. J.* **2011**, *47*, 61–69.
28. Zhang, L.; Bernard, J.; Davis, T. P.; Barner-Kowollik, C.; Stenzel, M. H. *Macromol. Rapid. Commun.* **2008**, *29*, 123–129.
29. Shinde, V. S.; Pawar, V. U. *J. Appl. Polym. Sci.* **2009**, *111*, 2607–2615.
30. Pasparakis, G.; Cockayne, A.; Alexander, C. *J. Am. Chem. Soc.* **2007**, *129*, 11014–11015.
31. Özyurek, Z.; Voit, B.; Krahl, F.; Arndt, K.-F. *e-Polymers* **2010**, *44*, 1–13.
32. Özyürek, Z.; Komber, H.; Gramm, S.; Schmaljohann, D.; Müller, A. H. E.; Voit, B. *Macromol. Chem. Phys.* **2007**, *208*, 1035–1049.
33. Min, E. H.; Ting, S. R. S.; Billon, L.; Stenzel, M. H. *J. Polym. Sci., Part A: Polym. Chem.* **2010**, *48*, 3440–3455.
34. Luo, Y.; Liu, L.; Wang, X.; Shi, H.; Lv, W.; Li, J. *Soft Matter* **2012**, *8*, 1634–1642.
35. Kumar, J.; McDowall, L.; Chen, G.; Stenzel, M. H. *Polym. Chem.* **2011**, *2*, 1879–1886.

36. Idota, N.; Ebara, M.; Kotsuchibashi, Y.; Narain, R.; Aoyagi, T. *Sci. Technol. Adv. Mater.* **2012**, *13*, 1–9.
37. Yusa, S.; Fukuda, K.; Yamamoto, T.; Iwasaki, Y.; Watanabe, A.; Akiyoshi, K.; Morishima, Y. *Langmuir* **2007**, *23*, 12842–12848.
38. Kusolkamabot, K.; Sae-ung, P.; Niamnont, N.; Wongravee, K.; Sukwattanasinitt, M.; Hoven, V. P. *Langmuir* **2013**, *29*, 12317–12327.
39. Firouzzare, M.; Wang, Q. *Talanta* **2012**, *101*, 261–266.
40. Kretschmer, F.; Mansfeld, U.; Hoeppener, S.; Hager, M. D.; Schubert, U. S. *Chem. Commun.* **2014**, *50*, 88–90.
41. Yohannes, G.; Jussila, M.; Hartonen, K.; Riekkola, M.-L. *J. Chromatogr. A* **2011**, *1218*, 4104–4116.
42. Cheng, H.; Shen, L.; Wu, C. *Macromolecules* **2006**, *39*, 2325–2329.

Publication 4

Detailed MALDI comparison of *N*iPAm glycopolymers

S. Crotty, C. von der Ehe, C. Weber, U. S. Schubert

Eur. Polym. J. **2015**, *71*, 325-335.

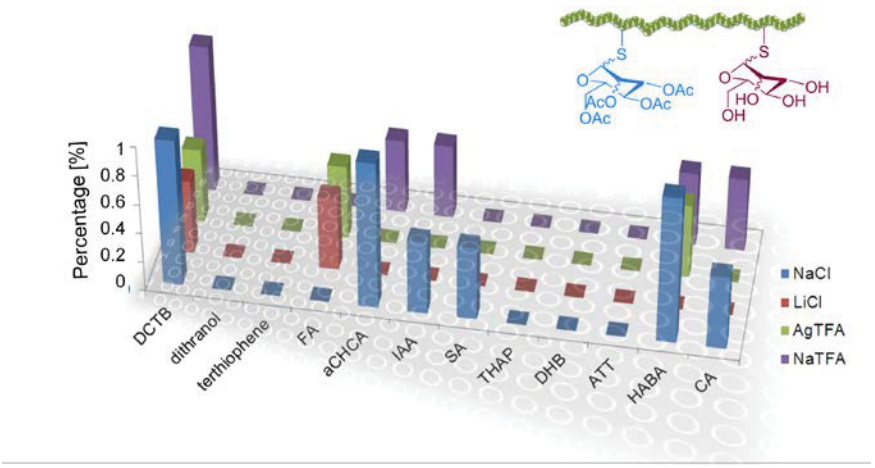

European Polymer Journal 71 (2015) 325–335

Contents lists available at ScienceDirect

European Polymer Journal

journal homepage: www.elsevier.com/locate/europolj

Macromolecular Nanotechnology

Detailed MALDI comparison of *N*iPAm glycopolymers

Sarah Crotty, Christian von der Ehe, Christine Weber *, Ulrich S. Schubert *

Laboratory of Organic and Macromolecular Chemistry (IOMC), Friedrich Schiller University Jena, Humboldstr. 10, 07743 Jena, Germany
Jena Center for Soft Matter (JCSM), Friedrich Schiller University Jena, Philosophenweg 7, 07743 Jena, Germany

ARTICLE INFO

Article history:
Received 2 July 2015
Received in revised form 7 August 2015
Accepted 9 August 2015
Available online 11 August 2015

Keywords:
Glycopolymers
MALDI-TOF MS
RAFT polymerization
Mannose
Glucose
*N-iso*propylacrylamide

ABSTRACT

A series of poly(*N*-isopropylacrylamide) (P*N*iPAm) statistical glycopolymers with either glucose or mannose based comonomers were analyzed in detail by matrix-assisted laser/desorption ionization time-of-flight mass spectrometry (MALDI-TOF MS). A systematic differentiation between first the protected copolymers and secondly the deprotected ones were performed. Furthermore, MALDI-TOF MS was exploited to investigate which matrix and cationization agent combination was best suited with respect to end group preservation, suppression of certain polymeric species as well as the signal to noise (S/N) ratio. The combination of the matrix DCTB and NaCl as cationization agent proved superior for all polymers, regardless whether in protected or deprotected form. Software analysis of the mass spectra using the computational tool COCONUT is shown to provide accurate information on the overall composition of the copolymers.

1. Introduction

Mass spectrometry (MS) has been widely used in a wide range of fields such as proteins and peptides as biological systems [1–4]. Eventually these advanced techniques reached out for none monodisperse analytes, such as natural as well as synthetic polymers [5]. The latter can be tailored to specific applications, which is possible because many different polymer types are accessible by living and controlled polymerization techniques. As a consequence, a great variety of polymeric architectures and end groups can be synthesized [6–8]. Offering great possibilities with respect to widespread applications, this makes the structural characterization much more demanding. As a consequence, MS techniques have evolved to provide structural features to highlight the complexity of synthetic polymer molecules [9]. Soft ionization techniques have been used to analyze polymers, circumventing the fragmentation observed for harsher ionization methods. Besides electrospray ionization (ESI) and atmospheric pressure chemical ionization (APCI), matrix-assisted laser desorption ionization (MALDI) is currently the most widely used technique in polymer analysis. Although valuable information such as the polydispersity index (PDI), molar masses (M_n and M_w), sequences and end groups can be determined, MALDI-TOF MS involves numerous steps to finally obtain a spectrum. Over the years the sample preparation has developed and the most common techniques are the dried droplet method [10–13], layering method [10] as well as spraying methods. The dried droplet is the simplest, fastest and mostly applied method for routine measurements. However, it is prone to the formation of heterogeneous crystals – so called 'hot spots' – and thus producing a commonly named coffee 'ring effect' at the sample surface [14]. MALDI-TOF MS has been used and developed with IR or UV [15] lasers to introduce the analyte ions into the gas phase [16]. The matrix

* Corresponding authors at: Laboratory of Organic and Macromolecular Chemistry (IOMC), Friedrich Schiller University Jena, Humboldstr. 10, 07743 Jena, Germany.
E-mail addresses: christine.weber@uni-jena.de (C. Weber), ulrich.schubert@uni-jena.de (U.S. Schubert).

http://dx.doi.org/10.1016/j.eurpolymj.2015.08.010
0014-3057/

represents a key item: A small molecule absorbing energy at the wavelength of the laser to volatilize the analyte [17]. While general trends for the choice of the matrix have been established over the years for the analysis of biological analytes such as lipids or proteins [4,18], this mostly remains a trial and error process for the synthetic polymers. Little efforts regarding systematic research are undertaken, but the polarity *i.e.* its hydrophobicity or hydrophilicity of a matrix relative to the analyte and a good co-crystallization of both seem to play an important role [19,20].

As shown in Fig. 1, commonly used matrices represent aromatic systems and exist with diverse functional groups. To provide an overview, the matrices used in this study have been divided in three categories regarding their polarity, ranging from carboxylic acids over alcohols to non-polar functional groups.

Moreover, MALDI-TOF mass spectra of polymers are usually acquired with cationization agents (salts) to enable the charging of the polymer in the gas phase, which represents a necessity in any MS method. As a consequence the peak intensities are increased and a complete ionization of the polymer chain is promoted. In this study, cationization agents based on sodium, lithium or silver cations were investigated systematically.

This contribution focuses on glycopolymers due to their significance in various fields such as the interaction with lectins (proteins) [21]. Fig. 2 shows the structure of the investigated copolymers, which were synthesized using the reversible-addition fragmentation chain transfer (RAFT) radical polymerization technique. The second comonomer present in the analyte, *N*iPAm is also interesting because of its lower critical solution temperature (LCST) behavior, which can be utilized to create "smart" materials whose properties respond to temperature changes [22,23]. A few examples exploring similar monomer structures have been studied with MALDI-TOF MS. In general, optimum matrix and measurement conditions were investigated for similar glycopolymers. Furthermore, mostly protected homopolymers or copolymers were investigated with MALDI while spectra of deprotected polymers are scarce [24–26]. Nonetheless, a 2D composition map was used to determine the microstructures of the copolymers but unfortunately without a sugar moiety [24]. Throughout these specific examples, deprotected forms of glycopolymers represent a challenging study for mass spectrometry, however, with specific conditions successful spectra could be obtained. Moreover, it has been observed that complementary methods have proven to be crucial to determine the molar mass, composition and conversions. Thus, to the best of our knowledge, no detailed investigations of synthetic glycopolymers with MALDI-TOF MS have been reported so far.

This study focusses on an in-depth characterization and discussion of the possibilities and drawbacks of MALDI-TOF MS of these copolymers. First, an extended screening that includes many matrices and cationization agents to ascertain the optimum measurement conditions will be presented. The obtained spectra will then be scrutinized with respect to end group preservation, suppression of certain polymeric species as well as the signal to noise (S/N) ratio. Finally, the copolymer composition will be elucidated based on MS data using the very recently developed software tool COCONUT [27].

2. Experimental section

2.1. Materials

The matrices used for the MALDI-TOF MS *trans*-2-[3-(4-*tert*-butylphenyl)-2-methyl-2-propenylidene]malononitrile (DCTB synthesized in house), 3-indoleacrylic acid (IAA, Sigma Aldrich), 2,5-dihydroxybenzoic acid (DHB, Sigma Aldrich), 4′-hydroxyazobenzene-2-carboxylic acid (HABA, Fluka), α-cyano-4-hydroxycinnamic acid (αCHCA, Sigma Aldrich), sinapinic acid (SA, Fluka), ferulic acid (FA, Fluka), caffeic acid (CA, Sigma Aldrich), dithranol (Sigma Aldrich), 6-aza-2-thiothymine (ATT, Sigma Aldrich), 2,4,6-trihydroxyacetophenone (THAP, Sigma Aldrich) and terthiophene (Sigma Aldrich), the cationization agents sodium chloride (NaCl, Sigma Aldrich), sodium trifluoroacetate (NaTFA, Sigma Aldrich), silver trifluoroacetate (AgTFA, Sigma Aldrich), lithium chloride (LiCl, Sigma Aldrich) as well as ethanol, tetrahydrofuran, methanol, chloroform and acetone (HPLC grade, Roth) were used as purchased.

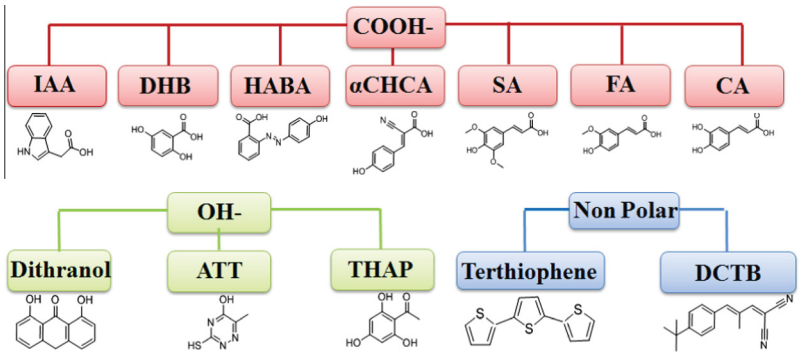

Fig. 1. Schematic representation of the matrices used in this study.

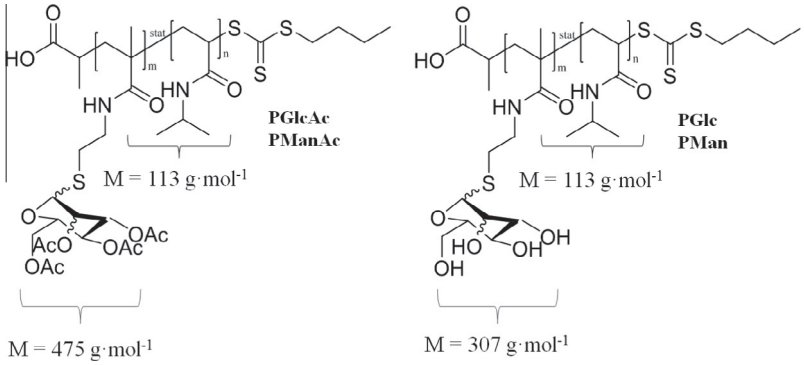

Fig. 2. Schematic representation of the glycopolymers investigated in this study.

2.2. General methods and instrumentation

Matrix-assisted laser desorption ionization time-of-flight mass spectrometry (MALDI-TOF MS) mass spectra were measured on an Ultraflex III TOF/TOF mass spectrometer (Bruker Daltonics) equipped with Nd:YAG laser and collision energy cell. Nuclear magnetic resonance (NMR) spectra were recorded at 298 K on a Bruker AC 300 (300 MHz) or a Bruker AC 250 (250 MHz) spectrometer, respectively. Size exclusion chromatograms (SEC) were measured using an Agilent 1200 series system with a PSS GRAM 1000/30 Å (10 µm particle size) column, a G1310A pump, a G1362A refractive index detector at 40 °C with a flow rate of 1 mL min^{-1}. *N,N*-Dimethylacetamide with 0.21% LiCl was used as eluent.

2.3. Synthesis

A more detailed description of the synthesis and characterization data of the polymers is provided in a previous publication [28].

2.3.1. RAFT polymerization

The monomers *N*iPAm and GlcMAm or ManMAm, the RAFT agent BTTCP and the initiator ACVA were dissolved in DMF ([M]:[CTA]:[AVCA] = 25:1:0.1, [monomer] = 2 mol L^{-1}) and the mixture was degassed by purging with argon for 1.5 h. After removal of an aliquot for conversion analysis the polymerization mixture was stirred at 80 °C for 15 h. Another aliquot (100 µL) was removed for conversion analysis by ^{1}H NMR spectroscopy. The polymers were purified by preparative size exclusion chromatography (BioBeads® column S-X1, eluent: THF) followed by precipitation into 15 mL of *n*-hexane and subsequently dried under reduced pressure. The polymers were characterized by means of SEC, NMR spectroscopy and MALDI-TOF MS [28].

2.3.2. Glycopolymer deprotection

The protected glycopolymer was dissolved in anhydrous methanol and catalytic amounts of sodium methoxide solution (0.5 M in methanol) were added. After the solution was stirred for 2 h at room temperature, the mixture was neutralized with 1 M hydrochloric acid. The polymers were purified by evaporation of the solvent, taking up the residue in ethanol, followed by filtration in order to remove the salt. After evaporation of the solvent the residue was re-dissolved in deionized water. Finally, all polymers were lyophilized. The deprotection was confirmed by SEC, NMR elemental analysis and mass spectrometry methods [28].

2.4. MALDI-TOF MS

MALDI-TOF MS experiments were performed with an Ultraflex III TOF/TOF (Bruker Daltonics, Bremen, Germany) equipped with a Nd:YAG laser (smartbeam, 200 Hz) and a collision cell. All spectra were measured in the positive reflector mode. The instrument was calibrated prior to each measurement with an external poly(methyl methacrylate) (PMMA) standard (*m/z* 410 or 2500) from PSS Polymer Standards Services GmbH (Mainz, Germany) in the required measurement range. MS data was processed using Flex Analysis 3.0, PolyTools 1.12 (beta version), Data Explorer 4.0 and an isotope pattern calculator. The ion abundances of several scans were summed up to obtain spectra with good signal/noise ratio for MS experiments. The quoted *m/z* values are monoisotopic. For the sample preparation, 10 µL of the polymer solution (10 mg mL^{-1}) in the specific solvent, 30 µL of the matrix solution (30 mg mL^{-1}) in the specific solvent, and 10 µL of the cationization agent in the specific solvent at a concentration of 100 mg mL^{-1} were mixed and the dried-droplet sample preparation method was applied. The presence of the potassium adducts could have been omitted by increasing the volume of the sodium salts. However, to keep the ratios of salt, matrix and analyte constant and, thus, comparable to the silver and lithium salts, the

salt concentration was not increased for the sodium salts. For the MALDI-TOF MS sample preparation, the matrices were prepared with DCTB (30 mg mL^{-1} in chloroform), IAA (30 mg mL^{-1} in chloroform), DHB (30 mg mL^{-1} in chloroform), HABA (30 mg mL^{-1} in chloroform), αCHCA (30 mg mL^{-1} in acetonitrile), SA (30 mg mL^{-1} in acetone), FA (30 mg mL^{-1} in methanol), CA (30 mg mL^{-1} in ethanol), dithranol (30 mg mL^{-1} in chloroform), ATT (30 mg mL^{-1} in methanol), THAP (30 mg mL^{-1} in methanol) and terthiophene (30 mg mL^{-1} in tetrahydrofuran), and of the cationization agents: NaCl (100 mg mL^{-1} in chloroform), NaTFA (100 mg mL^{-1} in acetone), LiCl (100 mg mL^{-1} in chloroform) and AgTFA (100 mg mL^{-1} in methanol) were prepared and subsequently mixed according to the dried-droplet spotting technique. In case of saturated solutions, only the supernatant was used. For each sample 1 μL of the mixture was spotted on a target plate. Each sample was spotted several times and allowed to air-dry at ambient conditions. The laser fired 10,000 shots per sample spot accumulated from the total spot using the random walk.

3. Results and discussion

The polymers used for this investigation have a rather low molar mass to ensure a sufficient quality of the MALDI-TOF mass spectra to be able to draw structural information from well resolved isotopic patterns. A low polydispersity index is another prerequisite that is met so that the entire sample can be ionized if appropriate conditions are applied. However, copolymers are challenging for detailed MS interpretations in general because the degrees of polymerization (DP) of both monomers will vary, which results in a much larger amount of peaks in the mass spectra in comparison to simple homopolymers. In this view, the advantage of the investigated polymers is the large mass difference of both monomers used (M(*N*iPAm) = 113.08 g mol^{-1}, M(Glycomonomer) = 475.15 g mol^{-1}). To further simplify the analysis the copolymers contain only 10 mol% sugar units. Thus, the large excess of the *N*iPAm and the high molar mass of the glycomonomer should significantly reduce the amount of overlapping isotopic patterns in the spectra. Furthermore, it should be noted that the deprotection of the sugar moieties represents a post-polymerization reaction and, therefore, does not influence the comonomer ratio in the polymer. However, the mass of the sugar repeating units is lowered because of the loss of the acetyl protection groups (M = 307.11 g mol^{-1}). All polymers are thoroughly characterized by means of SEC as relative method for M_n determination and NMR spectroscopy to confirm the purity and the copolymer composition [28]. Table 1 provides a short overview of the most important characterization data.

The first step in this study represented an extensive screening to identify the optimum measurement condition for MALDI-TOF MS. For this purpose, numerous matrices and cationization agents were used to evaluate similarities and, even more interestingly, the discrepancies. Fig. 1 represents the matrices used, for the ionization of statistical glycopolymers of P*N*iPAm containing either glucose or mannose in protected as well as its deprotected form (Fig. 2). In general, polar matrices are expected to favor the ionization of polar polymers, whereas nonpolar matrices would be used for measurement of nonpolar analytes [19]. In this view, it should be noted that the deprotected glycopolymer would be more polar than a P*N*iPAm homopolymer, while the acetyl protection groups render the protected glycopolymer less polar.

All polymers were cationized by using NaCl, LiCl, NaTFA and AgTFA, combined with all matrices as shown in Fig. 1. This resulted in 48 permutations per polymer. To ensure a uniform surface and provide a basis for a sufficient co-crystallization of matrix and analyte, the polymers were dissolved in chloroform, where most of the used matrices were soluble as well. In Tables 2 and 3 a resume of the ionization characteristics is displayed for both protected and deprotected polymers, respectively. The nomenclature on the side represented by colors and the percentages show how well the polymers were ionized. The green color indicates that all chains of the polymers were ionized, that the baseline was low, the signal to noise ratio was low and finally no suppression of high or low molar masses was observed. The blue color signifies that the polymer chains were ionized but one of the characteristics described above was not met. This is due to the increased laser power required for ionization, which enhances the occurrence of these undesired side effects. Finally, the red color shows that no ionization was possible or a very high laser power had to be used to obtain a spectrum.

As shown in Table 2, a general trend for the protected polymers can be observed irrespective of the type of protected sugar pendant on the P*N*iPAm. Most of all sodium adducts produced good ions in the gas phase whereas only a few lithium or silver adducts resulted in descent spectra. It should be noted that most of the non-polar and OH-based matrices do not ionize the protected polymer except of DCTB, which gave the best results among all matrices. However, in general matrices with acidic *i.e.* carboxylic acid functionalities were significantly more successful. This is in agreement with specific studies which show that DCTB provides cleaner spectra in comparison to more polar matrices *e.g.* DHB or dithranol, because of the

Table 1
Characterization data of the investigated polymers.[a]

	$M_{n,SEC}$ (g mol^{-1})	PDI_{SEC}	DP *N*iPAm	DP sugar
PGlcAc	7400	1.16	21.2	2.5
PGlc	8800	1.15	21.2	2.5
PManAc	6000	1.13	21.6	2.5
PMan	6700	1.13	21.6	2.5

[a] The given degrees of polymerization (DP) represent the expected values calculated from the [M]/[CTA] ratio and the monomer conversions. SEC data were obtained with RI detection and PMMA calibration from PSS Germany and measured in DMAc/LiCl.

Table 2
Screening of matrices and cationization agents for **PGlcAc** (above) and **PManAc** (below).

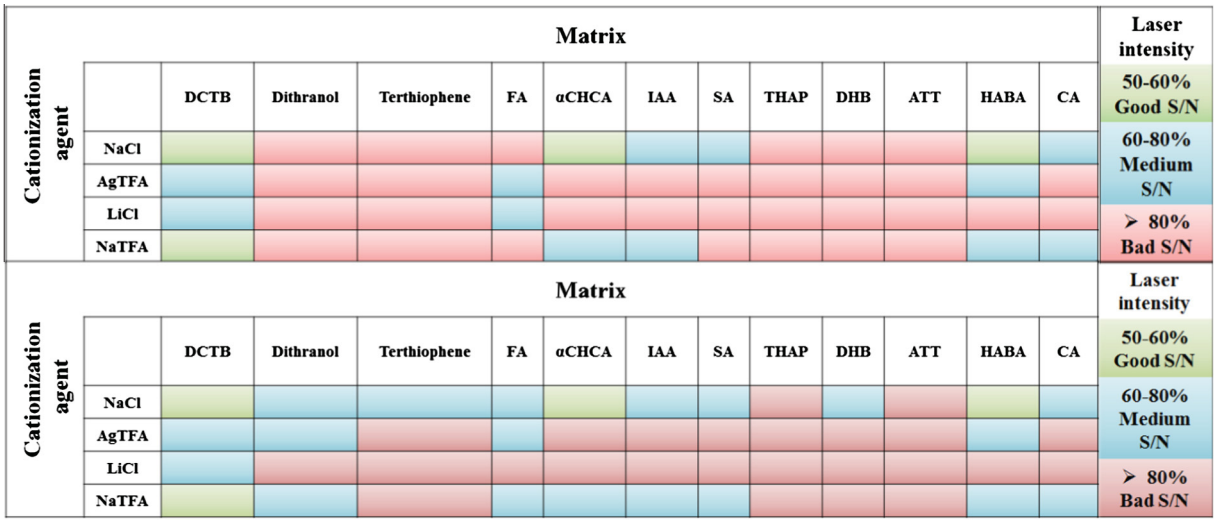

Table 3
Screening of matrices and cationization agents for **PGlc** (above) and **PMan** (below).

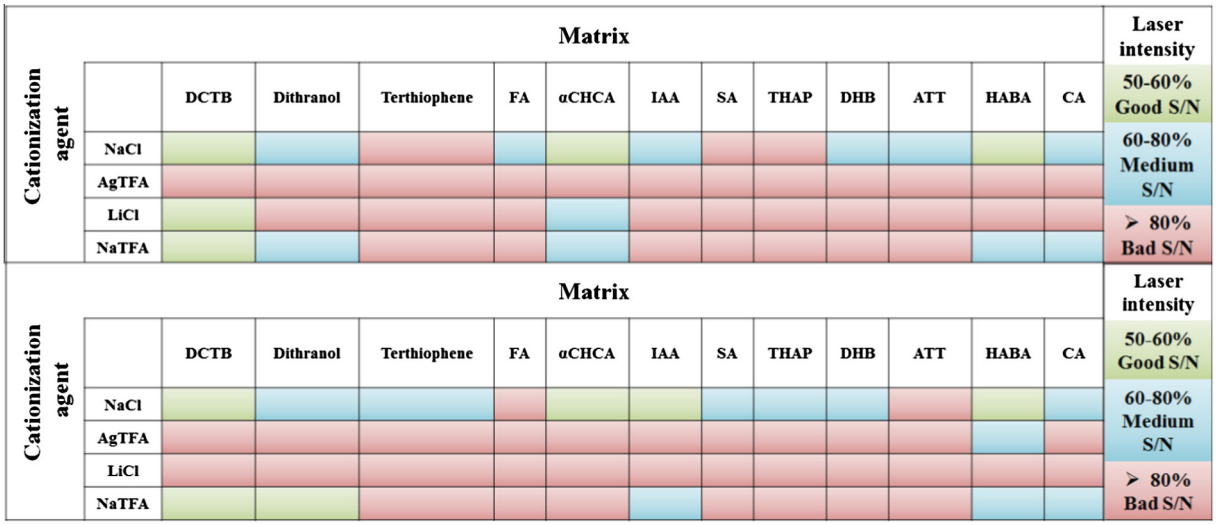

high signal intensities that can be achieved at lower laser powers [29,30]. It should be stressed that the ionization of the protected polymers **PGlcAc** and **PManAc** does not differ significantly from each other, thus indicating that the type of sugar moiety does not affect the optimum combination of matrix and salt.

As shown in Table 3, the analogue study was performed for the deprotected polymers. The results reveal that ionization of all polymer chains was restricted mainly to sodium adducts and fewer matrices resulted in good ionization in comparison to the ionization of the protected polymers. Although an MS spectrum of **PGlc** could be obtained with the combination LiCl/DCTB, the ionized species were restricted to P*N*iPAm homopolymers present in the sample (see below). Thus, only sodium salts enabled the ionization of the glycopolymers.

Moreover, NaTFA as cationization agent was significantly less efficient than NaCl. This shows that the anion of the ionization salt used to prepare the MALDI-TOF MS sample can play a significant role. Thus, it may not always be sufficient to

include only a variation of the cation in a screening to identify the optimum measurement conditions when the dried droplet spotting technique is applied. Insufficient miscibility that hinders the co-crystallization of analyte, salt and matrix can always be an issue that has to be considered when applying this spotting technique. These effects would be less pronounced using the spraying or layering technique. However, it is fast and easy when the dried droplet spotting technique is applied.

To be able to fully exploit the large amount of information that MALDI-TOF MS can provide in terms of structural analysis of polymers, a good signal to noise ratio and ionization of all species present in the sample without degradation represents a prerequisite. Fig. 3 shows the full spectra of **PGlcAc** obtained with the four most successful matrices DCTB, HABA, IAA and αCHCA with NaCl as cationization agent. The quality difference between these spectra is obvious on first glance: Both DCTB and αCHCA have significantly higher signal intensities in comparison to HABA and IAA, which resulted in very low intensities. Both HABA and IAA are less polar than αCHCA, however, αCHCA is only soluble in acetonitrile and not chloroform thus increasing the migration of matrix molecules to the outer parts of the spot and leaving the analyte mostly in the center [19]. The other major difference is the higher baseline and suppression of higher molar masses (*i.e.* polymer chains containing more **GlcAc** repeating units) that is observed in the spectra measured with HABA and IAA. These remarks also apply to **PManAc**, which has a strong difference in signal intensities for DCTB compared to the other matrices (Fig. S. 1).

Fig. 4 shows a similar overlay of the MALDI-TOF mass spectra of the deprotected glucose polymer **PGlc**, comparing the four best matrices dithranol, DCTB, αCHCA and DHB. NaCl was used as cationization agent for all four spectra. Remarkably, DHB and dithranol, which are commonly used matrices and are suitable for measurements of the deprotected polymers, did not ionize the protected polymers. Although having different polarities [19], DHB and dithranol show similar intensities, however, these are lower than for DCTB and αCHCA. In addition, both matrices result in a slightly low signal to noise ratio (S/N), which maybe could be attenuated by accumulating more shots, considering that a high laser intensity was required to obtain ions in the gas phase. However, it should be taken into account that high laser intensities applied for ionization often go along with a fragmentation of the polymeric analyte. Comparing the two best matrices αCHCA and DCTB, it appears that the former tends to suppress polymers with a higher number of sugar repeating units. As for the protected polymers, the type of sugar (glucose *vs.* mannose) attached to the copolymer was of little influence (Fig. S. 2).

Fig. 5 shows a magnified area of the mass spectra of **PManAc** where all major peaks have been assigned. The according overlays of the measured and theoretical isotopic patterns can be seen in Fig. S. 7. The zoomed area covers a m/z difference of 113.1 corresponding to one *N*iPAm repeating unit. The main series **A** represents polymer chains with intact trithiocarbonate end groups derived from the RAFT agent. Copolymer chains containing zero, one and two glycomonomers can be assigned in the selected m/z region of the spectra. Polymers with more sugar units occur at higher m/z values due to the high molar mass of these repeating units. Despite the use of NaCl as cationization agent, also potassium adducts could be detected, which are especially prominent when αCHCA and HABA are used as matrix, and which can be caused by the lower volume of the mixed solution of the sodium salts. The potassiated species possibly originate from solvent or glassware contamination or can be caused by trace impurities in the matrices or the cationization agent, respectively or by the concentration level of the sodium salts included in the premixed solution. In addition, a less abundant species (**B** in Fig. 5) can be assigned where the RAFT end

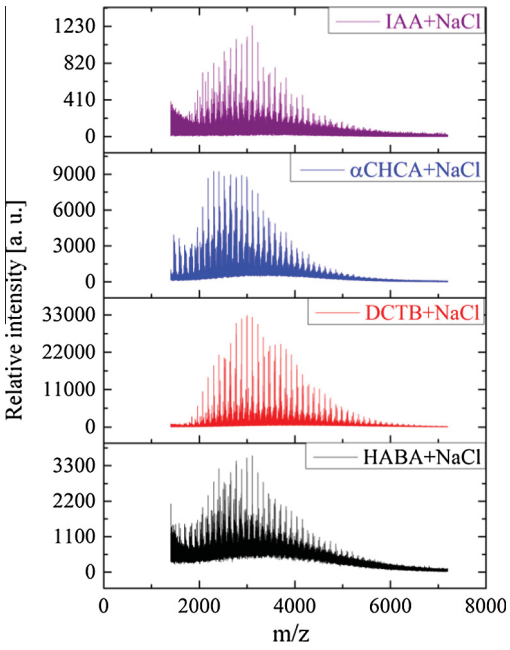

Fig. 3. Overlay of MALDI-TOF mass spectra of **PGlcAc** obtained with different matrices using NaCl as cationization agent.

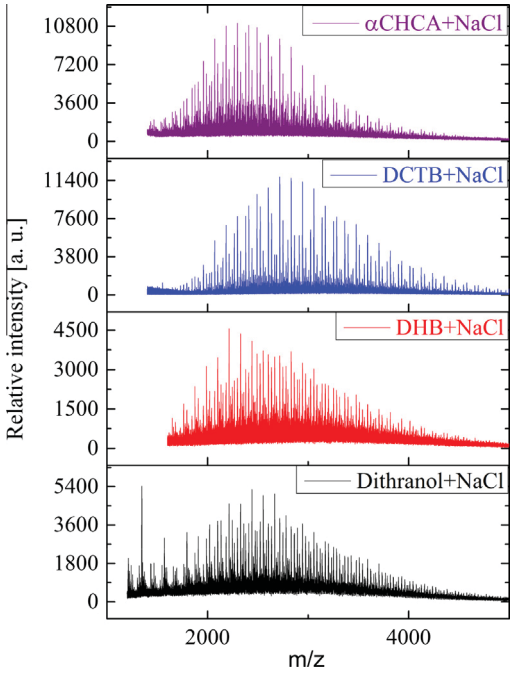

Fig. 4. Overlay of MALDI-TOF mass spectra of **PGlc** obtained with different matrices using NaCl as cationization agent.

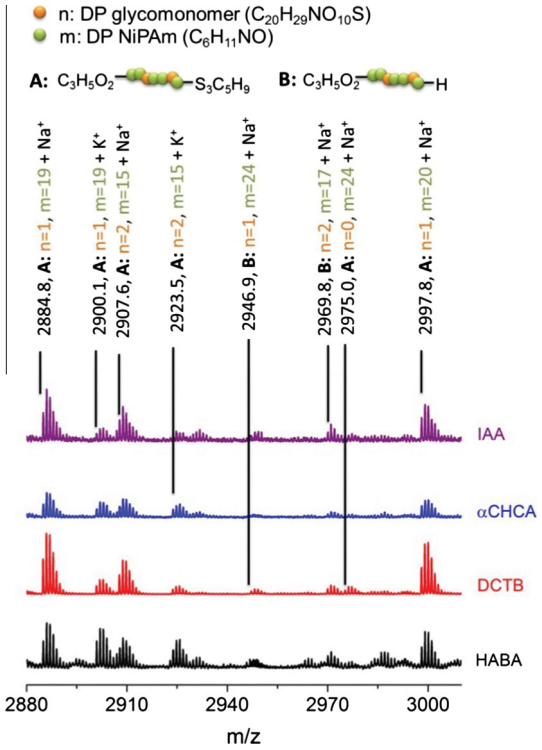

Fig. 5. Overlay of the normalized MALDI-TOF mass spectra of **PManAc** obtained with different matrices using NaCl as cationization agent. The zoom covers a *m*/*z* difference of 113.1 corresponding to one *N*iPAm repeating unit. Overlays of calculated and measured isotopic patterns can be found in the Supporting information.

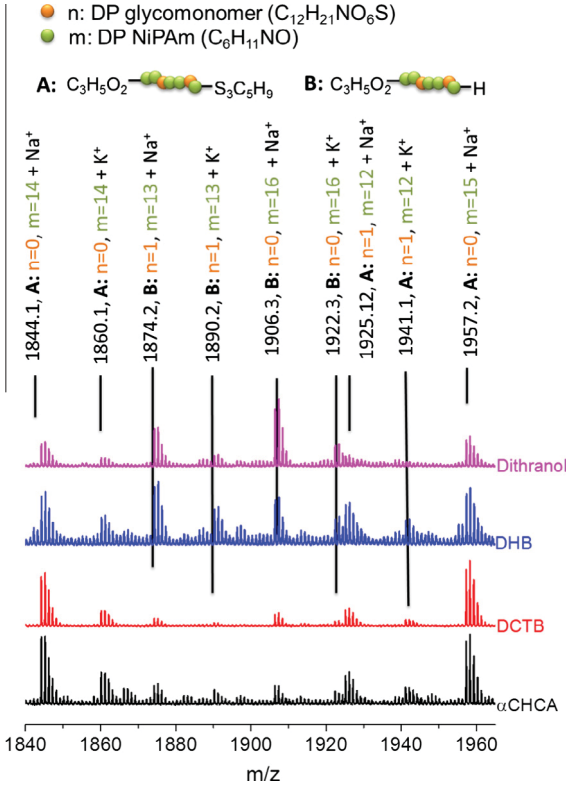

Fig. 6. Overlay of the normalized MALDI-TOF mass spectra of **PMan** obtained with different matrices using NaCl as cationization agent. The zoom covers a *m*/*z* difference of 113.1 corresponding to one *N*iPAm repeating unit. Overlays of calculated and measured isotopic patterns can be found in the Supporting information.

group is cleaved under MALDI-TOF MS conditions (see below). This fragmentation is more prominent in the spectra measured with HABA compared to the other matrices. As shown in Fig. S. 3, these observations hold true for the protected glucose containing polymer **PGlcAc** as well. Remarkably, the fragmented species **B** is slightly more abundant in the lower *m*/*z* regions of the spectra.

Fig. 6 shows a similar zoom into the mass spectra of the deprotected glycopolymer **PMan**. Basically the same end groups (species **A** and **B**) and cation adducts could be assigned as for the protected **PManAc**, taking into account the altered glycomonomer repeating unit. The RAFT end group fragmentation was more pronounced than for the protected polymers, in particular in the spectra obtained from DHB and dithranol and, thus, a proton as residual end group was present (species **B**). This phenomenon occurs readily for the ionization of RAFT polymers when studied with MALDI-TOF MS because this labile end group is prone to cleavage inside the spectrometer, which can also be due to the hardness of both matrices. DCTB's low ion production in comparison to DHB results in less production of fragments whereas the latter only reveals very weak molecular ions [29–31]. This usually happens upon a high laser power, which results in the cleavage of the weak C–S bond at the ω-chain end of polymers prepared by RAFT polymerization. In contrast, almost no end group fragmentation is observed when the polymers are analyzed by MALDI-TOF MS using αCHCA or DCTB as matrix. Among those two, DCTB reveals the spectrum with a remarkably better signal to noise ratio [29,30]. Differing from the protected species, dithranol and DCTB only resulted in sodiated species in contrary to the other matrices, where potassiated species were detected as well (Fig. S. 8). Again, the type of sugar did not have any influence since similar observations were made upon comparison of the spectra of the glucosylated polymer **PGlc** (Figs. S. 4 and S. 6).

The findings show that DCTB could on one hand overestimate the sugar enriched chains or on the other hand that the other matrices suppress these. To conclude, despite the difference in polarity of the analytes (protected *vs.* deprotected glycopolymer) DCTB seems to be the superior matrix, considering signal to noise ratio and end group preservation.

As a result from the discussion above, all other peaks could be assigned to copolymer chains with varied DP's of each repeating unit providing valuable information about the composition range present in the analyte. However, a manual assignment by alteration of both DP's to fit each isotopic pattern would be a tedious job. The computational tool COCONUT [27,32] is ideally suited to perform this task and able to provide the researcher with a composition map that shows the result of the analysis in a graphical form. Moreover, it has the ability to resolve isobars and overlapping peaks within an error of 0.2 Da, which represents a major issue in copolymer spectra. The program requires the chemical formula of each repeating unit (as a variable), the elemental composition of the polymer end groups and the cationization agent (as a constant) as input. However, it cannot handle the occurrence of different end groups or adduct ions present in one spectrum

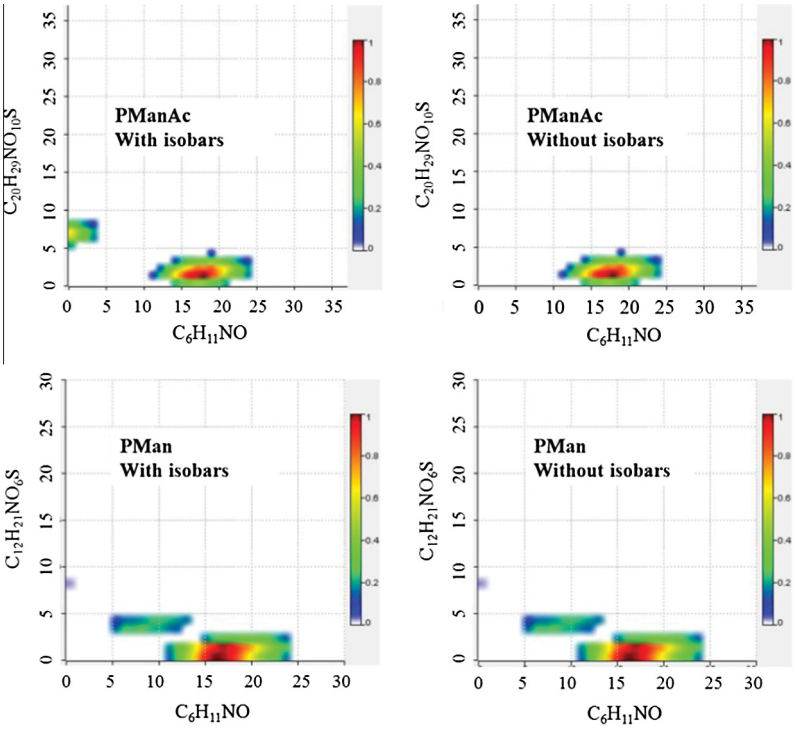

Fig. 7. Copolymer composition matrix obtained from the MALDI-TOF MS mass spectra (DCTB, NaCl) of the mannose based polymers **PManAc** and **PMan** using the COCONUT software tool.

simultaneously, *i.e.* the output will be only adequate for one distribution. In addition, the resolving of isobaric and overlapping species is performed using the peak areas and the centroid of each peak of the spectra. In case a peak in the spectrum cannot be fit to the input data, the software will exclude it from the resulting compositional matrix. As a result, well resolved isotopic patterns, a high S/N ratio and symmetrical peak shapes are required. Thus, the mass spectra obtained from the measurement with DCTB as matrix and NaCl as ionization salt were used for this analysis. The resulting 2D composition map computed by COCONUT for the mannose based systems **PManAc** and **PMan** is depicted in Fig. 7, showing the number of repeating units for each monomer, *i.e. N*iPAm and glycomonomer, as *x* and *y* axes, respectively. The color code translates the abundance of the respective compositions so that an average composition can be elucidated as well. As a matter of fact, only ionized species will be considered.

Isobaric species have the same *m*/*z* value but differ in their structural composition. For the discussed glycopolymers, this problem occurs only in the mass spectra of the protected polymers: *e.g.*, a homopolymer with 21 repeating units of *N*iPAm would be close to isobaric with a protected glyco-homopolymer with a DP of 5, because of the mass of the respective repeating units. Although these species are not exactly isobaric (the mass difference is 1 Da), the isotopic patterns will overlap (Fig. S. 10). For this reason, the theoretical possibility exists that a glyco-homopolymer is present underneath the isotopic pattern of the P*N*iPAm homopolymer. As a result, a second spot is visible in the composition map of **PManAc** (with isobars, top left in Fig. 7). However, both spots are not connected because the corresponding statistical copolymers in between these are not detected in the mass spectrum. Therefore, it is very unlikely that the glyco-homopolymer would be actually present in the analyte. Thus, the COCONUT software provides the option to re-fit all possible isotopic patterns, not taking into account the protected mannose-homopolymer. The resulting composition map is shown in Fig. 7 (top right, without isobars). Due to the changed molar mass of the deprotected mannose repeating unit, this is not an issue in the composition map of **PMan** (Fig. 7, bottom). As a consequence, both maps (with and without isobars) look identical. The second spot in the 2D compositional matrix of **PMan** has a rather low intensity and could be an artifact from the calculation.

While chains containing 11–24 *N*iPAm units are present in the sample, the COCONUT 2D maps for the mannose based polymers reveal that chains with a DP of 17 are most abundant for both protected and deprotected forms. However, the most abundant DP of the sugar repeating units is slightly decreased from 2 for **PManAc** to 1 for **PMan**. This might be caused by a more difficult ionization of chains that contain a higher number of deprotected sugars. However, a possible loss of sugar enriched chains during the purification after the deprotection of the polymer can provide an alternative explanation [28]. The corresponding plots for the glucosylated copolymers **PGlcAc** and **PGlc** are displayed in Fig. S. 9 and reveal an "average" number of twenty P*N*iPAm units for both the protected as well as the deprotected copolymer. Also in this case the most abundant number of sugar repeating units decreases from 2 in the protected polymer to 1 in the deprotected polymer.

These observations, which are based on MS data, correspond very well with the other characterization results from ^{1}H NMR spectroscopy and elemental analysis [28]. The number of glucose units results in an average number of two, which shows that DCTB does, in fact, not overestimate the number of sugar enriched chains for the protected forms.

4. Conclusion

In this contribution, detailed MALDI-TOF MS investigations were performed for the first time for *N*iPAm based statistical copolymers. Four copolymers synthesized by RAFT polymerization with mannose and glucose comonomers both in protected and deprotected form were studied with MALDI-TOF MS. First a screening was performed for these copolymers using twelve different matrices and four different cationization agents. The used matrices are the most commonly applied ones for biological molecules as well as ligands or complexes. Cationization agents were considered because polymers in general require cationization for MALDI-TOF MS. Major differences in the spectra were observed between protected and deprotected copolymers in the screening. For the protected polymers, the ionization was observed for the matrices DCTB, HABA, αCHCA, IAA with sodium, lithium and silver adducts. However, for the deprotected polymers a more restricted number of matrices was suitable. Remarkably, many very common matrices proved entirely unsuitable, whereas DCTB, a matrix not well-known in the field of "classical" protein or lipid analysis, was superior for all polymers investigated. Based on the detailed screening, the fragmentation of the RAFT end groups during the measurement could be minimized. Although MS is not a quantitative method, the composition of the analyzed copolymers was remarkably well consistent with the expectations from results as well as complementary characterization techniques.

Future efforts will concentrate on the transfer of the insights gained from this study to glycopolymers based on different polymer classes. Apart from this, the limits of the COCONUT software will be tested by applying this program to a wide range of other synthetic copolymers with more challenging mass spectra.

Acknowledgments

CW is thankful to the Carl Zeiss Foundation. The authors also acknowledge the Thuringian Ministry of Economic Affairs, Science and Digital Society (grant no. B515-07008) and the Ernst-Abbe Stiftung for financial support. The authors also thank Bruker Daltonics for their help and support.

Appendix A. Supplementary material

Supplementary data associated with this article can be found, in the online version, at http://dx.doi.org/10.1016/j.eurpolymj.2015.08.010.

References

[1] J.R. Yates, C.I. Ruse, A. Nakorchevsky, Proteomics by mass spectrometry: approaches, advances, and applications, Annu. Rev. Biomed. Eng. 11 (1) (2009) 49–79.
[2] R.J. Mishur, S.L. Rea, Applications of mass spectrometry to metabolomics and metabonomics: detection of biomarkers of aging and of age-related diseases, Mass Spectrom. Rev. 31 (1) (2012) 70–95.
[3] A. Bensimon, A.J.R. Heck, R. Aebersold, Mass spectrometry-based proteomics and network biology, Annu. Rev. Biochem. 81 (1) (2012) 379–405.
[4] H.C. Köfeler, A. Fauland, G.N. Rechberger, M. Trötzmüller, Mass spectrometry based lipidomics: an overview of technological platforms, Metabolites 2 (1) (2012) 19–38.
[5] P.O. Danis, D.E. Karr, F. Mayer, A. Holle, C.H. Watson, The analysis of water-soluble polymers by matrix-assisted laser desorption time-of-flight mass spectrometry, Org. Mass Spectrom. 27 (7) (1992) 843–846.
[6] T. Gruendling, S. Weidner, J. Falkenhagen, C. Barner-Kowollik, Mass spectrometry in polymer chemistry: a state-of-the-art up-date, Polym. Chem. 1 (5) (2010) 599–617.
[7] S.M. Weidner, S. Trimpin, Mass spectrometry of synthetic polymers, Anal. Chem. 80 (12) (2008) 4349–4361.
[8] S.M. Weidner, S. Trimpin, Mass spectrometry of synthetic polymers, Anal. Chem. 82 (12) (2010) 4811–4829.
[9] M.S. Montaudo, Mass spectra of copolymers, Mass Spectrom. Rev. 21 (2) (2002) 108–144.
[10] M. Karas, F. Hillenkamp, Laser desorption ionization of proteins with molecular masses exceeding 10,000 daltons, Anal. Chem. 60 (20) (1988) 2299–2301.
[11] S. Weidner, P. Knappe, U. Panne, MALDI-TOF imaging mass spectrometry of artifacts in "dried droplet" polymer samples, Anal. Bioanal. Chem. 401 (1) (2011) 127–134.
[12] M.A.R. Meier, N. Adams, U.S. Schubert, Statistical approach to understand MALDI-TOFMS matrices: discovery and evaluation of new MALDI matrices, Anal. Chem. 79 (3) (2007) 863–869.
[13] M.A.R. Meier, B.-J. de Gans, A.M.J. van den Berg, U.S. Schubert, Automated multiple-layer spotting for matrix-assisted laser desorption/ionization time-of-flight mass spectrometry of synthetic polymers utilizing ink-jet printing technology, Rapid Commun. Mass Spectrom. 17 (20) (2003) 2349–2353.
[14] S.J. Gabriel, C. Schwarzinger, B. Schwarzinger, U. Panne, S.M. Weidner, Matrix segregation as the major cause for sample inhomogeneity in MALDI dried droplet spots, J. Am. Soc. Mass Spectrom. 25 (8) (2014) 1356–1363.
[15] R. Knochenmuss, Ion formation mechanisms in UV-MALDI, Analyst 131 (9) (2006) 966–986.
[16] K. Dreisewerd, The desorption process in MALDI, Chem. Rev. 103 (2) (2003) 395–426.
[17] S.M.A.B. Batoy, E. Akhmetova, S. Miladinovic, J. Smeal, C.L. Wilkins, Developments in MALDI mass spectrometry: the quest for the perfect matrix, Appl. Spectrosc. Rev. 43 (6) (2008) 485–550.
[18] S.L. Cohen, B.T. Chait, Influence of matrix solution conditions on the MALDI-MS analysis of peptides and proteins, Anal. Chem. 68 (1) (1996) 31–37.
[19] A.J. Hoteling, W.J. Erb, R.J. Tyson, K.G. Owens, Exploring the importance of the relative solubility of matrix and analyte in MALDI sample preparation using HPLC, Anal. Chem. 76 (17) (2004) 5157–5164.
[20] S.D. Hanton, K.G. Owens, Using MESIMS to analyze polymer MALDI matrix solubility, J. Am. Soc. Mass Spectrom. 16 (7) (2005) 1172–1180.

[21] V. Vázquez-Dorbatt, J. Lee, E.-W. Lin, H.D. Maynard, Synthesis of glycopolymers by controlled radical polymerization techniques and their applications, ChemBioChem 13 (17) (2012) 2478–2487.
[22] G. Pasparakis, A. Cockayne, C. Alexander, Control of bacterial aggregation by thermoresponsive glycopolymers, J. Am. Chem. Soc. 129 (36) (2007) 11014–11015.
[23] E.-H. Min, S.R.S. Ting, L. Billon, M.H. Stenzel, Thermo-responsive glycopolymer chains grafted onto honeycomb structured porous films via RAFT polymerization as a thermo-dependent switcher for lectin Concanavalin a conjugation, J. Polym. Sci., A: Polym. Chem. 48 (15) (2010) 3440–3455.
[24] J. Huang, G. Habraken, F. Audouin, A. Heise, Hydrolytically stable bioactive synthetic glycopeptide homo- and copolymers by combination of NCA polymerization and click reaction, Macromolecules 43 (14) (2010) 6050–6057.
[25] S. Muthukrishnan, G. Jutz, X. André, H. Mori, A.H.E. Müller, Synthesis of hyperbranched glycopolymers via self-condensing atom transfer radical copolymerization of a sugar-carrying acrylate, Macromolecules 38 (1) (2005) 9–18.
[26] G. Gody, P. Boullanger, C. Ladavière, M.-T. Charreyre, T. Delair, Biotin α-end-functionalized gradient glycopolymers synthesized by RAFT copolymerization, Macromol. Rapid Commun. 29 (6) (2008) 511–519.
[27] M.S. Engler, S. Crotty, M.J. Barthel, C. Pietsch, K. Knop, U.S. Schubert, S. Böcker, COCONUT—an efficient tool for estimating copolymer compositions from mass spectra, Anal. Chem. 87 (10) (2015) 5223–5231.
[28] C. von der Ehe, F. Kretschmer, C. Weber, S. Crotty, S. Stumpf, S. Hoeppener, M. Gottschaldt, U.S. Schubert, RAFT copolymerization of thioglycosidic glycomonomers with *N*iPAm and subsequent immobilization onto gold nanoparticles, in: K. Matyjaszewski, B.S. Sumerlin, N.V. Tsarevsky, J. Chiefari (Eds.), Controlled Radical Polymerization: Material, American Chemical Society, Washington, DC, 2015, pp. 221–256.
[29] L. Ulmer, J. Mattay, H. Torres-Garcia, H. Luftmann, Letter: the use of 2-[(2E)-3-(4-tert-butylphenyl)-2-methylprop-2-enylidene]malononitrile as a matrix for matrix-assisted laser desorption/ionization mass spectrometry, Eur. J. Mass Spectrom. 6 (1) (2000) 49–52.
[30] M.F. Wyatt, B.K. Stein, A.G. Brenton, Characterization of various analytes using matrix-assisted laser desorption/ionization time-of-flight mass spectrometry and 2-[(2E)-3-(4-tert-Butylphenyl)-2-methylprop-2-enylidene]malononitrile matrix, Anal. Chem. 78 (1) (2006) 199–206.
[31] A. Favier, C. Ladavière, M.-T. Charreyre, C. Pichot, MALDI-TOF MS investigation of the RAFT polymerization of a water-soluble acrylamide derivative, Macromolecules 37 (6) (2004) 2026–2034.
[32] http://bio.informatik.uni-jena.de/software/coconut/ (last accessed 20.06.15).

Supplementary Information

Detailed MALDI comparison of *N*iPam glycopolymers

Sarah Crotty, [a,b] Christian von der Ehe, [a,b] Christine Weber, [a,b] * and Ulrich S. Schubert [a,b] *

[a] Laboratory of Organic and Macromolecular Chemistry (IOMC), Friedrich Schiller University Jena, Humboldstr. 10, 07743 Jena, Germany

[b] Jena Center for Soft Matter (JCSM), Friedrich Schiller University Jena, Philosophenweg 7, 07743 Jena, Germany

Corresponding author footnote: Fax. +49 3641 9-48202; Email: christine.weber@uni-jena.de ulrich.schubert@uni-jena.de

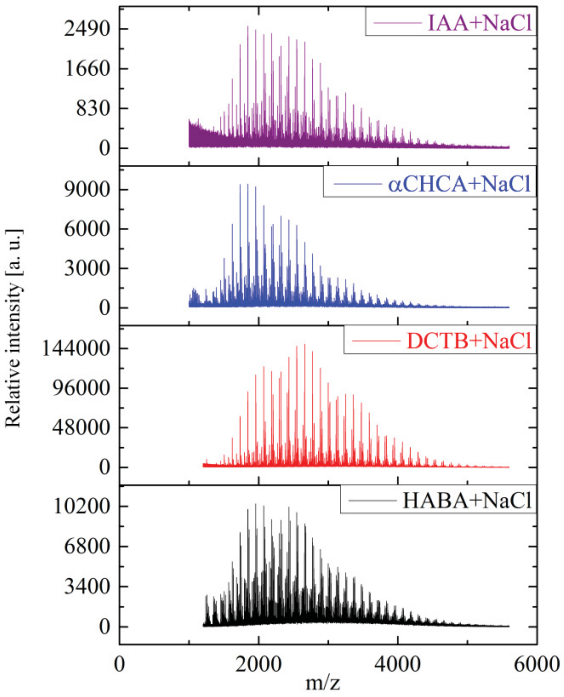

Figure S. 1. Overlay of MALDI-TOF mass spectra of **PManAc** obtained with different matrices using NaCl as cationization agent.

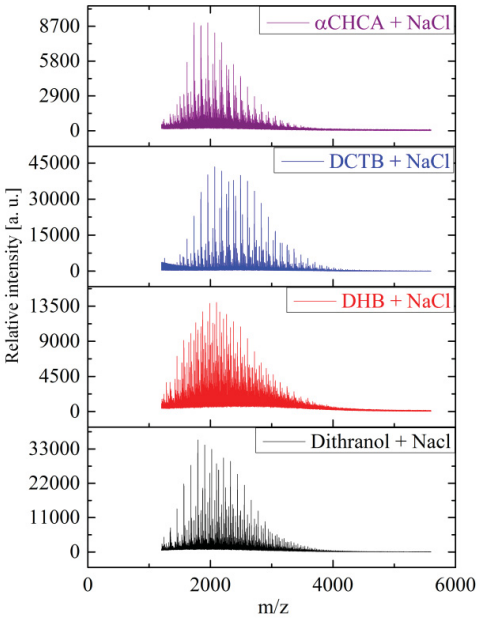

Figure S. 2. Overlay of MALDI-TOF mass spectra of **PMan** obtained with different matrices using NaCl as cationization agent.

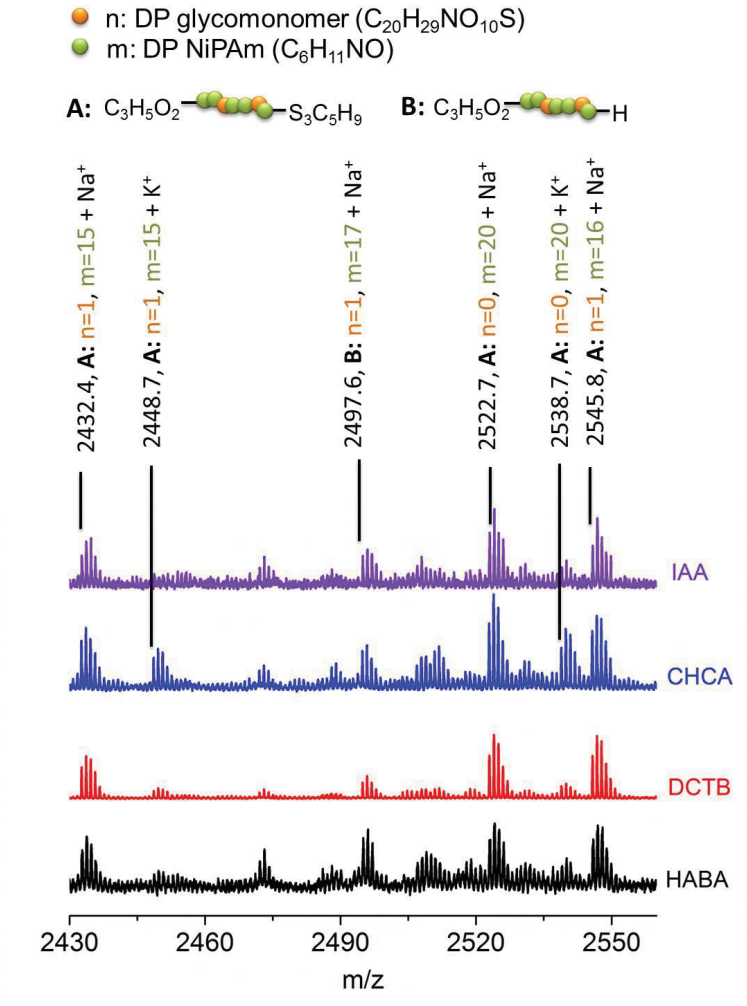

Figure S. 3. Overlay of the normalized MALDI-TOF mass spectra of **PGlcAc** obtained with different matrices using NaCl as cationization agent. The zoom covers a *m/z* difference of 113.1 corresponding to one *N*iPAm repeating unit. Overlays of calculated and measured isotopic patterns can be found in Figure S. 5.

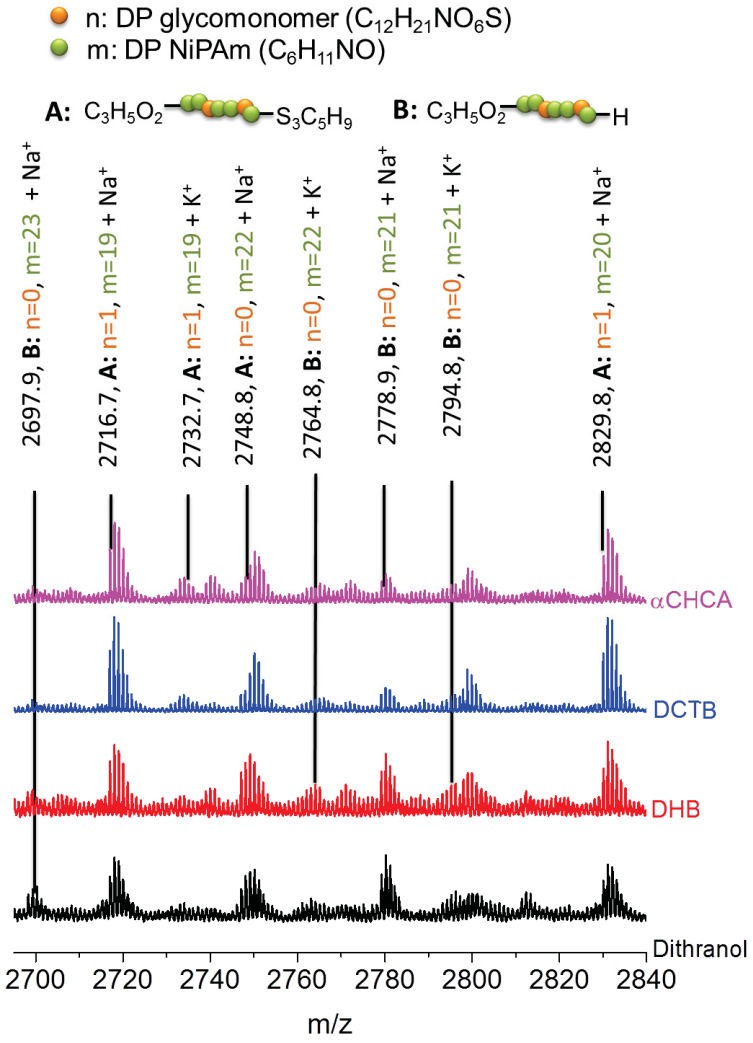

Figure S. 4. Overlay of the normalized MALDI-TOF mass spectra of **PGlc** obtained with different matrices using NaCl as cationization agent. The zoom covers a *m/z* difference of 113.1 corresponding to one *N*iPAm repeating unit. Overlays of calculated and measured isotopic patterns can be found in Figure S. 6.

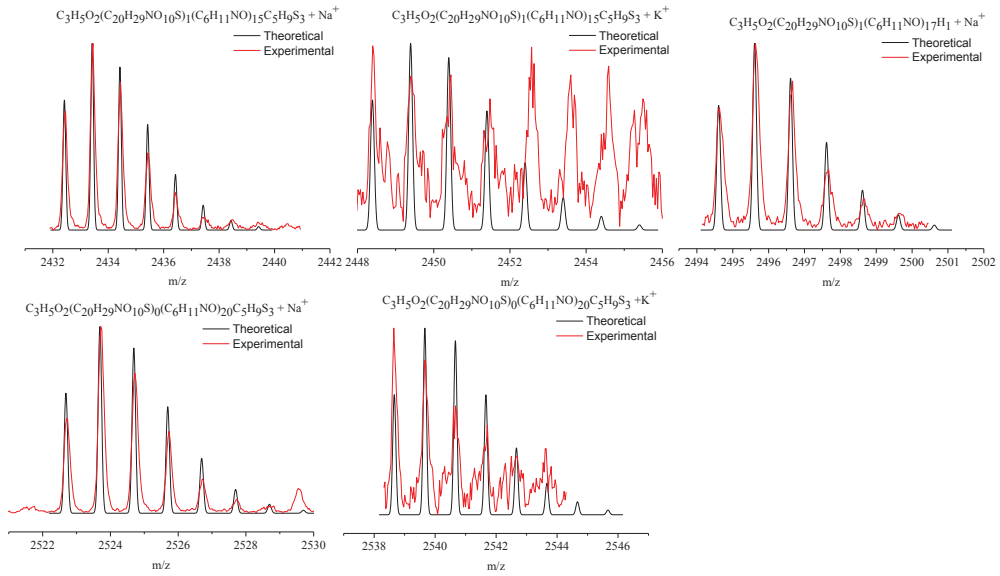

Figure S. 5. Overlay of the theoretical and experimental isotopic patterns from DCTB + NaCl for **PGlcAc**.

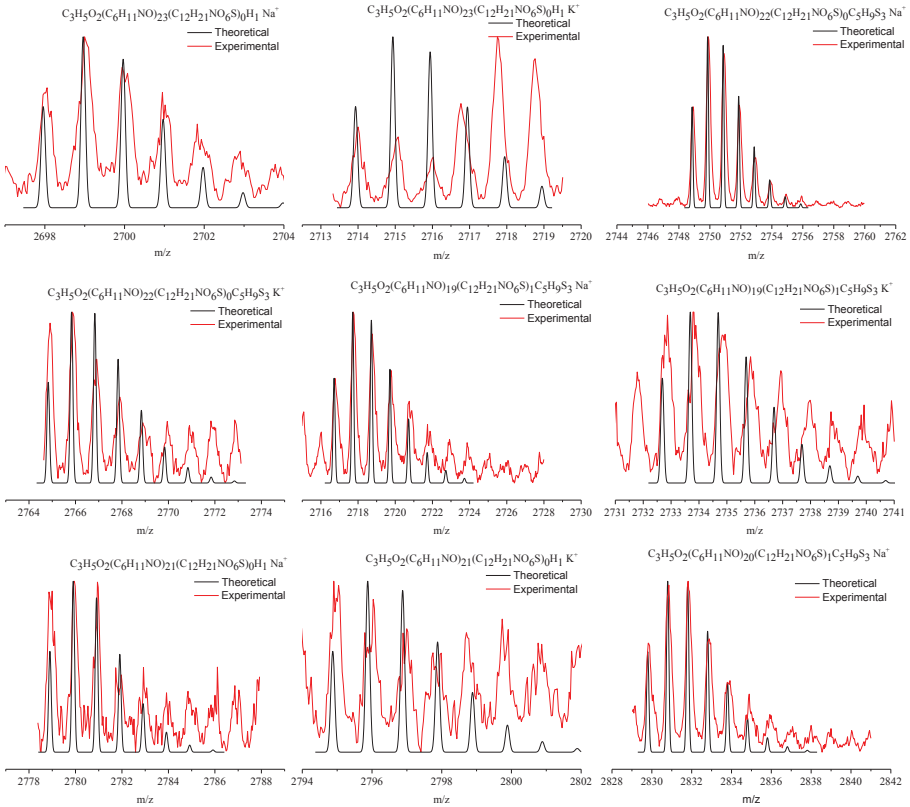

Figure S. 6. Overlay the theoretical and experimental isotopic patterns from DCTB + NaCl for **PGlc**.

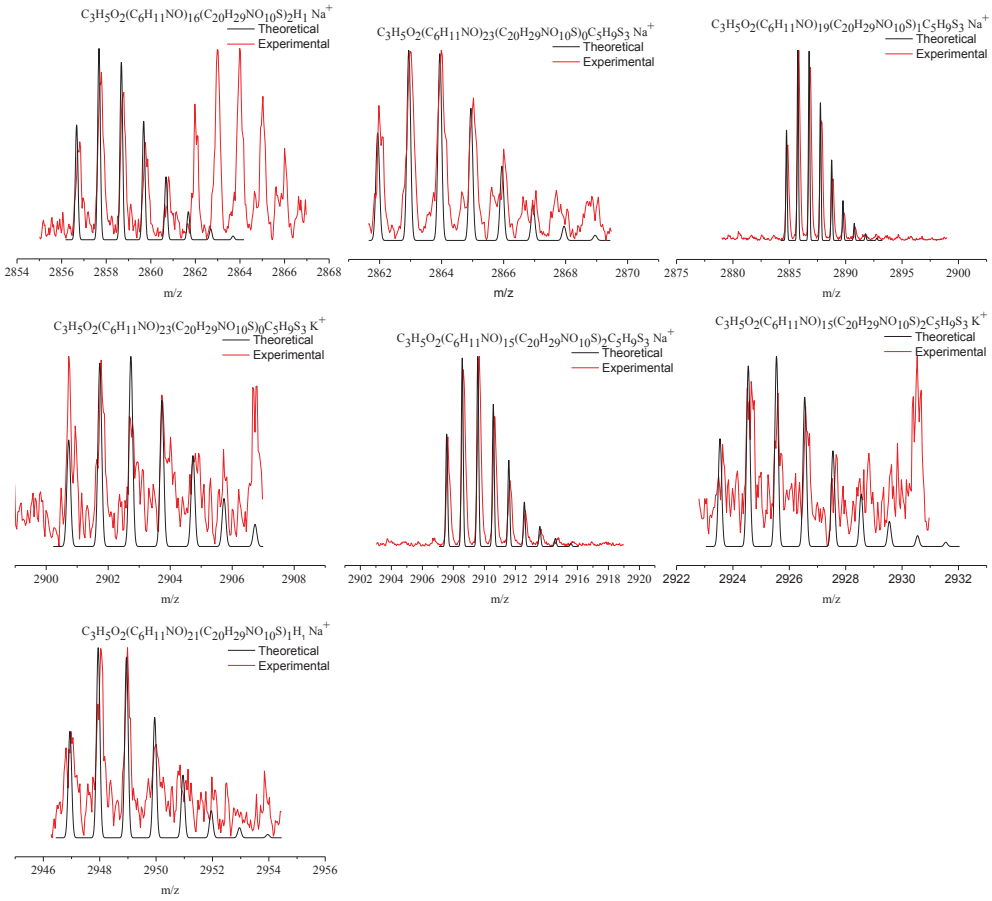

Figure S. 7. Overlay of the theoretical and experimental isotopic patterns from DCTB + NaCl for **PManAc**.

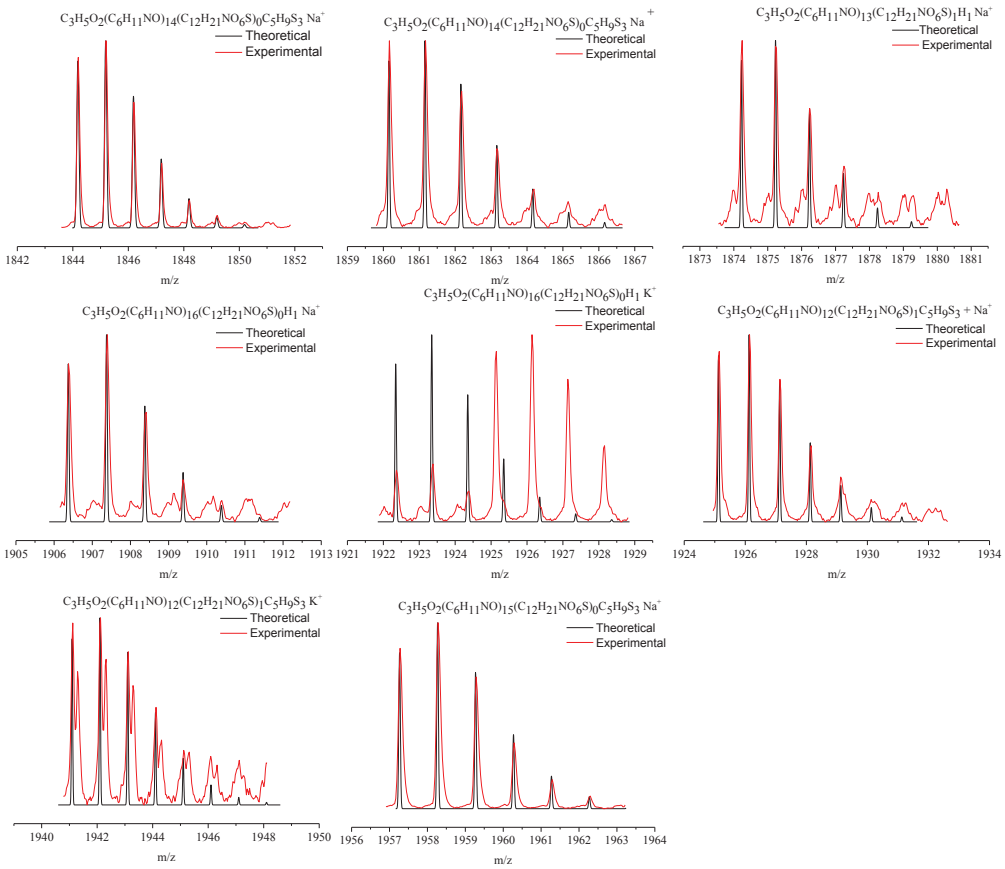

Figure S. 8. Overlay of the theoretical and experimental isotopic patterns from DCTB + NaCl for **PMan**.

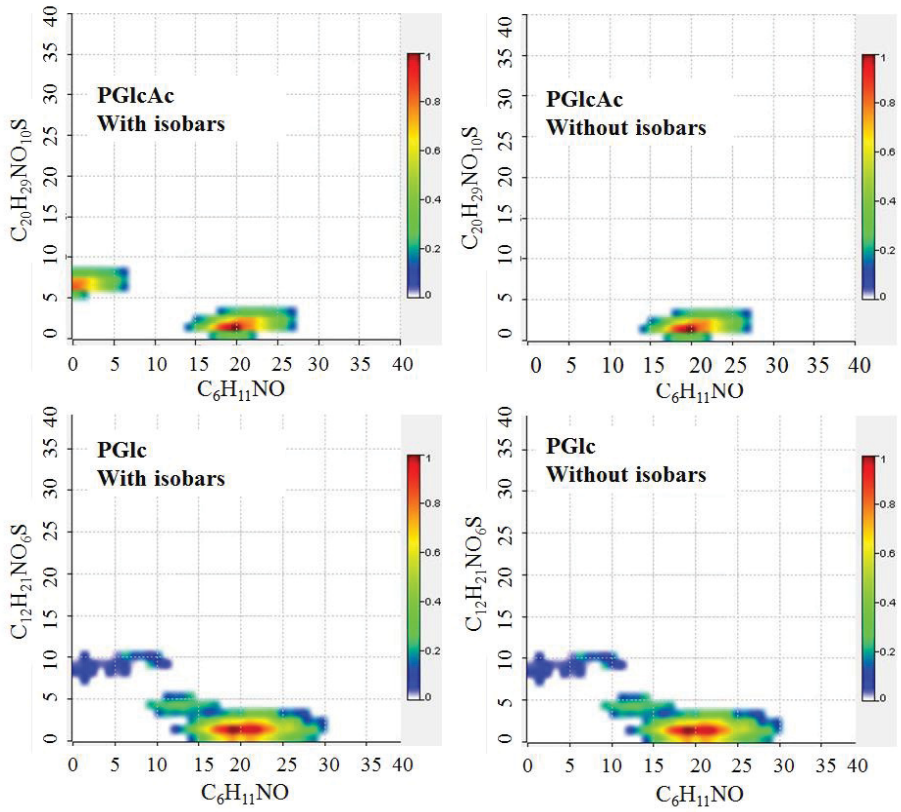

Figure S. 9. Copolymer composition matrix obtained from the MALDI-TOF mass spectra of the glucose based polymers (DCTB, NaCl) using the COCONUT software tool.

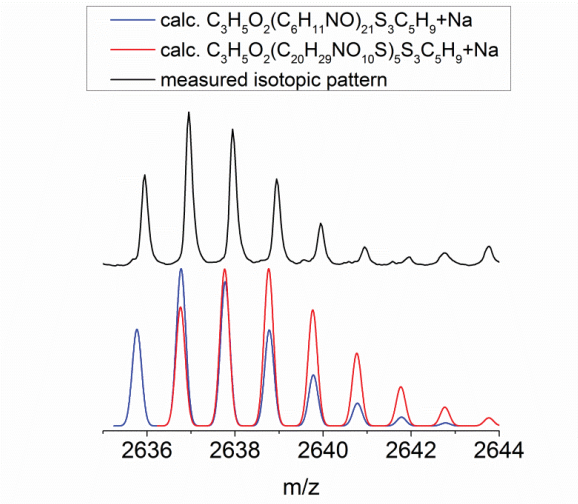

Figure S. 10. Overlay of the measured isotopic pattern for **PManAc** with the theoretical isotopic patterns of homopolymers.

Publication 5

Molecular and structural characterization of hybrid poly(ethylene oxide)–polyhedral oligomeric silesquioxanes star-shaped macromolecules

G. M.-E. Pozza, S. Crotty, M. Rawiso, U. S. Schubert, P. J. Lutz

J. Phys. Chem. B **2015**, *119*, 1669-1680.

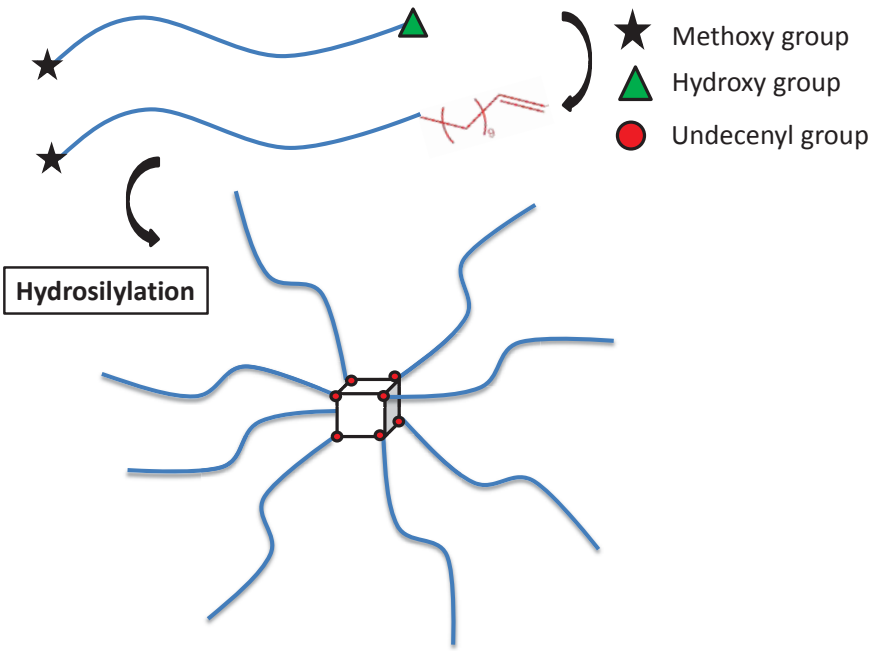

THE JOURNAL OF PHYSICAL CHEMISTRY B

Article

pubs.acs.org/JPCB

Molecular and Structural Characterization of Hybrid Poly(ethylene oxide)−Polyhedral Oligomeric Silesquioxanes Star-Shaped Macromolecules

Gladys M.-E. Pozza,[†,‡,§] Sarah Crotty,[‡] Michel Rawiso,[†] Ulrich S. Schubert,*[,‡,§,∥] and Pierre J. Lutz*[,†,§]

[†]University of Strasbourg, Institut Charles Sadron, CNRS UPR 22, 23, rue du Loess 67034, Strasbourg, France

[‡]Laboratory of Organic and Macromolecular Chemistry (IOMC), Friedrich Schiller University Jena, Humboldtstr. 10, 07743 Jena, Germany

[§]Dutch Polymer Institute (DPI), P.O. Box 902, 5600 AX Eindhoven, The Netherlands

[∥]Jena Center for Soft Matter (JCSM), Friedrich Schiller University, Philosophenweg 7, 07743 Jena, Germany

Supporting Information

ABSTRACT: Octafunctionalized spherosilsesquioxanes ($Q_8M_8^H$), decorated with Si−H functions, could be used to design, by coupling via hydrosilylation with α-methoxy-ω-undecenyl poly(ethylene oxide)s (PEOs), organic−inorganic nanocomposite structures. ^{1}H, ^{13}C, and ^{29}Si NMR; size exclusion chromatography; and Fourier transfrom infrared spectroscopy were used to follow the grafting reaction and determine the molar mass and the functionality of the different species. Hybrid star-shaped poly(ethylene oxide)s of precise molar mass and functionality could be isolated by fractional precipitation of the raw reaction product. Absolute molar masses of the purified star-shaped PEOs, calculated with the assumption of a functionality of 8, were comparable when measured by light scattering in methanol and by matrix-assisted laser desorption ionization time-of-flight mass spectrometry. Small-angle X-ray scattering was employed to determine their molecular and structural characteristics, representing the versatility and innovative aspect to this study. Both differential scanning calorimetry and optical microscopy were utilized to elaborate and analyze the thermal properties and crystallization, respectively, of the hybrid stars. Further ongoing work is being carried out currently to investigate and foresee the use of longer PEO branches onto the core.

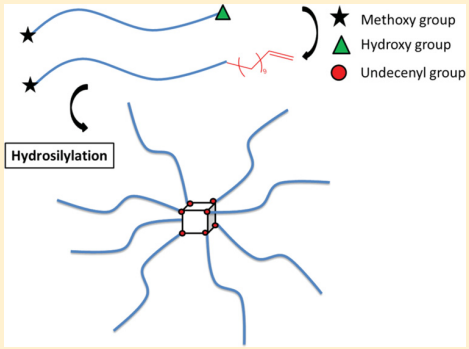

INTRODUCTION

Poly(ethylene oxide) (PEO) is a water-soluble polymer with outstanding properties and is the building block for a large number of macromolecular architectures designed for various applications.[1−3] PEO macromonomers are accessible either via anionic ring opening polymerization (AROP) of ethylene oxide in the presence of a heterofunctional unsaturated initiator or by chain-end modification of already existing PEOs.[4−6] Typically, ω-allyl PEO or α,ω-diallyl PEO macromonomers are obtained upon reaction of hydroxyl PEOs with allyl-bromide after transformation of the end-standing hydroxyl function into an alcoholate by reaction with a stoichiometric amount of diphenylmethyl potassium (DPMK),[7] sodium hydroxide (NaOH),[8,9] or sodium.[10] The interest for PEO macromonomers characterized by the presence of a flexible hydrophobic spacer between the terminal double bond and the PEO chain-end can be explained by the increased accessibility of the terminal double bonds. This would, in addition, enhance the amphiphilic character of the end-modified PEO. Preliminary attempts to synthesize ω-undecenyl PEO macromonomers by chain-end modification of existing PEOs based on the DPMK approach[11] failed. An explanation might be the occurrence of side reactions occurring during the metalation process. This stimulated us to search for more efficient ways to design PEO macromonomers, quantitatively fitted at least at one chain-end with undecenyl end-groups. The use of NaH has proven to be efficient for the chain-end functionalization of PEOs.[2,12]

PEOs or PEO-based star-shaped polymers covering a large range of molar masses and constituted of cores of different chemical nature and functionalities are accessible with a range of approaches.[13] PEO stars are of great interest as surface-modifying agents to improve the biocompatibility of surfaces designed for biomedical applications[13−15] or as building blocks for the synthesis of functional PEO hydrogels.[16]

Living anionic polymerization of ethylene oxide has been used for the preparation of a series of 4-arm, 8-arm, and 16-arm PEO stars starting from carbosilane dendrimers after appropriate modification of the hydroxy functions into alcoholate.[17] Eight-arm PEO stars can also be obtained via

Received: May 27, 2014
Revised: December 14, 2014
Published: December 22, 2014

DOI: 10.1021/jp505191d
J. Phys. Chem. B 2015, 119, 1669−1680

AROP of ethylene oxide in the presence of other octahydroxylated precursors.[18] Multiarm PEO-star polymers[19] with a purely aliphatic polyether structure have been synthesized in a direct "grafting from" polymerization of ethylene oxide using hyperbranched polyglycerol with different molar masses as a multifunctional initiator. The PEO arms were characterized by matrix-assisted laser desorption ionization time-of-flight mass spectrometry (MALDI-TOF MS), and the measurements confirmed that the arms of the star-shaped polymers possess homogeneous lengths.

Another possibility to access multiarm PEO stars based on the "arm-first" method was developed by Hou et al. The authors prepared six-arm PEO stars with 6 pyridyl or 12 hydroxyl end-groups.[20] The synthesis of dendrimer-like polymers is based on the combination of the AROP of ethylene oxide with three alcoholate functions as initiator and by branching reactions of PEO chain-ends that were repeated several times.[21]

Only a few examples of hybrid materials based on PEO and polyhedral oligomeric silesquioxanes (POSS) have been presented and discussed in the literature. POSS are three-dimensional nanometer-sized species and represent interesting reactive building blocks for the elaboration of organic−inorganic materials including hybrid macromolecular architectures.[22−28] The different ways, by copolymerization or grafting, to incorporate these POSS structures in polymers and the properties of the resulting hybrid materials have been discussed recently by Kuo et al.[26]

PEOs based on POSS may represent new water-soluble materials characterized by enhanced thermal and thermomechanical stability, mechanical toughness, or optical transparency.[11,29] A few years ago, monosubstituted cube-shaped spherosilsesquioxanes with amphiphilic properties, combining the relatively hydrophobic spherosilsesquioxane core with hydrophilic PEO segments,[30] could be prepared.

In this contribution, we discuss first the synthesis and the characterization of a series of heterofunctional α-methoxy-ω-undecenyl PEO macromonomers and their coupling with octafunctional silsesquioxanes ($Q_8M_8^H$) via hydrosilylation to yield hybrid star-shaped PEOs. The major part of the work will be devoted to a detailed investigation of the physicochemical characteristics of these star-shaped PEOs including small-angle X-ray scattering (SAXS) that allows investigation of their average internal structure through an increase of the spatial resolution. On the basis of SAXS results, some molecular and structural parameters will be determined and compared with those obtained by size exclusion chromatography (SEC) and static light scattering (SLS). Finally, some data on the thermal properties and on the crystallization of both the α-methoxy-ω-undecenyl PEO macromonomers and the hybrid star-shaped PEOs will be presented.

EXPERIMENTAL SECTION

Solvents, Monomers, Initiators, Deactivating Agents. Toluene (Aldrich) was purified by conventional methods and kept under argon atmosphere. Dichloromethane (Aldrich), tetrahydrofuran (THF) (Carbo Erba), and diethyl ether (Carbo Erba) were used as received. 11-Bromo-1-undecene (Aldrich, 95%) was purified by distillation over CaH_2 under reduced pressure and kept under argon atmosphere. Sodium hydride (NaH) (Aldrich, 95%) was used as received and stored in the glovebox. 1-Naphthyl isocyanate (Aldrich, 98%), 1,4-diazabicyclo[2.2.2]octan (DABCO) (Aldrich, 98%), and 1-undecene (Aldrich, 97%) were used without purification. The platinum(0)-1,3-divinyl-1,1,3,3-tetramethyldisiloxane Pt(dvs) catalyst (Aldrich) (Karstedt catalyst)[31] was used either as such (0.05 M in poly(dimethylsiloxane), vinyl terminate) or diluted to 5×10^{-4} M or 2×10^{-3} M solution with anhydrous toluene. Octakis(dimethylsilyloxy)silsesquioxane ($Q_8M_8^H$) (Aldrich) was utilized without further purification. Commercial PEOs were received as a gift from Clariant (molar masses of 1000, 1700, 4700, and 10 900 g mol^{-1} for the α-methoxy-ω-hydroxy and 6000 g mol^{-1} for the α,ω-dihydroxy PEO). The functionalization and hydrosilylation reactions were conducted in classical glass vessels under a slight argon pressure.

Synthesis of ω-Undecenyl PEO Macromonomers by Deactivation with 11-Bromo-1-undecene in the Presence of NaH. The commercial α-methoxy-ω-hydroxy PEO ($M_{n,SEC}$ = 1700 g mol^{-1}, 10 g, 5.88 mmol) was heated at 110 °C, and NaH (0.71 g, 29.41 mmol,) ([PEO]/[NaH] = 1/5 or 1/10) was added. After 20 min, 11-bromo-1-undecene (4 equiv, 5.16 mL, 23 mmol) was introduced, and the reaction was kept at 110 °C for 24 h. The PEO solution was then passed through alumina columns in dichloromethane (8 g/10 mL). After evaporation of dichloromethane and addition of THF, the PEO was precipitated in diethyl ether and filtered. The functionalized PEOs were characterized by SEC, ^{1}H NMR, and MALDI-TOF MS. The same experimental procedure was used for the synthesis of the α,ω-diundecenyl PEOs. ^{1}H NMR ($CDCl_3$, 400 MHz, δ): 5.8 (m, 1H, $-CH{=}CH_2$), 5.1 (m, 2H, $-CH{=}CH_2$), 3.6−3.8 (m, 4H*n, $-O-CH_2-CH_2-$), 3.3 (s, 3H, $-O-CH_3$), 2.0 (m, 2H, $-CH_2-CH{=}CH_2$), 1.5 (m, 2H, $-CH_2-(CH_2)_7-CH_2-CH{=}CH_2$), 1.1−1.3 (m, 2H*7, $-CH_2-(CH_2)_7-CH_2-CH{=}CH_2$).

PEO Star-Shaped Polymer ($Q_8M_8^{PEO}$). Several experimental conditions were tested for the grafting reactions. The Karstedt catalyst (0.05 M) was used either as such or diluted to 5×10^{-4} M or 2×10^{-3} M solution in anhydrous toluene. The reaction was conducted either at 40 or 80 °C for reaction times of 2 or 24 h, under air or inert atmosphere.

A 56.5 mg sample of $Q_8M_8^H$ (0.05 mmol) and 1 g of an α-methoxy-ω-undecenyl PEO macromonomer ($M_{n,SEC}$ = 1800 g mol^{-1}, 0.55 mmol) were dissolved in 0.7 mL of toluene (1 g for a total volume of 2.2 mL). A 0.5 mL portion of a 5×10^{-4} M Karstedt catalyst solution in toluene was added under atmosphere. The reaction mixture was kept at 40 °C for 2 h (see star 1 in Table 2). If not specified, 1 g PEO was used. The reaction was repeated under argon first with 0.5 mL (star 3) and then 1 mL (star 4) of a 5×10^{-4} M Karstedt catalyst solution. The influence of the concentration of catalyst was further investigated. One drop of the Karstedt catalyst (0.05 M) in 1 mL of polymer solution in toluene was used in reaction 2 (star 2). Then a 2×10^{-3} M Karstedt catalyst solution in toluene was used (0.15 mL) with 1 mL of polymer solution in toluene (star 5), and the reaction time was increased to 24 h (star 6). This reaction was also made at a lower polymer concentration (1 g for a total volume of 6.3 mL) (stars 7 and 8) with 0.3 mL of a 2×10^{-3} M Karstedt catalyst toluene solution at 40 °C. The reaction was made at higher temperatures 80 °C (1 g for a total volume of 6.15 mL) (star 9 and 12) with 0.15 mL of a 2×10^{-3} M Karstedt catalyst toluene solution.

At the end of the reaction, undecene (same quantity as that of the PEO mol number) was added to react with the Si−H functions of $Q_8M_8^H$ (star 10 at 12). This addition prevents the coupling between two Si−H functions. All the reaction products were treated as follows: they were precipitated

DOI: 10.1021/jp505191d
J. Phys. Chem. B 2015, 119, 1669−1680

directly in diethyl ether, filtered, dried under vacuum to constant weight, and characterized. ^{1}H NMR ($CDCl_3$, 400 MHz, δ): 3.6−3.8 (m, 4H*n, −O−CH_2−CH_2−), 3.3 (s, 3H, −O−CH_3), 2.1 (m, 2H, −CH_2−CH_2−CH_2−Si−), 1.5 (m, 2H, −CH_2−$(CH_2)_7$−CH_2−CH_2−CH_2−Si−), 1.1−1.3 (m, 2H*7, −CH_2−$(CH_2)_7$−CH_2−CH_2−CH_2−Si−), 0.5 (m, 2H, −Si-$(CH_3)_2$−CH_2−), 0 (t, 6H, −Si$(CH_3)_2$−). ^{13}C NMR ($CDCl_3$, 400 MHz, δ): 70.2−70.4 (−O−CH_2−CH_2−), 58.7 (−O−CH_3), 25.8−29.3−33.2 (−$(CH_2)_7$−), 22.7 (−Si$(CH_3)_2$−CH_2−CH_2−), 17.4 (−Si$(CH_3)_2$−CH_2−), 0.6 (−Si$(CH_3)_2$−). ^{29}Si NMR ($CDCl_3$, 400 MHz, δ): 12.55 (PEO−*Si*−), −108 (*Si*−O_4). IFTIR spectrum (ATR, cm^{-1}): 2880 (υ C−H), 1467 (δ CH_2), 1100 (υ C−O).

Fractionation of PEO Star-Shaped Polymers. Fractional precipitation was carried out in a tempered water circulating bath. The raw reaction product was dissolved in toluene in a conventional pear-like vessel (example, 0.95 g in 60 mL of toluene at T = 25 °C). Cyclohexane was added drop-by-drop from a buret until the medium became turbid. At that point the turbid solution was heated until the turbidity vanished. The temperature was decreased to 25 °C, and the solution was kept at that temperature for 24 h. The lower phase should contain the $Q_8H_8^{PEO}$ and the upper one the unreacted macromonomer. The fractions were recovered and analyzed by SEC to investigate the efficiency of the fractionation and grafting process.

Characterization Techniques. Number-average molar mass (M_n), weight-average molar mass (M_w), and the polydispersity index (PDI) value of the different PEO samples were determined by SEC at RT on a Shimadzu SIL-20A system controller with a LC-20AD pump, a RID-10A refractive index detector, and a Shimadzu SPD 10 Avp UV detector. THF with a flow rate of 1 mL min^{-1} was used as solvent. Calibration was made with PEO standards from Polymer Laboratories with molar masses from 194 to 22 800 g mol^{-1}).

Weight-average molar masses ($M_{w,LS}$) of the star PEOs were also determined by SLS. These measurements were carried out with a red He−Ne laser with a wavelength of λ_0 = 632.8 nm, a discrete-angle goniometer acting within the range from 20° to 155°, a Hamamatsu type photomultiplier as the detector, a photocounting device, and a toluene matching bath.[32] The dn/dc of α-methoxy-ω-undecenyl PEO in methanol solutions was measured by using a Wyatt Optilab Rex refractometer at a wavelength of 632.8 nm. dn/dc of α-methoxy-ω-undecenyl PEO solution in methanol is equal to 0.150 mL g^{-1} at 25 °C.

For nuclear magnetic resonance (NMR) spectroscopysolution ^{1}H NMR, ^{13}C NMR, and ^{29}Si NMR spectra were recorded on a Bruker DRX 400 MHz in deuterated chloroform ($CDCl_3$).

Fourier transform infrared (FTIR) spectroscopy was performed in the attenuated total reflection mode (ATR-FTIR) using a Vertex 70 spectrometer (Bruker, Germany) equipped with a DTGS detector and a single-reflection diamond ATR accessory (A225/Q Platinum ATR, Bruker, Germany). Reference (air) and sample spectra were taken by collecting 20 interferograms between 500 and 3000 cm^{-1} using a Blackman-Harris three-term apodization and the standard Bruker OPUS/IR software (version 5.0).

For the measurement of the matrix-assisted laser desorption/ionization (MALDI) spectra, an Ultraflex III TOF/TOF instrument (Bruker Daltonics, Bremen, Germany) was used. The instrument was calibrated prior to each measurement with poly(methyl methacrylate) (PMMA) as the external standard (PSS, Polymer Standards Service GmbH, Mainz, Germany). Samples were mixed with either 2-[(2E)-3-(4-*tert*-butylphenyl)-2-methylprop-2-enylidene]malononitrile (DCTB), or 2,5-dihydroxybenzoic acid (DHB) as matrix and the doping agent NaI (dried droplet method).

Ultaraviolet−visible spectroscopy was achieved on a Varian Cary 500 Scan spectrophotometer with ethanol as solvent. Low concentrations of PEO were chosen (7×10^{-2} to 2×10^{-1} g L^{-1}) to ensure the validity of Beer's law. The optical path length of the cell was 1 cm. A calibration curve was established using 1-naphthyl carbamate with an absorption maximum (λ max) observed at 291 nm and an extinction coefficient of 7060 mol^{-1} cm^{-1}.

Small-angle X-ray scattering experiments were performed with a diffractometer developed by Molecular Metrology (Elexience, France) that uses a Rigaku Micromax 007HF generator with a copper rotating anode. The wavelength of the incident X-ray beam is λ = 0.154 nm. This diffractometer operates with a pinhole collimation of the X-ray beam focused by a multilayer optic designed by Osmic and a two-dimensional gas-filled multiwire detector. The sample−detector distance was set at D = 0.7 m, leading to a range of scattering vectors covered by the experiment $0.1 < q < 3.2$ nm^{-1}. The scattering vector q is defined by $q = (4\pi/\lambda) \times \sin(\theta/2)$, where λ is the wavelength of the incident beam and θ is the scattering angle. Cells of 1 mm thickness and calibrated Mica windows were used as sample holders. Measurements were performed at room temperature.

Data were treated according to a standard procedure for isotropic SAXS. After radial averaging, spectra were corrected from the electronic noise of the detector, empty cell, absorption, and sample thickness. An ^{55}Ir source was used for the corrections of geometrical factors and detector cell efficiency. A Silver Behenate sample allowed the q-calibration, and the normalization to the unit incident flux was obtained using Lupolen as standard sample. Finally, the scattered intensities were corrected from the scattering of the solvent. According to such a procedure, a scattered intensity per unit volume, $I(q)$ (cm^{-1}), containing all the structural information is obtained for each polymer solution in methanol. Actually, $I(q)$ is the sum of an intramolecular term and an intermolecular one[33−35]

$$I(q) = K^2cN[g_1(q) + cg_2(q)] \quad (1)$$

where K (cm) is the contrast length of the ethylene oxide monomers with respect to the solvent, ($K = 2.16 \times 10^{-12}$ cm for methanol as solvent); K^2 (cm^2) the contrast factor ($K^2 = 4.67 \times 10^{-24}$ cm^2); c (mol cm^{-3}) the concentration of the polymer solution; and N Avogadro's number (mol^{-1}). $g_1(q)$ is the form factor, and $g_2(q)$ is the intermolecular correlation function. For PEO−POSS star-shaped macromolecules, we neglected the POSS core and kept the contrast length and contrast factor of PEO in methanol. This approximation is justified by the small volume fraction of POSS in the PEO−POSS stars and the close scattering length densities of both PEO and POSS ($\rho_X = 11.09 \times 10^{10}$ and 10.92×10^{10} cm^{-2}, respectively).

The scattered intensities measured from several solutions of distinct concentrations (as $c = 2.043 \times 10^{-4}$, 4.086×10^{-4}, and 6.129×10^{-4} mol cm^{-3} for the PEO stars $Q_8M_8^{PEO}$), in the dilute regime ($c < c^*$; c^* being the critical overlap concentration of the macromolecules), allow separation of the intra- and intermolecular terms. Specifically, as suggested by eq 1, the

DOI: 10.1021/jp505191d
J. Phys. Chem. B 2015, 119, 1669−1680

Scheme 1. Schematic Representation of the Synthesis of an ω-Undecenyl PEO Macromonomer by Deactivation with 11-Bromo-1-undecene in the Presence of NaH

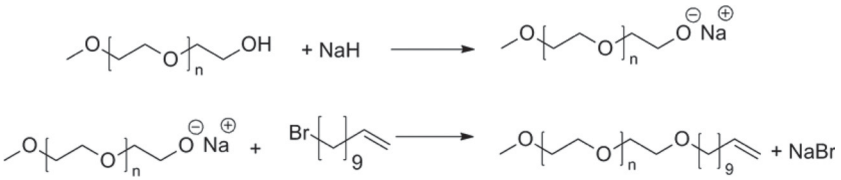

Table 1. Molecular Characteristics of the ω-Undecenyl PEO Macromonomers Obtained by Deactivation with 11-Bromo-1-undecene in the Presence of NaH

sample	M_n[a] (g mol^{-1}) SEC	M_n[b] (g mol^{-1}) SEC	M_w[c] (g mol^{-1}) SEC	M_n[d] (g mol^{-1}) MALDI	PDI[e]	f (%)[f] ^{1}H NMR
PEO1	1000	1200	1300	1300	1.04	100
PEO2	1700	1800	1900	2100	1.05	100
PEO3	1700	1800	1900	2000	1.05	95
PEO4[g]	1700	1800	1900	2000	1.05	100
PEO5[g]	1700	1800	1900	–	1.05	95
PEO6[g]	4600	5100	5500	5100	1.08	90
PEO7[g]	4600	5000	5300	–	1.06	99
PEO8	10900	7600	10400	10400	1.36	89
PEO9 (di OH)	6000	6500	7100	6500	1.09	100

[a]Number-average molar mass of the precursor PEOs, measured by SEC in THF, calibration with linear PEOs. [b]Number-average molar mass of the ω-undecenyl PEOs, measured by SEC in THF, calibration with linear PEOs. [c]Weight-average molar mass of the ω-undecenyl PEOs, measured by SEC in THF, calibration with linear PEOs. [d]Number-average molar mass M_n of the ω-undecenyl PEOs, measured by MALDI-TOF MS. [e]PDI of the ω-undecenyl PEOs (M_W /M_n) determined by SEC. [f]Yield of functionalization of the ω-undecenyl PEOs, measured by ^{1}H NMR (400 MHz) in $CDCl_3$. [g]PEO/NaH = 1/5.

extrapolation to $c = 0$ of $I(q)/K^2cN$ yields the form factor $g_1(q) = NP(q)$, characterizing the average conformation of the macromolecules dispersed in the solvent. N is the degree of polymerization of macromolecules; $P(q)$ is their form factor normalized in such a way that $P(0) = 1$. A typical curve of the scattered intensities $I(q, c)$ for distinct concentrations and form factor $g_1(q)$ of the PEO star 11 in methanol is presented in Figure SA in the Supporting Information. According to eq 1, the extrapolation to $c = 0$ of $I(q,c)/K^2cN$ leads to the form factor $g_1(q)$.

When the polydispersity is taken into account, it is actually the weight-average of the form factor $g_1(q)$, i.e. $\langle g_1(q)\rangle_w$, that is determined. We also have

$$\langle g_1(q)\rangle_w = N_w\langle P(q)\rangle_z \quad (2)$$

where N_w is the weight-average of the polymerization degree and $\langle P(q)\rangle_z$ is the z-average of the form factor $P(q)$.

At small q values, in the Guinier range $qR_g < 1$, where R_g is the radius of gyration of the macromolecules; a series expansion of the form factor $g_1(q)$ leads to

$$1/g_1(q) = (1/N_w)[1 + q^2\langle R_g^2\rangle_z/3 + o(q^2)] \quad (3)$$

At high q values, $qR_g > 1$, $g_1(q)$ is just related to the average conformation of the macromolecules and often obeys simple scaling laws. The strategy is then to compare the experimental curves with the predicted curves according to realistic structural models.

A PerkinElmer Diamond differential scanning calorimetry (DSC) instrument using stainless steel capsules under nitrogen atmosphere was used to determine thermal transitions. All the samples were dried under vacuum overnight before measurement. To remove any previous thermal history, all samples were heated to 100 °C with a fast heating rate of 20 °C min^{-1} and held for 1 min and then quenched to 0 or −60 °C. A heating rate of 10 °C min^{-1} was used in both first cases, followed by a heating rate of 5 °C min^{-1}.

The microscopy pictures were taken with a crossed polarized optical microscopy (Leica DMR-X microscope).

RESULTS AND DISCUSSION

Synthesis of ω-undecenyl PEO macromonomers by deactivation with 11-bromo-1-undecene in the presence of NaH.

As described in the Experimental Section, a series of ω-undecenyl PEO macromonomers were prepared by chain-end modification of commercial α-methoxy-ω-hydroxy PEOs ($M_{n,SEC}$ = 1000, 1700, 4600, 10 900 g mol^{-1}) or α-hydro-ω-hydroxy PEOs ($M_{n,SEC}$ = 6000 g mol^{-1}) with 11-bromo-1-undecene in the presence of NaH (Scheme 1).[2] The molecular characteristics of the precursor samples and of the resulting PEO macromonomers, determined by SEC and ^{1}H NMR, are collected in Table 1. A typical SEC diagram is also presented in Figure S5 in the Supporting Information.

From SEC it can be concluded that the sample is almost free of precursor polymer. The small shift in the elution volume reflects the addition of the undecenyl end-group. To confirm the absence of a degradation of the PEO chain during the functionalization process at 110 °C, we kept an α-methoxy-ω-hydroxy PEO at this temperature for 24 h. The sample was characterized by SEC and MALDI-TOF MS. The SEC curve is identical to that of the same PEO before heating. Hence, no degradation occurs during the chain-end modification of PEOs with 11-bromo-1-undecene in the presence of NaH. Moreover, the MALDI-TOF MS spectrum also remains unchanged. ^{1}H NMR spectroscopy (Figure S6 in the Supporting Information) was also used for end-group titration and to calculate the functionality of the different reaction products. In addition to the peaks characteristic for the precursor PEO, new peaks corresponding to the CH_2═CH− protons appear (CH_2═

DOI: 10.1021/jp505191d
J. Phys. Chem. B 2015, 119, 1669−1680

Scheme 2. Schematic Representation of the Synthesis of a $Q_8M_8^{PEO}$ Star by Coupling via Hydrosilylation Monofunctional α-Methoxy-ω-undecenyl PEO Macromonomers with $Q_8M_8^{H}$ in the Presence of a Karstedt Catalyst

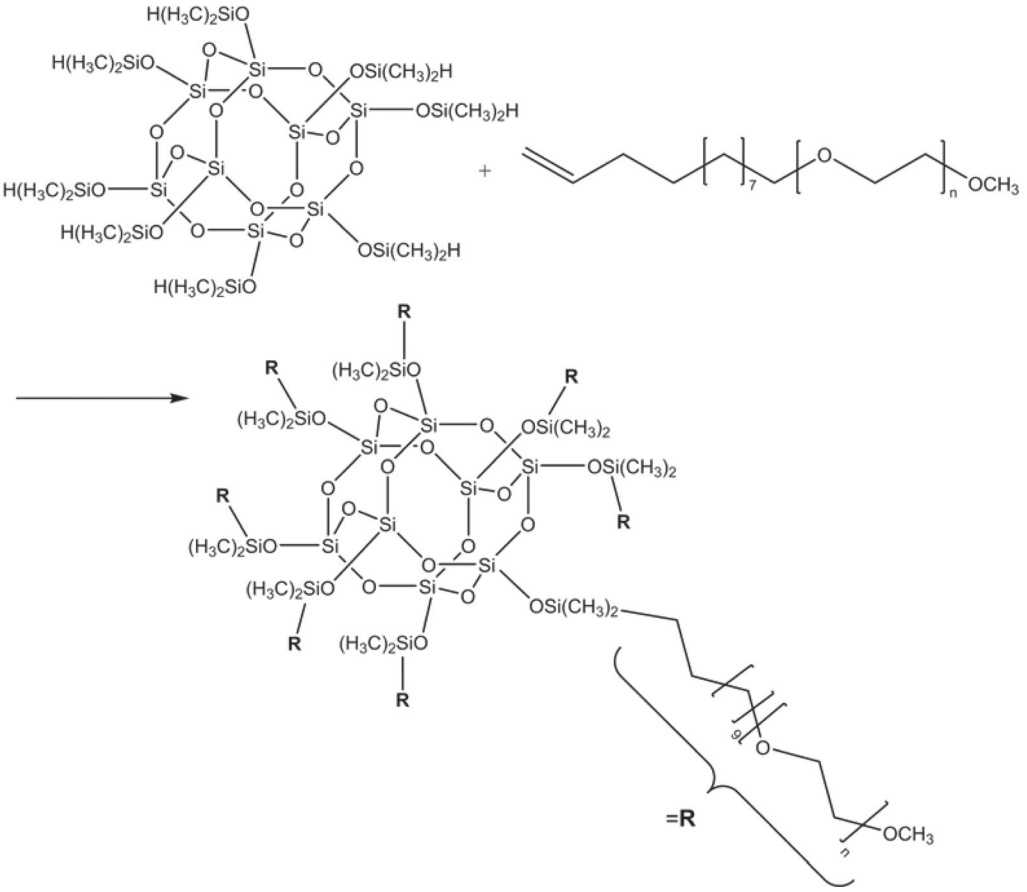

CH–, δ = 5.1 ppm; CH_2=C*H*–, δ = 5.8 ppm). The average functionality of the PEO macromonomers was determined by integrating the signals of the ^{1}H NMR spectra, i.e., the peaks at 5.1 ppm (double bond) and the peak at 3.3 ppm (CH_3O–) of the PEO chain. The different values are provided in Table 1. In most cases, the functionalization yield is close to 100%, independent of the molar mass of the precursor PEO. The M_n values obtained by SEC and determined by ^{1}H NMR are in good agreement. The presence of the undecenyl entity at the chain-end was confirmed by MALDI-TOF MS (Figure S7 in the Supporting Information). As expected, the molar mass of the ω-undecenyl PEO is higher than that of the precursor PEO. A difference of m/z of 152 could be noted, which confirms the presence of the undecenyl group and the almost quantitative functionalization of the PEOs. For the bifunctional PEO, a difference of m/z of 304 is observed. For the MALDI-TOF MS in Figure S7 in the Supporting Information, a "minor" distribution is visible. The distribution corresponds to the "protonated" but to neither the "sodiated" ω-undecenyl PEO nor the unfunctionalized PEOs.

To determine the detection limit of α-methoxy-ω-hydroxy PEOs by MALDI-TOF MS, 5, 10, 20, or 30 wt % of an α-methoxy-ω-hydroxy PEO was added to a selected α-methoxy-ω-undecenyl PEO ($M_{n,SEC}$ = 1800 g mol^{-1}). The presence of the α-methoxy-ω-hydroxy PEO in all contaminated samples could be confirmed by the clearly detected second distribution. Two typical MALDI-TOF MS spectra of the samples (M_n = 1800 g mol^{-1}) containing 5 and 20 wt % of α-methoxy-ω-hydroxy PEO are presented in Figure S8 in the Supporting Information. To determine the amount of contamination by ^{1}H NMR, we used the ratio of the integrals for the peak at 5.1 ppm (double bond) and the peak at 3.3 ppm (CH_3). These measurements attested the presence of α-methoxy-ω-hydroxy PEO for the samples contaminated with 10, 20, and 30 wt %. This is not the case for the 5 wt % sample. As a result, contaminations less than 10 wt % are not detectable by ^{1}H NMR spectroscopy. In conclusion, the chain-end modification of α-methoxy-ω-hydroxy PEOs or α-hydro-ω-hydroxy PEOs with 11-bromo-1-undecene in the presence of NaH represents a simple and efficient approach for decorating almost quantitatively PEOs with undecenyl end-groups. The reaction can be conducted in the absence of solvent. No degradation of the PEO chain takes places during the functionalization process, as demonstrated by SEC and MALDI-TOF MS.

PEO Star-Shaped Polymers Prepared with ω-Undecenyl PEO Macromonomers ($Q_8M_8^{PEO}$). Branched PEOs such as comb-shaped polymers,[36] star-shaped polymers,[13,37] hyperbranched polymers,[38] and dendrimers[13] have attracted much attention in the past 30 years because they constitute interesting species for physicochemical studies and can serve as building blocks for materials designed for many applications. A precise control of the functionality and the arm-length constitutes in most cases a prerequisite. In addition, the higher the functionality of the star-shaped polymers the better the

DOI: 10.1021/jp505191d
J. Phys. Chem. B 2015, 119, 1669−1680

Table 2. Molecular Characteristics of the PEO Star-Shaped Polymers Obtained by Grafting via Hydrosilylation of ω-Undecenyl PEOs onto $Q_8M_8^H$

sample	PEO (g)	time (h)	temp. (°C)	toluene (mL)	catalyst (5×10^{-4} M) (mL)	M_n[a] (g mol^{-1}) SEC	M_w[b] (g mol^{-1}) SEC	PDI[c]	% star SEC
star 1	1	2	40	0.7	0.5	14 300	16 100	1.12	33
star 2	1	2	40	1	1 drop	1 900	2 000	1.05	0
star 3	1	2	40	0.7	0.5	10 800	13 500	1.25	13
star 4	1	2	40	0.7	1	11 600	13 600	1.17	20
star 5	1	2	40	1	0.15[d]	14 300	21 100	1.48	50
star 6	1	24	40	1	0.15[d]	10 700	12 200	1.14	54
star 7	1	2	40	5	0.3[d]	10 080	11 700	1.16	65
star 8	1	2	40	5	0.3[d]	14 300	16 200	1.13	52
star 9	1	24	80	5	0.15[d]	12 700	13 600	1.07	83
star 10	1	24	80	5	0.15[d]	11 300	12 100	1.06	83
star 11	1.4	24	80	7	0.2[d]	11 700	12 500	1.07	83
star 12	1.7	24	80	9	0.25[d]	11 700	12 700	1.08	83

[a]Number-average molar mass of the PEO stars, measured by SEC, calibration with linear PEOs. [b]Weight-average molar mass of the PEO stars, measured by SEC, calibration with linear PEOs. [c]PDI of the PEO stars (M_W/M_n) determined by SEC in THF. [d]Catalyst at 2×10^{-3} M. Number-average molar mass of the ω-undecenyl PEO precursor measured by SEC in THF, calibration with linear PEOs: M_n = 1800 g mol^{-1}. Number-average molar mass of the PEO stars calculated taking into account the molar mass of the branch and the core and assuming a functionality of 8: 15 417 g mol^{-1}.

solubility in water provided the molar masses of the water-soluble PEO branches are sufficiently high. This can be explained by the protecting effect exerted in water by the PEO chains. Recently, we[11] and others[10] prepared PEO stars containing a central core by coupling via hydrosilylation of ω-allyl PEOs with $Q_8M_8^H$ in the presence of a hydrosilylation catalyst. The products $Q_8M_8^{PEO}$ could be characterized after purification by fractional precipitation as well-defined octafunctional PEO stars.

We propose in this contribution the use of ω-undecenyl PEO macromonomers. The undecenyl group should facilitate the accessibility of the double bond for subsequent applications. The reaction between these ω-undecenyl PEO macromonomers and $Q_8M_8^H$ is described in Scheme 2. The reaction products were systematically characterized by independent methods: SEC; ^{1}H, ^{13}C, and ^{29}Si NMR; infrared spectroscopy; MALDI-TOF MS; and SAXS. SEC with RI detection was used to evaluate the amount of PEO grafted onto the octafunctionalized silsesquioxane core. It has to be established whether or not all the ω-undecenyl PEO chains have reacted with the antagonist functions of the octafunctionalized silsesquioxane core. The results are presented in Table 2.

For the hydrosilylation reaction (star 1) carried out in the presence of oxygen, the SEC trace of the resulting product shows two well-separated peaks (Figure 1), one at low-volume elution corresponding to the $Q_8M_8^{PEO}$ and a second at higher-volume elution attributed to unreacted macromonomer introduction; 30 wt % of $Q_8M_8^{PEO}$ was obtained.

One drop of pure Karstedt catalyst (0.05 M) was added into a solution of ω-undecenyl PEO in 1 mL of toluene as discussed in the Experimental Section (40 °C for 2 h). The SEC trace of the resulting reaction product is characterized by the presence of only one peak which can be easily attributed to the unreacted PEO macromonomer (see Table 2, star 2). We tested also a diluted solution of the Karstedt catalyst (0.5 or 1 mL at 5×10^{-4} M). The SEC result confirmed the presence of two peaks corresponding to the unreacted macromonomer and to the star-shaped PEO. Samples of 30 wt % $Q_8M_8^{PEO}$ were obtained (stars 3 and 4). If one increases the catalyst concentration from 5×10^{-4} M to 2×10^{-3} M (0.15 mL), even better results are obtained. In this case, 50 wt % of $Q_8M_8^{PEO}$ was obtained (star 5). However, increasing the reaction time for the same catalyst concentration does not lead to high grafting yields (star 6). We decided then to increase the reaction temperature from 40 to 80 °C. Under these conditions (1 g PEO in 5 mL of toluene, 0.15 mL of a solution of the Karstedt catalyst (2×10^{-3} M)), we obtained far better results, around 80 wt % of $Q_8M_8^{PEO}$ (star 9 at 12). The reaction was repeated several times, and the results are approximately the same.

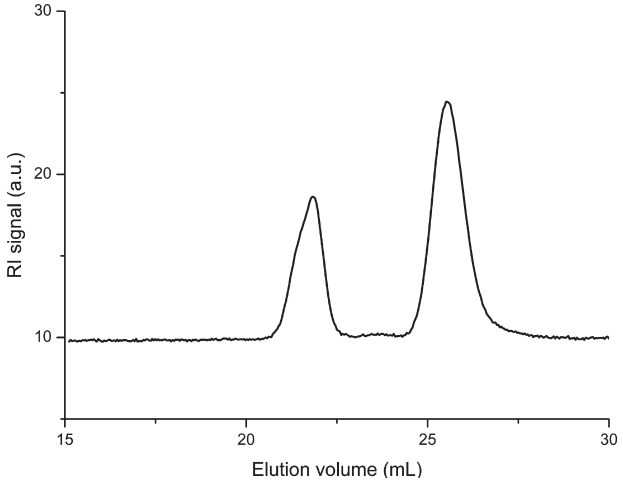

Figure 1. Typical SEC trace of $Q_8M_8^{PEO}$ ($M_{n,SEC,Macro}$ = 1800 g mol^{-1}).

Several Methods Can Be Used to Remove Undesired Compounds from Raw Polymers. Dialysis is known as a possible separation method in water by selective and passive diffusion through a semipermeable membrane. This technique has been used successfully to remove unreacted PEO in star-shaped PEOs.[37] Yen et al.[39] isolated pure star-shaped PEOs in aqueous solution of sodium carbonate, Cansell et al.[40] used supercritical fluids for the fractionation of PEOs. Trimpin et al.[41] utilized liquid adsorption chromatography at critical conditions combined with a MALDI-TOF MS characterization to achieve fractionation of mixtures of low molar mass PEOs (functionalized or not).

However, for $Q_8M_8^{PEO}$, the fractional precipitation is the best method to isolate the star-shaped product in a very effective

DOI: 10.1021/jp505191d
J. Phys. Chem. B 2015, 119, 1669−1680

way.[11] For this purpose toluene as solvent and cyclohexane as precipitant were utilized. The SEC curve shows (Figure 2) the

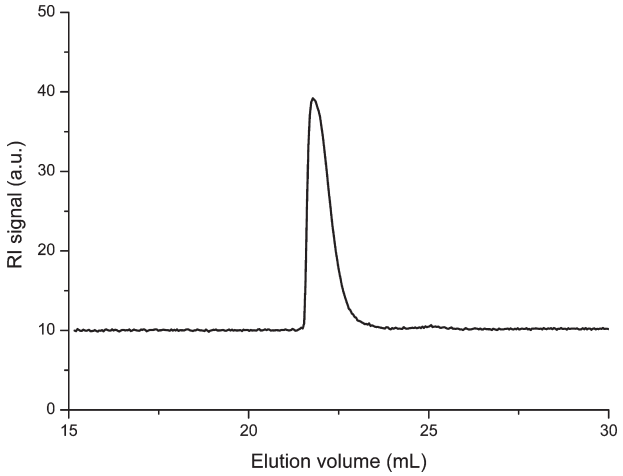

Figure 2. Typical SEC trace of fractionated $Q_8M_8^{PEO}$ ($M_{n,SEC,Macro}$ = 1800 g mol^{-1}).

successful isolation of the star-shaped PEOs. One peak is visible, and the elution volume peak corresponding to a maximum of 22.5 mL can be attributed to a M_n of 11 700 g mol^{-1}.

However, by SEC based on calibration with linear PEO, the apparent molar mass values are underestimated; in fact, star-shaped PEOs are known to exhibit a more compact structure in solution than the linear equivalent of the same molar mass. The determination of the absolute molar mass of $Q_8M_8^{PEO}$ by classical light-scattering (LS) in methanol revealed to be much more efficient. Star 10 was characterized by LS in methanol.[42−44] A typical LS diagram of a star-shaped PEO sample constituted of PEO chains ($M_{n,SEC}$ = 1800 g mol^{-1}) is presented in Figure S9 in the Supporting Information. From these measurements, a M_w value of 17 000 g mol^{-1} was obtained. From the ratio of the latter molar mass to the molar mass of the branch determined by SEC, an average functionality of 9.71 could be estimated. A functionality value of 8.5 is obtained from the ratio of the $M_{w,LS}$ of $Q_8M_8^{PEO}$ to the M_n of the branch determined by MALDI-TOF MS ($M_{n,MALDI\text{-}TOF\ MS}$ = 2000 g mol^{-1}). This value is in close agreement with the theoretical value taking into account the limits of characterization techniques.

The efficiency of the grafting of the ω-undecenyl PEOs on the silsesquioxane cores was also verified by ^{1}H NMR. The methyl group signals of $Q_8M_8^H$ appear at 0.23 ppm, and Si−H proton signals appear at 4.7 ppm. In the spectrum of the pure $Q_8M_8^{PEO}$ (Figure 3), the methyl proton signals are slightly shifted to low parts per million values, and the characteristic peaks of the double bond of the ω-undecenyl PEO macromonomer (at 5.7 and 4.9 ppm) disappeared. The peak at 4.7 ppm belonging to the Si−H function of the cage is absent. However, a new peak at 0.5 ppm appeared, confirming the formation of the bond between the cage and the PEO chain. The signals at 1.5 and 1.2 ppm characteristic of the 9 CH_2 entities are present, which confirms the grafting onto the cage. The new peak at 0.84 ppm corresponds to the protons of CH_3 of the undecene molecule grafted to the residual Si−H functions. ^{1}H NMR was also used to determine the number of PEO chains attached to $Q_8M_8^H$. ^{1}H NMR was also used to determine the number of PEO chains attached to $Q_8M_8^H$. A functionality of 7.2 could be calculated by considering the ratio between the integrals of the peak of the methyl group at 0.09 ppm (−Si(CH_3)$_2$) (on the core) and the methylene group at 0.56 ppm (−Si−CH_2−CH_2) (originating from the ω-undecenyl PEO) (star 11).

The ^{13}C NMR measurement shows the absence of the characteristic peaks for the double bond of the ω-undecenyl PEO. In Figure S10 in the Supporting Information, the carbon peaks of the double bond of ω-undecenyl PEO have disappeared (at 138.8 and 113.9 ppm). The peak at 0.6 ppm represents the methyl carbon of Si−CH_3, and the appearance of two carbon signals at 17.4 and 22.7 ppm in α and β of Si, respectively, due to the unsaturated carbons of the undecenyl group on the silsesquioxane core.

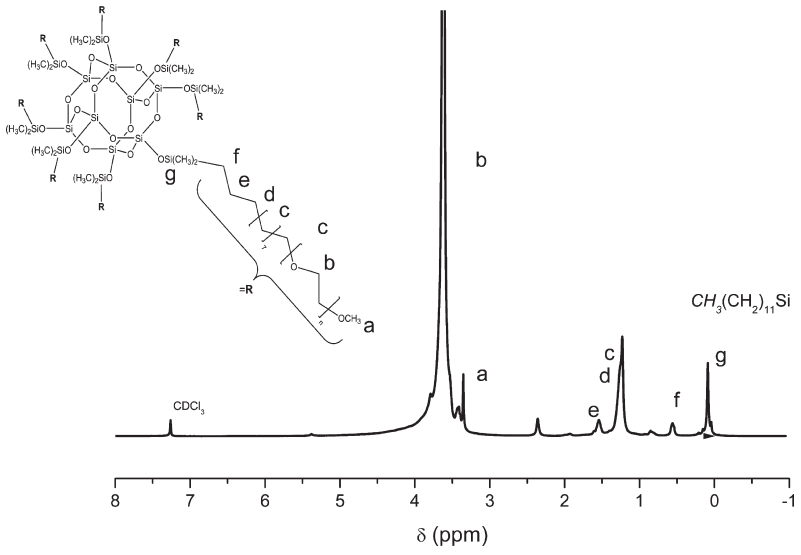

Figure 3. ^{1}H NMR spectrum of $Q_8M_8^{PEO}$ (400 MHz, $CDCl_3$).

DOI: 10.1021/jp505191d
J. Phys. Chem. B 2015, 119, 1669−1680

The ^{29}Si NMR allows the detection of the peak of Si groups. In Figure 4, at −1.42 ppm the peak characteristic of the *Si*−H

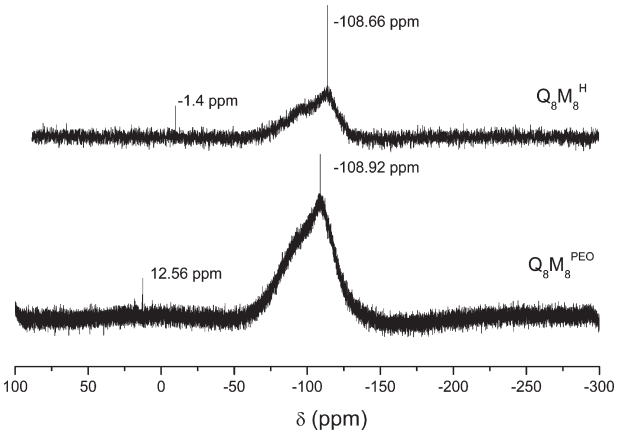

Figure 4. ^{29}Si NMR spectrum of $Q_8M_8^H$ and $Q_8M_8^{PEO}$ (400 MHz, $CDCl_3$).

and at −108 ppm the *Si*−O_4 group of the POSS are observed. On the spectrum of the $Q_8M_8^{PEO}$, the peak at −1.42 ppm is shifted to 12.55 ppm and corresponds to the bond between Si and PEO. The presence at 108 ppm of the *Si*−O_4 group confirms that the POSS core is not affected by the reaction. No signals characteristic of side products were detected.

The intense peak characteristics of the Si−H bond of $Q_8M_8^H$ is not present on the FTIR spectrum of $Q_8M_8^{PEO}$ (Figure 5).

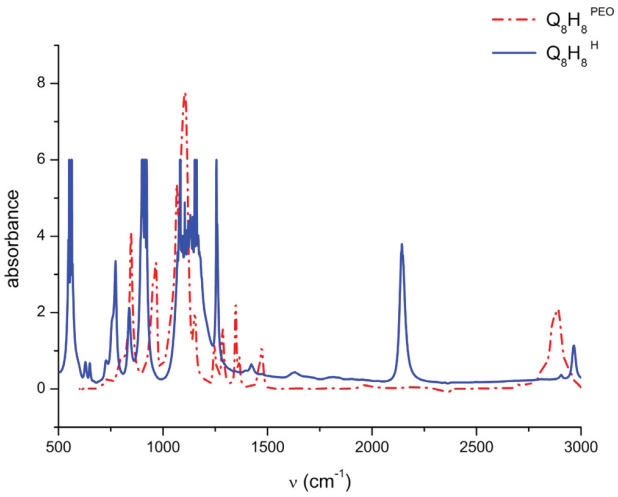

Figure 5. FTIR spectrum of (blue) $Q_8M_8^H$ and (red) $Q_8M_8^{PEO}$.

However, the characteristic peaks of PEO can be observed in the spectrum. The $Q_8M_8^H$ is completely surrounded by PEO chains. This is partially due to the shielding of PEO, and POSS represents only 6 wt % in weight in the star-shaped PEO.

An investigation by MALDI-TOF MS was performed on the pure star 12 (Figure 6). These MALDI-TOF MS measurements corroborate the results obtained by SEC and ^{1}H NMR. The sample is characterized by the presence of three peaks: a first one (peak A) present at m/z value of 2234, a second peak (peak B_1) at m/z value of 15 974 (with one shoulder at 14 040 (peak B_2)), and a last distribution (peak C) at 7773. This latter is the doubly charged species of the singly charged PEO (m/z

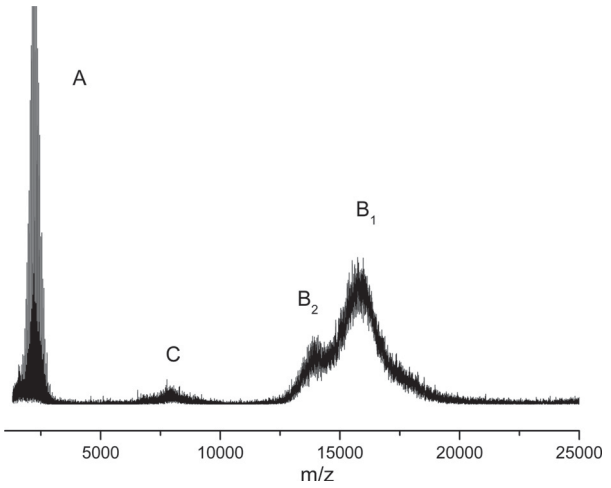

Figure 6. MALDI-TOF MS of $Q_8M_8^{PEO}$ (matrix: DCTB, NaI).

15974). In MALDI-TOF MS mostly singly charged species are observed, making the spectra much easier to analyze; however, doubly charged species are observed too and have been reported earlier.

In the MALDI-TOF MS spectrum, the distribution of chains corresponding to the PEO are visible. Peak A corresponds to a calculated value of 153.284 ($(CH_2)_9CHCH_2$) + 44.053 n (n = 46) (CH_2CH_2O) + 31.034 (CH_3O) + 22.990 (Na) (where n is the degree of polymerization) and can be assigned to the PEO macromonomer. A peak-to-peak mass increment of 44 corresponding to the molar mass of one ethylene oxide unit can be observed. However, the SEC and NMR measurements show the absence of PEO precursor. We assume that because of the difficult ionization of the $Q_8M_8^{PEO}$ a high laser intensity must be used, resulting in a fragmentation of the star molecule. However, it is unclear whether the seven-armed PEO (peak B_2), which was detected by MALDI-TOF MS, has been formed during the synthesis or results from a cleavage of the $Q_8M_8^{PEO}$ PEO under the MALDI conditions.

SAXS measurements are used[45] to obtain information about the structure of polystyrene stars as well as PMMA dendritic branched polymers. Specifically, they yield the average size and shape, or the internal structure, of these macromolecules. SAXS measurements also allowed to study the average structure of the styrene−butadiene−styrene triblock copolymers modified with POSS[46] and to characterize poly ethylene−polyhedral oligomeric silsesquioxanes nanocomposite blends.[47] The clustering phenomenon on PEO solution in various solvents is observed by small-angle neutron scattering.[48] Here, we present their use for characterizing the average conformation of the prepared PEO star-branched macromolecules.

The form factors, $g_1(q)$, of both the PEO stars $Q_8M_8^{PEO}$ and the PEO linear macromolecules corresponding to their arms, which results from our SAXS experiments, are shown in Figure 7. The form factor of PEO arms is characteristic of that of linear polymers.[33−35] At small q values, we observe a plateau and its height corresponds to an average degree of polymerization N_w close to 40. Beyond the Guinier range, the form factor can be described by a scaling law ($g_1(q) \propto q^{-5/3}$). It is close to the one characterizing the self-avoiding random walk chain model ($g_1(q) \propto q^{-1.7}$), i.e., the internal structure of a linear macromolecule in a good solvent provided its local structure can be neglected. However, such a condition is not fulfilled

DOI: 10.1021/jp505191d
J. Phys. Chem. B 2015, 119, 1669−1680

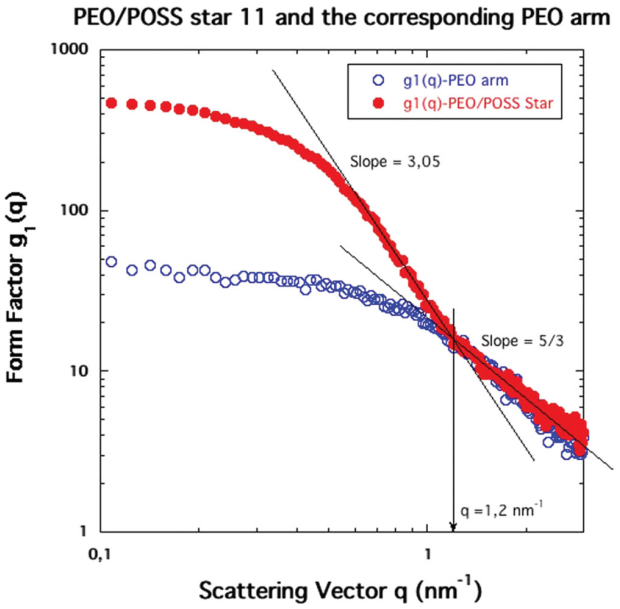

Figure 7. Form factors of PEO arms (ω-undecenyl PEO) and related PEO stars (star 11) in methanol.

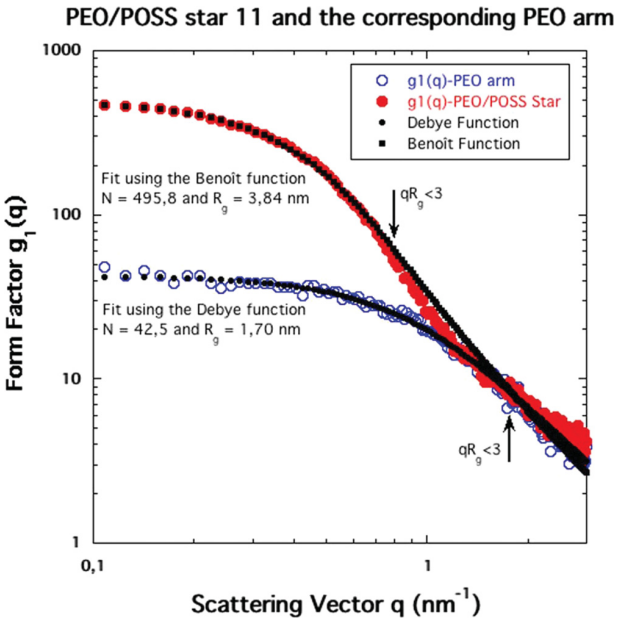

Figure 8. Fits of the PEO arm and star form factors to the Debye and Benoît functions, respectively.

because the range of scattering vectors in which the universal $q^{-1.7}$ scattering behavior is observed ($q > 1.2$ nm^{-1}) rather corresponds to a spatial scale comparable with the length of few monomers. The measured scattering decay can therefore only be related to the local structure of PEO chains (combination of chain local stiffness and cross-sectional effects). In contrast, the form factor of PEO stars displays two successive scaling laws beyond the Guinier range. This scattering behavior is characteristic of a star-branched polymer. At high q-values, the form factor is superimposed to that of PEO arms, displaying a similar scaling law. In the intermediate q-range, it is described by another power law ($g_1(q) \propto q^{-3.05}$) with an exponent that is close to double that of the one of the scaling law observed at high q-values. At this spatial scale, the form factor is actually proportional to the square of the amplitude scattered by the mean concentration profile inside a star. According to the Daoud−Cotton model of star-shaped macromolecules, the crossover between both scaling laws would occur at $q = 1/\xi(R)$, where $\xi(R)$ is the size of the largest blob associated with a star of geometric radius R.[34,49−53] With the relationship $\xi(R) = Rf^{-1/2}$, we would obtain $R = 2.36$ nm because the number of arms of PEO stars is $f = 8$. However, such a determination of the star radius is only approximative as the Daoud−Cotton model mainly concerns stars of large functionality and long arms. At small q-values, a plateau could form in the log representation, which leads to an estimation of N_w close to 500.

The polymerization degrees and radii of gyration of both PEO arms and PEO stars were mainly determined by fitting the form factors to the Debye function $g_D(q)$ and the Benoît function $g_B(q)$, respectively, in the q-range $qR_g < 3$. These fits are shown in Figure 8. They provide $N = 42.5$ and $R_g = 1.70$ nm for PEO arms; $N = 495.8$ and $R_g = 3.84$ nm for PEO stars.

The Debye function, which describes the form factor of a Gaussian chain of radius of gyration R_g, is

$$g_D(q) = (2N/x^2)[x - 1 + \exp(-x)] \quad (4)$$

where N is the degree of polymerization and $x = q^2R_g^2$.

The Benoît function, which describes the form factor of a Gaussian star-branched macromolecule of radius of gyration R_g, is

$$g_B(q) = (2N/x^2)[(f/2)(f-1)\exp(-2x/f) - f(f-2)\exp(-x/f) + x + (f/2)(f-3)] \quad (5)$$

where N and f are the degree of polymerization and the number of arms of the star, respectively; $x = (q^2R_g^2)[f^2/(3f-2)]$ this time.

Similar results are obtained using the Zimm representation of the data ($1/g_1(q)$ versus q^2) and eq 3 in the Guinier range $qR_g < 1$: $N_w = 4.31$ and $R_{g,z} = 1.84$ nm for PEO arms; $N_w = 495.2$ and $R_{g,z} = 3.89$ nm for PEO stars. This value of N_w is close to that measured by SLS (385).

Finally, the Kratky representation of the PEO arm and star form factors are presented in Figure 9. It emphasizes the increase in the internal density for star-branched polymers with respect to that of linear polymers.[53] In this representation, a maximum thus appears for the PEO star form factor at a q value which depends on the radius of gyration R_g and the functionality f. With $f = 8$, it appears at $qR_g = 2.13$.[34] This leads to $R_g = 4.1$ nm, in agreement with the R_g values previously determined for PEO stars using either a fit to the Benoît function in the q-range $qR_g < 3$ or the Zimm representation with eq 3 in the Guinier range $qR_g < 1$.

The incorporation of the POSS should improve in polymers the thermal stability compared to that of unmodified PEO polymers.[10] POSS are known for their thermal stability.[25]

We investigated first the thermal properties by DSC. The thermal properties of the ω-allyl and ω-undecenyl-functional PEOs and $Q_8M_8^{PEO}$ were studied by DSC. The crystallization temperatures (T_c) and the melting temperatures (T_m) were taken as the temperatures of the minima and the maxima of both exothermic and endothermic peaks, respectively and the values are noted in Table 3. Data were gathered on the second heating runs with scan rates of 10 °C min^{-1}. Linear PEOs were

DOI: 10.1021/jp505191d
J. Phys. Chem. B 2015, 119, 1669−1680

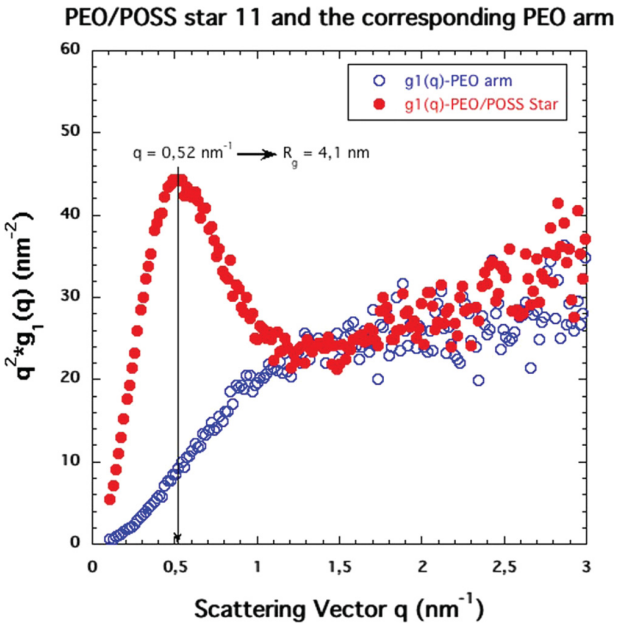

Figure 9. Kratky representation of the PEO arm and PEO star form factors.

Table 3. Thermal Properties of the ω-Undecenyl or ω-Allyl PEO Macromonomers and $Q_8M_8^{PEO}$ Prepared with Allyl or Undecenyl PEO

sample	T_m (°C)	T_c (°C)
α-methoxy-ω-hydroxy PEO (1700 g mol^{-1})	56.3	35.8
ω-allyl PEO (1800 g mol^{-1})	58.5	34.4
ω-undecenyl PEO (1800 g mol^{-1})	55.9	27.9
$Q_8M_8^{PEO}$ prepared with ω-allyl PEO	56.3	28.8
$Q_8M_8^{PEO}$ prepared with ω-undecenyl PEO	54.3	38.2

characterized by DSC measurements; the T_m values increased with the molar mass. In the literature, the T_m value of 53.8 °C is obtained for the α,ω-dihydroxy PEO (2000 g mol^{-1})[54] For α-methoxy-ω-hydroxy PEO precursors, the T_m value is 56.3 °C. Compared with ω-allyl PEO, no variations could be observed due at the short chain-end. With ω-undecenyl PEO, a second peak during the heating is visible, maybe caused by the hydrophobic part of undecenyl groups of the PEO.

For $Q_8M_8^{PEO}$ (based allyl or undecenyl PEO), a shoulder is present and most probably corresponding to the low crystallization of the $Q_8M_8^{PEO}$. The T_m value of $Q_8M_8^{PEO}$ based allyl PEO is at 56.3 °C and at 54.3 °C for $Q_8M_8^{PEO}$ based undecenyl PEO, compared to that of ω-allyl PEO (58.5 °C) or ω-undecenyl PEO (55.9 °C).

For the T_c values, the temperature of α-methoxy-ω-hydroxy PEO precursor are 37.6 °C and 34.4 °C for ω-allyl PEO and 27.9 °C for ω-undecenyl PEO. This difference can be explained by the presence of a flexible spacer between the double bond and the PEO chain. This spacer requires more time to organize during the crystallization. Considering the star compounds, the spacer has the same effect; the T_c value of allyl $Q_8M_8^{PEO}$ is 28.8 and 38.2 °C for undecenyl $Q_8M_8^{PEO}$.

WAXS was used to show the crystallization of peaks for linear and star PEOs.[55] Studies on the evolution of crystal patterns of single-layer lamellae of several star PEOs (3,4, and 8 arms) were reported.[56] The crystallization is observed in crossed polarized optical microscopy. Figure 10 represents the crystallization of different compounds: ω-undecenyl PEO and

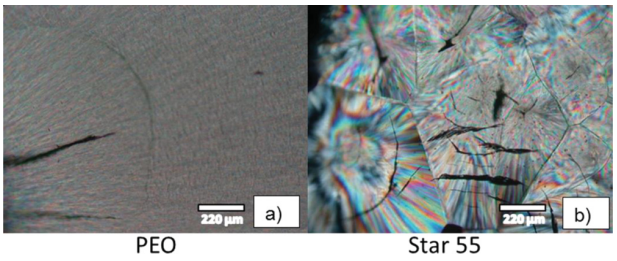

Figure 10. Sequence of micrographs obtained by optical microscopy with polarized light at distinct temperatures during a scanning melting process. The first crystallization point of ω-undecenyl PEO is observed at 39.8 °C (T = 4.33 min), and total crystallization is observed 36 °C (T = 5.4 min) (a). The first crystallization point of $Q_8M_8^{PEO}$ is observed at 38.5 °C (T = 4 min), and total crystallization is obtained 33 °C (T = 6.2 min) (b).

$Q_8M_8^{PEO}$ (see Figure S11 in the Supporting Information). In contrast to that of the ω-undecenyl PEO, on the image of the $Q_8M_8^{PEO}$, the existence of spherulites can be observed. The ω-undecenyl PEO crystallizes at 39.8 °C after a cooling period of 4.33 min. For $Q_8M_8^{PEO}$, this value is decreased to 38.5 °C after 4 min. $Q_8M_8^{PEO}$ takes more time to organize in crystals; this difference is caused by the structure of the star and by the presence of $(CH_2)_9$ spacer. The total crystallization of ω-undecenyl PEO is observed after T = 5.4 min at 36 °C and for $Q_8M_8^{PEO}$ after T = 6.2 min at 33 °C.

CONCLUSION

The aim of the present work was to design well-defined octafunctionalized spherosilsesquioxanes ($Q_8M_8^H$), decorated with Si−H functions by the coupling of α-methoxy-ω-undecenyl PEOs via hydrosilylation. These were successfully synthesized by the use of commercial PEOs with chain-end functionalized 11-bromo-1-undecene in the presence of NaH onto a POSS core. Advanced methods such as MALDI-TOF MS and light scattering in methanol obtained values which correlated to the theoretical molar masses taking into account an eight-arm star-shaped polymer. Furthermore, these were characterized by ^{1}H, ^{13}C, and ^{29}Si NMR and FTIR spectroscopy, which confirmed the covalently bonded branches onto the core. Moreover, their thermal properties and crystallization were concretized by DSC and optical microscopy. Finally, SAXS, by the determination of the radii of gyration and the degree of polymerization, has been shown to be flawless for affirming their architecture.

ASSOCIATED CONTENT

Supporting Information

Experimental section for the determination of the functionality of commercial PEOs via chemical modification of the chain-ends with 1-naphthyl isocyanate; typical SEC trace of an ω-undecenyl PEO macromonomer obtained by deactivation with 11-bromo-1-undecene in the presence of NaH; ^{1}H NMR spectrum of an ω-undecenyl PEO macromonomer obtained by deactivation with 11-bromo-1-undecene in the presence of NaH; MALDI-TOF MS of an ω-undecenyl PEO macromonomer obtained by deactivation with 11-bromo-1-undecene in the presence of NaH; MALDI-TOF MS of an ω-undecenyl

DOI: 10.1021/jp505191d
J. Phys. Chem. B 2015, 119, 1669−1680

PEO macromonomer with contamination of α-methoxy-ω-hydroxy PEO at 5 and 20 wt %; light scattering data of $Q_8M_8^{PEO}$ measured in methanol; ^{13}C NMR spectrum of $Q_8M_8^{PEO}$; sequence of micrographs obtained by optical microscopy with polarized light at distinct temperatures during a scanning melting process; and plot of scattered intensities, for distinct concentrations, and form factor of the PEO star 11 in methanol. This material is available free of charge via the Internet at http://pubs.acs.org.

AUTHOR INFORMATION

Corresponding Authors

*E-mail: pierre.lutz@ics-cnrs.unistra.fr. Phone:+33 (0)3 88 41 40 74

*E-mail: ulrich.schubert@uni-jena.de. Phone: +49 (0)3641 948200.

Notes

The authors declare no competing financial interest.

ACKNOWLEDGMENTS

We thank the Dutch Polymer Institute (DPI, technology area HTE, DPI project #690) and the Thüringer Ministerium für Bildung, Wissenschaft und Kultur (grants no. B515-07008) for financial support of this study. We thank Bruker Daltonics for their help and support. The authors thank Dr. D. Sarazin, L. Biniek, G. Fleith, C. Foussat, O. Gavat, and J. Quillé for their support with the polymer characterization, A. Collard and L. Oswald for her help in the preparation of some samples. The authors also acknowledge the CNRS and the Friedrich Schiller University Jena. The authors thank the French Ministry of Education and the DAAD for financial support (PROCOPE). P. J. Lutz thanks the Alexander von Humboldt Foundation for financial support.

REFERENCES

(1) Zhu, W.; Wang, B.; Zhang, Y.; Ding, J. Preparation of a Thermosensitive and Biodegradable Microgel *via* Polymerization of Macromonomers Based on Diacrylated Pluronic/Oligoester Copolymers. *Eur. Polym. J.* **2005**, *41*, 2161−2170.

(2) Zayed, G. M. S.; Tessmar, J. K. V. Heterobifunctional Poly(ethylene glycol) Derivatives for the Surface Modification of Gold Nanoparticles Toward Bone Mineral Targeting. *Macromol. Biosci.* **2012**, *12*, 1124−1136.

(3) Knop, K.; Hoogenboom, R.; Fischer, D.; Schubert, U. S. Poly(ethylene glycol) in Drug Delivery: Pros and Cons as Well as Potential Alternatives. *Angew. Chem., Int. Ed.* **2010**, *49*, 6288−6308.

(4) Ito, K.; Tsuchida, H.; Kitano, T. Poly(ethylene oxide) Macromonomers. *Polym. Bull.* **1986**, *15*, 425−430.

(5) Boutevin, B.; Boyer, C.; David, G.; Lutz, P. J. Synthesis of Macromonomers and Telechelic Oligomers by Living Polymerizations. In *Macromolecular Engineering*; Wiley-VCH Verlag: Weinheim, Germany, 2007; Vol. 2, pp 775−812.

(6) Yagci, Y.; Ito, K. Macromolecular Architecture Based on Anionically Prepared Poly(ethylene oxide) Macromonomers. *Macromol. Symp.* **2005**, *226*, 87−96.

(7) Harris, H.; Nohra, B.; Gavat, O.; Lutz, P. J. New Trends in Poly(ethylene oxide) or Polystyrene Macromonomer Based Networks Exhibiting Silsesquioxane Cross-Linking Points. *Macromol. Symp.* **2010**, *291−292*, 43−49.

(8) Lestel, L.; Cheradame, H.; Boileau, S. Crosslinking of Polyether Networks by Hydrosilylation and Related Side Reactions. *Polymer* **1990**, *31*, 1154−1158.

(9) Mya, K. Y.; Li, X.; Chen, L.; Ni, X.; Li, J.; He, C. Core−Corona Structure of Cubic Silsesquioxane-Poly(ethylene oxide) in Aqueous Solution: Fluorescence, Light Scattering, and TEM Studies. *J. Phys. Chem. B* **2005**, *109*, 9455−9462.

(10) Markovic, E.; Ginic-Markovic, M.; Clarke, S.; Matisons, J.; Hussain, M.; Simon, G. P. Poly(ethylene glycol)-Octafunctionalized Polyhedral Oligomeric Silsesquioxane: Synthesis and Thermal Analysis. *Macromolecules* **2007**, *40*, 2694−2701.

(11) Pozza, G. M. E.; Harris, H.; Barthel, M. J.; Vitz, J.; Schubert, U. S.; Lutz, P. J. Macromonomers as Well-Defined Building Blocks in the Synthesis of Hybrid Octafunctional Star-Shaped Poly(ethylene oxide)s. *Macromol. Chem. Phys.* **2012**, *213*, 2181−2191.

(12) Bosman, A. W.; Frechet, J. M. N.; Hawker, C. J. *Polym. Mater. Sci. Eng.* **2001**, *84*, 37.

(13) Lapienis, G. Star-Shaped Polymers Having PEO Arms. *Prog. Polym. Sci.* **2009**, *34*, 852−892.

(14) Gnanou, Y.; Lutz, P. J.; Rempp, P. Synthesis of Star-Shaped Poly(ethylene oxide). *Makromol. Chem.* **1988**, *189*, 2885−2892.

(15) Alexandre, E.; Schmitt, B.; Boudjema, K.; Merrill, E. W.; Lutz, P. J. Hydrogel Networks of Poly(ethylene oxide) Star Molecules Supported by Expanded Poly(tetrafluoroethylene) Membranes: Characterization, Biocompatibility Evaluation and Glucose Diffusion Characteristics. *Macromol. Biosci.* **2004**, *4*, 639−648.

(16) Keys, K. B.; Andreopoulos, F. M.; Peppas, N. A. Poly(ethylene glycol) Star Polymer Hydrogels. *Macromolecules* **1998**, *31*, 8149−8156.

(17) Comanita, B.; Noren, B.; Roovers, J. Star Poly(ethylene oxide)s from Carbosilane Dendrimers. *Macromolecules* **1999**, *32*, 1069−1072.

(18) Taton, D.; Saule, M.; Logan, J.; Duran, R.; Hou, S.; Chaikof, E. L.; Gnanou, Y. Polymerization of Ethylene Oxide with a Calixarene-Based Precursor: Synthesis of Eight-Arm Poly(ethylene oxide) Stars by the Core-First Methodology. *J. Polym. Sci., Part A: Polym. Chem.* **2003**, *41*, 1669−1676.

(19) Doycheva, M.; Berger-Nicoletti, E.; Wurm, F.; Frey, H. Rapid Synthesis and MALDI-ToF Characterization of Poly(ethylene oxide) Multiarm Star Polymers. *Macromol. Chem. Phys.* **2010**, *211*, 35−44.

(20) Hou, S.; Taton, D.; Saule, M.; Logan, J.; Chaikof, E. L.; Gnanou, Y. Synthesis of Functionalized Multiarm Poly(ethylene oxide) Stars. *Polymer* **2003**, *44*, 5067−5074.

(21) Feng, X.-S.; Taton, D.; Chaikof, E. L.; Gnanou, Y. Toward an Easy Access to Dendrimer-like Poly(ethylene oxide)s. *J. Am. Chem. Soc.* **2005**, *127*, 10956−10966.

(22) Baney, R. H.; Itoh, M.; Sakakibara, A.; Suzuki, T. Silsesquioxanes. *Chem. Rev. (Washington, DC, U.S.)* **1995**, *95*, 1409−1430.

(23) Marcolli, C.; Calzaferrit, G. Monosubstituted Octasilsesquioxanes. *Appl. Organometal. Chem.* **1999**, *13*, 213−226.

(24) Li, G.; Wang, L.; Ni, H.; Pittman, C. U., Jr. Polyhedral Oligomeric Silsesquioxane (POSS) Polymers and Copolymers: A Review. *J. Inorg. Organomet. Polym.* **2002**, *11*, 123−154.

(25) Cordes, D. B.; Lickiss, P. D.; Rataboul, F. Recent Developments in the Chemistry of Cubic Polyhedral Oligosilsesquioxanes. *Chem. Rev. (Washington, DC, U.S.)* **2010**, *110*, 2081−2173.

(26) Kuo, S.-W.; Chang, F.-C. POSS Related Polymer Nanocomposites. *Prog. Polym. Sci.* **2011**, *36*, 1649−1696.

(27) Xavier Perrin, F.; Viet Nguyen, T. B.; Margaillan, A. Linear and Branched Alkyl Substituted Octakis(dimethylsiloxy)-octasilsesquioxanes: WAXS and Thermal Properties. *Eur. Polym. J.* **2011**, *47*, 1370−1382.

(28) Wang, F.; Lu, X.; He, C. Some Recent Developments of Polyhedral Oligomeric Silsesquioxane (POSS)-Based Polymeric Materials. *J. Mater. Chem.* **2011**, *21*, 2775−2782.

(29) Maitra, P.; Wunder, S. L. Oligomeric Poly(ethylene oxide)-Functionalized Silsesquioxanes: Interfacial Effects on T_g, T_m, and ΔH_m. *Chem. Mater.* **2002**, *14*, 4494−4497.

(30) Knischka, R.; Dietsche, F.; Hanselmann, R.; Frey, H.; Mülhaupt, R.; Lutz, P. J. Silsesquioxane-Based Amphiphiles. *Langmuir* **1999**, *15*, 4752−4756.

(31) Karstedt, B. D. Platinum complexes of unsaturated siloxanes and platinum containing organopolysiloxanes. U.S. Patent 3,775,452, 1973.

DOI: 10.1021/jp505191d
J. Phys. Chem. B 2015, 119, 1669−1680

(32) Sarazin, D.; Schmutz, M.; Guenet, J. M.; Petitjean, A.; Lehn, J. M. Structure of Supramolecular Polymers Generated *via* Self-Assembly through Hydrogen Bonds. *Mol. Cryst. Liq. Cryst.* **2007**, *468*, 187−201.
(33) Higgins, J.; Benoit, H. *Polymers and Neutron Scattering*; Oxford University Press: Oxford, U.K., 1994.
(34) Rawiso, M. De l'Intensité à la Structure en Physico-Chimie des Polymères. *J. Phys. IV* **1999**, *9*, 147−195.
(35) Cotton, J. P. DNPA: Introduction et Variations sur le Contrast. *J. Phys. IV* **1999**, *9*, 21−49.
(36) Neugebauer, D. Graft Copolymers with Poly(ethylene oxide) Segments. *Polym. Int.* **2007**, *56*, 1469−1498.
(37) Knischka, R.; Lutz, P. J.; Sunder, A.; Mülhaupt, R.; Frey, H. Functional Poly(ethylene oxide) Multiarm Star Polymers: Core-First Synthesis Using Hyperbranched Polyglycerol Initiators. *Macromolecules* **2000**, *33*, 315−320.
(38) Lee, S.; Saito, K.; Lee, H.-R.; Lee, M. J.; Shibasaki, Y.; Oishi, Y.; Kim, B.-S. Hyperbranched Double Hydrophilic Block Copolymer Micelles of Poly(ethylene oxide) and Polyglycerol for pH-Responsive Drug Delivery. *Biomacromolecules* **2012**, *13*, 1190−1196.
(39) Yen, D. R.; Raghavan, S.; Merrill, E. W. Fractional Precipitation of Star Poly(ethylene oxide). *Macromolecules* **1996**, *29*, 8977−8978.
(40) Cansell, F.; Botella, P.; Six, J.-l.; Garrabos, Y.; Tufeu, R.; Gnanou, Y. Fractionation of Poly(ethylene oxide) Star Samples by Supercritical Fluids. *Polym. J.* **1997**, *29*, 910−913.
(41) Trimpin, S.; Weidner, S. M.; Falkenhagen, J.; McEwen, C. N. Fractionation and Solvent-Free MALDI-MS Analysis of Polymers Using Liquid Adsorption Chromatography at Critical Conditions in Combination with a Multisample On-Target Homogenization/Transfer Sample Preparation Method. *Anal. Chem.* **2007**, *79*, 7565−7570.
(42) Duval, M. Monitoring of Cluster Formation and Elimination in PEO Solutions. *Macromolecules* **2000**, *33*, 7862−7867.
(43) Vandermiers, C.; Damman, P.; Dosiere, M. Static and Quasielastic Light Scattering from Solutions of Poly(ethylene oxide) in Methanol. *Polymer* **1998**, *39*, 5627−5631.
(44) Zhou, P.; Brown, W. Static and Dynamic Properties of Poly(ethylene oxide) in Methanol. *Macromolecules* **1990**, *23*, 1131−1139.
(45) Jin, S.; Jin, K.; Yoon, J.; Heo, K.; Kim, J.; Kim, K.-W.; Ree, M.; Higashihara, T.; Watanabe, T.; Hirao, A. X-Ray Scattering Studies on Molecular Structures of Star and Dendritic Polymers. *Macromol. Res.* **2008**, *16*, 686−694.
(46) Fu, B. X.; Lee, A.; Haddad, T. S. Styrene−Butadiene−Styrene Triblock Copolymers Modified with Polyhedral Oligomeric Silsesquioxanes. *Macromolecules* **2004**, *37*, 5211−5218.
(47) Heeley, E. L.; Hughes, D. J.; El Aziz, Y.; Taylor, P. G.; Bassindale, A. R. Morphology and Crystallization Kinetics of Polyethylene/Long Alkyl-Chain Substituted Polyhedral Oligomeric Silsesquioxanes (POSS) nanocomposite blends: A SAXS/WAXS study. *Eur. Polym. J.* **2014**, *51*, 45−56.
(48) Hammouda, B.; Ho, D. L.; Kline, S. Insight into Clustering in Poly(ethylene oxide) Solutions. *Macromolecules* **2004**, *37*, 6932−6937.
(49) Daoud, M.; Cotton, J. P. Star Shaped Polymers: A Model for the Conformation and its Concentration Dependence. *J. Phys. (Paris)* **1982**, *43*, 531−538.
(50) Grest, G. S.; Kremer, K.; Witten, T. A. Structure of Many Arm Star Polymers: A Molecular Dynamics Simulation. *Macromolecules* **1987**, *20*, 1376−1383.
(51) Lairez, D.; Adam, M. Fractal Conformation of Polymers. *Fractals* **1993**, *01*, 149−169.
(52) Grest, G. S. Structure of Many-Arm Star Polymers in Solvents of Varying Quality: A Molecular Dynamics Study. *Macromolecules* **1994**, *27*, 3493−3500.
(53) Grest, G. S.; Fetters, L. J.; Huang, J. S.; Richter, D. Star Polymers: Experiment, Theory and Simulation. *Adv. Chem. Phys.* **2007**, *94*, 67−163.
(54) Kim, B.-S.; Mather, P. T. Amphiphilic Telechelics Incorporating Polyhedral Oligosilsesquioxane: 1. Synthesis and Characterization. *Macromolecules* **2002**, *35*, 8378−8384.
(55) Mya, K. Y.; Pramoda, K. P.; He, C. B. Crystallization Behavior of Star-Shaped Poly(ethylene oxide) with Cubic Silsesquioxane (CSSQ) Core. *Polymer* **2006**, *47*, 5035−5043.
(56) Zhang, G.-l.; Wen, X.-j.; Zhai, X.-m.; Wang, W. Evolution of Crystal Patterns of Single-Layer Lamellae of Star-Shaped PEO Samples. *Acta Polym. Sin.* **2013**, *0*, 398−405.

DOI: 10.1021/jp505191d
J. Phys. Chem. B 2015, 119, 1669−1680

Supporting Information

Molecular and Structural Characterization of Hybrid PEO/POSS Star-Shaped Macromolecules

Gladys M.-E. Pozza,[†,‡,§] Sarah Crotty,[‡] Michel Rawiso,[†] Ulrich S. Schubert,[,‡,§,] Pierre J. Lutz[*,†,§]*

[†] University of Strasbourg, Institut Charles Sadron, CNRS UPR 22, 23, rue du Loess 67034, Strasbourg, France

[‡] Laboratory of Organic and Macromolecular Chemistry (IOMC), Friedrich Schiller University Jena, Humboldtstr. 10, 07743 Jena, Germany

[§] Dutch Polymer Institute (DPI), P.O. Box 902, 5600 AX Eindhoven, the Netherlands

[#] Jena Center for Soft Matter (JCSM), Friedrich Schiller University, Philosophenweg 7, 07743 Jena, Germany

KEYWORDS: Hydrosilylation; macromonomers; MALDI-ToF MS; poly(ethylene oxide); Polyhedral Oligomeric Silsesquioxanes (POSS); SAXS

Experimental section for the determination of the functionality of commercial PEOs via chemical modification of the chain-ends with 1-naphthyl isocyanate

Table S1. Molecular characteristics of the ω-naphthyl carbamate PEOs

Figure S1. Typical SEC traces of an ω-naphthyl carbamate PEO ($M_{n,SEC}$ = 1800 g mol^{-1}).

Figure S2. UV spectrum of an ω-naphthyl carbamate PEO measured in ethanol.

Figure S3. ^{1}H NMR spectrum of an ω-naphthyl carbamate PEO (400 MHz, $CDCl_3$).

Figure S4. MALDI-ToF MS of an ω-naphthyl carbamate PEO ($M_{n,SEC}$ = 1200 g mol^{-1}) (Matrix: DCTB, NaI).

Figure S5.Typical SEC trace of an ω-undecenyl PEO macromonomer obtained by deactivation with 11-bromo-1-undecene in the presence of NaH ($M_{n,SEC}$ = 1800 g mol^{-1}).

Figure S6. ^{1}H NMR spectrum of an ω-undecenyl PEO macromonomer obtained by deactivation with 11-bromo-1-undecene in the presence of NaH (400 MHz, $CDCl_3$).

Figure S7. MALDI-ToF MS of an ω-undecenyl PEO macromonomer obtained by deactivation with 11-bromo-1-undecene in the presence of NaH ($M_{n,SEC}$ = 1900 g mol^{-1}) (Matrix: DCTB, NaI).

Figure S8. MALDI-ToF MS of an ω-undecenyl PEO macromonomer with contamination of α-methoxy-ω-hydroxy PEO at 5 and 20 wt % ($M_{n,SEC,\ Macro}$ = 1900 g mol^{-1}) (Matrix: DCTB, NaI).

Figure S9. Light scattering data of $Q_8M_8^{PEO}$ measured in methanol.

Figure S10. ^{13}C NMR spectrum of $Q_8M_8^{PEO}$ (400 MHz, $CDCl_3$).

Figure S11. Sequences of micrographs obtained by optical microscopy with polarized light at distinct temperatures, during a scanning melting process. The first point of the spherulite $Q_8M_8^{PEO}$ is observed at 38.5 °C after 4 min cooling (a) and the total crystallization is after 6.2 min at 33 °C (f).

Figure SA. Scattered intensities I(q, c), for distinct concentrations, and form factor $g_1(q)$ of the PEO star 11 in methanol. According to Eq. (1), the extrapolation to c=0 of $I(q,c)/K^2cN$ leads to the form factor $g_1(q)$.

Scheme S1. Schematical representation of the synthesis of an ω-naphthyl carbamate PEO

Determination of the functionality of commercial PEOs via chemical modification of the chain-ends with 1-naphthyl isocyanate.

Experimental section: Preparation of the samples.

The commercial α-methoxy-ω-hydroxy PEO (M_n = 1700 g mol^{-1}, 2 g, 1.18 μmol) was dissolved in 60 mL of dry THF under argon (T = 50 °C). One spatula of 1,4-diazabicyclo[2.2.2]octan (DABCO) was added, then 1-naphthyl isocyanate (20% molar excess, 0.202 mL, 1.41×10^{-3} mol) was introduced. The reaction was kept at 50 °C for 5 h. Afterwards, the THF was removed by evaporation under vacuum. The ω-naphthyl carbamate PEO was dissolved in THF:DMSO (50/50, v/v) and precipitated twice into cold diethyl ether (M_n < 4000 g mol^{-1}) and diethyl ether at room temperature for all the PEOs of higher molar masses. The resulting end-modified PEOs were characterized by SEC with RI and UV detection. ^{1}H NMR ($CDCl_3$, 400 MHz): δ 7.2–8 (m, 7H, Ar), 4.4 (m, 2H, –CO–O–CH_2–), 3.6–3.8 (m, 4H*n, –O–CH_2–CH_2–), 3.3 (s, 3H, –O–CH_3). The same experimental procedure was used for the modification of the bifunctional PEOs.

Discussion of the results.

The analysis of the hydroxyl content of commercial monofunctional PEOs revealed that they can be contaminated with critical amounts of bifunctional PEOs. Bifunctional PEOs are characterized by molar masses twice as high as the monofunctional PEO.

Their formation is attributed to the presence of water during the AROP process. They increase the PDI value of the supposedly “monofunctional” PEOs and further increase the average functionality. Moreover, the existence of bifunctional species may lead to undesired cross-linking during the copolymerization of the PEO macromonomers with low molar mass polymerizable

species. Hence, unexpected properties may be obtained. To overcome such difficulties, high osmotic pressure chromatography was used successfully to isolate the monofunctional PEO.[1] However, this strategy is time consuming and cannot be envisaged for the purification of large PEO quantities. As a consequence, it was important to determine the content of hydroxyl functions in the monofunctional PEOs used in the present study. Several approaches have been proposed in the literature to identify the chain-ends and to quantify the hydroxyl content of commercial monofunctional PEOs. This can be achieved directly by means of ^{1}H NMR[2] or after chain-end modification with trichloroacetyl isocyanate,[3] hexafluoroacetone,[4] or 1-naphthyl isocyanate.[5] Among the different possible approaches, we selected the method based on the modification of the hydroxyl chain-ends for a series of commercial PEOs with 1-naphthyl isocyanate. Naphthyl isocyanates are much more reactive than alkyl isocyanates. If appropriate experimental conditions are selected, the conversion of the hydroxyl functions into naphthyl carbamate groups is quantitative.[5] This reaction was applied to a series of commercial monofunctional PEOs covering a range of molar masses (M_n) from 1000 to 10900 g mol^{-1} and to a bifunctional sample with a M_n of 6000 g mol^{-1} (Scheme S1).

Insert Scheme S1

The functionalization reaction and the treatment of the end-modified PEOs are described below. It should be noted that the different samples had to be submitted to several precipitations to eliminate eventual traces of unreacted labeling agent leading to an overestimation of the functionalization rates. The different samples were characterized by three independent methods (SEC in THF with RI and UV detection, UV spectroscopic analysis and ^{1}H NMR) to assess the molar masses and polydispersity index values, and to confirm the presence of the naphthyl carbamate entity at the chain-end. MALDI-ToF MS measurements were also performed for all the

chain-end modified PEOs. The characterization data of the different naphthyl carbamate chain-end modified PEOs are presented in Table S1 together with the experimental conditions for the preparation of the samples. A typical SEC curve is presented in the supporting information section (Figure S1).

Insert Table S1 and Figure S1

Low PDI values, close to the precursor PEOs, were obtained by SEC (Figure S1 and Table S1). In most cases, the M_n values determined by SEC and based on calibration with linear α-hydro-ω-hydroxy PEOs, are in good agreement with the expected values. The slight increase in the molar mass with respect to the precursor PEO is attributed to the presence of the naphthyl carbamate entity at the chain-end. The results of the SEC with online UV detection (Figure S1) attested the presence of the naphthyl carbamate entity at the chain-end: A strong UV adsorption is observed at the elution volume corresponding to the PEO chain. Classical UV spectroscopy was also used to quantify the functionalization yield. The measurements were conducted in ethanol (Figure S2). This method allows the determination of the M_n values taking into account the chain-modified PEO concentration, the extinction coefficient (7060 mol^{-1} cm^{-1}) and the optical density. These values are presented in Table S1 and are consistent with the M_n values measured by SEC based on calibration with linear PEOs. The same remark is valid for the commercial bifunctional PEO sample with a molar mass (M_n) of 6000 g mol^{-1} and modified at the chain-end with 1-naphthyl isocyanate (Table S1).

Insert Figure S2

For the same samples, the functionality was determined by ^1H NMR measurements in $CDCl_3$. A typical ^1H NMR spectrum is presented in Figure S3. In addition to the signals of the methylene

protons [–O–C*H*$_2$–C*H*$_2$ (4H*n), δ = 3.6 to 3.8 ppm, PEO chain except the first methylene group], the spectrum is characterized by peaks assignable to the methoxy protons (initiator potassium methoxyethanolate). The corresponding peak of the hydroxyl function (in the precursor polymer at 4.70 ppm) disappeared. A new peak at 4.4 ppm appeared, corresponding to the bond-formation between the naphthyl carbamate group and the PEO chain (–CH$_2$–C*H*$_2$–O–CO–N–). ^{1}H NMR was also used to determine the functionalization yield. Considering the ratio between the integrals of the peak of the methyl group at 3.3 ppm (*CH*$_3$–O–PEO, outer chain) and the methylene group at 4.4 ppm (originating from the other end the PEO chain), a functionality value close to 1 was calculated.

Insert Figure S3

The same PEO samples were additionally analyzed by MALDI-ToF MS to verify the molar mass and to confirm the presence of the naphthyl carbamate entity at the chain-end (Figure S4). The measurements were systematically performed on the chain-end modified PEOs as well as on their precursors for comparison. The M_n values resulting from MALDI-ToF MS are shown in Table 1 together with the values determined by SEC and UV. A typical MALDI-ToF MS spectrum of a low molar mass naphthyl carbamate chain-end modified PEO ($M_{n,SEC}$ = 1200 g mol^{-1}) is presented in Figure S4. The M_n values determined for both, the precursor α-methoxy-ω-hydroxyl PEO and the α-methoxy-ω-naphthyl carbamate PEO, are in good agreement with the theoretical values. The signals between *m/z* 1236 and 1280 with a characteristic shift of *m/z* 44 are caused by the monofunctional PEO chain. The difference in the molar mass between the precursor PEO and the chain-end modified PEO (170 g mol^{-1}) corresponds exactly to the value of the naphthyl carbamate entity. However, besides these major peaks, a “minor” distribution is observed (see peaks at 1258

and 1303 g mol^{-1}). This distribution fits well with a monofunctional "protonated" naphthyl carbamate for the same number n, and not with a difunctional "protonated" or "sodiated" naphthyl carbamate PEO. The resulting mass spectrometrical signal appeared at *m/z* 1303: $CONHC_{10}H_7O(CH_2CH_2O)_{25}CH_3H$ (186.187 ($OC_{10}H_7NHCO$) + 44.053n (n = 25) (CH_2CH_2O) + 15.035 (CH_3) + 1.008 (H) (where n is the degree of polymerization)). The same "minor" distribution is observed for the PEO of molar mass 1700 g mol^{-1}. This "minor" distribution is not present in the chain-end modified PEO samples prepared from precursors of higher molar masses or from the bifunctional precursor of a molar mass of 6000 g mol^{-1}. These results confirm a nearly quantitative functionalization of the PEO chain-ends.

Insert Figure S4

Table S1. Molecular characteristics of the ω-naphthyl carbamate PEOs

Sample	[napht]/ [PEO][a)]	M_n[b)] (g mol^{-1}) SEC	M_n[c)] (g mol^{-1}) SEC	M_w[d)] (g mol^{-1}) SEC	M_n[e)] (g mol^{-1}) MALDI	M_n[f)] (g mol^{-1}) UV	F[g)] (%) ^{1}H NMR
PEONC1	1.2	1000	1100	1100	1200	1200	102
PEONC2	1.2	1700	1800	1900	2000	2000	101
PEONC3	1.2	4550	4700	5000	4900	4800	101
PEONC4	1.2	10900	11100	12400	10700	10600	105
PEONC5*	2.4	6000	5900	6400	6500	6100	103

[a)] Molar ratio 1-naphthyl isocyanate / PEO.

[b)] Number average molar mass of the precursor PEOs, measured by SEC in THF, calibration with linear PEOs.

[c)] Number average molar mass of the ω-naphthyl carbamate PEOs, measured by SEC in THF, calibration with linear PEOs.

[d)] Weight average molar mass of the ω-naphthyl carbamate PEOs, measured by SEC in THF, calibration with linear PEOs.

[e)] Number average molar mass of the ω-naphthyl carbamate PEOs, measured by MALDI ToF MS.

[f)] Number average molar mass of the ω-naphthyl carbamate PEOs, measured by UV.

[g)] Yield of functionalization of the ω-naphthyl carbamate PEOs, measured by ^{1}H NMR (400 MHz) in $CDCl_3$.

*PEO di OH.

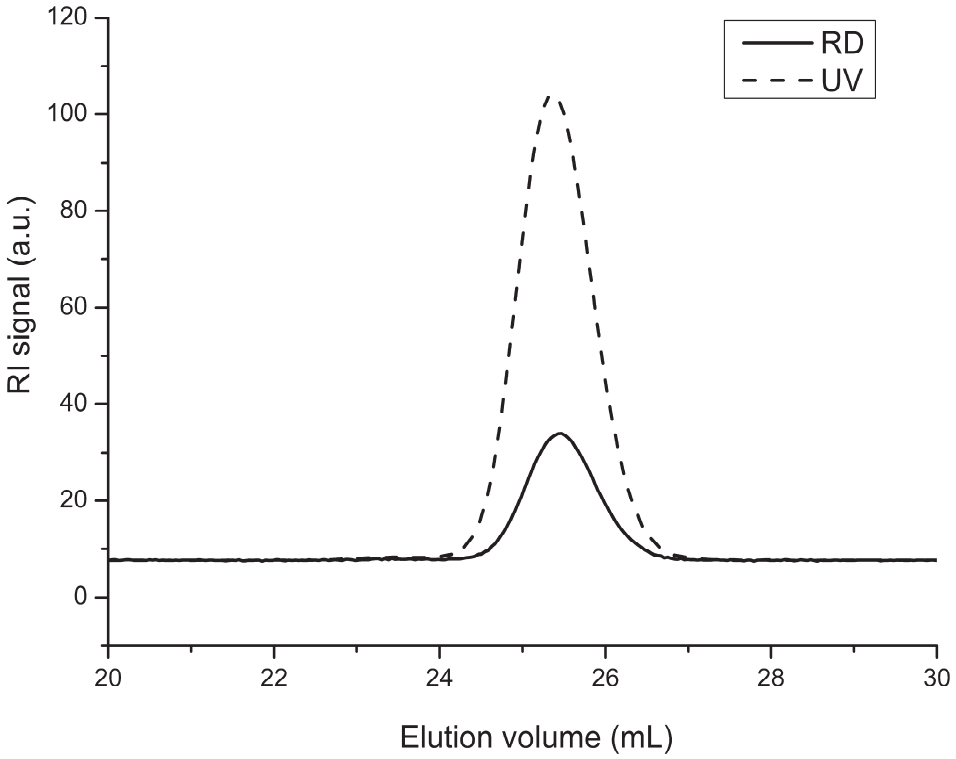

Figure S1. Typical SEC traces of an ω-naphthyl carbamate PEO ($M_{n,SEC}$ = 1800 g mol^{-1}).

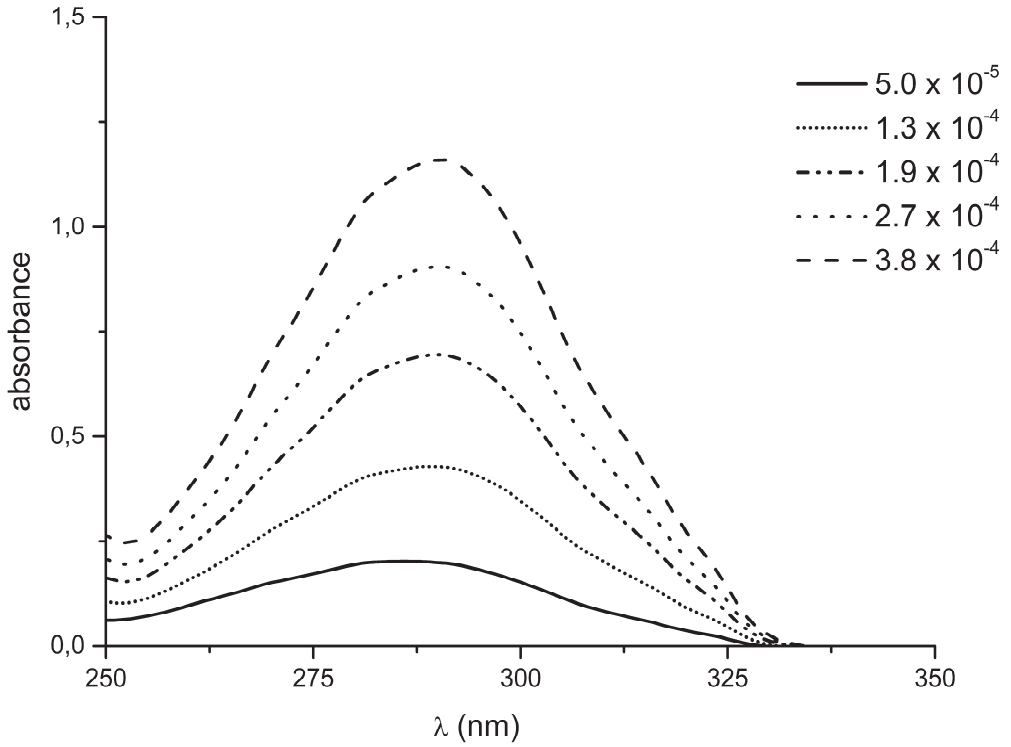

Figure S2. UV spectrum of an ω-naphthyl carbamate PEO measured in ethanol.

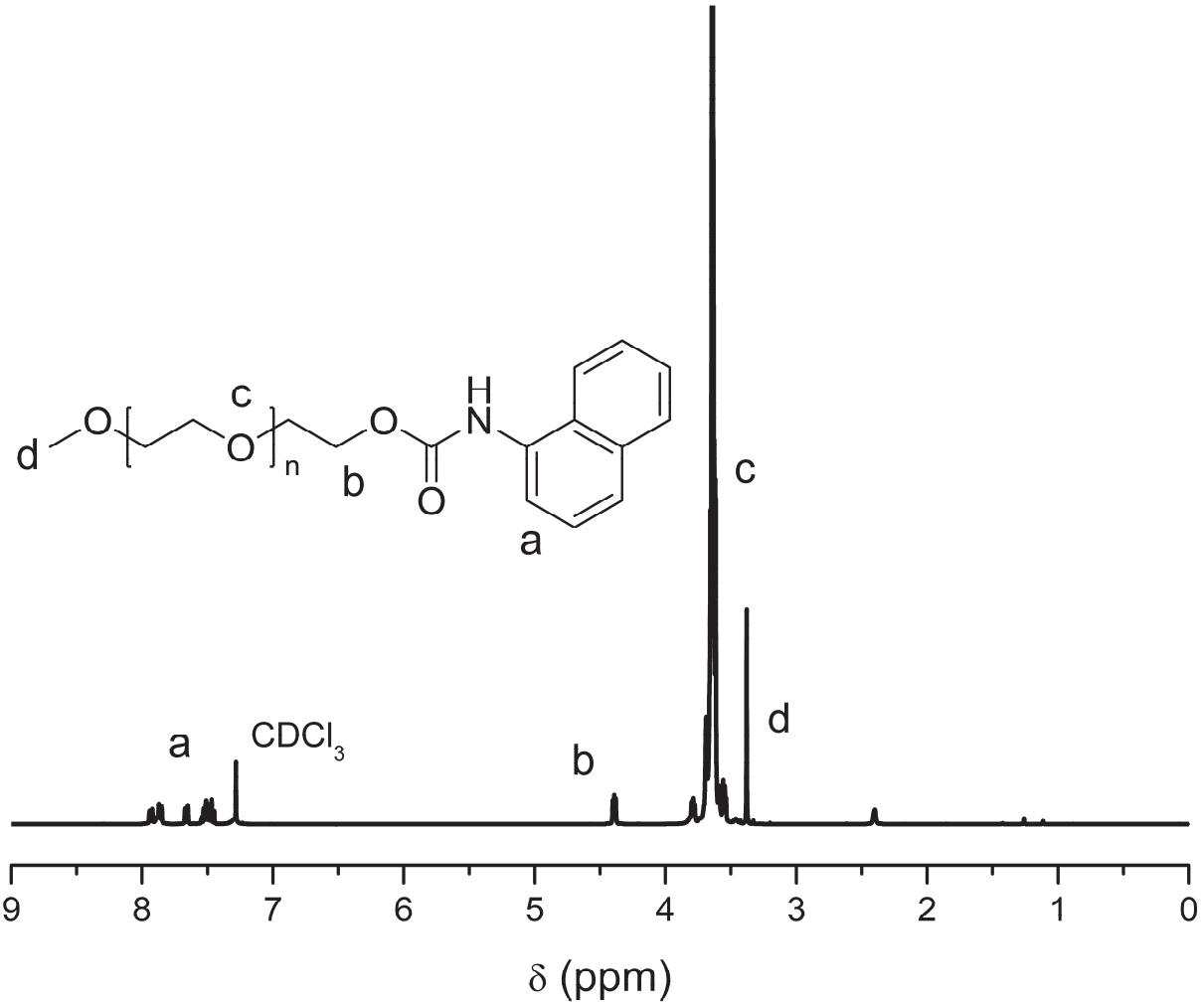

Figure S3. ^{1}H NMR spectrum of an ω-naphthyl carbamate PEO (400 MHz, $CDCl_3$).

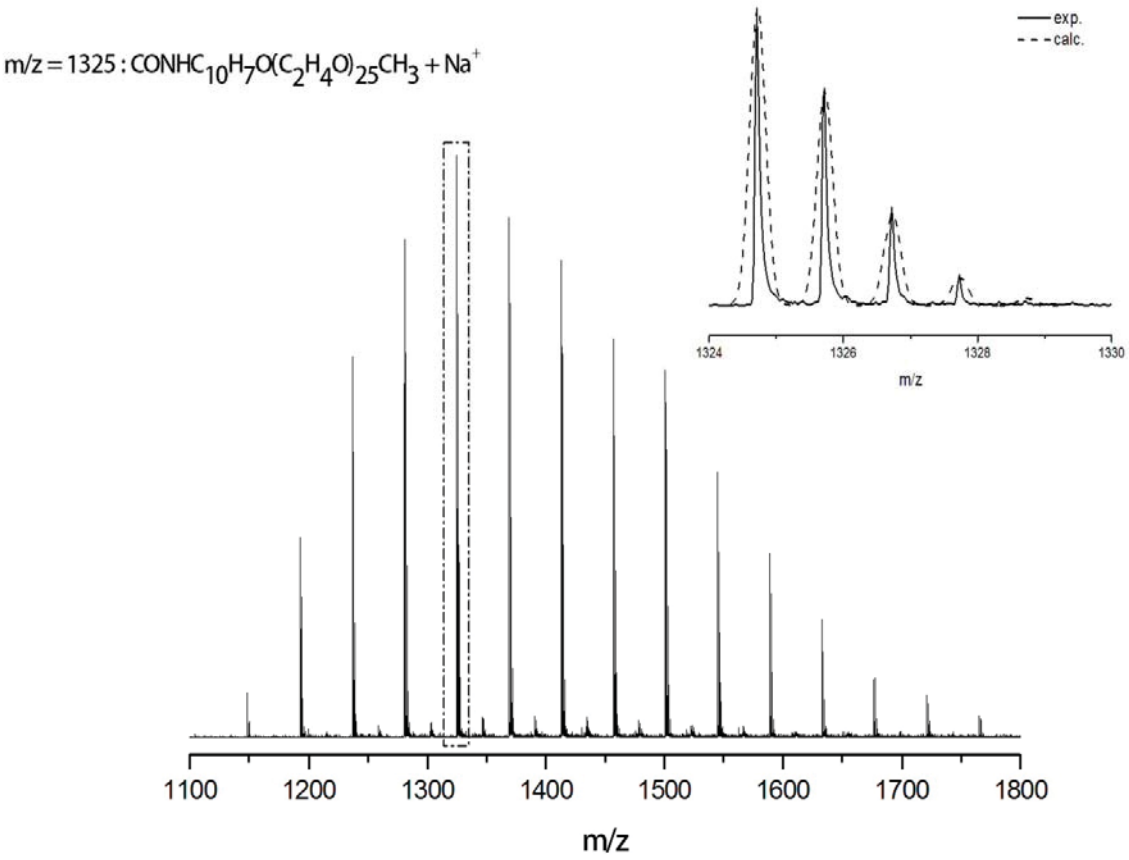

Figure S4. MALDI-ToF MS of an ω-naphthyl carbamate PEO ($M_{n,SEC}$ = 1200 g mol^{-1}) (Matrix: DCTB, NaI).

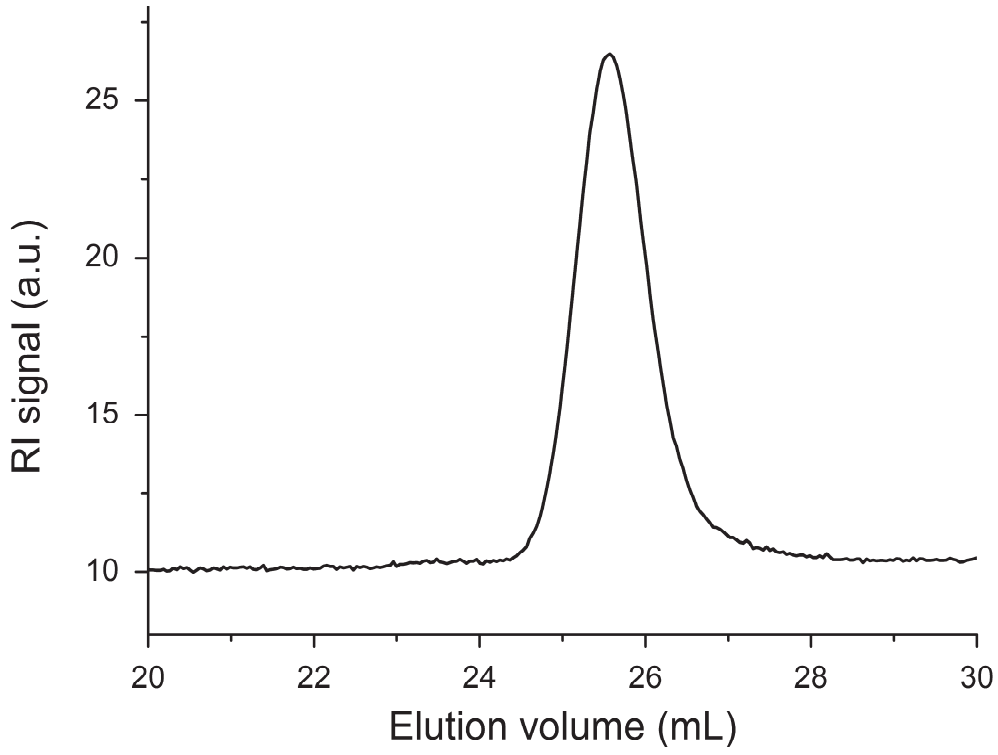

Figure S5.Typical SEC trace of an ω-undecenyl PEO macromonomer obtained by deactivation with 11-bromo-1-undecene in the presence of NaH ($M_{n,SEC}$ = 1800 g mol^{-1}).

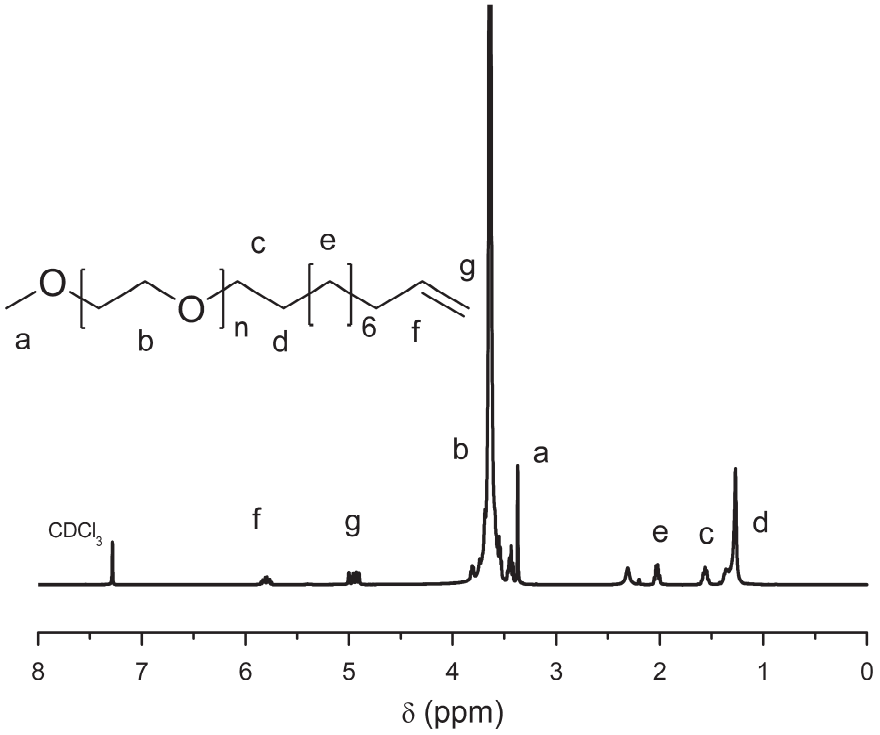

Figure S6. ^{1}H NMR spectrum of an ω-undecenyl PEO macromonomer obtained by deactivation with 11-bromo-1-undecene in the presence of NaH (400 MHz, $CDCl_3$).

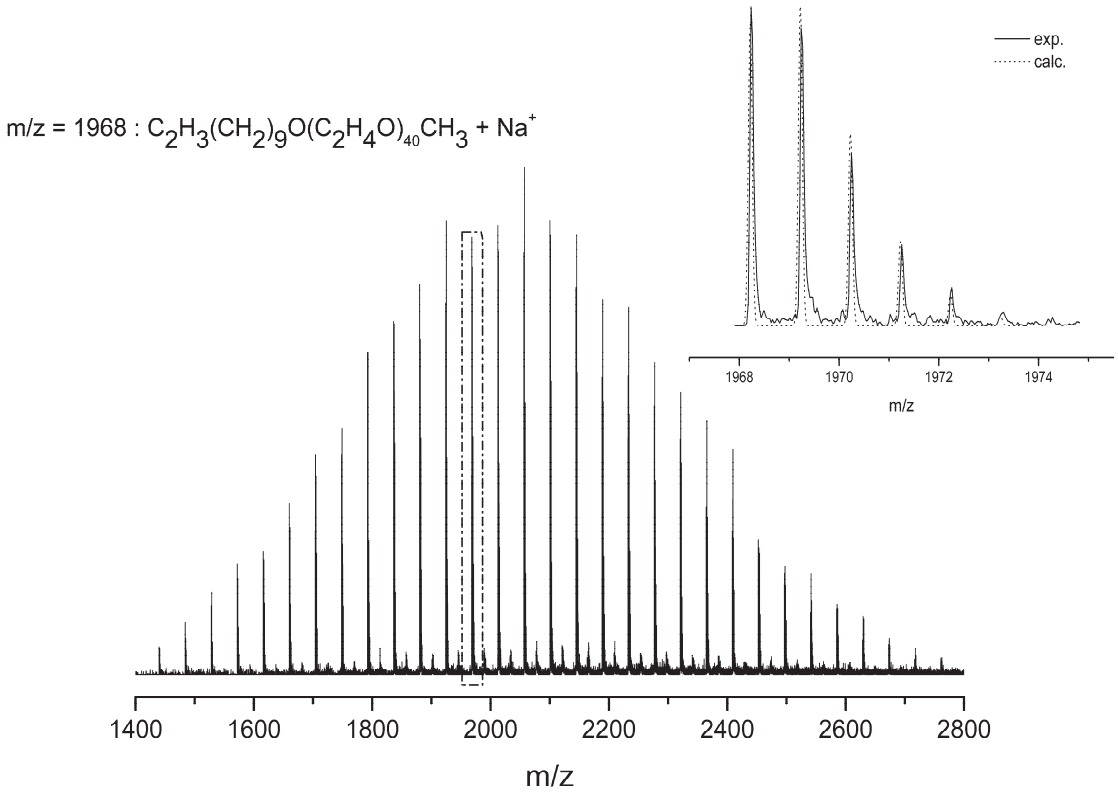

Figure S7. MALDI-ToF MS of an ω-undecenyl PEO macromonomer obtained by deactivation with 11-bromo-1-undecene in the presence of NaH ($M_{n,SEC}$ = 1900 g mol^{-1}) (Matrix: DCTB, NaI).

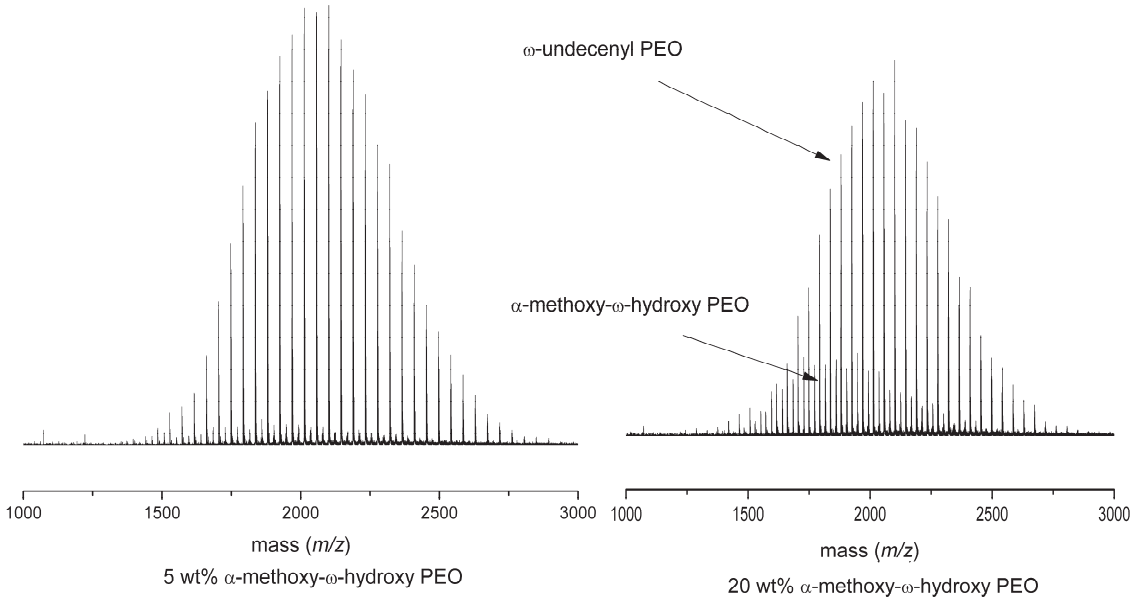

Figure S8. MALDI-ToF MS of an ω-undecenyl PEO macromonomer with contamination of α-methoxy-ω-hydroxy PEO at 5 and 20 wt % ($M_{n,SEC,\ Macro}$ = 1900 g mol^{-1}) (Matrix: DCTB, NaI).

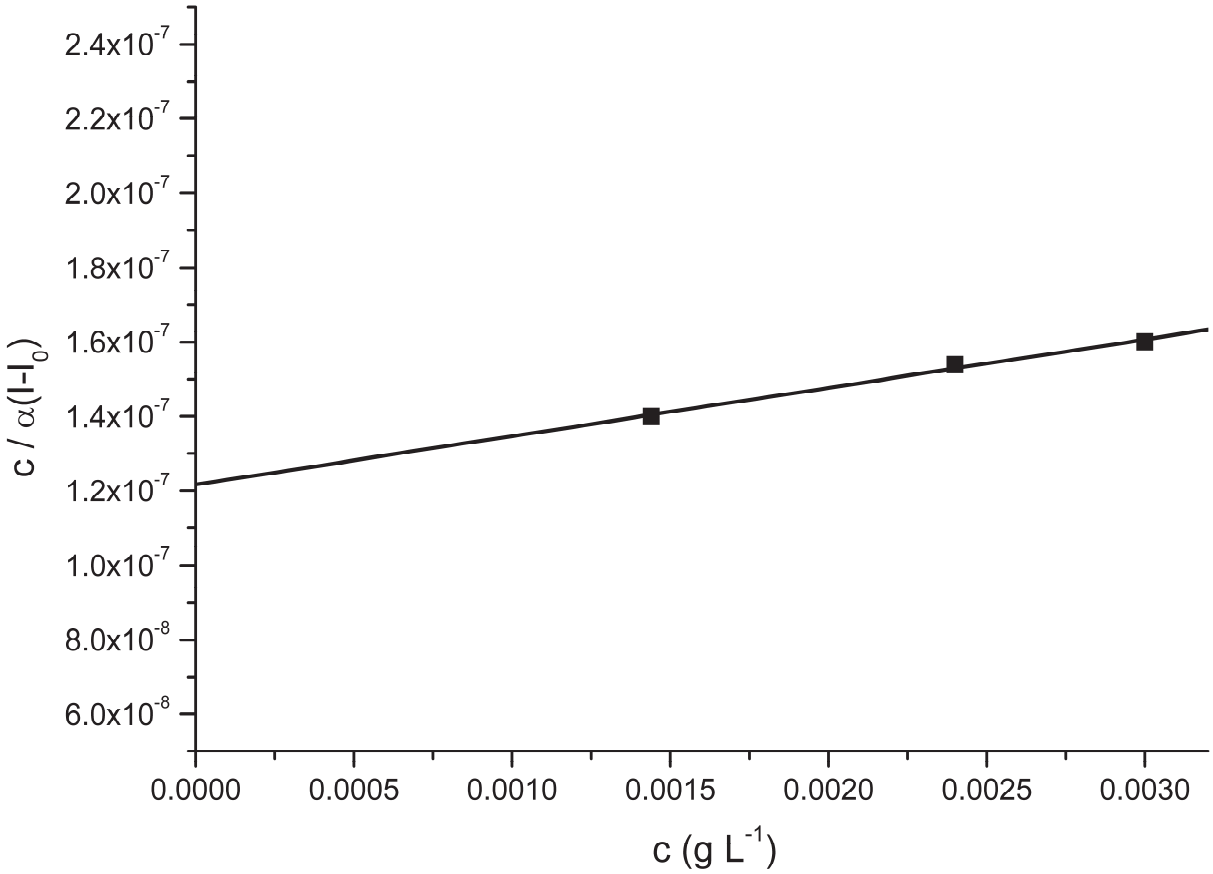

Figure S9. Light scattering data of $Q_8M_8^{PEO}$ measured in methanol.

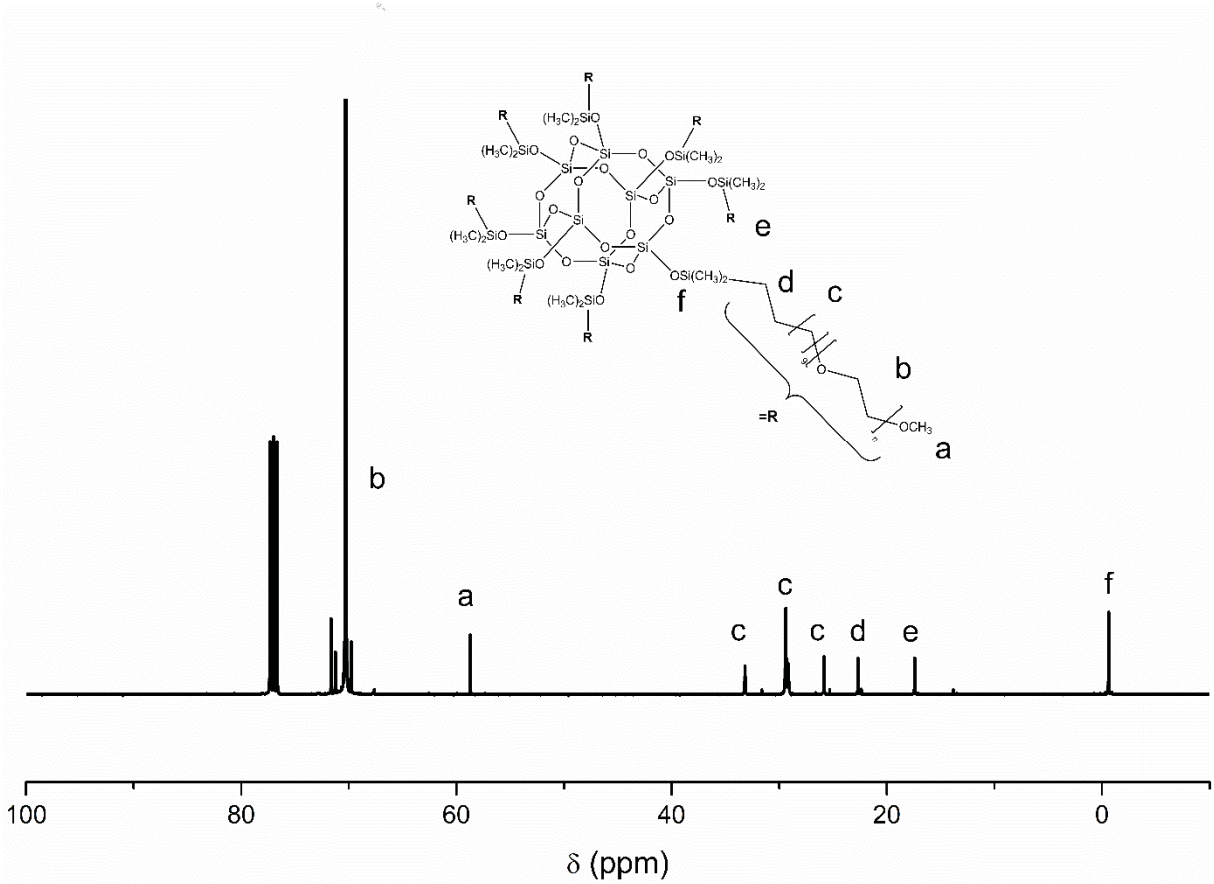

Figure S10. ^{13}C NMR spectrum of $Q_8M_8^{PEO}$ (400 MHz, $CDCl_3$).

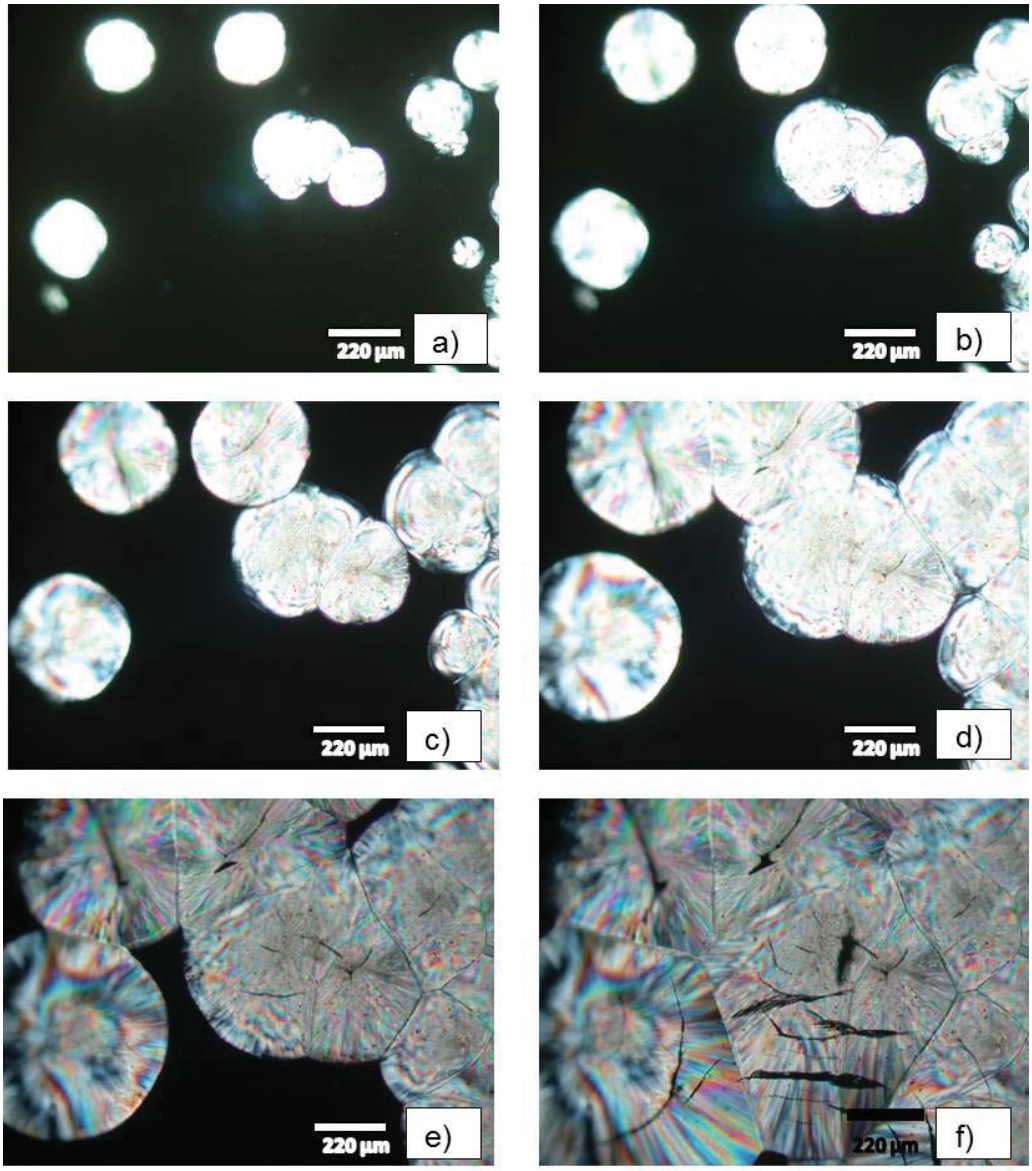

Figure S11. Sequences of micrographs obtained by optical microscopy with polarized light at distinct temperatures, during a scanning melting process. The first point of the spherulite $Q_8M_8^{PEO}$ is observed at 38.5 °C after 4 min cooling (a) and the total crystallization is after 6.2 min at 33 °C (f).

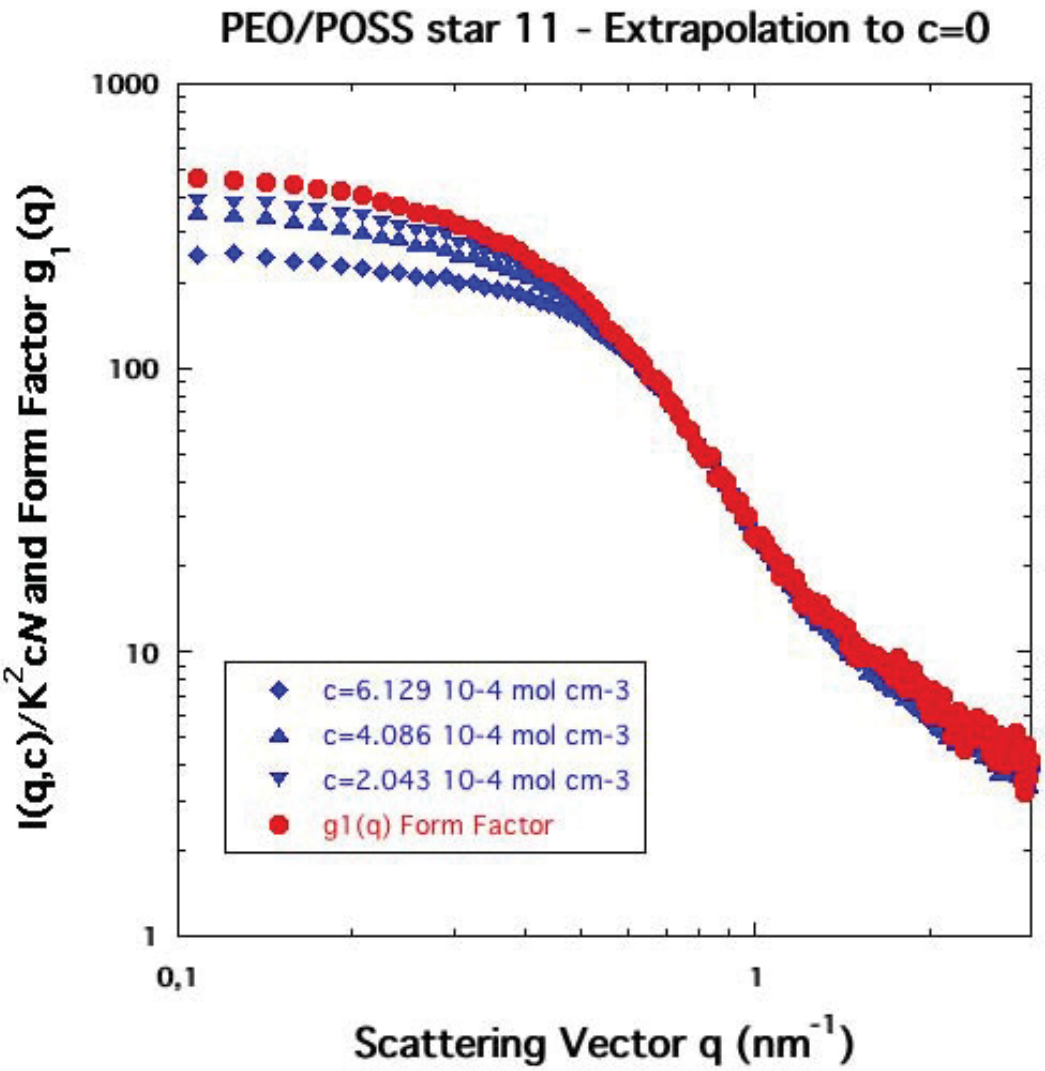

Figure SA. Scattered intensities I(q, c), for distinct concentrations, and form factor $g_1(q)$ of the PEO star 11 in methanol. According to Eq. (1), the extrapolation to c=0 of $I(q,c)/K^2cN$ leads to the form factor $g_1(q)$.

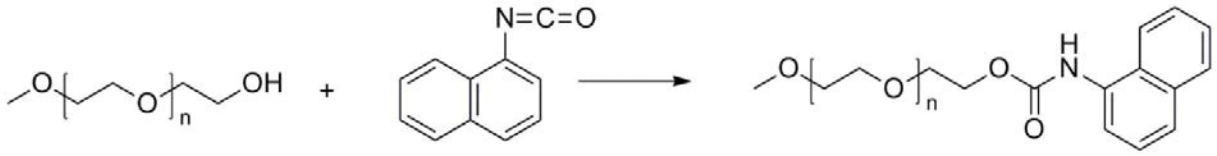

Scheme S1. Schematical representation of the synthesis of an ω-naphthyl carbamate PEO

(1) Lee, D.; Teraoka, I. Termini and main-chain composition of monomethoxy-terminated poly(ethylene glycol) studied by two-dimensional column chromatography. *Polymer* **2002**, *43*, 2691-2697.
(2) Dust, M. J.; Fang, Z.-H.; Harris, J. M. Proton NMR characterization of poly(ethylene glycols) and derivatives. *Macromolecules* **1990**, *23*, 3742-3746.
(3) De Vos, R.; Goethals, E. J. End group analysis of commercial poly(ethylene glycol) monomethyl ethers. *Polym. Bull.* **1986**, *15*, 547-549.
(4) Naraghi, K. S.; Sahli, N.; Franta, E.; Belbachir, M.; Lutz, P. J. Structured degradable poly(ether) hydrogels based on linear bifunctional macromonomers. *Polym. Int.* **2002**, *51*, 912-922.
(5) Beaudoin, E.; Hiorns, R. C.; Borisov, O.; François, J. Association of hydrophobically end-capped poly(ethylene oxide). 1. Preparation of polymers and characterization of critical association concentrations. *Langmuir* **2003**, *19*, 2058-2066.

Publication 6

Synthesis and solution properties of double hydrophilic poly(ethylene oxide)-*block*-poly(2-ethyl-2-oxazoline) (PEO-*b*-PEtOx) star block copolymers

T. Rudolph, S. Crotty, M. von der Luehe, D. Pretzel, U. S. Schubert, F. H. Schacher

Polymers **2013**, *5*, 1081-1101.

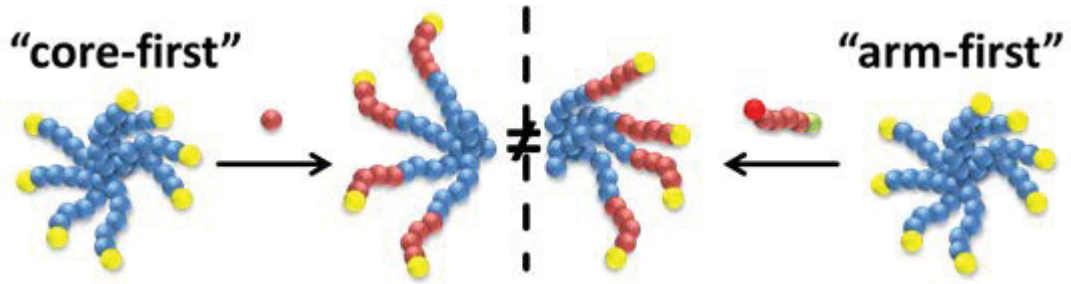

Polymers **2013**, *5*, 1081-1101; doi:10.3390/polym5031081

OPEN ACCESS

polymers

ISSN 2073-4360

www.mdpi.com/journal/polymers

Article

Synthesis and Solution Properties of Double Hydrophilic Poly(ethylene oxide)-*block*-poly(2-ethyl-2-oxazoline) (PEO-*b*-PEtOx) Star Block Copolymers

Tobias Rudolph [1,2], Sarah Crotty [1,2,3], Moritz von der Lühe [1,2], David Pretzel [1,2], Ulrich S. Schubert [1,2,3] and Felix H. Schacher [1,2,*]

[1] Laboratory of Organic and Macromolecular Chemistry (IOMC), Friedrich Schiller University Jena, Humboldtstr. 10, Jena 07743, Germany; E-Mails: tobias.rudolph@uni-jena.de (T.R.); sarah.crotty@uni-jena.de (S.C.); moritz.von-der-luehe@uni-jena.de (M.L.); david.pretzel@uni-jena.de (D.P.); ulrich.schubert@uni-jena.de (U.S.S.)

[2] Jena Center for Soft Matter (JCSM), Friedrich Schiller University Jena, Philosophenweg 7, Jena 07743, Germany

[3] Dutch Polymer Institute, P.O. Box 902, Eindhoven 5600 AX, The Netherlands

* Author to whom correspondence should be addressed; E-Mail: felix.schacher@uni-jena.de; Tel.: +49 (0) 3641-9-48250; Fax: +49 (0) 3641-9-48252.

Received: 28 June 2013; in revised form: 27 July 2013 / Accepted: 19 August 2013 / Published: 2 September 2013

Abstract: We demonstrate the synthesis of star-shaped poly(ethylene oxide)-*block*-poly(2-ethyl-2-oxazoline) $[PEO_m$-*b*-$PEtOx_n]_x$ block copolymers with eight arms using two different approaches, either the "arm-first" or the "core-first" strategy. Different lengths of the outer PEtOx blocks ranging from 16 to 75 repeating units were used, and the obtained materials $[PEO_{28}$-*b*-$PEtOx_x]_8$ were characterized via size exclusion chromatography (SEC), nuclear magnetic resonance spectroscopy (NMR), and Fourier-transform infrared spectroscopy (FT-IR) measurements. First investigations regarding the solution behavior in water as a non-selective solvent revealed significant differences. Whereas materials synthesized via the "core-first" method seemed to be well soluble (unimers), aggregation occurred in the case of materials synthesized by the "arm-first" method using copper-catalyzed azide-alkyne click chemistry.

Keywords: poly(2-ethyl-2-oxazoline); star-shaped block copolymers; double hydrophilic block copolymers

1. Introduction

The synthesis of polymer-based materials using different monomers, material compositions and macromolecular architectures can be realized via a multitude of synthetic methodologies. Mainly living and controlled polymerization techniques were developed to obtain polymers with narrow molar mass distributions, adjustable chain length and precisely positioned functional groups [1]. Thereby, the architecture has a large influence on the physical properties of the final material. Moreover, the monomer distribution and composition along the polymer backbone directly influences the solubility and other physical properties [2–4]. This has been demonstrated for random, gradient, graft and block copolymers synthesized by different polymerization techniques [5–9]. In the case of linear homo- and (block) copolymers, the solution behavior has become quite predictable after a manifold of systematic studies for different monomer combinations and sequences during the last few decades [10–14]. On the other hand, the combination of polymer chains in one central point leads to star-shaped materials and can result in unprecedented morphologies, as well as solution behavior in selective and non-selective solvents [15–18].

Star-shaped amphiphilic block copolymers are of special interest in drug delivery applications, due to the absence of a critical micellar concentration (cmc, depending on the hydrophilic-to-hydrophobic balance of the system) and the possibility to take up and release suitable drugs. The "load" can be encapsulated into the inner part (core, hydrophobic) of the materials, while the outer shell (hydrophilic) stabilizes the system in, e.g., aqueous solution [19]. If poly(ethylene oxide) (PEO) is used as the shell, "stealth"-behavior can be observed, also known as "PEGylation", preventing the recognition of such materials by our immune system. This renders such approaches suitable for the preparation of long-circulating polymer-based drug nanocontainers [20–22].

For the synthesis of star-shaped block copolymers, mainly two approaches have been employed, the divergent ("core-first") and the convergent ("arm-first") method [20,23–27]. The divergent approach uses a multifunctional initiator, but typically not all initiation sites are easily accessible, which drastically influences the number of arms and the overall degree of polymerization. Nevertheless, with increasing distance between the core and the initiation site, the initiation efficiency can be improved. Nevertheless, star-star coupling often occurs during, e.g., radical polymerizations, and limits the monomer conversion (arm length) in such attempts [2,4,28,29]. As an alternative, the convergent approach employs pre-synthesized arms, which are subsequently connected to the core covalently in the final step, often providing superior control over arm length and number; moreover, an in-depth characterization of the constituting building blocks prior to joining the core and shell is possible. Such approaches have been described in the literature via supramolecular chemistry [24,30,31], metal-complexation [32] or click-chemistry [23,33,34].

Herein, we demonstrate the synthesis of star-shaped poly(ethylene oxide)-*block*-poly(2-ethyl-2-oxazoline) $[PEO_m$-*b*-$PEtOx_n]_x$ block copolymers with eight arms using two different approaches, either the "arm-first" or the "core-first" strategy. Regarding the core block, PEO-based materials of different architectures have been thoroughly investigated concerning solution behavior [35,36] or the possibility of being scaffolds in medical applications [19,20,22]. The outer block, poly(2-ethyl-2-oxazoline) (PEtOx), is water-soluble and non-toxic, and the pseudo-peptide character of this material has been shown to induce similar "stealth" behavior, as observed for PEO [19,22,37–39]. PEtOx can be

synthesized with a wide range of functional groups, being present via cationic ring-opening polymerization (CROP) [40–43]. We used different lengths of the outer PEtOx blocks, and the obtained [PEO_{28}-*b*-$PEtOx_x$]$_8$ materials were characterized via size exclusion chromatography (SEC), nuclear magnetic resonance spectroscopy (NMR) and Fourier-transform infrared spectroscopy (FT-IR). Whereas similar compositions could be prepared using either "core-first" or "arm-first" approaches, first investigations regarding the solution behavior in water as a non-selective solvent revealed significant differences.

2. Experimental Section

2.1. Instruments

NMR: Proton nuclear magnetic resonance (^{1}H-NMR) spectra were recorded in $CDCl_3$ on a Bruker AC 300 MHz spectrometer at 298 K. Chemical shifts are given in parts per million (ppm, δ scale) relative to the residual signal of the deuterated solvent. Carbon NMR (^{13}C-NMR) spectra were recorded with 75 MHz.

SEC: Size exclusion chromatography was measured on a Shimadzu system equipped with a SCL-10A system controller, an LC-10AD pump, an RID-10A refractive index detector and both a PSS Gram30 and a PSS Gram1000 column [Polymer Standards Services GmbH (Mainz, Germany)] in series, whereby *N*,*N*-dimethylacetamide (DMAC) with 5 mmol of lithium chloride (LiCl) was used as an eluent at a 1 mL min^{-1} flow rate. The column oven was set to 60 °C. The system was calibrated with polystyrene (PS; 100 to 1,000,000 g mol^{-1}) standards. Furthermore, a Shimadzu system equipped with an SCL-10A system controller, an LC-10AD pump and an RID-10A refractive index detector using a solvent mixture containing chloroform ($CHCl_3$), triethylamine (TEA) and *iso*-propanol (*i*-PrOH) (94:4:2) at a flow rate of 1 mL min^{-1} on a PSS SDV linear M 5 µm column. The system was calibrated using PS (100 to 100,000 g mol^{-1}) and PEO (440 to 44,700 g mol^{-1}) standards.

MALDI-ToF MS: Matrix-assisted laser desorption/ionization time of flight mass spectrometry was performed on an Ultraflex III TOF/TOF (Bruker Daltonics, Bremen, Germany), equipped with a Nd:YAG laser and with *trans*-2-[3-(4-*tert*-butylphenyl)-2-methyl-2-propenylidene] malononitrile (DCTB) as the matrix and NaCl as the doping agent in reflector and linear mode. The instrument was calibrated prior to each measurement with an external poly(methyl methacrylate) (PMMA) standard from PSS Polymer Standards Services GmbH (Mainz, Germany).

FT-IR Infra-red spectroscopy: Dry powders of the copolymers were directly placed on the crystal of the ATR-FTIR (Affinity-1 FTIR, Shimadzu) for measurements in the range of 4000 to 600 cm^{-1}.

Microwave-assisted polymerizations were carried out utilizing an Initiator Sixty single-mode microwave synthesizer from Biotage, equipped with a non-invasive IR sensor (accuracy: 2%). Microwave vials (conical, 0.5 to 2 mL) were heated at 110 °C overnight and allowed to cool to room temperature under nitrogen atmosphere. All polymerizations were carried out using temperature control.

DLS: Dynamic light scattering was performed at a scattering angle of 90° on an ALV CGS-3 instrument equipped with a He-Ne laser operating at a wavelength of 633 nm at 25 °C. Tetrahydrofuran (THF) [polytetrafluoroethylene (PTFE); 0.45 µm] and MilliQ-water [glass faser (GF); 1–2 µm] were filtered before usage. The CONTIN algorithm was applied to analyze the obtained

correlation functions. For temperature control, the DLS is equipped with a Lauda thermostat. Apparent hydrodynamic radii were calculated according to the Stokes-Einstein equation. All CONTIN plots shown are number-weighted.

SLS: For static light scattering (SLS), different concentrations between 1.5 and 3.5 mg mL^{-1} were prepared in THF and measured at 25 °C and different scattering angles (30° to 150°). Prior to the measurements, the samples and all solvents were filtered with PTFE-syringe filters (0.45 μm).

Liquid Chromatography under Critical Conditions (LCCC): High-performance liquid chromatography (HPLC) was measured on an Agilent system (series 1200) equipped with a binary pump, an autosampler and an evaporative light scattering detector (ELSD, Softa Corporation, Model 400). For the LCCC separation, a Nucleosil octadecylsilyl (ODS) column (Knauer, 100 mm × 3 mm, particle size 5 μm, pore size 100 Å) was used. The mobile phase consisted of a mixture of acetonitrile (ACN) and water (55/45, v/v) delivered by the binary pump at a flow rate of 0.5 mL min^{-1}. The column oven temperature was set to 45 °C. For the detection part, the ELSD was used with an evaporator temperature of 90 °C. The samples were dissolved at a concentration of 2 mg mL^{-1} in the same solvent mixture as the mobile phase and for each measurement, 20 μL were injected. The data was acquired using the WINGPC Unity software from PSS. To characterize the star-shaped PEO samples prior to 2D measurements, size exclusion chromatography (SEC) was measured separately on a Shimadzu system equipped with an SCL-10A system controller, an LC-10AD pump and an RID-10A refractive index detector using 100% THF as the solvent at a flow rate of 3 mL min^{-1} on a PSS-SDV-linear S column (PSS GmbH Mainz, 300 mm × 8 mm, particle size 5 μm) at 45 °C. The system was calibrated with PEO (M_n = 1470 to 7000 g mol^{-1}) standards purchased from PSS.

Two-dimensional liquid chromatography (2D-LC): For the first dimension LCCC of PEO, the analytical conditions were used as described above, except that the flow rate was set to 0.02 mL min^{-1} to enable the subsequent SEC separation of the LCCC fractions for the 2D analysis. The different sample fractions of the LCCC separation were automatically transferred to the second dimension (SEC) via an eight-port valve system with 100 μL sample loops. On the SEC system, the fractions were separated on an SDV HighSpeed linear S column from PSS (50 mm × 20 mm, particle size 5 μm) using THF as eluent at a flow rate of 3 mL min^{-1} at 45 °C and the ELSD. For the 2D measurements, higher concentrated polymer solutions (7 mg mL^{-1}) were prepared, and 50 μL were used as the injection volume. The data acquisition was done by the PSS WINGPC unity software, including a 2D software module.

Transmission electron microscopy (TEM): The formed aggregates were analyzed using a TEM (Zeiss-CEM 902A, Oberkochen, Germany) operated at 80 kV. Images were recorded using a 1 k TVIPS FastScan CCD camera. TEM samples were prepared by applying a drop of an aqueous sample solution onto the surface of a plasma-treated carbon coated copper grid (Holey Carbon Grid + 2 nm C; Quantifoil Micro-Tools GmbH, Jena, Germany).

2.2. Materials

Star-shaped poly(ethylene oxide) ($[PEO\text{-}OH]_8$; supplier information: M_n = 10,000 g mol^{-1}; SEC ($CHCl_3$/*i*-PrOH/Et_3N): M_n = 6100 g mol^{-1}, Đ 1.07; SEC (DMAC/LiCl): M_n = 6800 g mol^{-1}; Đ= 1.11; MALDI-ToF MS: M_p = 9900 g mol^{-1}) (JenKem Technology, China) was dissolved in THF and

precipitated in cold diethyl ether, filtered and dried under vacuum before usage. Tetrahydrofuran (THF), acetonitrile (ACN) and dichloromethane (DCM) were purified using a Solvent Purification System (SPS, Innovative Technology, PM-400-3-MD) equipped with two activated alumina columns. 2-Ethyl-2-oxazoline (EtOx) and propargyl *p*-toluenesulfonate (Aldrich) were distilled over barium oxide under reduced pressure before polymerization and stored under argon. Triethylamine was distilled over CaH_2 and stored under argon. All other chemicals were used as purchased if not otherwise mentioned in the text.

2.2.1. Tosylation of Star-Shaped $[PEO_{28}\text{-}OH]_8$

The tosylation of $[PEO_{28}\text{-}OH]_8$ (6 g; 0.6 mmol) was achieved in a slightly modified way as described in the literature [44,45]. Briefly, the educts were dissolved in DCM and stirred at room temperature for at least 72 h, obtaining $[PEO_{28}\text{-}Ts]_8$ via extraction and precipitation in cold diethyl ether.

SEC ($CHCl_3$/*i*-PrOH/Et_3N): M_n = 6300 g mol^{-1}; Đ = 1.10 (PEO-calibration); SEC (DMAC/LiCl): M_n = 5800 g mol^{-1}; Đ = 1.22 (PEO-calibration); ^{1}H NMR (300 MHz, $CDCl_3$, δ): 7.84–7.14 (aromatic C*H*), 4.15 (t, Ts–CH_2–CH_2–O–), 3.80–3.46 (b, –CH_2–CH_2–O–), 2.44 (s, methyl) ppm; ^{13}C-NMR (75 MHz, $CDCl_3$, δ): 125–130 (aromatic *C*H), 71–70 (backbone), ppm 69.1 (–*C*H_2–CH_2–Ts), 68.5 (–CH_2–*C*H_2–Ts), 21.2 (Ts-*C*H_3) ppm.

2.2.2. Preparation of Star-Shaped $[PEO_{28}\text{-}N_3]_8$

$[PEO_{28}\text{-}Ts]_8$ (4 g; 0.4 mmol) was dissolved in DMF (10 mL) and stirred together with sodium azide (NaN_3, 20 equiv) overnight at room temperature. The solvent was removed under reduced pressure and the remainder diluted with chloroform and extracted with water, filtered and dried over sodium sulfate. The resulting $[PEO_{28}\text{–}N_3]_8$ was obtained as a brownish powder via precipitation in cold diethyl ether.

SEC ($CHCl_3$/*i*-PrOH/Et_3N): M_n = 7000 g mol^{-1}; Đ = 1.10 (PEO-calibration); SEC (DMAC/LiCl): M_n = 5800 g mol^{-1}; Đ = 1.21 (PEO-calibration); ^{1}H NMR (300 MHz, $CDCl_3$, δ): 3.80–3.46 (b, –CH_2–CH_2–O–) ppm; ^{13}C-NMR (75 MHz, $CDCl_3$, δ): 71–70 (backbone), ppm 69.8 (–*C*H_2–CH_2–N_3), 50.5 (–CH_2–*C*H_2–N_3) ppm; ATR-FT-IR: 2110 cm^{-1} (azide).

2.2.3. Synthesis of Alkyne-Functionalized TB-$PEtOx_x$

Propargyl *p*-toluenesulfonate and 2-ethyl-2-oxazoline (EtOx) were dissolved in acetonitrile (ACN) at different monomer to initiator ratios ([M]/[I] = 20, 60 and 80) at a monomer concentration of 4 M. The capped vials were placed in a microwave synthesizer at 140 °C. The polymerization was terminated via the addition of water. The polymers were obtained after extraction with $NaHCO_3$ solution, brine and dried under vacuum. After precipitation in cold diethyl ether, the polymer was filtered and dried under vacuum.

TB-$PEtOx_{18}$: SEC ($CHCl_3$/*i*-PrOH/Et_3N): M_n = 2700 g mol^{-1}; Đ = 1.12 (PS-calibration); SEC (DMAC/LiCl): M_n = 3900 g mol^{-1}; Đ = 1.18 (PS-calibration); TB-$PEtOx_{55}$: SEC ($CHCl_3$/*i*-PrOH/Et_3N): M_n = 5600 g mol^{-1}; Đ = 1.09 (PS-calibration); SEC (DMAC/LiCl): M_n = 9700 g mol^{-1}; Đ = 1.16 (PS-calibration); TB-$PEtOx_{75}$: SEC ($CHCl_3$/*i*-PrOH/Et_3N): M_n = 7000 g mol^{-1}; Đ = 1.10 (PS-calibration); SEC (DMAC/LiCl): M_n = 12,000 g mol^{-1}; Đ = 1.19 (PS-calibration); ^{1}H NMR

(300 MHz, $CDCl_3$, δ): 3.6–3.2 (br, –N–C*H*$_2$–C*H*$_2$–), 2.5–2.2 (br, CO–C*H*$_2$–CH_3), 1.2–0.9 (br, CO–CH_2–C*H*$_3$).

2.2.4. Copper catalyzed Azide-Alkyne Cycloaddition (CuAAC) Click Reaction between $[PEO_{28}\text{-}N_3]_8$ and TB-$PEtOx_x$

For the microwave-assisted copper-catalyzed azide-alkyne cycloaddition click chemistry (CuAAC) click reaction $[PEO_{28}\text{-}N_3]_8$ (1 equiv) and TB-$PEtOx_x$ (16 equiv) were dissolved in a solvent mixture of ethanol (EtOH) and THF (1:1 vol %). Copper bromide (CuBr; 10 equiv) and *N*,*N*,*N*′,*N*″,*N*‴-Pentamethyldiethylenetriamine (PMDETA; 10 equiv) were added under argon flux, purged for 15 min with argon and placed in the microwave-synthesizer for 30 min at 80 °C. The solvent was removed under reduced pressure, and the copper was removed via a short aluminum oxide (AlOxN) column. The homopolymer was removed via precipitation in THF at −30 °C.

$[PEO_{28}\text{-}b\text{-}PEtOx_{18}]_8$: SEC (DMAC/LiCl): M_n = 22,000 g mol^{-1}; Đ = 1.13 (PS-calibration); $[PEO_{28}\text{-}b\text{-}PEtOx_{55}]_8$: SEC (DMAC/LiCl): M_n = 46,000 g mol^{-1}; Đ = 1.18 (PS-calibration); $[PEO_{28}\text{-}b\text{-}PEtOx_{75}]_8$: SEC (DMAC/LiCl): M_n = 42,000 g mol^{-1}; Đ = 1.14 (PS-calibration); ^{1}H NMR (300 MHz, $CDCl_3$, δ): 4.0–3.0 (br, backbone), 2.6–2.2 (br, CO–C*H*2–CH3), 1.2–0.8 (br, CO–CH_2–C*H*$_3$).

2.2.5. Polymerization of 2-Ethyl-2-oxazoline using a Star-Shaped PEO Macroinitiator

For the polymerization of EtOx via a star-shaped macroinitiator $[PEO_{28}\text{-}Ts]_8$, different initiator to monomer ratios were chosen, and the polymerization was conducted in acetonitrile (1 M) in a microwave-synthesizer at 140 °C. The reaction was stopped via cooling the reaction mixture after 15 min and the addition of 0.2 mL of water. The final polymer was obtained via precipitation in THF at −30 °C.

$[PEO_{28}\text{-}b\text{-}PEtOx_{16}]_8$: SEC (DMAC/LiCl): M_n = 24,000 g mol^{-1}; Đ = 1.24 (PS-calibration); $[PEO_{28}\text{-}b\text{-}PEtOx_{50}]_8$: SEC (DMAC/LiCl): M_n = 35,000 g mol^{-1}; Đ = 1.15 (PS-calibration); ^{1}H NMR (300 MHz, $CDCl_3$, δ): 4.0–3.0 (br, backbone), 2.6–2.2 (br, CO–C*H*$_2$–CH_3), 1.2–0.8 (br, CO–CH_2–C*H*$_3$).

2.2.6. Kinetic Investigation of the Polymerization of 2-Ethyl-2-oxazoline using a Star-Shaped PEO-Macroinitiator

A stock solution of the macroinitiator $[PEO_{28}\text{-}Ts]_8$ and 2-ethyl-2-oxazoline (EtOx) were mixed with acetonitrile at a monomer to initiator ratio of 40 and a monomer concentration of 1 M. The capped vials were placed in a microwave synthesizer at 140 °C. The polymerization was terminated via the addition of water. The pure star-shaped block copolymers were received after precipitation in THF at −30 °C.

3. Results and Discussion

We were interested in the solution properties of well-defined star-shaped block copolymers containing two hydrophilic blocks. In particular, the influence of the length used for the outer block on the behavior in non-selective solvents (*i.e.*, water) for a system with a given arm number (here: eight

arms) was our focus for this study. We chose poly(ethylene oxide) as the core, due to its wide solubility in common solvents, its commercial availability and chemical inertness, enabling various chemical modifications. As the outer block (shell), we used poly(2-ethyl-2-oxazoline), a well-studied material with proven biocompatibility [22] and temperature-responsive properties (lower critical solution properties, LCST) above a threshold-molar mass in aqueous media [46,47].

Regarding the synthesis of star-shaped poly(ethylene oxide)-*block*-poly(2-ethyl-2-oxazoline) block copolymers with eight arms, we chose to compare two different strategies: for the "arm-first" approach, the macromolecular conjugation (azide-alkyne click reaction [27,48]) between azide-functionalized $[PEO_{28}\text{-}N_3]_8$ and alkyne-functionalized TB-$PEtOx_x$ of different molar mass was used. In the case of the "core-first" strategy, tosylated $[PEO_{28}\text{-}Ts]_8$ (the subscripts denote the degree of polymerization of the corresponding block, and the subscripts after the brackets represent the arm number of the herein described star-shaped block copolymers) was used as a macroinitiator for the cationic ring-opening polymerization (CROP) of 2-ethyl-2-oxazoline (EtOx). In both cases, the length of the PEtOx block can be easily varied within a certain range. In the following, first, both synthetic routes will be described separately, and afterwards, the solution properties in water as a non-selective solvent for both blocks will be compared.

3.1. Star Synthesis via Macromolecular Conjugation ("Arm-First"-Approach)

Core: First, a commercially available star-shaped poly(ethylene oxide) (PEO) with eight arms and a total molar mass (M_n) of 10,000 g mol^{-1} (1250 g mol^{-1} per arm) was modified. For this purpose, the hydroxyl end group was tosylated first by a nucleophilic substitution reaction using *p*-toluenesulfonyl chloride (Ts-Cl; Scheme 1), obtaining $[PEO\text{-}Ts]_8$. Whereas this modification for linear PEO is often described as being performed within a few hours [44,45], in our case, the reaction time needed to be increased to at least 72 h at room temperature to achieve full functionalization (determined via ^{1}H-NMR; Figure S1C).

Scheme 1. Preparation of $[PEO_{28}\text{-}Ts]_8$ and $[PEO_{28}\text{-}N_3]_8$.

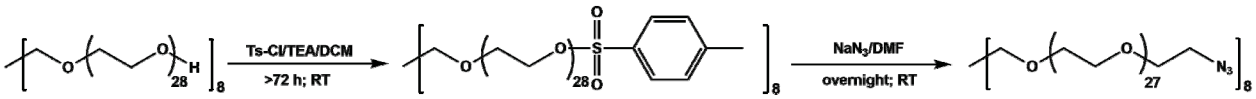

Afterwards, $[PEO_{28}\text{-}Ts]_8$ was converted to $[PEO_{28}\text{-}N_3]_8$ using sodium azide (Scheme 1). After purification, for $[PEO_{28}\text{-}N_3]_8$, slight amounts (<5%) of residual aromatic signals, corresponding to the tosyl-moiety, were observed via ^{1}H NMR (Figure S1C). Nevertheless, the azide group could be clearly detected by ATR FT-IR measurements (2110 cm^{-1}; Figure S1B).

To ensure full end-group conversion of the modified star-shaped macromolecules, the polymers were investigated via ^{13}C-NMR and 2D-LC (LCCC × SEC). In the latter case, liquid chromatography under critical conditions for PEO (LCCC) should enable the separation according to the end-group polarity and further coupled to SEC for the molar range [49–53]. After careful adjustment of the critical conditions for PEO (Figure S2), the stars with different end-groups ($[PEO_{28}\text{-}OH]_8$, $[PEO_{28}\text{-}Ts]_8$ and $[PEO_{28}\text{-}N_3]_8$) were investigated (Figure 1). As can be seen, $[PEO_{28}\text{-}OH]_8$ exhibits only one distribution, with a peak maximum at 0.62 mL (Figure 1A), whereas for $[PEO_{28}\text{-}Ts]_8$, two distributions

at 0.80 mL (97%) and 0.62 mL (3%, unfunctionalized material) were observed (Figure 1B). This is in good agreement with the error of the NMR spectroscopy, where no $[PEO_{28}\text{-}OH]_8$ could be detected. For $[PEO_{28}\text{-}N_3]_8$, also, two distributions at 0.80 mL (90%) and at 0.62 (10%) were observed (Figure 1C). We tentatively attribute this observation to a slow exchange of the azide functionality by hydroxyl groups under these conditions. This assumption can be confirmed by time-dependent investigations, leading to a ratio of 90:10 for both distributions directly after sample preparation, while 75:25 is found after 30 min (Figure S3). If the sample was stored overnight in solution, a ratio of 50:50 is observed. As many reactions using azides are described in the literature in water [49,54], this exchange process might be facilitated here, as the sample is heated to 45 °C and remains for 100 min within the system to elute/separate.

Figure 1. 2D-LC results (acetonitrile (ACN)/H_2O 55/45 v/v) for $[PEO_{28}\text{-}OH]_8$ (**A**), $[PEO_{28}\text{-}Ts]_8$ (**B**) and $[PEO_{28}\text{-}N_3]_8$ (**C**); in comparison with the SEC traces obtained for $[PEO_{28}\text{-}OH]_8$ (solid black line), $[PEO_{28}\text{-}Ts]_8$ (solid red line) and $[PEO_{28}\text{-}N_3]_8$ (solid blue line; THF was used as eluent).

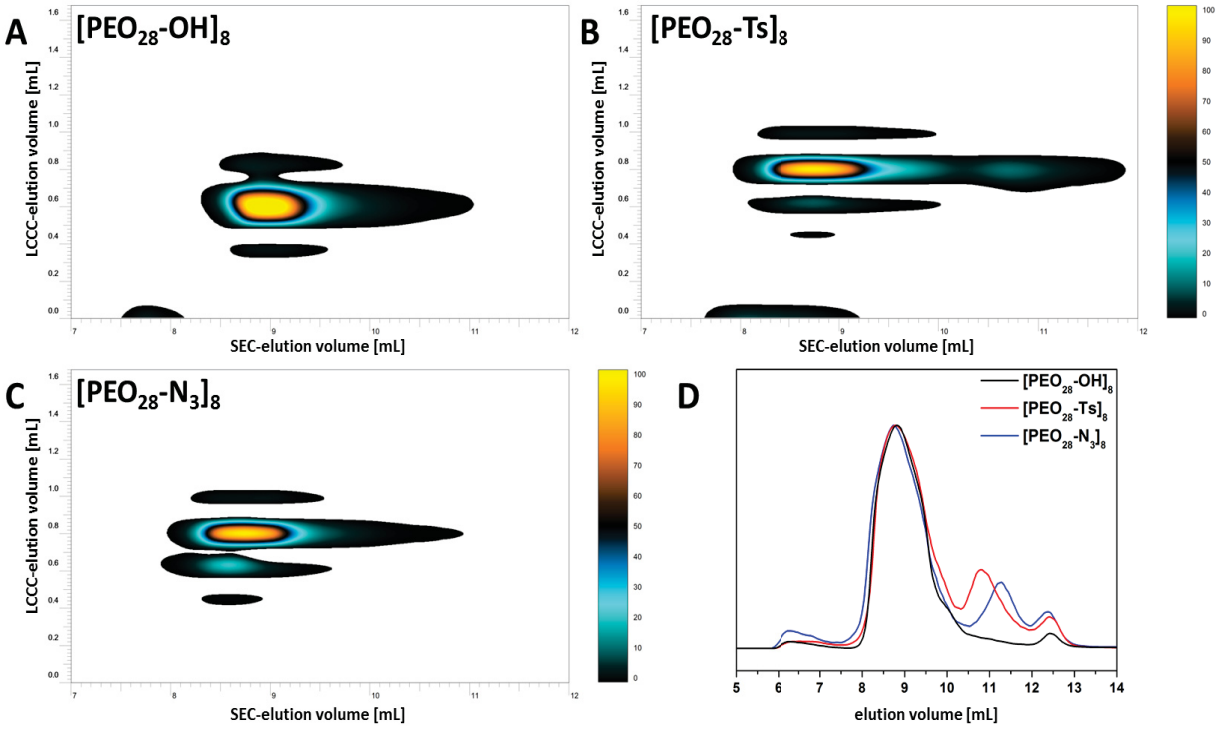

The elution behavior in LCCC was similar for $[PEO_{28}\text{-}Ts]_8$ and $[PEO_{28}\text{-}N_3]_8$, again, somewhat surprising. During SEC, further small distributions appear at higher elution volumes, which might be due to a higher flow rate of 3 mL min^{-1} (Figure 1D), as under flow rates of 1 mL min^{-1}, only monomodal distributions were observed.

Due to the results obtained for $[PEO_{28}\text{-}N_3]_8$ using 2D-LC experiments, additional ^{13}C-NMR measurements in $CDCl_3$ were carried out. Here, the signals for the tosyl-group, as well as the CH_2-group located next to the hydroxyl-end-group at 61.5 ppm are not observed, and also, two new signals for the two CH_2 groups next to the azide functionality at 50.5 and 79.8 ppm (Figure S4) confirm the successful conversion, at least within the experimental error of the NMR [45,55].

Arm: Alkyne-functionalized 2-ethyl-2-oxazoline homopolymers (TB-PEtOx$_x$) with different molar masses and low polydispersity indices (Đ; <1.1) were obtained via microwave-assisted cationic ring-opening polymerization (CROP) of 2-ethyl-2-oxazoline (EtOx) [25]. Therefore, solutions containing a functional initiator, propargyl *p*-toluenesulfonate, with different monomer-to-initiator ratios ([M]/[I]) at a constant monomer concentration of 4 M were prepared and polymerized in a microwave-synthesizer at 140 °C. The degrees of polymerization (DP) obtained via ^{1}H NMR and MALDI-ToF MS slightly differ from the theoretically calculated values, according to the feed ratios used for the polymerizations. For a theoretical DP of 20, a DP of 18 (TB-PEtOx$_{18}$), for a DP of 60, a DP of 55 (TB-PEtOx$_{55}$), and for a DP of 80, a DP of 75 (TB-PEtOx$_{75}$) were found (Table 1, SEC in Figure S6A).

Table 1. Selected characterization data for alkyne-functionalized poly(2-ethyl-2-oxazoline)s (TB-PEtOx$_x$) and star-shaped [PEO$_{28}$-Y]$_8$.

Sample	DP [a]	M_n [b] [g mol^{-1}]	M_n [c] [g mol^{-1}]	Đ [c]	M_p [d] [g mol^{-1}]	Building Block
TB-PEtOx$_{18}$ [b,e]	20	1800	2700	1.12	1500	**arm in chloroform**
TB-PEtOx$_{55}$ [b,e]	60	5500	5600	1.09	5400	
TB-PEtOx$_{75}$ [b,e]	80	7500	6700	1.10	7200	
TB-PEtOx$_{18}$ [e,f]	20	1800	3900	1.18	–	**arm in DMAC**
TB-PEtOx$_{55}$ [e,e]	60	5500	9700	1.16	–	
TB-PEtOx$_{75}$ [e,e]	80	7500	12,000	1.19	–	
[PEO$_{28}$-OH]$_8$ [b,e]	–	10,000	6100 [h]	1.07	9,900	**star-shaped core**
[PEO$_{28}$-Ts]$_8$ [b,e]	–	11,000	7000 [h]	1.04	–	
[PEO$_{28}$-N$_3$]$_8$ [b,e]	–	10,300	7000 [h]	1.07	–	
[PEO$_{28}$-N$_3$]$_8$ [e,g]	–	10,300	12,000 [g]	1.15	–	

[a] feed ratio [M]/[I]; [b] calculated from nuclear magnetic resonance spectroscopy (NMR) and Matrix-assisted laser desorption/ionization time of flight mass spectrometry (MALDI-ToF MS); [c] size exclusion chromatography (SEC) ($CHCl_3$/*i*-PrOH/TEA) (PS-calibration); [d] MALDI-ToF MS (matrix/doping agent *trans*-2-[3-(4-*tert*-butylphenyl)-2-methyl-2-propenylidene] malononitrile (DCTB) /NaCl); [e] subscripts denote the degree of polymerization; [f] SEC (DMAC/LiCl) (PS-calib.); [g] SEC (DMAC/LiCl) (PEO-calib.); [h] SEC ($CHCl_3$/*i*-PrOH/TEA) (PEO-calib.).

The molar masses of the polymers increase linearly with the monomer-to-initiator ratio and are also in good agreement with the values obtained by MALDI-ToF MS measurements (Table 1). As the molar masses of the star-shaped block copolymers after arm attachment will exceed the exclusion volume of the utilized $CHCl_3$ SEC, the homopolymers (arms) were also subjected to another SEC instrument featuring a higher molar mass range (here, *N*,*N*-dimethylacetamide (DMAc) was used as the eluent, Figure S6B). The slight broadening of the Đ-values can be ascribed to polymer-column interactions, and, furthermore, the apparent molar masses are higher in comparison to the values obtained using chloroform as the eluent.

For the synthesis of [PEO$_{28}$-*b*-PEtOx$_x$]$_8$, star-shaped block copolymers [PEO$_{28}$-N$_3$]$_8$ and different TB-PEtOx$_x$ were used in copper-catalyzed azide-alkyne cycloaddition reactions (CuAAC; Scheme 2). First, the conditions had to be optimized by variation of the solvent, the reaction temperature and the reaction time. The best conditions were obtained in a THF-ethanol mixture (1:1 v/v) at 80 °C using a four-fold excess of TB-PEtOx$_x$ in comparison to the azide-functionality and a reaction time of only 15 min in the microwave synthesizer. Under these conditions, it was possible to obtain the desired

$[PEO_{28}$-*b*-$PEtOx_x]_8$ materials. Purification was achieved via selective precipitation of the block copolymer in THF at −30 °C, while $PEtOx_x$ homopolymers are still soluble under these conditions. The obtained polymers were characterized using SEC (Table 2), FT-IR and NMR (Figure S7).

Scheme 2. Schematic representation of the synthesis of star-shaped $[PEO_{28}$-*b*-$PEtOx_x]_8$ block copolymers using copper-catalyzed azide-alkyne cycloaddition click chemistry (CuAAC).

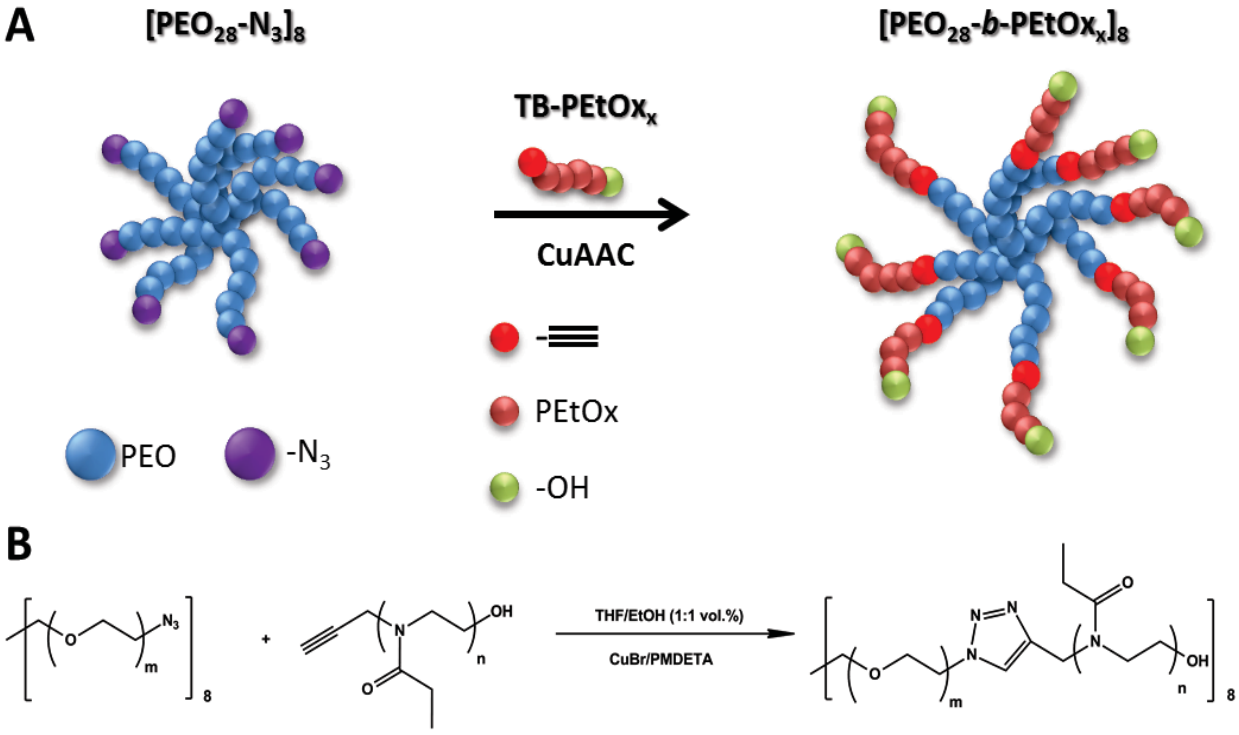

Table 2. Selected characterization data for star-shaped $[PEO_{28}$-*b*-$PEtOx_x]_8$ block copolymers obtained via the "core-first" or "arm-first" approach.

Sample	M_n [a] [g mol^{-1}]	Đ [a]	$M_{n,calc}$ [b] [g mol^{-1}]	$M_{w,SLS}$ [d] [g mol^{-1}]	Approach
$[PEO_{28}$-*b*-$PEtOx_{18}]_8$ [c]	22,000	1.13	22,000	–	
$[PEO_{28}$-*b*-$PEtOx_{55}]_8$ [c]	46,000	1.18	54,000	–	**arm-first**
$[PEO_{28}$-*b*-$PEtOx_{75}]_8$ [c]	42,000	1.14	67,000	–	
$[PEO_{28}$-*b*-$PEtOx_{16}]_8$ [c]	24,000	1.24	22,000	–	**core-first**
$[PEO_{28}$-*b*-$PEtOx_{50}]_8$ [c]	35,000	1.15	50,000	54,000	

[a] SEC (DMAC/LiCl) (PS-calib.); [b] calculated from the single compound molar masses obtained via MALDI-ToF MS ("arm-first") or ^{1}H-NMR ("core-first"); [c] subscripts denote the number of repeating units; [d] static light scattering at 25 °C in THF (dn/dc = 0.0915 mL g^{-1}; $A_2 = 1 \times 10^{-8}$ mol dm^3 g^{-2}).

SEC elution traces using DMAC/LiCl (0.21 wt % LiCl) as the eluent for the individual building blocks and the star-shaped block copolymers are shown in Figure 2. The corresponding characterization data are shown in Table 2. Via this approach, three different star-shaped block copolymers, $[PEO_{28}$-*b*-$PEtOx_{18}]_8$, $[PEO_{28}$-*b*-$PEtOx_{55}]_8$ and $[PEO_{28}$-*b*-$PEtOx_{75}]_8$, were obtained. Owing to the star architecture, the elution behavior of the star-shaped block copolymers leads to lower molar masses than expected during SEC measurements. This effect has already been described for other

star-shaped and branched systems [3]. According to the SEC traces, e.g., in the case of $[PEO_{28}$-*b*-$PEtOx_{18}]_8$, a clear shift for $[PEO_{28}$-*b*-$PEtOx_{18}]_8$, if compared to TB-$PEtOx_{18}$ and $[PEO_{28}$-$N_3]_8$, can be observed. Moreover, after purification, the sample contained neither an excess of the arm (TB-$PEtOx_{18}$) nor the core $[PEO_{28}$-$N_3]_8$. The apparent molar masses of $[PEO_{28}$-*b*-$PEtOx_{18}]_8$ obtained by SEC are 22,000 g mol^{-1} with a narrow Đ-value of 1.13 (PS-calibration). The apparent molar masses for $[PEO_{28}$-*b*-$PEtOx_{55}]_8$ and $[PEO_{28}$-*b*-$PEtOx_{75}]_8$ are in a comparable range with 46,000 and 42,000 g mol^{-1}. The composition of the star-shaped block copolymers was further confirmed using ^{1}H-NMR (Figure S7B).

Figure 2. SEC traces using DMAC/LiCl as the eluent for TB-$PEtOx_x$ (dotted line), $[PEO_{28}$-$N_3]_8$ (scattered line) and the obtained purified star-shaped $[PEO_{28}$-*b*-$PEtOx_x]_8$ (solid line): (**A**) $[PEO_{28}$-*b*-$PEtOx_{18}]_8$; (**B**) $[PEO_{28}$-*b*-$PEtOx_{55}]_8$; (**C**) $[PEO_{28}$-*b*-$PEtOx_{75}]_8$.

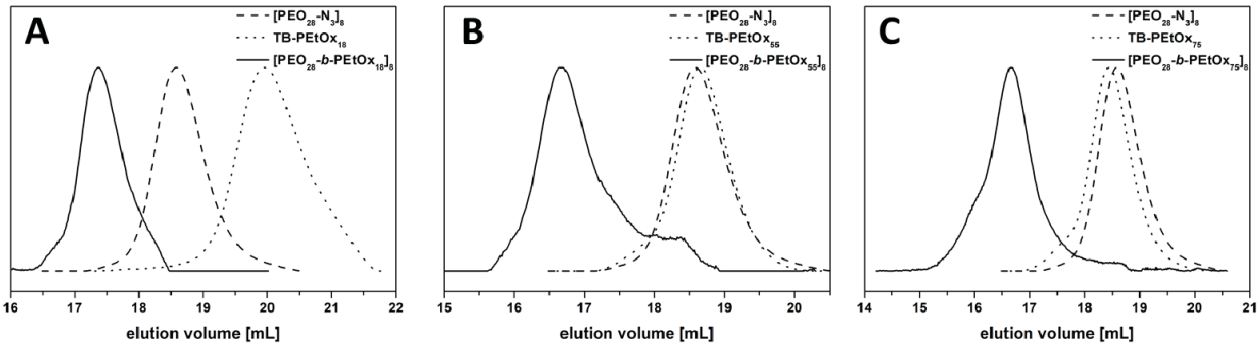

3.2. Star Synthesis via CROP of 2-Ethyl-2-oxazoline Using a Star-Shaped Macroinitiator ("Core-First"-Approach)

Furthermore, here, commercially available $[PEO_{28}$-$OH]_8$ was modified via tosylation as described above and purified until no further unreacted Ts-Cl could be observed in the ^{1}H-NMR spectra. As PEO is rather hydroscopic, the macroinitiator was co-evaporated with toluene, dried under vacuum for at least 24 h and stored in a glove box. After the preparation of the macroinitiator, we first carried out a kinetic study for the polymerization of EtOx (Figure 3). Therefore, a stock solution of $[PEO_{28}$-$Ts]_8$ and monomer ([M]/[I] = 40) was prepared in ACN (1M) and divided into several microwave vials. The vials were subsequently placed in the microwave-synthesizer and analyzed after different polymerization times at 140 °C via ^{1}H-NMR and SEC. A pseudo-linear first-order kinetic was observed for the monomer consumption over time, while in SEC elution traces, two distributions were observed (Figure 3B).

Taking into account the slope of the fit in Figure 3A, a propagation rate (k_p) of 337 L mol^{-1} s^{-1} × 10^{-3} can be calculated (corresponding to 42 L mol^{-1} s^{-1} × 10^{-3} per arm). However, as indicated by the second distribution in the SEC elution traces in Figure 3B, with increasing polymerization time, also homopolymer (PEtOx) is formed, presumably due to transfer reactions. Although $[PEO_{28}$-$Ts]_8$ has been extracted and co-evaporated with toluene several times prior to use, followed by drying for at least 24 h under vacuum, traces of impurities seem to persist.

Figure 3. First order time-conversion plot for the kinetic investigation of the microwave assisted polymerization of EtOx with $[PEO_{28}\text{-Ts}]_8$ as the initiator at 140 °C (**A**); comparison of the time-dependent SEC traces ($CHCl_3$) for the polymerization of EtOx (**B**).

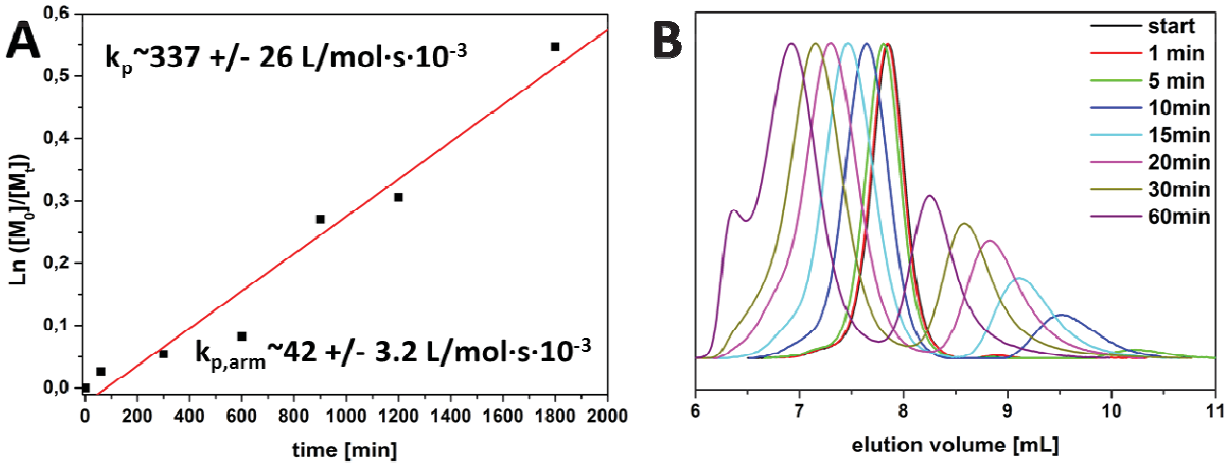

One way to determine the actual amount of incorporated PEtOx within the star-shaped $[PEO_{28}\text{-}b\text{-}PEtOx_x]_8$ block copolymers is to remove the generated homopolymer via fractionated precipitation in THF at −30 °C. The results are depicted in Figure 4. Therefore, differences of up to 50% between the expected and the real PEtOx content can be observed. The monomer conversion obtained from the reaction solution seems to be up to 50% (DP = 20), but the monomer conversion determined via NMR from the purified product leads to 25% (DP = 10).

Figure 4. Time-dependent EtOx conversion (black squares) and the corresponding degrees of polymerization per arm (red squares) determined from the reaction mixture (filled squares) and after purification of the star-shaped block copolymers (empty squares) via NMR (**A**); SEC traces before (dashed line) and after purification via fractionated precipitation (**B**) (solid lines; $CHCl_3$ was used as the eluent).

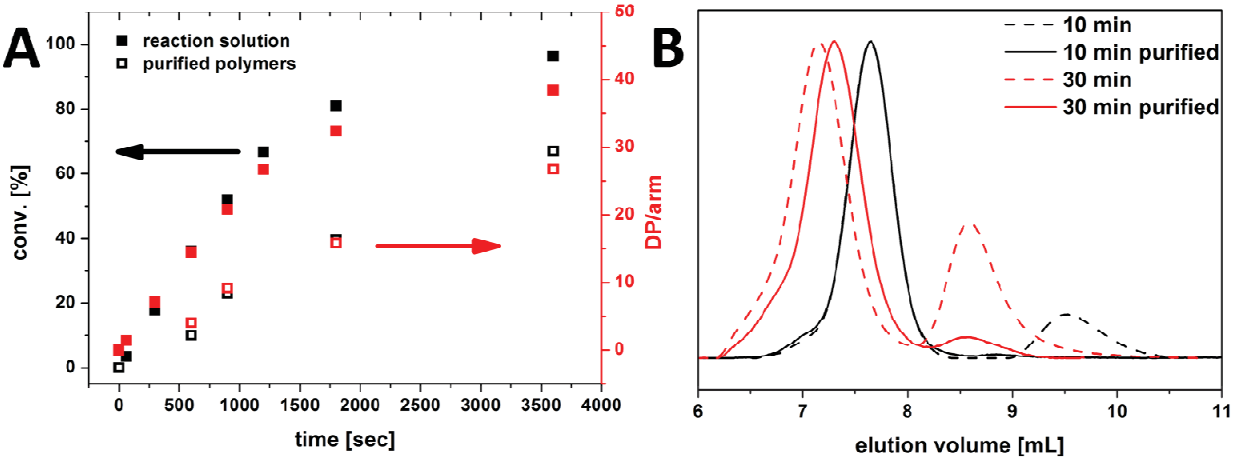

As can be seen in Figure 3B, after a polymerization time of 15 min, a considerable and clear shift of the desired product is visible in the elution traces and, at the same time, the amount of homopolymer formed is mediocre. The overall monomer conversion is around 50%, and we chose this as the conditions for the synthesis of samples with different PEtOx block lengths. Due to the fact that not

many differences were observed between $[PEO_{28}$-*b*-$PEtOx_{55}]_8$ and $[PEO_{28}$-*b*-$PEtOx_{75}]_8$ (Table 2), according to SEC measurements, $[PEO_{28}$-*b*-$PEtOx_{20}]_8$ and $[PEO_{28}$-*b*-$PEtOx_{60}]_8$ were targeted using the "core-first" approach, and the corresponding polymerizations were stopped at around 50% monomer conversion. The results are summarized in Table 2. In the case of the purified $[PEO_{28}$-*b*-$PEtOx_{50}]_8$, static light scattering (SLS) in THF was used in addition for the determination of the absolute molar mass (M_W). While in theory, a molar mass of 50,000 g mol^{-1} would be expected for $[PEO_{28}$-*b*-$PEtOx_{50}]_8$ by the [M]/[I]-ratio and NMR, SLS leads to a value of 54,000 g mol^{-1}, being in quite good agreement (Table 2).

We also compared the elution volume of star-shaped block copolymers with similar composition, but synthesized via two different approaches (Figure 5). As can be seen, for systems with a similar DP of roughly 20, the elution behavior is comparable via SEC (Figure 5A), as in NMR, the DP for the "arm-first" approach was 16, compared to 18 in the case of the "core-first" sample. For the star block copolymer with a higher amount of PEtOx (DP of 50), a shift to lower elution volume for the "core-first" product can be seen. Here, actual degrees of polymerization of 55 ("arm-first") and 50 ("core-first") for PEtOx were determined.

Figure 5. Comparison of the SEC traces obtained via the "core-first" (solid red lines) and the "arm-first" approach (solid black lines) in comparison to $[PEO_{28}$-Ts$]_8$ (dashed line) for two compositions: (**A**) $[PEO_{28}$-*b*-$PEtOx_{16}]_8$ (core-first; red curve) and $[PEO_{28}$-*b*-$PEtOx_{18}]_8$ (arm-first; black curve); and (**B**) $[PEO_{28}$-*b*-$PEtOx_{50}]_8$ (core-first; red curve) and $[PEO_{28}$-*b*-$PEtOx_{55}]_8$ (arm-first; black curve).

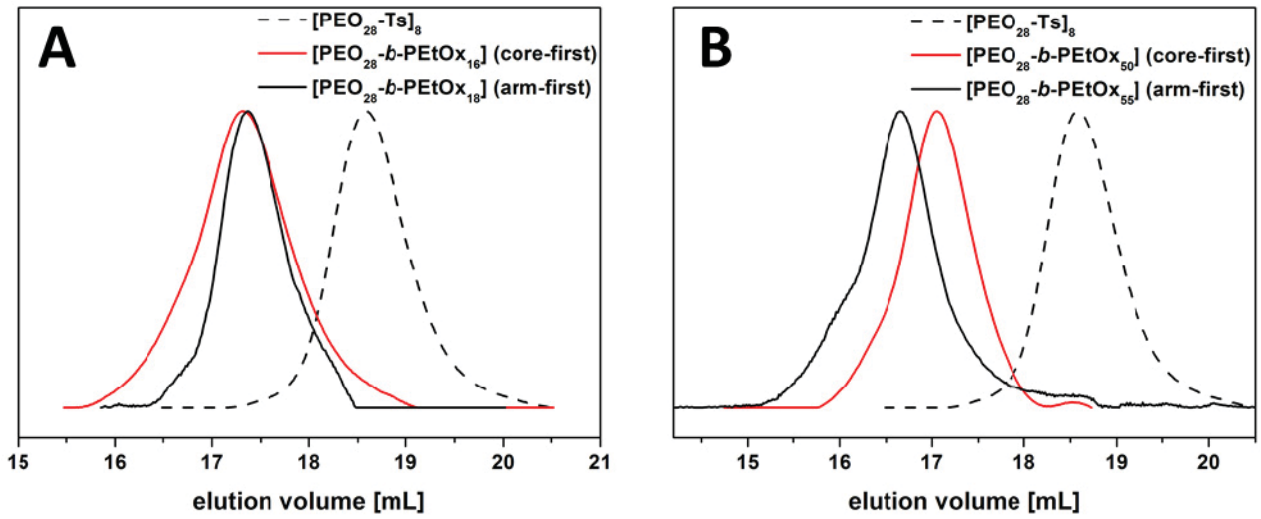

3.3. Study of Star-Shaped $[PEO_{28}$-b-$PEtOx_x]_8$ in Non-Selective Solvents

We were now interested in the solution properties of star-shaped $[PEO_{28}$-*b*-$PEtOx_x]_8$ block copolymers in non-selective solvents, for example, tetrahydrofuran (THF) or water. First, the hydrodynamic radii in solution were determined using dynamic light scattering (DLS). Therefore, the samples were dissolved in THF, filtered (0.45 µm, PTFE) and the size was compared to the crude $[PEO_{28}$-OH$]_8$ star polymer (Figure 6). According to the CONTIN plots depicted in Figure 6A, for $[PEO_{28}$-OH$]_8$, an apparent hydrodynamic radius of $<R_h>_{n,app}$ = 1.5 nm was observed, whereas for the

star-shaped block copolymers prepared via the "arm-first" approach, apparent hydrodynamic radii of 2.5 ([PEO_{28}-*b*-$PEtOx_{18}$]$_8$), 4 nm ([PEO_{28}-*b*-$PEtOx_{55}$]$_8$) and 5 nm ([PEO_{28}-*b*-$PEtOx_{75}$]$_8$) were determined under these conditions (Table 3). These results, in our opinion, both confirm the formation of unimers in THF and the elution behavior observed in SEC with increasing length of the outer PEtOx block. The hydrodynamic radii obtained for "core-first" [PEO_{28}-*b*-$PEtOx_{16}$]$_8$ (3 nm) and [PEO_{28}-*b*-$PEtOx_{50}$]$_8$ (3 nm) are comparable.

Figure 6. DLS CONTIN plot for "arm-first" approach stars in different solvents: in THF: [PEO_{28}-OH]$_8$ (dashed black line, $<R_h>_{n,app}$ = 1.5 nm), [PEO_{28}-*b*-$PEtOx_{18}$]$_8$ (red line, $<R_h>_{n,app}$ = 2.5 nm), [PEO_{28}-*b*-$PEtOx_{55}$]$_8$ (green line, $<R_h>_{n,app}$ = 4 nm) and [PEO_{28}-*b*-$PEtOx_{75}$]$_8$ (blue line, $<R_h>_{n,app}$ = 5 nm) (2 g L^{-1}) (**A**); in water [PEO_{28}-OH]$_8$ (dotted black line, $<R_h>_{n,app}$ = 3 nm), [PEO_{28}-*b*-$PEtOx_{18}$]$_8$ (red dashed, $<R_h>_{n,app}$ = 6 nm) and [PEO_{28}-*b*-$PEtOx_{75}$]$_8$ (blue line, $<R_h>_{n,app}$ = 14 nm) (0.5 g L^{-1}, filtered) (**B**).

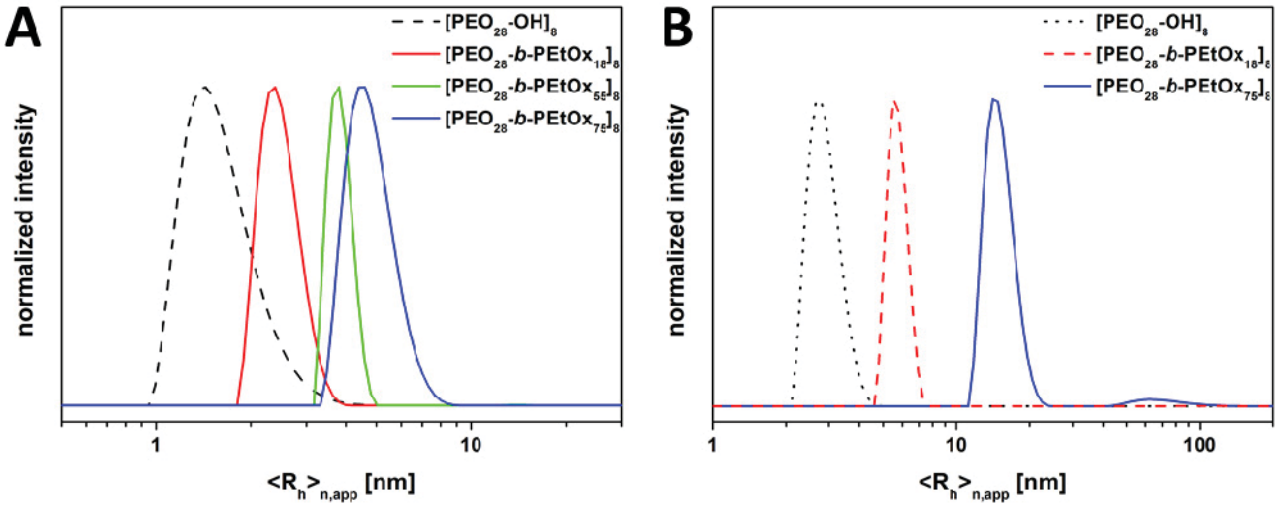

Table 3. Determination of the apparent hydrodynamic radius ($<R_h>_{n,app}$) for different star (block co-) polymer systems in non-selective solvents via DLS.

Sample	approach	$<R_h>_{n,app}$ [a] [nm] in THF	$<R_h>_{n,app}$ [a] [nm] in H_2O
[PEO_{28}-OH]$_8$	–	1.5	3
[PEO_{28}-*b*-$PEtOx_{18}$]$_8$	arm	2.5	6
[PEO_{28}-*b*-$PEtOx_{16}$]$_8$	core	3	3
[PEO_{28}-*b*-$PEtOx_{55}$]$_8$	arm	4	9
[PEO_{28}-*b*-$PEtOx_{50}$]$_8$	core	3	3
[PEO_{28}-*b*-$PEtOx_{75}$]$_8$	arm	5	14/62
[PEO_{28}-*b*-$PEtOx_{18}$]$_8$ [c]	arm	–	92/283 [b]
[PEO_{28}-*b*-$PEtOx_{75}$]$_8$ [c]	arm	–	72 [b]

[a] determined via CONTIN plot; [b] CONTIN plots in the Supporting Information part Figure S7; [c] non filtered sample.

However, if these "arm-first" materials are directly dissolved in water, again, a non-selective solvent for both PEO and PEtOx, turbid solutions are obtained. Transferring the materials from THF to water, via dialysis or evaporation of the organic co-solvent, leads to the same result. The turbidity did

not decrease after heating (up to 100 °C), cooling (~5 °C for one week), changing the pH (0 to 12), prolonged sonication or the addition of different salts (e.g., KSCN, NaCl, KCl). For these turbid solutions, hydrodynamic radii of up to several hundred nm were observed, even at very low concentrations (<0.5 g L^{-1}, Table 3, Figure S8). At this point, we assume that this turbidity originates from the aggregation of the star-shaped block copolymers, although both blocks are of hydrophilic nature. Such behavior has also been described for water-soluble homo- and block copolymers in the literature [12,19,56–58]. In some cases, the unexpected aggregation of double-hydrophilic block copolymers was explained by slight differences in the hydrophilicity of both blocks [50,58].

If, on the other hand, star-shaped $[PEO_{28}$-*b*-$PEtOx_x]_8$ block copolymers synthesized via the "core-first" approach were treated the same way, clear aqueous solutions with hydrodynamic radii of ~3 nm (both cases) are obtained. Somehow, the effect of aggregation in aqueous media is limited to samples prepared by click chemistry, for which we have no conclusive explanation up to now. No detectable amounts of copper were found in atom absorption spectroscopy (AAS), and therefore, an influence of residual copper from the CuAAC reaction can be excluded.

Applying shear forces via filtration (syringe filter, 1 µm, GF) to the turbid solutions of all described "arm-first" samples leads to clear solutions. To ensure that no material was removed by filtration, a defined concentration was filtered and dried afterwards, and the weight loss was below 5%. In Figure 6B, the DLS CONTIN plots for $[PEO_{28}$-OH$]_8$ (dashed black line, $<R_h>_{n,app}$ = 3 nm), $[PEO_{28}$-*b*-$PEtOx_{18}]_8$ (red line, $<R_h>_{n,app}$ = 6 nm) and $[PEO_{28}$-*b*-$PEtOx_{75}]_8$ (blue line, $<R_h>_{n,app}$ = 14 nm) are depicted. The obtained size distributions by DLS are slightly larger if compared to THF ($<R_h>_{n,app}$ = 1.5 nm, 2.5 nm and 5 nm), respectively. This might be an indication for the formation of aggregates by entanglements or that the star-shaped block copolymers are highly swollen.

It is well known that PEtOx materials exhibit lower critical solution temperatures (LCST), depending on the chain length [47,59]. To probe this for the herein described star-shaped systems, solutions of $[PEO_{28}$-*b*-$PEtOx_{20}]_8$ and $[PEO_{28}$-*b*-$PEtOx_{80}]_8$ (2.5 mg mL^{-1}, non-filtered aqueous solution) were heated up to 100 °C, and the turbidity was recorded. In both cases, the solutions did not show cloud points. We ascribe the absence of LCST behavior to the presence of a double-hydrophilic system and, in the case of $[PEO_{28}$-*b*-$PEtOx_{20}]_8$, to the short PEtOx arms.

As another peculiarity, it has been reported by Demirel *et al*. that PEtOx with a molar mass of 500 kg mol^{-1} (1 mg mL^{-1}) crystallizes after being heated in dilute solutions for several days at 70 °C [60]. We therefore were interested in whether similar observations can be made for star-shaped systems of different composition. Solutions of $[PEO_{28}$-*b*-$PEtOx_{18}]_8$ and $[PEO_{28}$-*b*-$PEtOx_{75}]_8$ were heated to 80 °C in water for three days. No changes could be detected for the materials synthesized using the "core-first" approach, whereas larger aggregates were found by DLS and transmission electron microscopy (TEM) for $[PEO_{28}$-*b*-$PEtOx_{18}]_8$ and $[PEO_{28}$-*b*-$PEtOx_{80}]_8$ prepared via the "arm-first" methodology (Figure 7, only if unfiltered solutions were used). The structure of such aggregates was different, depending on whether $[PEO_{28}$-*b*-$PEtOx_{18}]_8$ (55 wt % PEtOx) or $[PEO_{28}$-*b*-$PEtOx_{75}]_8$ (82 wt % PEtOx) was used. In the case of $[PEO_{28}$-*b*-$PEtOx_{18}]_8$, sharp, crystal-like structures were observed, possibly due to partial crystallization of PEtOx, which was also observed by Güner *et al*., [60] leading to an alignment in a rod-like fashion (Figure 7A). Assemblies of several hundred nm in length and ~200 nm width were obtained. For $[PEO_{28}$-*b*-$PEtOx_{75}]_8$, a slightly different aggregation mechanism might take place: here, the superstructures, rather, look like micellar clusters,

which might be the result of an initial formation of unimolecular micelles, followed by further agglomeration (Figure 7B) [61,62]. Tentatively, the hydrophilicity of PEtOx might be lower in comparison to PEO; we assume a partial collapse of the outer PEtOx shell over time, leading to aggregation. However, as this effect was only observed for star-shaped block copolymers prepared via the "arm first" approach and only if non-filtered solutions were used, we hypothesize that a certain pre-organization is required. The aggregation behavior of PEO depending on the treatment before was also discussed by Güner *et al*. for linear polymers [56], and differences in hydrophilicity were described by Ke *et al*. [50,60].

Figure 7. TEM micrographs of aggregates formed by $[PEO_{28}$-*b*-$PEtOx_{18}]_8$ (**top**) and $[PEO_{28}$-*b*-$PEtOx_{75}]_8$ (**bottom**) after heating for three days at 80 °C (unfiltered solutions, "arm-first" approach).

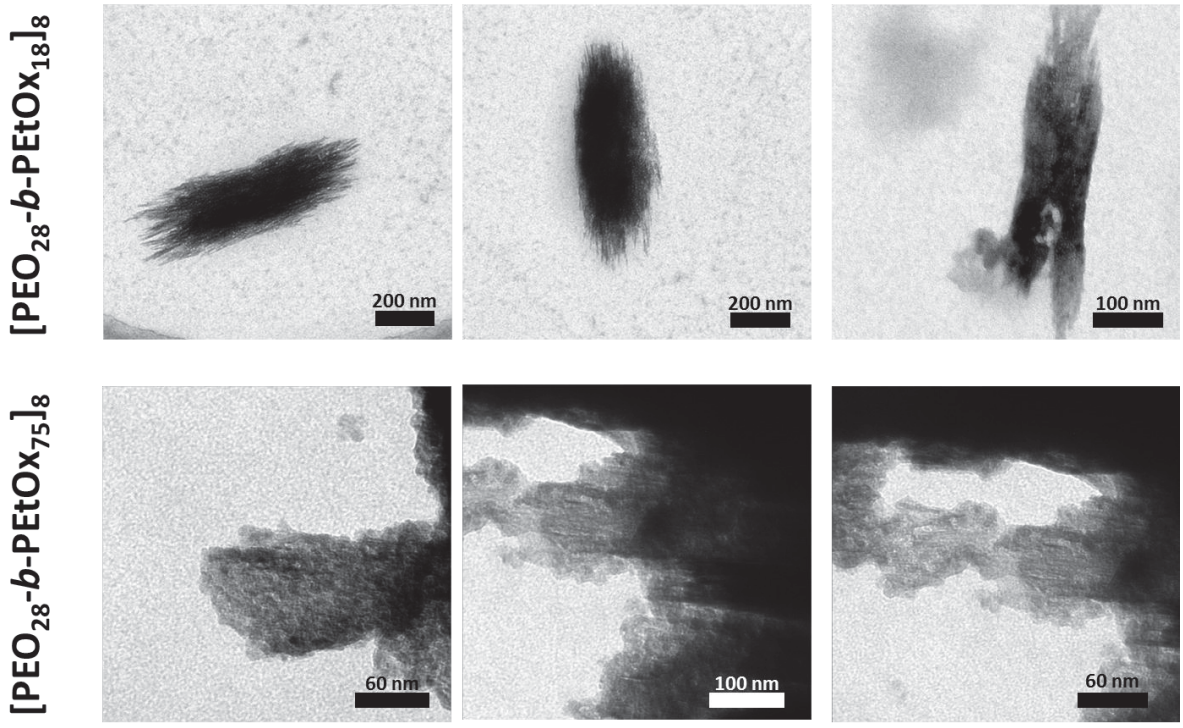

4. Conclusions

We demonstrated the synthesis of a series of well-defined star-shaped $[PEO_{28}$-*b*-$PEtOx_x]_8$ block copolymers using two different approaches, either "core-first" using $[PEO_{28}$-Ts$]_8$ as a macroinitiator for the CROP of EtOx or by copper-catalyzed azide-alkyne cycloadditions between $[PEO_{28}$-$N_3]_8$ and TB-$PEtOx_x$ ("arm-first"). In both cases, different block lengths for the outer PEtOx block were used, and comparable molar masses and hydrodynamic radii in THF as a non-selective solvent were observed. In dilute aqueous solutions, samples prepared via the "arm-first" approach showed aggregate formation, whereas this was not the case for the "core-first" materials. Although this behavior is not fully understood at this point, we could exclude several factors (salt, copper impurities, differences in the molar mass) as the origin of this peculiarity, and we could show that after filtration (1 μm pore size), also, here, smaller hydrodynamic radii are found. At this point, our hypothesis is that small differences in hydrophilicity are the main driving force for this behavior. More importantly, such loose

aggregates from star-shaped block copolymers could be used for the temperature-induced formation of larger agglomerates, where first investigations hint towards an influence of the weight ratio PEO:PEtOx on the morphology of the superstructures formed.

Acknowledgments

We thank Grit Festag for help with the SEC analysis, Sandra Köhn for AAS measurements, Nicole Fritz for help with the 2D-LC and Frank Steiniger and Christine Kämnitz (Electron Microscope Center Jena) for help with the TEM. F.H.S. and T.R. are further grateful to the Thuringian Ministry for Education, Science and Culture (TMBWK; #B515-10065, ChaPoNano) for financial support. F.H.S. thanks the VCI for a starting an independent researcher fellowship, and T.R. acknowledges the Carl-Zeiss foundation for a PhD-scholarship. We also wish to acknowledge the Dutch Polymer Institute (DPI, technology area high-throughput-experimentation, project #690) and the Thuringian Ministry for Education, Science and Culture (grants #B514-09051, NanoConSens, #B515-11028, SWAXS-JCSM and #03WKCB01C, BASIS and #B515-07008) for financial support of this study.

Conflicts of Interest

The authors declare no conflict of interest.

References

1. Barner-Kowollik, C.; Lutz, J.-F.; Perrier, S. New methods of polymer synthesis. *Polym. Chem.* **2012**, *3*, 1677–1679.
2. Pitsikalis, M.; Pispas, S.; Mays, J.W.; Hadjichristidis, N. Nonlinear Block Copolymer Architectures. In *Blockcopolymers–Polyelectrolytes–Biodegradation*; Advances in Polymer Science; Springer-Verlag: Berlin/Heidelberg, Germany, 1998; Volume 135, pp. 1–137.
3. Burchard, W. Solution Properties of Branched Macromolecules. *Adv. Polym. Sci.* **1999**, *143*, 113–194.
4. Hadjichristidis, N.; Pispas, S.; Pitsikalis, M.; Iatrou, H.; Vlahos, C. Asymmetric Star Polymers: Synthesis and Properties; In *Branched Polymers I*; Advances in Polymer Science; Roovers, J., Ed.; Springer: Berlin/Heidelberg, Germany, 1999; Volume 142, pp. 71–127.
5. Plamper, F.A.; McKee, J.R.; Laukkanen, A.; Nykanen, A.; Walther, A.; Ruokolainen, J.; Aseyev, V.; Tenhu, H. Miktoarm stars of poly(ethylene oxide) and poly(dimethylaminoethyl methacrylate): manipulation of micellization by temperature and light. *Soft Matter* **2009**, *5*, 1812–1821.
6. Hadjichristidis, N.; Pitsikalis, M.; Pispas, S.; Iatrou, H. Polymers with Complex Architecture by Living Anionic Polymerization. *Chem. Rev.* **2001**, *101*, 3747–3792.
7. Matyjaszewski, K.; Xia, J.H. Atom transfer radical polymerization. *Chem. Rev.* **2001**, *101*, 2921–2990.
8. Moad, G.; Rizzardo, E.; Thang, S.H. Living radical polymerization by the RAFT process. *Aust. J. Chem.* **2005**, *58*, 379–410.

9. Schacher, F.H.; Rupar, P.A.; Manners, I. Functional Block Copolymers: Nanostructured Materials with Emerging Applications. *Angew. Chem. Int. Ed.* **2012**, *51*, 7898–7921.
10. Zhang, J.; Lu, Z.-Y.; Sun, Z.-Y. Self-assembly structures of amphiphilic multiblock copolymer in dilute solution. *Soft Matter* **2013**, *9*, 1947–1954.
11. Gröschel, A.H.; Schacher, F.H.; Schmalz, H.; Borisov, O.V.; Zhulina, E.B.; Walther, A.; Müller, A.H.E. Precise hierarchical self-assembly of multicompartment micelles. *Nat. Commun.* **2012**, *3*, 710.
12. Riess, G. Micellization of block copolymers. *Prog. Polym. Sci.* **2003**, *28*, 1107–1170.
13. Schacher, F.; Walther, A.; Muller, A.H.E. Dynamic Multicompartment-Core Micelles in Aqueous Media. *Langmuir* **2009**, *25*, 10962–10969.
14. Förster, S.; Abetz, V.; Müller, A.H.E. *Polyelectrolyte Block Copolymer Micelles*; Springer Berlin: Heidelberg, Germany, 2004.
15. Iatridi, Z.; Tsitsilianis, C. Water-Soluble Stimuli Responsive Star-Shaped Segmented Macromolecules. *Polymers* **2011**, *3*, 1911–1933.
16. Schacher, F.H.; Elbert, J.; Patra, S.K.; Mohd Yusoff, S.F.; Winnik, M.A.; Manners, I. Responsive Vesicles from the Self-Assembly of Crystalline-Coil Polyferrocenylsilane-*block*-Poly(ethylene Oxide) Star-Block Copolymers. *Chem. Eur. J.* **2012**, *18*, 517–525.
17. Schacher, F.H.; Freier, U.; Steiniger, F. Hierarchical self-assembly of star-shaped organometallic crystalline-coil block copolymers in solution. *Soft Matter*. **2012**, *8*, 6968–6978.
18. Steinschulte, A.A.; Schulte, B.; Erberich, M.; Borisov, O.V.; Plamper, F.A. Unimolecular Janus Micelles by Microenvironment-Induced, Internal Complexation. *ACS Macro Lett.* **2012**, *1*, 504–507.
19. Knop, K.; Pavlov, G.M.; Rudolph, T.; Martin, K.; Pretzel, D.; Jahn, B.O.; Scharf, D.H.; Brakhage, A.A.; Makarov, V.; Mollmann, U.; Schacher, F.H.; Schubert, U.S. Amphiphilic star-shaped block copolymers as unimolecular drug delivery systems: investigations using a novel fungicide. *Soft Matter* **2013**, *9*, 715–726.
20. Lapienis, G. Star-shaped polymers having PEO arms. *Prog. Polym. Sci.* **2009**, *34*, 852–892.
21. Quaglia, F.; Ostacolo, L.; Nese, G.; Canciello, M.; de Rosa, G.; Ungaro, F.; Palumbo, R.; la Rotonda, M.I.; Maglio, G. Micelles based on amphiphilic PCL-PEO triblock and star-shaped diblock copolymers: Potential in drug delivery applications. *J. Biomed. Mater. Res. A* **2008**, *87A*, 563–574.
22. Knop, K.; Hoogenboom, R.; Fischer, D.; Schubert, U.S. Poly(ethylene glycol) in Drug Delivery: Pros and Cons as Well as Potential Alternatives. *Angew. Chem. Int. Ed.* **2010**, *49*, 6288–6308.
23. Hanisch, A.; Schmalz, H.; Müller, A.H.E. A Modular Route for the Synthesis of ABC Miktoarm Star Terpolymers via a New Alkyne-Substituted Diphenylethylene Derivative. *Macromolecules* **2012**, *45*, 8300–8309.
24. Altintas, O.; Vogt, A.P.; Barner-Kowollik, C.; Tunca, U. Constructing star polymers via modular ligation strategies. *Polym. Chem.* **2012**, *3*, 34–45.
25. Fijten, M.W.M.; Haensch, C.; van Lankvelt, B.M.; Hoogenboom, R.; Schubert, U.S. Clickable poly(2-oxazoline)s as versatile building blocks. *Macromol. Chem. Phys.* **2008**, *209*, 1887–1895.

26. Hadjichristidis, N.; Iatrou, H.; Pitsikalis, M.; Pispas, S.; Avgeropoulos, A. Linear and non-linear triblock terpolymers. Synthesis, self-assembly in selective solvents and in bulk. *Prog. Polym. Sci.* **2005**, *30*, 725–782.
27. Kempe, K.; Krieg, A.; Becer, C.R.; Schubert, U.S. "Clicking" on/with polymers: A rapidly expanding field for the straightforward preparation of novel macromolecular architectures. *Chem. Soc. Rev.* **2012**, *41*, 176–191.
28. Tsitsilianis, C.; Lutz, P.; Graff, S.; Lamps, J.P.; Rempp, P. Core-first synthesis of star polymers with potentially ionogenic branches. *Macromolecules* **1991**, *24*, 5897–5902.
29. Knischka, R.; Lutz, P.J.; Sunder, A.; Mülhaupt, R.; Frey, H. Functional Poly(ethylene oxide) Multiarm Star Polymers: Core-First Synthesis Using Hyperbranched Polyglycerol Initiators. *Macromolecules* **2000**, *33*, 315–320.
30. Schmidt, B.V.K.J.; Rudolph, T.; Hetzer, M.; Ritter, H.; Schacher, F.H.; Barner-Kowollik, C. Supramolecular three-armed star polymers via cyclodextrin host-guest self-assembly. *Polym. Chem.* **2012**, *3*, 3139–3145.
31. Altintas, O.; Tunca, U.; Barner-Kowollik, C. Star and miktoarm star block (co)polymers via self-assembly of ATRP generated polymer segments featuring Hamilton wedge and cyanuric acid. *Polym. Chem.* **2011**, *2*, 1146–1155.
32. Hochwimmer, G.; Nuyken, O.; Schubert, U.S. 6,6′-Bisfunctionalized 2,2′-bipyridines as metallo-supramolecular initiators for the living polymerization of oxazolines. *Macromol. Rapid Comm.* **1998**, *19*, 309–313.
33. Altintas, O.; Yankul, B.; Hizal, G.; Tunca, U. One-pot preparation of 3-miktoarm star terpolymers via click [3 + 2] reaction. *J. Polym. Sci. A Polym. Chem.* **2007**, *45*, 3588–3598.
34. Johnson, J.A.; Finn, M.G.; Koberstein, J.T.; Turro, N.J. Construction of Linear Polymers, Dendrimers, Networks, and Other Polymeric Architectures by Copper-Catalyzed Azide-Alkyne Cycloaddition "Click" Chemistry. *Macromol. Rapid Comm.* **2008**, *29*, 1052–1072.
35. Chen, C.H.; Wilson, J.; Chen, W.; Davis, R.M.; Riffle, J.S. A light-scattering study of poly(2-alkyl-2-oxazoline)s: effect of temperature and solvent type. *Polymer* **1994**, *35*, 3587–3591.
36. Carmichael, A.Y.; Caba, B.L.; Huffstetler, P.P.; Davis, R.M.; Riffle, J.S. Synthesis and solution properties of poly(ethylene oxide-*b*-2-ethyl-2-oxazoline) and poly(ethylene oxide-*b*-ethyleneimine). *Polym. Prepr.* **2004**, *45*, 476–477.
37. Schlaad, H.; Diehl, C.; Gress, A.; Meyer, M.; Demirel, A.L.; Nur, Y.; Bertin, A. Poly(2-oxazoline)s as Smart Bioinspired Polymers. *Macromol. Rapid Commun.* **2010**, *31*, 511–525.
38. Park, J.-S.; Kataoka, K. Comprehensive and Accurate Control of Thermosensitivity of Poly(2-alkyl-2-oxazoline)s via Well-Defined Gradient or Random Copolymerization. *Macromolecules* **2007**, *40*, 3599–3609.
39. Bauer, M.; Lautenschlaeger, C.; Kempe, K.; Tauhardt, L.; Schubert, U.S.; Fischer, D. Poly(2-ethyl-2-oxazoline) as Alternative for the Stealth Polymer Poly(ethylene glycol): Comparison of in vitro Cytotoxicity and Hemocompatibility. *Macromol. Biosci.* **2012**, *12*, 986–998.

40. Rudolph, T.; Kempe, K.; Crotty, S.; Paulus, R.M.; Schubert, U.S.; Krossing, I.; Schacher, F.H. A strong cationic Bronsted acid, $[H(OEt_2)_2][Al\{OC(CF_3)_3\}_4]$, as an efficient initiator for the cationic ring-opening polymerization of 2-alkyl-2-oxazolines. *Polym. Chem.* **2013**, *4*, 495–505.
41. Tauhardt, L.; Kempe, K.; Knop, K.; Altuntaş, E.; Jäger, M.; Schubert, S.; Fischer, D.; Schubert, U.S. Linear Polyethyleneimine: Optimized Synthesis and Characterization—On the Way to "Pharmagrade" Batches. *Macromol. Chem. Phys.* **2011**, *212*, 1918–1924.
42. Einzmann, M.; Binder, W.H. Novel functional initiators for oxazoline polymerization. *J. Polym. Sci. A Polym. Chem.* **2001**, *39*, 2821–2831.
43. Kobayashi, S.; Uyama, H.; Narita, Y.; Ishiyama, J. Novel multifunctional initiators for polymerization of 2-oxazolines. *Macromolecules* **1992**, *25*, 3232–3236.
44. Knop, K.; Jahn, B.O.; Hager, M.D.; Crecelius, A.; Gottschaldt, M.; Schubert, U.S. Systematic MALDI-TOF CID Investigation on Different Substituted mPEG 2000. *Macromol. Chem. Phys.* **2010**, *211*, 677–684.
45. Li, Z.; Chau, Y. A facile synthesis of branched poly(ethylene glycol) and its heterobifunctional derivatives. *Polym. Chem.* **2011**, *2*, 873–878.
46. Güner, P. T.; Demirel, A.L. Effect of Anions on the Cloud Point Temperature of Aqueous Poly(2-ethyl-2-oxazoline) Solutions. *J. Phys. Chem. B* **2012**, *116*, 14510–14514.
47. Christova, D.; Velichkova, R.; Loos, W.; Goethals, E.J.; Prez, F.D. New thermo-responsive polymer materials based on poly(2-ethyl-2-oxazoline) segments. *Polymer* **2003**, *44*, 2255–2261.
48. Kolb, H.C.; Finn, M.G.; Sharpless, K.B. Click Chemistry: Diverse Chemical Function from a Few Good Reactions. *Angew. Chem. Int. Ed.* **2001**, *40*, 2004–2021.
49. Rostovtsev, V.V.; Green, L.G.; Fokin, V.V.; Sharpless, K.B. A Stepwise Huisgen Cycloaddition Process: Copper(I)-Catalyzed Regioselective "Ligation" of Azides and Terminal Alkynes. *Angew. Chem. Int. Ed.* **2002**, *114*, 2708–2711.
50. Ke, F.; Mo, X.; Yang, R.; Wang, Y.; Liang, D. Association of Block Copolymer in Nonselective Solvent. *Macromolecules* **2009**, *42*, 5339–5344.
51. Malik, M.I.; Ahmed, H.; Trathnigg, B. Liquid chromatography under critical conditions: practical applications in the analysis of amphiphilic polymers. *Anal. Bioanal. Chem.* **2009**, *393*, 1797–1804.
52. Falkenhagen, J.; Much, H.; Stauf, W.; Müller, A.H.E. Characterization of Block Copolymers by Liquid Adsorption Chromatography at Critical Conditions. 1. Diblock Copolymers. *Macromolecules* **2000**, *33*, 3687–3693.
53. Jiang, W.; Khan, S.; Wang, Y. Retention Behaviors of Block Copolymers in Liquid Chromatography at the Critical Condition. *Macromolecules* **2005**, *38*, 7514–7520.
54. Sharghi, H.; Khalifeh, R.; Doroodmand, M.M. Immobilization of Porphyrinatocopper Nanoparticles onto Activated Multi-Walled Carbon Nanotubes and a Study of its Catalytic Activity as an Efficient Heterogeneous Catalyst for a Click Approach to the Three-Component Synthesis of 1,2,3-Triazoles in Water. *Adv. Synth. Catal.* **2009**, *351*, 207–218.
55. Ziegast, G.; Pfannemüller, B. Linear and star-shaped hybrid polymers, 1. A new method for the conversion of hydroxyl end groups of poly(oxyethylene) and other polyols into amino end groups. *Makromol. Chem.* **1984**, *5*, 363–371.

56. Özdemir, C.; Güner, A. Solubility profiles of poly(ethylene glycol)/solvent systems, I: Qualitative comparison of solubility parameter approaches. *Eur. Polym. J.* **2007**, *43*, 3068–3093.
57. Nakashima, K.; Bahadur, P. Aggregation of water-soluble block copolymers in aqueous solutions: Recent trends. *Adv. Col. Int. Sci.* **2006**, *123–126*, 75–96.
58. Casse, O.; Shkilnyy, A.; Linders, J.; Mayer, C.; Häussinger, D.; Völkel, A.; Thünemann, A.F.; Dimova, R.; Cölfen, H.; Meier, W.; Schlaad, H.; Taubert, A. Solution Behavior of Double-Hydrophilic Block Copolymers in Dilute Aqueous Solution. *Macromolecules* **2012**, *45*, 4772–4777.
59. Lambermont-Thijs, H.M.L.; Kuringen, H.P.C.V.; Put, J.P.W.V.D.; Schubert, U.S.; Hoogenboom, R. Temperature Induced Solubility Transitions of Various Poly(2-oxazoline)s in Ethanol-Water Solvent Mixtures. *Polymers* **2010**, *2*, 188–199.
60. Guner, P.T.; Miko, A.; Schweinberger, F.F.; Demirel, A.L. Self-assembled poly(2-ethyl-2-oxazoline) fibers in aqueous solutions. *Polym. Chem.* **2012**, *3*, 322–324.
61. Cheng, L.; Zhang, G.; Zhu, L.; Chen, D.; Jiang, M. Nanoscale tubular and sheetlike superstructures from hierarchical self-assembly of polymeric janus particles. *Angew. Chem. Int. Ed.* **2008**, *47*, 10171–10174.
62. Liu, C.; Zhang, K.; Chen, D.; Jiang, M.; Liu, S. Transforming spherical block polyelectrolyte micelles into free-suspending films via DNA complexation-induced structural anisotropy. *Chem. Commun.* **2010**, *46*, 6135–6137.

Supporting Information

Figure S1. Characterization data for the modification steps performed to obtain star-shaped $[PEO_{28}\text{-}N_3]_8$ via: (**A**) reaction scheme for the tosylation and azidation of $[PEO_{28}\text{-}OH]_8$ and the characterization via: (**B**) ATR-FT-IR; (**C**) ^{1}H-NMR $[PEO_{28}\text{-}OH]_8$ (black curve), $[PEO_{28}\text{-}Ts]_8$ (red curve), and $[PEO_{28}\text{-}N_3]_8$ (blue curve); (**D**) SEC (DMAC) of $[PEO_{28}\text{-}OH]_8$ (dashed line) and $[PEO_{28}\text{-}N_3]_8$ (solid line).

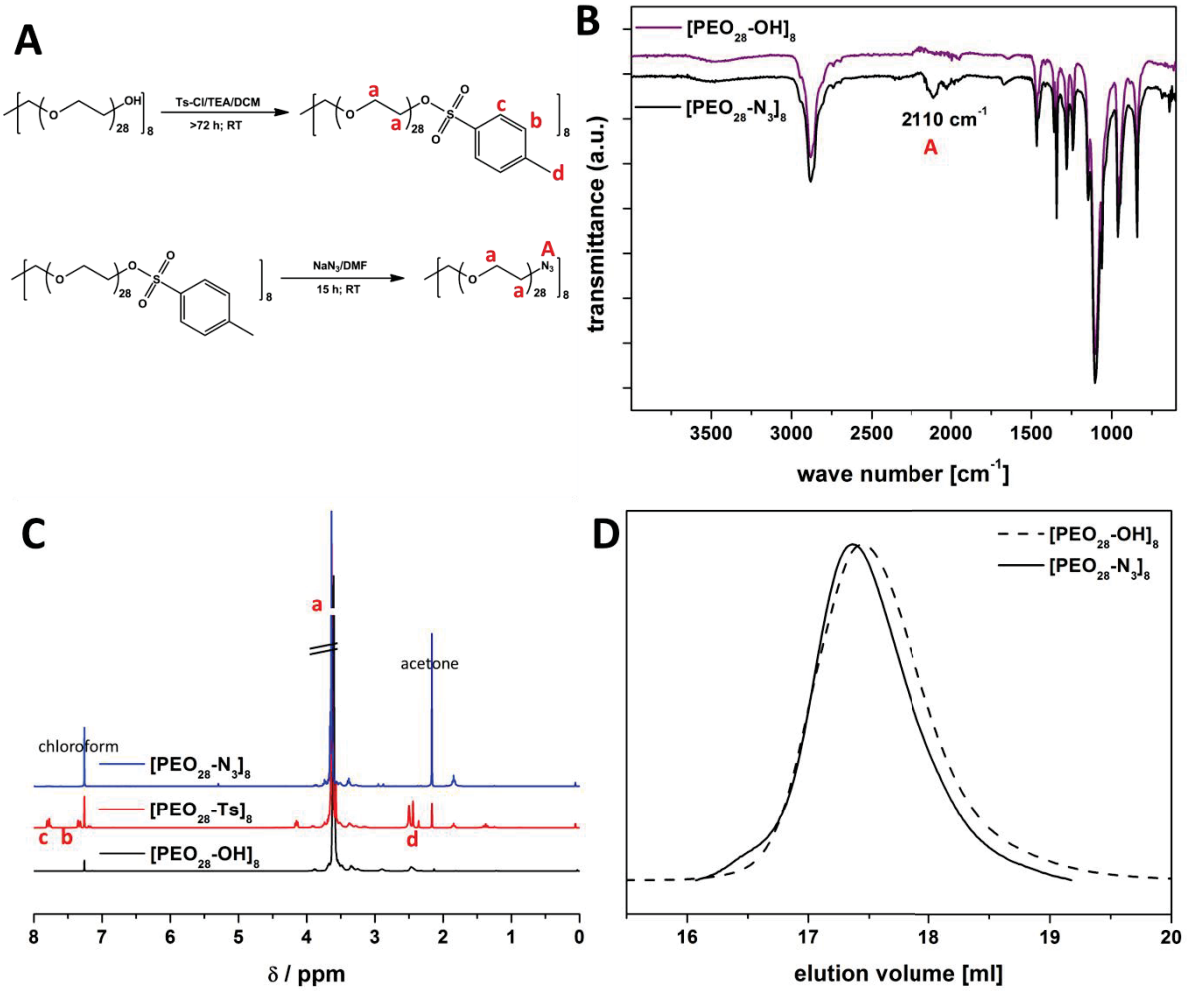

Figure S2. LCCC chromatograms at the critical conditions of PEO standards from PSS ($H(C_2H_4O)_nH$ (mobile phase composition acetonitrile and water (55/45, v/v))).

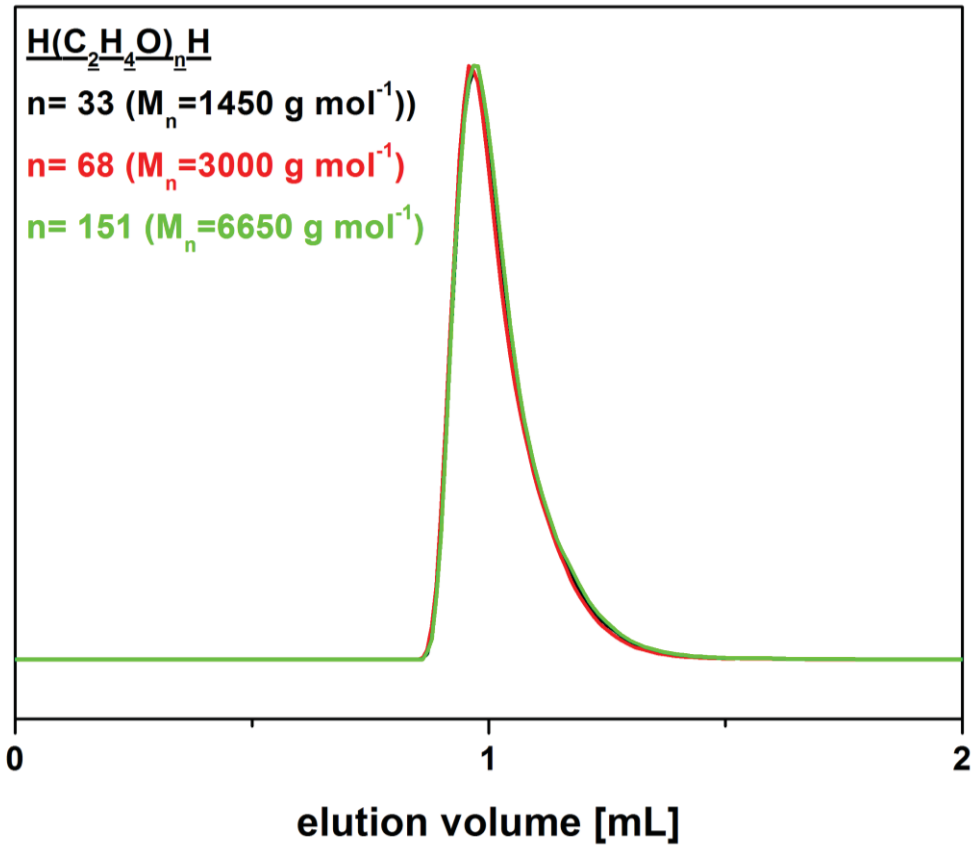

Figure S3. Comparison of 2D-LC results obtained for $[PEO_{28}\text{-}N_3]_8$ after different times in solution; (**A**) freshly prepared; (**B**) 30 min after preparation; (**C**) stored overnight in ACN/H_2O mixture of the eluent; *y*-axis elution at critical conditions (LCCC), *x*-axis SEC mode.

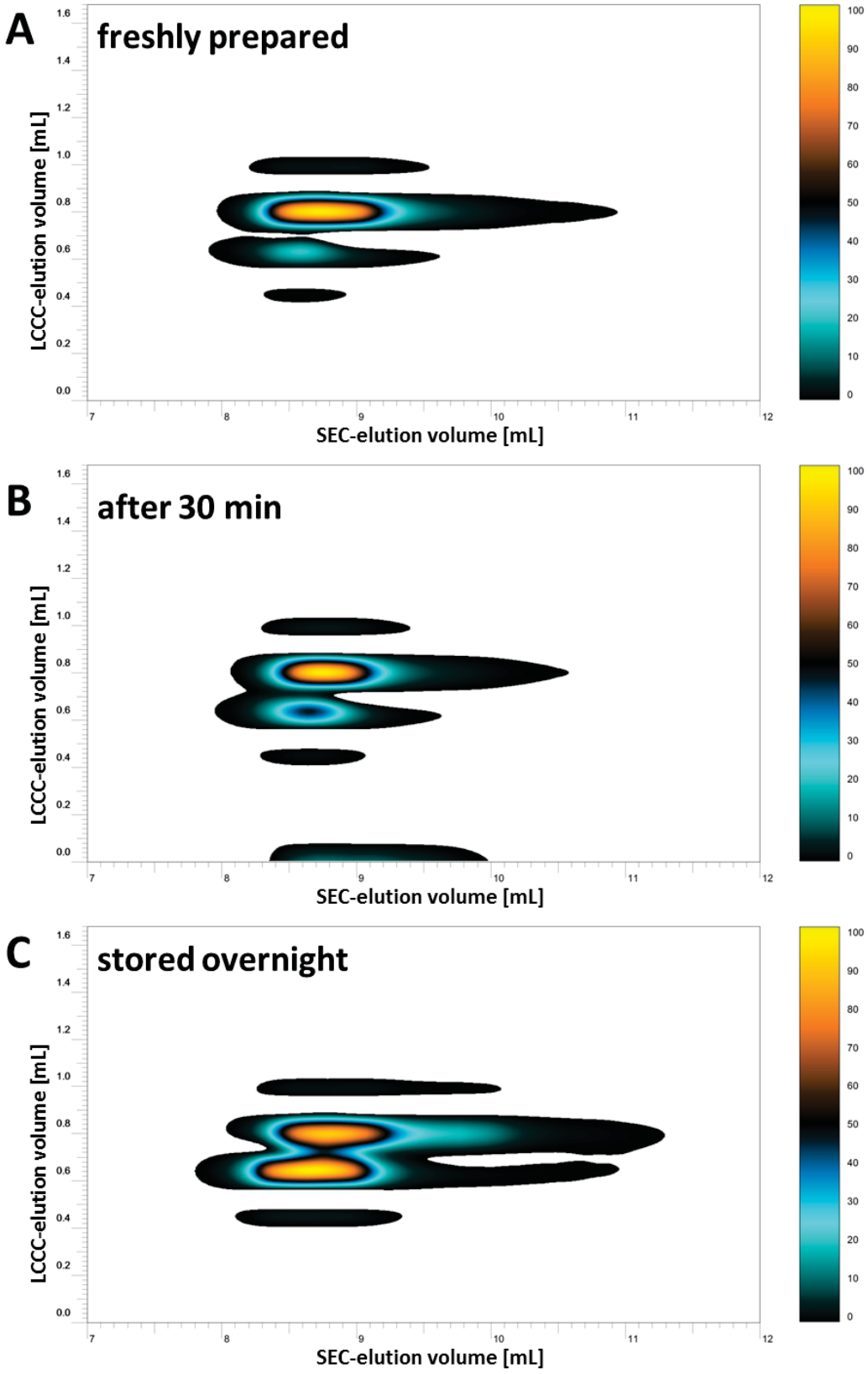

Figure S4. Comparison of characteristic signals in the ^{13}C-NMR spectra for $[PEO_{28}\text{-}OH]_8$ (black), $[PEO_{28}\text{-}Ts]_8$ (red), and $[PEO_{28}\text{-}N_3]_8$ (blue); (**A**) backbone $-CH_2-$ groups; (**B**) $-CH_2-OH$; (**C**) $-CH_2-N_3$.

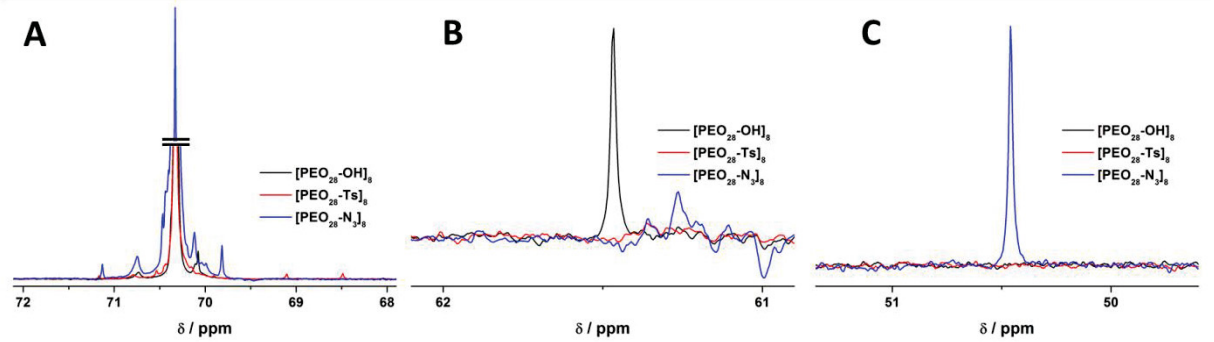

Figure S5. Schematic representation of the CROP of 2-ethyl-2-oxazoline initiated by $[PEO_{28}\text{-}Ts]_8$.

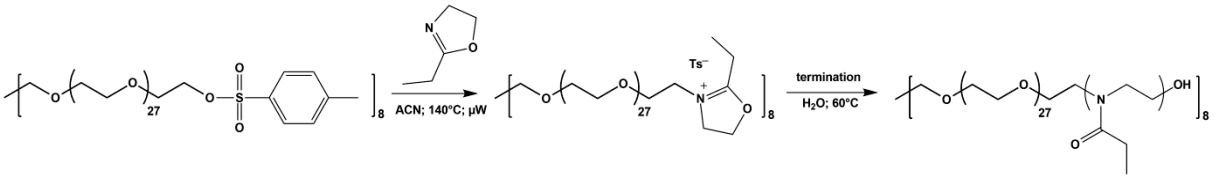

Figure S6. SEC traces for TB-$PEtOx_{20}$-OH (straight line), TB-$PEtOx_{60}$-OH (dashed line), and TB-$PEtOx_{80}$-OH (dotted line) on the chloroform (**A**) and dimethylacetamide (**B**) SEC.

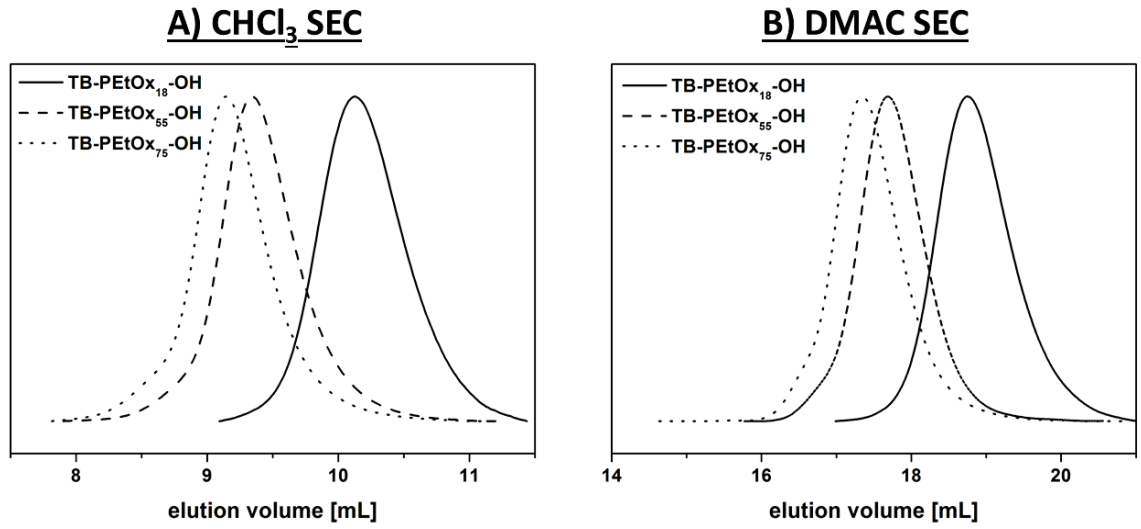

Figure S7. Characterization of the star-shaped block copolymer $[PEO_{28}$-*b*-$PEtOx_{55}]_8$ via: (**A**) NMR and (**B**) ATR-FT-IR.

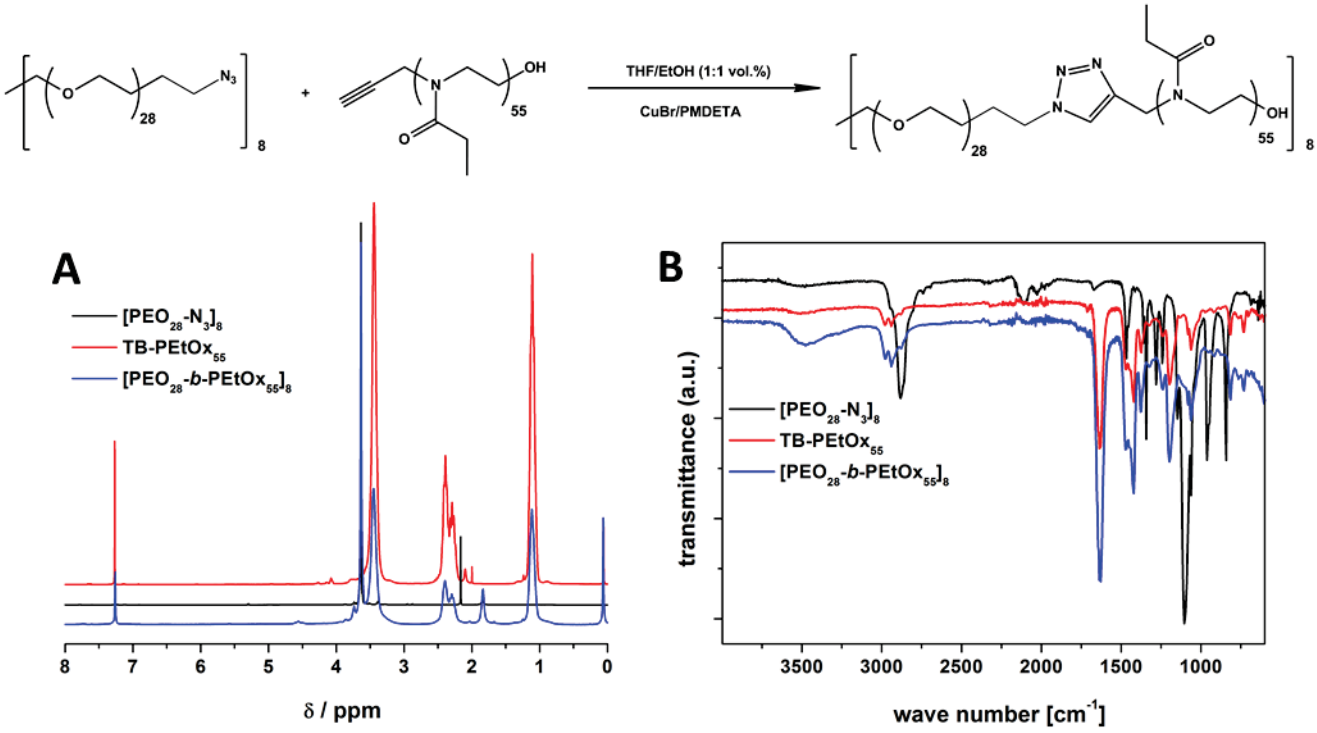

Figure S8. DLS CONTIN plots of the unfiltered samples of $[PEO_{28}$-*b*-$PEtOx_{18}]_8$ (black curve) and $[PEO_{28}$-*b*-$PEtOx_{75}]_8$ (red curve) in water.

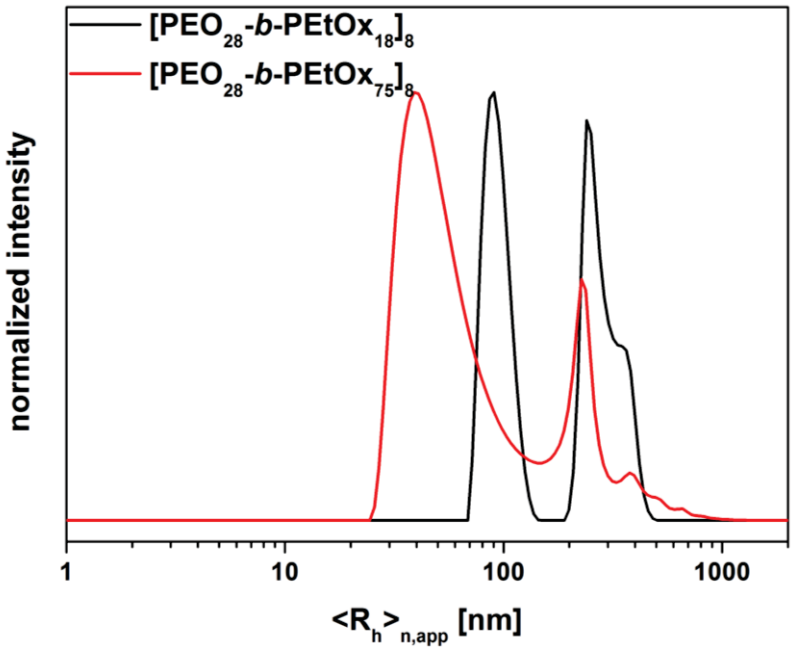

Publication 7

Semi-automated multi-dimensional characterization of synthetic copolymers

S. Crotty, C. Weber, A. Baumgaertel, N. Fritz, E. Altuntaş, K. Kempe, U. S. Schubert

Eur. Polym. J. **2014**, *60*, 153-162.

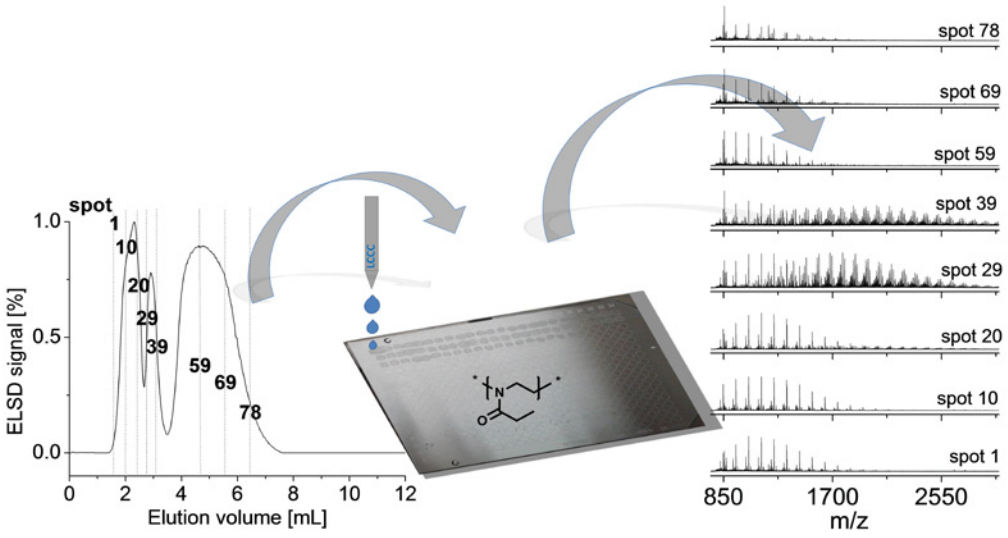

European Polymer Journal 60 (2014) 153–162

Contents lists available at ScienceDirect

European Polymer Journal

journal homepage: www.elsevier.com/locate/europolj

Semi-automated multi-dimensional characterization of synthetic copolymers

Sarah Crotty [a,b,c], Christine Weber [a,b,c], Anja Baumgaertel [a,b,c], Nicole Fritz [a,b,c], Esra Altuntaş [a,b], Kristian Kempe [a,b], Ulrich S. Schubert [a,b,c,*]

[a] Laboratory of Organic and Macromolecular Chemistry (IOMC), Friedrich Schiller University Jena, Humboldstr. 10, 07743 Jena, Germany
[b] Jena Center for Soft Matter (JCSM), Friedrich Schiller University Jena, Philosophenweg 7, 07743 Jena, Germany
[c] Dutch Polymer Institute (DPI), John F. Kennedylaan 2, 5612 AB Eindhoven, The Netherlands

ARTICLE INFO

Article history:
Received 10 April 2014
Received in revised form 12 July 2014
Accepted 27 July 2014
Available online 22 August 2014

Keywords:
Liquid adsorption chromatography under critical conditions (LACCC)
Automated robotic spotting
MALDI-ToF MS
ESI-Q-ToF-MS
Poly(2-oxazoline)s

ABSTRACT

Multi-dimensional high-throughput approaches are being transferred from biological to synthetic polymer systems due to the important increase of applications of polymers in life science. As a result, automated robotic spotting of poly(2-ethyl-2-oxazoline)s p(EtOx) was performed for the first time in combination with liquid adsorption chromatography at critical conditions (LACCC) and furthermore exploited for p(EtOx) block copolymers prepared for application as drug delivery systems. The LACCC is a complex and time-consuming process however, extremely helpful for the identification of the chemical functionality of polymers. The hyphenation between HPLC–MALDI-ToF MS *via* spotting and the subsequent analysis by ESI-Q-ToF MS/MS enabled the detailed characterization of side products occurring during the synthesis.

1. Introduction

Synthetic polymers have become more and more important for applications in life sciences since it has been discovered that they bear a great potential to support the delivery of bioactive substances or tracers in the human body. Such "drug delivery vehicles" in various forms provide multiple advantages during the curing of diseases: They can encapsulate hydrophobic drugs or tracers to enhance the biological uptake of the active substance or to protect/shield it during its way through the body [1]. In case the drug is toxic (as, e.g., cancer drugs) an encapsulation might help to decrease the negative side effects of the treatment if the polymeric drug carrier takes care that the drug is transported only to the place in the body where the treatment should take place. This can be done in a passive (non-functionalized nanoparticles or micelles) or active manner ("target" moieties are then attached to the polymeric carrier). Modern synthetic polymer chemistry allows the straightforward design of such complex carriers by the application of controlled and living polymerization techniques. Despite the large number of synthetically available polymer classes, the number of polymers that are actually applied in pharmaceutical devices on the market is rather limited. Poly(ethylene glycol) (PEG) is frequently used due to its protein repellent properties, which help to increase the circulation time of the drug in the blood [2]. Other examples are poly(lactic-*co*-glycolic acid) (PLGA) ("Resomer"® for the formation of degradable carriers) or certain polymetacrylates ("Eudragit"® for tailored release properties in the intestines after oral administration) [3].

A highly interesting alternative class of polymers for the development of new "smart" drug delivery systems are

* Corresponding author at: Laboratory of Organic and Macromolecular Chemistry (IOMC), Friedrich Schiller University Jena, Humboldstr. 10, 07743 Jena, Germany. Fax: +49 3641 9 48202.
E-mail address: ulrich.schubert@uni-jena.de (U.S. Schubert).

http://dx.doi.org/10.1016/j.eurpolymj.2014.07.030
0014-3057/

poly(2-oxazoline)s p(Ox) [4]. They can be obtained by the living cationic ring opening polymerization (CROP) [5], which represents an advantage for the tailoring of the carrier, because specific end groups can be attached at either end of the polymer chain by utilization of functional initiators and end-capping agents, respectively. In addition, the molar mass can be easily adjusted by the amount of initiator that is used for the CROP; and the properties of the entire macromolecule are determined by the substituent in 2-position of the cyclic monomer. Thus, the p(Ox) can vary from hydrophilic to hydrophobic, revealing lower critical solution temperature (LCST) behavior, can be fluorinated or carry moieties for post-polymerization functionalization processes. Finally, block copolymers can be obtained by simple sequential monomer addition due to the living character of the CROP. Moreover, p(MeOx) and p(EtOx) have been shown to reveal similar stealth behavior and low toxicity as PEG [6]. However, despite encouraging bio-studies being carried out in academia [7–9], p(EtOx) are not yet applied in real life because they are only approved by the FDA in the List of Indirect Additives Used in Food Contact Substances (Doc No. 6390). In order to be used for the development of pharmaceutical materials, by-products have to be identified and quantified [10].

A standard approach often applied for the analysis of proteins [11], lipids or other bio-based materials is the separation of (pre-digested)/[12,13] samples by reverse phase-high pressure liquid chromatography (RP-HPLC) (allowing to quantify the amount of compounds present) and the subsequent identification of the fractions by coupled mass spectrometry (MS) techniques [14]. The quality of the separation could even be improved by the application of multidimensional chromatography [14–16], whereas the advantage of the coupled MS technique is the additional possibility of sequencing the separated analyte by tandem MS.

Basically, MS methods (such as ESI [17] and MALDI-ToF MS [18,19]) have made its way from proteomics to synthetic polymers; however, LC is only slowly recognized by synthetic polymer chemists, especially when the separation of polymeric samples by LC (besides SEC) is further coupled to MS techniques (either offline or online). The main reason is the fact that, unlike proteins, even well-defined synthetic polymers are not monodisperse. This greatly affects the chromatographic behavior because a separation according to the composition of the sample may be accompanied by a separation according to the molar mass [20]. This can be overcome by the application of LACCC, where enthalpic and entropic effects for one homopolymer are delicately balanced out and, thus, one homopolymer elutes at the same time irrespective of its molar mass [21,22]. Therefore, one part of the analyte can be made "chromatographically invisible" [23,24]. However, the identification of the critical conditions for a specific polymer is laborious since it requires the testing of various solvent mixtures and columns. Having been adopted, the critical conditions may not always be suitable to analyze each sample in a straightforward manner because other parts of the sample might then show unfavorable elution, or end-group effects, which would complicate the assignment of the obtained peaks. Thus, the development of a standard analysis technique represents a difficult task. This problem requires a technique to identify the fractions from the LC run in a convenient and fast manner. The obvious choice would be a simple coupling of the LC [25] or SEC [26–28] system to ESI-Q-ToF MS [26,29]. However, ESI-Q-ToF MS may provide multiply charged species, which makes the interpretation of the resulting spectra complicated as synthetic polymers are not monodisperse (combination of molar mass distribution and charge distribution; see also above).

Since MALDI-ToF MS mostly provides singly charged species it is more frequently applied for synthetic polymers than ESI-Q-ToF MS, which is more applicable for oligomers in comparison to MALDI, which can ionize high M_n values [30]. However, due to the fact that it is measured from dried samples (composed of analyte, matrix and doping agent) this technique is not suitable for a direct on-line coupling to a LC method. Of course, fractions could be collected from the eluate and subsequently be analyzed, but this approach is far off from being reproducible and certainly will not allow a standardized high-throughput performance. To overcome this drawback, it is helpful to adopt the knowledge that has been created by the analysis of biological samples for synthetic polymer samples.

The most common spotting technique is where the eluate and the matrix are directly deposited onto the MALDI target in comparison to other older and rarely used techniques such as heated droplet and impulse driven heated droplet [31,32]. Moreover, other type of techniques have been elaborated such as electrospray deposition [33–40], plasma deposition [41], aerosol formation and evaporation formation. The specific reason for using the spotting technique is that we can reach a high-throughput application due to its online flow. (Fig. 1) In addition, the method can be reproduced several times on different targets to ensure reproducibility. For biological applications, automation has been demonstrated by, e.g., Iida et al. [42] using LC coupled to an automatic spotting system to transfer the fractions onto a MALDI target for serum applications. This is a powerful technique, which accomplishes separation in the column, but also spotting, and in the end, the analysis by mass spectrometry thus enabling a high-throughput and homogeneity in the sampling as well as spotting, therefore, acquiring reproducible results in the mass spectrum. Beside the already mentioned setup, Zarai et al. [43] used normal phase nano HPLC coupled to an automated spotting robot for the analysis of glycosphingolipids. An automated sheath flow assisted deposition was performed for peptides by Lechner et al. [44] to gain a higher quality of the mass spectra. However, the idea of automatically spotting the eluate from a LC system is rarely applied for the analysis of synthetic polymers. As first research group, Nielen et al. [45] coupled a MALDI-ToF MS to a micro SEC with a robotic interface for polybisphenol based polymers. Furthermore Keil et al. [46], coupled both LC and SEC to MALDI *via* a robot for the analysis of poly(propylene oxide)s.

In this contribution, we present the development of an automated spotting technique that enables a LC–MS hyphenation for the analysis of p(EtOx). Subsequently,

the analytical method is applied for the assignment of peaks in LACCC chromatograms of p(EtOx) containing block copolymers with different end groups. This general setup should promote the application of p(Ox) in life science and can be adequately used for the analysis of other synthetic polymers by adjustment of the chromatographical conditions.

2. Experimental

2.1. Synthesis of the poly(2-ethyl-2-oxazoline) p(EtOx)

The synthesis of the p(EtOx) standards is described in a previous publication [47], and the molecular characteristics are summarized in Table 1. According to ^{1}H NMR spectroscopy, all polymers were functionalized quantitatively with the desired acetyl end groups. Further information is supplied in the SI.

2.2. Synthesis of the poly(2-oxazoline) block copolymers

The diblock copolymer synthesis is discussed in an earlier publication [47,48]. Selected molecular characteristic data are listed in Table 2 (the SI).

2.3. Methods

2.3.1. Liquid adsorption chromatography under critical conditions (LACCC)

High performance liquid chromatography (HPLC) was measured on an Agilent system (series 1200) equipped with a binary pump, an autosampler and an evaporative light scattering detector (ELSD, Softa Corporation, Model 400). For the LACCC separation, a Macherey–Nagel (Nucleodur, 250 mm × 4 mm, particle size 5 μm, pore size 108 Å) RP-HPLC column was used. The mobile phase consisted of a mixture of 2-propanol (IPA) and water (75/25, v/v) delivered by a binary pump at a flow rate of 0.5 mL min^{-1}. The column oven temperature was set at 35 °C. The ELSD temperatures were adjusted according to the investigated mobile phase (e.g. 70 °C for IPA). The different (co)polymers samples were dissolved in the same solvent mixture as the mobile phase to achieve a sample concentration of 3–7 mg mL^{-1} and for each measurement 50 μL were injected. The data were acquired using the WINGPC Unity software from PSS.

Table 1
Selected characterization data of the used p(EtOx) standards.

DP (NMR)	M_n (NMR) in g mol^{-1}	M_n (SEC) in g mol^{-1}	PDI (SEC)
5	580	790	1.16
17	1750	2220	1.09
30	3050	3050	1.12

SEC was calibrated with polystyrene (PS; M_n = 374–128,000 g mol^{-1}) standards.

2.3.2. The Proteineer fc

Samples were spotted onto the MALDI target with a premix of the matrix and the doping agent. For the Proteineer fc, one spectrum was acquired per spot and all the spots were measured with the sample (3–7 mg mL^{-1}), the mixture of the matrix DHB (100 mg mL^{-1} in THF), and the doping agent: NaCl (50 mg mL^{-1} in THF) (volume of matrix:volume of doping agent = 300:50) are finally mixed at the end before spotting and then deposited onto the target. The total volume of the matrix/doping agent used for one run was 120 μL. To achieve completely separated spots on the target, a pulse of 7 s was chosen and the time slices for the spotting area varied according to the total elution volume of a sample. Subsequent to completion of the spotting procedure, the MALDI target was transferred to the Ultraflex III ToF/ToF instrument (Bruker Daltonics, Bremen, Germany) for MS measurements. The MALDI-ToF MS matrix 2,5-dihydroxybenzoic acid (DHB, Sigma Aldrich), sodium chloride (Acros Organics), sodium iodide (Sigma Aldrich) as well as tetrahydrofuran (HPLC grade, Roth) were used as purchased.

2.3.3. MALDI-ToF MS

For the measurement of the matrix-assisted laser desorption/ionization (MALDI) mass spectra, an Ultraflex III ToF/ToF instrument (Bruker Daltonics, Bremen, Germany) was used. The instrument is equipped with a Nd-YAG laser and a collision cell. All spectra were measured in the positive ion reflector mode. The instrument was calibrated prior to each measurement with an external standard PMMA from PSS (Polymer Standards Service GmbH, Mainz, Germany). For the MALDI-ToF MS calibration standards preparation, separate solutions of polymer (10 mg mL^{-1} in chloroform), *trans*-2-[3-(4-tert-butylphenyl)-2-methyl-2-propenylidene]malononitrile (DCTB) (30 mg mL^{-1} in chloroform), and NaI (100 mg mL^{-1} in acetone) were prepared and mixed following the dried droplet spotting technique. For the calibration, 1 μL of the mixture was spotted onto the target plate. The MALDI-ToF MS matrix DCTB, (synthesized in house), sodium iodide (Sigma Aldrich) as well as chloroform and acetone (HPLC grade, Roth) were used as purchased.

2.3.4. ESI-Q-ToF MS

All samples were analyzed by using a microTOF Q-II (Bruker Daltonics) mass spectrometer equipped with an automatic syringe pump from KD Scientific for sample injection. The ESI-Q-ToF mass spectrometer was operating at 4.5 kV, at a desolvation temperature of 180 °C, in the positive ion mode. Nitrogen was used as the nebulizer and drying gas. All fractions were injected using a constant flow rate (3 μL min^{-1}) of sample solution. The ESI-Q-ToF MS instrument was calibrated in the *m/z* range 50–3000 using a calibration standard (Tunemix solution), which was supplied from Agilent. All data were processed *via* Bruker Data Analysis software version 4.0.

3. Results and discussion

Applying critical conditions in combination with MS has become a powerful characterization tool in recent years for

Table 2
Characterization data of the used diblock copolymers.

	DP (NMR)		M_n (NMR) in g mol^{-1}	M_n (SEC) in g mol^{-1}	PDI (SEC)
	n	*m*			
p(EtOx)$_n$-*b*-p(*o*DFOx)$_m$	10	2	1400	2010	1.20
p(EtOx)$_n$-*b*-p(EPOx)$_m$	10	3	1540	1800	1.13

SEC was calibrated with polystyrene (PS; M_n = 374–128,000 g mol^{-1}) standards.

the separation of different functionalized homopolymers from each other or block copolymer species from its side products [14]. Unfortunately, only semi-online or offline spotting and spraying techniques have been used up to now for polymeric samples were MALDI is concerned [49]. Therefore, the Proteineer fc, which can be used as automated spotting instrument, was adopted for the simpler analysis of spectra of different poly(2-oxazoline) homopolymers (*i.e.* p(EtOx) and p(*i*PropOx) as well as two kinds of block copolymers with well-defined end groups. The homopolymer samples differ only by one methyl group. The two block copolymers have been chosen specifically because they have the same starting block (p(EtOx)) and possess a short hydrophobic second block. Thus, they serve as models for polymers that could be used as micellar drug delivery systems [9].

3.1. Spotting of homopolymers under LACCC of p(EtOx)

The first step involved in the study was the correct adjustment of the mobile phase composition during the HPLC measurements to enable the performance of LACCC for p(EtOx). For this purpose, three p(EtOx)-standard polymers with the same end groups but varying molar masses were eluted over a RP-HPLC column [47]. The composition of the mobile phase was subsequently varied until all polymers eluted at the same retention time irrespective of their molar masses. A LACCC run for a homopolymer of p(EtOx) with M_n = 790 g mol^{-1} was performed, and the resulting chromatogram shows one signal at an elution volume (V_{el}) of 2.94 mL. The exact critical conditions are difficult to meet, necessitate significant efforts in terms of columns, temperatures and solvents adjustments and require a lot of time. However, near critical conditions could be found at a mobile phase combination of 2-propanol/H_20 = 75/25 (v, v) (Fig. S.1), and served well for the present study due to the fact that a straightforward analysis of the eluate by MS was performed.

In a second run, the eluate, which corresponds to the complete signal derived from the p(EtOx) sample, was then spotted onto the MALDI target with the Proteineer fc with a specific spotting time depending on the total elution volume of the sample. The total experiment was finished with about 30 spots using a premixed matrix and a doping agent. The spotting method was equivalent to the dried droplet method because single sample parts were finally mixed and spotted onto the target plate to then be analyzed by MALDI-ToF MS using the same laser intensities for each spot. Only a few spots were used out of the total number of spots for the MALDI spectra stack (Fig. 2) to show the increase and the decrease of the distribution intensity over the spotting run. In the corresponding MALDI spectra, a difference of 99.1*m*/*z* units could be found, which corresponds to the desired p(EtOx) homopolymer with a methyl initiating group and an –OAc terminating end group with a sodiated adduct. As the spectrum shows the same molar mass for all spectra this confirms that the critical adsorption point (CAP) was met. On the other hand we can observe a similar trend of the maximum count for each spot for the same *m*/*z* value and the chromatogram. This is no quantification but a way to show that there is gradient in the concentration spotted onto the target during the elution from the analytical column. The loss in counts at the highest point may surely be due to the sweet spot effect where the sample was not uniformly deposited and measured. In addition, a slight band spreading could be observed due to the fact that, outside the ELSD trace of the eluate, ions could be detected before and after the elution of the polymer, nonetheless pointing out the sensitiveness of mass spectrometry.

Prior to the analysis of complex copolymer samples, the concept of spotting the eluted sample and the straightforward analysis by MALDI-ToF MS was further tested by the analysis of another poly(2-oxazoline) homopolymer sample: p(*i*PropOx) with a $M_{n,SEC}$ of 2000 g mol^{-1} ((Fig. 3). This polymer contains the same end groups as the p(EtOx) but a different substituent at the nitrogen atom in the polymer chain. This specific p(*i*PropOx) chosen here was analyzed under p(EtOx) LACCC mode, which cannot be used for functionality determination of p(*i*PropOx). Nonetheless, this polymer was selected due to its similarities in terms of polymerization technique (identical end groups and narrow molar mass distribution) and a straightforward ionization *via* MALDI-ToF MS. It is clear that the critical conditions for p(*i*PropOx) would be different from the critical conditions of p(EtOx) but the analysis of a slightly less polar p(Ox) sample allowed first impressions on the elution behavior of more hydrophobic samples under LACCC of p(EtOx) and on the applicability and reproducibility of the spotting technique. The chromatogram shows one signal eluting at a retention time of 2.87 mL (V_{el} p(EtOx)) = 2.94 mL). Considering the reduced polarity of the p(*i*PropOx) compared to p(EtOx) and the application of a RP column in a polar mobile phase, this is surprising and stresses the necessity to confirm the molecular structure of the eluting polymer in detail. Whilst the LACCC of p(EtOx) is met, p(*i*PropOx) could run in SEC mode under the same conditions. This could indeed explain the observed elution behavior. Fig. S.2 displays an overlay of the elugram of p(*i*PropOx) with p(EtOx) standards, despite their different polarity, it is practically co-eluting. Thus, the

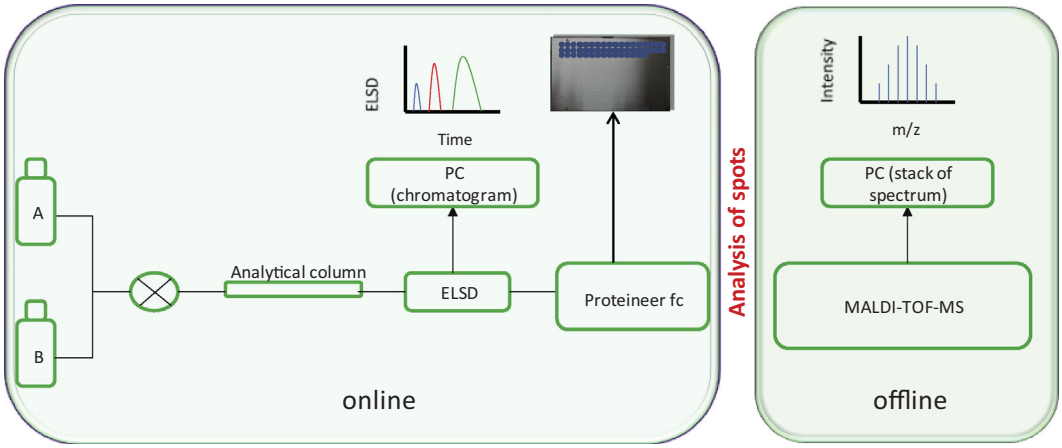

Fig. 1. Schematic diagram of the experimental setup.

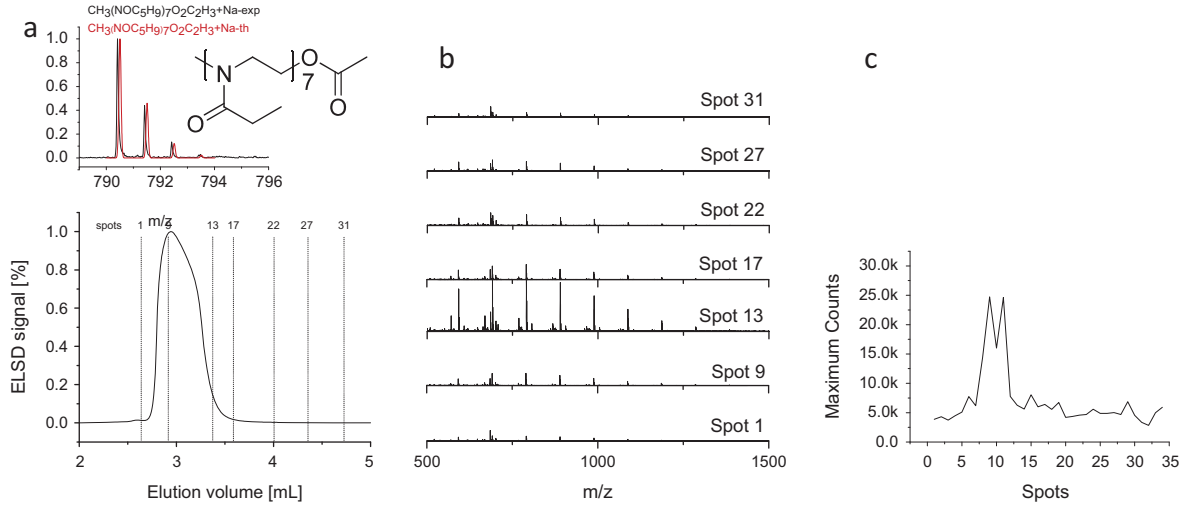

Fig. 2. (a) Chromatogram and isotopic pattern, (b) spectra stack and (c) the maximum count for each spot of p(EtOx) at LACCC at mobile phase composition 2-propanol/H_2O = 75/25 (v/v) of the p(EtOx), *i.e.* critical conditions (ELSD evaporator temperature: 70 °C).

sample was investigated by MALDI-ToF MS using the same settings for the spotter as described above. The desired polymeric structure could be confirmed from the acquired spectra (Fig. 3). In this case, the intensity of the peaks in the MALDI correlated with the intensity of the peak in the chromatogram. The peaks have a $\Delta m/z$ value of 113.1, corresponding to the mass of one *i*PropOx repeating unit and the calculated and measured isotopic patterns match for a polymer with both a $-CH_3$ and an –OAc end group being ionized with sodium cations. The maximum count graph shows that counts became drastically minimal closer to the end of the elution.

However, synthetic polymers that are used in pharmacy and medicine usually do not represent such simple homopolymers. In most cases they are composed of block copolymers (or other polymeric architectures), functionalized with additional biologically active moieties, or loaded with drugs that are not attached covalently. A useful separation and characterization method should be able to handle this sample complexity. Thus, the next step involved the investigation of p(EtOx) containing block copolymer samples under critical conditions for the p(EtOx) block to eliminate the influence of the molar mass of one component on the elution behavior of the entire block copolymer. The CROP technique also forms proton initiated chains, which is a result from chain transfer reactions during the polymerization.

3.2. Spotting of block copolymers

Based on the LACCC experiments with the automated spotting procedure for homopolymers, two different kinds of block copolymers were investigated. Both copolymers are composed of a moderately hydrophilic p(EtOx) block and a short hydrophobic (p(EtOx)-*b*-p(EPOx)) or fluorophilic (p(EtOx)-*b*-p(*o*DFOx)) block. As such they represent potential candidates for a prospective application as micellar drug delivery vehicles [50]. The spotted signals in the

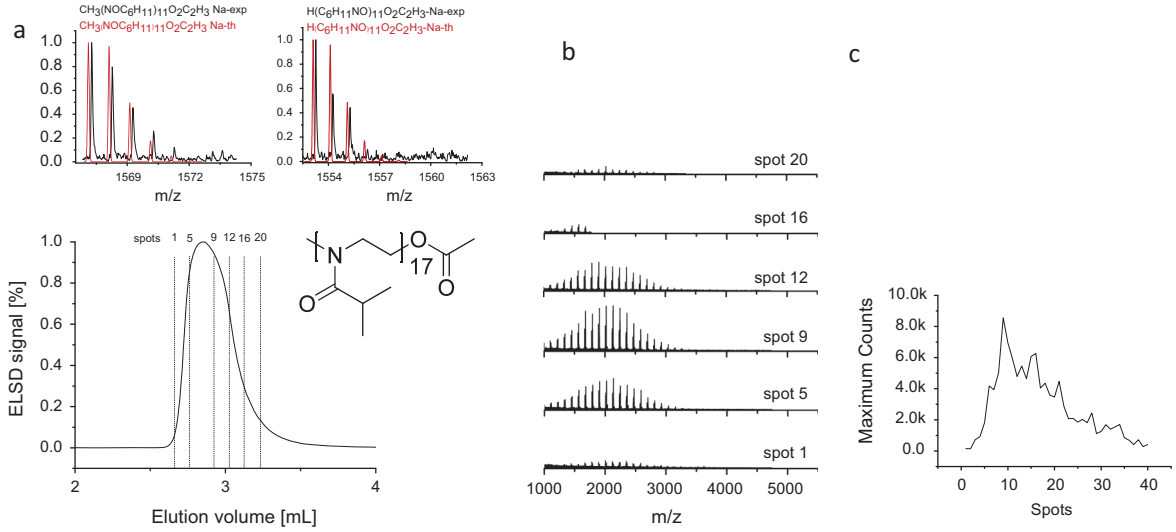

Fig. 3. (a) Chromatogram and isotopic pattern, (b) MALDI spectra stack and (c) the maximum count for each spot of p(*i*PropOx) at LACCC of p(EtOx) at mobile phase composition 2-propanol/H_2O = 75/25 (v/v) of the p(EtOx), *i.e.* critical conditions (ELSD evaporator temperature: 70 °C).

LACCC chromatograms were further analyzed by MALDI-ToF MS and (after manual fractionation) with ESI-Q-ToF MS/MS for the end group analysis.

3.2.1. Spotting of (p(EtOx)-b-p(oDFOx))

Applying LACCC for a p(EtOx)-*b*-p(oDFOx) block copolymer sample, three signals in the chromatogram were delivered (Fig. 4(a)), which were spotted automatically with the specific spotting settings according to the total elution time onto the MALDI target. An overview about the measured MALDI spectra is shown in Fig. 4(b). As for the other samples analyzed, the MALDI measurement conditions were kept constant for the entire investigations and as shown in Fig. 4(c) the maximum count for three specific *m*/*z* values were chosen. We could observe three distinct regions and the peak assignments will be discussed in the following paragraph. The p(EtOx) amino/ester homopolymer is shown with (★), the copolymer with (★) and the hydroxyl homopolymer p(EtOx) is characterized with (★). We could observe a prominent high ionization for the p(EtOx) amino/ester homopolymer, in comparison to the copolymer and the hydroxyl p(EtOx) homopolymer, where both have a fairly low count.

Peak 1 and peak 3 both correspond to a p(EtOx) homopolymer, and only peak 2 corresponds to the block copolymer. To note from the spots 29–39 both copolymer and homopolymer are observed due to the close elution observed in the chromatogram. In general, in MALDI spectra where copolymers are concerned, many distributions and therefore many peaks are present leading to a time

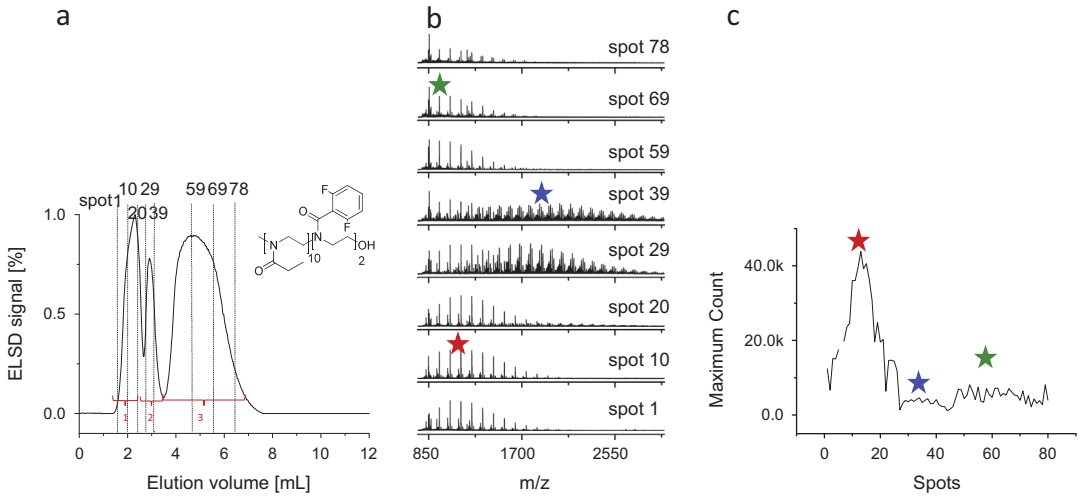

Fig. 4. (a) LACCC chromatogram (p(EtOx)-*b*-p(oDFOx)), (b) stacked MALDI-ToF MS spectra of the spots generated by the Proteineer fc (none normalized) and (c) maximum count at three specific *m*/*z* values. (★ *m*/*z* = 1243, ★ *m*/*z* = 2144, ★ *m*/*z* = 1144).

consuming and many possibilities for peak assignments. Thus, it is obvious that the block copolymer p(EtOx)-*b*-p(*o*DFOx) copolymer elutes in peak 2. The main peaks in the related MALDI spectra can be assigned to the block copolymer with both, a $-CH_3$ and a –OH end group that are ionized with sodium cations, respectively (Fig. 5). Two other distributions can be assigned to p(EtOx)-*b*-p(*o*DFOx) chains that are initiated by a proton (a result from chain transfer reactions during the CROP).

However, the interesting question to be answered is related to the origin of two p(EtOx) homopolymer peaks in the chromatogram (peak 1 and 3). Since the LC analysis was performed under LACCC conditions for p(EtOx) it is unlikely that the p(EtOx) homopolymer is separated due to variations in molar mass. Instead, the significantly different elution behavior should result from different end groups of p(EtOx). At this point benefit could be taken from the hyphenation of the LC system with MALDI-ToF MS since this method does not only allow a determination of the polymer type but, in addition, for an assignment of the polymer end groups. Upon comparison of the corresponding peaks in both spectra (from peaks 1 and 3, respectively) it appears that the main distribution occurs at the same *m*/*z* values, which is contradictory to the elution behavior during the LACCC. The presence of isobaric species would explain this contradiction: During the termination of the CROP with water, the water molecules can quench the cationic species either in 2-position or in 4-position of the oxazolinium ring, which results in the two different end groups that are depicted in Fig. 5(a) and (c) respectively. The mechanism of this formation is shown in Figs. S.4 and S.5 [51].

To rule out which isobaric species corresponds to which peak, another LC run of the sample was performed, and the eluate was fractionated for an off-line analysis by ESI-Q-ToF MS/MS [47]. In this approach, the parent ion of interest (*m*/*z* value of 847.55) was selected in the instrument and fragmented by collision with nitrogen gas (collision induced dissociation). The resulting fragments were subsequently analyzed with respect to *m*/*z* by the TOF detector. Since the two different end groups are fragmented by different end group cleavage mechanisms [52] it was possible to distinguish between the two isobaric species: As assigned in Fig. 5 peak 1 contains p(EtOx) with the amine/ester end group, whereas peak 3 an be associated with p(EtOx)-OH. These results are in accordance with detailed investigations, regarding the separation of both species on a CN column [47].

Thus, to summarize the identification of the observed peaks in the chromatogram the peak a.1. (V_{el} = 2.45 mL) corresponds to the p(EtOx)-amino/ester group, the peak a.2. (V_{el} = 3.09 mL) is from the copolymer: p(EtOx)-*b*-p(*o*DFOx) and finally a.3. (V_{el} = 4.5 mL) relates to p(EtOx)-OH.

Despite the possibility of 'sweet' spots once spotted onto the target (even with an automated system), the intensity of the MALDI spectra nicely increases and decreases for each distribution one after the other, as was the case for the analyzed homopolymers. In comparison to ELSD and MALDI counts (Fig. 5), no correlation could be observed (Fig. 4). This clearly demonstrates the necessity to apply complementary methods for quantification and identification of the eluates. To summarize, the developed method could be well applied for the analysis of a fluorinated sample that contained two different species of one homopolymer and help to clearly assign the observed peaks.

3.2.2. Spotting of (p(EtOx)-b-p(EPOx))

As next step, the spotting of a block copolymer containing a hydrophobic block with branched alkyl substituents (p(EtOx)-*b*-p(EPOx)) was performed to test the versatility of the new method. The chromatogram for p(EtOx)-*b*-p(EPOx) shows two signals with maxima at V_{el} = 2.09 mL (peak 1) and V_{el} = 2.9 mL (peak 2), respectively (Fig. 6(a)). According to the established LACCC conditions, an elution of p(EtOx) homopolymer impurities would be expected at V_{el} = 2.9 mL, which would suggest that the p(EtOx) homopolymer is separated from the copolymer. This is likely because the block copolymer was synthesized by sequential monomer addition with p(EtOx) as the first block. The presence of p(EtOx) homopolymer in the analyzed sample could then be simply explained by a non-quantitative initiation of the second block during the synthesis. As for p(*i*PropOx), the more hydrophobic block copolymer would then elute prior to the hydrophilic p(EtOx), despite the applied RP stationary phase. However, peak 1 displays a slight fronting, which might indicate a co-elution of two different components within the sample, despite the application of critical conditions for one block

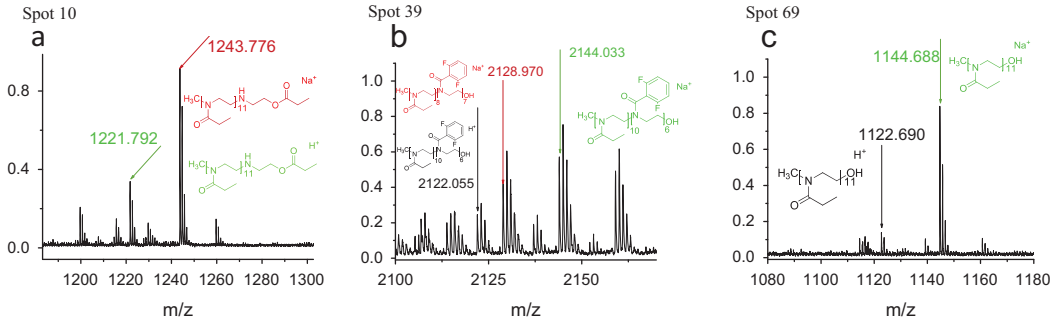

Fig. 5. MALDI-ToF MS spectra of different spots of p(EtOx)-*b*-p(*o*DFOx) and the maximum count for each spot: (a) First spot of the p(EtOx) amino/ester homopolymer, (b) p(EtOx)-*b*-p(*o*DFOx) copolymer and (c) p(EtOx) homopolymer with hydroxyl end group.

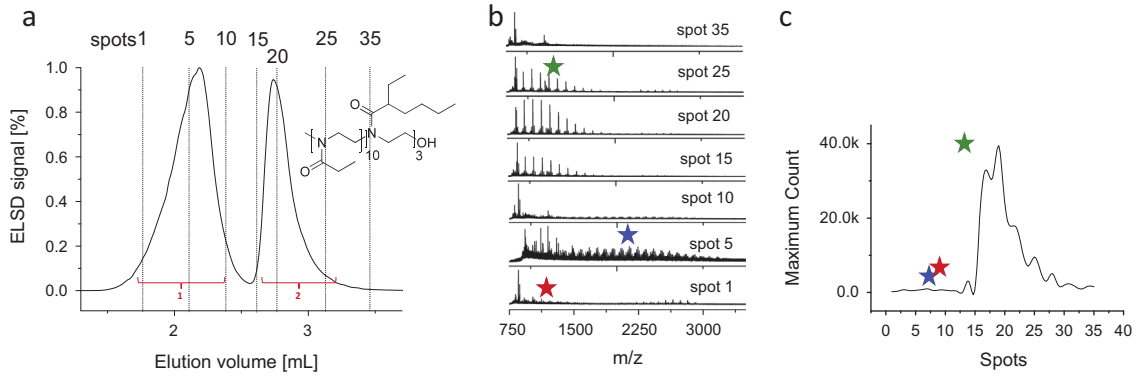

Fig. 6. (a) LACCC chromatogram of p(EtOx)-*b*-p(EPOx), (b) stacked MALDI-ToF MS spectra of the spots generated by the Proteineer fc (none normalized) and (c) maximum counts for each spot at three specific *m*/*z* values. (★ *m*/*z* = 1144, ★ *m*/*z* = 2144, ★ *m*/*z* = 1045).

during the LC analysis. Thus, the application of hyphenation is required to understand fully the elution behavior of the polymer systems. Indeed, once spotted onto the MALDI target three distributions were observed in the stack (Fig. 6(b)). Peak 2 corresponds to a p(EtOx) homopolymer, but in peak 1 the block copolymer and a p(EtOx) homopolymer are co-eluting (Fig. S.3).

Similar to the other p(EtOx) block copolymer, p(EtOx)-*b*-p(EPOx) was fractionated and studied *via* ESI-Q-ToF MS. As a result two fractions resulting from p(EtOx) homopolymer were observed: One eluting at the beginning (peak 1, amine-ester end group) as shown in Fig. S.6 and the other eluting last from the LACCC run (peak 2, –OH end group) as shown in Fig. S.7. The block copolymer was eluting in between both p(EtOx) homopolymers (peak 1). The chromatogram shows that the p(EtOx) with the amino/ester group is co-eluting with the block copolymer. Whilst the block copolymer and the p(EtOx)-OH are also well separated in the chromatogram, the application of the spotting/MALDI technique improved the visibility of the underlying second p(EtOx) species in peak 1. The developed analytical method could even be applied to identify the species involved in the co-eluting peak. However, the interpretation of the resulting MALDI-ToF MS spectra was more difficult compared to the p(EtOx)-*b*-p(EPOx) since some spectra contained more than one species. In addition, all spectra acquired after spotting were recorded with a higher constant laser intensity due to the low concentration of the mixture on the spot in comparison to a normal one spot approach of the whole copolymer where the concentration of copolymer is higher. A comparison of the elugram and the maximum count graph clearly demonstrates that the p(EtOx) homopolymers is much easier ionized than the two co-eluting species (homo- and block copolymer) in peak 1 when the laser intensity is kept constant. However, the block copolymer could still be well detected, even without an adjustment of the MALDI measurement conditions.

Thus, the analysis protocol, which was established for one block copolymer sample, could be easily transferred to a different block copolymer comprising a similar p(EtOx) block but a completely different second block. This encourages the application of the developed analytical method for the investigation of other p(EtOx) containing materials suitable for life science applications.

The results obtained from both block copolymer samples clearly show the necessity for an in depth characterization of fractions eluting from LC of p(EtOx)-based copolymer samples for a correct peak assignment and demonstrate the power of hyphenated MS techniques to fulfill this task.

4. Conclusion

In this study, LACCC was combined with an automated spotting robot to place the samples onto a MALDI target followed by a semi-online hyphenation to MALDI-ToF MS. LACCC is a time-consuming method requiring large quantities of graded HPLC solvents; however, providing extremely important characterization data. The developed workflow allowed a full application of the system in hand in a high-throughput separation and characterization process. The results clearly demonstrate that the CAP of p(EtOx), once determined, cannot be simply applied to assign the resulting peaks from LACCC of the p(EtOx)-*b*-p(EPOx) block copolymer because the elution behavior is strongly dependent on the polymer end group. As a matter of fact "real" samples will not always contain the well-defined end groups of the standards that are applied to identify the CAP. However, the present approach of spotting the eluate and subsequent analysis by MALDI-ToF MS and ESI-Q-ToF MS ascertained to be suitable not only for peak assignments but also for providing a detailed picture of side products, which are correlated to side reactions during the synthesis. Taking into account the large diversity that will be present in p(EtOx)-containing polymers for life science applications, the established analysis protocol was extended to a block copolymer containing a fluorinated block. The results show that multiple dimensions are important to analyze polymer systems in detail. Therefore, this advanced setup represents an important step towards high-throughput multidimensional measurements for complex copolymers and its reproducibility, quantifiability aspect and structurally informative, making it amenable for pharmaceutical polymers. This highly developed

approach can be transferred to other polymer classes as well, which is also very useful for complementing 2D-LC experiments. In case samples contain analytes that require different matrices or salts to be ionized in MALDI-ToF MS measurements, several HPLC runs under identical conditions would have to be performed. Nonetheless, the eluates could be spotted onto the same MALDI target ensuring the analysis of the analyte under optimum conditions in a HTE manner. Finally, and most importantly this allows new ways for an intellectual property (IP) protection and the next steps would be to monitor and the analysis of pharmaceutical polymers and drug loaded carriers.

Acknowledgments

The authors acknowledge the Dutch Polymer Institute (DPI, technology area HTE, project #668) and the Thüringer Ministerium für Bildung, Wissenschaft und Kultur (Grants No. B515-07008 and B715-08011) for financial support of this study. Kristian Kempe is grateful to the Landesgraduiertenförderung Thüringen (Germany) for financial support. Christine Weber is grateful to the Carl-Zeiss foundation. We thank Bruker Daltonics for their help and support.

Appendix A. Supplementary material

Supplementary data associated with this article can be found, in the online version, at http://dx.doi.org/10.1016/j.eurpolymj.2014.07.030.

References

[1] Vollrath A, Schubert S, Schubert US. Fluorescence imaging of cancer tissue based on metal-free polymeric nanoparticles - a review. J Mater Chem B 2013;1(15):1994–2007.
[2] Knop K, Hoogenboom R, Fischer D, Schubert US. Poly(ethylene glycol) in drug delivery: pros and cons as well as potential alternatives. Angew Chem Int Ed 2010;49(36):6288–308.
[3] Lee H, Chang T, Lee D, Shim MS, Ji H, Nonidez WK, et al. Characterization of poly(L-lactide)-*block*-poly-(ethylene oxide)-*block*-poly(L-lactide) triblock copolymer by liquid chromatography at the critical condition and by MALDI-TOF mass spectrometry. Anal Chem 2001;73(8):1726–32.
[4] Adams N, Schubert US. Poly(2-oxazolines) in biological and biomedical application contexts. Adv Drug Delivery Rev 2007;59(15):1504–20.
[5] Hoogenboom R. Poly(2-oxazoline)s: a polymer class with numerous potential applications. Angew Chem Int Ed 2009;48(43):7978–94.
[6] Gaertner FC, Luxenhofer R, Blechert B, Jordan R, Essler M. Synthesis, biodistribution and excretion of radiolabeled poly(2-alkyl-2-oxazoline)s. J Control Release 2007;119(3):291–300.
[7] Mero A, Pasut G, Via LD, Fijten MWM, Schubert US, Hoogenboom R, et al. Synthesis and characterization of poly(2-ethyl 2-oxazoline)-conjugates with proteins and drugs: suitable alternatives to PEG-conjugates? J Control Release 2008;125(2):87–95.
[8] Viegas TX, Bentley MD, Harris JM, Fang Z, Yoon K, Dizman B, et al. Polyoxazoline: chemistry, properties, and applications in drug delivery. Bioconjugate Chem 2011;22(5):976–86.
[9] Luxenhofer R, Schulz A, Roques C, Li S, Bronich TK, Batrakova EV, et al. Doubly amphiphilic poly(2-oxazoline)s as high-capacity delivery systems for hydrophobic drugs. Biomaterials 2010;31(18):4972–9.
[10] http://www.accessdata.fda.gov/scripts/fcnDetailNavigation.cfm?rpt=iaListing&id=2151.
[11] Anhalt JP, Fenselau C. Identification of bacteria using mass spectrometry. Anal Chem 1975;47(2):219–25.
[12] Calleri E, Temporini C, Perani E, De Palma A, Lubda D, Mellerio G, et al. Trypsin-based monolithic bioreactor coupled on-line with LC/MS/MS system for protein digestion and variant identification in standard solutions and serum samples. J Proteome Res 2005;4(2):481–90.
[13] O'Farrell PH. High resolution two-dimensional electrophoresis of proteins. J Biol Chem 1975;250(10):4007–21.
[14] Baumgaertel A, Altuntaş E, Schubert US. Recent developments in the detailed characterization of polymers by multidimensional chromatography. J Chromatogr A 2012;1240:1–20.
[15] Chojnacka A, Kempe K, van de Ven HC, Englert C, Hoogenboom R, Schubert US, et al. Molar mass, chemical-composition, and functionality-type distributions of poly(2-oxazoline)s revealed by a variety of separation techniques. J Chromatogr A 2012;1265:123–32.
[16] Hu L, Ye M, Jiang X, Feng S, Zou H. Advances in hyphenated analytical techniques for shotgun proteome and peptidome analysis – a review. Anal Chimica Acta 2007;598(2):193–204.
[17] Fenn JB. Electrospray wings for molecular elephants (Nobel lecture). Angew Chem Int Ed 2003;42(33):3871–94.
[18] Tanaka K, Waki H, Ido Y, Akita S, Yoshida Y, Yoshida T, et al. Protein and polymer analyses up to *m/z* 100 000 by laser ionization time-of-flight mass spectrometry. Rapid Commun Mass Spectrom 1988;2(8):151–3.
[19] Karas M, Hillenkamp F. Laser desorption ionization of proteins with molecular masses exceeding 10,000 daltons. Anal Chem 1988;60(20):2299–301.
[20] Pasch H. Analysis of complex polymers by interaction chromatography. Springer-Verlag BH; 1997. p. 1–45.
[21] Belenky BG, Gankina ES, Tennikov MB, Vilenchik LZ. Fundamental aspects of adsorption chromatography of polymers and their experimental verification by thin-layer chromatography. J Chromatogr A 1978;147:99–110.
[22] Entelis S, Evreinov V, Gorshkov A. Functionality and molecular weight distribution of telechelic polymers pharmacy/thermomechanics/elastomers/telechelics. Berlin, Heidelberg: Springer; 1986.
[23] Gorbunov AA, Vakhrushev AV. Theory of chromatographic separation of linear and star-shaped binary block-copolymers. J Chromatogr A 2005;1064(2):169–81.
[24] Jiang X, van der Horst A, Lima V, Schoenmakers PJ. Comprehensive two-dimensional liquid chromatography for the characterization of functional acrylate polymers. J Chromatogr A 2005;1076(1–2):51–61.
[25] Girod M, Phan TNT, Charles L. On-line coupling of liquid chromatography at critical conditions with electrospray ionization tandem mass spectrometry for the characterization of a nitroxide-mediated poly(ethylene oxide)/polystyrene block copolymer. Rapid Commun Mass Spectrom 2008;22(23):3767–75.
[26] Voll D, Junkers T, Barner-Kowollik C. A qualitative and quantitative post-mortem analysis: studying free-radical initiation processes via soft ionization mass spectrometry. J Polym Sci, Part A: Polym Chem 2012;50(14):2739–57.
[27] Prokai L, Aaserud DJ, Simonsick Jr WJ. Microcolumn size-exclusion chromatography coupled with electrospray ionization mass spectrometry. J Chromatogr A 1999;835(1–2):121–6.
[28] Prokai L, Simonsick WJ. Electrospray ionization mass spectrometry coupled with size-exclusion chromatography. Rapid Commun Mass Spectrom 1993;7(9):853–6.
[29] Barqawi H, Ostas E, Liu B, Carpentier J-F, Binder WH. Multidimensional characterization of α,ω-telechelic poly(ε-caprolactone)s via online coupling of 2D chromatographic methods (LC/SEC) and ESI-TOF/MALDI-TOF-MS. Macromolecules 2012;45(24):9779–90.
[30] Barner-Kowollik C, Gruendling T, Falkenhagen J, Weidner S. Mass spectrometry in polymer chemistry. 1st ed. Germany: Wiley-VCH Verlag GmbH and Co KGaA-Weinheim; 2012.
[31] Young JB, Li L. Impulse-driven heated-droplet deposition interface for capillary and microbore LC-MALDI MS and MS/MS. Anal Chem 2007;79(15):5927–34.
[32] Zhang B, McDonald C, Li L. Combining liquid chromatography with MALDI mass spectrometry using a heated droplet interface. Anal Chem 2004;76(4):992–1001.
[33] Kassis CE, DeSimone JM, Linton RW, Remsen EE, Lange GW, Friedman RM. A direct deposition method for coupling matrix-assisted laser desorption/ionization mass spectrometry with gel permeation chromatography for polymer characterization. Rapid Commun Mass Spectrom 1997;11(10):1134–8.
[34] Esser E, Keil C, Braun D, Montag P, Pasch H. Matrix-assisted laser desorption/ionization mass spectrometry of synthetic polymers. 4.

Coupling of size exclusion chromatography and MALDI-TOF using a spray-deposition interface. Polymer 2000;41(11):4039–46.
[35] Hensel RR, King RC, Owens KG. Electrospray sample preparation for improved quantitation in matrix-assisted laser desorption/ionization time-of-flight mass spectrometry. Rapid Commun Mass Spectrom 1997;11(16):1785–93.
[36] Axelsson J, Hoberg A-M, Waterson C, Myatt P, Shield GL, Varney J, et al. Improved reproducibility and increased signal intensity in matrix-assisted laser desorption/ionization as a result of electrospray sample preparation. Rapid Commun Mass Spectrom 1997;11(2):209–13.
[37] Hanton SD, Hyder IZ, Stets JR, Owens KG, Blair WR, Guttman CM, et al. Investigations of electrospray sample deposition for polymer MALDI mass spectrometry. J Am Soc Mass Spectrom 2004;15(2):168–79.
[38] Lou X, van Dongen JLJ. Direct sample fraction deposition using electrospray in narrow-bore size-exclusion chromatography/matrix-assisted laser desorption/ionization time-of-flight mass spectrometry for polymer characterization. J Mass Spectrom 2000;35(11):1308–12.
[39] Wetzel SJ, Guttman CM, Flynn KM. The influence of electrospray deposition in matrix-assisted laser desorption/ionization mass spectrometry sample preparation for synthetic polymers. Rapid Commun Mass Spectrom 2004;18(10):1139–46.
[40] Wang Y-X, Zhou Y, Balgley BM, Cooper JW, Lee CS, DeVoe DL. Electrospray interfacing of polymer microfluidics to MALDI-MS. Electrophoresis 2005;26(19):3631–40.
[41] Wang L, May SW, Browner RF, Pollock SH. Low-flow interface for liquid chromatography-inductively coupled plasma mass spectrometry speciation using an oscillating capillary nebulizer. J Anal Atom Spectrom 1996;11(12):1137–46.
[42] Iida T, Kuyama H, Watanabe M, Toda C, Matsuo E-i, Kido A, et al. Rapid and efficient MALDI-TOF MS peak detection of 2 nitrobenzenesulfenyl labeled peptides using the combination of HPLC and an automatic spotting apparatus. J Biol Tech 2006;17:333–41.
[43] Zarei M, Kirsch S, Müthing J, Bindila L, Peter-Katalinić J. Automated normal phase nano high performance liquid chromatography/matrix assisted laser desorption/ionization mass spectrometry for analysis of neutral and acidic glycosphingolipids. Anal Biochem 2008;391(1):289–97.
[44] Lechner M, Seifner A, Rizzi AM. Capillary isoelectric focusing hyphenated to single-and multistage matrix-assisted laser desorption/ionization-mass spectrometry using automated sheath-flow-assisted sample deposition. Electrophoresis 2008;29(10):1974–84.
[45] Nielen MWF. Polymer analysis by micro-scale size-exclusion chromatography/MALDI time-of-flight mass spectrometry with a robotic interface. Anal Chem 1998;70(8):1563–8.
[46] Keil C, Esser E, Pasch H. Matrix-assisted laser desorption/ionization mass spectrometry of synthetic polymers, 5. Analysis of Poly(propylene oxide)s by coupled liquid chromatography at the critical point of adsorption and MALDI-TOF mass spectrometry. Macromol Mate Eng 2001;286(3):161–7.
[47] Baumgaertel A, Weber C, Fritz N, Festag G, Altuntaş E, Kempe K, et al. Characterization of poly(2-oxazoline) homo- and copolymers by liquid chromatography at critical conditions. J Chromatogr A 2011;1218(46):8370–8.
[48] Kempe K, Baumgaertel A, Hoogenboom R, Schubert US. Design of new amphiphilic triblock copoly(2-oxazoline)s containing a fluorinated segment. J Polym Sci, Part A: Polym Chem 2010;48(22):5100–8.
[49] Falkenhagen J, Weidner SM. Detection limits of matrix-assisted laser desorption/ionisation mass spectrometry coupled to chromatography – a new application of solvent – free sample preparation. Rapid Commun Mass Spectrom 2005;19(24):3724–30.
[50] Rosen BM, Wilson CJ, Wilson DA, Peterca M, Imam MR, Percec V. Dendron-mediated self-assembly, disassembly, and self-organization of complex systems. Chem Rev 2009;109(11):6275–540.
[51] Kobayashi S, Masuda E, Shoda S, Shimano Y. Synthesis of acryl- and methacryl-type macromonomers and telechelics by utilizing living polymerization of 2-oxazolines. Macromolecules 1989;22(7):2878–84.
[52] Baumgaertel A, Altuntaş E, Kempe K, Crecelius A, Schubert US. Characterization of different poly(2-oxazoline) block copolymers by MALDI-TOF MS/MS and ESI-Q-TOF MS/MS. J Polym Sci, Part A: Polym Chem 2010;48(23):5533–40.

Supporting Information

Semi-Automated Multi-Dimensional Characterization of Synthetic Copolymers

Sarah Crotty,[a,b,c] Christine Weber,[a,b,c] Anja Baumgaertel,[a,b,c] Nicole Fritz,[a,b,c] Esra Altuntaş,[a,b] Kristian Kempe,[a,b] and Ulrich S. Schubert[a,b,c,*]

Received (in XXX, XXX) Xth XXXXXXXXX 20XX, Accepted Xth XXXXXXXXX 20XX
DOI: 10.1039/b000000x

Notes and references

[a] *Laboratory of Organic and Macromolecular Chemistry (IOMC), Friedrich Schiller University Jena, Humboldstr. 10, 07743 Jena, Germany*

[b] *Jena Center for Soft Matter (JCSM), Friedrich Schiller University Jena, Philosophenweg 7, 07743 Jena, Germany*

[c] *Dutch Polymer Institute (DPI), John F. Kennedylaan 2, AB Eindhoven, The Netherlands*

Experimental

Materials

All solvents were obtained from standard suppliers and used as received if not otherwise noted. *i*PropOx was synthesized and purified similar to a procedure described elsewhere.[1] 2-(2,6-Difluorophenyl)-2-oxazoline (*o*DFOx) and 2-(1-ethyl-pentyl)-2-oxazoline (EPOx) were synthesized as described previously.[2, 3] Acetonitrile (CH_3CN, extra dry) was purchased from Acros Organics and stored over molecular sieves under argon atmosphere. Methyl tosylate (98%, Sigma Aldrich, MeTos) was distilled under reduced pressure and stored under argon. Triethylamine was dried over potassium hydroxide and distilled under argon. The components of the mobile phase for HPLC (2-propanol, water, all HPLC grade) were obtained from Sigma Aldrich.

Synthesis of the p(*iso*-propyl-oxazoline) p(*i*PropOx)

MeTos (0.22 mmol, 42 mg), *i*PropOx (4.2 mmol, 470 mg) and CH_3CN (0.51 mL) were weighed into a pre-dried microwave vial under inert conditions. The monomer concentration was adjusted to 4 $mol \cdot L^{-1}$. The vial was capped and heated to 140 °C for 2.5 min using microwave irradiation. Subsequently, the polymerization was quenched by the addition of acetic acid (1.5 fold excess to initiator, 0.33 mmol, 20 µL) and triethylamine (2-fold excess to initiator, 0.45 mmol, 63 µL). The vials were placed in an oil bath overnight at 40 °C. After completion of the end capping protocol, ^{1}H NMR spectroscopy was used to determine the conversion and the degree of polymerization (DP). The polymers were purified by dissolving the reaction mixture in chloroform and washed with saturated aqueous sodium hydrogen carbonate as well as brine. The organic layer was dried over sodium sulfate and filtered. Subsequently, the chloroform was removed under reduced pressure to yield the final polymer. SEC ($CHCl_3$, RI detection, PS calibration): M_n = 1,360 $g \cdot mol^{-1}$, PDI = 1.04; ^{1}H NMR (300 MHz, $CDCl_3$): DP = 21.5 (corresponding to M_n = 2,450 $g \cdot mol^{-1}$), degree of functionalization with -OAc was 100% according to ^{1}H NMR.

Methods

The polymerization of 2-oxazoline monomers was performed in a Biotage Initiator Sixty microwave synthesizer. ^{1}H NMR spectra were recorded in $CDCl_3$ on a Bruker Avance 300 MHz using the residual solvent resonance as internal standard. For the initial characterization of all polymers, size exclusion chromatography (SEC) was applied using a Shimadzu system

equipped with a SCL-10A VP system controller, a LC-10AD VP pump, and a RID-10A refractive index (RI) detector with a solvent mixture containing chloroform, triethylamine, and isopropanol (94:4:2) at a flow rate of 1 mL·min^{-1} on a PSS-SDV-linear S 5 µm column at 40 °C. The system was calibrated with polystyrene (PS; M_n = 374 to 128,000 g·mol^{-1}) standards.

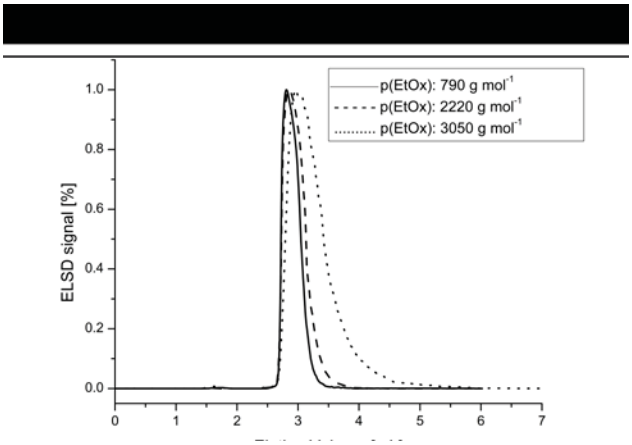

Fig. S.1. LACCC chromatograms of a series poly(2-ethyl-2-oxazoline) homopolymers at mobile phase composition 2-propanol/H_2O = 75/25 (v/v), *i.e.* critical conditions (ELSD evaporator temperature: 70 °C).

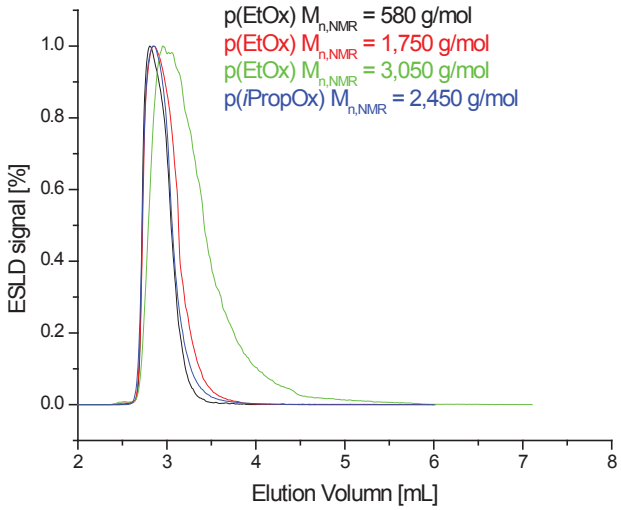

Fig. S.2. Overlay of LC chromatograms of a p(EtOx)s and of p(*i*PropOx) under p(EtOx) LACCC conditions at mobile phase composition 2-propanol/H_2O = 75/25 (v/v), *i.e.* critical conditions (ELSD evaporator temperature: 70 °C).

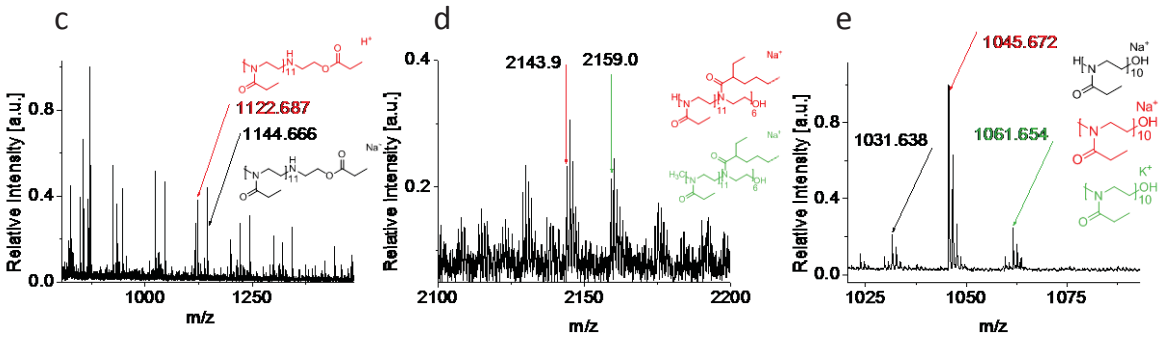

Fig. S.3. MALDI-ToF MS spectra of different spots of p(EtOx)-*b*-p(EPOx): (c, d) First spot the p(EtOx) amine/ester homopolymer and copolymer: p(EtOx)-*b*-p(EPOx), (e) p(EtOx) homopolymer with hydroxyl end group.

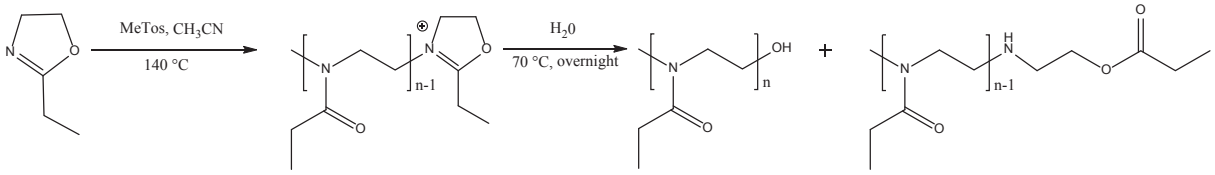

Fig. S.4. Schematic representation of the formation of both end groups.

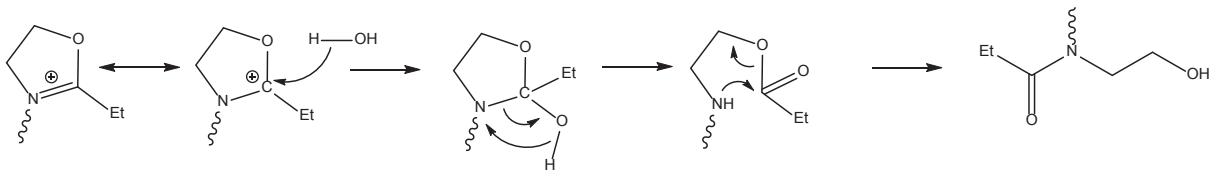

Fig. S.5. Schematic representation of the formation of the hydroxyl end group of the hydroxyl terminated oligo(2-ethyl-2-oxazoline)s.[4]

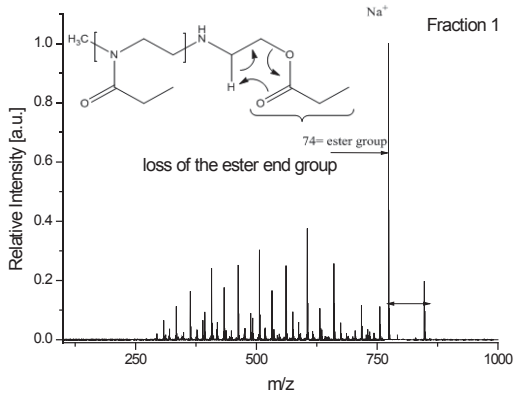

Fig. S.6. ESI-Q-ToF MS/MS spectra of the p(EtOx)-*b*-p(EPOx) of peak 1.

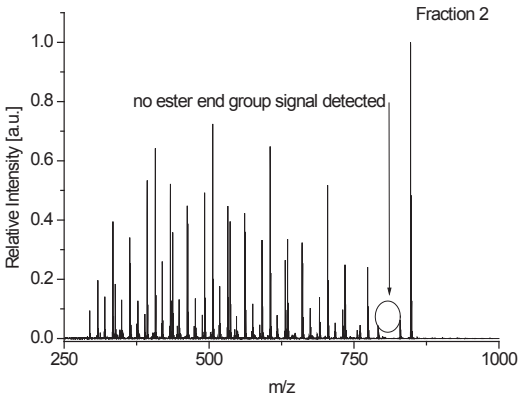

75

76 Fig. S.7. ESI-Q-ToF MS/MS spectra of the p(EtOx)-*b*-p(EPOx) of peak 2.

77

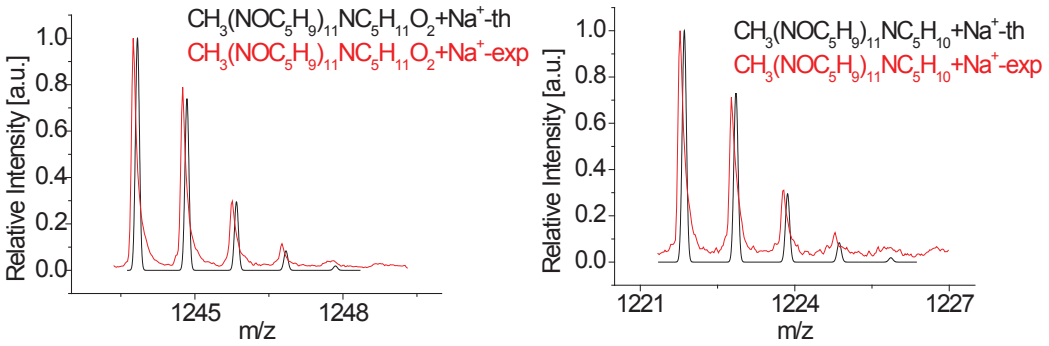

78

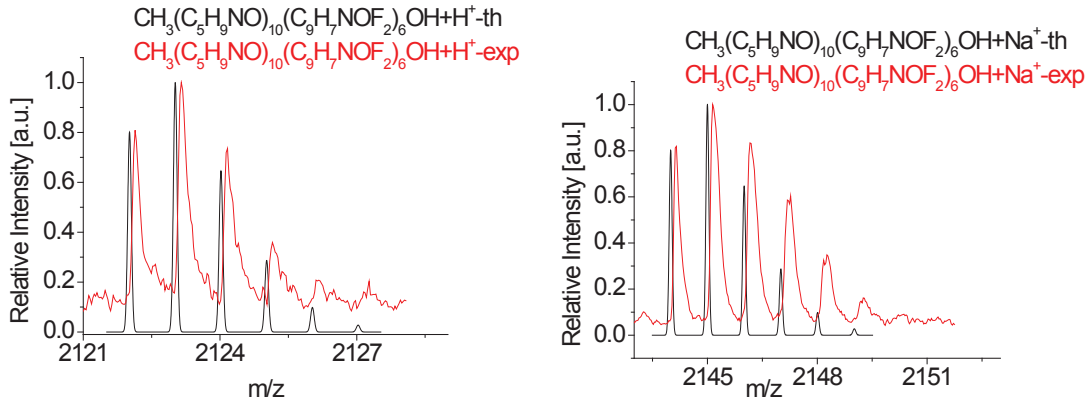

79

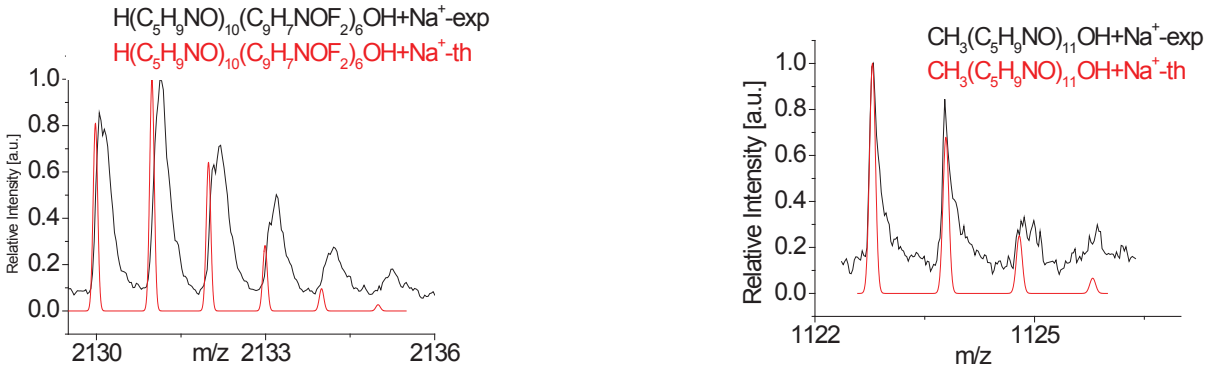

80

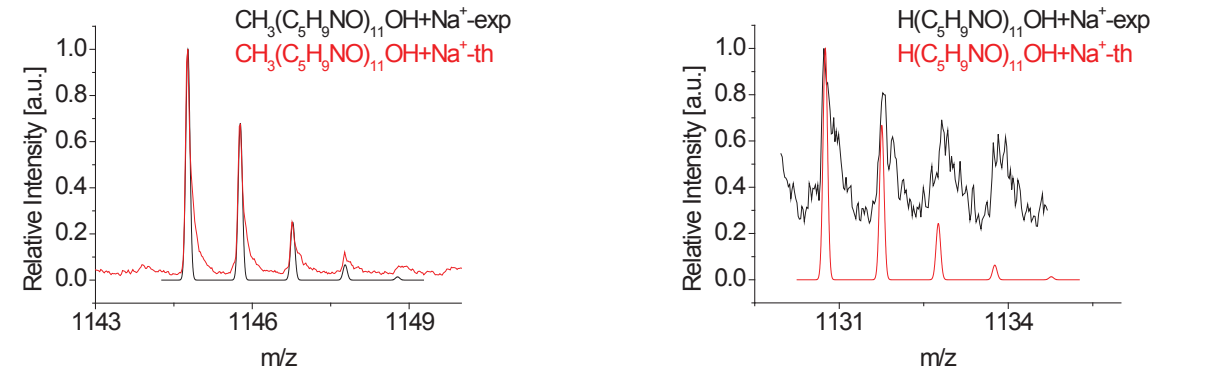

81

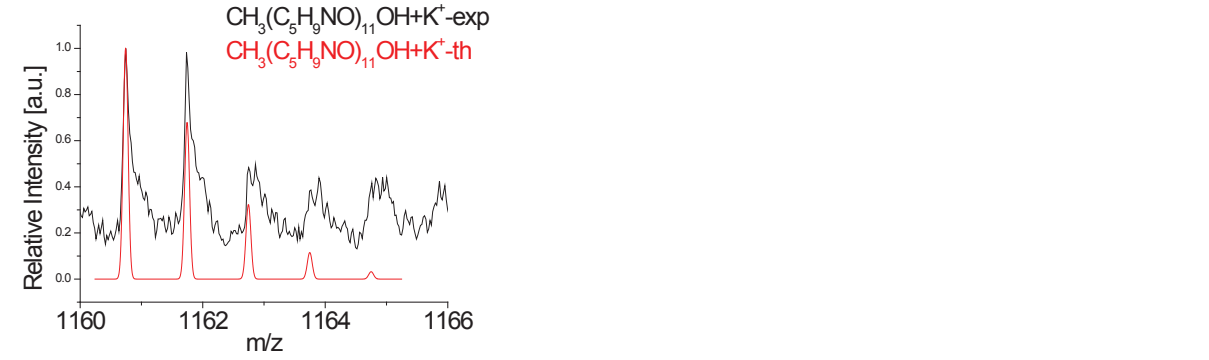

82

83 Fig. S.8. Isotopic patterns for (p(EtOx)-*b*-p(oDFOx).

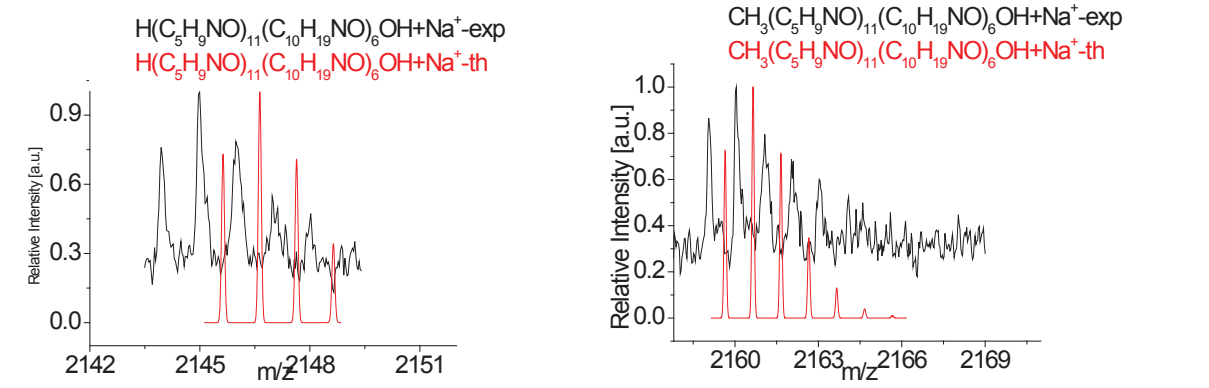

84

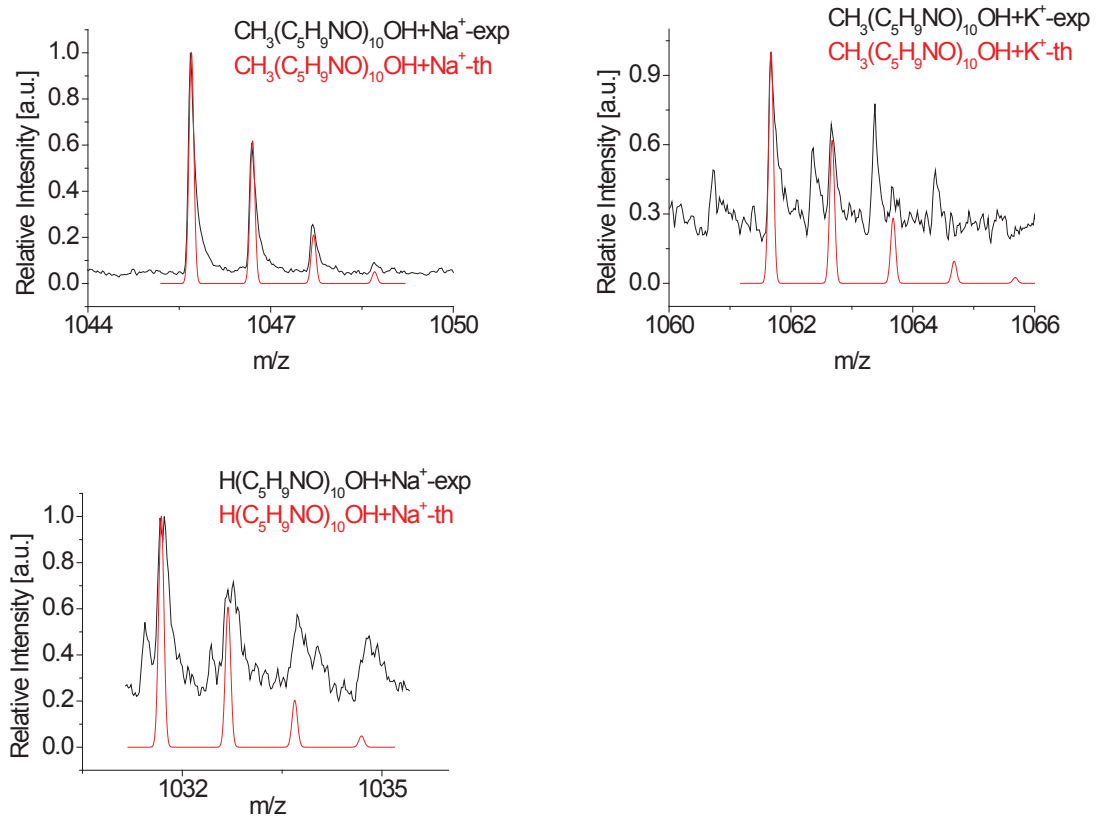

Fig. S.9. Isotopic patterns for (p(EtOx)-*b*-p(EPOx).

References

[1] Baumgaertel A, Weber C, Fritz N, Festag G, Altuntaş E, Kempe K, Hoogenboom R, Schubert US. Characterization of poly(2-oxazoline) homo- and copolymers by liquid chromatography at critical conditions. J Chromatogr, A 2011;1218(46):8370-78.

[2] Weberskirch R, Preuschen J, Spiess HW, Nuyken O. Design and synthesis of a two compartment micellar system based on the self-association behavior of poly(N-acylethyleneimine) end-capped with a fluorocarbon and a hydrocarbon chain. Macromol Chem Phys 2000;201(10):995-1007.

[3] Lutz J-F, Laschewsky A. Multicompartment Micelles: Has the Long-Standing Dream Become a Reality? Macromol Chem Phys 2005;206(8):813-17.

[4] Kobayashi S, Masuda E, Shoda S, Shimano Y. Synthesis of acryl- and methacryl-type macromonomers and telechelics by utilizing living polymerization of 2-oxazolines. Macromolecules 1989;22(7):2878-84.

Publication 8

COCONUT − an efficient tool for estimating copolymer compositions from mass spectra

M. S. Engler,[#] S. Crotty,[#] M. J. Barthel, C. Pietsch, K. Knop,
U. S. Schubert, S. Boecker

Anal. Chem. **2015**, *57*, 5223-5231.

[#] both contributed equally to this work

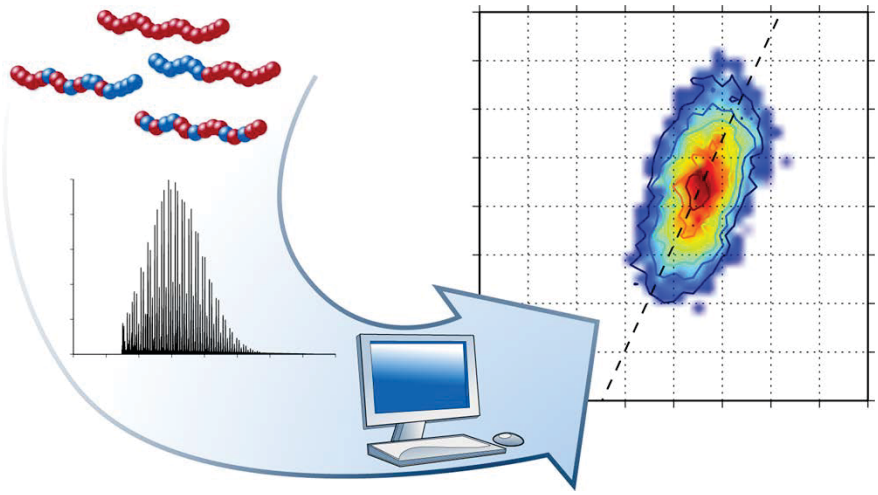

analytical chemistry

Article

pubs.acs.org/ac

COCONUT—An Efficient Tool for Estimating Copolymer Compositions from Mass Spectra

Martin S. Engler,[†] Sarah Crotty,[‡,¶] Markus J. Barthel,[‡,¶,∥] Christian Pietsch,[‡,¶] Katrin Knop,[‡,¶] Ulrich S. Schubert,[‡,¶] and Sebastian Böcker*[,†,¶]

[†]Chair of Bioinformatics, Friedrich Schiller University Jena, Ernst-Abbe-Platz 2, 07743 Jena, Germany

[‡]Laboratory of Organic and Macromolecular Chemistry (IOMC), Friedrich Schiller University Jena, Humboldtstr. 10, 07743 Jena, Germany

[¶]Jena Center for Soft Matter (JCMS), Friedrich Schiller University Jena, Philosophenweg 7, 07743 Jena, Germany

Supporting Information

ABSTRACT: The accurate characterization of synthetic polymer sequences represents a major challenge in polymer science. Matrix-assisted laser desorption/ionization time-of-flight mass spectrometry (MALDI-TOF MS) is frequently used for the characterization of copolymer samples. We present the COCONUT software for estimating the composition distribution of the copolymer. Our method is based on Linear Programming and is capable of automatically resolving overlapping isotopes and isobaric ions. We demonstrate that COCONUT is well suited for analyzing complex copolymer MS spectra. COCONUT is freely available and provides a graphical user interface.

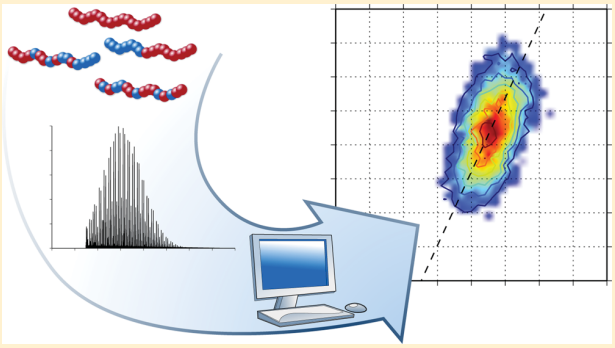

Mass spectrometry (MS) is increasingly used for analyzing synthetic polymers,[1] utilizing soft ionization techniques, such as matrix-assisted laser desorption/ionization (MALDI),[2] electrospray ionization, or atmospheric pressure chemical ionization. MS techniques can highlight different features of polymers such as molecular weight distribution[3] or end-groups.[4] MS is frequently used to determine compositional drift,[5] or the average composition,[6−10] which then can be verified by other techniques, such as nuclear magnetic resonance (NMR).

Quantifying the relative abundances of copolymers in a sample provides insightful information: Wilczek-Vera et al.[11] introduced the copolymer composition matrix, representing the relative abundance of all compositions of monomers. The copolymer composition matrix provides information about the copolymer architecture,[12,13] the distribution of block lengths in block copolymers,[11,14−16] or the reactivity ratio of the consumed monomers.[17] It has been used to study degradation[10] and MALDI matrix effects.[18] The composition matrix is related to the bivariate distribution of monomer ratio and degree of polymerization, which can be used to highlight compositional drift.[9,19,20]

Here, we focus on linear copolymer architectures. Several assignment methods have been introduced to estimate the copolymer composition matrix from MS data.[10−18] For these methods, the abundance of each copolymer molecule is assigned to the height of some measured peak, being closest to the most abundant theoretical isotope peak for this copolymer. However, this approach has certain drawbacks:[14,21] First, since peak shapes change with increasing mass, abundance of the molecule is not correlated to the peak height but to the area of the peak. However, for very high masses above the reported masses in this publication, peak resolution becomes poorer. For such mass regions, peak intensities should be used. Second, overlapping isotopes of different copolymers may result in imprecise polymer abundance assignments. Third, isobaric molecules may prohibit to resolve copolymer abundances.

Weidner et al.[22,23] presented a method to determine the copolymer composition matrix using liquid adsorption chromatography at critical condition (LACCC) MS measurements. By using intensity information from chromatography, the authors evade the nonlinear relationship between MS signals and molecule abundances. Fractions are separately analyzed and assembled in silico to form single composition matrices. Unfortunately, LACCC-MS is time-consuming, and critical conditions have to be known for at least one of the polymers. Vivó-Truyols et al.[21] presented a regression method to determine the copolymer composition from a single MS measurement. The method fits peak curves to the raw data, and can resolve overlapping isotopes. Because fitting the complete MS spectrum is computationally expensive, the method

Received: January 12, 2015
Accepted: April 17, 2015
Published: April 17, 2015

DOI: 10.1021/acs.analchem.5b00146
Anal. Chem. 2015, 87, 5223−5231

truncates the spectrum into strips. This truncation complicates quantification of isotopes on the strip borders.

In this contribution, we propose a method to infer the copolymer composition matrix from a single MS measurement. Our method uses peak areas instead of peak heights, and can handle overlapping isotopes. We also propose an approach to resolve isobaric molecules, which is a frequently occurring issue in copolymer MS. To the best of our knowledge, this has previously been possible only by using complementary measurements, such as NMR investigations.

We demonstrate the validity of our method using several synthesized copolymers measured with MALDI time-of-flight (TOF) MS. To evaluate our method's power to resolve isotope overlaps and isobaric molecules, we have simulated mass spectra for different monomers. We evaluate our software to the approach of Vivó-Truyols et al.,[21] which is the most recent for this problem. Our method is implemented in the COCONUT (Copolymer Composition Numbering Tool) software, which is provided free and open-source, and offers a graphical user interface.

COMPUTATIONAL METHODS

Overview. In the first step of our method, we centroid the spectra, that is, we identify peaks and their area-under-peak. We do not provide details for this approach, as it has been discussed extensively in the literature. For the following steps of our analysis, we will use the representation of the spectrum as a list of peaks and peak areas, as this allows us faster processing of the data. To reduce noise, we remove peaks below a certain threshold. We assume that all molecules in the MALDI spectrum are singly-charged. The *mass range* is the interval from the smallest mass to the largest mass of any observed peak, but can be further restricted if required. Further, we assume that the absolute mass error in the measured spectrum is at most $\Delta_m < 0.5\ m/z$; we will call this fixed Δ_m the *mass accuracy*. This implies that measured peaks can be uniquely assigned to one theoretical peak of an isotopic pattern. To simplify our presentation, we assume that the mass of the initiating and terminating end-groups plus cationization agent is a constant which is ignored in our presentation: As a consequence, the mass of a monomer composition A_iB_j is the sum of its monomer masses $m = i{\cdot}m_A + j{\cdot}m_B$.

Different compositions of monomer repeating units A and B can result in copolymers with similar monoisotopic masses. To this end, we often observe peaks with multiple potential explanations. We define two monomer compositions as *isobaric* if the difference of their monoisotopic masses is less than the mass accuracy. In this case, mass differences of the peaks of the theoretical isotope patterns for these two monomer compositions will usually be smaller than the mass accuracy, too. As the last step of our method, we present an approach for untangling the isotope patterns of isobaric monomer compositions. But even if the monoisotopic masses of two monomer compositions is above the mass accuracy, it is possible that some isotope peaks of their theoretical isotope patterns have mass difference below the mass accuracy. We say that two isotope patterns are *overlapping*, if there exist two peaks in the patterns with mass difference below the mass accuracy.

Our method estimates relative abundances of all possible monomer compositions A_iB_j in the MS spectrum. It proceeds in four steps: (i) Generate all candidate isotopic patterns; (ii) assign candidate peaks to the MS spectrum; (iii) compute the abundances and simultaneously resolve overlapping isotopes; and (iv) resolve isobaric molecules.

Candidate Generation. We first compute theoretical isotope distributions for all monomer compositions A_iB_j with monoisotopic mass within the mass range. We compute the first n peaks of each isotope pattern by convolving the elemental isotopic distributions.[24]

Next, we identify isobaric monomer compositions. Consider the monomer compositions A_iB_j and $A_{i-\Delta i}B_{j+\Delta j}$ for natural numbers $i,j \geq 0$ and $\Delta i, \Delta j > 0$. Masses m_1 and m_2 of these two monomer compositions are:

$$m_1 = i{\cdot}m_A + j{\cdot}m_B$$
$$m_2 = (i - \Delta i){\cdot}m_A + (j + \Delta j){\cdot}m_B \quad (1)$$

Recall that two monomer compositions are isobaric if their mass difference is less than the mass error, $|m_1 - m_2| < \Delta_m$. Substituting m_1 and m_2 using eq 1 we infer $|\Delta i{\cdot}m_A - \Delta j{\cdot}m_B| < \Delta_m$. Thus, given $\Delta j > 0$, any natural number $\Delta i > 0$ with

$$\frac{\Delta j{\cdot}m_B - \Delta_m}{m_A} < \Delta i < \frac{\Delta j{\cdot}m_B + \Delta_m}{m_A} \quad (2)$$

leads to isobaric monomer compositions A_iB_j and $A_{i-\Delta i}B_{j+\Delta j}$. This is independent of the choice of $i,j \geq 0$. To this end, we call any such tuple $(\Delta i, \Delta j)$ an *isobaric series*.

We determine all isobaric series; then, we use the isobaric species to arrange the monomer compositions (and, hence, the corresponding isotope patterns) into isobaric sets. For each monomer composition A_iB_j, we iterate over all isobaric series $(\Delta i, \Delta j)$. If there is another monomer composition $A_{i-\Delta i}B_{j+\Delta j}$ within the mass range, these two are grouped into the same isobaric set. Note that an isobaric set can also contain only a single monomer composition. For each isobaric set, we compute an average isotope pattern for all the theoretical isotope patterns of the monomer compositions in the isobaric set; this will be our *candidate* isotope patterns. In the following, we assume that for any isobaric set, abundances for all monomer compositions but one are set to zero during fitting the matrix. We will split abundances of these monomer compositions in Resolving Isobaric Molecules section.

Template Matching. In this step, we want to assign the candidate isotope pattern peaks to the measured peaks in the experimental MS spectrum. However, measured peaks with a distance less than Δ_m can lead to ambiguous assignments: These peaks may be caused by overlapping raw peaks, or errors during the centroiding (usually caused by shoulder peaks) which have been falsely identified as separate peaks. Thus, we assume centroids with a distance less than Δ_m to originate from one continuous peak area, and merge them. The mass of the merged peak is the area-weighted average of the masses of its component peaks. The area of the new peak is the sum of areas of its components. Naturally, we may accidentally merge two actually separate peaks or signal with noise peaks. However, the estimation of the composition in the next step is robust toward this kind of error, and noisy data in general.

Each measured peak is now assigned to zero, one, or several peaks of the candidate isotope patterns. We match an isotope pattern peak to a measured peak if their distance is less than Δ_m. Formally, let $m'_{i,j,k}$ be the mass and $I'_{i,j,k}$ the intensity of the kth peak in the isotopic pattern of monomer composition A_iB_j. Let m_l and I_l be the mass and area under curve of the l th measured peak. Then, the set of matching peaks is:

DOI: 10.1021/acs.analchem.5b00146
Anal. Chem. 2015, 87, 5223−5231

$$S_l = \{(i, j, k): |m_l - m'_{i,j,k}| < \Delta_m\} \quad (3)$$

We define S_0 as the set of all unmatched candidate peaks:

$$S_0 = \{(i, j, k): \text{there is no } l \text{ with } (i, j, k) \in S_l\} \quad (4)$$

These sets form a partition of all candidate isotope pattern peaks.

Composition Estimation. We now describe how to estimate the composition matrix. For each monomer composition A_iB_j we want to find the matrix of relative abundances R, with $0 \le R_{i,j} \le 1$, which minimizes the distance of its theoretical isotopic pattern to the assigned measured peaks. Formally, we solve the following optimization problem:

$$\arg\min_R \sum_l \left| \sum_{(i,j,k)\in S_l} R_{i,j}\cdot I'_{i,j,k} - I_l \right| + \sum_{(i,j,k)\in S_0} R_{i,j}\cdot I'_{i,j,k} \quad (5)$$

The first term of 5 tries to minimize the distance of the measured area under peak I_l to all its matching potentially overlapping candidate peaks, that is, the sum of polymer abundance times theoretical isotopic intensities $R_{i,j}\cdot I'_{i,j,k}$. The second term of 5 considers all candidate isotope peaks that have no matching measured peak. Since these are not represented in the spectrum and, hence, should also not exist in the model, we minimize the distance of the sum of their intensities times polymer abundance $R_{i,j}\cdot I'_{i,j,k}$ to a zero peak area.

The number of free parameters $R_{i,j}$ is determined by the number of possible template isotope patterns, which increases quadratic in mass: There exist $m + 1$ compositions of two monomers for a given integer mass $m = i\cdot A + j\cdot B$.[25] The sum of all compositions with integer mass at most m can be estimated by $\sum_{k=1}^{m}(k + 1) = ((m(m + 3))/2) \in O(m^2)$.

We efficiently solve this high-dimensional optimization problem by transforming it to a linear program (LP). We introduce distance coefficients, d_0 for the unmatched theoretical peaks and a coefficient d_l for each measured peak. Then, solving the linear program

$$\min \quad \sum_l d_l$$

$$\text{s.t.} \quad \sum_{(i,j,k)\in S_l} R_{i,j}\cdot I'_{i,j,k} + d_l \ge I_l \;\forall\, l \quad (6a)$$

$$\sum_{(i,j,k)\in S_l} R_{i,j}\cdot I'_{i,j,k} - d_l \le I_l \;\forall\, l \quad (6b)$$

$$\sum_{(i,j,k)\in S_0} R_{i,j}\cdot I'_{i,j,k} + d_0 \ge 0 \quad (6c)$$

$$\sum_{(i,j,k)\in S_0} R_{i,j}\cdot I'_{i,j,k} - d_0 \le 0 \quad (6d)$$

estimates the optimal abundances $R_{i,j}$. We omitted the upper and lower limit constraints for all coefficients. Constraints 6a and 6b correspond to the first term of 5, and constraints 6c and 6d to the second term. In case there are isobaric monomer compositions with $R_{i,j} > 0$, we will resolve them in the next step.

Resolving Isobaric Molecules. Isobaric monomer compositions have almost identical monoisotopic mass, so there are competing possible explanations for certain measured peaks. Given any two isobaric monomer compositions, then the differences in isotope abundances of the corresponding theoretical isotopic patterns are usually too small to split the measured abundances. Therefore, we suggest an alternate approach to split corresponding entries in the composition matrix R. Obviously, this is not necessary if there are no isobaric monomer compositions present.

Our task is to split abundances $R_{i,j}$ that correspond to more than one monomer composition, that is, that belong to isobaric sets with two or more elements. It has been suggested repeatedly that distributions of polymer abundances follow some common probability distribution such as Poisson distribution or Schulz–Zimm distribution. Wilczek-Vera et al.[11] suggested that monomer composition abundances can be modeled by a suitable bivariate distribution, and also suggested to use Poisson or Schulz–Zimm distributions as the marginal distributions. To simplify our computations, we further approximate this using a normal distribution: For example, the Poisson distribution $P(\lambda)$ with parameter λ can be approximated by a normal distribution $\mathcal{N}(\lambda, (\lambda)^{1/2})$. The joint distribution of two normal distributions is a bivariate normal distribution. We now use the bivariate normal distribution to split abundances of isobaric sets with more than one monomer composition.

In principle, we may do this splitting by the following procedure: (1) Estimate the mean $\mu = (\mu_1,\mu_2)$ and covariance matrix Σ of the bivariate normal distribution $F = \mathcal{N}(\mu, \Sigma)$ from the matrix R. In the first round, we consider only those entries of R where the corresponding isobaric set has cardinality one. (2) Do the following for each isobaric set B of cardinality two or more: Let r be the sum of abundances of all monomer compositions in B. Now, we distribute this abundance over all monomer compositions in B:

$$R_{i,j} := \frac{F(i, j)}{\sum_{(x,y)\in B} F(x, y)}\cdot r \quad (7)$$

Repeat this until R converges. We found that this approach is often too slow in practice; to this end, we instead use a general purpose optimizer[26] that combines both of these steps (estimating the bivariate normal and splitting the abundances) into one. We leave out the tedious technical details.

EXPERIMENTAL METHODS

Overview. We evaluated our method on two different data sets. First, we synthesized three different random copolymers (Figure 1), consisting of two macromers with both a different ratio of styrene and isoprene (Tables 1, 2). We measured the first macromers (**I1** to **I3**) and the complete (PS-*r*-PI)-*r*-(PS-*r*-PI) copolymers (**P1** to **P3**). Second, to assess the accuracy of our method, we evaluated it with simulated data sets, as this is the only way to compare the result to a know ground truth. We

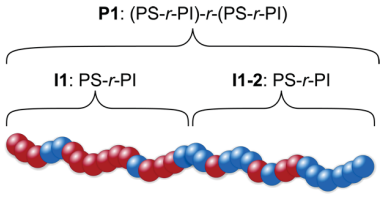

Figure 1. Schematic representation of the synthesized (PS-*r*-PI)-*r*-(PS-*r*-PI) copolymer **P1**. **P2** and **P3** have the same architecture, but different PS to PI ratios.

DOI: 10.1021/acs.analchem.5b00146
Anal. Chem. 2015, 87, 5223–5231

Table 1. Summary of Theoretical Values of Each First Macromer

	I1		I2		I3	
	PS	PI	PS	PI	PS	PI
percent [%]	80	20	70	30	60	40
molar mass [g mol^{-1}]	2000	500	1750	750	1500	1000
DP	19	7	17	11	14	15
mass (monomer) [g]	0.79	0.19	0.71	0.30	0.58	0.41
volume (monomer) [mL]	0.87	0.28	0.78	0.44	0.64	0.60

Table 2. Summary of Theoretical Values of Each Second Macromer

	I1−2		I2−2		I3−2	
	PS	PI	PS	PI	PS	PI
percent [%]	20	80	30	70	40	60
molar mass [g mol^{-1}]	500	2000	750	1750	1000	1500
DP	5	29	7	26	10	22
mass (monomer) [g]	0.21	0.79	0.29	0.71	0.42	0.60
volume (monomer) [mL]	0.23	1.16	0.32	1.04	0.46	0.88

simulated PMMA-*co*-P*n*BA and PMMA-*co*-PHEMA spectra as numerous overlapping isotopes and isobaric molecules appear in these copolymers.

Materials and Polymerization Procedures. The first (**I1**, **I2**, **I3**) and second macromers (**I1−2**, **I2−2**, **I3−2**) are constituted of a random copolymer of styrene and isoprene.[27] The copolymers (**P1**, **P2**, **P3**) were synthesized in Schlenk tubes under dry argon atmosphere. Solvents were dried over sodium/benzophenone and freshly distilled. Isoprene was dried over sodium whereas styrene was dried over calcium hydride. Both monomers were freshly distilled before reaction. *sec*-Butyllithium (1.4 mol in hexane) was used as received. All chemicals were obtained from Aldrich. The Schlenk flasks were heated and dried under vacuum and each filled with 10 mL of cyclohexane and 0.09 mL (1.2 mmol) of tetrahydrofuran as randomizer. To the solution, 0.29 mL of *sec*-butylithium solution (0.4 mmol) was added and allowed to stir for 15 min resulting in a slightly pink solution. Subsequently, each flask was heated to 40 °C, and the monomer mixtures (Table 1) for the first macromer were added. After it was stirred for 1.5 h, the second monomer mixture (Table 2) was added for the formation of the second macromer.[27] Theoretical molar masses (Mn) of 5000 g mol^{-1} (2500 g mol^{-1} for each macromer) were targeted and 2 g of final product were aimed for. Differences between the theoretical and observed values for the DP in particular for isoprene can be explained by the difficult handling of the monomer, the related inaccurate added volume and the Ag^+ cluster suppression in the MS spectra. All copolymers showed PDI values lower than 1.1, indicating a living character of the polymerization. All molar masses (Mn) of **I1** to **I3** were obtained in the range of 2500 g mol^{-1} and **P1** to **P3** of 5000 g mol^{-1} using a polystyrene calibration. **I1**: M_n = 2310 g mol^{-1}. **I2**: M_n = 1960 g mol^{-1}. **I3**: M_n = 2153 g mol^{-1}. **P1**: M_n = 4546 g mol^{-1}. **P2**: M_n = 4058 g mol^{-1}. **P3**: M_n = 4380 g mol^{-1}.

Instrumentation. ^{1}H NMR spectra were recorded on a Bruker AC 300 MHz. Size exclusion chromatography was performed on either a Shimadzu SCL-10 A system (with a LC-10AD pump, a RID-10A refractive index detector, and a PL gel 5 μm mixed-D column at 25 °C) where the eluent was a mixture of chloroform:triethylamine/isopropanol (94:4:2) with a flow rate of 1 mL/min. The system was calibrated with PS standards purchased from PSS Standard.

An Ultraflex III TOF/TOF (Bruker Daltonics, Bremen, Germany) was used for the MALDI-TOF-MS analysis. The instrument was equipped with a Nd:YAG laser and a collision cell. All spectra were measured in the positive reflector mode. The instrument was calibrated prior to each measurement with an external standard PMMA from PSS Polymer Standards Services GmbH (Mainz, Germany). MS data were processed using PolyTools 1.0 (Bruker Daltonics) and Data Explorer 4.0 (Applied Biosystems). Before applying our computational methods for estimating the copolymer composition, the spectra were centroided and baseline-corrected. The compositions were estimated using the COCONUT software.

Sample Preparation. For the sample preparation, all polymers (10 mg mL^{-1}) in chloroform, dithranol (50 mg mL^{-1}) in chloroform, and silver trifluoroacetate (AgTFA) dissolved in chloroform at a concentration of 100 mg mL^{-1} were mixed and the dried-droplet sample preparation method was applied.

Simulating Mass Spectra. To compare our results against some ground truth, we have to simulate mass spectra. Although we can not simulate all aspects of the physical processes of an MS instrument, we have tried to capture several fundamental aspects. We start by simulating a composition matrix; here, we use five bivariate normal distributions with randomly chosen parameters (Supporting Information Table S1). Given the composition matrix, we iterate over all monomer compositions: We add the appropriate end groups, and simulate the first 12 peaks of the isotope pattern, estimating both intensities and mean peak masses.[24] We disturb each isotope peak by adding normally distributed noise with mean zero and variance $\sigma/2$ to the masses, and multiplying intensities by log-normal distributed random noise with mean zero and variance σ, where the noise parameter σ is given below. For an isotope peak with mass m and intensity I, we add a Gaussian function with mean m, variance 1/5, and height (multiplier) I to the simulated spectrum. We then sample this spectrum at sampling points with mass difference 0.1 Da. Finally, this sampled (discretized) spectrum is again perturbed using multiplicative noise following a log-normal distribution with mean zero and variance $\sigma/2$.

We simulated spectra for copolymers PMMA-*co*-P*n*BA and PMMA-*co*-PHEMA. Here, PMMA-*co*-P*n*BA results in a large number of overlapping isotope patterns, whereas PMMA-*co*-PHEMA results in many isobaric molecules. To demonstrate that our method can resolve overlapping isotopes and isobaric monomer compositions, we simulated noise-free spectra with σ = 0. To evaluate the robustness of our method, we additionally use four noise levels σ = 0.05, 0.1, 0.2, 0.5. For each copolymer, all five composition matrices and all five noise levels, we simulated five mass spectra; resulting in 250 spectra in total.

RESULTS AND DISCUSSION

Experimental (PS-*r*-PI)-*r*-(PS-*r*-PI). The shown materials were synthesized by living anionic polymerization, which is widely used with other monomers such as ethylene oxide (EO), allyl glycidyl ether (AGE), (meth)acrylate, etc. This polymerization technique produces well-defined polymers with low polydispersity index values, which is required for MS analysis to ionize all polymer chains. The chosen copolymers have also

DOI: 10.1021/acs.analchem.5b00146
Anal. Chem. 2015, 87, 5223−5231

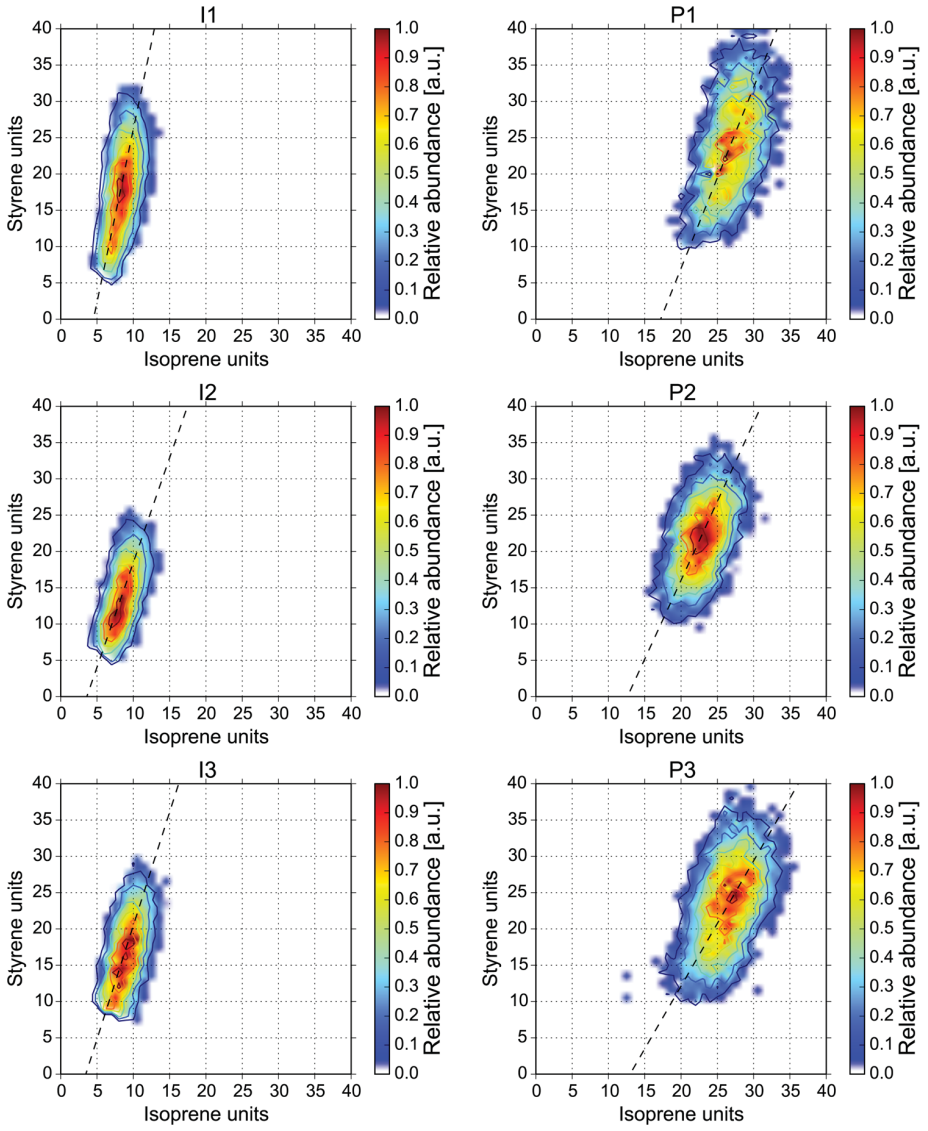

Figure 2. Copolymer composition matrix of the (PS-*r*-PI) macromers **I1** to **I3** (left) and the final (PS-*r*-PI)-*r*-(PS-*r*-PI) copolymers **P1** to **P3** (right).

been used as potential membranes applications when having high molar masses.[28−30]

Copolymers were synthesized with two random macromers with different ratios of styrene and isoprene (Figure 1), analyzed by MALDI-TOF MS (Supporting Information Figure S3) and the COCONUT software (Supporting Information Figure S4). The estimated composition matrices (Figure 2) were transformed to distributions of chain sizes and compositions (Figure 3) by calculating the isoprene ratios and interpolating them for each antidiagonal of the composition matrix. They show a compositional drift, indicating a high conversion rate, since the distribution is not symmetric with respect to the monomer fractions.[19]

Table 3 shows the theoretical ratios between styrene and isoprene in the first macromer and the complete copolymer, the values obtained by ^{1}H NMR and the ratios estimated from the composition matrices (Figure 2). The maximal value in the matrix correlates to the highest intensity in the MS spectrum. It is thus the maximum of the copolymer distribution, the M_p value. We computed the M_n value by taking the average of the marginal distributions of the composition matrices (Supporting Information Figure S5). The COCONUT and ^{1}H NMR values are slightly lower than the theoretical values for both monomers, which may be due to some deactivation of the initiator by impurities in the solvent and also the challenging usage of isoprene. The M_n values of COCONUT and ^{1}H NMR are in a good correlation for the first macromer and are slightly shifted for the entire copolymers because of Ag^+ clusters. The clusters form when Ag^+ is used as cationization agent and thus ion suppression was used to have less interference with the polymer signal.

Nevertheless, a living character of the polymerization can be assumed as well-defined polymers with a narrow molar mass distribution were obtained (Supporting Information Figure S1). Isoprene as a monomer has three different microstructures (cis/trans: 1,4-:1,2-:3,4), where the 1,4 regiospecificity is mostly abundant. The different microstructures can induce slight errors in the NMR spectra (Supporting Information Figure S2).[31] In addition, when THF was added to act as a randomizer, we did observe overlapping isotopes in the MS spectra and multiple

DOI: 10.1021/acs.analchem.5b00146
Anal. Chem. 2015, 87, 5223−5231

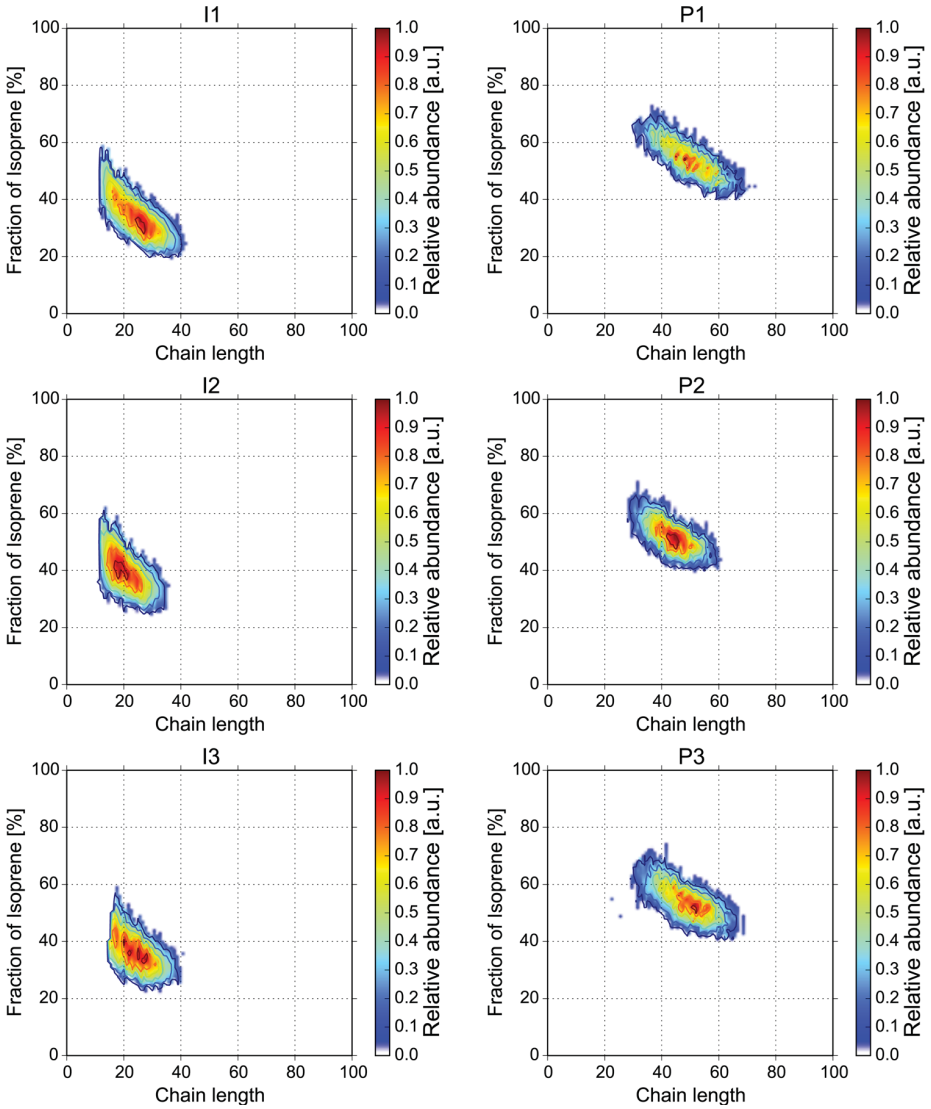

Figure 3. Copolymer composition as a function of degree of polymerization and the ratio of isoprene of the (PS-*r*-PI) macromers **I1** to **I3** (left) and the final (PS-*r*-PI)-*r*-(PS-*r*-PI) copolymers **P1** to **P3** (right).

Table 3. Summary of M_n and M_p Values

	theoretical		M_n (^{1}H NMR)		M_n (COCONUT)		M_p (COCONUT)	
	PS	PI	PS	PI	PS	PI	PS	PI
I1	19	7	17	9	17.4	8.2	17	8
I2	17	11	12.5	11	13.7	8.3	11	8
I3	14	15	16	13	16.7	8.9	18	9
P1	24	36	21	35	23.6	26.6	25	26
P2	24	37	21	29	21.7	22.5	22	22
P3	24	37	22	33	23.1	26.0	24	26

isobaric distributions in the composition matrix. As shown in Figure 4 overlapping isotopes were resolved. Moreover, for each copolymer, one isobaric distribution was determined by our method, which we confirmed by comparing both average monomer composition from NMR and COCONUT (Table 3).

Huijser et al.,[12] Staal,[32] and Willemse[33] suggested a quick way to provide an indication of the microstructure from the slope of a line, fitted through the composition matrix. In reference to the composition matrices from **I1** to **I3** (Figure 2), we can observe straight lines, which correlate to a block like structure. However, we expected a random copolymer, where the line should go through the origin with a constant slope. Possibly due to intensity deviations in the high m/z range the origin of the line could have a slight offset, which explains the uncertainty in the microstructure determination. However, this deviation could also occur during the synthesis where THF

DOI: 10.1021/acs.analchem.5b00146
Anal. Chem. 2015, 87, 5223−5231

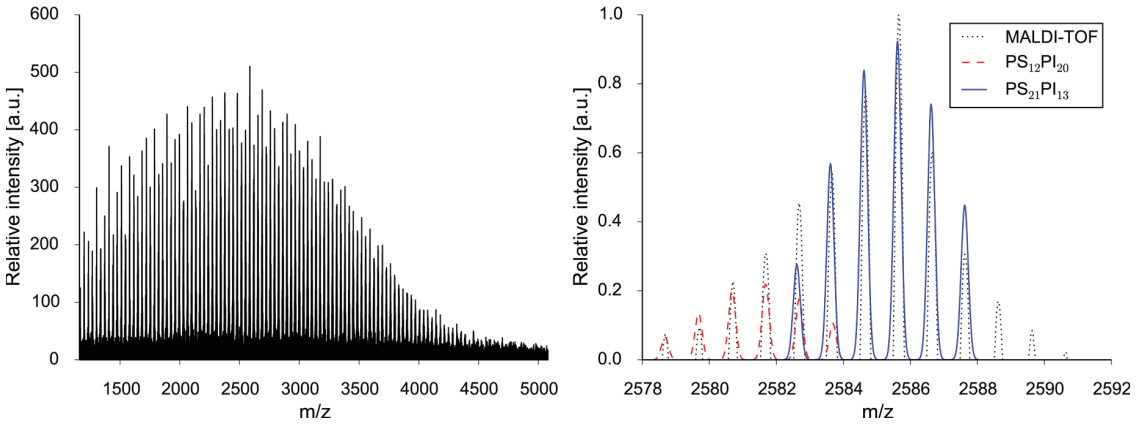

Figure 4. Left: MALDI-TOF spectrum of the (PS-*r*-PI) copolymer **I1**. Right: Detail of the spectrum overlaid with the estimated theoretical isotopes. We used six isotopic peaks per pattern to estimate the abundances.

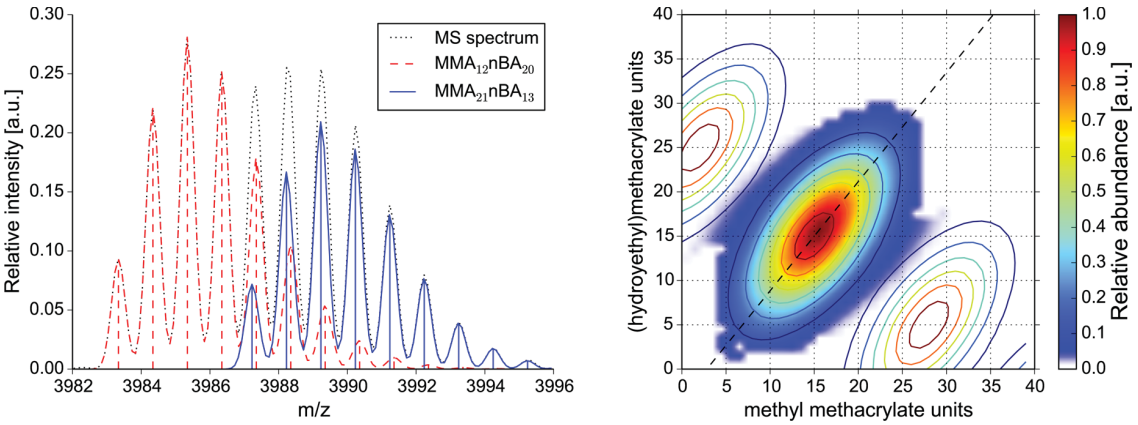

Figure 5. Left: Detail of the simulated MS spectrum of PMMA-*co*-P*n*BA showing overlapping isotopes. The relative molecule abundances estimated by COCONUT are represented by the centroid intensities. Right: Copolymer composition matrix estimated from a simulated MS spectrum of a PMMA-*co*-PHEMA copolymer overlaid with all isobaric distributions (contours).

is considered as randomizer. Nonetheless the **P1** to **P3** do correlate to block like structures as was desired.

Simulated PMMA-*co*-P*n*BA/PMMA-*co*-PHEMA. First, we analyzed two noise-free spectra of PMMA-*co*-P*n*BA and PMMA-*co*-PHEMA using COCONUT with intensity threshold 0.05. The abundances of the overlapping isotopes in PMMA-*co*-P*n*BA spectrum were correctly calculated (Figure 5). The distribution was almost perfectly reconstructed, only isotopes below the intensity threshold were not considered by our method and, thus, lost (Supporting Information Figure S6). In the simulated spectrum of PMMA-*co*-PHEMA (Supporting Information Figure S7), there exist three neighboring isobaric distributions that may explain the data; from these, COCONUT chose the correct distribution located in the center of the composition matrix (Figure 5). Both simulations indicate that our method can reconstruct the true copolymer distribution, given that the input spectrum is free of noise.

To assess the robustness of our method we use the second simulated data set with noise. We stress that for noise parameter $\sigma = 0.5$, resulting signal-to-noise ratios are below 50% on average, resulting in very challenging instances for any quantification method. We also applied the "strip-based regression" (SBR) method[21] to this simulated data set. To the best of our knowledge, this is the only freely available software for this purpose; at the same time, it is the newest approach reported in the literature and, hence, arguably the most advanced to date.

We evaluated results by calculating the Pearson correlation coefficient of each estimated composition matrices against the original composition matrix (Figure 6). For each method, noise level and data set, we calculated the median over all coefficients. We find that for both data sets, our method is capable of

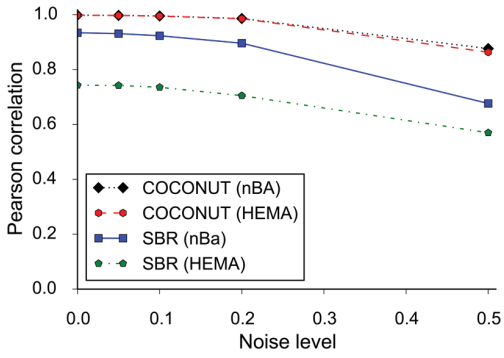

Figure 6. Median Pearson correlation coefficient for each method and copolymer data set, PMMA-*co*-P*n*BA and PMMA-*co*-PHEMA, at five different noise levels.

DOI: 10.1021/acs.analchem.5b00146
Anal. Chem. 2015, 87, 5223−5231

reconstructing the correct composition matrix with very high accuracy (Pearson correlation close to one) for noise parameter up to 0.2. Only for noise parameter σ = 0.5, we observe a significant deviation between estimated and original composition matrix. We see a similar pattern for the SBR method, with no significant correlation differences for noise parameter between 0 and 0.2, and a pronounced drop for noise parameter σ = 0.5. But SBR reaches smaller Pearson correlation for both copolymers: for PMMA-*co*-P*n*BA correlation is between 0.89 and 0.93, and for PMMA-*co*-PHEMA it is between 0.70 and 0.74, leaving out noise parameter σ = 0.5. Examining the composition matrices calculated by SBR for individual spectra, it appears that SBR cannot redistribute abundances of isobaric monomer compositions, what explains the decreased Pearson correlation for PMMA-*co*-PHEMA copolymers.

On average, COCONUT required 8.7 s per PMMA-*co*-P*n*BA spectrum, and 46.0 s per PMMA-*co*-PHEMA spectrum. The difference was caused by the numerous isobaric isotopes, which had to be resolved in the second data set. SBR required an average of 203.2 s per spectrum for both data sets.

Software. Our software called COCONUT (Copolymer Composition Numbering Tool) was implemented in the Groovy language and runs on the Java platform. It is freely available for download at http://bio.informatik.uni-jena.de/software/coconut. The core is formed by efficient algorithms for calculating the isotope patterns, estimating the copolymer composition and resolving isobaric species. It is distributed with the free open source LP solver lp_solve (http://sourceforge.net/projects/lpsolve/). Our software also supports the efficient commercial Gurobi LP solver (Gurobi Optimization, Inc., Houston, USA). Furthermore, we included algorithms for spectral preprocessing (peak smoothing, centroiding and baseline correction) based on the routines implemented in the open source MS framework MzMine 2.[34]

COCONUT combines these algorithms with a user-friendly interface (Supporting Information Figure S8). At the starting point of an analysis, the user can choose to import either a previously centroided or a raw MS spectrum. If necessary, noise in the raw signal peaks can be reduced by smoothing them with a Savitzky−Golay filter.[35] Baseline bias and noise peaks are filtered by a baseline correction and setting an intensity threshold. The raw spectrum is then centroided by estimating the area under the curve of the detected peaks. To calculate the copolymer composition, the molecular formulas of the monomers and initiating, as well as terminating end-groups plus cationization agent are required. If there are isobaric species, the program resolves them automatically.

The supported file formats include, among others, the open standards mzML and mzXML for mass spectra and the Open Document, as well as the Excel format for the copolymer compositions. Graphics can be exported as bitmaps.

CONCLUSIONS

Mass spectrometry has become an indispensable tool for analyzing copolymers. Copolymer spectra are highly complex and contain numerous peaks. Often occurring challenges include isobaric species, overlapping isotopes, background noise, and peak shape perturbations. Computational methods have proven to be a remarkable efficient tool to counteract these recurring troublesome points. We have presented a robust algorithm to estimate composition matrices of linear copolymers from any type of MS spectra. A remaining open challenge in quantifying copolymers from single mass spectra is mass and composition-dependent ionization.

In this contribution, we have demonstrated the power of our tool COCONUT using several synthesized copolymers. In addition, we have evaluated our software on simulated data sets, as this is the only way to compare the result to a known ground truth. We demonstrated COCONUT is swift and accurate for the simulated spectra. We argue that COCONUT is well suited for complex copolymer spectra, as we strove to incorporate their characteristic features in the simulated spectra.

COCONUT is freely available for polymer scientists to investigate composition and linear architectures for designing smart polymers. Our software fulfills chemists demand for computational support in an efficient manner.

ASSOCIATED CONTENT

Supporting Information

Additional information as noted in text. This material is available free of charge via the Internet at http://pubs.acs.org.

AUTHOR INFORMATION

Corresponding Author

*E-mail: sebastian.boecker@uni-jena.de.

Present Address

[‖]M.J.B.: Drug Discovery and Development Department, Istituto Italiano di Tecnologia (IIT), via Morego 30, 16163 Genova, Italy

Author Contributions

M.S.E. and S.C. contributed equally to this work

Notes

The authors declare no competing financial interest.

ACKNOWLEDGMENTS

Funding by the Thüringer Ministerium für Bildung, Wissenschaft und Kultur (Grants B515-07008, 12038-514) and the Ernst-Abbe Stiftung. We thank Bruker Daltonics for help and support, Dr. Gabriel Vivó-Truyols for providing the SBR software, and Alexander Meier for his help with the polymerization experiments.

REFERENCES

(1) Montaudo, M. S. *Mass Spectrom Rev.* **2002**, *21*, 108−144.
(2) Pasch, H., Schrepp, W., Eds. *MALDI-TOF Mass Spectrometry of Synthetic Polymers*; Springer: Berlin, 2003.
(3) Guttman, C. M.; Blair, W. R.; Danis, P. O. *J. Polym. Sci., Part B: Polym. Phys.* **1997**, *35*, 2409−2419.
(4) Crecelius, A. C., Schubert, U. S. *Mass Spectrometry in Polymer Chemistry*; Wiley-VCH Verlag GmbH & Co. KGaA: Weinheim, Germany, 2011; pp 281−318.
(5) Montaudo, M. S. *J. Am. Soc. Mass Spectrom.* **2004**, *15*, 374−384.
(6) Montaudo, M. S.; Montaudo, G. *Makromol. Chem., Macromol. Symp.* **1993**, *65*, 269−278.
(7) Montaudo, M. S.; Puglisi, C.; Samperi, F.; Montaudo, G. *Macromolecules* **1998**, *31*, 8666−8676.
(8) Alhazmi, A. M.; Mayer, P. M. *Rapid Commun. Mass Spectrom.* **2007**, *21*, 3392−3394.
(9) Zagar, E.; Krzan, A.; Adamus, G.; Kowalczuk, M. *Biomacromolecules* **2006**, *7*, 2210−2216.
(10) Kasperczyk, J.; Li, S.; Jaworska, J.; Dobrzynski, P.; Vert, M. *Polym. Degrad. Stab.* **2008**, *93*, 990−999.
(11) Wilczek-Vera, G.; Danis, P. O.; Eisenberg, A. *Macromolecules* **1996**, *29*, 4036−4044.
(12) Huijser, S.; Staal, B. B. P.; Huang, J.; Duchateau, R.; Koning, C. E. *Biomacromolecules* **2006**, *7*, 2465−2469.

DOI: 10.1021/acs.analchem.5b00146
Anal. Chem. 2015, 87, 5223−5231

(13) Huijser, S.; Staal, B. B. P.; Huang, J.; Duchateau, R.; Koning, C. E. *Angew. Chem., Int. Ed.* **2006**, *45*, 1521−3773.
(14) Wilczek-Vera, G.; Yu, Y.; Waddell, K.; Danis, P. O.; Eisenberg, A. *Rapid Commun. Mass Spectrom.* **1999**, *13*, 764−777.
(15) Wilczek-Vera, G.; Yu, Y.; Waddell, K.; Danis, P. O.; Eisenberg, A. *Macromolecules* **1999**, *32*, 2180−2187.
(16) Willemse, R. X. E.; Staal, B. B. P.; Donkers, E. H. D.; van Herk, A. M. *Macromolecules* **2004**, *37*, 5717−5723.
(17) Huijser, S.; Mooiweer, G. D.; van der Hofstad, R.; Staal, B. B. P.; Feenstra, J.; van Herk, A. M.; Koning, C. E.; Duchateau, R. *Macromolecules* **2012**, *45*, 4500−4510.
(18) Terrier, P.; Buchmann, W.; Cheguillaume, G.; Desmazières, B.; Tortajada, J. *Anal. Chem.* **2005**, *77*, 3292−3300.
(19) Montaudo, M. S.; Montaudo, G. *Macromolecules* **1999**, *32*, 7015−7022.
(20) Montaudo, M. S. *Macromolecules* **2001**, *34*, 2792−2797.
(21) Vivó-Truyols, G.; Staal, B.; Schoenmakers, P. J. *J. Chromatogr. A* **2010**, *1217*, 4150−4159.
(22) Weidner, S.; Falkenhagen, J.; Krueger, R.-P.; Just, U. *Anal. Chem.* **2007**, *79*, 4814−4819.
(23) Weidner, S. M.; Falkenhagen, J.; Maltsev, S.; Sauerland, V.; Rinken, M. *Rapid Commun. Mass Spectrom.* **2007**, *21*, 2750−2758.
(24) Böcker, S.; Letzel, M.; Lipták, Zs.; Pervukhin, A. *Bioinformatics* **2009**, *25*, 218−224.
(25) Böcker, S.; Lipták, Zs. *Algorithmica* **2007**, *48*, 413−432.
(26) Powell, M. J. D. *The BOBYQA Algorithm for Bound Constrained Optimization without Derivatives*; Department of Applied Mathematics and Theoretical Physics, Centre for Mathematical Sciences: Cambridge, U.K., 2009
(27) Nakahara, A.; Satoh, K.; Kamigaito, M. *Polym. Chem.* **2012**, *3*, 190−197.
(28) Schacher, F.; Ulbricht, M.; Müller, A. H. E. *Adv. Funct. Mater.* **2009**, *19*, 1040−1045.
(29) Phillip, W. A.; Dorin, R. M.; Werner, J.; Hoek, E. M. V.; Wiesner, U.; Elimelech, M. *Nano Lett.* **2011**, *11*, 2892−2900.
(30) Schacher, F.; Rudolph, T.; Wieberger, F.; Ulbricht, M.; Müller, A. H. E. *ACS Appl. Mater. Interfaces* **2009**, *1*, 1492−1503.
(31) Worsfold, D. J.; Bywater, S. *Can. J. Chem.* **1964**, *42*, 2884−2892.
(32) Staal, B. Characterization of (co)polymers by MALDI-TOF-MS, Ph.D. Thesis, University of Technology Eindhoven, the Netherlands, 2005.
(33) Willemse, R. X. E. *New Insights into Free-Radical (Co) Polymerization Kinetics*. Ph.D. thesis, University of Technology Eindhoven2005.
(34) Pluskal, T.; Castillo, S.; Villar-Briones, A.; Oresic, M. *BMC Bioinf.* **2010**, *11*, 395.
(35) Savitzky, A.; Golay, M. J. E. *Anal. Chem.* **1964**, *36*, 1627−1639.

DOI: 10.1021/acs.analchem.5b00146
Anal. Chem. 2015, 87, 5223−5231

Supporting information for:

COCONUT — An Efficient Tool for Estimating Copolymer Compositions from Mass Spectra

Martin S. Engler,[†,§] Sarah Crotty,[‡,¶,§] Markus J. Barthel,[‡,¶,‖] Christian Pietsch,[‡,¶] Katrin Knop,[‡,¶] Ulrich S. Schubert,[‡,¶] and Sebastian Böcker[*,†,¶]

Chair of Bioinformatics, Laboratory of Organic and Macromolecular Chemistry, and Jena Center for Soft Matter, Friedrich Schiller University Jena, Germany

E-mail: sebastian.boecker@uni-jena.de

[*]To whom correspondence should be addressed

[†]Chair of Bioinformatics, Friedrich Schiller University Jena, Ernst-Abbe-Platz 2, 07743 Jena, Germany

[‡]Laboratory of Organic and Macromolecular Chemistry (IOMC), Friedrich Schiller University Jena, Humboldtstr. 10, 07743 Jena, Germany

[¶]Jena Center for Soft Matter (JCMS), Friedrich Schiller University Jena, Philosophenweg 7, 07743 Jena, Germany

[§]Contributed equally to this work

[‖]Present address: Drug Discovery and Development Department, Istituto Italiano di Tecnologia (IIT), via Morego 30, 16163 Genova, Italy

Table S1: Parameters of the simulated composition matrices used for evaluation. The five bivariate normal distributions were generated with randomly chosen parameters (means μ uniformly drawn from $[6, 22]$, variances σ uniformly drawn from $[2, 6]$, shape ρ uniformly drawn from $[-0.5, 0.5]$).

	μ_A	μ_B	σ_A	σ_B	ρ
1	11.0	9.0	2.4976131963448998	2.3899262596580195	-0.4501784953590977
2	6.0	12.0	2.532897843117028	4.349914949331601	0.40217536504947726
3	8.0	9.0	3.5328177424903933	2.8424627024892173	0.25925811791731745
4	19.0	13.0	5.192975793306746	4.12753685222484	0.2624095395236721
5	13.0	10.0	5.571620004044149	5.313466676925163	-0.05731275108645284

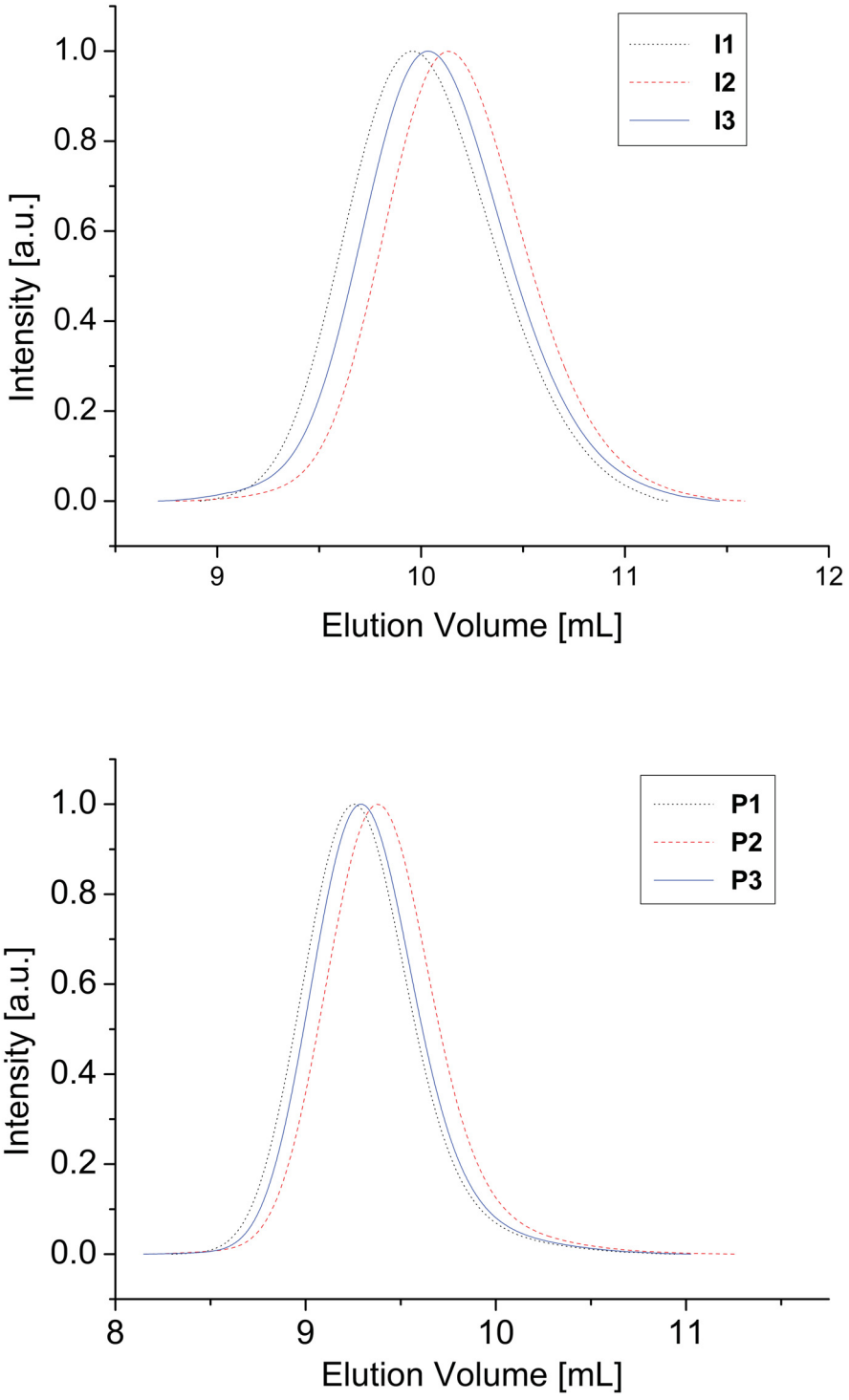

Figure S1: SEC curves of the (PS-*r*-PI) macromers **I1 to I3** (top) and the final (PS-*r*-PI)-*r*-(PS-*r*-PI) copolymers **P1 to P3** (bottom).

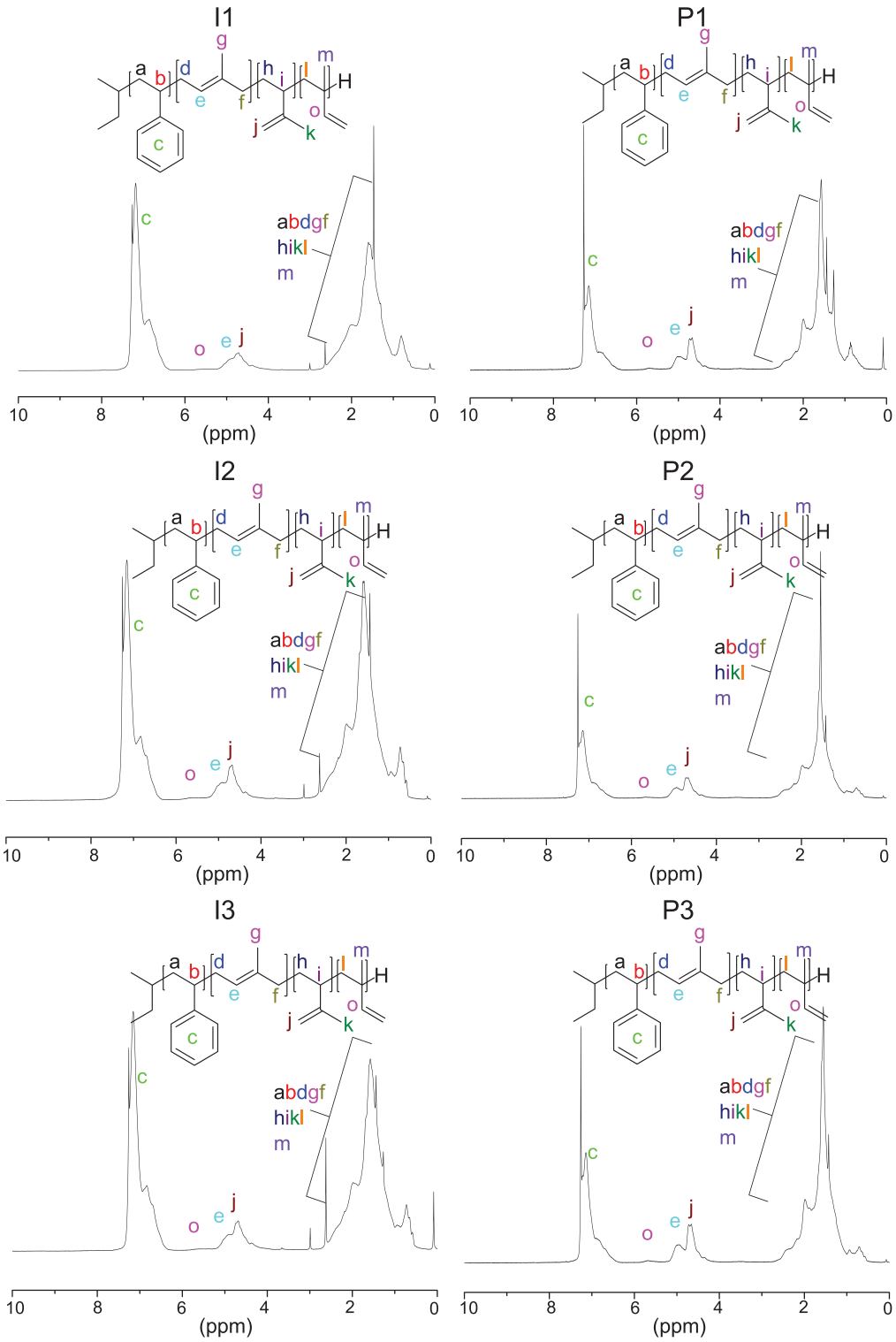

Figure S2: NMR spectra of the (PS-*r*-PI) macromers **I1 to I3** (left) and the final (PS-*r*-PI)-*r*-(PS-*r*-PI) copolymers **P1 to P3** (right).

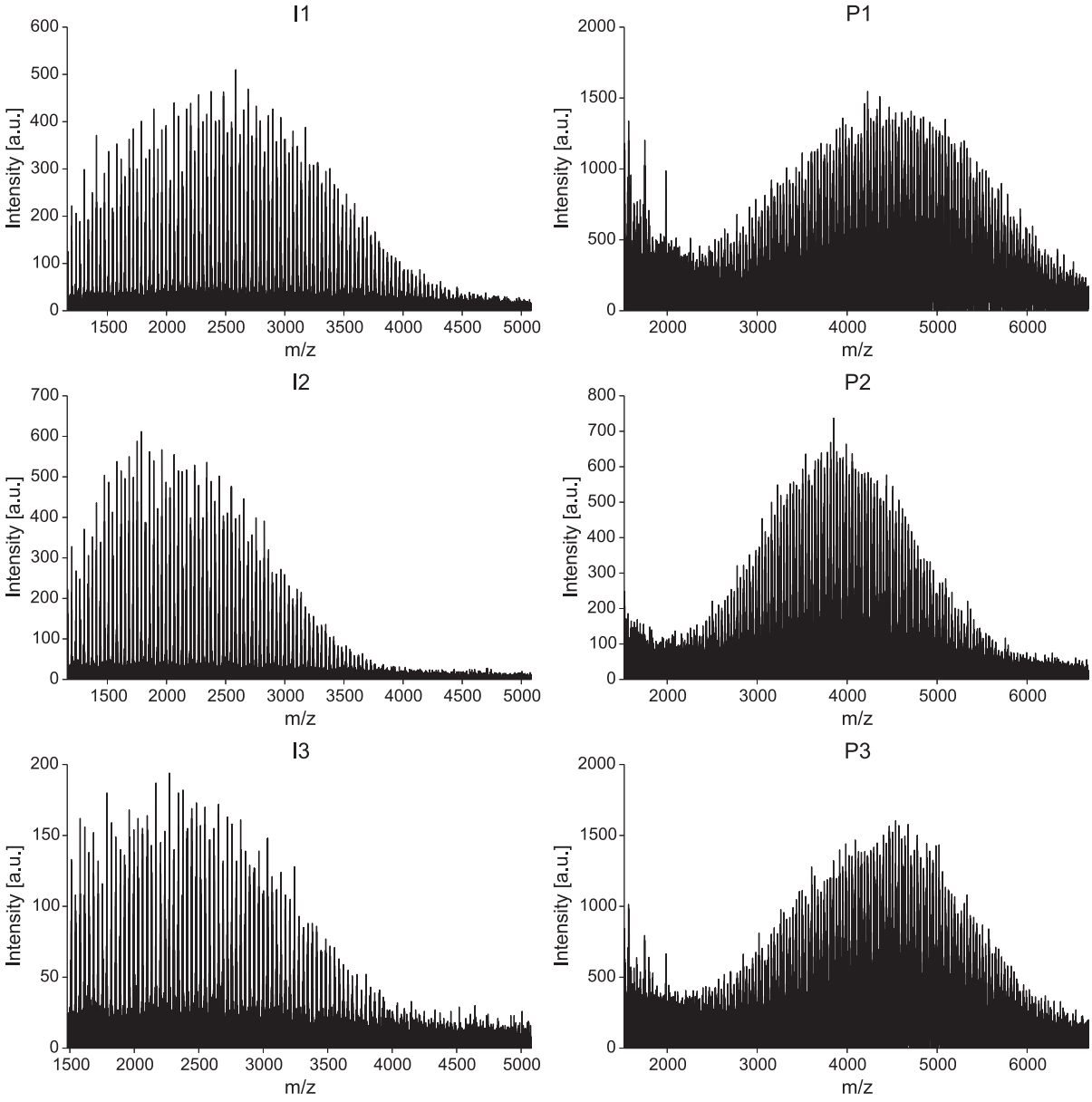

Figure S3: MALDI-TOF spectra of the (PS-*r*-PI) macromers **I1 to I3** (left) and the final (PS-*r*-PI)-*r*-(PS-*r*-PI) copolymers **P1 to P3** (right).

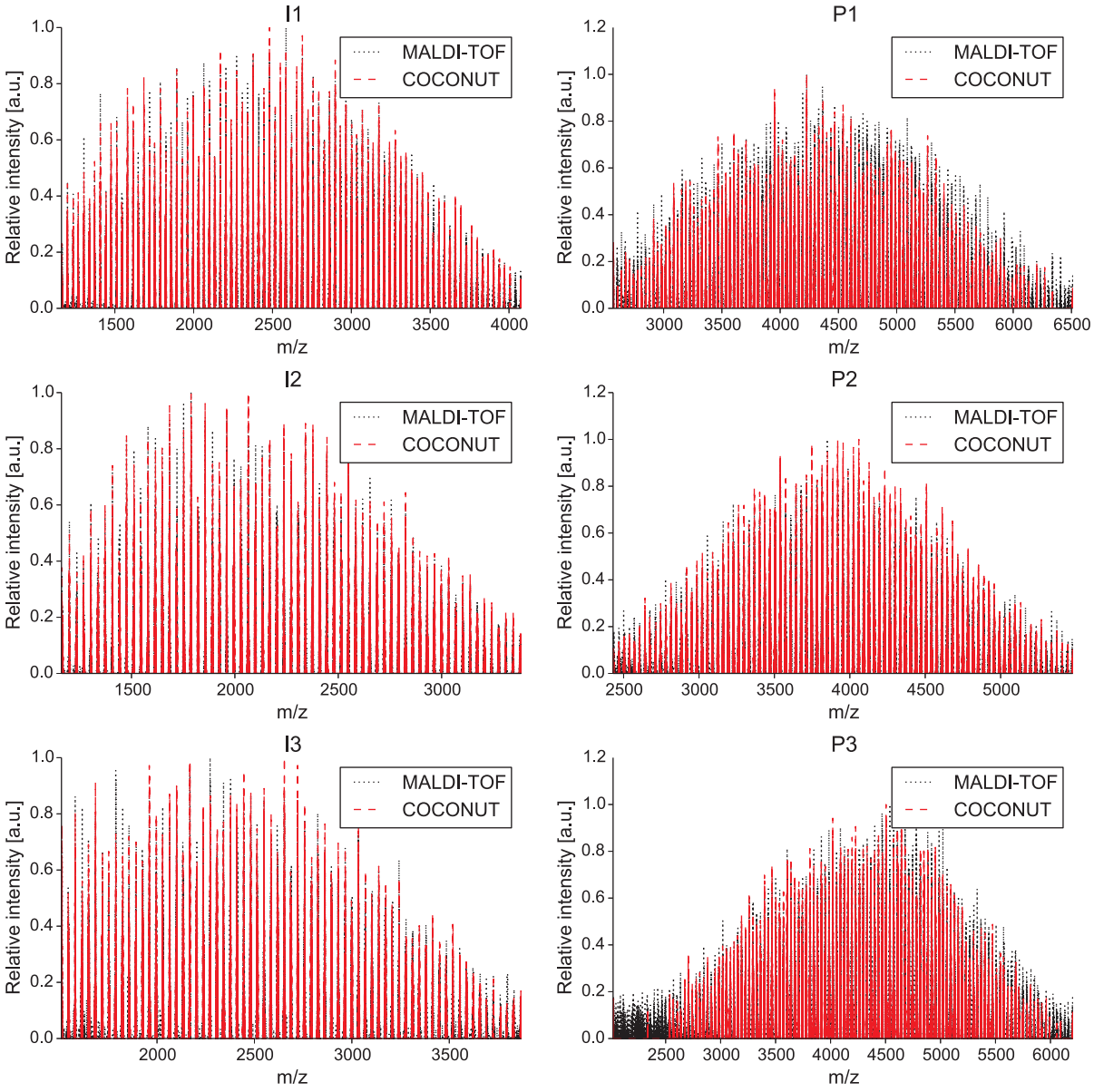

Figure S4: MALDI-TOF spectra after baseline-correction overlayed with the isotopes estimated by COCONUT of the (PS-*r*-PI) macromers **I1 to I3** (left) and the final (PS-*r*-PI)-*r*-(PS-*r*-PI) copolymers **P1 to P3** (right).

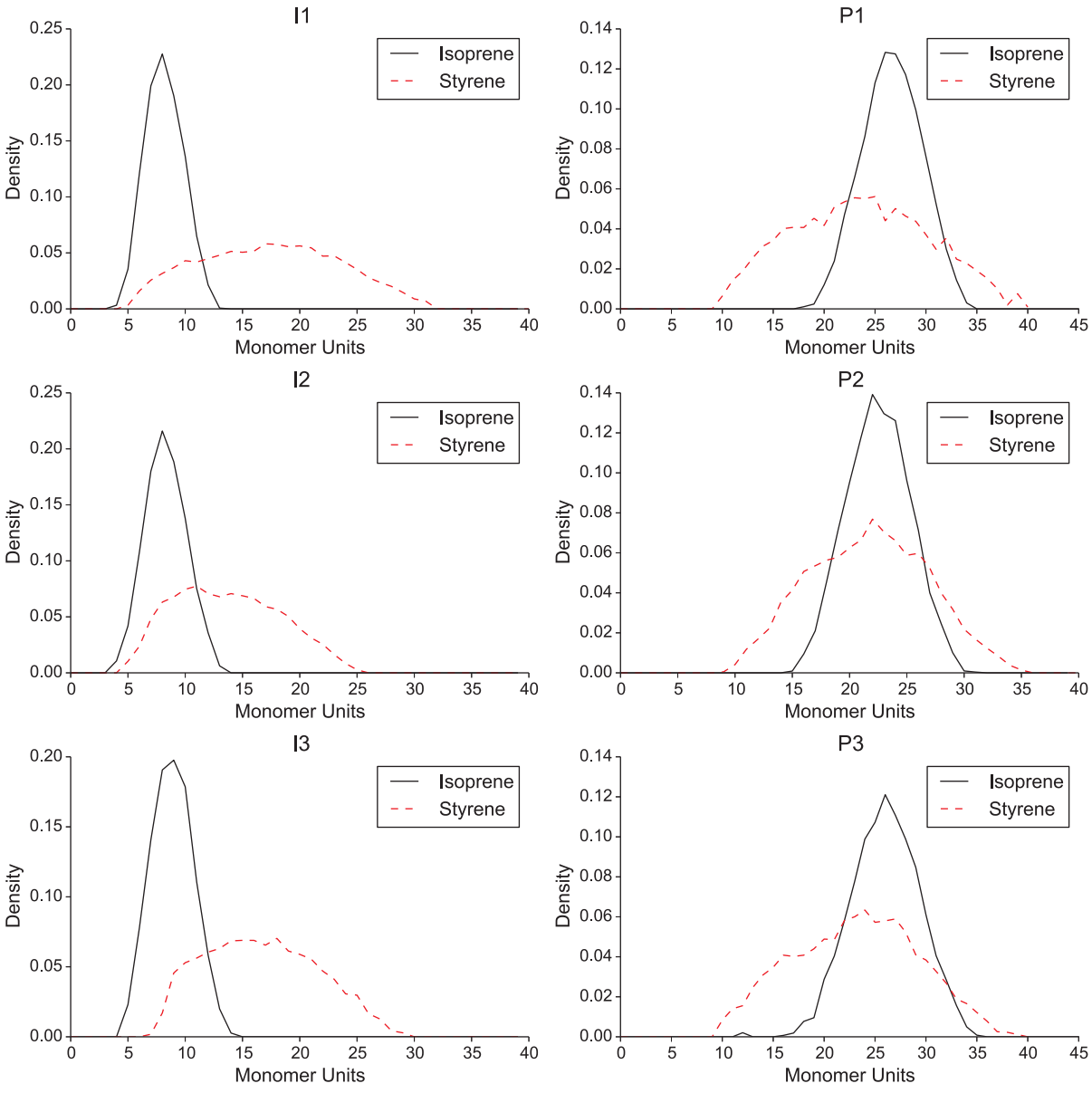

Figure S5: Marginal distributions of the (PS-*r*-PI) macromers **I1 to I3** (left) and the final (PS-*r*-PI)-*r*-(PS-*r*-PI) copolymers **P1 to P3** (right).

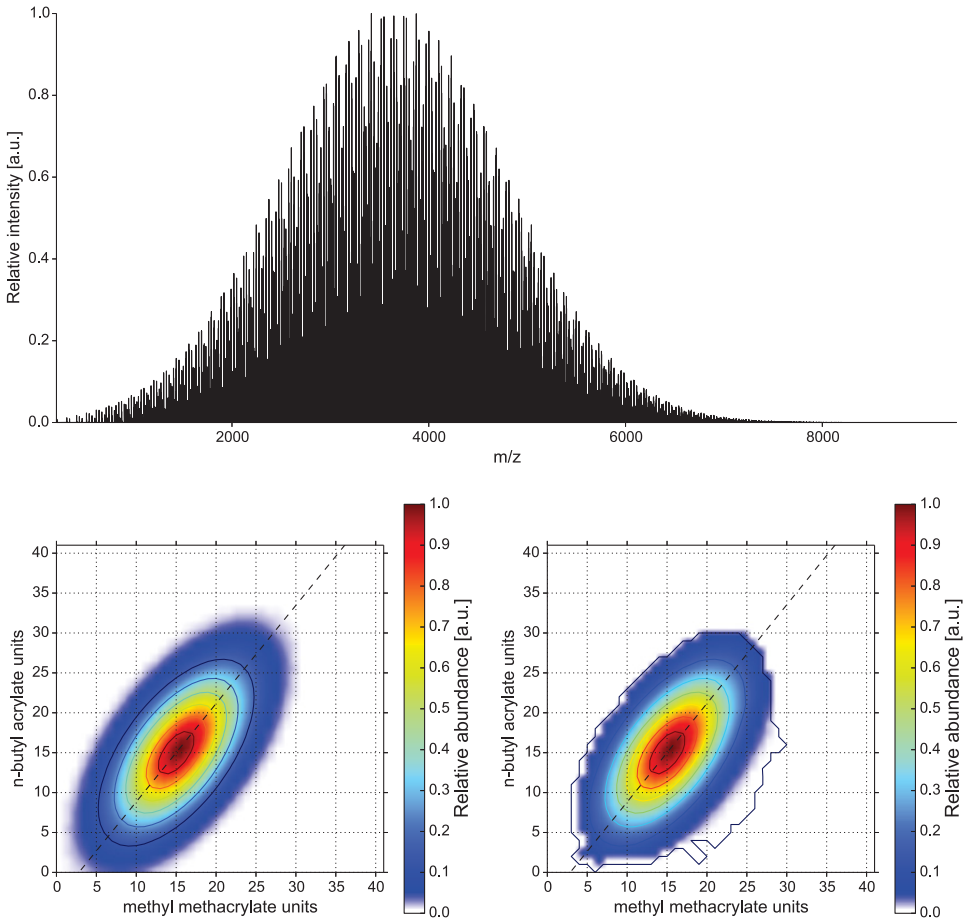

Figure S6: Simulated composition (bottom left), the resulting MS spectrum (top) of a PMMA-*co*-P*n*BA copolymer and the copolymer composition estimated by COCONUT (bottom right).

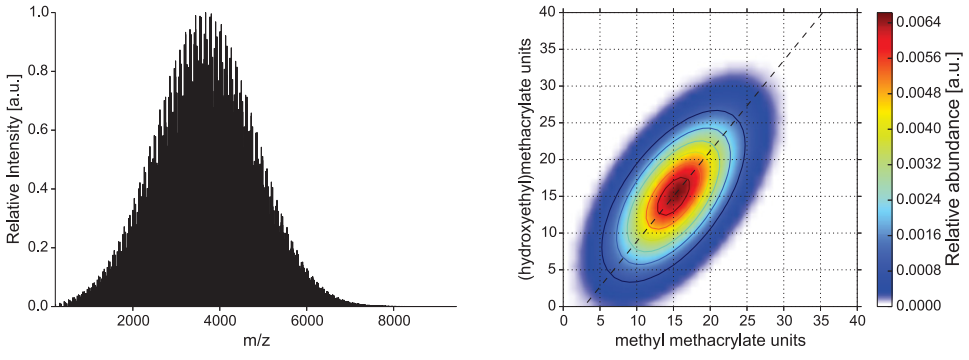

Figure S7: Simulated copolymer composition (right) and the resulting MS spectrum (left) of a PMMA-*co*-PHEMA copolymer.

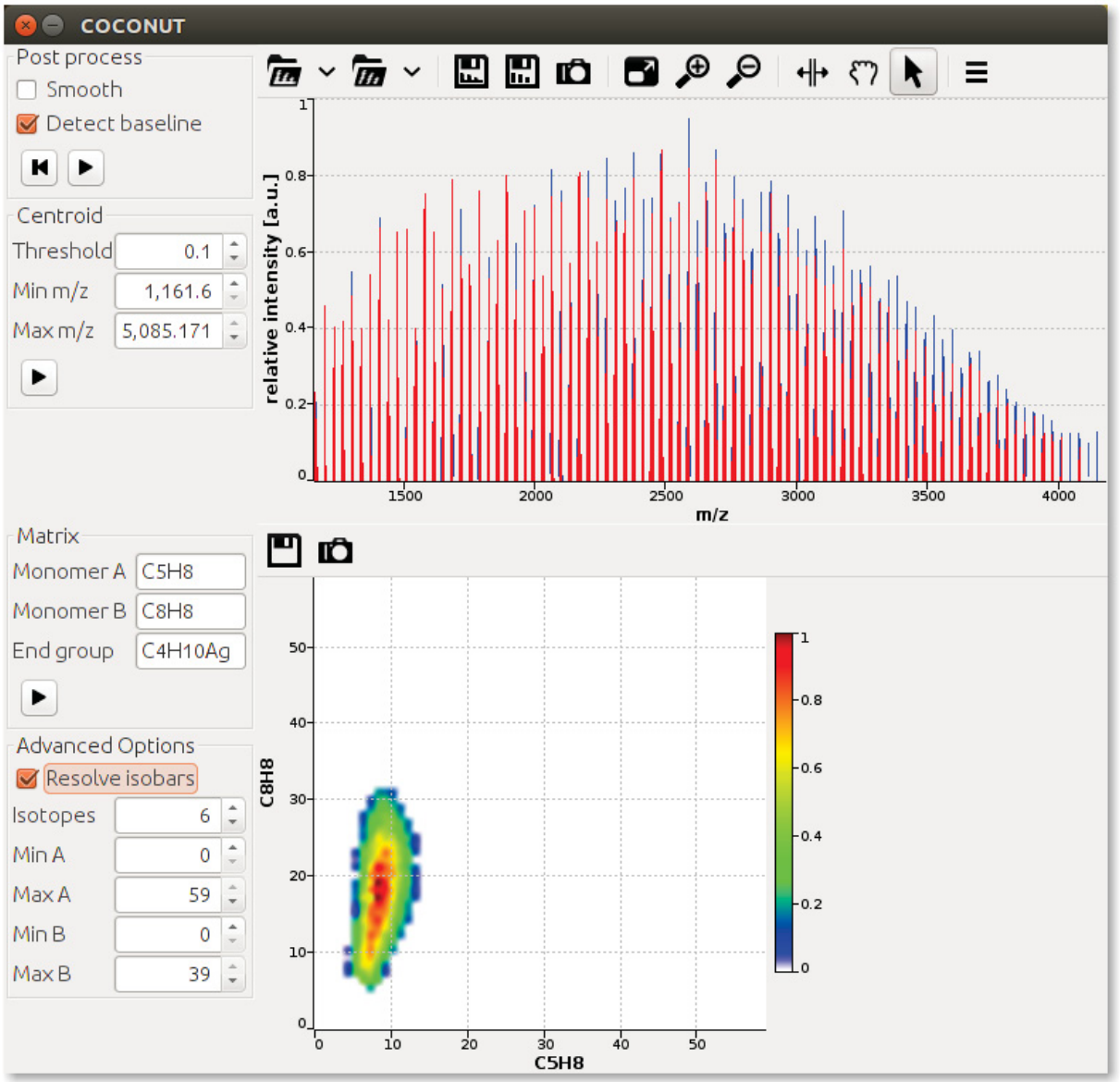

Figure S8: Screenshot of the COCONUT user interface.

Publication 9

Abundance correction for mass discrimination effects in polymer mass spectra

M. S. Engler,[#] S. Crotty,[#] M. J. Barthel, C. Pietsch, U. S. Schubert, S. Boecker

Rapid Commun. Mass Spectrom. **2016**, *30*, 1233-1241.

[#] both contributed equally to this work

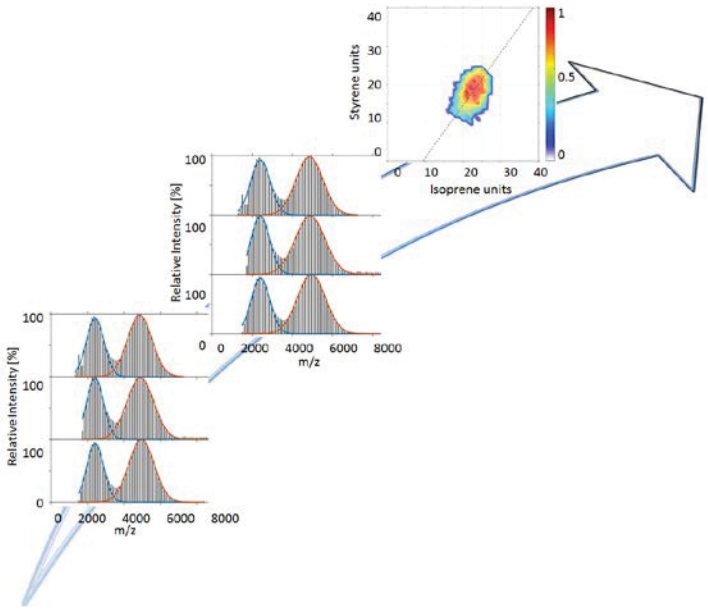

Research Article

Rapid Communications in Mass Spectrometry

Received: 16 December 2015 Revised: 28 February 2016 Accepted: 4 March 2016 Published online in Wiley Online Library

Rapid Commun. Mass Spectrom. **2016**, *30*, 1233–1241
(wileyonlinelibrary.com) DOI: 10.1002/rcm.7553

Abundance correction for mass discrimination effects in polymer mass spectra

Martin S. Engler[1†], Sarah Crotty[2,3†], Markus J. Barthel[2,3‡], Christian Pietsch[2,3], Ulrich S. Schubert[2,3] and Sebastian Böcker[1,3*]

[1]Chair of Bioinformatics, Friedrich Schiller University Jena, Ernst-Abbe-Platz 2, 07743 Jena, Germany
[2]Laboratory of Organic and Macromolecular Chemistry (IOMC), Friedrich Schiller University Jena, Humboldstr. 10, 07743 Jena, Germany
[3]Jena Center for Soft Matter (JCSM), Friedrich Schiller University Jena, Humboldstr. 10, 07743 Jena, Germany

RATIONALE: Matrix-assisted laser desorption/ionization time-of-flight mass spectrometry (MALDI-TOFMS) is frequently used to analyze homo- and copolymers, i.e. for computing copolymer fingerprints. However, the oligomer abundances are influenced by mass discrimination, i.e. mass- and composition-dependent ionization. We have developed a computational method to correct the abundance bias caused by the mass discrimination.
METHODS: MALDI-TOFMS in combination with computational methods was used to investigate three random copolymers with different ratios of styrene and isoprene. Furthermore, equimolar high- and low-mass styrene and isoprene homopolymers (2500 and 4200 Da) were mixed and also analyzed by MALDI-TOFMS. The abundances of both copolymers and homopolymers were corrected for mass discrimination effects with our new method.
RESULTS: The novel computational method was integrated into the existing COCONUT software. The method was demonstrated using the measured styrene and isoprene co- and homopolymers. First, the method was applied to homopolymer spectra. Subsequently, the copolymer fingerprint was computed from the copolymer MALDI mass spectra and the correcting function applied. The changes in the composition are plausible, indicating that correction of copolymer abundances was reasonable.
CONCLUSIONS: Our computational method may help to avoid erroneous conclusions when analyzing copolymer MS spectra. The software is freely available and represents a step towards comprehensive computational support in polymer science. Copyright © 2016 John Wiley & Sons, Ltd.

Mass spectrometry (MS) represents a widely used method to characterize molecules. In particular, matrix-assisted laser desorption/ionization time-of-flight (MALDI-TOF) MS is applied frequently in polymer science.[1,2] Most recently, we introduced COCONUT, a new openly available software, to estimate the copolymer fingerprint, or copolymer composition matrix.[3] The fingerprint is an alternative representation of a copolymer mass spectrum, and it displays the abundances of all combinations of monomer repeating units. COCONUT applies Linear Programming to assign the copolymer composition frequencies and to resolve overlapping isotopes. To the best of our knowledge, it is the only tool capable of automatically resolving isobaric molecules, which are a major problem in copolymer fingerprinting,[4] using only MS data.

* *Correspondence to*: S. Böcker, Chair of Bioinformatics, Friedrich Schiller University Jena, Ernst-Abbe-Platz 2, 07743 Jena, Germany.
E-mail: sebastian.boecker@uni-jena.de

‡ Current address: Drug Discovery and Development Department, Istituto Italiano di Tecnologia, Via Morego 30, 16163 Genova, Italy.

† These authors contributed equally to this work.

However, there is a fundamental challenge, which is the focus of this paper. Like all similar approaches,[5–9] COCONUT determines the abundances from mass spectra – but the task of estimating the entire copolymer fingerprint from MALDI-TOF mass spectra turns out to be only semi-quantitative due to the mass and composition-dependent ionization.[3,10–13] The differential ionization leads to mass discrimination, i.e. peaks at certain m/z values, which are less intense than expected. This discrimination phenomenon is very pronounced against peaks at higher masses and it is best observed when the analyte ion peaks span a wide mass range.[12,13] The mass discrimination depends on instrumental parameters such as the time-lag setting, the laser energy, and the wire-voltage setting.[14] Furthermore, the mass discrimination depends on the polydispersity index (PDI) of the analyte, and the crystal homogeneity,[15] as well as on the monomer and matrix polarity.[16] In addition, it may be influenced by other factors, for example, the matrix/salt ratio and matrix/analyte ratio,[17] or the matrix solubility.[18] In consequence, many groups have used hyphenated techniques such as size-exclusion chromatography (SEC), high-pressure liquid chromatography (HPLC), 2D × LC, or ion mobility spectrometry, linked with MS, as methods for quantification.[19–22] However, in our opinion, MALDI-MS is still a strong competitor in this area; for example, the use of solvent-free MALDI-MS

Table 1. Summary of M_n, PDI, and S/N values for PS and PI (top) and the M_n, PDI and S/N values for copolymers PS-*r*-PI: P1 to P3 (bottom). ^{1}H NMR and SEC measurements of the copolymers P1 to P3 were performed before degradation,[3] therefore show higher M_n values than MALDI. The PI SEC values are higher due to using PS calibration standards. Homopolymer MALDI values of PDI, M_n and S/N were averaged over the replicate spectra

	Theoretical	M_n[a], (^{1}H NMR) [g·mol^{-1}]	M_n[b], (SEC) [g·mol^{-1}]	M_n[c], (MALDI) [g·mol^{-1}]	$PDI_{(MALDI)}$	$S/N_{(MALDI)}$
PS-2500	2,000	2,540	2,350	2,416	1.03	780.8
PS-4200	5,000	4,650	4,420	4,770	1.03	
PI-2500	2,000	2,540	3,920	2,482	1.03	482.3
PI-5000	5,000	4,770	8,160	5,067	1.02	

	Theoretical		M_n[a], (^{1}H NMR) [g·mol^{-1}]		M_n[b], (SEC) [g·mol^{-1}]	M_n[d] (MALDI) [g·mol^{-1}]	$PDI_{(MALDI)}$	$S/N_{(MALDI)}$
	PS	**PI**	**PS**	**PI**				
P1	24	36	21	35	4,550	3,456	1.04	52.6
P2	24	37	21	29	4,060	3,445	1.02	134.1
P3	24	37	22	33	4,380	3,563	1.02	72.7

[a]$CDCl_3$, 300 MHz.
[b]$CHCl_3$:*i*-Prop.:TEA 94:4:2, using PS standards.
[c]Dithranol or DCTB with AgTFA for PS or PI, respectively, using PMMA standards.
[d]Dithranol with AgTFA, using PMMA standards.

led to significant improvements in reliability and quantitation.[23] Our focus was to obtain similar results using exclusively MALDI-TOFMS.

In this contribution, the focus is on the analysis of linear copolymers and their respective homopolymers. We describe in detail a novel computational method to counteract the differential mass discrimination against higher masses and investigate its limits with respect to the PDI. We demonstrate our new approach using two homopolymer mixtures and, for comparison, new MALDI-TOFMS measurements of the copolymers previously reported by Engler *et al.*[3] The developed method was added as a new module to the COCONUT software.

EXPERIMENTAL

Polymerization procedures

We synthesized three copolymers, P1, P2 and P3 (Table 1, bottom, and Supplementary Table S2, Supporting Information), which were composed of two macromers with different ratios of styrene (PS) and isoprene (PI).[24] A more detailed description of the synthesis and characterization data of the copolymers (Fig. 1) was provided in a previous publication.[3]

The PS and PI homopolymers (Table 1, top, and Supplementary Table S1, Supporting Information) were freshly synthesized. [See the Polymerization Procedures section in the Supporting Information for a detailed description.] All the homopolymers showed PDI values lower than 1.1, indicating the living character of the polymerization. The M_n values of the homopolymers are near their theoretical molar masses (Table 1), and this was confirmed by SEC and ^{1}H NMR investigations (Supplementary Figs. S1–S4, Supporting Information).

Sample preparation

Equimolar mixtures of 2500 g/mol and 5000 g/mol homopolymers were prepared from the respective stock solutions of PI and PS (10 mg·mL^{-1} in chloroform). For the sample preparation, dithranol (50 mg·mL^{-1} in chloroform) and silver trifluoroacetate (AgTFA) dissolved in chloroform at a concentration of 100 mg·mL^{-1} were used for the PS homopolymers. For the PI homopolymers, *trans*-2-[3-(4-*tert*-butylphenyl)-2-methyl-2-propenylidene]malononitrile (DCTB) (50 mg·mL^{-1} in chloroform) and AgTFA dissolved in chloroform at a concentration of 100 mg·mL^{-1} were used. The matrix, the cationization agent and the analyte were mixed by volume in a ratio of 3:1:1, respectively. The salt did not completely

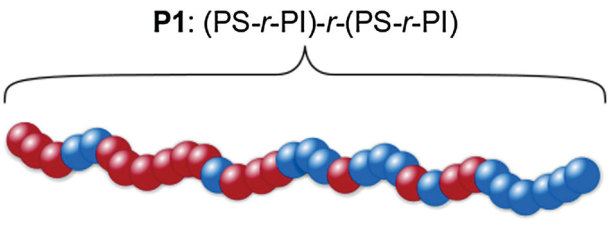

Figure 1. Schematic representation of the synthesized (PS-r-PI)-r-(PS-r-PI) copolymer P1. P1 consists of two macromers of random copolymers with 80% PS and 20% PI in the first macromer, and 20% PS and 80% PI in the second macromer. P2 and P3 similar, but have different PS to PI ratios.

Rapid Communications in Mass Spectrometry

dissolve, producing a saturated solution, from which the supernatant was pipetted out. The high proportion of matrix is an important factor for the dried-droplet technique, reducing segregation and the coffee ring effect.[25] All the polymers were spotted onto the MALDI target plate and the dried-droplet sample preparation method was applied.

Instrumentation

^{1}H NMR spectra were recorded on a Bruker AC 300 MHz instrument (Bruker BioSpin, Rheinstetten, Germany) as described in Engler *et al*.[3]

SEC was performed on a system from Shimadzu (Duisburg, Germany) equipped with a SCL-10A system controller (with a LC-10AD pump, a RID-10A refractive index detector and a PL gel 5 µm mixed-D column at 25 °C) where the eluent was a mixture of chloroform, triethylamine and isopropanol (94:4:2) at a flow rate of 1 mL·min^{-1}. The system was calibrated with PS standards purchased from Polymer Standard Services GmbH (PSS, Mainz, Germany).

An Ultraflex III TOF/TOF mass spectrometer (Bruker Daltonics, Bremen, Germany) was used for the MALDI-TOFMS analysis. The instrument was equipped with a Nd:YAG laser and a collision cell. All spectra were measured in the positive reflector mode. The instrument was calibrated prior to each measurement with an external standard, PMMA from PSS. The homopolymer measurements were replicated three times with 33,000 laser shots and the copolymers were measured once, with 30,000 shots for P1, 83,000 shots for P2 and 92,000 shots for P3. All the measurements used a random walk on three different spots.

Data processing

The MS data were processed using PolyTools 1.0 (Bruker Daltonics) and Data Explorer 4.0 (Applied Biosystems, Foster City, CA, USA). The averaging of the replicates was performed using in-house built Groovy scripts; all other computations were performed using COCONUT 1.4.[3]

RESULTS AND DISCUSSION

Overview

First, we discuss the experimental results, the polymerization and MALDI mass spectra of the homopolymer mixtures and copolymers. Secondly, we discuss in detail the new computational method: We show how to estimate the molecular weight distribution (MWD) of a homopolymer mixture, and investigate the limits of this approach with respect to the PDI. Next, we describe how to estimate an abundance-correcting function from the MWD to counteract the discrimination against higher masses in the homopolymer spectra. Thereafter, we apply the correction to the homopolymer spectra and describe a method to correct the copolymer spectra, based on the previously estimated homopolymer correction parameters. Finally, we present the new module for the COCONUT software implementing the new method.

Polymerization and MALDI-TOFMS

In a previous study, (PS-*r*-PI)-*r*-(PS-*r*-PI) random copolymers with two random macromers with different ratios of styrene and isoprene (Table 1, bottom) were synthesized with the same molar masses of around 4250 g mol^{-1}.[3] Compared with the previously reported spectra and M_n values (Table 1, bottom), the newly measured spectra clearly show degradation products (Supplementary Fig. S7, Supporting Information), resulting in lower M_n values (Table 3). The degradation products are known to consist of depolymerized styrene and isoprene, as several pyrolysis studies have shown.[26,27] The degradation could be explained by random chain scissions, cyclization, or the splitting of monomers or low molecular weight oligomers. The degradation products accumulated in the lower mass regions of the spectra and have not been taken into account in computing the copolymer fingerprints (Fig. 5). Nevertheless, all the polymers synthesized by anionic polymerization showed narrow and well-defined distributions in MALDI with PDI values lower than 1.1 and signal-to-noise (S/N) ratios above 50 (Table 1).

Mixtures of two different molar masses of both the PS and the PI homopolymers were measured at several laser intensities with the same number of laser shots over the whole sample preparation of three different spots. The minimum and maximum laser intensities were determined for a good S/N ratio taking into consideration possible in-source fragmentation or detector saturation when the laser intensity is too high. Furthermore, the laser intensities were chosen to be near the laser intensities used for the copolymers, as the subsequent data analysis predicts the copolymer mass discrimination based on the homopolymer behavior. The laser intensities for the PS homopolymers were 48%, 51% and 54% and for the PI homopolymers they were 36%, 45%% and 54%, while the copolymer laser intensities were 46% and 49%. The intensities in the MALDI-TOFMS spectra reveal a dependency upon laser intensity and a discrimination against high molar masses particularly at low laser powers. This discrimination is observed when mixtures or blends of homopolymers with different masses are analyzed, and it is also influenced by the sample preparation or polymer class and is more pronounced when the polymers are of a polydisperse nature (Supplementary Fig. S5, Supporting Information). The PS spectra were expected to show less discrimination against higher masses at higher laser intensities,[12,14] although we did not observe this behavior, perhaps because of the sample preparation method – the dried-droplet method being hindered by matrix segregation and a coffee ring effect.[25] The PS homopolymers were analyzed with dithranol and AgTFA whereas DCTB and AgTFA were used to ionize both PI homopolymer mixtures. The change in the matrix was necessary, as no spectra with signals over the whole mass range could be obtained for the PI homopolymer mixtures when analyzed with dithranol. Both the solvent and the cationization agent remained identical to reduce differences in the co-crystallization. For each MALDI-TOF spectrum of the PS and PI homopolymers (Supplementary Fig. S5, Supporting Information) an m/z threshold at around 1500 was applied to cut off low mass noise such as matrix ions and, more significantly, the Ag clusters interfering with the peak intensities,[28] and possible in-source fragmentation. Use of a mass cut-off will prevent low mass ions from

saturating the detector.[29] Averaging the homopolymer abundances over the three replicates shows that the influence of the cut-off is negligible in our case, because the intensity differences from the average are small. Subsequently, we identified the baselines for each spectrum by fitting a Loess curve to the signal 'valleys', and these baselines were subtracted from the spectra. We identified isotope patterns and quantified the abundances of the oligomers using the average peak heights of the isotopic patterns (Supplementary Fig. S5, Supporting Information). To reduce stochastic errors, the resulting peak lists were averaged over the three replicates for each laser intensity.

Molecular weight distribution

We suggest that an abundance correcting function *f* should be applied to mitigate mass discrimination effects. However, since the mass discrimination is an undetermined function, we propose using a data-driven approach to estimate the correction parameters. To this end, we need to estimate the MWD of the homopolymer mixtures.

Textbooks in polymer science[30] state that the MWD of a homopolymer can be characterized by the Gamma distribution:

$$Gamma(\alpha,\beta) = \frac{\beta^{\alpha}}{\Gamma(\alpha)} x^{\alpha-1} e^{-\beta x} \tag{1}$$

The two dimensionless parameters can be transformed into parameters with dimensions of M_n and M_w, i.e. g/mol. The parameter change is $\alpha = \frac{DP_w}{DP_n}$ and $\beta = \alpha - 1$, where DP_n and DP_w are proportional to M_w and M_n, respectively. The resulting distribution is known as the Schulz-Zimm distribution. Thus, given a mixture of homopolymers, the MWD can be described by a mixture of Gamma distributions. However, our goal is to obtain an estimation technique, which is insensitive to small departures from the idealized assumptions. We use the symbols $\mathcal{N}(x_0,\sigma)$ to indicate a Gaussian curve with variance σ^2, centered at x_0. It is known that, given a mixture distribution with well-separated modes, estimating a mixture of normal (i.e. Gaussian) distributions is more robust than using a mixture of Gamma distributions.

The question is, what is the error in the normal approximation to the Gamma distribution? We are interested in the cumulative distribution function (cdf), i.e. the integral. The upper and lower integeration limits are usually $-\infty$ and x, respectively. However, in our case, there is no need for negative numbers and thus the integration limits are 0 and x.Let $F(x)$ be the error between the cdf of the Gamma distribution $Gamma(\alpha,\beta)$, and $\Phi(x)$ the cdf of the normal distribution $\mathcal{N}\left(\frac{\alpha}{\beta},\frac{\alpha}{\beta^2}\right)$. The Gamma distribution is the sum of α exponential distributions. The central limit theorem tells us that the sum of any independent and identically distributed random variables converges to a normal distribution as the number of random variables approaches infinity. Thus, in general, the error in the approximation decreases, as α grows large. More specifically, according to the findings by Shevtsova,[31] the maximal error between both cdfs is:

$$\sup_{x\in\mathbb{R}} |F(x) - \Phi(x)| \le \frac{0.3328\ (\rho + 0.429\sigma^3)}{\sigma^3\sqrt{\alpha}} \tag{2}$$

Inserting $\sigma = \frac{\sqrt{\alpha}}{\beta}$ and the third absolute moment $\rho = \frac{\alpha(\alpha+1)(\alpha+2)}{\beta^3}$ of the Gamma distribution yields:

$$\sup_{x\in\mathbb{R}} |F(x) - \Phi(x)| \le 0.3328\left(\alpha + \frac{2}{\alpha} + \frac{0.429}{\sqrt{\alpha}} + 3\right) \tag{3}$$

Since this a rather pessimistic upper limit, we also calculated the actual maximal error numerically by computing the maximum of $|F(x) - \Phi(x)|$ as a function of α. Figure 2 shows both error estimates as functions of the PDI $\frac{M_W}{M_N}$.

In the following, we briefly recall the well-known relationship between the PDI and the Gamma distribution. Let E be the expected value of the distribution of masses M. Then, the variance is:

$$\sigma^2 = E(M^2) - E(M)^2 = M_W \cdot M_N - M_N^2 \tag{4}$$

Thus, the PDI is:

$$\frac{M_W}{M_N} = \frac{\sigma^2}{M_N^2} + 1 = \frac{\sigma^2}{\mu^2} + 1 = \frac{1}{\alpha} + 1 \tag{5}$$

Using the numerically calculated error in the normal approximation to the Gamma distribution (Fig. 2), we determined the limitations of this approach. The error is less than 4% for PDI ≤1.1, which is satisfied by the homopolymers that we used. Also, the error is less than 10% for PDI ≤1.56, and less than 16% for PDI ≤2. Therefore, a normal approximation is applicable to most living polymerizations and the MWD of a mixture of such homopolymers can be described by a mixture of normal distributions $\sum_i w_i \mathcal{N}(\mu_i,\sigma_i)$, with scaling factor w, mean μ and variance σ for each homopolymer in the mixture. We estimated the MWD of the PS and PI homopolymer mixtures for all laser intensities using least-squares nonlinear regression.Formally, let I be homopolymers in the mixture, and K the indices of the observed abundances Y in the MS spectra. As usual, we assume that the observed abundances are normalized to 1. The regression minimized for each laser intensity j the squared error:

$$SE_j = \left| \sum_{i\in I, k\in K} w_{i,j}\mathcal{N}(\mu_i,\sigma_i) - Y_{j,k} \right|_2^2 \tag{6}$$

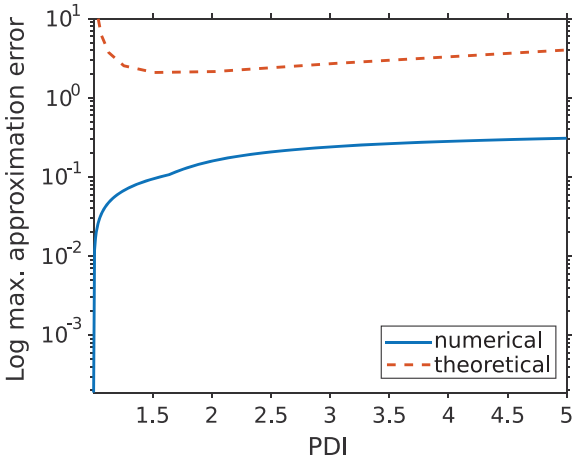

Figure 2. Numerically determined error in the normal approximation to the gamma distribution and its theoretical upper limit on a logarithmic scale as a function of the PDI.

Rapid Communications in Mass Spectrometry

Abundance correcting function

We estimated the MWD of the homopolymer mixtures using normal mixture distributions. In the following, we describe how to compute the abundance correction function from the MWDs. Supposing that there were no mass discrimination effects, the areas under the curve of all homopolymers of each mixture should be equal, because the homopolymers in the mixtures are equimolar and the relationship between intensity and abundance is linear in homopolymers.[32] Thus, the ideal theoretical MWDs can be estimated by equalizing the areas of homopolymers with a normalizing factor.

Let I be the homopolymers in the mixture and J the laser intensities. The theoretical MWD is:

$$\sum_{i \in I} c_{i,j} w_{i,j} \mathcal{N}(\mu_i, \sigma_i), \tag{7}$$

with $j \in J$ and the normalizing factors $c_{i,j}$. We calculate the normalizing factor $c_{i,j}$ by taking the ratio of the largest area in the mixture to the area of the current homopolymer $i \in I$, such that:

$$c_{i,j} = \frac{\max_{i' \in I} \int w_{i',j} \mathcal{N}\left(\mu_{i'}, \sigma_{i'}\right)}{\int w_{i,j} \mathcal{N}(\mu_i, \sigma_i)} \tag{8}$$

The mass discrimination is an unknown function. Other important parameters, such as matrix/analyte and matrix/salt ratios, should have been constant throughout our experiments. Thus, the observed mass discrimination depends on the laser intensity and the mass. However, in principle, other parameters, such as matrix/analyte and matrix/salt ratios, can be included by conducting more experiments with varying ratios.

To correct for the mass discrimination effects, the correcting function $f(m, l)$ (which takes different values as the mass m and laser intensity l change) can be calculated by dividing the ideal theoretical MWD by the observed MWD. We collected the sample points in the intervals $\mu_i \pm \frac{k\,\sigma_i}{c_{i,j}}$ for each component and laser intensity with the sample interval width $1 \leq k \leq 3$, which is automatically chosen with a hill climbing optimization to minimize the distance of area ratios to 1. We estimated the abundance-correcting functions $f_{PS}(m, l)$ and $f_{PI}(m, l)$ for PS and PI by fitting a Thin Plate Spline (TPS) to the sample points (Supplementary Fig. S6, Supporting Information).[33] TPS is a standard technique for interpolating data with more than one dimension. It is able to provide a good fit to the sample points and avoids the oscillation problems that occur when interpolating using polynomials.

Abundance correction

After calculating the correcting function, we applied it to the homopolymer spectra of PS and PI (Figs. 3 and 4, respectively). The areas under the curve of the homopolymers are now nearly equal (Table 2, Fig. 3 and Fig. 4, right). This indicates that

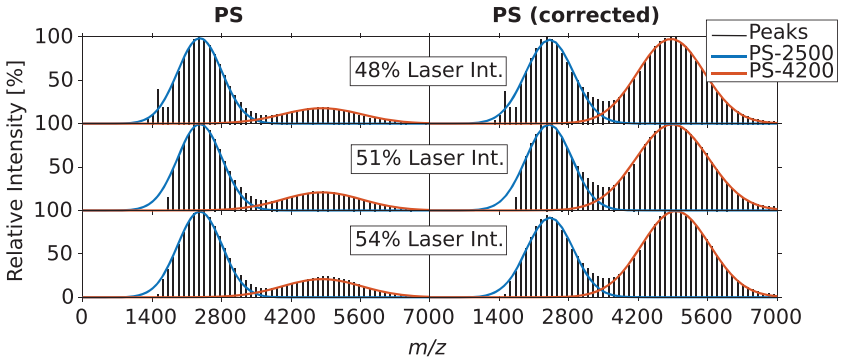

Figure 3. Measured (left) and corrected (right) peak lists of PS, with the estimated MWDs of PS-2500 and PS-4200.

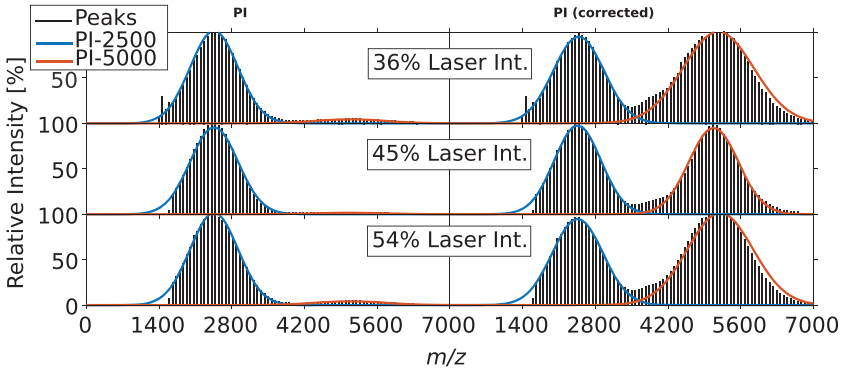

Figure 4. Measured (left) and corrected (right) peaks lists of PI, with the estimated MWDs of PI-2500 and PI-5000.

Table 2. Ratios of the area under curve (AUC) of the MWDs of the homopolymers in the PS and PI mixtures before and after correction. With no mass discrimination, both AUCs should be equal and the ratio one, because the homopolymers are equimolar

Laser Int.	PS-4200/PS-2500		Laser Int.	PI-4200/PI-2500	
[%]	**Uncorrected**	**Corrected**	[%]	**Uncorrected**	**Corrected**
48	0.1731	1.0634	**36**	0.0446	1.0594
51	0.2146	1.0006	**45**	0.0161	0.9474
54	0.2179	1.0542	**54**	0.0419	1.0484

thespectra could be corrected for the contributions of both investigated parameters (mass and laser intensity) to the mass discrimination, which favored the low masses und underestimated the abundances of the higher masses.

Before correction the PS homopolymers show a slight discrimination against higher masses for PS-4200, which is less pronounced at higher laser powers, possibly due to 'hot spots' of the analyte on the MALDI target plate. (Fig. 3, left) The measured spectra for the PI mixtures show a strong discrimination against higher mass even with DCTB as the matrix (Fig. 4, left). At first sight, this result may seem not to be in line with the results obtained by Yalcin *et al.*,[34] who used a copper salt with a different matrix and measured less discrimination against higher masses. However, it should be noted that the many differences in the ionization of the mixtures would significantly affect the signal intensities and, thus, the copolymer evaluations.[28] Nonetheless, a correction for the mass discrimination effects depending on mass and laser intensity was achieved with the PI mixtures, despite the strong discrimination in favor of low masses, which is more challenging for the estimation of the correcting function. In addition, our approach is limited by the mass spectrometer being used: the larger the mass range, the more peaks at higher mass might be suppressed or discriminated against.[14] Where the high-mass signals are discriminated against to the point of being indistinguishable from the noise, additional experiments such as blanking out lower masses (i.e. suppressing the signals from lower masses) or fractionation could be performed.

Mass discrimination favoring low masses over high masses is a known effect in polymer MS and it has been studied carefully for homopolymers.[14–18] Although the mass discrimination in copolymers has been experimentally observed, there is, to the best of our knowledge, no comprehensive theory to explain the mass discrimination phenomenon in copolymer MS. In the following, we assume that mass and monomer frequency are the predominant analyte factors for the copolymer ionization properties. In contrast, we assume that sequence plays only a subordinate role. We also assume that the influence of the three-dimensional structure is negligible, because this work focuses on linear polymers.To account for the influence of the monomer frequency to the mass discrimination in copolymers, we indicate with *#PS* and *#PI* the copolymer composition (number of PS and PI monomer repeating units, respectively) and we propose to apply the correction in the simplest way, as a weighted sum according to their fraction of monomers in the chain:

$$f(m,l) = \frac{\#PS \cdot f_{PS}(m,l) + \#PI \cdot f_{PI}(m,l)}{\#PS + \#PI} \quad (9)$$

Applying the correction resulted in higher average numbers of PS and PI monomers (Table 3). Instead of a compact circular shape, the distribution now shows a narrow oval shape (Fig. 5). However, the upper parts are 'lost', as the higher mass peaks have dropped below the noise threshold and the distribution is less smooth due to the increased influence of the noise in the higher mass regions. The narrow shape is typical for living polymerizations,[35] which is also supported by the PDI values of less than 1.1. Fitting a line through the most abundant oligomers before and after correction results in a straight line off center for both which hints at the desired random-like structure.[36]

However, due to the sharp slope of the correcting function for larger numbers of PI units, the measured copolymers are less affected in the PI dimension than the non-degraded copolymers would be. Also, there is the possible issue of underestimating PI even after correcting the abundances, due to the differences between the copolymer and homopolymer MALDI matrices, which were necessary to obtain good quality PI mass spectra due to the high mass discrimination in the homopolymer mixtures. The experimental setup for homo- and copolymers should be kept as similar as possible, because we assumed that discrimination against higher mass ions affects them similarly. Generally, a new measurement of homopolymers and re-computation of the correcting function should be performed before major changes such as a change in monomers or MALDI matrices. Also, as the instrument laser and detector degrade over time, homopolymer measurements should be repeated regularly.

Table 3. M_n values computed from the copolymer fingerprints of P1 to P3

	$M_{n(Uncorrected)}$			$M_{n(Corrected)}$		
	PS	**PI**	**[g mol^{-1}]**	**PS**	**PI**	**[g mol^{-1}]**
P1	15.9	25.2	3.533	18.0	26.5	3.838
P2	17.3	22.2	3.472	17.9	22.5	3.561
P3	17.1	24.7	3.623	18.3	25.3	3.787

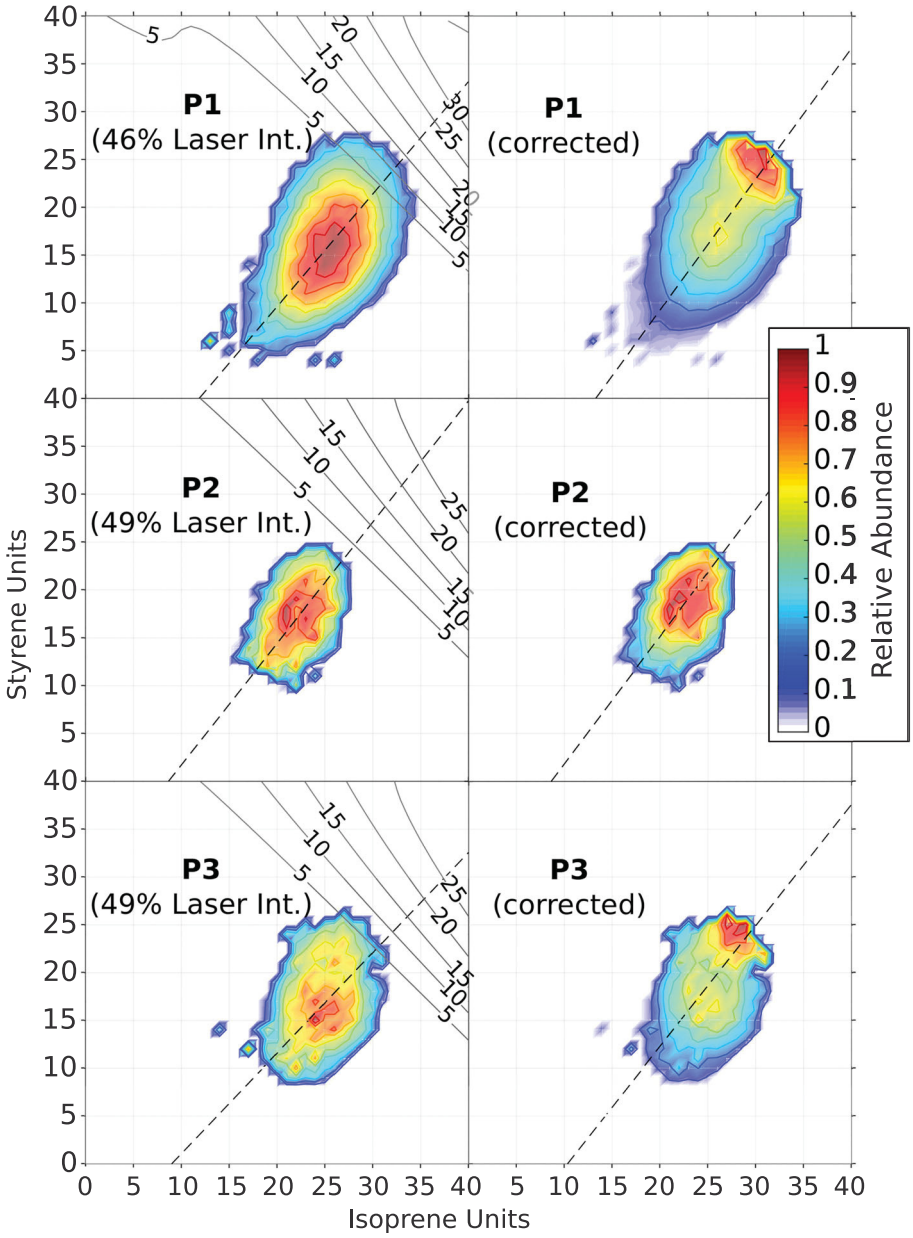

Figure 5. Measured (left) and corrected (right) copolymer fingerprints of P1 to P3. The overlaid contour lines on the left side represent the intensity correcting function, i.e. the correcting factor for each monomer combination of the fingerprint. Dashed lines represent the average compositions computed by fitting a line through the most abundant fingerprint entries.

Software

We integrated the algorithms demonstrated in this publication into the open source software COCONUT 1.4,[3] which is freely available.[37] It is implemented in the Groovy language and runs on the Java platform.

A typical analysis consists of two parts. First, the user needs to import homopolymer mass spectra and specify the parameters, such as laser intensities and the formulae of the monomers and end-groups. The software will compute the correcting function and save it in a machine-readable format. Secondly, the user can apply the saved correcting function to a copolymer fingerprint, which was computed beforehand with any suitable tool, such as COCONUT.

CONCLUSIONS

Mass discrimination is a major challenge in computing copolymer fingerprints. In this contribution, we described an experimental protocol and a software to correct the measured abundances. Because our method uses a Gaussian approximation to Gamma distribution to compute the MWDs, it is applicable to narrowly distributed homopolymers up to PDI values of around 2. The Gaussian approximation is more robust, but, if the need arises, in the future broader homopolymers could be analyzed by using Gamma distributions.

Crucial to advancing MALDI-MS from a semi-quantitative to a quantitative technique for copolymers is a carefully planned experimental setup with the best possible matching

conditions for homo- and copolymers. Most importantly, the MS instrument needs to able to detect both homo- and copolymer signals over the whole investigated mass and laser intensity ranges. Acquiring such data is challenging, and the homopolymer spectra in this contribution did not perfectly conform to these stringent requirements. We invite all interested scientists to further evaluate our method. A full-scale evaluation on, for example, the applicable ranges, polymer classes, and ionization types remains to be conducted in the future.

The software demonstrated in this contribution is openly available for polymer scientists to investigate synthesized linear polymers.

Acknowledgements

Funding was provided by the Thüringer Ministerium für Bildung, Wissenschaft und Kultur (Grant Nos. B515-07008, 12038-514) and the Ernst-Abbe Stiftung. We thank Bruker Daltonics for help and support, and Alexander Meier for his support with the polymerization experiments.

REFERENCES

[1] M. S. Montaudo. Mass spectra of copolymers. *Mass Spectrom. Rev.* **2002**, *21*, 108.
[2] H. Pasch, W. Schrepp. *MALDI-TOF Mass Spectrometry of Synthetic Polymers*. Springer, Berlin Heidelberg, **2003**.
[3] M. S. Engler, S. Crotty, M. J. Barthel, C. Pietsch, K. Knop, U. S. Schubert, S. Böcker. COCONUT – An efficient tool for estimating copolymer compositions from mass spectra. *Anal. Chem.* **2015**, *87*, 5223.
[4] J. Horský, Z. Walterová. Fingerprint multiplicity in MALDI-TOF mass spectrometry of copolymers. *Macromol. Symp.* **2014**, *339*, 9.
[5] R. X. E. Willemse, B. B. P. Staal, E. H. D. Donkers, A. M. van Herk. Copolymer fingerprints of polystyrene-block-polyisoprene by MALDI-ToF-MS. *Macromolecules* **2004**, *37*, 5717.
[6] S. Huijser, B. B. P. Staal, J. Huang, R. Duchateau, C. E. Koning. Topology characterization by MALDI-ToF-MS of enzymatically synthesized poly(lactide-co-glycolide). *Biomacromolecules* **2006**, *7*, 2465.
[7] S. Weidner, J. Falkenhagen, R.-P. Krueger, U. Just. Principle of two-dimensional characterization of copolymers. *Anal. Chem.* **2007**, *79*, 4814.
[8] G. Vivó-Truyols, B. Staal, P. J. Schoenmakers. Strip-based regression: a method to obtain comprehensive co-polymer architectures from matrix-assisted laser desorption ionisation-mass spectrometry data. *J. Chromatogr. A* **2010**, *1217*, 4150.
[9] G. Wilczek-Vera, Y. Yu, K. Waddell, P. O. Danis, A. Eisenberg. Detailed structural analysis of diblock copolymers by matrix-assisted laser desorption/ionization time-of-flight mass spectrometry. *Rapid Commun. Mass Spectrom.* **1999**, *13*, 764.
[10] S. M. Weidner, J. Falkenhagen, S. Maltsev, V. Sauerland, M. Rinken. A novel software tool for copolymer characterization by coupling of liquid chromatography with matrix-assisted laser desorption/ionization time-of-flight mass spectrometry. *Rapid Commun. Mass Spectrom.* **2007**, *21*, 2750.
[11] T. Gruendling, S. Weidner, J. Falkenhagen, C. Barner-Kowollik. Mass spectrometry in polymer chemistry. *Polym. Chem.* **2010**, *1*, 599.
[12] K. Martin, J. Spickermann, H. J. Räder, K. Müllen. Why does matrix-assisted laser desorption/ionization time-of-flight mass spectrometry give incorrect results for broad polymer distributions? *Rapid Commun. Mass Spectrom.* **1996**, *10*, 1471.
[13] H. Räder, W. Schrepp. MALDI-TOF mass spectrometry in the analysis of synthetic polymers. *Acta Polym.* **1998**, *49*, 272.
[14] D. C. Schriemer, L. Li. Mass discrimination in the analysis of polydisperse polymers by MALDI time-of-flight mass spectrometry. 2. Instrumental issues. *Anal. Chem.* **1997**, *69*, 4176.
[15] D. C. Schriemer, L. Li. Mass discrimination in the analysis of polydisperse polymers by MALDI time-of-flight mass spectrometry. 1. Sample preparation and desorption/ionization issues. *Anal. Chem.* **1997**, *69*, 4169.
[16] S. D. Hanton, K. G. Owens. Using MESIMS to analyze polymer MALDI matrix solubility. *J. Am. Soc. Mass Spectrom.* **2005**, *16*, 1172.
[17] A. J. Hoteling, T. H. Mourey, K. G. Owens. Importance of solubility in the sample preparation of poly(ethylene terephthalate) for MALDI TOFMS. *Anal. Chem.* **2005**, *77*, 750.
[18] A. J. Hoteling, W. J. Erb, R. J. Tyson, K. G. Owens. Exploring the importance of the relative solubility of matrix and analyte in MALDI sample preparation using HPLC. *Anal. Chem.* **2004**, *76*, 5157.
[19] S. M. Weidner, J. Falkenhagen, I. Bressler. Copolymer composition determined by LC-MALDI-TOF MS coupling and "MassChrom2D" data analysis. *Macromol. Chem. Phys.* **2012**, *213*, 1521.
[20] H. J. Philipsen. Determination of chemical composition distributions in synthetic polymers. *J. Chromatogr. A* **2004**, *1037*, 329.
[21] E. Uliyanchenko, S. van der Wal, P. J. Schoenmakers. Challenges in polymer analysis by liquid chromatography. *Polym. Chem.* **2012**, *3*, 2313.
[22] S. Trimpin, D. E. Clemmer. Ion mobility spectrometry/mass spectrometry snapshots for assessing the molecular compositions of complex polymeric systems. *Anal. Chem.* **2008**, *80*, 9073.
[23] S. Trimpin, S. Keune, H. J. Räder, K. Müllen. Solvent-free MALDI-MS. *J. Am. Soc. Mass Spectrom.* **2006**, *17*, 661.
[24] A. Nakahara, K. Satoh, M. Kamigaito. Random copolymer of styrene and diene derivatives via anionic living polymerization followed by intramolecular Friedel–Crafts cyclization for high-performance thermoplastics. *Polym. Chem.* **2012**, *3*, 190.
[25] S. J. Gabriel, C. Schwarzinger, B. Schwarzinger, U. Panne, S. M. Weidner. Matrix segregation as the major cause for sample inhomogeneity in MALDI dried droplet spots. *J. Am. Soc. Mass Spectrom.* **2014**, *25*, 1356.
[26] S. Meng, S. I. Kuchanov, J. Xu, T. Kyu. Collaborative studies of thermo-oxidative degradation of styrene–isoprene diblock copolymer. *Polymer* **2005**, *46*, 5580.
[27] J. Hacaloglu, M. M. Fares, S. Suzer. Pyrolysis mass spectrometric analysis of styrene–isoprene–styrene copolymer. *Eur. Polym. J.* **1999**, *35*, 939.
[28] S. F. Macha, P. A. Limbach. Matrix-assisted laser desorption/ionization (MALDI) mass spectrometry of polymers. *Curr. Opin. Solid State Mater. Sci.* **2002**, *6*, 213.
[29] G. J. van Rooij. Laser desorption analyses in trapped ion mass spectrometry systems. *PhD thesis*, University of Amsterdam, **1999**.
[30] P. C. Painter, M. M. Coleman. *Essentials of Polymer Science and Engineering*. DEStech Publications, Lancaster, **2008**.

[31] I. Shevtsova. *On the absolute constants in the Berry-Esseen type inequalities for identically distributed summands*. Technical report, Cornell University Library, arXiv:1111.6554, **2011**.
[32] Z. Walterová, J. Horský. Quantification in MALDI-TOF mass spectrometry of modified polymers. *Anal. Chim. Acta* **2011**, *693*, 82.
[33] F. L. Bookstein. Principal warps: thin-plate splines and the decomposition of deformations. *IEEE T. Pattern Anal.* **1989**, *11*, 567.
[34] T. Yalcin, D. C. Schriemer, L. Li. Matrix-assisted laser desorption ionization time-of-flight mass spectrometry for the analysis of polydienes. *J. Am. Soc. Mass Spectrom.* **1997**, *8*, 1220.
[35] S. Huijser, G. D. Mooiweer, R. van der Hofstad, B. B. P. Staal, J. Feenstra, A. M. van Herk, C. E. Koning, R. Duchateau. Reactivity ratios of comonomers from a single MALDI-ToF-MS measurement at one feed composition. *Macromolecules* **2012**, *45*, 4500.
[36] S. Huijser, B. B. P. Staal, J. Huang, R. Duchateau, C. E. Koning. Chemical composition and topology of poly(lactide-co-glycolide) revealed by pushing MALDI-TOF MS to its limit. *Angew. Chem. Int. Ed.* **2006**, *45*, 4104.
[37] Available: http://www.bio.informatik.uni-jena.de/software/coconut.

SUPPORTING INFORMATION

Additional supporting information may be found in the online version of this article at the publisher's website.

Supporting Information

Abundance correction for mass discrimination effects in polymer mass spectra

Martin S. Engler,[a,†] Sarah Crotty,[b,c,†] Markus J. Barthel,[b,c,#] Christian Pietsch,[b,c] Ulrich S. Schubert,[b,c] and Sebastian Böcker,[a*]

[a] Chair of Bioinformatics, Friedrich Schiller University Jena, Ernst-Abbe-Platz 2, 07743 Jena, Germany

[b] Laboratory of Organic and Macromolecular Chemistry (IOMC), Friedrich Schiller University Jena, Humboldstr. 10, 07743 Jena, Germany

[c] Jena Center for Soft Matter (JCSM), Friedrich Schiller University Jena, Humboldstr. 10, 07743 Jena, Germany

[#] current address: Drug Discovery and Development Department, Istituto Italiano di Tecnologia, Via Morego 30, 16163 Genova, Italy

[†] equal contribution

E-mail: sebastian.boecker@uni-jena.de

Polymerization Procedures

The PS and PI homopolymers (**Table 1, top** and **Supplementary Table S. 1**) for this publication were synthesized in Schlenk tubes under dried argon atmosphere. Solvents were dried over sodium/benzophenone and freshly distilled. Isoprene was dried over sodium whereas styrene was dried over calcium hydride. Both monomers were freshly distilled before reaction. *sec*-Butylithium (*s*-BuLi) (1.4 mol in hexane) was used as received. All chemicals were obtained from Aldrich (Sigma-Aldrich, Munich, Germany). In a classical synthesis 15 mL of freshly distilled cyclohexane was transferred in the Schlenk tube and the calculated amount of *s*-BuLi (**Supplementary Table S. 1.**) was added via a syringe. The mixture was heated to 40 °C and the calculated amount of the monomer (styrene or isoprene, **Supplementary Table S. 1.**) was added. The reaction mixture was allowed to stir for 1 h at 40 °C and the polymerization was terminated by the addition of 1 mL of methanol.

Tables

Table S. 1. Summary of theoretical values for PS and PI.

	Amount of initiator [mL]	**Molar mass [g·mol^{-1}]**	**DP**	**Mass (monomer) [g]**	**Volume (monomer) [mL]**
PS-2500	0.54 mL (0.75 mmol)	2,000	19	1.50	1.66
PS-4200	0.21 mL (0.3 mmol)	5,000	48	1.50	1.66
PI-2500	0.54 mL (0.75 mmol)	2,000	29	1.50	2.20
PI-5000	0.21 mL (0.3 mmol)	5,000	73	1.50	2.20

Table S. 2. Summary of theoretical values for P1, P2 and P3

	Molar mass [g·mol^{-1}]		DP		Mass (monomer) [g]		Volume (monomer) [mL]	
	PS	PI	PS	PI	PS	PI	PS	PI
P1	2,500	2,500	24	36	1.00	0.98	1.1	1.44
P2	2,500	2,500	24	37	1.00	1.01	1.1	1.48
P3	2,500	2,500	24	37	1.00	1.01	0.64	0.68

Figures

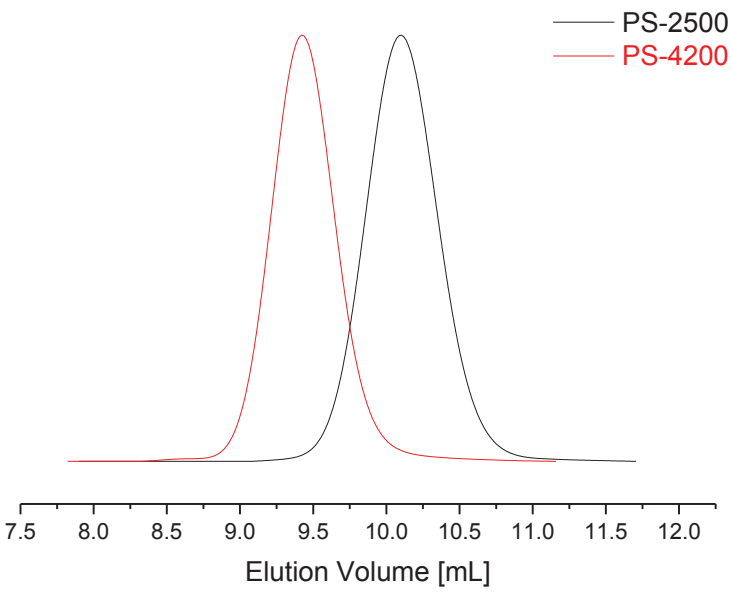

Figure S .1. Overlay of SEC chromatograms of PS 2500 (black curve) and PS 4200 (red curve).

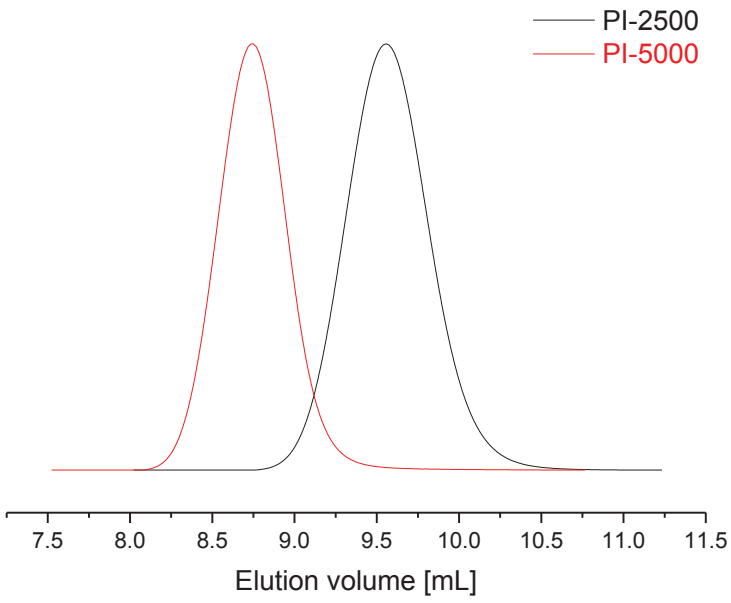

Figure S. 2. Overlay of SEC chromatograms of PI 2500 (black curve) and PI 5000 (red curve).

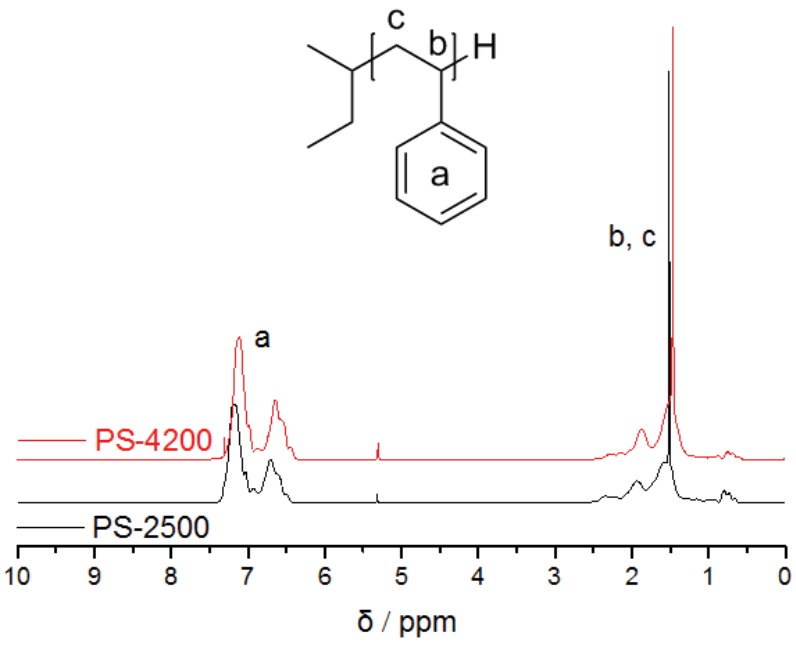

Figure S. 3. Overlay of ^{1}H NMR spectra of PS-2500 (black curve) and PS-4200 (red curve).

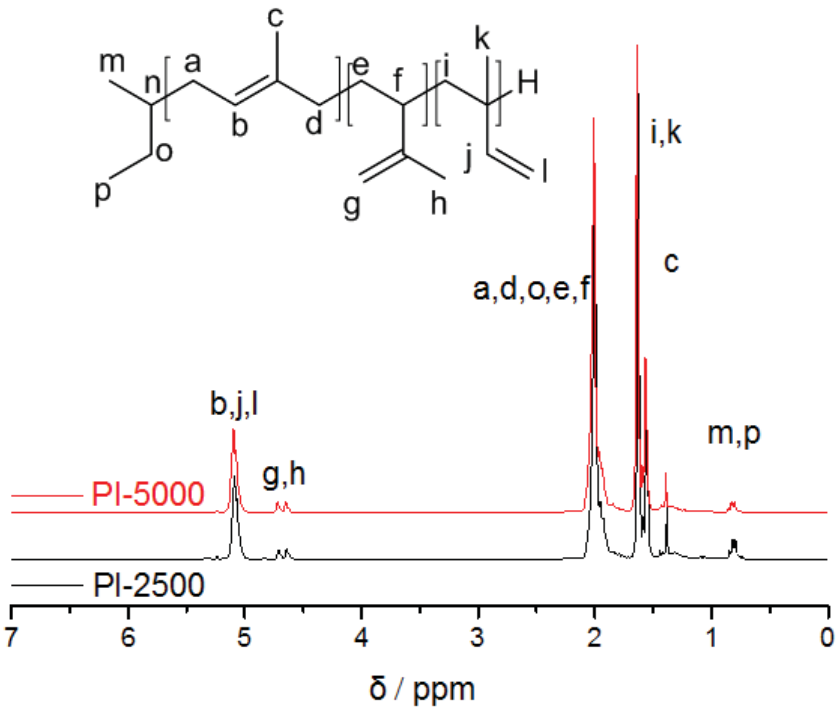

Figure S. 4. Overlay of ^{1}H NMR spectra of PI-2500 (black curve) and PI-5000 (red curve).

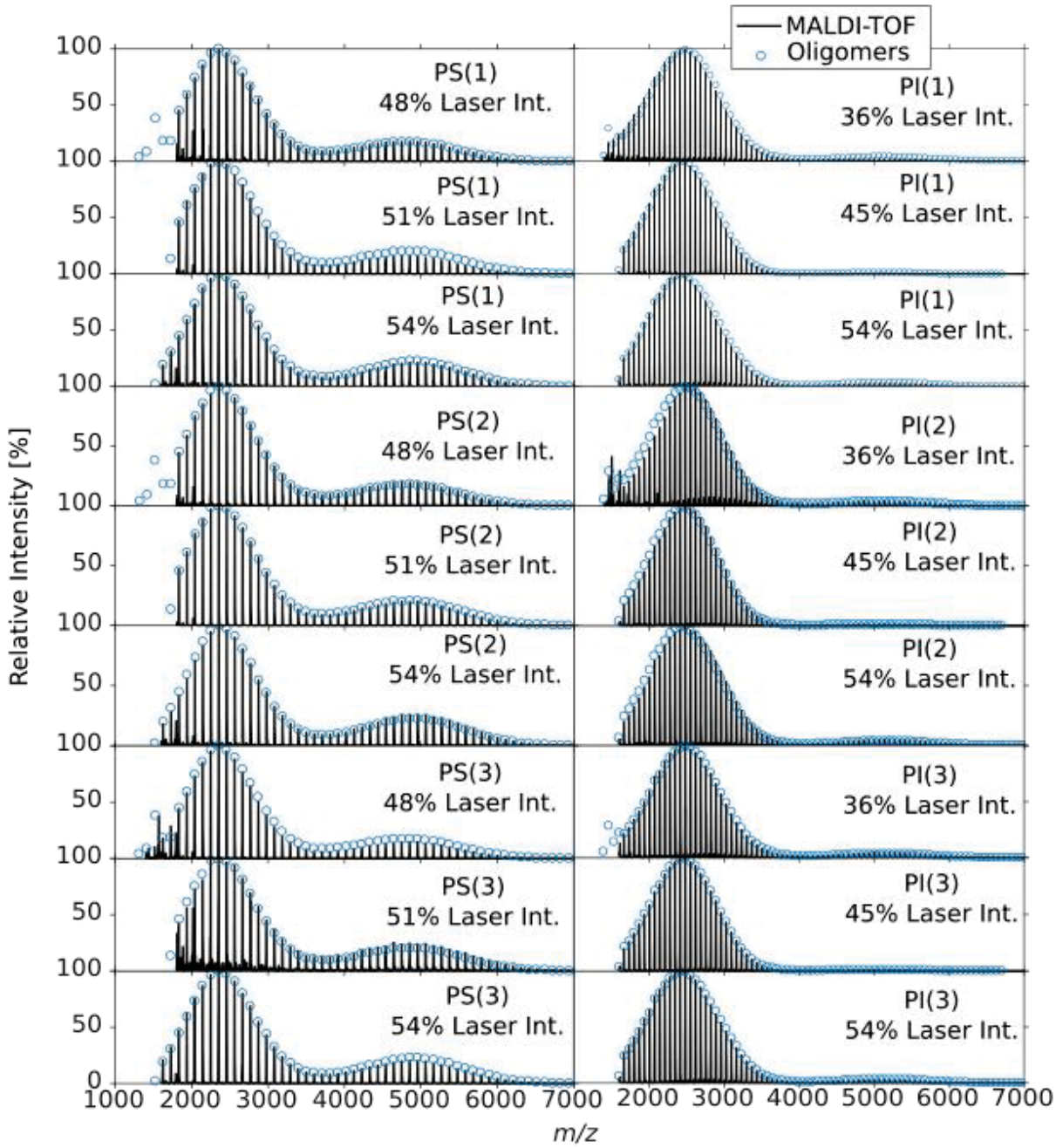

Figure S. 5 MALDI-TOF mass spectra of PS and PI homopolymers overlaid with the oligomer peaks. The oligomer abundances were averaged over the three replicated spectra for each laser intensity.

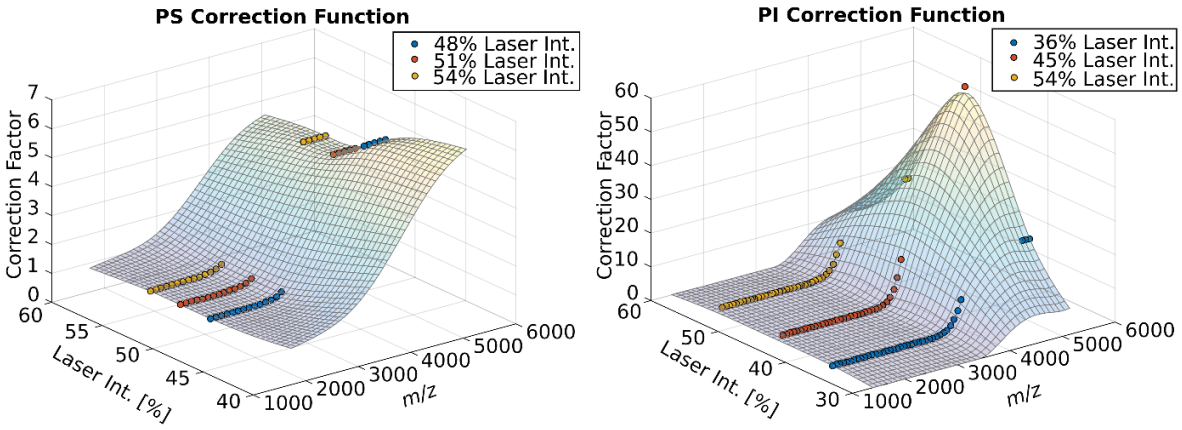

Figure S. 6 Estimated correction factors for PS (left) and PI (right) as a bivariate function of mass and laser intensity.

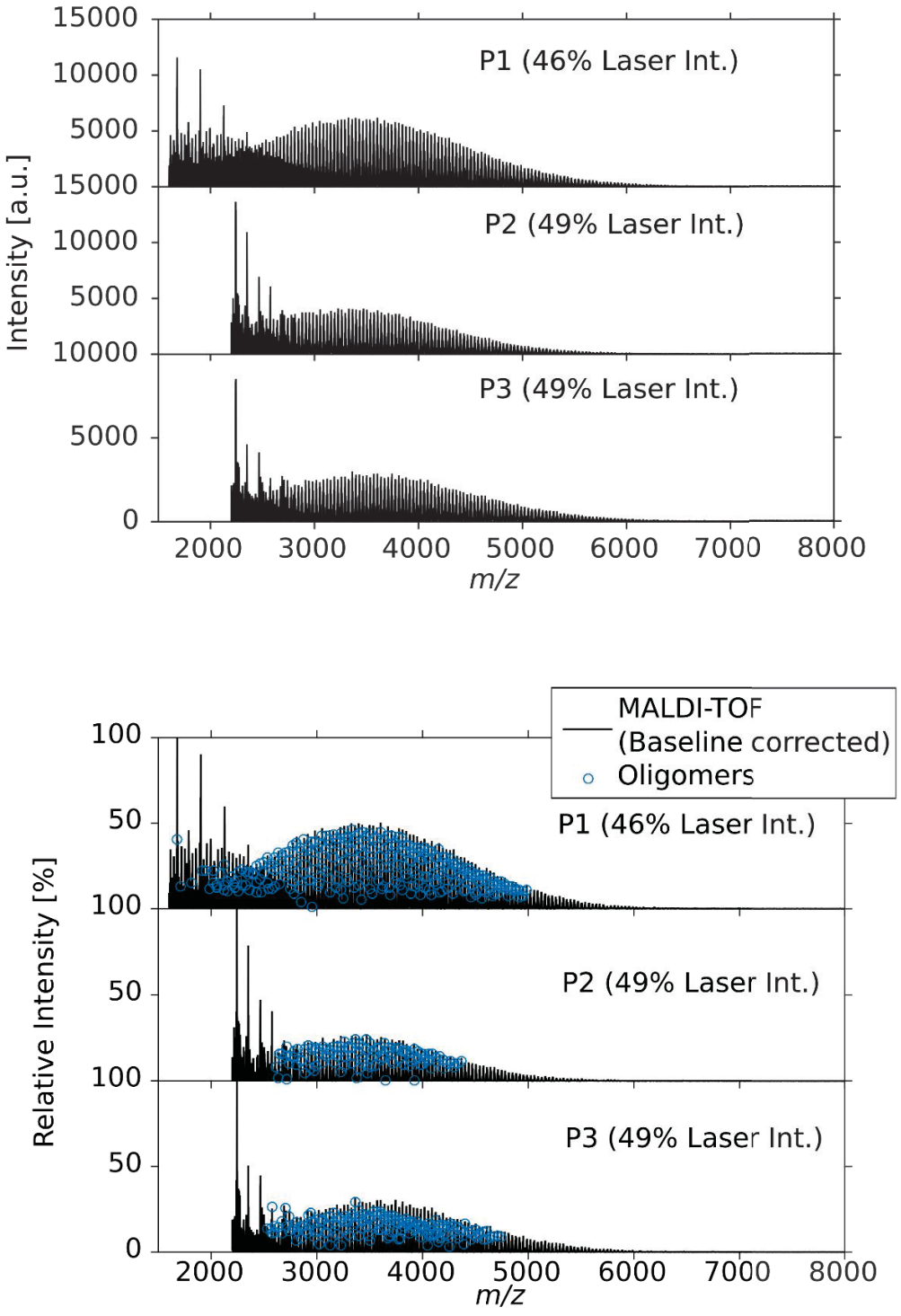

Figure S. 7. Top: MALDI-TOF mass spectra of copolymers P1 to P3, bottom: mass spectra after baseline correction overlaid with oligomer peaks computed by COCONUT.